

TOTAL SYNTHESIS OF GOMBAMIDE A AND ACTINOPHENANTHROLINE A.  
DISCOVERY, OPTIMIZATION AND CHARACTERIZATION OF NOVEL POSITIVE  
ALLOSTERIC MODULATORS FOR THE METABOTROPIC GLUTAMATE RECEPTOR  
SUBTYPE 1.

By

Pedro M. Garcia Barrantes

Dissertation

Submitted to the Faculty of the  
Graduate School of Vanderbilt University  
in partial fulfillment of the requirements  
for the degree of

DOCTOR OF PHILOSOPHY

in

Chemical & Physical Biology

December, 2016

Nashville, Tennessee

Approved:

Craig W. Lindsley, Ph.D.

Gary A. Sulikowski, Ph.D.

Stephen W. Fesik, Ph.D.

J. Scott Daniels, Ph.D.

Henry Charles Manning, Ph.D.

A Rosanna, el amor de mi vida y mi compañera de aventuras.

A mi papá, mi mamá y hermanos por estar siempre conmigo, aún en la distancia.

## ACKNOWLEDGEMENTS

I have been really fortunate for all the opportunities I have had in my career, and I am very thankful to God for this. Also, I would like to acknowledge my family, colleagues and mentors during these years, this journey would have not been possible without them.

First, I would like to say thanks to my advisor Dr. Craig Lindsley. Even before joining his lab, Craig has always been there to provide me with help and guidance, encouraging me to do great research, while allowing me to explore new frontiers. Craig's productivity and passion for science is contagious, I can assure his keen academic and professional advice will accompany me for the rest of my career, along with a developed palate for good scotch.

I would also like to recognize my committee members. To Dr. Gary Sulikowski, who instructed me in the art of organic synthesis and classic rock. I am very thankful he accepted to be my chair. To Dr. Stephen Fesik, who was the first person to open me the doors of his lab in Vanderbilt. I will always treasure the opportunity he gave me to perform medicinal chemistry during my rotation, as well as his advice throughout the years. To Dr. Scott Daniels, for inspiring me to learn more about pharmacokinetics and to be a more informed medicinal chemist. And to Dr. H. Charles Manning, for his career advice and his valuable input during our meetings.

I would also like to acknowledge Dr. P. Jeffrey Conn and Dr. Colleen Niswender for allowing me to perform the pharmacological assays of my project in their lab. I appreciate the input that both have gave to my research and their willingness to collaborate and make me feel welcomed in their laboratory. Their leadership in the VCNDD is invaluable. I would also like to thank Hyekyung P. Cho for being my experimental pharmacology mentor and for all the help provided for mutant and selectivity assays, without her previous work developing the mGlu<sub>1</sub> TR-Ex® 293 cell line this work would have not been possible.

To my collaborators in the pharmacokinetics group of the VCNDD, Ryan Morrison, Dr. Tom Bridges, Dr. Chuck Locuson and Dr. Annie Blobaum, who have been fundamental for this project and have been always willing to answer my DMPK questions.

I would also like to thank all individuals within the VCNDD and the past and current members of the Lindsley lab. They made coming to the lab fun and enjoyable and I am certain that we have forged a friendship that will last longer than our graduate years.

I am also very thankful to the Vanderbilt International Scholar Program (VISP), which convinced me of coming to Vanderbilt and offered me support and assistance over these years. I am especially thankful to Dr. Kathy Gould and the leadership committee, as well as to Amanda Connolly and Leslie Pitman. Also, special thanks to the QCB/CPB program, especially Dr. David Piston, Lindsay Meyers, Dr. Bruce Damon and Patty Mueller.

También agradezco a mi familia. A mis padres, por estar siempre presentes y por apoyarme en este viaje, siento su amor y cariño en la distancia. A mi hermana Graciela y a mi hermano Marco por su comprensión y apoyo incondicional.

Finalmente, a mi querida esposa Rosanna, testigo y participe de esta aventura. Un agradecimiento infinito por tener la valentía de dar un paso adelante a lo incierto y desconocido, tener la paciencia de vivir con este aprendiz de científico y compartir las dificultades y los triunfos en estos cuatro años; se me hace imposible imaginar este proyecto sin ella. Su amor y cariño son parte importante de la fuerza que motiva la investigación descrita en este documento.



## TABLE OF CONTENTS

	Page
DEDICATION .....	ii
ACKNOWLEDGEMENTS .....	iii
LIST OF TABLES .....	viii
LIST OF FIGURES .....	xii
LIST OF SCHEMES.....	xvi
LIST OF EQUATIONS .....	xix
LIST OF ABBREVIATIONS.....	xx
Chapters	
I. TOTAL SYNTHESIS OF GOMBAMIDE A .....	1
Introduction.....	1
Retrosynthetic analysis for the synthesis of Gombamide A .....	7
Dehydration route for Gombamide A .....	9
Copper-catalyzed amidation route for Gombamide A.....	15
Metathesis route for Gombamide A.....	17
Grieco elimination route for Gombamide A .....	19
Summary and future directions .....	30
Experimental methods .....	31
II. TOTAL SYNTHESIS OF ACTINOPHENANTHROLINE A .....	50
Introduction.....	50
Retrosynthetic analysis for the synthesis of Actinophenanthroline A .....	53
Synthesis of Actinophenanthroline A .....	54
Summary and future directions .....	62
Experimental methods .....	63
III. METABOTROPIC GLUTAMATE RECEPTOR SUBTYPE 1 ACTIVATION AND OPTIMIZATION EFFORTS AROUND RO 07-11401 .....	77
Metabotropic glutamate receptor subtype 1 .....	77
Glutamate in the nervous system .....	77
Structural features of the metabotropic glutamate receptor subtype 1.....	79
Signaling of the metabotropic glutamate receptor subtype 1 .....	81
Normal distribution of the mGlu <sub>1</sub> receptor in the brain .....	81

Role of the mGlu <sub>1</sub> receptor in brain function and psychiatric conditions.....	83
Role of the mGlu <sub>1</sub> receptor in memory and learning .....	83
Role of the mGlu <sub>1</sub> receptor in the motor activity .....	87
Role of the mGlu <sub>1</sub> receptor in anxiety .....	90
Role of the mGlu <sub>1</sub> receptor in hyperexcitability and seizures.....	90
Role of the mGlu <sub>1</sub> receptor in addiction .....	92
Role of the mGlu <sub>1</sub> receptor in schiziphrenia.....	95
Ligands for the metabotropic glutamate receptor subtype 1 .....	96
Orthosteric agonists .....	96
Orthosteric antagonists .....	98
Allosteric ligands .....	100
Negative allosteric modulators .....	101
Positive allosteric modulators.....	107
Study of the structure-activity relationship around Ro 07-11401.....	108
Development of Ro 07-11401.....	108
Modifications to the Ro 07-11401 scaffold .....	111
Computational efforts to optimize Ro 07-11401 .....	130
Summary and future directions.....	135
Experimental methods .....	137

#### IV. DISCOVERY OF POSITIVE ALLOSTERIC MODULATORS FOR THE METABOTROPIC GLUTAMATE RECEPTOR SUBTYPE 1 AROUND A NEW CHEMOTYPE..... 151

Identification of a starting point for a campaign to develop an mGlu <sub>1</sub> positive allosteric modulator.....	151
Medicinal chemistry around CDPBB and VU-71 structure.....	151
Dual mGlu <sub>1</sub> /mGlu <sub>4</sub> PAMs as starting point for development of selective mGlu <sub>1</sub> PAMs ....	153
Exploration of the structure-activity relationship around VU0405622.....	154
Medicinal chemistry strategy for the exploration of VU0405622 .....	154
Modification on the eastern picolinamide of VU0405622.....	156
Exploration of the SAR in the phthalimide in the context of <b>4.51</b> , <b>4.28</b> and <b>4.22</b> .....	167
Additional SAR around scaffold VU0405622 and its picolinamide derivatives .....	175
Evaluation of the new mGlu <sub>1</sub> PAMs in the wild type and mutated receptors.....	181
Pharmacokinetic characterization of the new mGlu <sub>1</sub> PAMs.....	191
<i>In vitro</i> pharmacokinetic properties and brain penetrance of novel mGlu <sub>1</sub> PAMs .....	191
Plasma biotransformation analysis of a compound around VU0405622 scaffold.....	193
Designing of mGlu <sub>1</sub> PAMs with better plasma stability.....	195
Summary and future directions.....	199
Experimental methods .....	201

#### V. DISCOVERY OF VU0486321, A POTENT, PREFERENTIAL AND BRAIN PENETRANT MGLU1 PAM..... 225

Finding a more potent eastern piece as a replacement of the VU0405622's picolinamide ....	225
Bioisostere replacements for the picolinamide .....	225
Exploration of the SAR around the furan .....	230
Discovery and characterization of VU0486321 .....	234
Phthalimide modifications around VU0474633 .....	234

Pharmacodynamic characterization of VU0474633 analogs .....	237
Pharmacokinetic characterization of VU0474633 analogs .....	244
Adverse event propensity of VU0474633 analogs .....	248
Summary and future directions .....	251
Experimental methods .....	254

VI. LEAD OPTIMIZATION OF VU0486321 SERIES: DISCOVERY OF VU0487351 AND VU6004909, MGLU1 PAMS WITH AN IMPROVED PHARMACOKINETIC PROFILE .... 263

SAR exploration for the replacement of the furan ring.....	263
Screening of different methyl substituted rings as replacements of the furan .....	263
Modification of the phthalimide in the context of methyl-substituted furan replacements from <b>6.9, 6.10, 6.12</b> and <b>6.14</b> .....	266
Exploration of different heteroaromatic rings in the context of a methylene linker.....	273
SAR exploration in the central phenyl ring .....	274
Study of substituents in the central phenyl ring.....	274
Homologation of the anilines in the central phenyl ring.....	293
Cycloalkanes replacement for the central phenyl ring.....	296
Substitution pattern in the central phenyl ring.....	297
SAR exploration for the replacement of the phthalimide .....	298
Fused rings as substitutes of the phthalimide ring .....	298
Reverse amides as replacements of the phthalimide.....	299
Ring opening of the phthalimide.....	304
Tied-back rings as replacements of the phthalimide.....	308
Other replacements of the phthalimide .....	309
Isoindolinones as replacements of the phthalimide .....	315
Summary and future directions .....	324
Experimental methods .....	327

Appendix

A. NMR spectra relevant to chapter I .....	337
B. NMR spectra relevant to chapter II .....	369
C. NMR spectra relevant to chapter III.....	382
D. NMR spectra relevant to chapter IV .....	389
E. NMR spectra relevant to chapter V .....	458
F. NMR spectra relevant to chapter VI.....	479
REFERENCES .....	506

## LIST OF TABLES

Table	Page
<b>Table 1.1.</b> One pot Boc-deprotection/dehydration of derivative <b>1.40</b> .....	10
<b>Table 1.2.</b> Tandem deprotection/cyclization of <b>1.81</b> .....	29
<b>Table 1.3.</b> NMR data comparison between isolated and synthetic Gombamide A .....	47
<b>Table 2.1.</b> NMR data comparison between isolated and synthetic Actinophenanthroline.....	68
<b>Table 2.2.</b> Atomic coordinates and equivalent isotropic displacement parameters.....	71
<b>Table 2.3.</b> Anisotropic displacement parameters. ....	73
<b>Table 2.4.</b> Geometric parameters.. ....	74
<b>Table 3.1.</b> Representative orthosteric agonists for the mGlu <sub>1</sub> receptor. ....	97
<b>Table 3.2.</b> Representative orthosteric antagonists for the mGlu <sub>1</sub> receptor. ....	99
<b>Table 3.3.</b> Representative negative allosteric modulators for the mGlu <sub>1</sub> receptor. ....	104
<b>Table 3.4.</b> Representative positive allosteric modulators for the mGlu <sub>1</sub> receptor .....	107
<b>Table 3.5.</b> Structures of the aromatic amine library analogs <b>3.114-3.162</b> and associated PAM activity from the single point screening at 10 μM in human mGlu <sub>1</sub> .....	116
<b>Table 3.6.</b> Potencies in human and rat forms of mGlu <sub>1</sub> for the active compounds obtained from the aromatic amine library .....	124
<b>Table 3.7.</b> Effect of the VU6000790 <b>3.152</b> , VU6000799 <b>3.156</b> and Ro 07-11401 <b>3.43</b> at 10 μM in the potency and efficacy of glutamate in the human mGlu <sub>1</sub> receptor in a fold-shift .....	129
<b>Table 3.8.</b> <i>In vitro</i> pharmacokinetic characterization and brain penetrance evaluation of VU6000790 <b>3.152</b> , VU6000799 <b>3.156</b> and Ro 07-11401 <b>3.43</b> . ....	130
<b>Table 4.1.</b> Structures of the amide library analogs <b>4.13-4.65</b> and associated PAM activity from the single point screening at 10 μM in human mGlu <sub>1</sub> .....	158
<b>Table 4.2.</b> Potencies in human and rat forms of mGlu <sub>1</sub> and human mGlu <sub>4</sub> for the active compounds obtained from the amide library single point screen... ..	166

<b>Table 4.3.</b> Potencies in human mGlu <sub>1</sub> and mGlu <sub>4</sub> of compounds derived from the matrix library <b>4.76a-4.78g</b> .....	170
<b>Table 4.4.</b> Structures of phenyl ring modified analogs <b>4.84-4.89</b> and associated PAM activity from the single point screening at 3 μM in rat mGlu <sub>1</sub> . .....	177
<b>Table 4.5.</b> Maximal efficacy of agonists glutamate and DHPG in wild type and mutant mGlu <sub>1</sub> receptors obtained in kinetic calcium mobilization assays .....	184
<b>Table 4.6.</b> Effect of PAMs on the parameters of concentration-response curve of glutamate and DHPG in hmGlu <sub>1</sub> . .....	185
<b>Table 4.7.</b> Effect of PAMs on the parameters of concentration-response curve of glutamate in hmGlu <sub>1</sub> mutant constructs .....	188
<b>Table 4.8.</b> Effect of PAMs on the parameters of concentration-response curve of DHPG in hmGlu <sub>1</sub> mutant constructs. ....	191
<b>Table 4.9.</b> Intrinsic clearance and predicted hepatic clearance for the new mGlu <sub>1</sub> PAMs.....	192
<b>Table 4.10.</b> Potencies in human mGlu <sub>1</sub> and mGlu <sub>4</sub> of isoindolinone analogs <b>4.145-4.146</b> and <b>4.150-4.151</b> .....	198
<b>Table 5.1.</b> Structures of the pyridine bioisostere library, analogs <b>5.1-5.17</b> and associated PAM activity from the single point screening at 10 μM in human mGlu <sub>1</sub> . .....	227
<b>Table 5.2.</b> Structures of the pyridine bioisostere library, analogs <b>5.18-5.32</b> and associated PAM activity from the single point screening at 10 μM in human mGlu <sub>1</sub> .....	231
<b>Table 5.3.</b> Potencies in human mGlu <sub>1</sub> and mGlu <sub>4</sub> of VU0474633 analogs <b>5.35a-5.35g</b> .....	236
<b>Table 5.4.</b> Effect of VU0486287 <b>5.35g</b> , VU0486320 <b>5.35e</b> and VU0486321 <b>5.35c</b> on the parameters of concentration-response curve of glutamate in hmGlu <sub>1</sub> . .....	241
<b>Table 5.5.</b> Effect of VU0486287 <b>5.35g</b> , VU0486320 <b>5.35e</b> and VU0486321 <b>5.35c</b> on the parameters of concentration-response curve of glutamate in hmGlu <sub>1</sub> mutant constructs. ....	244
<b>Table 5.6.</b> <i>In vitro</i> pharmacokinetic properties of analogs VU0486287 <b>5.35g</b> , VU0486320 <b>5.35e</b> and VU0486321 <b>5.35c</b> .....	245

<b>Table 5.6.</b> <i>In vivo</i> rat pharmacokinetic properties of analogs VU0486287 <b>5.35g</b> , VU0486320 <b>5.35e</b> and VU0486321 <b>5.35c</b> .....	247
<b>Table 6.1.</b> Structures of the amide library analogs <b>6.1-6.14</b> and associated PAM activity from the single point screening at 10 $\mu$ M in human mGlu <sub>1</sub> .....	265
<b>Table 6.2.</b> Potencies in human mGlu <sub>1</sub> and mGlu <sub>4</sub> of compounds derived from the matrix library <b>6.23a-6.26g</b> .....	268
<b>Table 6.3.</b> Potencies in human mGlu <sub>1</sub> and mGlu <sub>4</sub> of compounds derived from the matrix library with modifications in the central phenyl ring, <b>6.37a</b> , <b>6.37b</b> , <b>6.37c</b> , <b>6.37d</b> and <b>6.37m</b> . .....	277
<b>Table 6.4.</b> Potencies in human mGlu <sub>1</sub> and mGlu <sub>4</sub> of compounds derived from the matrix library with modifications in the central phenyl ring, <b>6.37n</b> , <b>6.37o</b> and <b>6.37l</b> . .....	281
<b>Table 6.5.</b> Potencies in human mGlu <sub>1</sub> and mGlu <sub>4</sub> of compounds derived from modifications in the central phenyl ring, <b>6.37e-k</b> .....	284
<b>Table 6.6.</b> Potencies in human mGlu <sub>1</sub> and mGlu <sub>4</sub> of compounds derived from modifications of the phthalimide in VU6002194, <b>6.45-6.51</b> .....	288
<b>Table 6.7.</b> <i>In vitro</i> pharmacokinetic properties of analogs <b>6.45-6.48</b> and <b>6.50</b> .....	289
<b>Table 6.8.</b> <i>In vivo</i> pharmacokinetic properties of analogs <b>6.45-6.48</b> and <b>6.50</b> .....	290
<b>Table 6.9.</b> Comparison of the single point screen result for PAM activity in human mGlu <sub>1</sub> at 10 $\mu$ M for compounds derived from modifications in the furan region of VU6002194, analogs <b>6.53-6.67</b> . .....	292
<b>Table 6.10.</b> Structures of the reverse amide analogs <b>6.116-6.140</b> and associated PAM activity from the single point screening at 10 $\mu$ M in human mGlu <sub>1</sub> .....	301
<b>Table 6.11.</b> Structures of the open ring analogs <b>6.141-6.148</b> and <b>6.158-6.163</b> , and associated PAM activity from the single point screening at 10 $\mu$ M in human mGlu <sub>1</sub> .....	307
<b>Table 6.12.</b> Structures of the phthalimide replacement analogs <b>6.168-6.171</b> and <b>6.187-6.193</b> , and associated PAM activity from the single point screening at 10 $\mu$ M in human mGlu <sub>1</sub> .....	311

<b>Table 6.13.</b> Potencies in human mGlu <sub>1</sub> of VU0486321phthalimide replacements analogs <b>6.168-6.171</b> and <b>6.187-6.193</b> .....	313
<b>Table 6.14.</b> Potencies in human mGlu <sub>1</sub> of isoindolinone related analogs <b>6.194-6.212</b> .....	316
<b>Table 6.15.</b> <i>In vitro</i> pharmacokinetic properties of isoindolinone <b>6.197</b> VU0487351.....	320
<b>Table 6.16.</b> <i>In vivo</i> pharmacokinetic properties of isoindolinone <b>6.197</b> VU0487351.....	321
<b>Table 6.17.</b> Potencies in human mGlu <sub>1</sub> of isoindolinone related analogs <b>6.214-6.225</b> .....	322

## LIST OF FIGURES

Figure	Page
<b>Figure 1.1.</b> Natural products isolated from marine sponges of the <i>Clathria</i> genus with confirmed biological activity.....	2
<b>Figure 1.2.</b> Marine sponge <i>Clathria gombawuensis</i> and examples of isolated natural products from this organism .....	3
<b>Figure 1.3.</b> Structure of Gombamide A ( <b>1.16</b> ), a thiohexapeptide with unusual amino acids and a rare disulfide-containing, 17-membered macrocycle.....	4
<b>Figure 1.4.</b> Example of natural products with <i>p</i> HSA in its structure .....	5
<b>Figure 1.5.</b> Representative structures of macrocyclic peptides containing 17 ( <b>1.26</b> and <b>1.27</b> ) and 18-member rings ( <b>1.28</b> and <b>1.29</b> ).....	6
<b>Figure 1.6.</b> <sup>1</sup> H-NMR monitoring of the oxidation of <b>1.75</b> to produce enamide <b>1.76</b> .....	25
<b>Figure 2.1.</b> Representative examples of natural products isolated from marine actinomycetes ...	51
<b>Figure 2.2.</b> Structures of actinobenzoquinoline ( <b>2.5</b> ) and actinophenanthroline A-C ( <b>2.6-2.8</b> )....	52
<b>Figure 2.3.</b> X-ray crystal structure of synthetic actinophenanthroline A ( <b>2.6</b> ) .....	61
<b>Figure 3.1.</b> The glutamatergic synapse. ....	79
<b>Figure 3.2.</b> Diagram and 3-D model based on X-Ray crystal structures of the mGlu <sub>1</sub> receptor ...	80
<b>Figure 3.3.</b> Discovery of compound Ro 67-4853 <b>3.45</b> .....	109
<b>Figure 3.4.</b> Bioisosteric replacement of the carbamate in the Ro 67-4853 <b>3.45</b> series .....	110
<b>Figure 3.5.</b> Discovery of compound Ro 07-11401 <b>3.43</b> .....	111
<b>Figure 3.6.</b> Possible chemical modifications to study the SAR around Ro 07-11401 .....	112
<b>Figure 3.7.</b> Saturated acyclic amines that yield inactive compounds for mGlu <sub>1</sub> PAM activity, analogs <b>3.49-3.67</b> .....	113
<b>Figure 3.8.</b> Saturated cyclic amines that yield inactive compounds for mGlu <sub>1</sub> PAM activity, analogs <b>3.68-3.113</b> .....	114
<b>Figure 3.9.</b> Comparison of the single point screen result for PAM activity in human mGlu <sub>1</sub> at 10 μM for the aromatic amine library, analogs <b>3.114-3.162</b> . ....	116
<b>Figure 3.10.</b> Xanthene replacements that yield inactive compounds for mGlu <sub>1</sub> PAM activity, analogs <b>3.165-3.180</b> .....	127



<b>Figure 3.11.</b> Glutamate concentration-response curve fold-shift experiments for compound VU6000790 <b>3.152</b> , VU6000799 <b>3.156</b> and Ro 07-11401 <b>3.43</b> .....	128
<b>Figure 3.12.</b> Flow diagram of the ligand-based approach to improve the properties of RO 07-11401 .....	132
<b>Figure 3.13.</b> Machine-learning neural network model performance.....	133
<b>Figure 3.14.</b> Synthesized virtual screening hits, analogs <b>3.181-3.195</b> .....	134
<b>Figure 3.15.</b> Summary of the results of the structure-activity relationship study around Ro 07-11401 <b>3.43</b> .....	135
<b>Figure 3.16.</b> Initial compound selection from the virtual screening by the artificial neural network. ....	149
<b>Figure 3.17.</b> The highest-scoring Surflex-Sim binding hypothesis using Ro 07-11401 <b>3.43</b> and Ro 67-4853 <b>3.45</b> .....	150
<b>Figure 4.1.</b> CDPPB analogs that potentiate the rat mGlu <sub>1</sub> receptor .....	152
<b>Figure 4.2.</b> VU-71 <b>4.4</b> activity in the rat mGlu <sub>1</sub> receptor.....	153
<b>Figure 4.3.</b> Dual mGlu <sub>1</sub> /mGlu <sub>4</sub> PAMs derived from mGlu <sub>4</sub> PAM drug discovery program at the VCNDDD .....	154
<b>Figure 4.4.</b> Chemical modifications to explore the SAR around VU0405622 scaffold.....	155
<b>Figure 4.5.</b> Optimization work flow for the development of adequate mGlu <sub>1</sub> PAMs for <i>in vivo</i> target validation studies. ....	156
<b>Figure 4.6.</b> Comparison of the single point screen result for PAM activity in rat and human mGlu <sub>1</sub> at 10 μM for the amide library, analogs <b>4.13-4.65</b> . ....	158
<b>Figure 4.7.</b> Potency of analogs <b>4.76b</b> (VU0483737) and <b>4.77b</b> (VU0483605) in the rat and human mGlu <sub>1</sub> receptor .....	173
<b>Figure 4.8.</b> Selectivity of VU0483605 <b>4.77b</b> against the mGlu receptors determined in fold-shift mode.....	174
<b>Figure 4.9.</b> Comparison of the single point screen result for PAM activity in human mGlu <sub>1</sub> at 3 μM for the phenyl ring modified analogs <b>4.84-4.89</b> . ....	176
<b>Figure 4.10.</b> Comparison of the single point screen result for PAM activity in human mGlu <sub>1</sub> at 10 μM for the phenyl ring modified analogs <b>4.97-4.104</b> .....	179
<b>Figure 4.11.</b> Analogs to assess the effect of the removal of the carbonyl group in the picolinamide side of VU0405622 .....	180

<b>Figure 4.12.</b> Distribution of mutations in the hmGlu <sub>1</sub> gene that are enriched in schizophrenic and bipolar patients.....	181
<b>Figure 4.13.</b> Effect of mutations in the mGlu <sub>1</sub> response of glutamate and DHPG, with respect to wild type in fold shift experiments. ....	183
<b>Figure 4.14.</b> Effect of PAMs on the concentration-response curve of glutamate and DHPG in hmGlu <sub>1</sub> .....	185
<b>Figure 4.15.</b> Effect of the application of mGlu <sub>1</sub> PAMs on the concentration response curve of glutamate in hmGlu <sub>1</sub> mutant constructs .....	187
<b>Figure 4.16.</b> Effect of the application of mGlu <sub>1</sub> PAMs on the concentration response curve of DHPG in hmGlu <sub>1</sub> mutant constructs.....	190
<b>Figure 4.17.</b> Biotransformation analysis of VU0405623 <b>1.141</b> in rat and human plasma.....	194
<b>Figure 4.18.</b> Identification of metabolites for plasma degradation of VU0405623 <b>4.141</b> .....	195
<b>Figure 4.19.</b> Exploration of SAR in the VU0405622 <b>4.8</b> scaffold.....	199
<b>Figure 5.1.</b> Comparison of the single point screen result for PAM activity in human mGlu <sub>1</sub> at 10 μM for the pyridine bioisostere library, analogs <b>5.1-5.17</b> .....	227
<b>Figure 5.2.</b> Comparison of the concentration-response of curve for PAM activity of <b>5.2</b> (VU0487495) and <b>5.13</b> (VU0474567) in human mGlu <sub>1</sub> .....	230
<b>Figure 5.3.</b> Comparison of the single point screen result for PAM activity in human mGlu <sub>1</sub> at 10 μM for the pyridine bioisostere library, analogs <b>5.18-5.32</b> .....	231
<b>Figure 5.4.</b> Concentration-response of curve for PAM activity of VU0474633 <b>5.27</b> in human and rat mGlu <sub>1</sub> .....	234
<b>Figure 5.5.</b> Concentration-response of curve for PAM activity of VU0486321 <b>5.35c</b> ,VU0486320 <b>5.35e</b> and VU0486287 <b>5.35g</b> in human and rat mGlu <sub>1</sub> .....	238
<b>Figure 5.6.</b> Selectivity of VU0486321 <b>5.35c</b> ,VU0486320 <b>5.35e</b> and VU0486287 <b>5.35g</b> against the mGlu receptors determined in fold-shift mode .....	239
<b>Figure 5.7.</b> Effect of VU0486287 <b>5.35g</b> , VU0486320 <b>5.35e</b> and VU0486321 <b>5.35c</b> on the concentration-response curve of glutamate in hmGlu <sub>1</sub> .....	240
<b>Figure 5.8.</b> Effect of the application of mGlu <sub>1</sub> PAMs VU0486287 <b>5.35g</b> , VU0486320 <b>5.35e</b> and VU0486321 <b>5.35c</b> on the concentration response curve of glutamate in hmGlu <sub>1</sub> mutants.....	243
<b>Figure 5.9.</b> Biotransformation analysis of VU0486321 <b>5.35c</b> in rat and human plasma .....	246
<b>Figure 5.10.</b> mGlu <sub>1</sub> ago-PAM VU0486321 <b>5.35c</b> did not induce epileptiform activity in CA3 region of the hippocampus.....	249
<b>Figure 5.11.</b> mGlu <sub>1</sub> PAMs do not induce behavioral convulsions in mice .....	250

<b>Figure 5.12.</b> SAR summary for the obtention of analogs <b>5.35c</b> , <b>5.35e</b> and <b>5.35g</b> .....	251
<b>Figure 5.13.</b> Summary of VU0486287 <b>5.35g</b> , VU0486320 <b>5.35e</b> and VU0486321 <b>5.35c</b> properties .....	253
<b>Figure 6.1.</b> SAR exploration around the central phenyl ring of the VU0486321 scaffold .....	274
<b>Figure 6.2.</b> Comparison of the pharmacodynamic and pharmacokinetic properties of analogs VU6002194 <b>6.37f</b> and VU0487104 <b>6.37g</b> .....	286
<b>Figure 6.3.</b> Comparison of the single point screen result for PAM activity in human mGlu <sub>1</sub> at 10 μM for reverse amide analogs <b>6.116-6.140</b> .....	301
<b>Figure 6.4.</b> Comparison of the single point screen result for PAM activity in human mGlu <sub>1</sub> at 10 μM for open ring analogs <b>6.141-6.148</b> and <b>6.158-6.163</b> .....	306
<b>Figure 6.5.</b> Comparison of the single point screen result for PAM activity in human mGlu <sub>1</sub> at 10 μM for different phthalimide replacements, analogs <b>6.168-6.171</b> and <b>6.187-6.193</b> .....	311
<b>Figure 6.6.</b> Structure activity relationship around VU0486321 <b>5.35c</b> .....	324
<b>Figure 6.7.</b> Pharmacodynamic and pharmacokinetic profile of VU6004909 <b>6.48</b> and VU0487351 <b>6.197</b> .....	325

## LIST OF SCHEMES

Scheme	Page
<b>Scheme 1.1.</b> Retrosynthetic strategy for the total synthesis of Gombamide A .....	8
<b>Scheme 1.2.</b> Synthesis of <b>1.40</b> en route to intermediate <b>1.41</b> .....	9
<b>Scheme 1.3.</b> Synthesis of pentapeptide <b>1.43</b> .....	12
<b>Scheme 1.4.</b> Synthesis of the acyclic hexapeptide <b>1.49</b> and first attempt to prepare <b>1.16</b> .....	14
<b>Scheme 1.5.</b> Synthesis of carboxamide <b>1.51</b> .....	16
<b>Scheme 1.6.</b> Synthesis of vinyl iodide <b>1.53</b> through a Takai olefination reaction .....	16
<b>Scheme 1.7.</b> Application of alkene metathesis in the synthesis of Paliurine E .....	17
<b>Scheme 1.8.</b> Obtention of intermediate <b>1.58</b> and attempts for production of <b>1.59</b> .....	18
<b>Scheme 1.9.</b> Synthesis of intermediate <b>1.62</b> through isomerization of <b>1.61</b> .....	19
<b>Scheme 1.10.</b> Application of Grieco elimination in the synthesis of Zizyphine A .....	20
<b>Scheme 1.11.</b> Efforts for the synthesis of intermediate <b>1.68</b> .....	21
<b>Scheme 1.12.</b> Efforts to synthesize intermediate <b>1.70</b> .....	21
<b>Scheme 1.13.</b> Synthesis of phenylselenoamine <b>1.74</b> .....	22
<b>Scheme 1.14.</b> Synthesis of fragment A via Grieco elimination procedure.....	24
<b>Scheme 1.15.</b> Synthesis of acyclic precursor <b>1.81</b> .....	27
<b>Scheme 1.16.</b> Completion of the synthesis of Gombamide A .....	28
<b>Scheme 2.1.</b> Retrosynthetic analysis for obtention of <b>2.5</b> .....	54
<b>Scheme 2.2.</b> Synthesis of 1,7-phenanthroline <b>2.10</b> .....	55
<b>Scheme 2.3.</b> Synthesis of aminohydroxyphenanthroline <b>2.9</b> .....	58
<b>Scheme 2.4.</b> Efforts for the protection of the phenol in <b>2.15</b> .....	59
<b>Scheme 2.5.</b> Synthesis of Actinophenanthroline A <b>2.6</b> .....	60
<b>Scheme 3.1.</b> Synthesis of diverse amines library, analogs <b>3.49-3.162</b> .....	112
<b>Scheme 3.2.</b> Synthesis of xanthene replacements library, analogs <b>3.165-3.180</b> .....	126

<b>Scheme 4.1.</b> Synthesis of picolinamide analogs <b>4.13-4.65</b> .....	156
<b>Scheme 4.2.</b> Synthesis of the matrix library with variations on the picolinamide and phthalimide region, analogs <b>4.76a-4.78g</b> .....	168
<b>Scheme 4.3.</b> Synthesis of phenyl ring modified analogs <b>4.84-4.87</b> .....	175
<b>Scheme 4.4.</b> Synthesis of reverse amide analogs <b>4.97-4.104</b> .....	178
<b>Scheme 4.5.</b> Synthesis of analogs <b>4.105-4.140</b> to assess the effect of the removal of the carbonyl group in the picolinamide side of VU0405622.....	179
<b>Scheme 4.6.</b> Synthesis of isoindolinone analogs <b>4.145-4.146</b> and <b>4.150-4.151</b> .....	197
<b>Scheme 5.1.</b> Synthesis of pyridine bioisostere analogs <b>5.1-5.17</b> .....	226
<b>Scheme 5.2.</b> Synthesis of analogs <b>5.35a-g</b> derived from VU0474633 <b>5.27</b> with modifications on the phthalimide .....	235
<b>Scheme 6.1.</b> Synthesis of analogs <b>6.1-6.14</b> .....	264
<b>Scheme 6.2.</b> Synthesis of matrix library analogs <b>6.23a-6.26g</b> to assess alternatives to the 3-methylfuran carboxamide in VU0486321 <b>5.35c</b> .....	267
<b>Scheme 6.3.</b> Synthesis of analogs <b>6.27-6.33</b> to assess the effect of the removal of the carbonyl group in the furancarboxamide side of VU0486321 scaffold.....	273
<b>Scheme 6.4.</b> Synthesis of analogs <b>6.37a-6.37o</b> to assess the effect of modifications on the central phenyl ring of VU0486321 scaffold. ....	276
<b>Scheme 6.5.</b> Synthesis of analogs of VU6002194 <b>6.37f</b> with modifications in the phthalimide, <b>6.45-6.51</b> .....	287
<b>Scheme 6.6.</b> Synthesis of analogs of VU6002194 <b>6.37f</b> with modifications in the furan ring, <b>6.53-6.67</b> .....	291
<b>Scheme 6.7.</b> Synthesis of homologues of VU0486321 <b>5.35c</b> , analogs <b>6.71-6.74</b> , <b>6.77-6.80</b> and <b>6.83-6.86</b> .....	295
<b>Scheme 6.8.</b> Synthesis of analogs of VU0486321 <b>5.35c</b> with a cycloalkyl central ring, analogs <b>6.89A-6.89D</b> .....	297
<b>Scheme 6.9.</b> Synthesis of analogs of VU0486321 <b>5.35c</b> with <i>meta</i> distribution in the central phenyl ring, analogs <b>6.99-6.101</b> . Description .....	298
<b>Scheme 6.10.</b> Synthesis of analogs of VU0486321 <b>5.35c</b> to replace the phthalimide with fused ring amides, analogs <b>6.102-6.112</b> .....	299
<b>Scheme 6.11.</b> Synthesis of analogs of VU0486321 <b>5.35c</b> to replace the phthalimide with reverse amides, analogs <b>6.116-6.140</b> .....	300

<b>Scheme 6.12.</b> Synthesis of analogs of VU0486321 <b>5.35c</b> to replace the phthalimide with open ring variants, analogs <b>6.141-6.148</b> and <b>6.158-6.163</b> .....	305
<b>Scheme 6.13.</b> Synthesis of analogs of VU0486321 <b>5.35c</b> to replace the phthalimide with a tied back ring strategy, analogs <b>6.167A-6.167G</b> .....	309
<b>Scheme 6.14.</b> Synthesis of analogs of VU0486321 <b>5.35c</b> with different phthalimide replacements, analogs <b>6.168-6.171</b> and <b>6.187-6.193</b> .....	310
<b>Scheme 6.15.</b> Synthesis of analogs of VU0486321 <b>5.35c</b> to replace the phthalimide with an isoindolinone, analogs <b>6.194-6.206</b> .....	315
<b>Scheme 6.16.</b> Synthesis of isoindolinone analogs of VU0486321 <b>5.35c</b> with additional modifications in the central phenyl ring, analogs <b>6.223-6.225</b> .....	321

## LIST OF EQUATIONS

Equation	Page
<b>Equation 3.1.</b> Determination of half-life.....	142
<b>Equation 3.2.</b> Determination of intrinsic clearance. ....	142
<b>Equation 3.3.</b> Determination of predicted hepatic clearance. ....	143
<b>Equation 3.4.</b> Determination of fraction unbound in plasma.....	143

## LIST OF ABBREVIATIONS

AcOH	Acetic acid
ACN	Acetonitrile
AMPA	Amino-3-hydroxy-5-methyl-4-isoxazolepropionate
Bz	Benzene
HATU	1-[Bis(dimethylamino)methylene]-1H-1,2,3-triazolo[4,5-b]pyridinium 3-oxid hexafluorophosphate
TDMS	<i>t</i> -Butyldimethylsilyl
CNS	Central Nervous System
TMP	2,4,6-collidine
CRC	Concentration-reponse curve
Cys	Cysteine
CRD	Cysteine rich-domain
CFTR	Cystic Fibrosis Transmembrane Conductance Regulator chloride channel
°C	Degree Celsius
PIDA	(diacetoxyiodo)benzene
DAG	Diacylglycerol
DCE	Dichloroethane
DCM	Dichloromethane
DEA	Diethylamine
DME	1,2-Dimethoxyethane
DMF	<i>N,N</i> -Dimethylformamide
EtOH	Ethanol
EDCI	1-Ethyl-3-(3-dimethylaminopropyl)carbodiimide
ELSD	Evaporative light scattering detector
EPSC	Excitatory postsynaptic currents



ERK	Extracellular receptor kinase
FDA	Food and Drug Administration
GPCR	G protein-coupled receptor
Glu	Glutamate
FITM	4-Fluoro-N-(4-(6-(isopropylamino)pyrimidin-4-yl)thiazol-2-yl)- <i>N</i> -Methylbenzamide
EAAT	High-affinity excitatory amino acid transporters
HPLC	High-performance liquid chromatography
HRMS	High resolution mass spectrometry
HOAt	1-Hydroxy-7-azabenzotriazole
HOBt	Hydroxybenzotriazole
IP <sub>3</sub>	1,4,5-Inositol trisphosphate
JNK	c-Jun N-terminal kinase (JNK)
LC-MS	Liquid chromatography coupled to mass spectrometry
LTP	Long-term potentiation
LTD	Long-term depression
mTOR	Mammalian target of rapamycin
mGlu	Metabotropic glutamate receptor
MeOH	Methanol
mRNA	Messenger RNA
NMDA	<i>N</i> -methyl-D-aspartate
MAPK	Mitogen-activated protein kinase
Mrp3	Multidrug-resistance protein 3
NCATS	National Center for Advancing Translational Sciences
NIH	National Institute of Health
NMR	Nuclear magnetic resonance
<i>p</i> HSA	<i>para</i> -hydroxystyrylamide

PIP <sub>2</sub>	Phosphatidylinositol biphosphate
PLC <sub>β</sub>	Phospholipase C <sub>β</sub>
PLD	Phospholipase D
PET	Positive emission tomography
PKC	Protein kinase C
THF	Tetrahydrofuran
TLC	Thin layer chromatography
Tol	Toluene
TRP	Transient receptor potential channels
TMD	Transmembrane-spanning domain
TFA	Trifluoroacetic acid
TMSN <sub>3</sub>	Trimethylsilylazide
UV	Ultraviolet
VFD	Venus flytrap domain
VGLUT	Vesicular glutamate transportes
VOCC	Voltage operated calcium channel

## CHAPTER I

### TOTAL SYNTHESIS OF GOMBAMIDE A

#### Introduction

Marine organisms have demonstrated to be the source of chemically diverse secondary metabolites which, due to its structural uniqueness and biological properties, represent interesting scaffolds for drug discovery.<sup>1-3</sup> In this realm, marine sponges have been a prolific source, yielding natural products in different structural groups from polyketides to polypeptides, including the FDA approved anticancer drug Eribulin (Halaven<sup>®</sup>).<sup>4</sup>

The genus *Clathria* provides a good example of chemical diversity in products isolated from marine sponges. Initial research of organic fractions from some species proved that the extracts inhibited quorum sensing, and had antibacterial activity as well as antiplasmodium properties,<sup>5-8</sup> while subsequent isolation reports showed the discovery of chemically diverse compounds with interesting biological activity such as clathsterol **1.1**,<sup>9</sup> mirabilin G **1.2**,<sup>10</sup> clathriol **1.3**,<sup>11</sup> microacionamide A **1.4** and B **1.5**,<sup>12</sup> clathriadic acid **1.6**, norbatzelladine L **1.7**,<sup>13</sup> clathric acid **1.8**,<sup>14</sup> and crambescindin 800 **1.9** (Fig.1.1).<sup>15</sup>

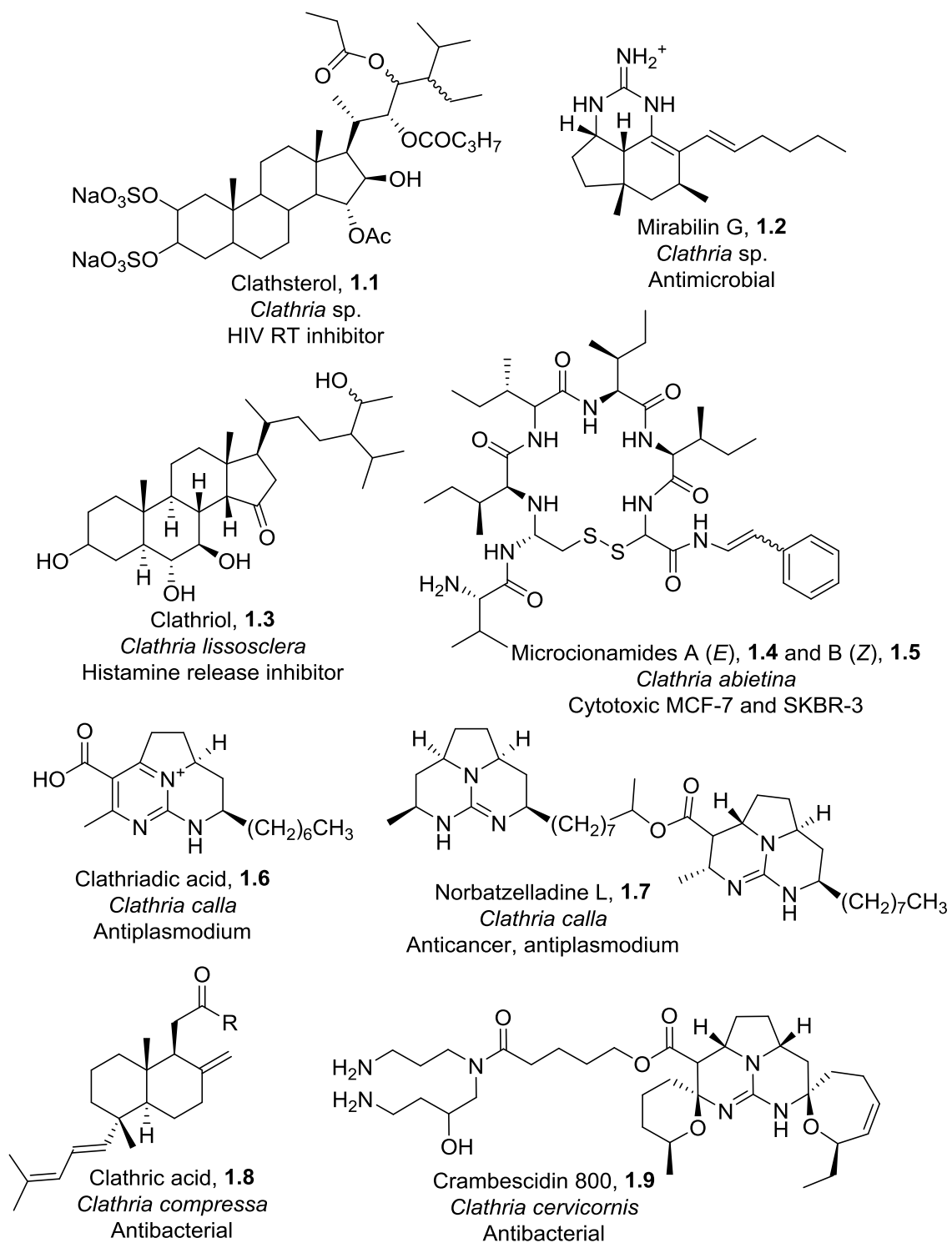


**Figure 1.1.** Natural products isolated from marine sponges of the *Clathria* genus with confirmed biological activity.

*Clathria gombawuiensis* is a red encrusting marine sponge from the order Poecilosclerida, family Microcionidae. This sponge has provided unique sesterterpenes with cytotoxic activity such as phorone B **1.10**, ansellone B **1.11**, gombaspiroketal A-C **1.12-1.14**, saponin gombaside A **1.15** and the peptide derived Gombamide A **1.16**. While **1.12**, **1.14** and **1.15** have also shown antibacterial activity (Fig. 1.2).<sup>16-18</sup>

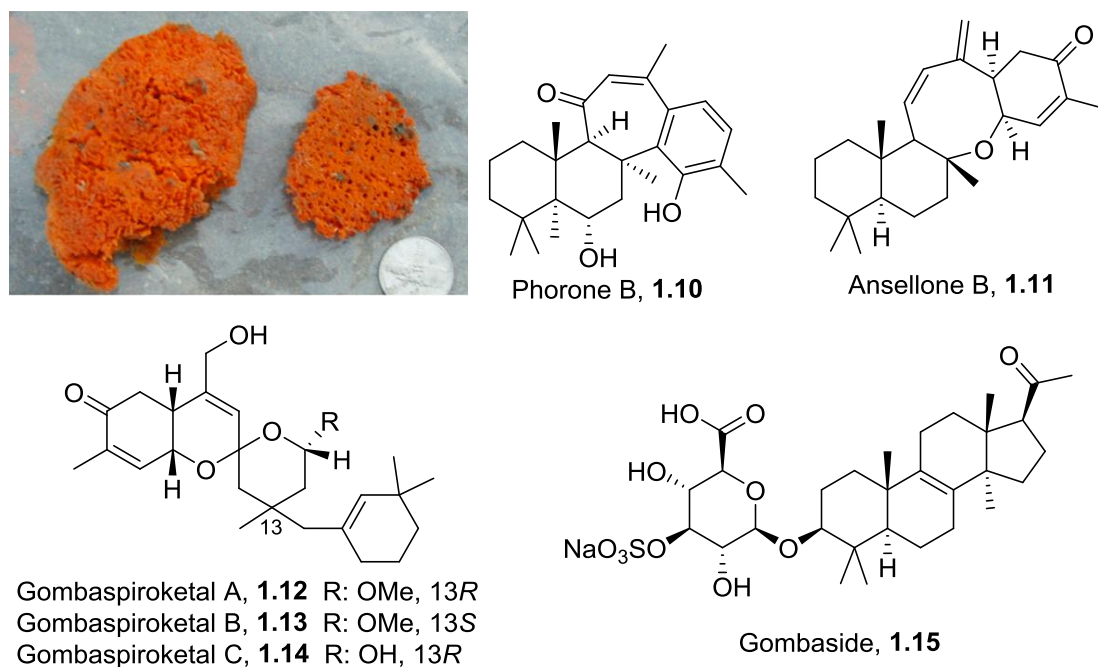


**Figure 1.2.** Marine sponge *Clathria gombawuiensis* and examples of isolated natural products from this organism.

Gombamide A (**1.16**, Fig. 1.3) was the first reported metabolite from this marine sponge. This cyclopeptide was isolated by Jongheon Shin's research group at Seoul National University, from specimens of *C.gombawuiensis* collected in the coast of Gaheo-Do, South Korea. **1.16** displayed cytotoxic activity against A549 (epithelial lung carcinoma) and K562 (chronic myelogenous leukemia) cell lines with LC<sub>50</sub>s of 7.1 μM and 6.9 μM, respectively. Furthermore, this natural product displayed inhibitory activity of the Na<sup>+</sup>/K<sup>+</sup>-ATPase pump with an IC<sub>50</sub> of 17.8 μM, only 2-fold less potent with respect to the positive control ouabaine (IC<sub>50</sub> = 9.4 μM).<sup>18</sup>

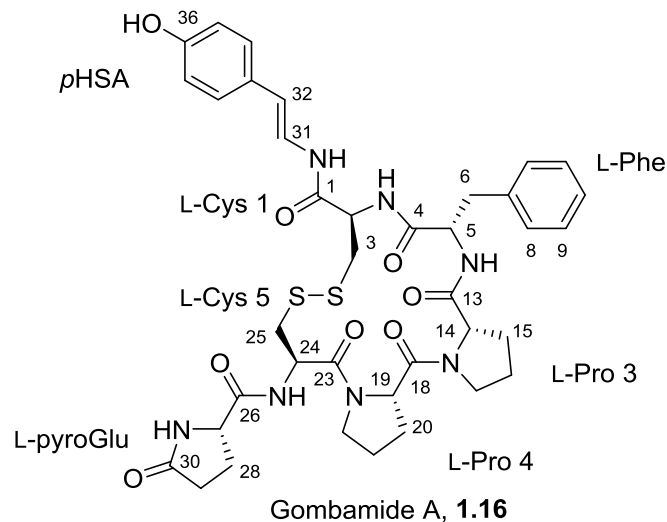


**Figure 1.3.** Structure of Gombamide A (**1.16**), a thiohexapeptide with unusual amino acids and a rare disulfide-containing, 17-membered macrocycle.

Remarkably, **1.16** presents various distinctive chemical features in its structure. Gombamide A is a rare, 17-membered macrocycle with a disulfide bond forming part of the cycle and two uncommon exocyclic substitutions: an L-pyrroglutamic amide (pyroGlu) and an (*E*)-*para*-hydroxystyrylamide (*p*HSA).

The O-substituted *p*HSA feature has been observed in macrocyclic peptides, primarily forming part of the 14-member cycle of cyclopeptide alkaloids in the *Z* configuration, like Sanjoinine A **1.17**;<sup>19–21</sup> while the only endocyclic *E* example has been found in the non-peptidic bastadins **1.18** and **1.19**.<sup>22</sup> The uncapped *p*HSA has only been reported in small, linear natural products **1.20-1.25**,<sup>23–30</sup> and **1.16** is the sole reported molecule where this moiety is present in a cyclic peptide (Fig. 1.4). Moreover, **1.16** is the first reported sulfur-containing molecule with an enamide functionality.

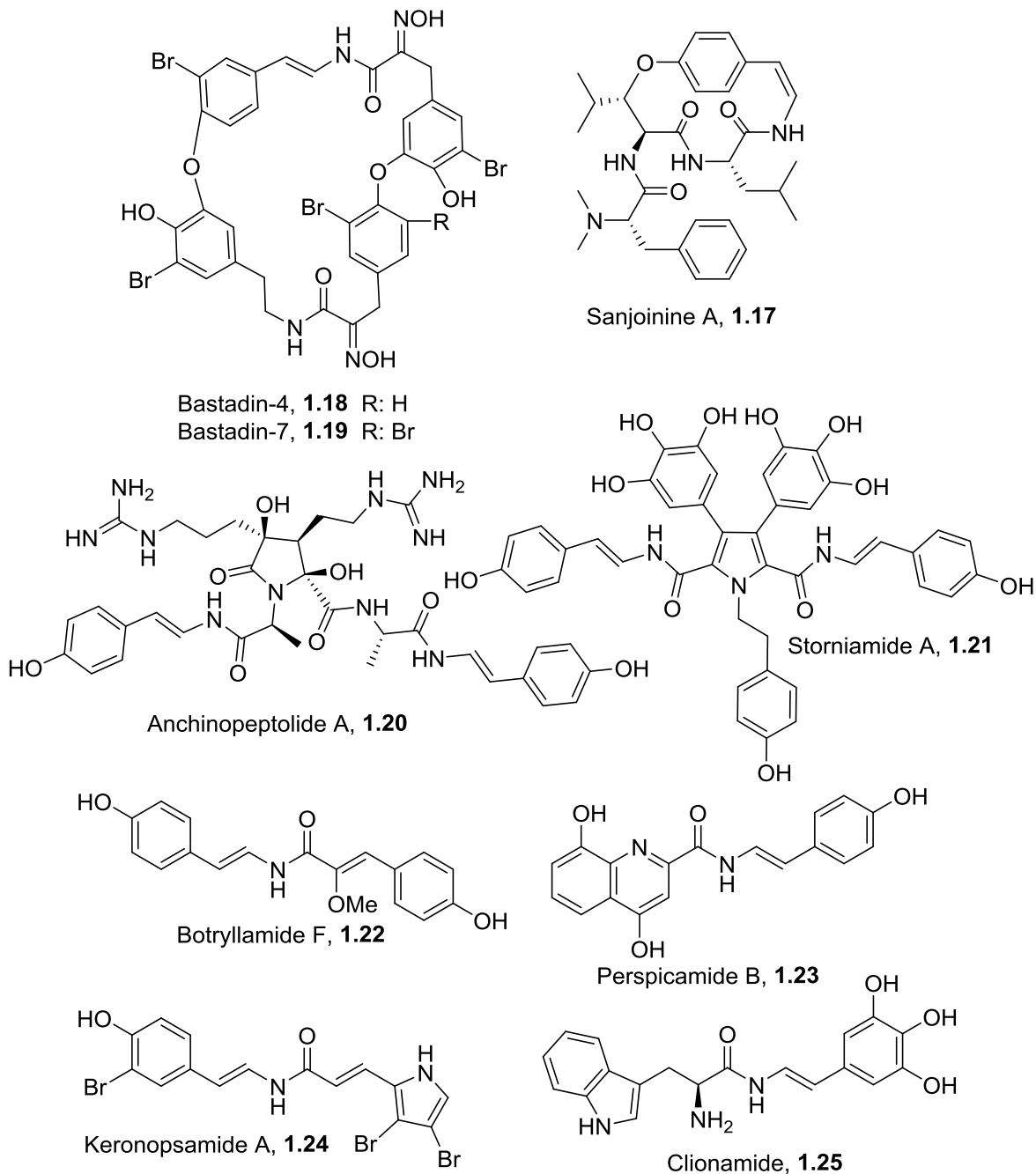


**Figure 1.4.** Examples of natural products with pHSA in its structure.

The examples of cyclic peptides with disulfide linkages isolated from marine sponges are scant.<sup>12,31,32</sup> Moreover, the 17-member ring thiopeptide cycle has only been reported before in two classes of peptide molecules: the eudistomide lipopeptides from the fijian ascidian *Eudistoma* sp. **1.26**,<sup>33</sup> and the malformins metabolites **1.27** from the *Aspergillus niger*; which are stimulants of

plant growth and possess cytotoxic and antibacterial activity (Fig. 1.5).<sup>34,35</sup> The structure of the antitumor antibiotics related to quinomycin, like Triostin A **1.28** and SW-163C **1.29**, have an 18-membered macrocycle which could be considered the homologue of the ring in **1.16**; these cyclopeptides act as topoisomerase and DNA polymerase inhibitors.<sup>36</sup> Considering that malformins and quinomycin analogs present a bicyclic arrangement, it would be possible that the monocyclic structure of **1.16** would represent a simpler pharmacophore for cytotoxic activity.

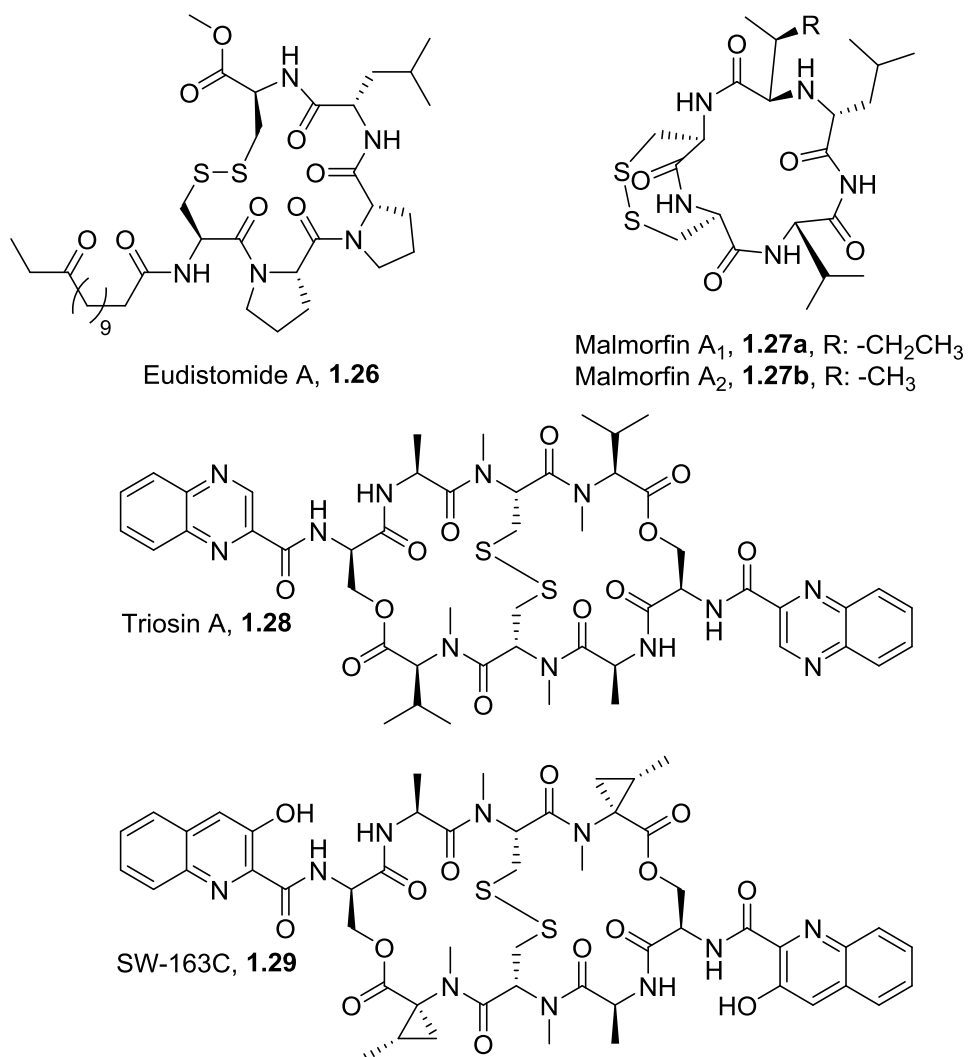


**Figure 1.5.** Representative structures of macrocyclic peptides containing 17 (**1.26** and **1.27**) and 18-member rings (**1.28** and **1.29**).



The mechanism for the cytotoxic activity of Gombamide A is unknown. In order to carry out the required experiments to study the biological effects of this natural product and elucidate its mechanism of action, the compound should be available in reasonable quantities. Obtaining this substance just by isolation from the marine sponge specimens would be an inefficient strategy, as **1.16** is produced in very small amounts from these organisms and can only be isolated after labor intensive purification of the material. Hence, a synthetic route to obtain Gombamide A appears as a promising way to solve the compound supply problem. A target oriented synthesis of this molecule additionally opens the possibility to explore the structure-activity relationships of this natural product, and to learn about chemical modifications that can eventually improve its anticancer or pharmacokinetic properties. Therefore, due to synthetic intrigue and our interest in the biological activity of this rare cyclic thiopeptide, we decided to embark in the total synthesis of Gombamide A.

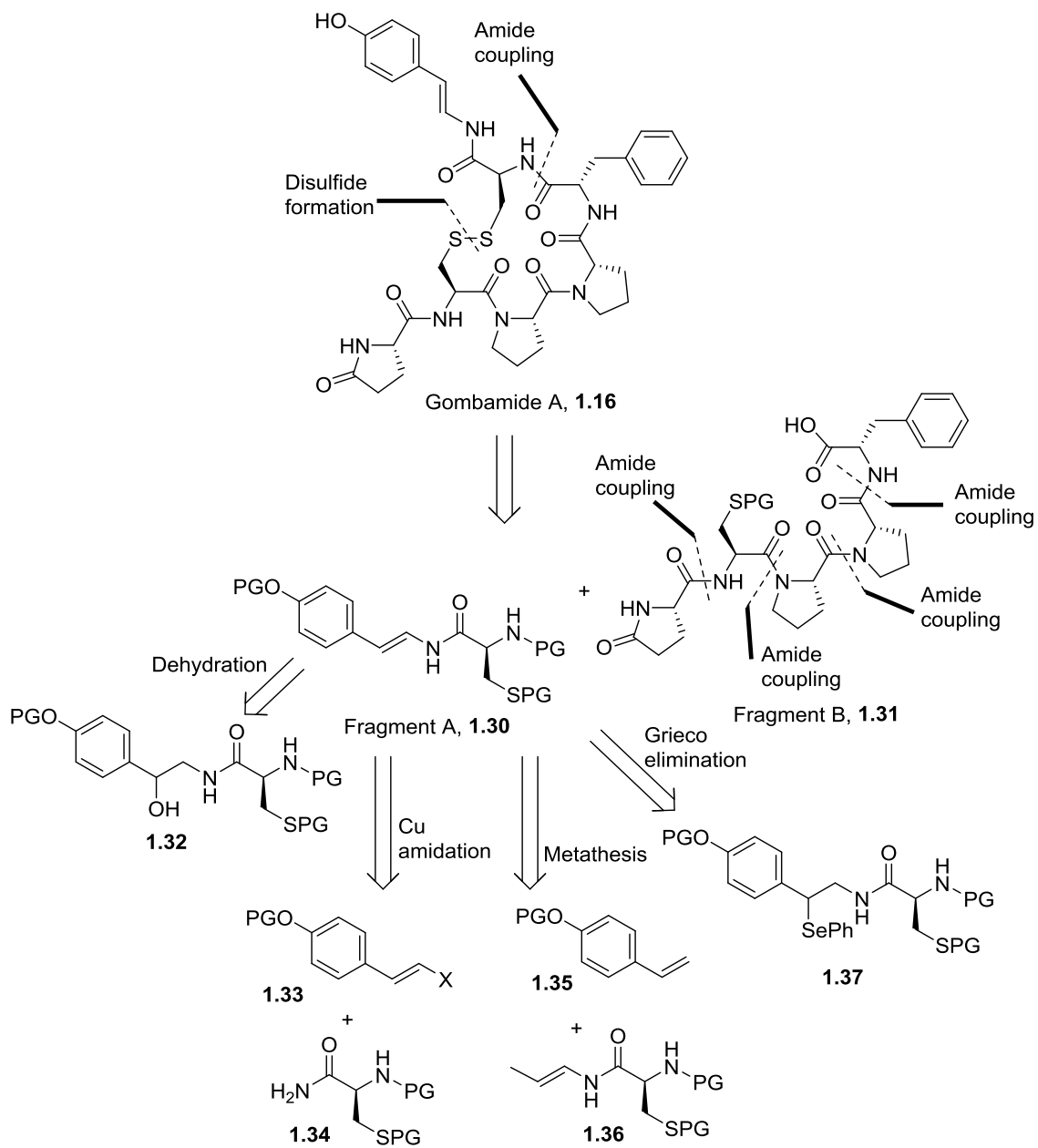
### **Retrosynthetic analysis for the synthesis of Gombamide A**

The analysis of the retrosynthesis of **1.16** led us to propose the formation of the disulfide bond as final step. Having as the final intermediate the enamide acyclic hexapeptide with the cysteines protected, it was envisioned that the 17-membered macrocycle could be accessed through an oxidative deprotection/disulfide formation cascade (Scheme 1.1).

The acyclic precursor for this reaction would originate from the amide coupling between L-Phe and L-Cys-1 which will bring together Fragments A **1.30** and Fragment B **1.31**, facilitating a convergent synthetic route. Fragment B **1.31** could be readily prepared by employing suitable protected versions of L-phenylalanine, two L-prolines, L-cysteine and L-pyroglutamic acid.

The synthesis of Fragment A **1.30** is limited by the formation of the *p*HSA feature and this enamide could be accessed by several different approaches. Between these options, we selected the dehydration of octopamine derived amide **1.32**, the copper catalyzed-amidation of

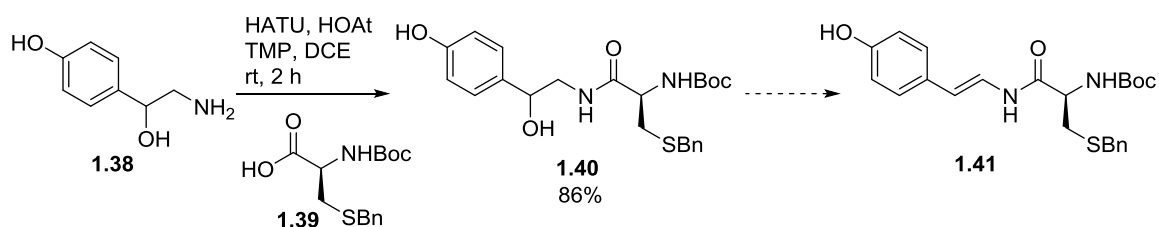
vinyl halide **1.33** with carboxamide **1.34**, intermolecular metathesis of styrene **1.35** with enamide **1.36** and Grieco elimination of phenylselenide **1.37**.



**Scheme 1.1.** Retrosynthetic strategy for the total synthesis of Gombamide A, **1.16**.

## Dehydration route for Gombamide A

The first attempts to accomplish the synthesis of fragment A were performed around the dehydration approach. In order to obtain intermediate **1.40** and being able to evaluate different dehydration strategies, a HATU-mediated amide coupling was performed using ( $\pm$ )-octopamine **1.38** and L-cysteine **1.39** (Scheme 1.2). The reaction proceeded smoothly at room temperature in multi-gram scale and without the need of using a protection group on the alcohols, to provide **1.40** in 86% yield.



**Scheme 1.2.** Synthesis of **1.40** en route to intermediate **1.41**.

Here, the benzylthioether was chosen as the protecting group in the cysteine due to its great stability, as it allows for the exploration of a diverse array of dehydration conditions. When testing different alcohol dehydration methods, we tried to avoid base-promoted methodologies, as the cysteine residue has a high tendency for racemization. The first efforts involved the use of the specific dehydrating agents, Burgess reagent<sup>37</sup> and Martin sulfurane;<sup>38</sup> however, after several trials varying the number of equivalents employed and reaction temperature, the formation of the desired product **1.41** was not observed. Other dehydration conditions such as trifluoroacetic acid, trifluoroacetic anhydride, *p*-toluenesulfonic acid, *p*-toluenesulfonic anhydride, *p*-toluenesulfonyl chloride in pyridine or thionyl chloride in pyridine were screened but they led to decomposition of starting material or no reaction.

Then, the dehydration reaction was performed employing  $\text{BF}_3 \cdot \text{OEt}_2$  in *N,N*-dimethylformamide (DMF), conditions reported for the introduction of the olefin in makaluvamine E.<sup>39</sup> Following the literature procedure, it was possible to observe by LC-MS the formation of the desired enamide along with the deprotection of the Boc group (**1.42**) (entry 1, Table 1.1) and no remaining starting material; however, the product was recovered only in small amounts and it was not possible to obtain a yield for the reaction. As the original procedure required 10 equivalents of the Lewis acid along with heating for 24 hours at 100 °C, we thought that it would be possible to increase the yield of this reaction using milder conditions.

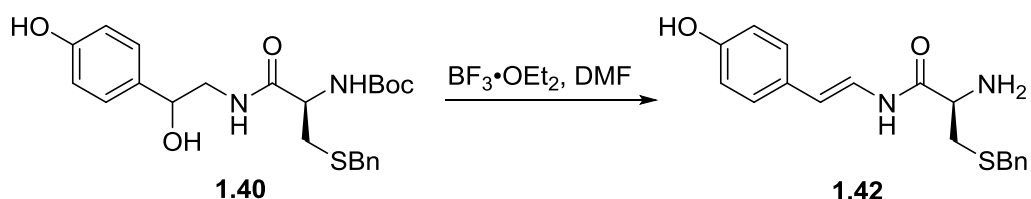


**Table 1.1.** One pot Boc-deprotection/dehydration of derivative **1.40**.<sup>a</sup>

Entry	$\text{BF}_3 \cdot \text{OEt}_2$ equiv.	Time	Temperature (°C)	Yield
1	10.0	24 h	100	Trace
2	5.0	24 h	100	27%
3	2.0	24 h	100	19%
4	2.0	24 h	50	Trace
5	2.0	24 h	rt	0%
6	5.0	30 min	100 <sup>b</sup>	44%
7	2.0	30 min	100 <sup>b</sup>	52%
8	2.0	40 min	100 <sup>b</sup>	47%
9	2.0	20 min	100 <sup>b</sup>	Trace

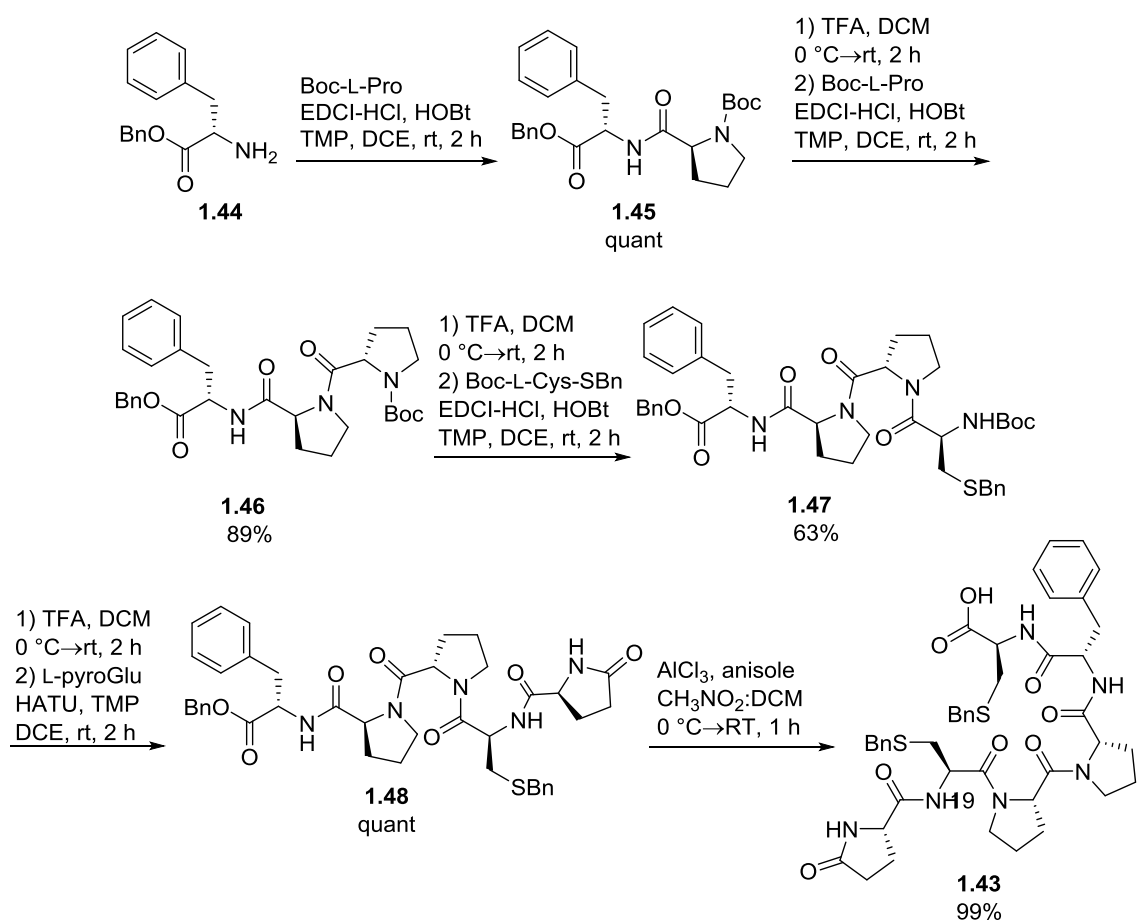
<sup>a</sup>Reactions were performed in DMF at a concentration of 0.09 M. <sup>b</sup>Microwave heating.

Decreasing the amount of  $\text{BF}_3 \cdot \text{OEt}_2$  to five equivalents, led to an increase in yield to 27% (entry 2, Table 1.1), but further reduction to two equivalents of Lewis acid did not provide additional advantage (entry 3, Table 1.1). Lowering the temperature did not prove to be successful increasing the yield of this transformation, only achieving traces of the desired product at 50 °C (entry 4, Table 1.1). Thinking that a more efficient heat source could improve the results of this reaction, conventional thermal heating was switched for microwave-assisted heating. Effectively, microwave promoted internal heating was accompanied by an increase in yield to 44% when using five equivalents of  $\text{BF}_3 \cdot \text{OEt}_2$  and a remarkable shortening of reaction time from 24 hours to 30 minutes without modifying the reaction temperature (entry 6, Table 1.1). In this setting, reduction of the amount of Lewis acid to two equivalents was slightly beneficial increasing the yield of the dehydration/deprotection to 52% yield (entry 7, Table 1.1). After this, different reaction times were evaluated but had no further improvement in the yield of this chemical transformation (entry 8 and 9, Table 1.1).

After approaching successfully the synthesis of fragment A **1.42**, our attention shifted to building fragment B. During the first attempts, a convergent approach was carried out by coupling a Phe-Pro dipeptide with a Pro-Cys-Pyr tripeptide; although, in this case the amide coupling of this pieces led to racemization and formation of diastereomers. Therefore, the construction of the pentapeptide **1.43** was performed linearly, starting from the C-terminal to the N-terminal, as it has been demonstrated that this approach is less prone to racemization of the aminoacids.<sup>40</sup> Following this strategy, we observed racemization when using diisopropylethylamine (DIEA) as a base for the amide couplings. We eventually set in the use of 2,4,6-collidine (TMP) as a base, which being a pyridine derivative possesses a lower  $\text{pK}_a$  than the tertiary alkylamines and it has been reported as a suitable base for peptide synthesis, especially in the presence of cysteine residues.<sup>41</sup>

Then, synthesis of fragment B **1.43** started with the amide coupling between benzyl L-phenylalaninate **1.44** and Boc-L-proline using EDCI/HOBt conditions to obtain dipeptide **1.45** in

quantitative yield (Scheme 1.3). Trifluoroacetic acid (TFA) deprotection of the Boc group, and a second EDCI/HOBt-mediated coupling with another Boc-L-proline delivered tripeptide **1.46** in 89% yield over two steps. Introduction of the cysteine residue was performed after TFA deprotection of the Boc group in **1.46**, through EDCI/HOBt-mediated coupling with Boc-L-Cysteine-SBn to give tetrapeptide **1.47** in 63% yield for the two steps. Repetition of this two steps with **1.47** but employing L-pyroglutamic acid and HATU-mediated amide coupling conditions afforded the key pentapeptide **1.48** in quantitative yield for the two-step deprotection/coupling sequence.



**Scheme 1.3.** Synthesis of pentapeptide **1.43**.

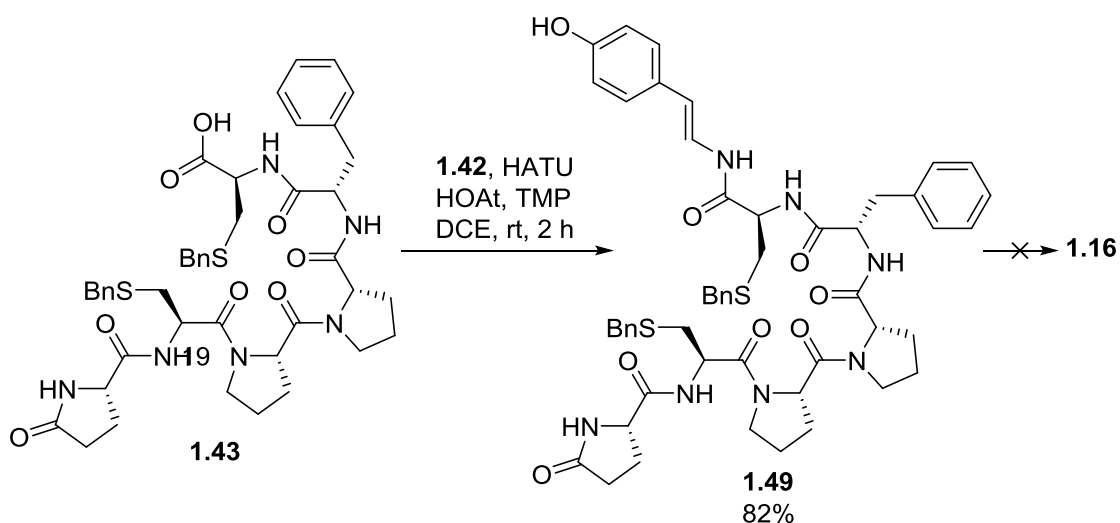
Initially, the pentapeptide was prepared using methyl L-phenylalaninate. When it came to the hydrolysis deprotection step, regular basic hydrolysis led to production of diastereoisomers identified as different peaks in the LC-MS chromatogram. This led to a change in the protecting group to the benzyl ester in **1.48**.

The benzyl gives the advantage of not requiring basic hydrolysis for its removal and being stable during the amide coupling and Boc-deprotection steps. However, benzyl deprotection of **1.48** proved to be challenging as standard conditions were not successful in removing the protecting group. Hydrogenolysis procedures catalized with palladium/carbon did not provide the deprotected product, even when using Brønsted acids (formic acid) as additives. Intact starting material was recovered during these reactions, pointing probably to poisoning of the palladium by the sulfur in the cysteine residue of **1.48**.

Exploring different procedures, it was found that neither heating in neutral or acidic alumina achieved the transformation effectively.<sup>42</sup> Then, the use of Lewis acid based deprotections was assessed. Executing the deprotection with boron trichloride in DCM did not provide the desired product when carried at 0 °C,<sup>43</sup> while it only achieved 20% conversion at room temperature (determined by LC-MS) after 16 hours of reaction. Aluminum trichloride was subsequently tested as the deprotecting reagent; although, performing the reaction with 3 equivalents at 0 °C and room temperature did not provide the desired product. Increasing the amount of AlCl<sub>3</sub> to six equivalents showed clean and full conversion of starting material to the desired carboxylic acid **1.43**. This reaction was carried out in a mixture of nitromethane:DCM (1:1), a solvent system that allows the dissolution of AlCl<sub>3</sub>.<sup>44</sup> Further enhancement in the efficiency of the reaction was observed by adding three equivalents of anisole, shortening the reaction time to close to two hours and allowing the obtention of fragment A **1.43** in almost quantitative yields.

With both fragments in hand, the acyclic precursor of Gombamide A **1.49** was assembled during a HATU-mediated amide coupling of **1.42** and **1.43**. This reaction proceeded smoothly

and delivered **1.49** in good yield (82%) (Scheme 1.4), setting the stage to assay conditions that achieve the deprotection of the thioethers and cyclization to obtain the natural product **1.16**. The tandem deprotection/cyclization was attempted employing the trichloromethylsilane-diphenylsulfoxide system in trifluoroacetic acid at 0 °C, conditions that proved useful to remove benzyl thioethers and form the disulfide bond in good yields according to the literature;<sup>45-47</sup> however, no desired product was obtained after multiple variables were modified, and the result was a complex mixture from which the main substances were the unreacted starting material and overoxidation products of the starting material, detected by the appearance of masses with +16 and +32 m/z during the LC-MS analysis. This transformation was also tried using iodine<sup>48,49</sup> and with a procedure based on magnesium/ammonium formate,<sup>50</sup> both without success and recovering only starting material. Sodium in liquid ammonia at -78 °C was the only methodology in which the deprotection of the starting material was observed;<sup>51,52</sup> though, the intermediate product decomposed quickly during the course of the reaction and it was not possible to isolate it from the mixture or to obtain the natural product **1.16**.



**Scheme 1.4.** Synthesis of the acyclic hexapeptide **1.49** and first attempt to prepare **1.16**.

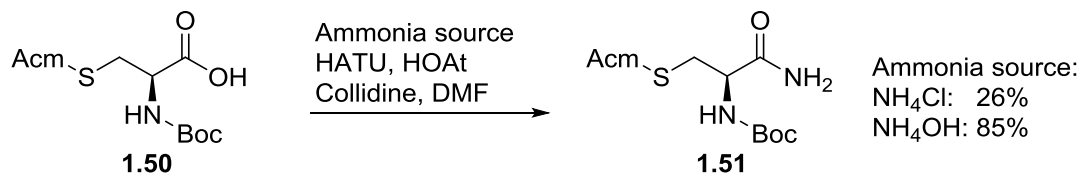


Therefore, despite the advantages in stability that provides the benzylthioether protecting group, the difficulties found during its removal made us look for a more labile substitute that could allow the final cyclization. This effort was performed using L-cysteines protected with benzylthioether derivatives, such as *p*-methylbenzyl, *p*-methoxybenzyl and the trityl group, as well as the acetamidomethyl protecting groups. Starting by the preparation of fragment A, no issues were observed with the formation of the amide coupling with octopamine **1.38**; however, none of these more labile protecting groups were stable enough to survive the  $\text{BF}_3 \cdot \text{OEt}_2$  dehydration conditions previously used to obtain **1.42**, hindering the evaluation of its applicability in the tandem deprotection/cyclization reaction.

### Copper-catalized amidation route for Gombamide A

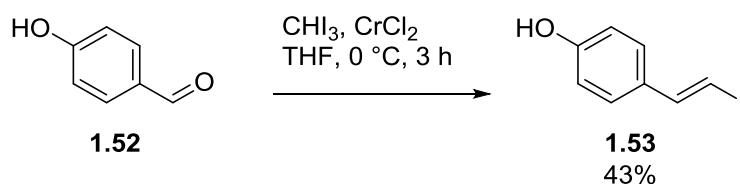
As the dehydration route did not produce satisfactory results to achieve the synthesis of Gombamide, we proceeded to study other routes presented in the retrosynthetic analysis (Scheme 1.1). Independently, Buchwald and Porco have described the synthesis of enamides through the copper-catalyzed amidation of vinyl halides with primary carboxamides.<sup>53,54</sup> The applicability of this procedure in total synthesis has been demonstrated by Porco in the preparation of the antitumor macrolide lobatamide C and close analogs of this natural product.<sup>55</sup>

To assess this alternative, the new synthesis of fragment A started with L-cysteine-S-Acm **1.50** to form the respective carboxamide **1.51** (Scheme 1.5). For this reaction, two ammonia sources were tried, solid ammonium chloride and 28% ammonium hydroxide aqueous solution. The reaction was performed using HATU as the amide coupling reagent and DCE as solvent, offering the opportunity of accessing **1.51** in good yields (85%).



**Scheme 1.5.** Synthesis of carboxamide **1.51**.

After the synthesis of the carboxamide **1.51**, vinyl iodide **1.53** was synthesized en route to the evaluation of the amidation procedure. **1.53** was obtained through a Takai olefination reaction using 4-hydroxybenzaldehyde **1.52**, this procedure allowed the obtention of the *E* alkene selectively but in moderate yields.<sup>56</sup>

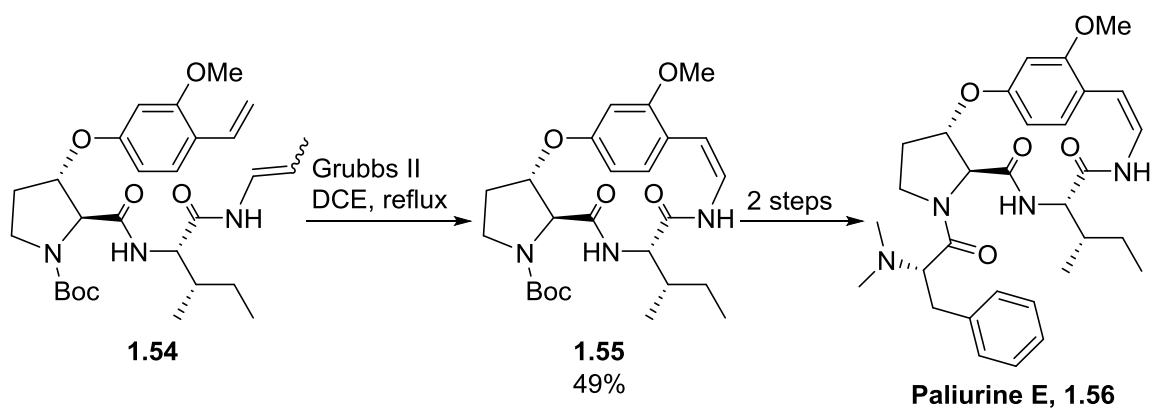


**Scheme 1.6.** Synthesis of vinyl iodide **1.53** through a Takai olefination reaction.

The amidation procedure was evaluated using carboxamide **1.51** and iodide **1.53**. For this reaction, two different copper sources were tried: copper iodide and copper oxide; additionally, different ligands were screened: *N,N*-dimethylglycine, ethylenediamine, *N,N*-diethylamine and *N,N'*-diethylamine. The reactions were carried in refluxing dioxane for 24 hours without sign of formation of the desire product, with decomposition of the vinyl iodide and recovering the carboxamide starting material. This approach was also attempted using the bromide version of **1.53** and with the TBDMS phenoxysilane protected iodide, but formation of the enamine was not observed, which led us to abandon this strategy.

## Metathesis route for Gombamide A

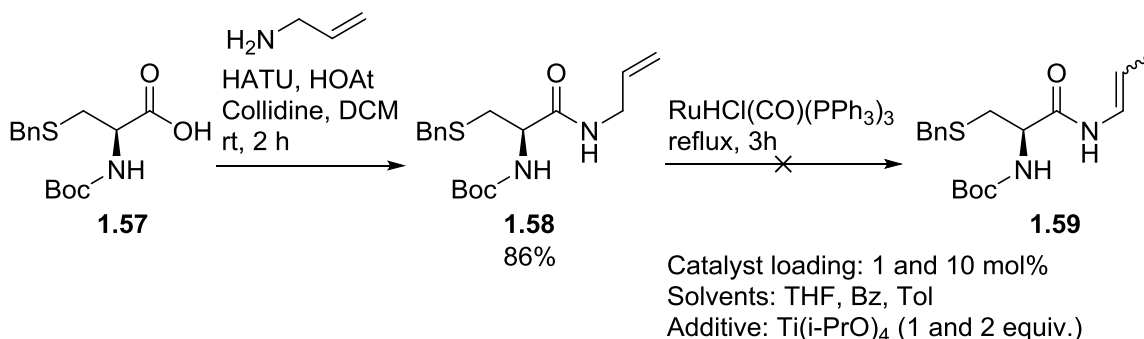
The synthesis of the enamide in the cyclopeptide alkaloid Paliurine E has been achieved by a Grubbs metathesis procedure (Scheme 1.7). In this case, when using intermediate **1.54**, the metathesis occurred intramolecularly between a 4-phenoxy styrene and a simple vinyl amide to provide the core of the natural product in moderate yields.<sup>57</sup> This alternative presents as an interesting strategy for the construction of the fragment A, necessary to obtain Gombamide A. Being aware that in our case the metathesis reaction would be intermolecular and the limitations of this approach, we advanced into the synthesis of the necessary intermediates to evaluate this route.



**Scheme 1.7.** Application of alkene metathesis in the synthesis of Paliurine E.<sup>57</sup>

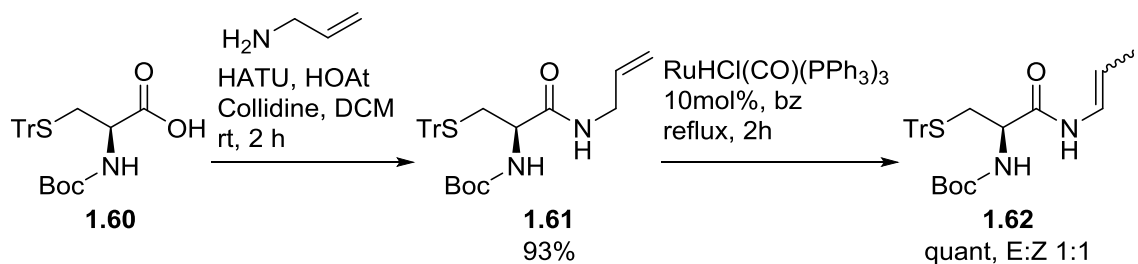
The preparation of the vinyl amide was envisioned as a two-step process with the formation of an amide between a protected cysteine and allylamine, followed by isomerization of the double bond to the vinylamide. Initial trials to perform the HATU-mediated amide coupling between allylamine and cysteine **1.57** provided a low yielding transformation. Here, prior distillation of the allylamine proved to enhance the yield of this coupling, allowing the obtention of **1.58** in good yields (86%) (Scheme 1.8). Then, isomerization of the double bond to obtain **1.59** was attempted using a ruthenium(II) monohydride catalyst. In this case, no reaction was observed

when using different amounts of  $\text{RuHCl}(\text{CO})(\text{PPh}_3)_3$  and different solvents at refluxing temperature. Also, the use of titanium isopropoxide as a Lewis acid additive did not improve the results.



**Scheme 1.8.** Obtention of intermediate **1.58** and attempts for production of **1.59**.

As we were evaluating the results of the isomerization, it was thought that the presence of sulfur might be poisoning the ruthenium catalyst by complexing with the metal. This could be also the reason why the copper amidation methodology did not yield positive results. In an effort to improve upon this observation, it was decided to use a bulkier protecting group in the sulfur that diminishes the possibility of interaction with the metal; therefore, the trityl thioether was selected. The amide coupling between Boc-L-cysteine-STr **1.60** and the distilled allylamine proceeded smoothly and providing **1.61** in excellent yield (93%) (Scheme 1.9). The isomerization of the double bond to obtain **1.62** was performed using two different sources of ruthenium(II) hydride,  $\text{RuHCl}(\text{CO})(\text{PPh}_3)_3$  and  $\text{RuH}_2\text{CO}(\text{PPh}_3)_3$ , and refluxing in benzene for two hours. In this case, effective transformation from the allylamide to the vinylamide **1.62** in quantitative yields was confirmed with both catalysts; with the only difference being that the monohydride provided a 1:1 mixture *E:Z* enamides, while with the dihydride catalyst the ratio was 3:1 *E:Z*. It was confirmed that this mixture of alkenes could be separated by silica gel flash chromatography and semipreparative HPLC.

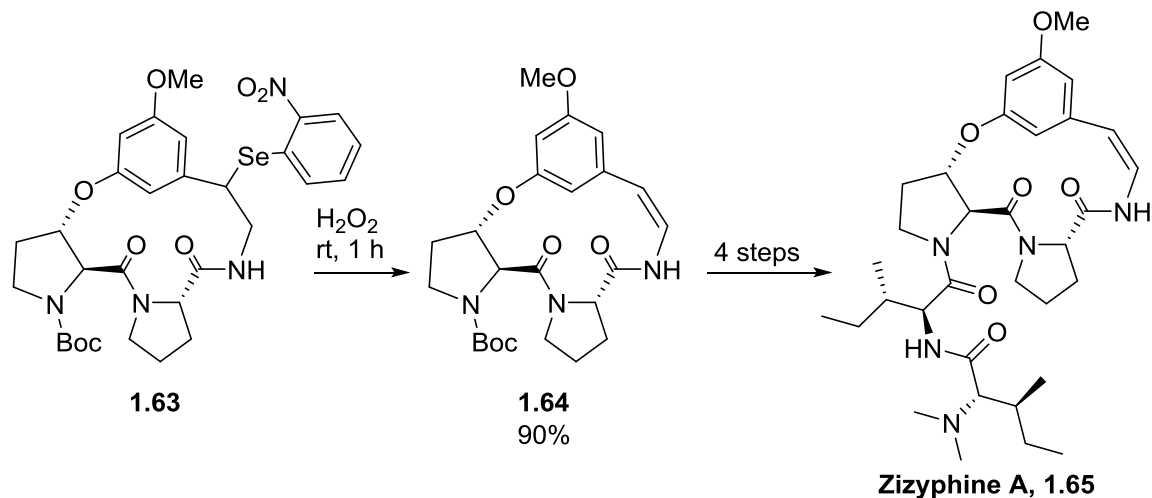


**Scheme 1.9.** Synthesis of intermediate **1.62** through isomerization of **1.61**.

The assessment of the metathesis reaction was performed with the vinylamide **1.62** mixture and 4-hydroxystyrene using 10 mol% Grubbs' second generation as the catalyst. No formation of product was observed after executing the reaction in DCE or toluene at reflux, or increasing the catalyst loading to 20 mol%. The use of Hoveyda-Grubbs' second generation provide similar results, as well as the addition of titanium isopropoxide as Lewis acid additive. Protecting the phenol group with an acetyl, did not produce any improvement in the reaction, and only starting material was isolated from the reaction matrix.

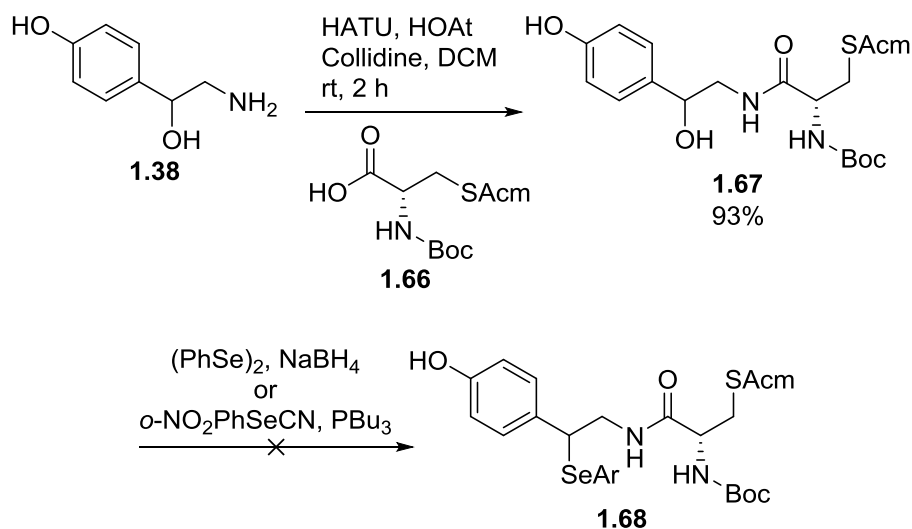
### Grieco elimination route for Gombamide A

Efforts then shifted towards the preparation of the required intermediates to pursue the Grieco elimination procedure to access the unusual *p*HSA moiety of **1.16**. This methodology has been employed in the synthesis of different cyclopeptide alkaloids such as Zizyphine A **1.65** (Scheme 1.10).<sup>58</sup> In this case, the transformation was performed in the advance intermediate **1.63** with the selenide substituent in one carbon of the macrocycle, providing the *Z* olefin **1.64**. We believed that a non-cyclic intermediate carrying the adequate substituents would allow us to access the *E* enamide.



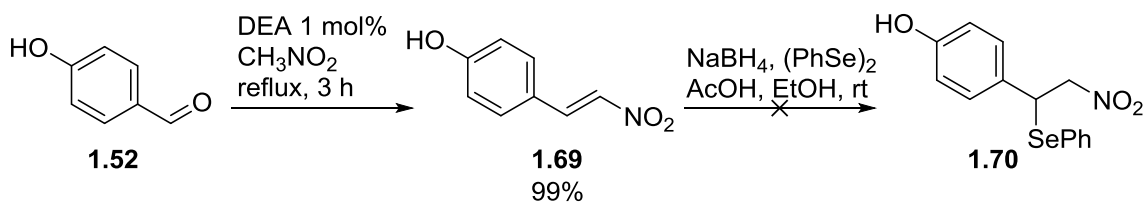
**Scheme 1.10.** Application of Grieco elimination in the synthesis of Zizyphine A.<sup>58</sup>

To obtain the selenide, the amide obtained after the coupling of ( $\pm$ )-octopamine **1.38** and Boc-L-Cys-Sacm was employed. The HATU-facilitated procedure provided amide **1.67** in excellent yields. However, the introduction of the required arylselenide for the Grieco elimination proved to be difficult, and regular conditions using diphenyldiselenide and sodium borohydride or nitrophenylselenocyanate with tributylphosphine were not fruitful. These procedures are supposed to occur through a nucleophilic substitution mechanism, and the highly functionalized **1.67** might pose a challenge for the nucleophilic attack. Therefore, it was decided to evaluate the formation of the selenide prior to the amide coupling.



**Scheme 1.11.** Efforts for the synthesis of intermediate **1.68**.

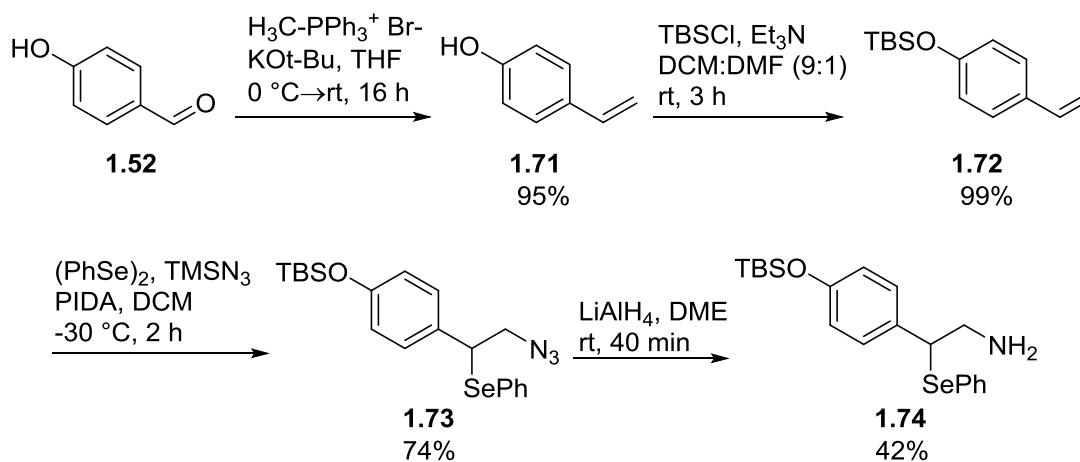
A new method to form the aryl selenide was pursued based on the formation of a styrene and then the addition of phenylselenide to the double bond.<sup>59</sup> Starting with 4-hydroxybenzaldehyde, a Henry reaction was performed, using nitromethane and catalytic amounts of diethylamine to obtain the nitrostyrene **1.69** in excellent yields. In the next step, addition of the selenide was carried out by adding the Henry product **1.69** into a solution of preformed phenylselenide. Monitoring of the reaction showed formation of the desired product; however, the product **1.70** demonstrated to decompose with time during and after purification. It was possible to observe the generation of the starting material and diphenyldiselenide from the purified product, indicating that this reaction is probably reversible.



**Scheme 1.12.** Efforts to synthesize intermediate **1.70**.

As intermediate **1.70** decomposed quickly, we sought to install a different nitrogenated group that could give a handle for the synthesis of the proper selenoamine to advance to the synthesis of fragment A. An option to do this was the development of a selenoazide intermediate for which a synthetic procedure has been described by Tingoli and collaborators starting from an olefin.<sup>60-63</sup> This procedure has been employed for the azido-phenylselenylation of aliphatic and aromatic double bonds, as well as with protected glycols. The reaction is believed to occur through a radical mechanism and gives an anti-markonikov regiochemistry in unsymmetric olefins, positioning the phenylselenide in the most substituted carbon.

In order to evaluate this methodology, the synthesis of styrene **1.72** was performed in two steps (Scheme 1.13). Starting with 4-hydroxybenzaldehyde, **1.71** was obtained in excellent yields (95%) after the formation of the olefin through a Wittig reaction with methyltriphenylphosphonium bromide. Subsequent TBS protection allowed to access styrene **1.72** in almost quantitative yield.



**Scheme 1.13.** Synthesis of phenylselenoamine **1.74**.

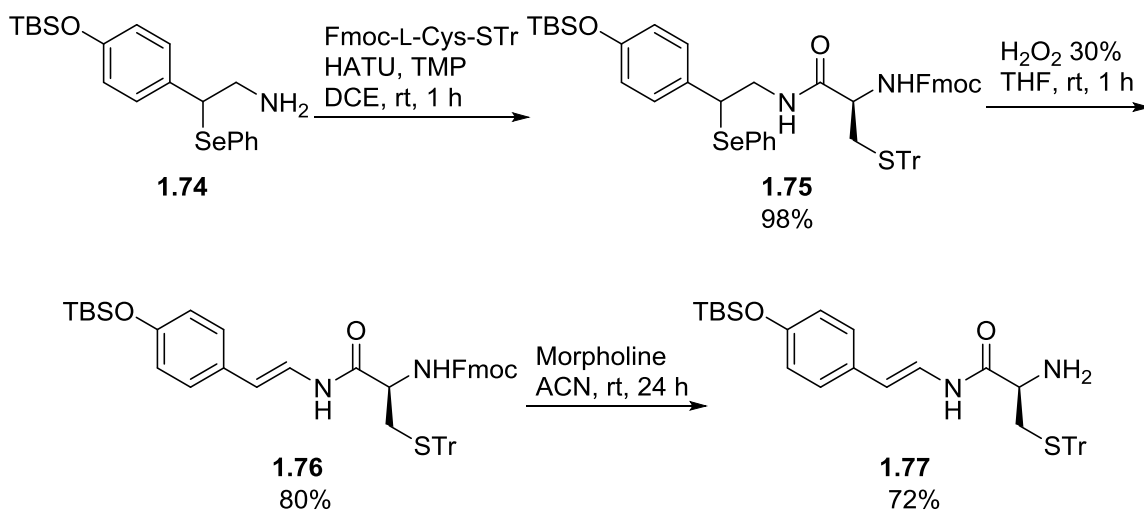
Then, the azidophenylselenylation procedure was evaluated using olefin **1.72** as starting material. The process which requires sodium azide and (diacetoxyiodo)benzene (PIDA),



generated an heterogenous matrix and, in our case, it was carried out at room temperature to afford  $\alpha$ -selenoazide **1.73** in low yields (30-40%). Switching the sodium azide for trimethylsilylazide rendered the reaction homogenous,<sup>64,65</sup> giving more robust scalability and improving the yield to 74%.

Phenylselenoamine **1.74** was obtained through the reduction of intermediate **1.73**. The use of lithium aluminum hydride at room temperature quickly provided amine **1.74** in modest yields (42%). Looking for a higher yield in this transformation, Staudinger reduction conditions were tested, but this method produced the amine only in 29% yield. The one pot procedure (azidophenylselenylation/LAH reduction) provided the desired product **1.74** in 31% over the two steps, similarly to the combination of the two reactions performed separately.

Then, amine **1.74** was coupled via HATU with different protected L-cysteines to obtain different fragments A. Three cysteines were chosen: Boc-L-cysteine-SAc<sub>m</sub>, Boc-L-cysteine-S<sub>Tr</sub> and Fmoc-L-cysteine-S<sub>Tr</sub>; the three residues provided good yields for the amide coupling (70%, 96% and 98%, respectively). The three compounds were submitted to oxidation by the addition of aqueous 30% hydrogen peroxide and stirring at room temperature. The experiment showed that the S-Ac<sub>m</sub> protected compound yield no desired product with apparent oxidation of the molecule, while with the S-<sub>Tr</sub> compounds clean transformation of the selenide to the olefin was observed (Scheme 1.14).



**Scheme 1.14.** Synthesis of fragment A via Grieco elimination procedure.

The yield for the elimination was 91% for the Boc-protected cysteine adduct, while the Fmoc variant gave 80% of the product. In both, formation of the *E* enamide was observed without production of the *Z* isomer. This is probably explained by the steric bulk of the trityl group which destabilized the conformation with the larger substituents on the same side of the molecule, disfavoring the *cis* geometry.

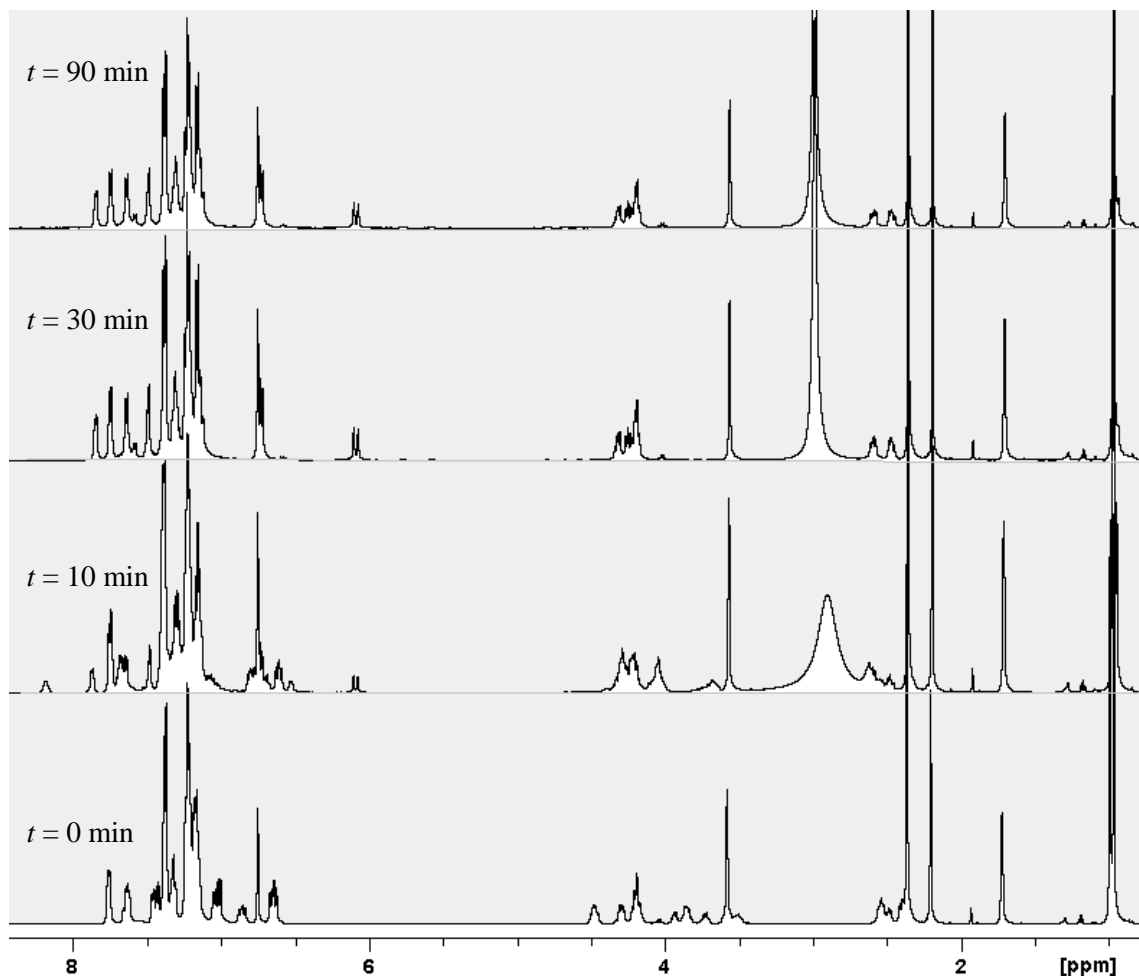


**Figure 1.6.** <sup>1</sup>H-NMR monitoring of the oxidation of **1.75** to produce enamide **1.76**. The reaction was performed in *d*<sub>8</sub>-THF.

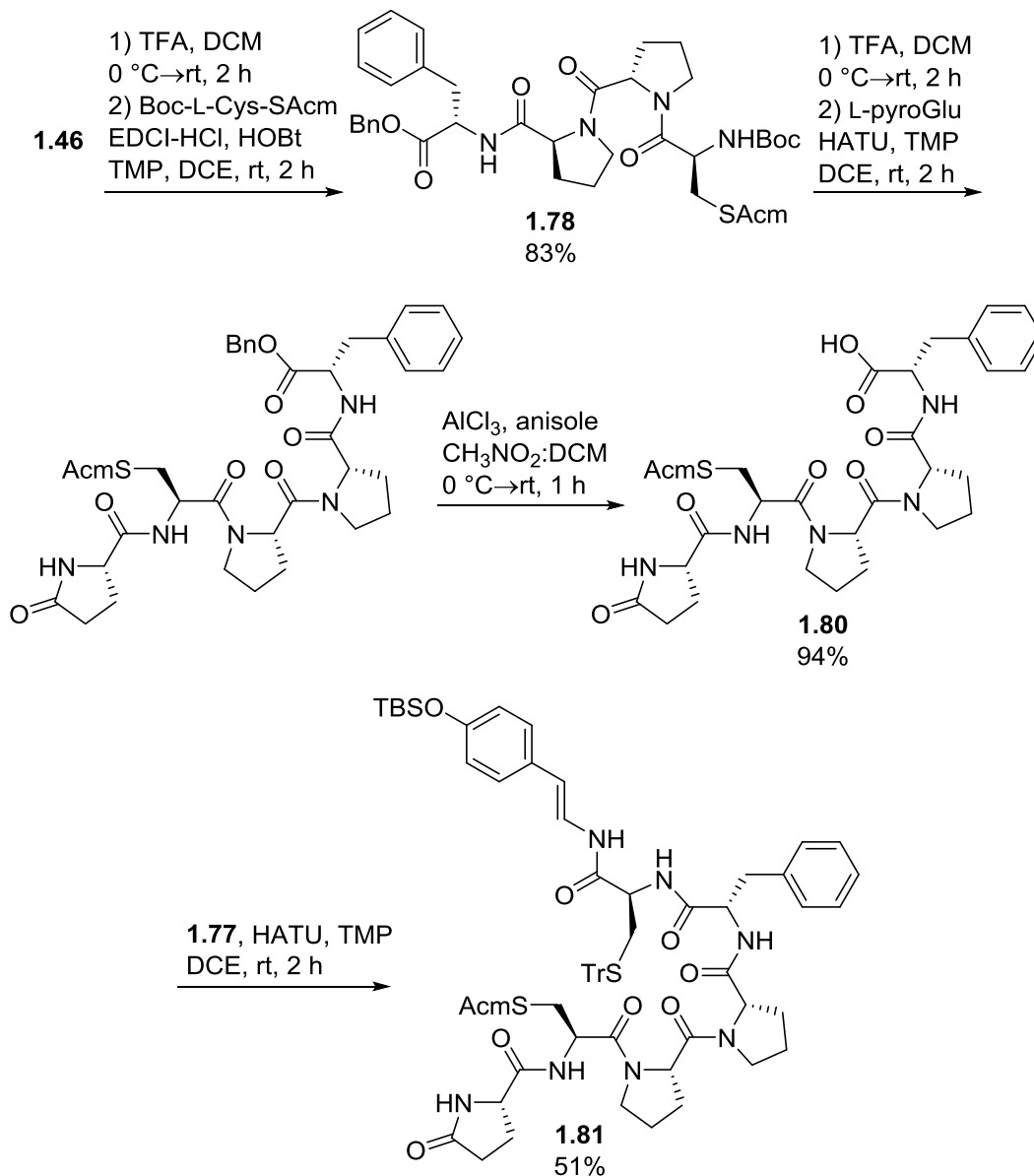
As overoxidation was observed with the S-Acm protecting group, the propensity for formation of byproducts was assessed with the trytil protected cysteine. Using the Fmoc congener **1.75**, the oxidation reaction was carried out in deuterated THF (*d*<sub>8</sub>-THF) and monitored by <sup>1</sup>H-NMR (Figure 1.6). NMR monitoring indicated that the reaction was completed in less than 30 minutes. Additionally, monitoring for up to 90 minutes showed no further changes in the spectrum after conversion of the starting material to the desired olefin, demonstrating no over oxidation or formation of byproducts.

With the enamides in hand, the amino protecting groups were removed and fragment A was generated. The removal of the Boc group was challenging, as TFA deprotection conditions led to decomposition of the starting material. Therefore, we focused our attention on the Fmoc protected **1.76**. For this deprotection, we tried to avoid the common piperidine ( $pK_a = 11.2$ ) conditions, as racemization has been an issue in the past, and instead employed morpholine, a weaker base ( $pK_a = 8.4$ ). The use of this base in acetonitrile at room temperature allowed clean deprotection of **1.76** to obtain amine **1.77** in 72% yield (Scheme 1.14).

After achieving the synthesis of fragment A, the construction of a new fragment B was initiated. This time, instead of the S-benzyl group, the more labile S-Tr and S-Acm were employed to construct fragment B in parallel. The synthesis of fragment B started by Boc-deprotection of the previously prepared Phe-Pro-Pro **1.46**, followed by the amide coupling with the corresponding cysteine. The amide coupling with Fmoc-L-cysteine-S-Tr was performed successfully with EDCI/HOBt, proceeding in 82% isolated yield over two steps. Then, the Fmoc group was removed with the morpholine conditions previously employed for **1.76**, and a HATU-mediated amide coupling with L-pyroglutamic acid gave the desired pentapeptide in 58% yield. Deprotection of the ester was needed for accessing fragment B; however, the conditions previously employed to execute this transformation did not provide positive results with this substrate, as  $AlCl_3$  caused decomposition of the starting material and early deprotection of the trityl thioether.

The synthesis of fragment B using Boc-L-cysteine-Sacm started by the EDCI/HOBt mediated amide coupling with the deprotected amine from **1.46** to obtain **1.78** in good yield (83% over two steps). Then, it was followed by the deprotection of the Boc group with TFA and a second amide coupling with the L-pyroglutamic acid, to afford the ester **1.79** in 87% isolated yield for the two-step sequence. In this case, the deprotection of the benzylic ester was carried out using the  $AlCl_3$ /anisole system, providing fragment B **1.80** in excellent yield. Next, formation of

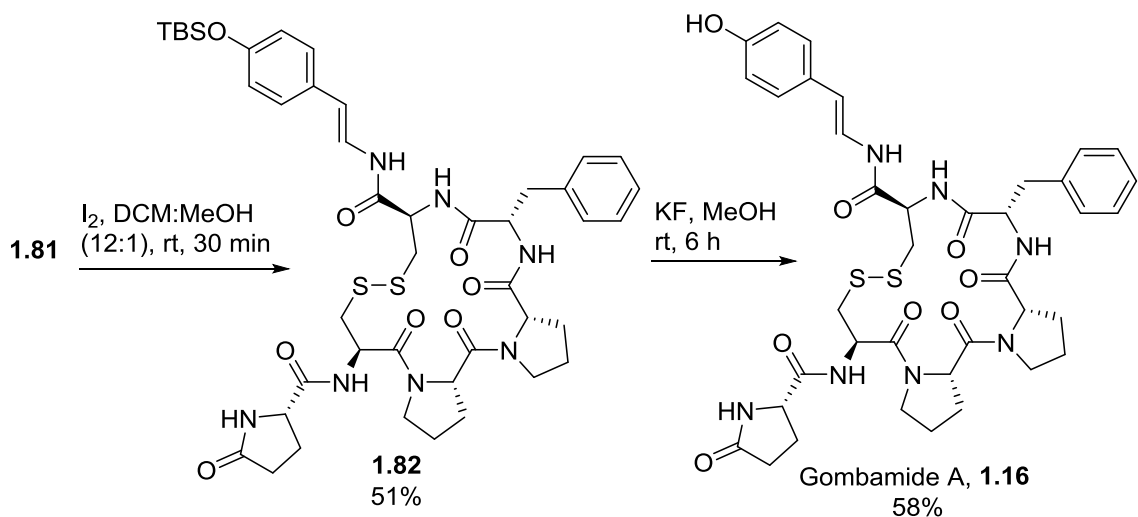
the protected acyclic precursor of Gombamide A was performed by the coupling of fragment A **1.77** and fragment B **1.80**, providing **1.81** in 51% yield



**Scheme 1.15.** Synthesis of acyclic precursor **1.81**.

With **1.81** in hand, the stage was set to attempt the formation of the 17-membered macrocycle. For this transformation, we selected to employ an iodine-mediated oxidative

cyclization protocol.<sup>48,49</sup> The iodine will promote tandem removal of the S-Acm and S-Tr protecting groups and formation of the disulfide bond (Scheme 1.16). Following the literature procedure describe by Boger and collaborators (entry 1, Table 1.2), the reaction was run with 10 equivalents of iodine and fairly diluted (0.0008M). These conditions proved to deprotect quickly both S-Acm and S-Tr groups, but also caused over oxidation of the intermediate species which did not allow the isolation of the desired product. By decreasing the amount of iodine to five equivalents (entry 2, Table 1.2), the tandem deprotection/cyclization reaction occurred without observable over oxidation byproducts, while maintaining short reaction times. This procedure permitted the synthesis of **1.82** in moderate isolated yield. Further decrease in the amount of iodine (entry 3, Table 1.2) caused a decrease in yield and longer times to achieve full consumption of the starting material. The reaction was also run at higher concentration (entries 4 and 5, Table 1.2), and despite fast formation of **1.82** was observed, no improvement in yield was achieved with respect to the diluted conditions.



**Scheme 1.16.** Completion of the synthesis of Gombamide A.

**Table 1.2.** Tandem deprotection/cyclization of **1.81**.<sup>a</sup>

Entry	I <sub>2</sub> equiv.	Concentration (M)	Time <sup>b</sup>	Yield
1	10.0	0.0008	5 min	0% <sup>c</sup>
2	5.0	0.0008	30 min	51%
3	2.0	0.0008	22 h	28%
4	5.0	0.008	15 min	34%
5	2.0	0.008	2 h	43%

<sup>a</sup>Reactions were performed in a mixture of DCM:MeOH (12:1) at room temperature. <sup>b</sup>Time to achieve consumption of starting material. <sup>c</sup>Deprotection along with overoxidation was observed.

The final step to obtain **1.16** was the deprotection of TBS-phenoxy silane **1.82**. The assessment of several conditions to achieve the formation of **1.16** showed that using tetrabutylammonium fluoride or HCl in methanol caused mainly product degradation; while HF-pyridine or KF in methanol proved to effectively produced **1.16**. Ultimately, KF in methanol was selected, as this method had the advantage of faster reaction times (6 hours to completion, compared to 24 hours for HF-pyridine), and it provided for the first time, Gombamide A **1.16** in 58% yield (Scheme 1.16). The produced synthetic material displayed identical spectroscopic data with respect to the reported isolated Gombamide A.

## Summary and future directions

In summary, the first total synthesis of Gombamide A **1.16** has been completed, employing a convergent synthetic route that required a total of 18 steps, with an overall yield of 2.5% from *p*-hydroxybenzaldehyde **1.52** (10 linear step sequence), and 9.1% from benzyl L-phenylalaninate **1.44** (11 linear step sequence).

The presented synthesis shows how the introduction of sulfur in a natural product molecule is harmful for the majorities of methodologies currently developed for the production of enamides. At the same time, this synthesis exemplified the non-trivial task of protecting group selection in the presence of distinct functionalities in Gombamide A **1.16**.

The developed synthetic route highlights the azidophenylselenylation and Grieco elimination procedures as useful methods in the synthesis of *E* enamides in the presence of sulfur, and a tandem deprotection/cyclization procedure to achieve the formation of the 17-membered macrocycle in **1.16**.

The synthetic natural product will allow exploring further the biological effect of these molecules. The obtained material is in the process of being submitted to the CANVASS panel assay, a program run by the National Center for Advancing Translational Sciences (NCATS) of the National Institute of Health (NIH). In these assays, the compound will be tested for its anticancer, antibacterial and antiinflammatory activity.

Finally, this synthetic route provides a way to start questioning the SAR of Gombamide A. The use of the synthetic procedure for formation of the enamide and cyclization of the natural product, in combination with fast solid-phase peptide synthesis, would allow the production of analogs libraries where the impact of multiple chemical modifications on the activity of Gombamide A could be evaluated.

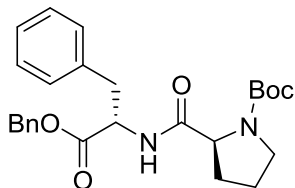


## EXPERIMENTAL METHODS

### *General*

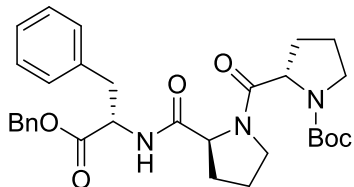
All reagents and solvents were commercial grade and purified prior to use when necessary. Thin layer chromatography (TLC) was performed on glassbacked silica gel. Visualization was accomplished with UV light and/or the use of iodine or ninhydrin solution followed by charring on a hot-plate. Flash chromatography on silica gel was performed using Silica Gel 60 (230-400 mesh) from Sorbent Technologies.  $^1\text{H}$  and  $^{13}\text{C}$  NMR spectra were recorded on Bruker DRX-400 (400 MHz) instrument. Chemical shifts are reported in ppm relative to residual solvent peaks as an internal standard at the following chemical shifts ( $^1\text{H}$  and  $^{13}\text{C}$  respectively): 7.26 and 77.0 ppm for  $\text{CDCl}_3$ ; 2.50 and 39.52 ppm for  $\text{DMSO}-d_6$ , 3.31 and 49.2 ppm for  $\text{CD}_3\text{OD}$ . Data are reported as follows: chemical shift, multiplicity (s = singlet, d = doublet, t = triplet, q = quartet, dd = doublet of doublets, br = broad, m = multiplet), coupling constant (Hz), integration. Optical rotations were measured on a JASCO P-2000 digital polarimeter. Concentration in g/100 ml and solvent are given in parentheses and the reported value is an average of  $n=3$  independent measurements. Low resolution mass spectra were obtained on an Agilent 6130 mass spectrometer with ESI source. MS parameters were as follows: fragmentor: 100, capillary voltage: 3000 V, nebulizer pressure: 40 psig, drying gas flow: 11 L/min, drying gas temperature: 350° C. Samples were introduced via an Agilent 1200 HPLC comprised of a degasser, G1312A binary pump, G1367B HP-ALS, G1316A TCC, G1315D DAD, and a Varian 380 ELSD. UV absorption was generally observed at 215 nm and 254 nm with a 4 nm bandwidth. Column: Thermo Accucore C18, 2.1 x 30 mm, 2.6  $\mu\text{m}$ . Gradient conditions, Method A: 7% to 95%  $\text{CH}_3\text{CN}$  in  $\text{H}_2\text{O}$  (0.1% TFA) over 1.6 min, hold at 95%  $\text{CH}_3\text{CN}$  for 0.35 min, 1.5 mL/min, 45° C. Gradient conditions, Method B: 40% to 95%  $\text{CH}_3\text{CN}$  in  $\text{H}_2\text{O}$  (0.1% TFA) over 1.1 min, hold at 95%  $\text{CH}_3\text{CN}$  for 0.25 min, 1.5 mL/min, 45° C. A Micromass Qtof API-US mass spectrometer was used to acquire high-resolution mass

spectrometry (HRMS) data. The value  $\Delta$  is the error in the measurement (in ppm) given by the equation  $\Delta = [(ME - MT) / MT] \times 106$ , where  $ME$  is the experimental mass and  $MT$  is the theoretical mass. The HRMS results were obtained with ES as the ion source and leucine enkephalin as the reference.



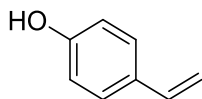
**Benzyl *N*-(*tert*-butoxycarbonyl)-L-prolyl-L-phenylalaninate (1.45).** In a flask, Boc-L-proline (1.844 g, 8.568 mmol) and hydroxybenzotriazole (1.737 g, 12.85 mmol) were weighed and suspended in 75 mL of DCE. Then, while in an ice bath, EDCI hydrochloride was added (1.969 g, 10.28 mmol) followed by 2,4,6-collidine (3.4 mL, 25.71 mmol), and finally benzyl L-phenylalaninate hydrochloride (2.500 g, 8.568 mmol). The mixture was warmed to room temperature and stirred for two hours. The reaction was worked up by washing the mixture with HCl 1.0 M twice, then the aqueous phase was extracted thrice with DCM. The organic phases were combined, washed with brine, dried with magnesium sulfate and filtered. The volatiles were eliminated *in vacuo* and the crude was purified by silica gel flash chromatography (0-20% EtOAc/Hex). A clear oil was obtained (3.890 g, *quant.*). LC-MS retention time (Method A): 1.201 min,  $m/z$  352.9 (M-Boc), 396.9 (M-O-*t*-Bu), 452.9 (M+H).  $^1\text{H}$  NMR (600.1 MHz,  $\text{CDCl}_3$ )  $\delta$  (ppm): 7.34 (m, 5H), 7.20 (m, 3H), 7.02 (m, 2H), 6.50 (br s, 1H, NH), 5.14 (m, 2H), 4.79-4.98 (m, 1H), 4.13-4.56 (m, 1H), 3.22-3.48 (m, 2H), 3.16 (dd,  $J_{\text{ABX}} = 13.9$  Hz, 5.9 Hz, 1H), 3.02 (dd,  $J_{\text{ABX}} = 13.9$  Hz, 6.6 Hz, 1H), 1.50-2.34 (m, 4H), 1.40 (m-rotamers, 9H).  $^{13}\text{C}$  NMR (150.0 MHz,  $\text{CDCl}_3$ )  $\delta$  (ppm) rotamers were observed and denoted with \*: 172.2\*, 171.8\*, 171.1, 155.7\*, 154.6\*, 136.0\*, 135.7\*, 135.2, 129.3\*, 129.2\*, 128.6, 128.5, 127.1\*, 126.9\*, 80.8\*, 80.3\*, 67.2, 61.0\*, 59.9\*, 53.4\*, 52.7\*, 46.9, 38.0, 30.6, 28.3\*, 28.2\*, 24.5\*, 23.4\*.  $^1\text{H}$ -NMR corresponds to:

*Arch. Pharm. Pharm. Med. Chem.* 334, 167–172 (2001).  $[\alpha]_D^{25}$ : -66.5 (c 1.0, CHCl<sub>3</sub>); HRMS (TOF,ES+) C<sub>26</sub>H<sub>32</sub>N<sub>2</sub>O<sub>5</sub> [M] calculated 452.2311, found 452.2309,  $\Delta$  = -0.42 ppm.



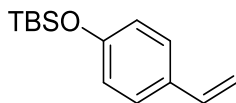
**Benzyl *N*-(*tert*-butoxycarbonyl)-L-prolyl-L-prolyl-L-phenylalaninate (1.46).** In a flask, **1.45** (3.842 g, 8.490 mmol) was dissolved in 72 mL of DCM, to this mixture 8 mL of TFA were added drop wise while in an ice bath and the reaction was allowed to warm until room temperature. After two hours of stirring, full deprotection of starting material was confirmed by LC-MS. The reaction was worked-up by evaporating the solvent and TFA *in vacuo*. The generated amine was used without further purification for the next reaction. Then, in a new flask, the Boc-L-proline (2.741 g, 12.734 mmol) and hydroxybenzotriazole (2.581 g, 19.100 mmol) were weighted and suspended in 50 mL of DCE. Then, while in an ice bath, EDCI hydrochloride was added (2.927 g, 15.284 mmol) followed by 2,4,6-collidine (3.37 mL, 25.491 mmol), and finally a solution of the deprotected amine obtained from **1.45** in 20 mL of DCE. The mixture was warmed to room temperature and stirred for 1.5 hours. The reaction was worked up by washing the mixture with HCl 1.0 M twice, then the aqueous phase was extracted thrice with DCM. The organic phases were combined, washed with brine, dried with magnesium sulfate and filtered. The volatiles were eliminated *in vacuo* and the crude was purified by silica gel flash chromatography (0-50% EtOAc/Hex). A clear solid was obtained (4.140 g, 89%). LC-MS retention time (Method A): 1.150 min, *m/z* 450.1 (-Boc), 550.2 (M+H), 572.1 (M+Na). <sup>1</sup>H NMR (600.1 MHz, CDCl<sub>3</sub>)  $\delta$  (ppm): 8.58 (d, *J* = 8.3 Hz, 1H, NH), 7.28-7.38 (m, 5H), 7.24-7.28 (m, 2H), 7.17-7.23 (m, 2H), 7.03-7.08 (m, 1H), 5.06-5.18 (m, 2H), 4.81 (m, 0.5H), 4.72 (m, 0.5H), 4.63 (m, 0.5H), 4.43 (dd, *J* = 7.8 Hz, *J* = 3.2 Hz, 0.25H), 4.31 (dd, *J* = 8.2 Hz, *J* = 4.7 Hz, 0.25H),

4.17 (m, 1H), 3.69 (q,  $J = 8.6$  Hz, 0.25H), 3.56-3.62 (m, 0.25H), 3.48-3.56 (m, 1H), 3.35-3.48 (m, 2H), 3.29-3.34 (m, 0.5H), 3.23-3.28 (m, 0.5H), 3.13-3.20 (m, 1H), 3.01-3.09 (m, 0.5H), 2.22-2.42 (m, 1H), 1.52-2.07 (m, 6.5H), 1.32-1.52 (m, 9H), 0.86-0.99 (m, 0.5H).  $^{13}\text{C}$  NMR (150.0 MHz,  $\text{CDCl}_3$ )  $\delta$  (ppm): 173.1, 172.7, 171.7, 171.3, 171.21, 171.16, 171.0, 170.9, 154.7, 154.5, 153.6, 137.7, 136.1, 136.0, 135.6, 135.2, 129.21, 129.18, 129.1, 128.53, 128.49, 128.4, 128.4, 128.2, 128.0, 128.8, 126.6, 79.9, 79.6, 79.5, 67.14, 67.09, 66.96, 60.8, 59.84, 59.78, 58.0, 57.52, 57.47, 54.3, 53.45, 53.39, 47.00, 46.98, 46.97, 46.85, 46.62, 46.58, 37.63, 37.57, 36.0, 31.3, 30.2, 29.4, 28.9, 28.53, 28.50, 28.39, 27.1, 27.0, 25.2, 25.1, 24.4, 24.2, 23.7, 21.5;  $[\alpha]_{\text{D}}^{25}$ : -84.4 (c 1.0,  $\text{CHCl}_3$ ); HRMS (TOF,ES+)  $\text{C}_{31}\text{H}_{39}\text{N}_3\text{O}_6$  [M] calculated 549.2839, found 549.2838,  $\Delta = -0.23$  ppm.

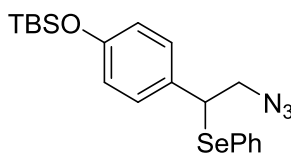


**4-Vinylphenol (1.71).** In a flask, methyltriphenylphosphonium bromide (25.01 g, 70.01mmol) was suspended in 80 mL of THF. Then, potassium *tert*-butoxide (15.71 g, 140.0 mmol) was added and the reaction was stirred at room temperature for 10 minutes. After this time, a solution of 4-hydroxybenzaldehyde (8.550 g, 70.01mmol) dissolved in THF (40 ml) was added dropwise. The reaction was stirred for 16 hours at room temperature, consumption of starting material and formation of product was confirmed by LC-MS. The reaction was worked up by addition of HCl 1.0 M and successive extractions with DCM. The organic phase was reextracted with a solution of  $\text{K}_2\text{CO}_3$  20%, diluted in water to obtain a pH of 10. Then, the aqueous phase was neutralized and acidified to pH=5, and extracted with  $\text{CHCl}_3$ :IPA (3:1). These last organic phases were combined, dried with  $\text{MgSO}_4$  and filtered. The volatiles were eliminated *in vacuo* and the crude was purified by silica gel flash chromatography (0-20% EtOAc/Hex). A white solid was obtained (8.00 g, 95%). LC-MS retention time (Method A): 0.778 min.  $^1\text{H}$  NMR (600.1 MHz,  $\text{CDCl}_3$ )  $\delta$  (ppm): 7.31 (d,  $J = 8.5$  Hz, 2H), 6.80 (d,  $J = 8.6$  Hz, 2H), 6.66 (dd,  $J =$

17.6, 10.9 Hz, 1H), 5.61 (dd,  $J = 17.6, 0.84$  Hz, 1H), 5.13 (dd,  $J = 10.9, 0.84$  Hz, 1H), 4.88 (s, 1H, OH).  $^{13}\text{C}$  NMR (150.0 MHz,  $\text{CDCl}_3$ )  $\delta$  (ppm): 155.1, 136.1, 130.6, 127.6, 115.3, 111.6. HRMS (TOF,ES+)  $\text{C}_8\text{H}_8\text{O}$  [M] calculated 120.0575, found 120.0571,  $\Delta = -3.25$  ppm.

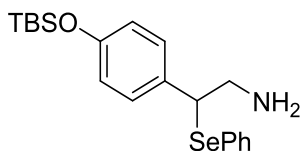


***tert*-Butyldimethyl(4-vinylphenoxy)silane (1.72).** In a flask, **1.71** (1145 mg, 9.530 mmol) was weighted and suspended in a mixture of DCM (36 mL) and DMF (4mL). Then, triethylamine (2.66 mL, 19.06 mmol) was added, followed by *tert*-butyldimethylchlorosilane (2873 mg, 19.06 mmol). The reaction was stirred at room temperature for 3 hours, after this time LC-MS showed full consumption of the starting material and formation of product. The reaction was worked up by addition of water and successive extractions with DCM. The organic phases were combined, dried with  $\text{MgSO}_4$ , filtered. The volatiles were eliminated *in vacuo* and the crude was purified by silica gel flash chromatography (0-10% EtOAc/Hex). A clear colorless oil was obtained (2202 mg, 99%). LC-MS retention time (Method A): 1.477 min.  $^1\text{H}$  NMR (400.1 MHz,  $\text{CDCl}_3$ )  $\delta$  (ppm): 7.35 (d,  $J = 8.5$  Hz, 2H), 6.88 (d,  $J = 8.6$  Hz, 2H), 6.72 (dd,  $J = 17.6, 10.9$  Hz, 1H), 5.67 (dd,  $J = 17.6, 0.9$  Hz, 1H), 5.19 (dd,  $J = 10.9, 0.9$  Hz, 1H), 1.08 (s, 9H), 0.28 (s, 6H).  $^{13}\text{C}$  NMR (100.0 MHz,  $\text{CDCl}_3$ )  $\delta$  (ppm): 155.5, 136.3, 131.0, 127.3, 111.6, 25.7, 18.2, -4.4; HRMS (TOF,ES+)  $\text{C}_{14}\text{H}_{22}\text{Osi}$  [M] calculated 234.1440, found 234.1430,  $\Delta = -4.38$  ppm.



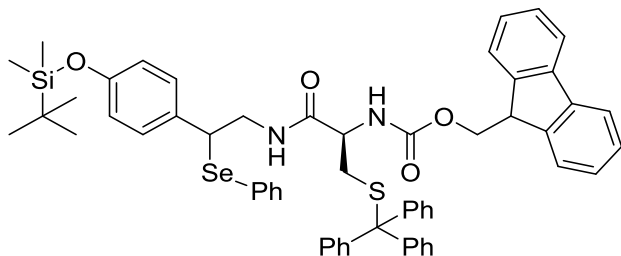
**(4-(2-azido-1-(phenylselanyl)ethyl)phenoxy)(*tert*-butyl)dimethylsilane (1.73).** In a flask, **1.72** (1000 mg, 4.266 mmol) was dissolved in 21 mL DCM. The mixture was cooled to  $-30$   $^\circ\text{C}$ , then, the diphenyl diselenide (1332 mg, 4.266 mmol) was added. To this solution,

iodobenzene diacetate (1374 mg, 4.266mmol) and azidotrimethylsilane (1.12 mL, 8.53mmol) were added sequentially. After two hours, LC-MS showed full consumption of starting material along with formation of the desired product. The solvent was evaporated and the crude product was purified by silica gel flash chromatography (0-3% EtOAc/Hex). A yellow oil was obtained (1368 mg, 74%). LC-MS retention time (Method B): 1.159 min, m/z 276.2 (M-PhSe), 391.0 (M-N<sub>3</sub>). <sup>1</sup>H NMR (400.1 MHz, CDCl<sub>3</sub>) δ (ppm): 7.44-7.50 (m, 2H), 7.35-7.22 (m, 3H), 7.11 (d, *J* = 8.5 Hz, 2H), 6.78 (d, *J* = 8.5 Hz, 2H), 4.40 (dd, *J* = 9.6, 5.7 Hz, 1H), 3.84 (dd, *J* = 12.6, 9.6 Hz, 1H), 3.66 (d, *J* = 12.6, 5.7 Hz, 1H), 1.00 (s, 9H), 0.21 (s, 6H). <sup>13</sup>C NMR (100.0 MHz, CDCl<sub>3</sub>) δ (ppm): 155.3, 135.6, 131.3, 129.1, 128.9, 128.4, 128.3, 120.3, 55.5, 45.9, 25.6, 18.2, -4.5. HRMS (TOF,ES+) C<sub>57</sub>H<sub>58</sub>N<sub>2</sub>O<sub>4</sub>SseSi [M] calculated 433.1081, found 433.1089, Δ = -1.83 ppm.

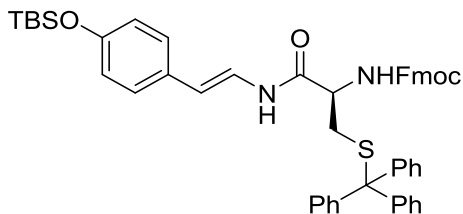


**2-(4-((*tert*-butyldimethylsilyl)oxy)phenyl)-2-(phenylselanyl)ethan-1-amine (1.74).** In a flask, **1.73** (2500 mg, 5.781 mmol) was weighted and suspended in THF (29 mL). Then, a solution of lithium aluminum hydride 1.0 M in THF (5.8 mL, 5.781 mmol) was added, partial consumption of the azide product was observed after 30 minutes of reaction. Another 1.0 equivalent of LiAlH<sub>4</sub> was added and after 10 minutes of stirring, full consumption of the starting material was observed. The reaction was quenched using Glauber's salt, stirred for 30 minutes and filtered. The solvent was evaporated and the crude product was purified by silica gel flash chromatography (0-5% MeOH in DCM). A yellow oil was obtained (979 mg, 42%). LC-MS retention time (Method A): 1.150 min, m/z 391.0 (M-NH<sub>2</sub>). <sup>1</sup>H NMR (400.1 MHz, CDCl<sub>3</sub>) δ (ppm): 7.23-7.29 (m, 2H), 7.00-7.13 (m, 3H), 6.89 (d, *J* = 8.5 Hz, 2H), 6.59 (d, *J* = 8.5 Hz, 2H), 4.05 (dd, *J* = 8.3, 6.3 Hz, 1H), 3.04 (dd, *J* = 13.4, 8.4 Hz, 1H), 2.97 (dd, *J* = 13.4, 6.3 Hz, 1H), 0.82 (s, 9H), 0.03 (s, 6H). <sup>13</sup>C NMR (100.0 MHz, CDCl<sub>3</sub>) δ (ppm): 154.8, 135.5, 132.6, 129.0,

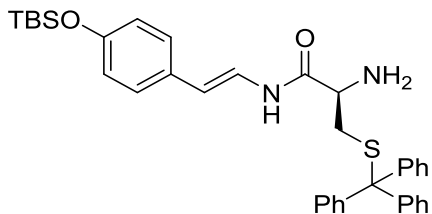
128.8, 128.7 127.8, 120.1, 51.1, 46.8, 25.6, 18.1, -4.5. HRMS (TOF,ES+) C<sub>57</sub>H<sub>58</sub>N<sub>2</sub>O<sub>4</sub>SseSi [M]  
calculated 407.1183, found 407.1184,  $\Delta$  = -0.21 ppm.



**(9H-fluoren-9-yl)methyl ((2R)-1-((2-(4-((tert-butyl)dimethylsilyl)oxy)phenyl)-2-(phenylselanyl)ethyl)amino)-1-oxo-3-(tritylthio)propan-2-yl)carbamate (1.75).** In a flask, Fmoc-L-cysteine-S-trityl (1506 mg, 2.571 mmol) and HATU (1066 mg, 2.804 mmol), were weighted and suspended in 13 mL of DCE. Then, 2,4,6-trimethylpyridine (0.93 mL, 7.011 mmol) was added and the mixture was stirred for 2 minutes. After this time, a solution of **1.74** (950 mg, 2.337 mmol) in 10 mL of DCE was added. The reaction was stirred for 1 h at room temperature. The reaction was quenched by addition of water and extracted with DCM thrice. The organic phases were combined, dried with MgSO<sub>4</sub> and filtered. The solvent was evaporated and the crude product was purified by silica gel flash chromatography (0-25% EtOAc in Hex). A white solid was obtained (2240 mg, 98%). LC-MS retention time (Method B): 1.450 min, m/z 996.6 (M+Na). <sup>1</sup>H NMR (600.1 MHz, CDCl<sub>3</sub>)  $\delta$  (ppm): 7.63 (t,  $J$  = 7.4 Hz, 2H), 7.39-7.46 (m, 2H), 7.23-7.29 (m, 10H), 7.03-7.18 (m, 14H), 6.82 (d,  $J$  = 8.4 Hz, 2H), 6.48-6.54 (m, 2H), 5.73-5.85 (m, 1H), 4.69-4.79 (m, 1H), 4.13-4.26 (m, 3H), 4.00-4.07 (m, 1H), 3.59-3.69 (m, 1H), 3.42-3.54 (m, 1.5H), 3.29-3.36 (m, 0.5H), 2.38-2.54 (m, 2H), 0.83-0.88 (m, 9H), 0.03-0.07 (m, 6H). <sup>13</sup>C NMR (150.0 MHz, CDCl<sub>3</sub>)  $\delta$  (ppm): 169.82, 169.79, 155.8, 155.7, 155.1, 155.0, 144.3, 143.73, 143.67, 141.3, 135.5, 135.3, 131.8, 129.6, 129.04, 129.00, 128.9, 128.1, 127.8, 127.1, 126.92, 126.91, 125.04, 120.22, 120.18, 120.0, 67.38, 67.33, 66.92, 66.86, 53.97, 53.88, 47.1, 45.9, 44.1, 43.9, 33.8, 25.7, 18.2, -4.4.



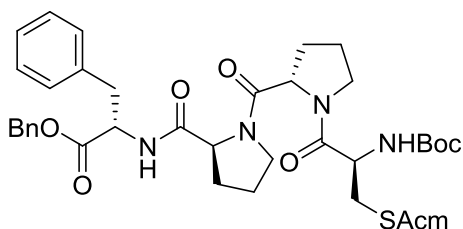
**(9H-fluoren-9-yl)methyl (R,E)-1-((4-((tert-butyldimethylsilyl)oxy)styryl)amino)-1-oxo-3-(tritylthio)propan-2-yl)carbamate (1.75)**. In a flask, **1.75** (1000 mg, 1.027 mmol) was added and suspended in THF (20 mL). Then, an aqueous solution of hydrogen peroxide 30% (127  $\mu$ L, 1.23 mmol) was added. The reaction was stirred for 1 hour at room temperature. LC-MS shows consumption of the starting material and formation of the desired product. The solvent was evaporated and the crude product was purified by silica gel flash chromatography (0-20% EtOAc in Hex). A colorless solid was obtained, (673 mg, 80%). LC-MS retention time (Method B): 1.285 min,  $m/z$  838.9 (M+Na).  $^1\text{H}$  NMR (600.1 MHz,  $\text{CDCl}_3$ )  $\delta$  (ppm): 7.75 (m, 2H) 7.52-7.64 (m, 2H), 7.34-7.43 (m, 8H), 7.24-7.29 (m, 8H), 7.15-7.22 (m, 5H), 7.13 (d,  $J = 8.4$  Hz, 2H), 6.74 (d,  $J = 8.4$  Hz, 2H), 6.00 (d,  $J = 14.6$  Hz, 1H), 4.93-5.0 (m, 1H), 4.38-4.46 (m, 2H), 4.18 (t,  $J = 6.6$  Hz, 1H), 3.78-3.84 (m, 1H), 2.69-2.74 (m, 1H), 2.62-2.68 (m, 1H), 0.97 (s, 9H), 0.18 (s, 6H).  $^{13}\text{C}$  NMR (150.0 MHz,  $\text{CDCl}_3$ )  $\delta$  (ppm): 167.3, 156.3, 154.8, 144.3, 143.6, 141.3, 129.6, 128.9, 128.2, 127.8, 127.1, 127.0, 126.8, 125.0, 120.35, 120.30, 120.1, 114.2, 67.5, 67.1, 54.1, 47.1, 33.5, 25.7, 18.2, -4.4.  $[\alpha]_D^{25}$ : -8.8 (c 1.0,  $\text{CHCl}_3$ ); HRMS (TOF,ES+)  $\text{C}_{51}\text{H}_{52}\text{N}_2\text{O}_4\text{S}$  [M] calculated 816.3417, found 816.3390,  $\Delta = -3.29$  ppm.



**(R,E)-2-amino-N-(4-((tert-butyldimethylsilyl)oxy)styryl)-3-(tritylthio)propanamide (1.77)**. In a vial, **1.76** (2043 mg, 2.5 mmol) was added and dissolved in 60 mL of acetonitrile.

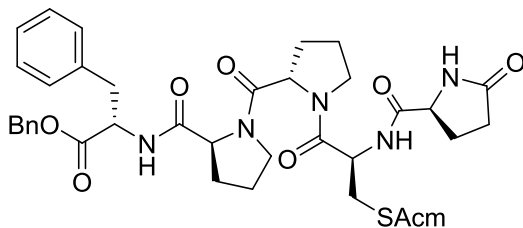


Then, morpholine (647  $\mu\text{L}$ , 7.5 mmol) was added while stirring. The reaction was stirred at room temperature for 24 hours, formation of product and full conversion was confirmed by LC-MS. The reaction was quenched by addition of water and extracted with DCM. The organic phases were combined and washed with aqueous LiCl 5%, dried with sodium sulfate and filtered. The solvent was evaporated and the crude product was purified by silica gel flash chromatography (0-5% MeOH in DCM). A pale yellow oil was obtained, (1067 mg, 72%). LC-MS retention time (Method B): 0.932 min,  $m/z$  243.0 (Tr), 633.0 (M+K), 1189.1 (2M+H).  $^1\text{H}$  NMR (600.1 MHz,  $\text{CDCl}_3$ )  $\delta$  (ppm): 8.97 (d,  $J = 8.4$  Hz, 1H), 7.45-7.50 (m, 6H), 7.28-7.35 (m, 6H), 7.21-7.27 (4H), 7.18 (d,  $J = 8.6$  Hz, 2H), 6.77 (d,  $J = 8.6$  Hz, 2H), 6.08 7 (d,  $J = 14.6$  Hz, 1H), 3.11-3.16 (m, 1H), 2.77-2.82 (m, 1H), 2.60-2.67 (m, 1H), 1.00 (s, 9H), 0.21 (s, 6H).  $^{13}\text{C}$  NMR (150.0 MHz,  $\text{CDCl}_3$ )  $\delta$  (ppm): 170.2, 154.6, 144.5, 129.5, 129.2, 128.0, 126.8, 126.6, 120.5, 120.2, 113.3, 67.1, 53.7, 37.0, 25.6, 18.1, -4.5.  $[\alpha]_{\text{D}}^{25}$ : -17.1 (c 1.0,  $\text{CHCl}_3$ ); HRMS (TOF,ES+)  $\text{C}_{36}\text{H}_{42}\text{N}_2\text{O}_2\text{S}$  [M] calculated 594.2736, found 594.2729,  $\Delta = -1.22$  ppm.



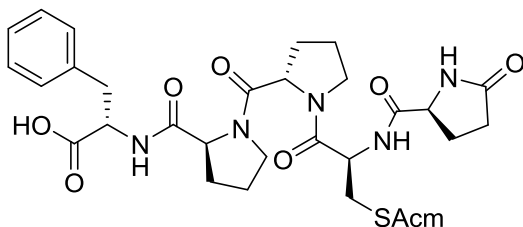
**Benzyl *S*-(acetamidomethyl)-*N*-(*tert*-butoxycarbonyl)-*L*-cysteinyl-*L*-prolyl-*L*-prolyl-*L*-phenylalaninate (1.78).** In a flask, **1.46** (670 mg, 1.219 mmol) was dissolved in 18 mL of DCM; to this mixture, 2 mL of TFA were added drop wise while in an ice bath and the reaction was allowed to warm until room temperature. After two hours of stirring, full deprotection of starting material was confirmed by LC-MS. The reaction was worked-up by evaporating the solvent and TFA *in vacuo*. The generated amine was used without further purification for the next reaction. Then, in a new flask, the Boc-*L*-cysteine-SAcM (535 mg, 1.828 mmol) and hydroxybenzotriazole (371 mg, 2.743 mmol) were weighted and suspended in 10 mL of DCE.

Then, while in an ice bath, EDCI hydrochloride was added (420 mg, 2.194 mmol) followed by 2,4,6-collidine (483  $\mu$ L, 3.657 mmol), and finally a solution of the deprotected amine obtained from **16** in 10 mL of DCE. The mixture was warmed to room temperature and stirred for 2 hours. The mixture was worked up by washing with HCl 1.0 M twice, then the aqueous phase was extracted thrice with DCM. The organic phases were combined, washed with brine, dried with magnesium sulfate and filtered. The volatiles were eliminated *in vacuo* and the crude was purified by silica gel flash chromatography (0-70% EtOAc/Hex). A white solid was obtained (730 mg, 83%). LC-MS retention time (Method A): 1.197 min, m/z 724.3 (M+H).  $^1\text{H}$  NMR (600.1 MHz,  $\text{CDCl}_3$ )  $\delta$  (ppm): 8.40 (d,  $J = 8.3$  Hz, 0.5H, NH), 7.61 (m, 0.5H, NH), 7.49 (m, 0.5H, NH), 7.31-7.38 (m, 3H), 7.27-7.30 (m, 2H), 7.22-7.25 (m, 1H), 7.16-7.21 (m, 3H), 6.97-7.02 (m, 1H), 6.82 (d,  $J = 7.1$  Hz, 0.5H, NH), 5.48-5.65 (m, 1H, NH), 5.02-5.19 (m, 2H), 4.79-4.84 (m, 0.5H), 4.70-4.76 (m, 0.5H), 4.56-4.64 (m, 1H), 4.48-4.51 (m, 0.5H), 4.23-4.47 (m, 2.5H), 4.12-4.17 (m, 1H), 3.64-3.76 (m, 2H), 3.51-3.58 (m, 0.5H), 3.44-3.49 (m, 0.5H), 3.33-3.41 (m, 1H), 3.19-3.25 (m, 0.5H), 3.10-3.18 (m, 1H), 3.03-3.09 (m, 0.5H), 2.82-2.98 (m, 2H), 2.61-2.66 (m, 0.5H), 2.21-2.41 (m, 1H), 1.79-2.12 (m, 7H), 1.62-1.76 (m, 2H), 1.40-1.50 (m, 9H), 1.014-1.14 (m, 0.5H).  $^{13}\text{C}$  NMR (150.0 MHz,  $\text{CDCl}_3$ )  $\delta$  (ppm): 173.4, 171.9, 171.2, 171.1, 170.72, 170.67, 170.63, 170.58, 170.1, 169.9, 155.42, 155.37, 154.7, 137.3, 135.7, 137.5, 135.0, 129.3, 129.1, 128.63, 128.61, 128.54, 128.45, 128.41, 128.34, 128.1, 127.1, 126.8, 123.6, 80.4, 80.1, 67.3, 67.1, 61.1, 60.1, 59.1, 58.2, 54.1, 53.2, 51.5, 51.1, 47.7, 47.5, 47.2, 46.9, 42.2, 41.6, 41.4, 37.5, 36.4, 35.3, 32.9, 32.7, 31.4, 28.44, 28.41, 28.35, 28.33, 28.2, 27.6, 24.99, 24.96, 24.94, 23.2, 23.0, 21.6, 21.5, 21.0.  $[\alpha]_{\text{D}}^{25}$ : -38.9 (c 1.0,  $\text{CHCl}_3$ ); HRMS (TOF,ES+)  $\text{C}_{37}\text{H}_{49}\text{N}_5\text{O}_8\text{S}$  [M] calculated 723.3302, found 723.3295,  $\Delta = -0.94$  ppm.



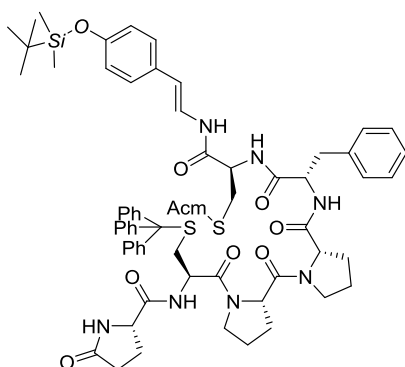
**Benzyl S-(acetamidomethyl)-N-((S)-5-oxopyrrolidine-2-carbonyl)-L-cysteinyl-L-prolyl-L-prolyl-L-phenylalaninate (1.79).** In a flask, **1.78** (485 mg, 0.670 mmol) was dissolved in 7.6 mL of DCM; to this mixture, 0.4 mL of TFA were added drop wise while in an ice bath and the reaction was allowed to warm until room temperature. After two hours of stirring, full deprotection of starting material was confirmed by LC-MS. The reaction was worked-up by evaporating the solvent and TFA *in vacuo*. The generated amine was used without further purification for the next reaction. Then, in a new flask, the L-pyroglutamic (95 mg, 0.737 mmol) and 1-hydroxyl-7-azabenzotriazole (137 mg, 1.005 mmol) were weighted and suspended in 7 mL of DCE. Then, while in an ice bath, HATU was added (306 mg, 0.804 mmol) followed by 2,4,6-collidine (266  $\mu$ L, 2.010 mmol), and finally a solution of the deprotected amine obtained from 28 in 7 mL of DCE. The reaction was warmed to room temperature and stirred for 2 hours. The mixture was worked up by washing with HCl 1.0 M twice, then the aqueous phase was extracted thrice with DCM. The organic phases were combined, washed with brine, dried with magnesium sulfate and filtered. The volatiles were eliminated *in vacuo* and the crude was purified by reverse phase C18 flash chromatography (0-50% ACN/water 0.1% TFA). A white solid was obtained (428 mg, 87%). LC-MS retention time (Method A): 0.891 min,  $m/z$  735.0 (M+H).  $^1\text{H}$  NMR (600.1 MHz,  $\text{CDCl}_3$ )  $\delta$  (ppm): 8.37 (d,  $J = 9.0$  Hz, 0.5H, NH), 7.60 (d,  $J = 7.7$  Hz, 0.5H, NH), 7.45-7.50 (m, 0.5H, NH), 7.32-7.38 (m, 3H), 7.26-7.32 (m, 3H), 7.22-7.25 (m, 1H), 7.16-7.21 (m, 3H), 7.03-7.06 (m, 0.5H, NH), 6.97-7.03 (m, 1H), 6.92 (d,  $J = 7.0$  Hz, 0.5H, NH), 6.77 (s, 1H, NH), 5.01-5.21 (m, 1.5H), 4.83-4.96 (m, 2H), 4.76-4.82 (m, 0.5H), 4.59-4.66 (m, 0.5H), 4.51-4.56 (m, 0.5H), 4.37 (d,  $J = 6.1$  Hz, 1H), 4.27-4.33 (m, 0.5H), 4.21-4.21 (m, 1H), 4.11-4.18 (m,

1H), 3.99-4.05 (m, 0.5H), 3.62-3.78 (m, 1.5H), 3.49-3.55 (m, 0.5H), 3.42-3.48 (m, 1H), 3.32-3.39 (m, 0.5H), 3.23-3.29 (m, 0.5H), 2.79-3.16 (m, 4H), 2.52-2.59 (m, 0.5H), 2.40-2.50 (m, 1.5H), 2.15-2.37 (m, 3H), 1.90-2.13 (m, 7H), 1.71-1.79 (m, 0.5H), 1.60-1.70 (m, 1.5H), 1.39-1.48 (m, 0.5H), 0.97-1.07 (m, 0.5H). <sup>13</sup>C NMR (150.0 MHz, CDCl<sub>3</sub>) δ (ppm): 179.1, 178.8, 172.4, 172.0, 171.4, 171.2, 171.0, 170.92, 170.86, 170.23, 170.18, 137.1, 135.8, 135.3, 135.0, 129.3, 129.1, 128.7, 128.61, 128.57, 128.45, 128.41, 128.36, 127.0, 126.7, 67.3, 67.1, 61.2, 60.1, 59.2, 58.3, 57.12, 57.06, 53.3, 53.1, 50.7, 50.2, 47.7, 47.6, 47.2, 46.9, 41.4, 41.1, 37.5, 36.3, 32.0, 31.6, 31.5, 29.35, 29.26, 28.4, 28.1, 27.9, 26.0, 25.6, 25.0, 24.9, 24.8, 23.1, 23.0, 21.5. [α]<sub>D</sub><sup>25</sup>: -73.9 (c 1.0, CHCl<sub>3</sub>); HRMS (TOF,ES+) C<sub>37</sub>H<sub>46</sub>N<sub>6</sub>O<sub>8</sub>S [M] calculated 734.3098, found 734.3092, Δ = -0.86 ppm.



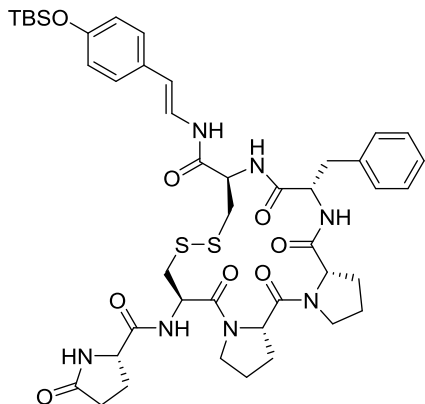
**S-(acetamidomethyl)-N-((S)-5-oxopyrrolidine-2-carbonyl)-L-cysteinyl-L-prolyl-L-prolyl-L-phenylalanine (1.80).** In a flask, **1.79** (2.360 g, 3.211 mmol) was dissolved in 30 mL of DCM. Then, a solution of aluminum chloride (2.569 g, 19.26 mmol) in nitromethane was added dropwise while in an ice bath. The reaction was warmed to room temperature and stirred for 1 hour. After this time, formation of product and consumption of starting material was confirmed by LC-MS. The reaction was quenched by addition of water and it was worked up by successive extractions with CHCl<sub>3</sub>:IPA (3:1). The organic phases were combined, washed with brine, dried with magnesium sulfate and filtered. The volatiles were eliminated *in vacuo* and the crude was purified by reverse phase C18 flash chromatography (0-60% ACN/water 0.1% TFA). A white solid was obtained (1.950 g, 94%). LC-MS retention time (Method A): 0.748 min, m/z 645.0

(M+H). <sup>1</sup>H NMR (600.1 MHz, CDCl<sub>3</sub>) δ (ppm): 8.16 (d, *J* = 8.9 Hz, 1H), 7.71 (s, 1H), 7.68 (t, *J* = 5.8 Hz, 1H), 7.27 (t, *J* = 7.3 Hz, 2H), 7.18-7.23 (m, 3H), 6.98 (d, *J* = 8.6 Hz, 1H), 4.89-5.00 (m, 2H), 4.64 (dd, *J*<sub>ABX</sub> = 13.5 Hz, *J* = 6.8 Hz, 1H), 4.21-4.32 (m, 3H), 4.11 (dd, *J*<sub>ABX</sub> = 13.6 Hz, *J* = 5.6 Hz, 1H), 3.76-3.87 (m, 1H), 3.65-3.73 (m, 1H), 3.46 (dd, *J*<sub>ABX</sub> = 14.1 Hz, *J* = 4.6 Hz, 1H), 3.38-3.43 (m, 1H), 3.21-3.27 (m, 1H), 2.93-3.00 (m, 2H), 2.74 (dd, *J*<sub>ABX</sub> = 14.3 Hz, *J* = 5.3 Hz, 1H), 2.56-2.64 (m, 2H), 2.42-2.50 (m, 2H), 2.12-2.26 (m, 3H), 2.06 (s, 3H), 1.85-2.01 (m, 3H), 1.57-1.64 (m, 1H), 0.80-0.90 (m, 1H). <sup>13</sup>C NMR (150.0 MHz, CDCl<sub>3</sub>) δ (ppm): 181.0, 175.1, 171.6, 171.4, 170.6, 170.4, 168.6, 136.9, 129.0, 128.6, 127.0, 61.4, 59.6, 57.6, 53.0, 51.7, 47.9, 46.9, 42.9, 38.0, 33.1, 31.7, 29.5, 28.8, 25.6, 25.2, 22.8, 21.4. [α]<sub>D</sub><sup>25</sup>: -86.7 (c 1.0, CHCl<sub>3</sub>); HRMS (TOF,ES+) C<sub>30</sub>H<sub>40</sub>N<sub>6</sub>O<sub>8</sub>S [M] calculated 644.2628, found 644.2630, Δ = +0.26 ppm.



(*S*)-*N*-((*S*)-1-((1-3-((acetamidomethyl)thio)-1-((*E*)-4-((*tert*-butyldimethylsilyloxy)styryl)amino)-1-oxopropan-2-yl)amino)-1-oxo-3-phenylpropan-2-yl)-1-(*N*-((*S*)-5-oxopyrrolidine-2-carbonyl)-*S*-trityl-*L*-cysteinyl-*L*-prolyl)pyrrolidine-2-carboxamide (**1.81**). In a flask, **1.80** (1149 mg, 1.781 mmol) and HATU (813 mg, 2.138 mmol), were weighted and suspended in 30 mL of DCE. Then, 2,4,6-trimethylpyridine (0.353 mL, 2.673 mmol) was added and the mixture was stirred for 2 minutes. Then, while in an ice bath, a solution of **1.77** (1060 mg, 1.781 mmol) in 15 mL of DCE was added dropwise. The reaction was warmed to room temperature and stirred for 1 hour; formation of product and consumption of starting material was confirmed by LC-MS. The reaction was quenched by

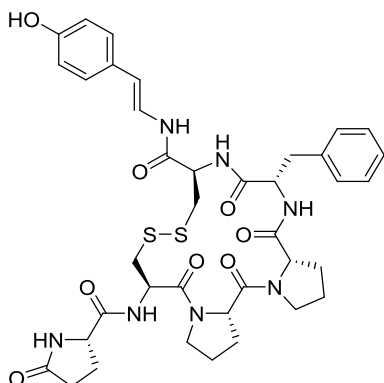
addition of water. Then, it was worked up by successive extractions with  $\text{CHCl}_3$ :IPA (3:1). The organic phases were combined, dried with  $\text{MgSO}_4$  and filtered. The solvent was evaporated and the crude product was purified by reverse phase C18 flash chromatography (0 to 60% ACN in water-TFA 0.1%). A white solid was obtained (1129 mg, 51%). LC-MS retention time (Method A): 1.368 min,  $m/z$  243.0 (Tr+), 979.2 (M-Tr) 1243.2 (M+Na).  $^1\text{H}$  NMR (600.1 MHz,  $\text{CDCl}_3$ )  $\delta$  (ppm): 8.66 (d,  $J = 10.3$  Hz, 1H), 8.24-8.37 (m, 1H), 7.37-7.42 (m, 3H), 7.31-7.36 (m, 6H), 7.27-7.31 (m, 5H), 7.07-7.25 (m, 13H), 6.70-6.77 (m, 2H), 6.10-6.23 (m, 1H), 4.94-5.02 (m, 0.6H), 4.74-4.82 (m, 0.4H), 4.61-4.67 (m, 0.6H), 4.56-4.61 (m, 0.6H), 4.49-4.53 (m, 0.4H), 4.43-4.48 (m, 0.4H), 4.24-4.36 (m, 0.8H), 4.17-4.24 (m, 1.6H), 4.06-4.17 (m, 2H), 3.92-3.98 (m, 0.6H), 3.72-3.79 (m, 1H), 3.55-3.64 (m, 1H), 3.14-3.41 (m, 3H), 2.92-3.11 (m, 2H), 2.79-2.87 (m, 1H), 2.63-2.69 (m, 1H), 2.27-2.59 (m, 3H), 2.15-2.26 (m, 2H), 1.55-2.07 (m, 11H), 0.94-0.99 (m, 9H), 0.16-0.19 (m, 6H).  $^{13}\text{C}$  NMR (150.0 MHz,  $\text{CDCl}_3$ )  $\delta$  (ppm): 178.8, 172.7, 172.5, 172.4, 172.2, 171.1, 170.9, 170.7, 170.6, 170.2, 169.2, 169.1, 167.5, 167.3, 154.9, 154.6, 144.4, 144.1, 136.9, 135.7, 129.8, 129.6, 129.5, 129.36, 129.32, 129.1, 129.02, 129.97, 128.6, 128.2, 128.1, 127.08, 127.03, 126.9, 126.7, 120.4, 120.3, 114.5, 114.3, 67.6, 67.5, 61.4, 61.2, 59.3, 58.3, 57.2, 57.0, 54.9, 54.5, 53.6, 53.1, 51.2, 50.7, 47.9, 47.5, 46.9, 42.1, 41.8, 36.3, 33.8, 33.1, 32.9, 32.1, 31.5, 29.6, 29.4, 28.7, 28.4, 28.2, 26.0, 25.7, 25.4, 25.3, 25.0, 23.1, 23.0, 21.5, 18.3, -4.4.  $[\alpha]_D^{25}$ : -31.7 (c 1.0,  $\text{CHCl}_3$ ).



**(6*R*,11*R*,14*S*,16*aS*,21*aS*)-14-benzyl-*N*-((*E*)-4-((*tert*-butyldimethylsilyl)oxy)styryl)-5,13,16,21-tetraoxo-6-((*S*)-5-oxopyrrolidine-2-carboxamido)hexadecahydro-1*H*,5*H*,10*H*-dipyrrolo[2,1-*j*:2',1'-*m*][1,2]dithia[5,8,11,14]tetraazacycloheptadecine-11-carboxamide**

**(1.82)**. In a flask, iodine (104 mg, 0.410mmol) was dissolved in 80 mL of a mixture of DCM:MeOH (9:1). A solution of **1.81** (100 mg, 0.082 mmol) in 16 mL of DCM was added dropwise and while stirring. The reaction was stirred for 30 minutes, formation of product and consumption of starting material was confirmed by LC-MS. The reaction was quenched with 5% sodium thiosulfate solution, then water was added to the mixture and extractions with DCM were performed. The organic phases were combined, dried with MgSO<sub>4</sub> and filtered. The solvent was evaporated and the crude product was purified by reverse phase C18 column flash chromatography (0 to 70% ACN in water-TFA 0.1%). A white solid was obtained (37.9 mg, 51%). LC-MS retention time (Method A): 1.243 min, m/z 906.2 (M+H). <sup>1</sup>H NMR (600.1 MHz, CDCl<sub>3</sub>) δ (ppm): 9.64 (br s, 1H), 9.16 (br d, *J* = 7.1 Hz), 7.88-8.16 (m, 2H), 7.27-7.34 (m, 3H), 7.18-7.25 (m, 5H), 7.06 (t, *J* = 7.1 Hz, 1H), 6.76 (d, *J* = 8.3 Hz, 1H), 6.38 (t, *J* = 7.1 Hz, 1H), 4.90-4.99 (m, 1H), 4.62-4.85 (m, 3H), 4.32-4.39 (m, 1H), 4.19-4.30 (m, 1H), 3.69-3.82 (m, 1H), 3.50-3.61 (m, 1H), 3.30-3.39 (m, 1H), 3.19-3.29 (m, 2H), 3.10-3.19 (m, 2H), 2.97-3.07 (m, 1H), 2.87-2.96 (m, 1H), 2.61-2.75 (m, 2H), 2.18-2.35 (m, 4H), 1.75-1.98 (m, 5H), 1.32-1.44 (m, 1H), 0.97 (s, 9H), 0.25-0.35 (m, 1H), 0.19 (s, 6H). <sup>13</sup>C NMR (150.0 MHz, CDCl<sub>3</sub>) δ (ppm): 180.5, 172.7, 171.6, 171.4, 169.9, 169.1, 166.7, 154.7, 136.9, 129.4, 129.3, 128.8, 126.9, 120.9, 120.6,

120.2, 115.1, 61.0, 59.8, 56.6, 54.0, 51.3, 49.4, 47.0, 46.8, 42.4, 38.6, 33.7, 32.3, 30.9, 29.6, 25.9, 25.7, 22.3, 20.0, 18.2, -4.4.  $[\alpha]_D^{25}$ : 29.6 (c 1.0, CHCl<sub>3</sub>); HRMS (TOF,ES+) C<sub>44</sub>H<sub>59</sub>N<sub>7</sub>O<sub>8</sub>S<sub>2</sub>Si [M] calculated 905.3636, found 905.3634,  $\Delta$  = -0.24 ppm.



**Gombamide A, (6R,11R,14S,16aS,21aS)-14-benzyl-N-((E)-4-hydroxystyryl)-5,13,16,21-tetraoxo-6-((S)-5-oxopyrrolidine-2-carboxamido)hexadecahydro-1H,5H,10H-dipyrrolo[2,1-j:2',1'-m][1,2]dithia[5,8,11,14]tetraazacycloheptadecine-11-carboxamide (1.16).** In a flask, **1.82** (29.0 mg, 0.032 mmol) was weighed and dissolved in methanol (1.60 mL). Then, potassium fluoride (1.9 mg, 0.032 mmol) was added to the mixture and the reaction was stirred for 6 hours at room temperature. Consumption of starting material and formation of product was confirmed by LC-MS. The solvent was evaporated and the crude product was purified by reverse phase C18 column flash chromatography (0 to 40% ACN in water-TFA 0.1%). A white solid was obtained (14.6 mg, 58%). LC-MS retention time (Method A): 0.951 min, m/z 792.1 (M+H). For <sup>1</sup>H NMR (600.1 MHz, CDCl<sub>3</sub>)  $\delta$  (ppm) and <sup>13</sup>C NMR (150.0 MHz, CDCl<sub>3</sub>)  $\delta$  (ppm) see Table S1.  $[\alpha]_D^{25}$ : 79.8 (c 1.0, CHCl<sub>3</sub>); HRMS (TOF,ES+) C<sub>44</sub>H<sub>59</sub>N<sub>7</sub>O<sub>8</sub>S<sub>2</sub>Si [M] calculated 791.2771, found 791.2767,  $\Delta$  = -0.54 ppm.



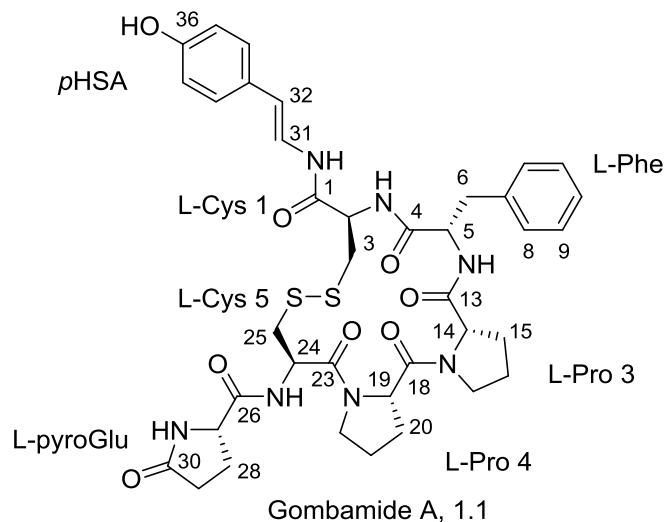


**Table 1.3.** NMR data comparison between isolated<sup>a</sup> and synthetic<sup>b</sup> Gombamide A (**1.16**).

Position	Isolated		Synthetic		
	$\delta_C$	$\delta_H$ (J in Hz)	$\delta_C$	$\delta_H$ (J in Hz)	
Cys 1	1	167.4, C	-	167.5, C	-
	2	51.5, CH	4.62, ddd (12.0, 8.7, 3.2)	51.6, CH	4.62, m (3.2, 8.7)
	3	41.8, CH <sub>2</sub>	3.15, dd (14.1, 3.2)	41.8, CH <sub>2</sub>	3.14, dd (14.6, 3.4)
			2.91, dd (14.1, 12.0)		2.90, dd (13.9, 12.2)
2-NH		7.67, d (8.7)		7.67, d (8.6)	
Phe	4	171.0, C	-	171.1, C	-
	5	53.2, CH	4.88, ddd (12.7, 8.8, 4.3)	53.2, CH	4.88, dd (8.8, 4.3)
	6	33.8, CH <sub>2</sub>	3.07, dd (14.2, 12.7)	33.9, CH <sub>2</sub>	3.07, dd (13.7, 13.2)
			2.96, dd (14.2, 4.3)		2.96, dd (14.0, 3.7)
	7	138.1, C	-	138.1, C	-
	8/12	129.5, CH	7.39, br d (7.4)	129.6, CH	7.38, br d (7.4)
	9/11	128.0, CH	7.22, dd (7.7, 7.4)	128.1, CH	7.22, t (7.4)
	10	126.0, CH	7.16, t (7.7)	126.0, CH	7.15, dd (8.0, 6.6)
5-NH		9.14, d (8.8)		9.14, d (8.6)	
Pro 3	13	171.4, C	-	171.5, C	-

	14	60.3, CH	4.35, br d (8.0)	60.4, CH	4.34, br d (7.9)
	15	31.1, CH <sub>2</sub>	1.83, m 1.70, m	31.1, CH <sub>2</sub>	1.83, m 1.69, m
	16	19.7, CH <sub>2</sub>	1.31, m 0.23, m	19.7, CH <sub>2</sub>	1.30, m 0.22, m
	17	45.8, CH <sub>2</sub>	3.22, ddd (11.0, 8.6, 3.2) 3.02, br dd (11.0, 9.0)	45.8, CH <sub>2</sub>	3.22, m, (11.0, 8.5) 3.02, dd (11.5, 10.2)
Pro 4	18	169.4, C	-	169.5, C	-
	19	59.3, CH	4.86, dd (8.9, 3.3)	59.3, CH	4.86, dd (8.9, 3.1)
	20	30.3, CH <sub>2</sub>	2.23, m 1.87, m	30.4, CH <sub>2</sub>	2.22, m 1.86, m
	21	21.8, CH <sub>2</sub>	1.77, m 1.71, m	21.8, CH <sub>2</sub>	1.76, m 1.71, m
	22	46.4, CH <sub>2</sub>	3.50, ddd (11.7, 8.2, 4.1) 3.35, m	46.5, CH <sub>2</sub>	3.49, ddd (11.4, 8.3, 4.1) 3.35, m
Cys 5	23	168.0, C	-	168.1, C	-
	24	48.5, CH,	4.59, ddd (11.6, 10.0, 5.5)	48.5, CH	4.58, m (5.5, 10.1)
	25	37.6, CH <sub>2</sub>	3.19, dd (12.0, 5.5) 2.62, dd (12.0, 11.6)	37.6, CH <sub>2</sub>	3.18, m 2.62, t (11.8)
	24-NH		8.64, d (10.0)		8.63, d (9.7)
pyroGlu	26	172.0 C	-	172.0, C	-
	27	54.9, CH	4.12, br dd (9.1, 1.5)	54.9, CH	4.11, br d (9.2)
	28	25.5, CH <sub>2</sub>	2.24, m 2.09, m	25.6, CH <sub>2</sub>	2.23, m 2.08, m
	29	28.8, CH <sub>2</sub>	2.36, m 2.06, ddd (12.5, 9.7, 2.7)	28.9, CH <sub>2</sub>	2.36, m 2.05, m

	30	177.9, C	-		178.0, C	-
	27-NH		7.93, br s			7.93, s
<i>p</i> HSA	31	120.4, CH	7.15, dd (14.8, 10.0)	120.4, CH	7.13, d (15.0)	
	32	113.6, CH	6.26, d (14.8)	113.7, CH	6.25, d (14.6)	
	33	126.9, C	-	127.0, C	-	
	34/38	115.6, CH	6.71, d (8.7)	115.6, CH	6.70, d (8.5)	
	35/37	126.5, CH	7.18, d (8.7)	126.6, CH	7.17, d (8.6)	
	36	156.4, C	-	156.3, C	-	
	31-NH		10.21, d (10.0)		10.21, d (9.8)	
	36-OH		9.40, s		9.39, s	

<sup>a</sup>600 MHz for <sup>1</sup>H-NMR and 150 for <sup>13</sup>C-NMR, from Woo, J-K.; Jeon, J.; Kim, C-K.; Sim, C.J.; Oh, D-C.; Oh, K-B.; Shin, J. *J. Nat. Prod.* **2013**, *76*, 1380-1383. <sup>b</sup>600 MHz for <sup>1</sup>H-NMR and 150 for <sup>13</sup>C-NMR.

## CHAPTER II

### TOTAL SYNTHESIS OF ACTINOPHENANTHROLINE A

#### Introduction

As mentioned in Chapter I, the marine ecosystems are widely recognized for being the source of chemically diverse and biologically active natural products. Until recently, marine plants and invertebrates were the principle species studied from this habitats, leaving the microorganism of the sea vastly unexplored. This was due in part to the difficulty to collect the samples from deep-sea sediments, perform the purification and classification of the organism, and culture these species *in vitro*; however, due to technological advances in sequencing and molecular biology multiple marine microbial have been isolated and characterized.<sup>66</sup>

The actinomycetes class of bacteria has been an abundant source of antibiotics. After being discovered in the earth soil, the exploration of the marine actynomicetes has led to the discovery of a novel species in the class. Within these new species, new genres have also been found like the salt water-dependent *Salinospora*. Additionally, new species of known genres have been discovered, for example within the *Streptomyces*.<sup>67</sup>

Efforts to characterize the biology and chemistry of these new species of *Streptomyces* have led to the discovery of numerous interesting and uncommon natural products, by different research groups. The molecules isolated from these *Streptomyces* species are structurally diverse and exemplify most different classes of metabolites, as illustrated by the natural products in Fig. 2.1. An example, is the polyketide metabolite nahuoic acid A **2.1**, that has been isolated from *Streptomyces spp* (isolate RJA2928) from marine sediments of Papua New Guinea and it has shown inhibition of SETD8, a protein methyl transferase involve in epigenetic regulation and overexpressed in various types of cancer.<sup>68</sup> From the terpenoids class, the meroterpenoid

actinoranone **2.2** was isolated from a non-described species of *Streptomyces*, strain CNQ-027, and it proved to have cytotoxic activity in the HCT-116 cell line.<sup>69</sup> In this same strain, peptidic metabolites have also been found, such as actinoramide A **2.3**.<sup>70</sup> While from the alkaloids group, the cytotoxic marineosin A **2.4** has also been isolated from the marine *Streptomyces* spp. (CNQ-617).<sup>71</sup>

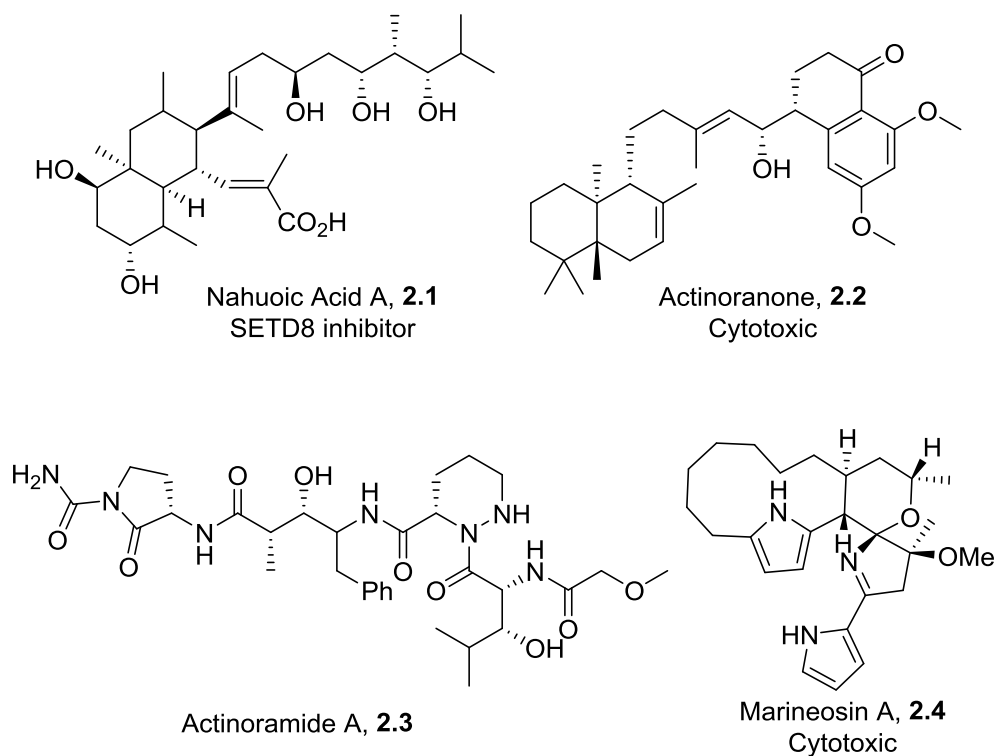


**Figure 2.1.** Representative examples of natural products isolated from marine actinomycetes.

In 2015, Fenical and collaborators reported the isolation of a non described actinomycete bacterium from the marine sediments of the coast of La Jolla, San Diego. The bacterial strain, which required seawater for growth and culture, was described as a likely member of the genus *Streptomyces* based on available sequence data and was coded as CNQ-149. Large scale fermentation and LC-MS analysis of crude extracts identified several compounds with a UV pharmacophore at low wavelength and with molecular weight between 300 and 400 amu. This

effort led to the identification of four new alkaloids: actinobenzoquinoline **2.5** and actinophenanthrolines A-C **2.6-2.8** (Figure 2.2).<sup>72</sup>

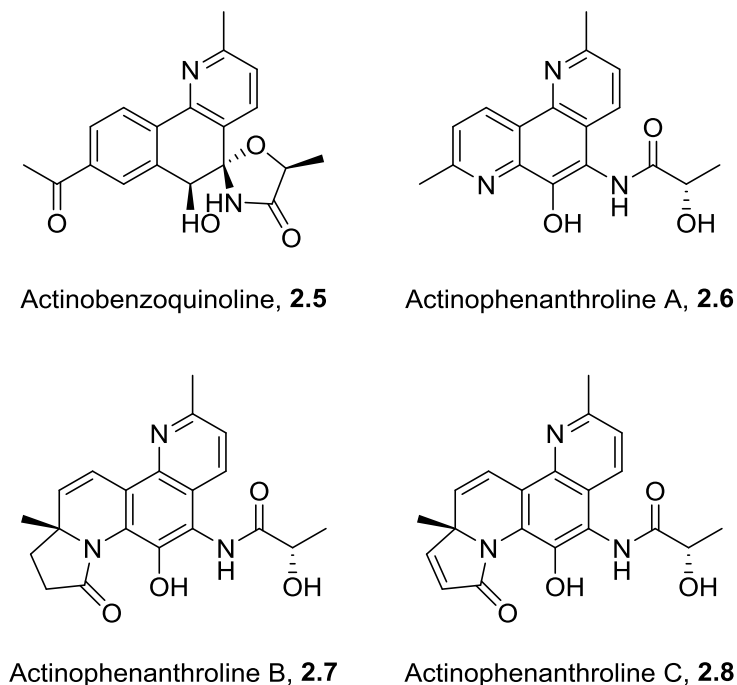


**Figure 2.2.** Structures of actinobenzoquinoline (**2.5**) and actinophenanthrolines A-C (**2.6-2.8**), unprecedented marine sediment alkaloids.

Actinophenanthroline A **2.6** is the first 1,7-phenanthroline alkaloid isolated from a natural source, and one of the rare examples of phenanthroline natural products. Compound **2.6** did not show general cytotoxicity in HCT-116 cell line, as well as alkaloids **2.7-2.8**. However, synthetic 1,7-phenanthrolines have demonstrated biological activity.

There have been reports of the anticancer and mutagenic activities of 1,7-phenanthrolines analogs,<sup>73-81</sup> and other biological effects have also been described. 1,7-phenanthroline promotes epithelial chloride secretion by opening of the Cystic Fibrosis Transmembrane Conductance Regulator (CFTR) chloride channel.<sup>82</sup> It has also been observed that administration of naked 1,7-phenanthroline in mice causes induction of drug metabolizing enzymes. This heterocycle

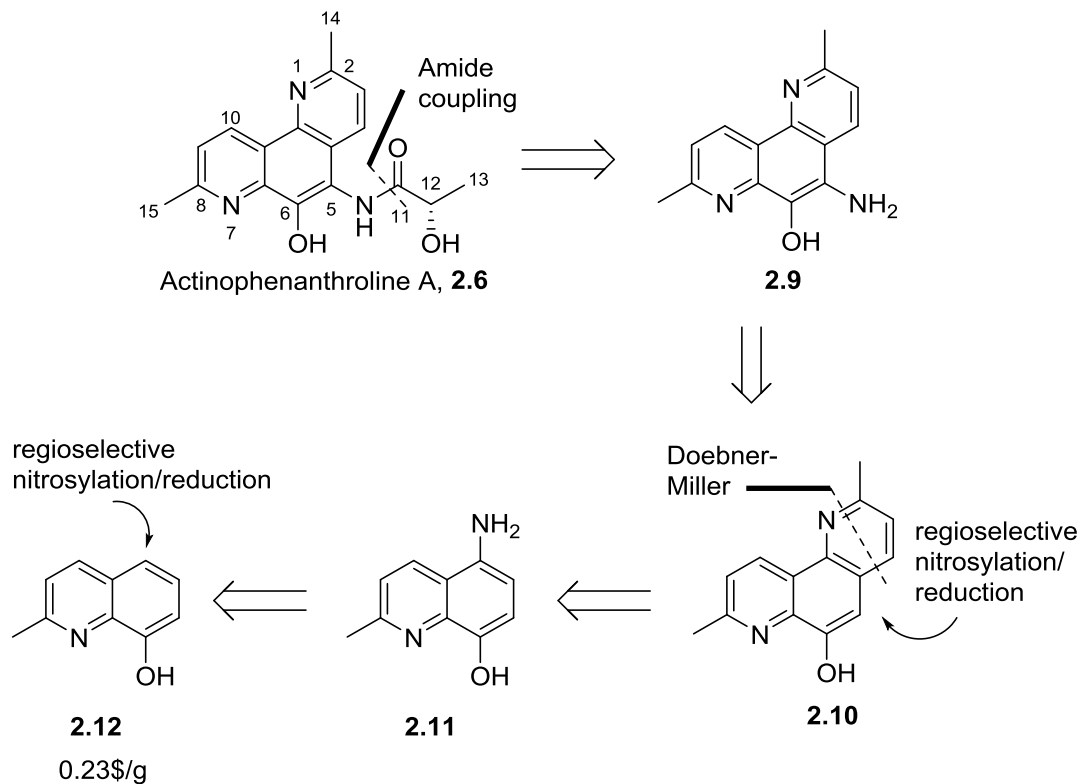
increased the activity of glutathione S-transferase and NADPH-quinone reductase in mice, while not affecting P450 metabolism.<sup>83,84</sup> The compound also proved to increase the transcription of quinone reductase, glucuronyltransferases (UGT1A6, UGT2B1), along with mRNA levels of the transporter Mrp3 in rat liver and kidney.<sup>85</sup> Besides, the phenanthroline derived bufrolin acts as an agonist of GPR35 receptor and has antiallergic and mast cell stabilizing properties.<sup>86</sup> 1,7-phenanthroline analogs have shown weak antimicrobial activity against *Mycobacterium tuberculosis* and *Plasmodium falciparum*.<sup>87,88</sup> Moreover, this type of compounds have also shown anti-HIV-1 integrase activity.<sup>89,90</sup>

The precedent of diverse biological activity of secondary metabolites from strains related to CNQ-149, along with the presence of various bioactive synthetic 1,7-phenanthrolines, argues for further exploration of the effects of actinophenanthrolines. The isolation of **2.6-2.8** in milligram quantities required large fermentation volumes (70 L) and lengthy purification, and we believed that the obtention of this natural products could be achieve more efficiently through a synthetic procedure. Therefore, because of its potential biological activity and their unprecedented structure, it was decided to start the synthesis of actinophenanthrolines. As Actinophenanthroline A **2.6** presents the simpler core from this set of compounds and might provide a route that can be used later for the building of **2.7** and **2.8**, we decide to embark in its total synthesis first.

### **Retrosynthetic analysis for the synthesis of Actinophenanthroline A**

For the retrosynthesis of compound **2.6**, we envisioned a short and linear route where the (*S*)-2-hydroxypropanamide would be installed in the last step through the coupling between aminohydroxyphenanthroline **2.9** and L-lactic acid (Scheme 2.1). The intermediate **2.9** would be derived from the directed nitrosylation of **2.10** followed by the reduction to the amino. Meanwhile, the phenanthroline core and installation of carbon 14 would be performed following

a Brønsted acid-catalyzed Doebner-Miller procedure, with **2.11** as starting material. The first steps would involve the regioselective nitrosylation of 8-hydroxyquinoline **2.12** and further reduction to obtain 5-amino-8-hydroxyquinoline **2.11**. This route would provide quick access to the natural product **2.5** from inexpensive commercial material (8-hydroxyquinoline **2.12**, \$0.23 per gram) and it potentially would not require the use of protection/deprotection steps.



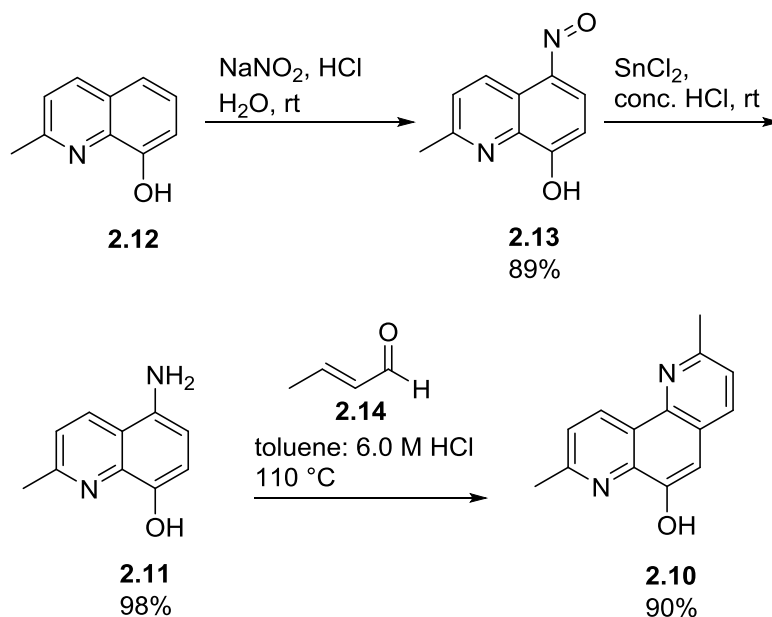
**Scheme 2.1.** Retrosynthetic analysis for obtention of **2.6**.

### Synthesis of Actinophenanthroline A

The synthesis of actinophenanthroline A **2.6** started with the regioselective *para*-directed nitrosylation reaction of **2.12** using sodium nitrite and concentrated HCl in water (Scheme 2.2). This procedure provided a regioisomeric mixture of 5-nitroso **2.13** and the undesired 7-nitroso



compound, in a ratio of 10:1. The preference for the *para*-substituted regioisomer has been described in the literature,<sup>91–94</sup> and it can be explained by considering the stabilization of the sigma complex after the introduction of the nitroso group in the ring. In the case of an unsubstituted quinoline, the most reactive positions are 5 and 8, while electrophilic substitution is less favored in 6 and 7. The introduction of the hydroxyl group in position 8, besides blocking this position for nitrosylation favors even more electrophilic substitution in position 5 due to electron donation by resonance and the possibility of more resonance forms that stabilize the sigma complex.



**Scheme 2.2.** Synthesis of 1,7-phenanthroline **2.10**.

It was attempted to separate the mixture of regioisomers rate through silica gel flash chromatography; however, formation of a complex matrix and decomposition of the nitrosylation products was observed during the purification, which led to little recovery of pure **2.13**. Eventually, it was found that the regioisomers could be separated by trituration with cold water, as the 7-nitroso isomer presumably has a larger dipole moment. This operation allowed obtaining **2.13** in 89% isolated yield.

Reduction of **2.13** to the amine **2.11** was attempted through hydrogenation with palladium on carbon as the catalyst and ethanol as solvent. Monitoring of the reaction demonstrated the formation of product; although, decomposition was observed after filtration of the reaction matrix through a celite pad during the workup that led to no isolation of the desired product. Then, it was found that the reaction could also be performed effectively with tin(II) chloride in concentrated HCl with dioxanes. However, the purification of compound **2.11** proved to be difficult as it showed very high solubility in water during extractive workup. Attempts to increase the pH of the aqueous phase also led to the decomposition of the product and once enough crude material could be recovered the electron rich **2.11** compound decomposed during silica gel chromatography.

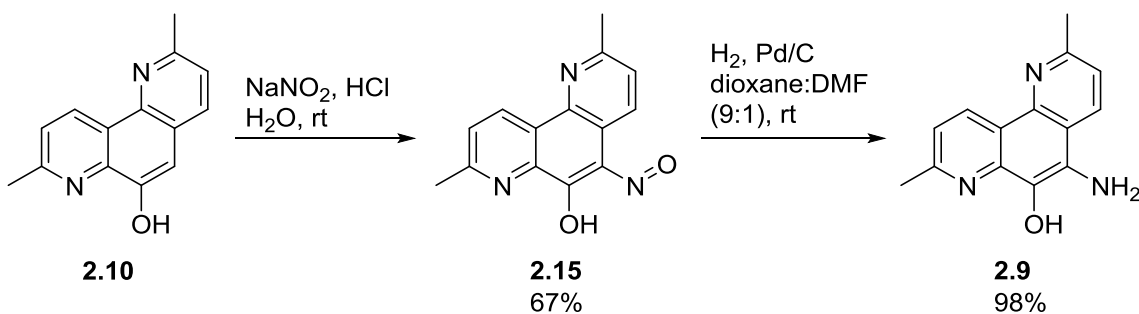
At this point, it was thought that the possible decomposition process was caused by the oxidation of **2.11** to the corresponding reactive iminoquinone, and that protecting the phenol group might be beneficial to impede this transformation. Before adding more steps to our sequence, the modification of the purification operations was explored. In order to circumvent column chromatography and maintaining an acidic media to avoid degradation of the product, it was decided to perform the reaction in conditions that favored the precipitation of the product in the reaction media. The concentration of starting material was increased gradually and it was found that an organic solvent was not necessary for the transformation to occur. The reaction was carried out in concentrated hydrochloric acid at a concentration of 2.2 M of **2.13**, which favored the precipitation of product **2.11** from the media; this permitted the purification of **2.11** as the hydrochloride salt in excellent isolated yields (98%). Moreover, this synthetic protocol demonstrated to be robust as it afforded comparable yields and purities when performed on either a 20 mg or 10 g scale.

After the obtention of **2.11**, we studied the use of a Doebner-Miller pyridine ring annulation reaction to construct the 1,7-phenantholine core. The procedure was performed in conjunction with *trans*-crotonaldehyde to provide the tricycle and introduce the C14 methyl

group. Using classic Brønsted acid-catalyzed conditions,<sup>95,96</sup> employing HCl in an aqueous media and heating to reflux temperature, did not prove effective to achieve the transformation as mainly polymerization of the crotonaldehyde was observed.

To decrease the aldehyde decomposition, the reaction was carried out in a biphasic solvent system of toluene:aqueous acid. Although this modification improved the reaction productivity, the yield of **2.10** was still very low (17%). In an effort to increase the yield, a solution of crotonaldehyde in toluene was added slowly *via* syringe pump over one hour to a stirred a solution of **2.11** in 6.0 M HCl at 110 °C, followed by reflux. This procedure demonstrated to give excellent isolated yields of **2.10**. The reaction time was a critical parameter during this step, as thermal decomposition of the 1,7-phenanthroline **2.10** was detected after one hour of the addition of the crotonaldehyde solution. The optimized protocol delivered intermediate **2.10** in 90% isolated yield robustly in scales of up to 10 grams.

The second nitrosylation procedure to provide intermediate **2.15** was performed following the procedure for the synthesis of **2.13**. **2.10** was nitrosylated with NaNO<sub>2</sub> in aqueous HCl, and the low solubility in water of the product was profited to obtain the hydrochloride salt of **2.15** in 67% yield (Scheme 2.3). The selectivity of the reaction for the C5 position of the 1,7-phenanthroline is given by the low reactivity of the pyridine rings toward electrophilic substitution and the hydroxyl electron donating that direct the substitution to the *ortho* position.



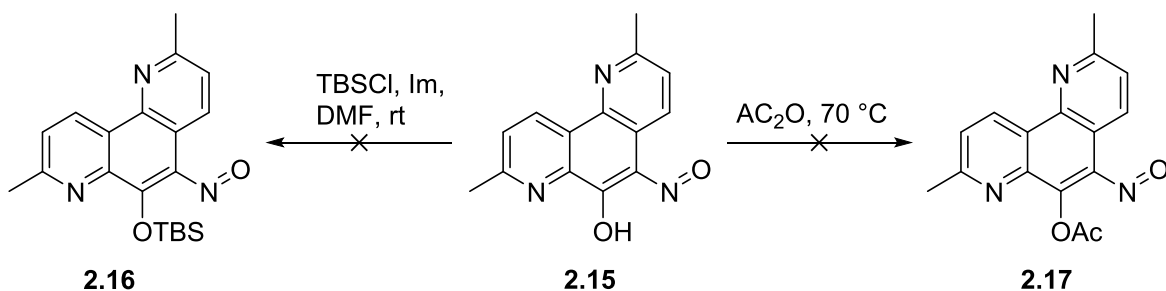
**Scheme 2.3.** Synthesis of aminohydroxyphenanthroline **2.9**.

For the transformation of nitroso **2.15** to the aniline **2.9**, the tin(II) chloride reduction procedure proved to be useful. Although, **2.9** demonstrated to be difficult to purify, as its good solubility in water and aqueous HCl did not allow the implementation of purification techniques based on the precipitation of the product. On top of this, extractive and column chromatography led to decomposition of the product.

At this point, it was decided to reevaluate the catalytic hydrogenation procedure for the obtention of **2.9**. As decomposition of **2.11** was observed when using ethanol, we explored the use of alternative aprotic polar solvents and found that the reaction could be carried out effectively in DMF at room temperature. Under these conditions, full consumption of the starting material to the desired product was observed within one hour, but the purification proved inconvenient as operations for the removal of the DMF complicated the isolation of product **2.9**. Exploration of more solvents for this reaction led to find that 1,4-dioxane was also effective to perform this hydrogenation, even though the process was substantially more inefficient than using DMF, as the reaction occurred more slowly showing only around 20% of conversion after one hour. This behavior is probably caused by the little solubility of **2.15** in dioxane. This observation prompted us to assess a cosolvent strategy, where it was found that the use of a 9:1 dioxane:DMF mixture as solvent improved the solubility of **2.15** and enabled efficient and effective standard hydrogenation conditions. This led to straightforward purification of **2.9** in 98% isolated yield.

With **2.9** in hand, we proceeded to try the amide coupling between this aromatic amine and (*S*)-2-hydroxypropanoic acid, the last step to achieve the total synthesis of **2.6**. Initial conditions that involved the use of HATU and three equivalents of Hünig's base in either DCE or DMF, caused the formation of a complex mixture from which formation of **2.6** and the diacylated amide ester by-product were identified.

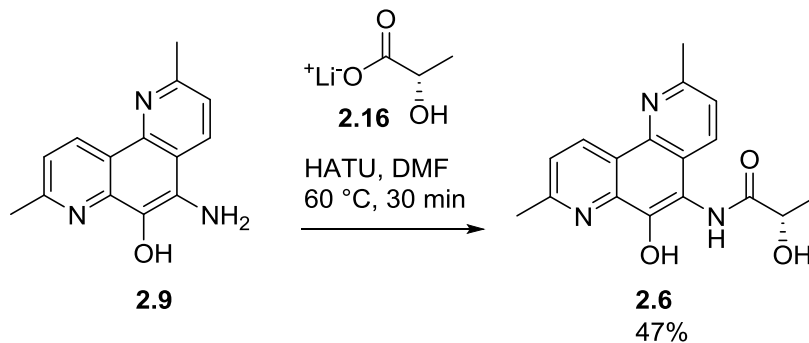
Considering the results from the amide coupling, it was decided to test the effect of protecting the phenol group, as this would avoid the diacylation observed with aminohydroxy **2.9**. For this experiment, we selected TBS and acetyl protecting groups and tried to introducing them in intermediate **2.15**, just before the formation of the aromatic amine. In this case, TBS protection under regular conditions proved difficult and this approach was discarded. Acetylation of the phenol in **2.15** proved also difficult, and formation of product was only achieved after heating at 70 °C in neat acetic anhydride for 18 hours. However, purification through silica gel caused the deprotection of **2.17** and only **2.15** was isolated.



**Scheme 2.4.** Efforts for the protection of the phenol in **2.15**.

At this stage, it was determined that the oxygen in **2.15** was poorly nucleophilic and not amenable for protection and it was decided to revisit the amide coupling methodology. As most intermediates in this route showed instability under basic conditions, the amount of Hünig base was decreased to just one equivalent, but the change did not translate to an improvement in the reaction. The procedure then was run without exogenous, organic amine base, and employed instead the lithium salt of L-lactic acid **2.16**. This approach was highly dependent on both solvent and temperature. The amide coupling in DCE led to no consumption of starting material, while mild heating at 60 °C caused only decomposition. Clean but slow formation of **2.5** was observed when the reaction was carried out in DMF at room temperature. In this case, heating the

reaction to 60 °C caused rapid formation of the desired product delivering Actinophenanthroline in moderate isolated yield (47%) (Scheme 2.5).



**Scheme 2.5.** Synthesis of Actinophenanthroline A **2.6**.

After synthetic actinophenanthroline A **2.6** was fully characterized, it was found that it displayed identical physical and spectroscopic properties with respect to the isolated compound. To unequivocally establish the structure of synthetic **2.6** and its stereochemistry, crystals of the compound were obtained and the X-Ray structure was determined in collaboration with Dr. Joel M. Harp from Vanderbilt's Center for Structural Biology. The crystal structure was identical to the reported by Fenical and collaborators,<sup>72</sup> and the (*S*)-configuration of C12 in our synthetic material was confirmed (Fig. 2.3).

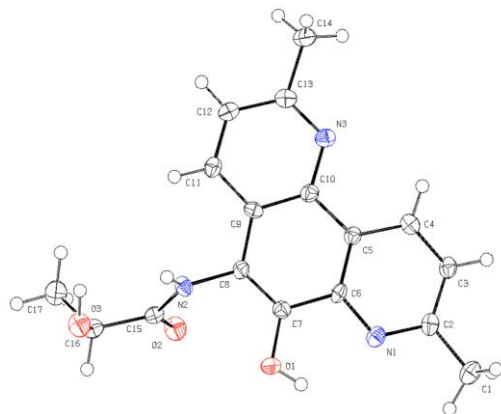


**Figure 2.3.** X-ray crystal structure of synthetic actinophenanthroline A (**2.6**).

## Summary and future directions

In this chapter, the first total synthesis of Actinophenanthroline A **2.6** was described. Overall, this approach presents a protecting group free six-step process that proceeds in 24.2% overall yield from inexpensive and commercial available starting material 8-hydroxyquinoline **2.12**. This procedure features two regioselective nitrosylation/reduction sequences and a Brønsted acid catalyzed Doebner-Miller reaction, and the use of no chromatographic purifications until the last step.

The availability of this synthetic natural product will allow exploring further its biological properties. As with Gombamide A, this material is in the process of being submitted to the CANVASS panel assay. In this assays, the compound will be tested for its anticancer, antibacterial and antiinflammatory activity.

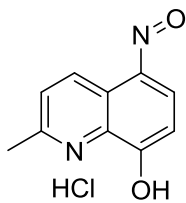
If the compound demonstrates to have interesting biological activity, our synthetic strategy provides a feasible route for the generation of analogs providing three points of diversity just by using different quinolines,  $\alpha,\beta$ -unsaturated aldehydes and different carboxylic acids. Hopefully, our synthetic route to access **2.5** will also facilitate the synthesis of the other actinophenanthrolines **2.7-2.8**.



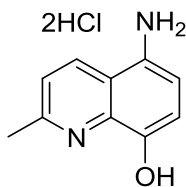
## EXPERIMENTAL METHODS

### *General*

All reagents and solvents were commercial grade and purified prior to use when necessary. Thin layer chromatography (TLC) was performed on glass-backed silica gel. Visualization was accomplished with UV light and/or the use of iodine or ninhydrin solution followed by charring on a hot-plate. Chromatography on silica gel was performed using Silica Gel 60 (230-400 mesh) from Sorbent Technologies.  $^1\text{H}$  and  $^{13}\text{C}$  NMR spectra were recorded on Bruker DRX-400 (400 MHz) instrument. Chemical shifts are reported in ppm relative to residual solvent peaks as an internal standard at the following chemical shifts ( $^1\text{H}$  and  $^{13}\text{C}$  respectively): 7.26 and 77.0 ppm for  $\text{CDCl}_3$ ; 2.50 and 39.52 ppm for  $\text{DMSO}-d_6$ , 3.31 and 49.2 ppm for  $\text{CD}_3\text{OD}$ . Data are reported as follows: chemical shift, multiplicity (s = singlet, d = doublet, t = triplet, q = quartet, dd = doublet of doublets, br = broad, m = multiplet), coupling constant (Hz), integration. Optical rotations were measured on a JASCO P-2000 digital polarimeter. Concentration in g/100 ml and solvent are given in parentheses and the reported value is an average of  $n=3$  independent measurements. Low resolution mass spectra (LCMS) were obtained on an Agilent 1200 LCMS with electrospray ionization. A Micromass Qtof API-US mass spectrometer was used to acquire high-resolution mass spectrometry (HRMS) data. The value  $\Delta$  is the error in the measurement (in ppm) given by the equation  $\Delta = [(ME - MT) / MT] \times 106$ , where  $ME$  is the experimental mass and  $MT$  is the theoretical mass. The HRMS results were obtained with ES as the ion source and leucine enkephalin as the reference.

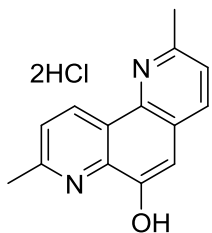


**2-methyl-5-nitrosoquinolin-8-ol hydrochloride (2.13).** In a flask, 8-hydroxyquinoline (10.00 g, 62.82 mmol) was dissolved in 60 mL of water. The mixture was cooled down to 0 °C in an ice bath, and 15 mL of concentrated HCl were added. Then, slowly and with stirring, sodium nitrite (4.33 g, 62.82 mmol) was added. The mixture was let warm to room temperature and stirred for 4 hours. A yellow solid was formed in the reaction and the mixture was filtered through a medium glass fritted funnel and triturated with cold water. 2-methyl-5-nitrosoquinolin-8-ol hydrochloride was obtained as a yellow solid (12.55 g, 55.90 mmol, 89% yield). <sup>1</sup>H NMR (400.1 MHz, DMSO-*d*<sub>6</sub>) δ (ppm): 8.73 (d, *J* = 8.3 Hz, 1H), 8.46 (br), 8.06 (d, *J* = 10.4 Hz, 1H), 7.85 (d, *J* = 8.4 Hz, 1H), 6.81 (d, *J* = 10.4 Hz, 1H), 2.73 (s, 3H); <sup>13</sup>C NMR (100.6 MHz, DMSO-*d*<sub>6</sub>) δ (ppm): 181.43, 159.68, 144.51, 140.94, 135.16, 131.38, 129.15, 129.07, 126.38, 22.86; HRMS (TOF, ES+) C<sub>10</sub>H<sub>8</sub>N<sub>2</sub>O<sub>2</sub> [M] calculated 188.0586, found 188.0583, Δ = -1.48 ppm.

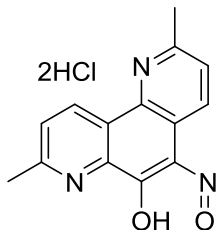


**5-amino-2-methylquinolin-8-ol dihydrochloride (2.11).** In a flask, **2.13** (8.26 g, 43.89 mmol) was added and suspended in 10 mL of concentrated HCl. Then, a solution of tin chloride (16.6 g, 87.79 mmol) in 10 mL of concentrated HCl was added while in an ice bath. The reaction was warmed to room temperature and stirred for 30 minutes, after full conversion was confirmed by LC-MS. The suspension was cooled to 0 °C again for 30 minutes to favor precipitation of the product, and the mixture was filtered through a medium glass fritted funnel and triturated with cold concentrated HCl. 5-amino-2-methylquinolin-8-ol dihydrochloride was obtained as a pale

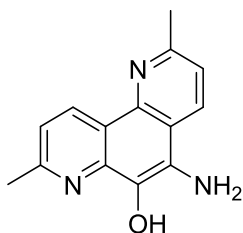
cream solid (10.65 g, 43.08 mmol, 98% yield).  $^1\text{H}$  NMR (400.1 MHz,  $\text{CD}_3\text{OD}$ )  $\delta$  (ppm): 9.05 (d,  $J= 8.9$  Hz, 1H), 8.17 (d,  $J= 8.9$  Hz, 1H), 7.85 (d,  $J= 8.4$  Hz, 1H), 7.53 (d,  $J= 8.4$  Hz, 1H), 3.16 (s, 3H);  $^{13}\text{C}$  NMR (100.6 MHz,  $\text{CD}_3\text{OD}$ )  $\delta$  (ppm): 158.96, 148.17, 139.66, 129.26, 125.28, 124.39, 122.43, 118.99, 115.12, 19.53; HRMS (TOF,ES+)  $\text{C}_{10}\text{H}_{10}\text{N}_2\text{O}_2$  [M] calculated 174.0793, found 174.0792,  $\Delta = -0.39$  ppm.



**2,8-dimethyl-1,7-phenanthroline-6-ol (2.10).** In a flask, **2.11** (10.35 g, 41.87 mmol) was dissolved in HCl 6 M (480 mL). The mixture was refluxed at 110 °C while a solution of *trans*-crotonaldehyde (4.16mL, 50.24 mmol) in 60 mL of toluene was slowly added with a syringe pump over 60 minutes. After refluxing for an additional hour, the reaction was stopped and cool down to 0 °C to favor precipitation of product. The reaction produced a crystalline brown solid, which was filtrated under vacuum through a medium glass fritted funnel and washed with DCM and cold water. 2,8-dimethyl-1,7-phenanthroline-6-ol dihydrochloride was obtained as brown crystals (11.26 g, 37.89 mmol, 90 % yield).  $^1\text{H}$  NMR (400.1 MHz,  $\text{DMSO}-d_6$ )  $\delta$  (ppm): 9.89 (d,  $J= 8.6$  Hz, 1H), 8.40 (d,  $J= 8.3$  Hz, 1H), 8.13 (d,  $J= 8.6$  Hz, 1H), 7.71 (s, 1H), 7.68 (d,  $J= 8.3$  Hz, 1H), 3.02 (s, 3H), 2.79 (s, 3H);  $^{13}\text{C}$  NMR (100.6 MHz,  $\text{DMSO}-d_6$ )  $\delta$  (ppm): 158.4, 157.2, 145.9, 140.7, 137.2, 136.7, 134.3, 125.9, 125.5, 125.2, 111.8, 24.6, 21.2; HRMS (TOF,ES+)  $\text{C}_{14}\text{H}_{12}\text{N}_2\text{O}$  [M] calculated 224.0950, found 224.0949,  $\Delta = -0.07$  ppm.

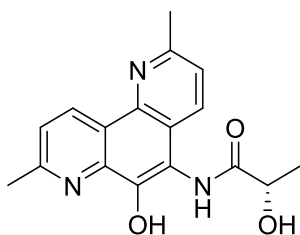


**2,8-dimethyl-5-nitroso-1,7-phenanthrolin-6-ol (2.15).** In a flask, **2.10** (9.49 g, 31.93 mmol) was dissolved in 20 mL of water and cool down to 0 °C with an ice bath. The mixture was cool down to 0 °C in an ice bath, and 6.7 mL of concentrated HCl were added. Then, slowly and with stirring, sodium nitrite (2.42 g, 35.13 mmol) was added. The reaction was allowed to warm to room temperature and stirred for 1 hour. The mixture was a suspension and the flask was cold in an ice bath to favor precipitation of product. The solid was filtered *in vacuo* through a medium glass fritted funnel, and washed with cold water. 2,8-dimethyl-5-nitroso-1,7-phenanthrolin-6-ol dihydrochloride was obtained as a yellow solid (6.94 g, 21.28 mmol, 67% yield). <sup>1</sup>H NMR (400.1 MHz, DMSO-*d*<sub>6</sub>) δ (ppm): 9.05 (d, *J* = 8.4 Hz, 1H), 9.00 (d, *J* = 8.2 Hz, 1H), 7.87 (d, *J* = 8.2 Hz, 1H), 7.41 (d, *J* = 8.4 Hz, 1H), 2.73 (s, 3H), 2.57 (s, 3H); <sup>13</sup>C NMR (100.6 MHz, DMSO-*d*<sub>6</sub>) δ (ppm): 178.3, 159.8, 159.7, 143.8, 143.4, 143.2, 137.8, 136.5, 132.1, 129.7, 124.0, 119.4, 24.3, 22.6; HRMS (TOF,ES+) C<sub>14</sub>H<sub>11</sub>N<sub>3</sub>O<sub>2</sub> [M] calculated 253.0851, found 253.0853, Δ = 0.57 ppm.



**5-amino-2,8-dimethyl-1,7-phenanthrolin-6-ol (2.9).** In a flask, **2.15** (1000 mg, 3.95 mmol) was added and suspended in 40 mL of a 1,4-Dioxane:DMF (9:1) mixture. Then, palladium (10%) on activated carbon (197 mg, 0.19 mmol) was added. The mixture was stirred at room temperature under 1 atm of H<sub>2</sub> for one hour. The reaction was worked up by filtration over a short Celite pad and washed DCM. Volatiles were evaporated *in vacuo*, and the remaining DMF was

eliminated through distillation under reduced pressure. 5-amino-2,8-dimethyl-1,7-phenanthroline-6-ol was obtained as a bright red solid (926 mg, 3.87 mmol, 98% yield). <sup>1</sup>H NMR (400.1 MHz, DMSO-*d*<sub>6</sub>) δ (ppm): 10.11 (br, 1H), 9.46 (d, *J*= 7.2 Hz, 1H), 8.70 (d, *J*= 7.8 Hz, 1H), 7.66 (d, *J*= 7.8 Hz, 1H), 7.48 (d, *J*= 7.1 Hz, 1H), 7.24 (br, 2H), 2.89 (s, 3H), 2.74 (s, 3H); <sup>13</sup>C NMR (100.6 MHz, DMSO-*d*<sub>6</sub>) δ (ppm): 158.4, 155.9, 139.8, 139.5, 138.0, 135.0, 131.5, 124.5, 123.8, 119.5, 117.7, 117.6, 25.1, 20.5; HRMS (TOF,ES+) C<sub>14</sub>H<sub>13</sub>N<sub>3</sub>O [M] calculated 239.1059, found 239.1059, Δ = 0.29 ppm.



**(S)-2-hydroxy-N-(6-hydroxy-2,8-dimethyl-1,7-phenanthroline-5-yl)propanamide**

**(Actinophenanthroline A, 2.6).** In a vial, **2.9** (40.0 mg, 0.170 mmol), HATU (63.6 mg, 0.170 mmol) and lithium (*S*)-2-hydroxypropanoate (16.1 mg, 0.170 mmol) were weighted and suspended in 2 mL of DMF. The mixture was stirred for 10 minutes at 60 °C. The reaction was worked up by addition of water and successive extractions with CHCl<sub>3</sub>:IPA (3:1). The organic phases were recovered and combined, washed with LiCl 5%, dried with MgSO<sub>4</sub>, filtered and concentrated *in vacuo*. The crude was dissolved in DMSO and purified by Gilson HPLC prep, C18 column, gradient 0.1% TFA in water:ACN, from 0 to 45% ACN. (*S*)-2-hydroxy-N-(6-hydroxy-2,8-dimethyl-1,7-phenanthroline-5-yl)propanamide was obtained as a pale yellow solid (24.6 mg, 0.0790 mmol, 47% yield). <sup>1</sup>H and <sup>13</sup>C-NMR (400 MHz, DMSO-*d*<sub>6</sub>), see Table S1. [α]<sub>D</sub><sup>25</sup>: -19.0 (c 0.5, MeOH); HRMS (TOF,ES+) C<sub>17</sub>H<sub>13</sub>N<sub>3</sub>O<sub>3</sub> [M] calculated 311.1270, found 311.1270, Δ = 0.11 ppm.

**Table 2.1.** NMR data comparison between isolated<sup>a</sup> and synthetic<sup>b</sup> Actinophenanthroline A (**2.6**).

Isolated		Synthetic	
$\delta_C$	$\delta_H$ (J in Hz)	$\delta_C$	$\delta_H$ (J in Hz)
174.6	9.50, br	174.6	9.56, br
158.8	ND	158.9	9.41, s
154.5	9.30, d (8.5)	154.8	9.30, d (8.3)
145.8	7.99, d (8.5)	145.2	8.00, d (8.3)
141.2	7.66, d (8.5)	140.8	7.67, d (8.3)
138.9	7.49, d (8.5)	139.1	7.50, d (8.4)
132.7	5.90, br	132.7	5.82, s
131.3	4.32, q (6.8)	131.4	4.33 (6.5)
123.2	2.79, s	123.2	2.79, s
123.1	2.71, s	123.1	2.71, s
122.8	1.44, q (6.8)	122.9	1.45 (6.7)
122.5		122.5	
114.2		114.3	
67.7		67.7	
24.6		24.60	
24.6		24.57	
21.3		21.3	

<sup>a</sup>500 MHz for <sup>1</sup>H-NMR and 75 for <sup>13</sup>C-NMR, from Nam, S-J.; Kauffman, C.A.; Jensen, P.R.; Moore, C.E.; Rheingold, A.L.; Fenical, W. *Org. Lett.* **2015**, *17*, 3240-3243. <sup>b</sup>400 MHz for <sup>1</sup>H-NMR and 100 for <sup>13</sup>C-NMR.

## Crystallographic Data of **2.6**

### Crystal Data

$C_{17}H_{17}N_3O_3$

$M = 311.34$

Monoclinic,  $P 2_1 2_1 2_1$

Hall symbol:  $P 2ac 2ab$

$a = 4.732 \text{ \AA}$

$b = 11.317 \text{ \AA}$

$c = 27.570 \text{ \AA}$

$V = 1476.4 \text{ \AA}^3$

$Z=4$

$F(000) = 656$

$D_x = 1.401 \text{ Mg M}^{-3}$

Cu  $K\alpha$  radiation,  $\lambda = 1.54178 \text{ \AA}$

Cell parameters from 10878 reflections

$\Theta = 3.2\text{-}66.59^\circ$

$\mu = 0.805 \text{ mm}^{-1}$

$T = 293 \text{ K}$

Needle

$0.19 \times 0.04 \times 0.01 \text{ mm}$

### Data Collection

Bruker X8 Proteum 135 diffractometer

Radiation source: Bruker Microstar rotating-anode

Monochromator: confocal, multilayer

17619 measured reflections

3641 independent reflections

3544 reflections with  $I > 2\sigma(I)$

$R_{\text{int}} = 0.086$

$\Theta_{\text{max}} = 133.17^\circ$ ,  $\Theta_{\text{min}} = 6.41^\circ$

$h = -5 \rightarrow 5$

$k = -12 \rightarrow 13$

$l = -31 \rightarrow 21$

### Refinement

Refinement on  $F^2$

Least-squares matrix: full

$R[F^2 > 2\sigma(F^2)] = 0.0494$

$wR(F^2) = 0.1201$

$S = 0.981$

2412 reflections

213 parameters	$(\Delta/\sigma)_{\max} = 0.001$
0 restraint	$\Delta\rho_{\max} = 0.15 \text{ e } \text{\AA}^{-3}$
Primary atom site location: structure-invariant direct methods	$\Delta\rho_{\min} = -0.27 \text{ e } \text{\AA}^{-3}$
Secondary atom site location: difference Fourier map	Absolute structure: Flack x determined using 528 quotients [(I+)-(I-)]/[(I+)+(I-)] (Parsons, Flack and Wagner, Acta Cryst. B69 (2013) 249-259).
Hydrogen site location: inferred from neighboring sites	
H atoms treated by a mixture of independent and constrained refinement	Flack parameter: -0.1 (4)
$w = 1/[\sigma^2(F_0^2) + (0.050P)^2 + 0.6517P]$ where	
$P = (F^2 + 2F^2_3) /$	

### Special Details

#### **Geometry.**

All esds (except the esd in the dihedral angle between two l.s. planes) are estimated using the full covariance matrix. The cell esds are taken into account individually in the estimation of esds in distances, angles and torsion angles; correlations between esds in cell parameters are only used when they are defined by crystal symmetry. An approximate (isotropic) treatment of cell esds is used for estimating esds involving l.s. planes.

#### **Refinement.**

Refinement of  $F^2$  against ALL reflections. The weighted R-factor wR and goodness of fit S are based on  $F^2$ , conventional R-factors R are based on F, with F set to zero for negative  $F^2$ . The threshold expression of  $F^2 > 2\text{sigma}(F^2)$  is used only for calculating R-factors(gt) etc. and is not

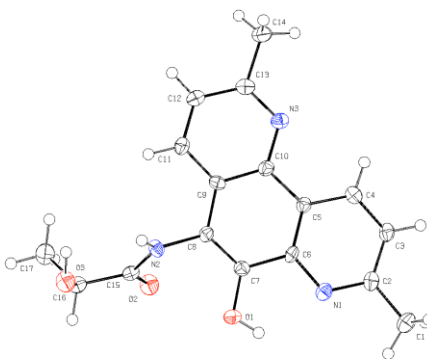


relevant to the choice of reflections for refinement. R-factors based on  $F^2$  are statistically about twice as large as those based on  $F$ , and R- factors based on ALL data will be even larger.

### Computing:

Data reduction and scaling were done using PROTEUM2 (Bruker,2010). Structure solution was done by direct methods using SIR2014 (Burla, et al., 2015). The structure was refined using SHELXL (Sheldrick, 2014) and visualized with COOT (Emsley, et al., 2010). The structure was examined and figures produced using PLATON (Spek, 2009).

**Table 2.2.** Atomic coordinates ( $\text{\AA} \times 10^5$ ) and equivalent isotropic displacement parameters ( $\text{\AA}^2 \times 10^4$ ).  $U(\text{eq})$  is defined as one third of the trace of the orthogonalized  $U_{ij}$  tensor. E.s.ds are in parentheses.



	x	y	z	U(eq)	S.o.f.#
O(3)	73630(60)	93000(30)	9049(12)	289(8)	1
O(2)	11260(60)	107580(30)	13172(11)	276(8)	1
O(1)	12240(70)	123680(30)	4056(11)	263(8)	1
N(1)	-6410(70)	145530(30)	4229(13)	210(9)	1
N(3)	54500(80)	154920(30)	17757(13)	212(9)	1
N(2)	52780(80)	115270(30)	10597(13)	201(9)	1
C(6)	13160(90)	142860(40)	7646(15)	180(10)	1

C(9)	54610(90)	135130(40)	14290(15)	181(10)	1
C(5)	23520(100)	150760(40)	11122(15)	177(9)	1
C(8)	43160(90)	127260(40)	10656(16)	188(10)	1
C(10)	44740(90)	146900(40)	14510(16)	191(10)	1
C(4)	12050(90)	162220(40)	10977(16)	205(10)	1
C(2)	-16790(90)	156530(40)	4173(16)	212(10)	1
C(7)	23320(100)	130930(40)	7490(15)	185(10)	1
C(11)	75360(100)	131760(40)	17623(16)	210(10)	1
C(3)	-7740(90)	165070(40)	7589(16)	211(11)	1
C(13)	74580(100)	151490(40)	20811(16)	220(10)	1
C(16)	48790(90)	93770(40)	11789(15)	207(10)	1
C(15)	36090(90)	106120(40)	11848(15)	193(10)	1
C(12)	85370(100)	139890(40)	20869(16)	224(10)	1
C(1)	-37980(100)	159340(40)	357(16)	273(11)	1
C(17)	52030(110)	89400(40)	16948(17)	317(12)	1
C(14)	86250(110)	160770(40)	24175(17)	298(12)	1

# - site occupancy, if different from 1

\* - U(iso) ( $\text{\AA}^2 \diamond 10^4$ )

**Table 2.3.** Anisotropic displacement parameters ( $\text{\AA}^2 \times 10^4$ ) for the expression:  $\exp -\pi^2 (h^2 a^{*2}U_{11} + \dots + 2hka^*b^*U_{12})$ . E.s.ds are in parentheses.

	$U_{11}$	$U_{22}$	$U_{33}$	$U_{23}$	$U_{13}$	$U_{12}$
O(3)	195(15)	286(18)	390(20)	-5(16)	39(17)	8(16)
O(2)	180(17)	277(17)	370(19)	4(15)	43(15)	3(15)
O(1)	272(19)	247(17)	271(18)	-68(15)	-103(15)	28(15)
N(1)	150(19)	250(20)	230(20)	6(17)	15(17)	35(17)
N(3)	214(19)	240(20)	180(20)	7(17)	0(17)	-31(18)
N(2)	146(18)	166(19)	290(20)	-28(16)	31(17)	18(16)
C(6)	140(20)	220(20)	180(20)	26(19)	-2(19)	60(20)
C(9)	180(20)	170(20)	190(20)	-11(19)	10(20)	-49(18)
C(5)	150(20)	180(20)	200(20)	12(19)	0(20)	6(18)
C(8)	120(20)	190(20)	260(20)	2(19)	-18(19)	25(18)
C(10)	150(20)	200(20)	220(20)	10(20)	-20(20)	-17(19)
C(4)	210(20)	200(20)	210(20)	-20(20)	50(20)	0(20)
C(2)	180(20)	220(20)	250(20)	50(20)	40(20)	20(20)
C(7)	160(20)	190(20)	210(30)	-10(19)	0(20)	-12(19)
C(11)	180(20)	220(20)	230(30)	20(20)	-10(20)	30(20)
C(3)	150(20)	210(20)	270(30)	20(20)	30(20)	40(20)
C(13)	190(20)	270(30)	200(20)	-30(20)	20(20)	-30(20)
C(16)	140(20)	260(20)	210(20)	0(20)	20(20)	-10(20)
C(15)	160(20)	230(20)	190(20)	0(20)	-20(20)	-10(20)
C(12)	200(20)	270(20)	200(20)	0(20)	-30(20)	-10(20)
C(1)	260(20)	340(30)	230(30)	50(20)	0(20)	30(20)
C(17)	340(30)	300(30)	310(30)	20(20)	10(20)	30(20)
C(14)	320(30)	300(30)	280(30)	0(20)	-100(20)	-50(20)

**Table 2.4.** Geometric parameters. Bond lengths are in Ångstroms, angles in degrees. E.s.d's are in parentheses.

O(3)–C(16)	1.400(5)	C(4)–H(4)	0.95
O(3)–H(3)	0.84	C(2)–C(3)	1.416(6)
O(2)–C(15)	1.241(5)	C(2)–C(1)	1.488(6)
O(1)–C(7)	1.358(5)	C(11)–C(12)	1.369(6)
O(1)–H(1)	0.84	C(11)–H(11)	0.95
N(1)–C(2)	1.338(5)	C(3)–H(3)	0.95
N(1)–C(6)	1.355(5)	C(13)–C(12)	1.409(6)
N(3)–C(13)	1.328(6)	C(13)–C(14)	1.506(6)
N(3)–C(10)	1.356(5)	C(16)–C(17)	1.514(6)
N(2)–C(15)	1.347(5)	C(16)–C(15)	1.521(6)
N(2)–C(8)	1.432(5)	C(16)–H(16)	1
N(2)–H(2)	0.88	C(12)–H(12)	0.95
C(6)–C(5)	1.400(6)	C(1)–H(1A)	0.98
C(6)–C(7)	1.434(6)	C(1)–H(1B)	0.98
C(9)–C(11)	1.398(6)	C(1)–H(1C)	0.98
C(9)–C(10)	1.413(6)	C(17)–H(17A)	0.98
C(9)–C(8)	1.445(6)	C(17)–H(17B)	0.98
C(5)–C(4)	1.407(6)	C(17)–H(17C)	0.98
C(5)–C(10)	1.439(6)	C(14)–H(14A)	0.98
C(8)–C(7)	1.347(6)	C(14)–H(14B)	0.98
C(4)–C(3)	1.362(6)	C(14)–H(14C)	0.98

C(16)–O(3)–H(3)	109.5	C(4)–C(3)–H(3)	119.9
C(7)–O(1)–H(1)	109.5	C(2)–C(3)–H(3)	119.9
C(2)–N(1)–C(6)	117.8(4)	N(3)–C(13)–C(12)	122.7(4)
C(13)–N(3)–C(10)	117.8(4)	N(3)–C(13)–C(14)	116.7(4)
C(15)–N(2)–C(8)	122.6(4)	C(12)–C(13)–C(14)	120.6(4)
C(15)–N(2)–H(2)	118.7	O(3)–C(16)–C(17)	113.7(4)
C(8)–N(2)–H(2)	118.7	O(3)–C(16)–C(15)	113.2(4)
N(1)–C(6)–C(5)	124.9(4)	C(17)–C(16)–C(15)	109.3(4)
N(1)–C(6)–C(7)	114.7(4)	O(3)–C(16)–H(16)	106.7
C(5)–C(6)–C(7)	120.3(4)	C(17)–C(16)–H(16)	106.7
C(11)–C(9)–C(10)	117.4(4)	C(15)–C(16)–H(16)	106.7
C(11)–C(9)–C(8)	123.5(4)	O(2)–C(15)–N(2)	121.9(4)
C(10)–C(9)–C(8)	119.1(4)	O(2)–C(15)–C(16)	119.9(4)
C(6)–C(5)–C(4)	115.8(4)	N(2)–C(15)–C(16)	118.2(4)
C(6)–C(5)–C(10)	119.7(4)	C(11)–C(12)–C(13)	119.6(4)
C(4)–C(5)–C(10)	124.6(4)	C(11)–C(12)–H(12)	120.2
C(7)–C(8)–N(2)	120.4(4)	C(13)–C(12)–H(12)	120.2
C(7)–C(8)–C(9)	121.4(4)	C(2)–C(1)–H(1A)	109.5
N(2)–C(8)–C(9)	118.2(4)	C(2)–C(1)–H(1B)	109.5
N(3)–C(10)–C(9)	123.2(4)	H(1A)–C(1)–H(1B)	109.5
N(3)–C(10)–C(5)	117.5(4)	C(2)–C(1)–H(1C)	109.5
C(9)–C(10)–C(5)	119.3(4)	H(1A)–C(1)–H(1C)	109.5
C(3)–C(4)–C(5)	120.2(4)	H(1B)–C(1)–H(1C)	109.5
C(3)–C(4)–H(4)	119.9	C(16)–C(17)–H(17A)	109.5
C(5)–C(4)–H(4)	119.9	C(16)–C(17)–H(17B)	109.5

N(1)–C(2)–C(3)	121.1(4)	H(17A)–C(17)–H(17B)	109.5
N(1)–C(2)–C(1)	117.0(4)	C(16)–C(17)–H(17C)	109.5
C(3)–C(2)–C(1)	121.9(4)	H(17A)–C(17)–H(17C)	109.5
C(8)–C(7)–O(1)	122.3(4)	H(17B)–C(17)–H(17C)	109.5
C(8)–C(7)–C(6)	120.3(4)	C(13)–C(14)–H(14A)	109.5
O(1)–C(7)–C(6)	117.4(4)	C(13)–C(14)–H(14B)	109.5
C(12)–C(11)–C(9)	119.3(4)	H(14A)–C(14)–H(14B)	109.5
C(12)–C(11)–H(11)	120.3	C(13)–C(14)–H(14C)	109.5
C(9)–C(11)–H(11)	120.3	H(14A)–C(14)–H(14C)	109.5
C(4)–C(3)–C(2)	120.2(4)	H(14B)–C(14)–H(14C)	109.5

## CHAPTER III

### METABOTROPIC GLUTAMATE RECEPTOR SUBTYPE 1 ACTIVATION AND OPTIMIZATION EFFORTS AROUND THE RO 07-11401 SCAFFOLD

#### **Metabotropic glutamate receptor subtype 1**

##### *Glutamate in the nervous system*

Glutamate ((*S*)-2-aminopentanedioic acid) is a non-essential amino acid that plays an important role as an excitatory neurotransmitter in the nervous system. Its excitatory action was recognized in the brain and spinal cord of mammals back to the 1950s,<sup>97,98</sup> and it accounts for approximately 70% of synaptic transmission in the central nervous system (CNS).<sup>99</sup> Glutamate has been involved in several cognitive functions, such as learning and memory, and dysregulation in its release, uptake, metabolism and signaling are associated with neuropsychiatric disorders.<sup>100</sup>

Glutamate is stored in vesicles in presynaptic terminals and its release occurs via a calcium mediated process that requires the activation of N- and P/Q-type voltage-dependent calcium channels.<sup>101</sup> Also, the cystine-glutamate antiporter, mainly expressed in glial cells, acts as a non-vesicular source of glutamate as it exchanges intracellular glutamate for extracellular cystine.<sup>99,100</sup>

Brain intracellular concentration of glutamate is approximately 10 mM, and can be up to 500000 times higher in comparison to the basal concentration in the synaptic cleft, which is approximately 20 nM. However, following an action potential the concentration in the synaptic space can exceed 1 mM.<sup>102,103</sup> Therefore, the concentration of glutamate in the synapse needs to be tightly regulated.

There are different transporters in charge of maintaining homeostasis of glutamate levels. After release of glutamate in the synapse, the high-affinity excitatory amino acid transporters

(EAATs) are in charge of its reuptake and are located on glutamatergic terminals and glial cells. EAATs are sodium dependent and have five isoforms (EAAT1-5) in humans. The storage of glutamate in these vesicles is carried on by the vesicular glutamate transporters (VGLUTs), for which three different isoforms have been reported (VGLUT1-3).<sup>99,104</sup> These transporters are selective for glutamate and driven by a proton gradient.<sup>101</sup>

Once released into the synaptic cleft, glutamate exerts its actions through ionic and metabotropic receptors. The ionotropic glutamate receptors (iGluRs) mediate fast postsynaptic potentials and are divided in three types, named by the ligand that prompted its discovery: amino-3-hydroxy-5-methyl-4-isoxazolepropionate (AMPA), *N*-methyl-D-aspartate (NMDA), and kainite receptors. AMPA receptors are tetramers formed by GluR (Glu1-4) subunits. These receptors have lower affinity for glutamate than the NMDA receptors but faster kinetics, and they mediate the fast initial component of the excitatory postsynaptic potentials (EPSP). NMDA receptors are tetramers composed by NR1, NR2 (NR2A-D) and NR3 subunits and their activation requires removal of magnesium, facilitated by partial membrane depolarization as well as binding of glutamate and glycine.<sup>99,101,105</sup>

The metabotropic glutamate receptors (mGlu) are G protein-coupled receptors that mediate slower neurotransmission, allowing modulation of synaptic activity and intracellular metabolic processes via second messenger signaling cascades.<sup>106,107</sup> There are eight different mGlu that have been classified in three groups based on their signaling transduction pathway, sequence homology and pharmacological selectivity. Group I is composed by mGlu<sub>1</sub> and mGlu<sub>5</sub>, group II consist of mGlu<sub>2</sub> and mGlu<sub>3</sub>, while Group III entails mGlu<sub>4</sub>, mGlu<sub>6</sub>, mGlu<sub>7</sub> and mGlu<sub>8</sub>. Group I receptors are mainly localized postsynaptically and are usually coupled too G<sub>q/11</sub>, while groups II and III are generally present in presynaptic glutamate terminals and glial cells and coupled to G<sub>i/o</sub>, serving as feedback and decreasing glutamate release in the synapse (Fig. 3.1).<sup>99</sup>



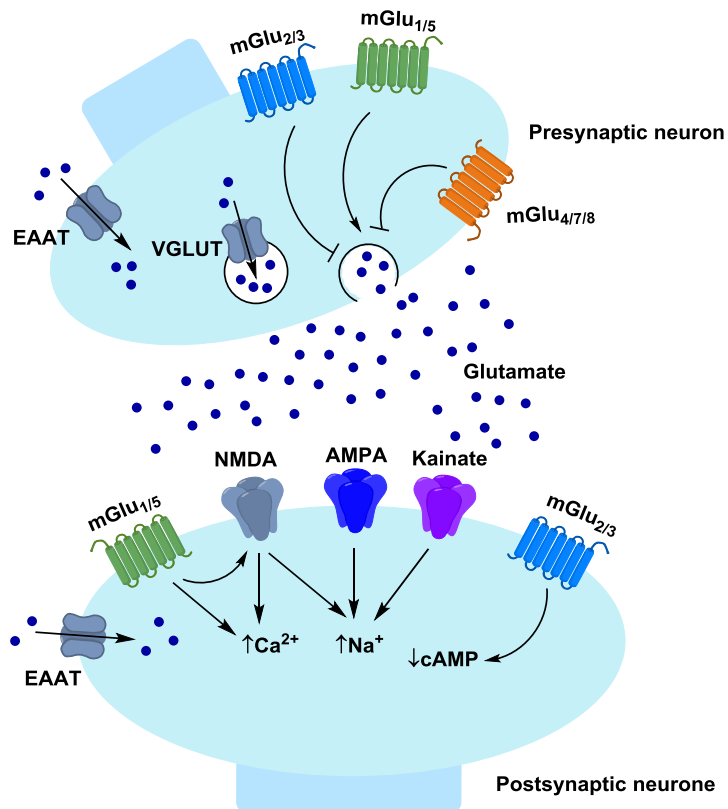


**Figure 3.1.** The glutamatergic synapse. mGlu are depicted as monomers for simplicity, but they are functional dimers in the neurone.<sup>108</sup>

### *Structural features of the metabotropic glutamate receptor subtype 1*

The mGlu<sub>1</sub> receptor is part of the class C family of GPCRs. The receptor has an intracellular C-terminus, a transmembrane-spanning domain (TMD) and a distinctive large extracellular N-terminal domain (Fig. 3.2).<sup>109</sup> This extracellular domain is known as the Venus Flytrap Domain (VFD) which has two lobes disposed in a clam shell-like structure. The glutamate binding site is located in the center of this domain. Dimerization of VFD from two different mGlu<sub>1</sub> is required for activation of the receptor.<sup>110,111</sup> The closure of the VFD lobes is directly related to the binding of glutamate and it causes significant conformational changes that translate to the rest of the protein. These conformational changes are propagated from the VFD to the TMD, through a cysteine rich-domain (CRD). The CRD contains nine cysteine residues, eight forming disulfide bonds within the domain while the remaining ninth cysteine (Cys518) is

involved in a disulfide bond with Cys234 in one of the lobes of the VFD. These interactions occur after agonist binding in the receptor's VFD and disruptive mutations cause a cease in intracellular signaling events that has no effect in expression, dimerization or recognition of orthosteric ligands.<sup>107,108</sup> Recently, the X-ray crystallography determination of the structure of the TMD in complex with the negative allosteric modulator FITM was accomplished.<sup>112</sup> The TMD is composed by seven  $\alpha$ -helices connected by intra- and extracellular flexible loops. Interactions between TM6 and TM7 hold the receptor in an inactive state and a change in the conformation of these motifs is essential for activation of the receptor after agonist binding. The TMD is the place where most allosteric modulators (positive and negative) bind to the receptor.<sup>107</sup> Finally, the intracellular C-terminus is a region where multiple protein-protein interactions occur. This area is subject to phosphorylation and it modulates G-protein coupling and the expression in the cell surface as well as the interaction with scaffolding proteins (Homer, tubulin).<sup>113,114</sup> The alternative splicing variants of the mGlu<sub>1</sub> receptor are differentiated mainly, by changes in the C-terminal region.<sup>115,116</sup>

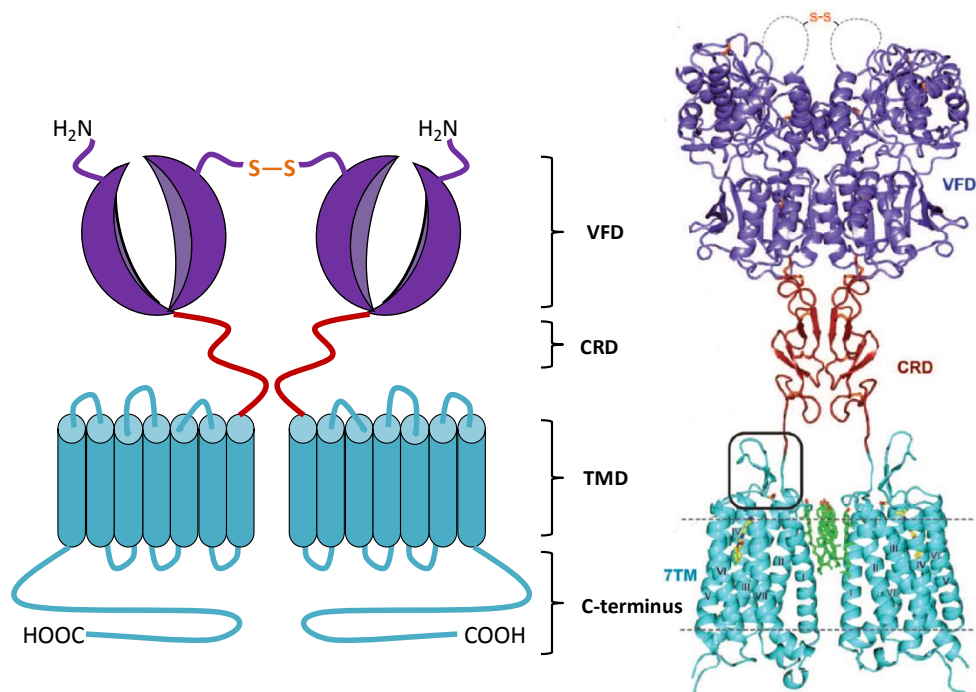


**Figure 3.2.** Diagram and 3-D model based on X-Ray crystal structures of the mGlu<sub>1</sub> receptor.<sup>112</sup>

### *Signaling of the metabotropic glutamate receptor subtype 1*

The mGlu<sub>1</sub> receptor is predominantly coupled to G<sub>αq/11</sub> causing the activation of phospholipase C<sub>β</sub> (PLC<sub>β</sub>), leading to the hydrolysis of phosphatidylinositol bisphosphate (PIP<sub>2</sub>). The reaction produces 1,4,5-trisphosphate (IP<sub>3</sub>) and diacylglycerol (DAG), important second messengers that together can activate protein kinase C (PKC) and trigger the calcium release from the endoplasmic reticuli.<sup>108</sup> Potential for alternative or additional coupling to other G proteins (e.g. G<sub>i/o</sub>) has also been reported.<sup>117</sup> This phenomena varies substantially depending on the neuronal population or cell line background, and while in the beginning it was believed to be caused by overexpression of the receptor in *in vitro* systems, later studies have shown that it can be of physiological relevance.<sup>109</sup> Additionally, the mGlu<sub>1</sub> receptor has shown to promote arachidonate formation through several paths, including: activation of phospholipase A<sub>2</sub>, stimulation of conductance of L-type voltage operated calcium channel (VOCC) (independently of PLC activation), phospholipase D (PLD) activation in a PKC-dependent way, recruitment of beta-arrestin,<sup>118</sup> activation of c-Jun N-terminal kinase (JNK) and mitogen-activated protein kinase/extracellular receptor kinase (MAPK/ERK) cascades, and the mammalian target of rapamycin pathway (mTOR).<sup>119,120</sup> The fact that these different signal transduction pathways may converge synergistically and antagonizing each other, to modulate the biological effects of the receptor, provides fine tuning to the observed overall cellular response and also increases the complexity of the analysis of the consequences of receptor activation.

### *Normal distribution of the mGlu<sub>1</sub> receptor in the brain*

The mGlu<sub>1</sub> receptor is expressed in different regions of the brain. Studies with rats through immunocytochemical and radioligand autoradiography approaches have shown that it is specially enriched in the olfactory bulb, stratum oriens/alveus areas of CA1 and polymorph layer of dentate gyrus in hippocampus, globus pallidus in the basal ganglia, thalamus, substantia nigra pars reticulata, superior colliculus and cerebellum. Lower levels were observed in the neocortex,

striatum, amygdala, hypothalamus, medulla, and principal cells of cerebral cortex and hippocampus.<sup>121,122</sup> The distribution in human brain of mGlu<sub>1</sub> mRNA is similar to the rat, where the highest levels are observed in the cerebellum followed by the cerebral cortex, thalamus, subthalamic nucleus and amygdala, and lower levels are detected in the hippocampus, substantia nigra, caudate nucleus and putamen.<sup>123</sup>

Dendrites, spines and neuronal cell bodies contain mGlu<sub>1</sub>. Ultrastructure studies in rat hippocampus and cerebellum showed higher density in postsynaptic membranes, with some densities in perisynaptic and extrasynaptic membranes.<sup>124</sup> On dendritic spines, the receptor is highly compartmentalized in plasma membrane domains, showing the highest density in the perisynaptic annulus (50%, 60 nm of the edge of the synapse), followed by a decrease extrasynaptically (60-900 nM).<sup>125</sup> Also, there is substantial cytoplasmic immunostaining associated with organelles, especially the endoplasmic reticulum.<sup>126</sup>

*In situ* hybridization of messenger RNA (mRNA) has detected intense mGlu<sub>1</sub> labeling in Purkinje cells of the cerebellum, mitral and tufted cells of the olfactory bulb, hippocampus, lateral septum, thalamus, globus pallidus, substantia nigra, dorsal cochlear nucleus; while moderate labeled neurons were detected in the dentate gyrus, striatum, islands of Calleja, superficial layers of the retrosplenial, cingulate and entorhinal cortices, mammillary nuclei, red nucleus, and superior colliculus.<sup>127</sup>

There is redistribution and reorganization of mGlu<sub>1</sub> with age. Expression of the mGlu<sub>1</sub> receptor gradually increases in early post-natal days, in accordance with maturation of neuronal elements. Studies in rat pups showed that mGlu<sub>1</sub> mRNA increases during the first few weeks and does not decrease up to the 5<sup>th</sup> postnatal week. On day 3, little mRNA is observed and is confined in the pyramidal cell layer of CA1-3 in the hippocampus, granular cell layers of the dentate gyrus, Purkinje cells and in the olfactory bulb region.<sup>128</sup> Additionally, mGlu<sub>1</sub> is present in thalamus since the first day after the rat's birth, but it can only be activated by corticothalamic stimulation after the second postnatal week. During the first postnatal week, mGlu<sub>1</sub> is mainly found in proximal

dendrites and somata and not usually associated with synaptic contacts. On the second postnatal week, the receptor is found in distal dendrites but remains mainly confined to somata and proximal dendrites, more synapses are observed but they are still immature with presynaptic terminal of irregular shape and containing few vesicles. By week four, the terminals contained more vesicles, and they are preferentially associated with corticothalamic synapses. In postnatal week seven, the synapses are prominent with mGlu<sub>1</sub> immunoreactivity concentrated in postsynaptic densities of asymmetric synapses or in perisynaptic areas. At 21 weeks after birth, the receptor is localized only in small distal dendrites and specifically concentrated at postsynaptic densities of corticothalamic type synapses.<sup>129,130</sup>

During rat adulthood, mGlu<sub>1</sub> mRNA and protein expression increases in the thalamic nuclei, caudate-putamen and hippocampal CA1 and CA3; a slight increase is observed in cerebral cortex and striatum, while a slight decrease occurs in Purkinje cells and cerebellum.<sup>131</sup>

### **Role of the mGlu<sub>1</sub> receptor in brain function and psychiatric conditions**

#### *Role of the mGlu<sub>1</sub> receptor in memory and learning*

The hippocampus plays a key role in relational, contextual, spatial or declarative learning and memory. The hippocampus is one of the main brain regions related to cognitive processes, and is especially involved with distinct types of learning. In the hippocampus, mGlu<sub>1</sub> is mainly expressed in the dentate gyrus and CA3, and is weaker in the CA1 region, being located in the perisynaptic area and in dendrites and dendritic spines.<sup>132-134</sup>

Memory and learning are dependent on synaptic plasticity, defined as the change of intensity in synapse output with time. These changes can occur in tens of milliseconds (short-term) to a few minutes (long-term). Hippocampal long-term potentiation (LTP) has been associated as a mechanism involved in learning and memory. NMDA activation and calcium influx are necessary but not sufficient for LTP in the CA1 region. The effect of mGlu<sub>1</sub> in these

processes has been studied in the hippocampus and it has been observed that direct excitatory effect of CA1 pyramidal cells is mediated through group I mGlu receptors.<sup>135</sup> DHPG, a non-selective mGlu<sub>1</sub>/mGlu<sub>5</sub> agonist evoked a transient increase in intracellular calcium levels with relatively long lasting inward current in CA1 pyramidal neurons, which were enhanced by depolarization.<sup>136</sup>

Although expressed at lower levels than mGlu<sub>5</sub>, mGlu<sub>1</sub> receptors are also involved in certain functions within the CA1 regions of hippocampus.<sup>137</sup> Experiments showed that mGlu<sub>1</sub> was not required to maintain the normal gross anatomy of the hippocampus, as well as to generate short-term potentiation and LTD on CA1 pyramidal cells; however, absence of the *GRM1* gene in mice diminishes considerably the magnitude of LTP and causes moderate impairment in the acquisition of memory in a context-dependent fear conditioning task (context specific associative learning).<sup>138,139</sup> LTP in Schaffer collateral-CA1 synapses requires inhibition of SK channels by mGlu<sub>1</sub>, which removes a negative feedback loop that constitutively regulates NMDAR. Rather than being controlled simply by the magnitude of the postsynaptic calcium rise, LTP induction requires activation of distinct sources of calcium and mGlu<sub>1</sub> dependent facilitation.<sup>140</sup> Additionally, mGlu<sub>1</sub> antagonists impaired both induction and late phases of LTP and LTD in the CA1 region of the hippocampus of adult male rats when applied before high-frequency tetanization or low frequency stimulation, but no effect if applied after. These effects were reduced with a protein synthesis inhibitor.<sup>141</sup>

The hippocampal CA1 inhibitory interneurons control the excitability of pyramidal cells and hippocampal plasticity. LTP of excitatory postsynaptic currents (EPSC) in stratum oriens/alveus (O/A) interneurons is induced after pairing theta burst stimulation with postsynaptic depolarization. This LTP is significantly reduced in mGlu<sub>1</sub> knock-out mice, is blocked by mGlu<sub>1/5</sub> antagonists and is independent of NMDAR activation.<sup>142,143</sup> mGlu<sub>1</sub> activation elicits dendritic calcium signals in CA1 hippocampus and in O/A interneurons, resulting from calcium influx via transient receptor potential (TRP) channels and calcium release from intracellular stores, and

ERK1/2 activation; these biochemical features play an important role to control LTP at interneuron synapses.<sup>144</sup>

DHPG enhances NMDA, AMPA and kainate responses in CA1 pyramidal neurons; although, a brief perfusion of DHPG can induce a robust LTD in this area, along with an enhancement in the paired-pulse facilitation ratio. DHPG facilitates postsynaptic responses but also suppress synaptic transmission, and the observed net effect is a reduction of the response. DHPG also reduces calcium-dependent responses in CA3 pyramidal neurons (presynaptic to CA1).<sup>145,146</sup> Blockade of both mGlu<sub>1</sub> and mGlu<sub>5</sub> is required to block induction of LTD by DHPG, and the inhibition of mGlu<sub>1</sub>, but not mGlu<sub>5</sub>, reduces expression of LTD and the associated decrease in AMPA expression in cell surface; this is observed as well with the deletion of the *GRM1* gene.<sup>147</sup> This form of synaptic plasticity has been observed in both young and adult rats in the CA1 region, and is facilitated by corticosterone during periods of acute stress.<sup>148,149</sup>

In the dentate gyrus of the wild-type mice, stimulation of the medial perforant path produced paired-pulse depression of inter-pulse intervals (IPIs) up to 30 ms. The mGlu<sub>1</sub> knock-out mice, showed significantly longer IPI depression, up to 50 ms. Paired-pulse depression results from the activation of inhibitory interneurons and it is facilitated by GABA<sub>B</sub> agonists. Mice lacking mGlu<sub>1</sub> have reduced LTP in dentate gyrus compared to wild-type, and these effects have been confirmed with the mGlu<sub>1</sub> antagonist LY367385 *ex vivo* and *in vivo*. This effect is mediated via an inhibitory feedback loop onto the granule cells.<sup>137,150,151</sup>

Also in the dentate gyrus, LTD induced by low frequency stimulation of the medial perforant path was prevented by mGlu<sub>1</sub> antagonism, while DHPG induced LTD was blocked by both antagonism of mGlu<sub>1</sub> and mGlu<sub>5</sub>, and was impaired by NMDA antagonism.<sup>152</sup> Acute and long-term effects of DHPG are restricted to a subset of GABA afferents that are sensitive to depolarization-induced suppression of inhibition (DSI), an effect that depends on activation of CB<sub>1</sub>. Here, antagonist work suggested the effect is mGlu<sub>1</sub> dependent.<sup>153</sup>

Coactivation of NMDA and group I mGlu is required for learning. The coapplication of an mGlu<sub>1</sub> antagonist and an NMDA antagonist blocked acquisition of passive avoidance (PA) during the acquisition phase. These antagonists were not effective in acquisition during the Fear-Potentiated Startle (FPS) Paradigm. The mGlu<sub>1</sub> knock-out mice exhibited reduced LTP and impaired context-specific learning, but it shows no change in cue-dependent fear conditioning. Contextual learning depends both in hippocampus and amygdala, while cue-dependent is a hippocampus-independent process.<sup>154,155</sup> It has also been observed that an mGlu<sub>1</sub> antagonist did not affect the behavior in the passive avoidance test when administered post-training.<sup>156,157</sup> Moreover, infusion of DHPG in the amygdala (BLA) prior to fear conditioning, enhances freezing memory.<sup>158</sup>

In classical eye blink conditioning, a test of associative learning where hippocampal circuits are involved in trace conditioning acquisition and consolidation, it was confirmed the role of mGlu<sub>1</sub> as the acquisition to evoke eyelid responses was impaired in the mGlu<sub>1</sub><sup>+/-</sup> mice and abolished in the mGlu<sub>1</sub><sup>-/-</sup> animal, when using conditioned or unconditioned stimulus. This acquisition correlates with potentiation of synaptic transmission in the hippocampal circuit, reflected by an increase in the slope of fEPSP at the CA3-CA1 synapse.<sup>159</sup> In a single-trial passive discrimination avoidance task in young chicks, blockade of mGlu<sub>1</sub> and IP<sub>3</sub> receptors impaired retention 90 minutes post-training; disturbing memory consolidation and reconsolidation, but not memory recall. In this model, intracellular calcium release and protein synthesis was required for the formation of long-term memory.<sup>160,161</sup>

The mGlu<sub>1</sub> deficient mice have also impaired ability to learn spatial tasks. In the eight-arm radial maze, LY367385 (a selective mGlu<sub>1</sub> antagonists) induced deficits in reference but not working-memory, while leaving rearing, grooming and locomotor activity unaffected.<sup>151</sup> In a mouse water maze study, the mGlu<sub>1</sub> antagonist BAY 36-720 increased the escape latency and impaired the water escape task acquisition during the first 4 days.<sup>162</sup> In rats that showed increase learned capacity, the effect of group I mGlu agonist DHPG was dependent on the time of



administration of the treatment; pre-training injection caused impaired acquisition in a water maze task or amnesia of spatial alternation, whereas post-training injection of the same drug enhanced retention of memory.<sup>163</sup>

In a spatial three-choice reward-finding test, bilateral prelimbic injections of an mGlu<sub>1</sub> antagonist before training sessions blocked the acquisition of correct performance behavior, while after full training it impaired correct performance without causing a complete block in the learning of the task; the antagonist also prevented normal adaptation of spontaneous exploration in the open-field test.<sup>164</sup>

However, studies using an appetitive/positively reinforced tasks protocol (delayed non-matching to position, DNMT; differential reinforcement of low rates of responding 18 s, DRL 18-s) showed that mGlu<sub>1</sub> blockade improved working memory and reduced impulsive choices at the doses that have no effect on time perception but appear to facilitate impulsive action. These results highlights the intricacies of the role of mGlu<sub>1</sub> in memory and learning.<sup>165,166</sup>

Additionally, a genetic study of an Azeri population looking to identify candidate genes for autosomal recessive intellectual disorder (ARID), identified a rare missense variant in the *GRM1* gene. The mutation was located in the Venus fly-trap domain in a residue conserved (Leu454Phe) in the throughout the animal kingdom and it was predicted to be damaging for the function of the receptor. In the affected individuals, the mutation was homozygous and they presented moderate to severe intellectual disability, delayed developmental milestones and derangement of speech, ataxia, frequent convulsions, aggressive behavior, and increased number of cerebellar cisterns and cerebellar atrophy were observed during brain MRI.<sup>167</sup>

#### *Role of the mGlu<sub>1</sub> receptor in the motor activity*

Through different genetic studies, it has been observed that mGlu<sub>1</sub> has a prominent role in maintaining normal motor behavior. The mGlu<sub>1</sub> knock-out mice can be identified by having ataxia as soon as 2 weeks after birth and complete loss of righting reflex as adults.<sup>168</sup> Besides,

although these animals can still sit, upon initiation of movement, they exhibit tremors of significant amplitude that persists for the duration of the movement. These changes altered significantly the performance of the animal in the open field-test and rota-rod experiments.<sup>169</sup> Also, these animals showed severe spatial learning deficits in the hidden-platform task in the Morris test.<sup>168</sup> The introduction of the *GRM1* gene back in the animals demonstrated to rescue this motor phenotype.<sup>170</sup>

Conditional mGlu<sub>1</sub> knockout mice can reach adulthood with a normal phenotype, but selective blockade of mGlu<sub>1</sub> expression in Purkinje cells causes impaired motor coordination, suggesting that mGlu<sub>1</sub> is not only essential during development but also for maintaining cerebellar function during adulthood.<sup>171</sup>

It is estimated that these characteristics have their origin in the deficient development and function of the cerebellum, but changes in the anatomy of this brain structure anatomy are not evident.<sup>137,172</sup> Pharmacological studies with antagonists (LY367385 and CPCCOEt) showed that both group I mGlu are required for differentiation and survival of cerebellar Purkinje cells.<sup>173</sup> In knock-out mice, excitatory transmission in the parallel fiber-Purkinje cells and climbing fiber-Purkinje cells appears functional, but this does not extend to synaptic plasticity.<sup>172</sup> So, while short-term plasticity presents no change, activation of mGlu<sub>1</sub> is necessary to induce long-term depression in the parallel fiber-Purkinje cells synapse, an important structure for motor learning.<sup>131</sup> These synaptic deficits are also reversed by reintroduction of the *GRM1* gene.<sup>170</sup> This type of long-term depression has demonstrated to be important for producing conditioned eye blink reflex and relies in the functional integrity of the cerebellar motor circuitry.<sup>172,174</sup>

These deficits have also been observed in other animal models, such as the *crv4* mice, that carries an autosomal recessive mutation, *cervelet-4*, in the context of the BALB/c strain. The homozygous mutant mice display reduced body size, along with ataxic gait and intention tremor.<sup>175</sup> This effects are also describe in different mammal species and have been characterized

in Coton de Tulear dogs that present Bandera's neonatal ataxia (BNAt), a disease caused by a retrotransposon inserted into exon 8 of *GRM1*.<sup>176</sup>

Spinocerebellar ataxia type 1 mice have lower mGlu<sub>1</sub> mRNA and protein levels in the cerebellum. These mice also show high expression of mGlu<sub>5</sub> in cerebellar Purkinje cells, which normally present low density of these receptors. Pharmacological studies showed that Ro 07-11401, a mGlu<sub>1</sub> positive allosteric modulator, improved the motor performance of these animals, while further impairment was observed after dosing JNJ16259685, an mGlu<sub>1</sub> antagonist. The improvement with Ro 07-11401 was prolonged and was associated to neuroadaptive changes in the cerebellum, such as reduction in mGlu<sub>5</sub> expression and changes in the length of spines in distal dendrites of Purkinje cells.<sup>177,178</sup>

In humans, the reduction of mGlu<sub>1</sub> in cerebellum with age can be associated with age-dependent decrease in motor learning and coordination.<sup>131</sup> Also, patients with Hodgkin's lymphoma have presented paraneoplastic ataxia due to the production of mGlu<sub>1</sub> antibodies.<sup>131,179</sup> Although more uncommon, this finding has been extended to individuals with subacute cerebellar ataxia but with no tumor precedent.<sup>180</sup>

Mutations in the *GRM1* have transduced into a form of autosomal-recessive congenital cerebellar ataxia in Roma patients. These subjects also presented global developmental delay, stance and gait ataxia, dysarthria, dysdiadochokinesia, dysmetria and tremors, intellectual deficit, and mild pyramidal signs; and a subset of them showed progressive cerebellar atrophy through brain imaging analysis.<sup>181</sup>

Finally, in cerebellum samples of mice with autoimmune-induced encephalomyelitis and multiple sclerosis patients, progressive loss of mGlu<sub>1</sub> was found in Purkinje cells, along with increase mGlu<sub>5</sub>. Treatment of these animals with Ro 07-11401 demonstrated to improve motor coordination.<sup>174,182</sup>

### *Role of the mGlu<sub>1</sub> receptor in anxiety*

The findings that point to a function of mGlu<sub>1</sub> in anxiety are less straightforward. Although the mGlu<sub>1</sub> knock-out mice appear more agitated and prone to stress, there are conflicting studies that show that mGlu<sub>1</sub> antagonist can be anxiolytic.<sup>137</sup> The mGlu<sub>1</sub> antagonist AIDA had anxiolytic activity in the conflict drinking test and the elevated plus maze in rats without affecting motor coordination.<sup>183</sup> The negative allosteric modulator JNJ16259685 increased the number of licks but no anxiolytic effects were observed in the elevated plus maze.<sup>184</sup> EMQMCM results for anxiolytic activity are mixed as it could inhibit fear-potentiated startle, but it had no effects on the Geller-Seifter conflict test, and mixed effects in elevated plus maze test.<sup>185,186</sup>

A study showed that in DBA/2 mice, which display a high anxiety phenotype, amygdala neurons express asynchronous activity with diverse excitability, and weak transmission in GABAergic synapses compared to low anxiety FVB/N mice. mGlu<sub>1/5</sub> activation with DHPG improved anxiety-like behaviors in the DBA/2 mice, synchronized the activity of amygdala neurons and strengthened the GABAergic synapses.<sup>187</sup> These results demonstrate how the outcome of mGlu<sub>1</sub> activation can vary depending on the initial condition of the individual.

Also, in experiments where social isolation stress is produced to induce anxious-depressive like behavior, a decrease expression of mGlu<sub>1</sub> in the prefrontal cortex was observed; however, this study did not elucidate if this finding could be a driver of the observed behavior or a compensatory mechanism.<sup>188</sup>

### *Role of the mGlu<sub>1</sub> receptor in the hyperexcitability and seizures*

Group I mGlu receptors have been involved in neuron hyperexcitability and the induction of seizures. The application of DHPG in the CA3 region of the hippocampus transforms normal neuronal activity into prolonged epileptiform discharges (interictal discharges and longer synchronous seizure-like), an effect that persists after removal of the agonist.<sup>189</sup> Group I agonists

induce seizure discharges *in vivo* and cause prolonged ictal-like activity in brain slices in a mechanism believed to be related to PLC $\beta$  and ERK1/2 activation.<sup>190</sup> So, it has been stated that mGlu<sub>1</sub> contributes to long-lasting plastic changes associated with seizure activity.<sup>191</sup>

The use of an mGlu<sub>1</sub> antagonist suppressed the induction of ictal activity but showed almost no effect on maintenance of epileptiform activity, inhibition of PLC and TRPC displayed a similar effect.<sup>192,193</sup> DPHG induced an increase in burst frequency up to 300% in the hippocampal CA1 region, along with a decrease in amplitude and duration. LY367385, AIDA and MPEP prevented these changes.<sup>194,195</sup> LY367385 decreased the duration of these discharges, and the effect is additive when an mGlu<sub>5</sub> antagonist is employed.<sup>196</sup>

*In vivo*, group I mGlu agonists have shown convulsant activity, while antagonists impede DHPG generalized motor seizures.<sup>197</sup> It has been found that activation of mGlu<sub>5</sub>, but not mGlu<sub>1</sub>, induced epileptogenesis, while synaptic activation of both maintains group I mGlu-induced epileptogenesis.<sup>198</sup>

Studies with antagonists LY367385 and AIDA showed that mGlu<sub>1</sub> inactivation transiently suppressed sound-induced clonic seizures in the DBA/2 mice, an epilepsy prone strain; and also reduced spontaneous spike and wave discharges in lethargic mice (*lh/lh*).<sup>199</sup> Additionally, animal models have shown that kindled seizures can increase mGlu<sub>1</sub> mRNA and protein expression in different regions of the brain (e.g. dentate gyrus, CA3, supraoptic nucleus).<sup>191,200</sup> Kainate-induction of status epilepticus caused also an increase in mGlu<sub>1</sub> expression in inhibitory interneurons of the CA1 stratum oriens/alveus. This increase may be a compensatory mechanism that contributes to the resistance and tolerance of the immature hippocampus from damage. Excessive stimulation of excitatory synapses enhances the inhibitory drive of the immature brain by increasing GABA release.<sup>201</sup> However, different studies have reported that status epilepticus did not alter expression of mGlu<sub>1</sub> in hippocampal neurons, while causing mGlu<sub>5</sub> downregulation in the hippocampus and losing its induced long-term depression.<sup>202,203</sup>

Contrasting results have been observed in absence seizures. A spontaneously epileptic rat strain that develops tonic convulsions and absence-like seizures at 8-weeks, showed increase glutamate and low mGlu<sub>1</sub> mRNA in hippocampus, with lower expression of mGlu<sub>1</sub> in CA3 and dentate gyrus.<sup>204</sup> The WAG/Rij rats develop spontaneous absence seizures and it was found in these animals that mGlu<sub>1</sub> response and expression were decreased in the thalamus. This finding was especially important in the reticular thalamic nucleus. Administration of Ro 07-11401 reduced the spontaneous spike and spike-wave discharges (incidence and duration), while dosing the JNJ16259685 increased these discharges.<sup>205,206</sup> This effect was also observed with mGlu<sub>5</sub> PAM VU0360172. When administered chronically, animals develop tolerance for Ro 07-11401 after the third day of treatment, while this was not observed with VU0360172. The application of Ro 07-11401 increased the expression of mGlu<sub>1</sub> and mGlu<sub>5</sub> in the thalamus and cortex. Interestingly, in non-epileptic rats repeated injections of Ro 0711401 down-regulated the expression of mGlu<sub>1</sub> and mGlu<sub>5</sub> receptors.<sup>207</sup>

#### *Role of the mGlu<sub>1</sub> receptor in addiction*

The role of mGlu<sub>1</sub> in addiction is still not clear. Several single nucleotide polymorphisms in *GRM1* found in populations of the Detroit Neighborhood Health Study and Grady Trauma Project were linked to an increment in alcohol consumption.<sup>208</sup> Chronic ethanol consumption caused a decrease in expression of mGlu<sub>1</sub> mRNA in the CA3 region of the hippocampus and cerebellum; and upregulation of Homer2 and mGlu<sub>1</sub> in the nucleus accumbens.<sup>209,210</sup> Meanwhile, history of binge alcohol drinking led to higher expression of mGlu<sub>1</sub>, GluN2B, Homer2 and PLCβ in the central nucleus of the amygdala, but not in the adjacent basolateral amygdala.<sup>211</sup>

In ethanol consumption studies, mixed results have been observed with mGlu<sub>1</sub> antagonists. EMQMCM attenuated ethanol-induced conditioned place preference and ethanol withdrawal audiogenic seizures in rats, the antagonist also potentiated the inhibitory effect of MK-801 on the expression of ethanol induced sensitization.<sup>212</sup> Administration of CPCCOEt in a

chronic intermittent ethanol consumption model has shown that ethanol activates mGlu<sub>1</sub> to promote withdrawal-associated cytotoxicity *in vitro* and physical dependence *in vivo*.<sup>213</sup> CPCCOEt also resulted in reduced instrumental responding for ethanol, free-choice ethanol drinking and ethanol-induced locomotor sedation in mice in one study; however, these actions are not robust, as different reports have shown how the treatment with this compound resulted in no effect.<sup>210,214</sup> In the case of JNJ16259685, intra-CeA infusions moderately reduced binge intake, without influencing sucrose drinking, and the effect was enhanced with the use of mGlu<sub>5</sub> and PLC inhibitors.<sup>211</sup> This compound also reduced ethanol self-administration, dose dependently, in alcohol preferring inbred rats; although, it was concluded that the effect was due to motor impairment, even with the lowest effective dose.<sup>215-217</sup>

The effect of mGlu<sub>1</sub> in the action of stimulants has also been studied and conflicting results have emerged. Activation of group I mGlu<sub>s</sub> is necessary for acquisition and expression of amphetamine induced conditioned place preference, and it has been observed that it is inhibited by MPEP but not to by mGlu<sub>1</sub> NAM JNJ16259685.<sup>218</sup> Additionally, EMQMCM attenuated expression of behavioral sensitization cocaine in rats.<sup>210,214</sup> Antagonism of mGlu<sub>1</sub> receptors in the dorsal hippocampus has been reported to attenuate the reinstatement of cocaine-seeking behavior evoked by cocaine-associated contextual cues.<sup>219</sup> Moreover, intra-accumbens administration of DHPG promoted cocaine seeking in rats, while the mGlu<sub>1</sub> antagonist YM298198 attenuated drug-induced reinstatement of cocaine seeking.<sup>220</sup>

Group I mGlu is believed to be involved in drug-related learning. Cocaine-experienced animals exhibited a time-dependent intensification of cue-induced cocaine seeking and impaired extinction, an effect that was associated with reduction in mGlu<sub>1/5</sub> within ventromedial PFC. Dosing of mGlu<sub>1</sub> antagonists in cocaine-experienced rats did not affect drug-seeking behavior, while application of DHPG before the test after 30-day withdrawal facilitated extinction learning. Deficits in mGlu<sub>1</sub> in PFC mediate resistance to extinction and stimulation of mGlu<sub>1</sub> could facilitate learned suppression of drug-seeking behavior, helping drug abstinence.<sup>221</sup>

It has also been observed that application of DHPG in the medial prefrontal cortex increased glutamate levels in cocaine-sensitized rats, indicating that group I mGlu activation may contribute to the increased excitability in neurons in sensitized animals.<sup>222</sup> However, the Homer2 knock-out mice, which has reduced mGlu<sub>1</sub> function, also exhibited increased sensitivity to the psychomotor activation and conditioned rewarding effects of cocaine, and an enhanced capacity to increase glutamate in the striatum. Deletion of mGlu<sub>1</sub> also blunted ethanol reward and place conditioning, causing reduced reward and aversion of ethanol, with higher sensitivity to motor-impairing/sedative effects.<sup>223</sup>

Acute and chronic cocaine use decreases expression of mGlu<sub>1</sub> in dendrites of nucleus accumbens, with no change in mGlu<sub>5</sub>.<sup>224</sup> Repeated cocaine injections for 3 weeks, decreased the capacity of DHPG to induce glutamate release in the nucleus accumbens and reduced the increase in locomotor activity, a change associated to reduction in Homer1b/c.<sup>225</sup>

High conductance calcium-permeable AMPAR are normally low in the nucleus accumbens synapses, but levels increase with cocaine administration and it has been found that they mediate cue-induced cocaine craving. Stimulation of mGlu<sub>1</sub> inhibits synaptic transmission by these receptors in several brain regions (e.g. VTA, cerebellum, and amygdala). Specifically in the nucleus accumbens, mGlu<sub>1</sub> activation eliminates the contribution of these receptors in synaptic transmission, and facilitates transmission with calcium-impermeable AMPAR, reducing cue-induced cocaine craving, an effect that could be beneficial for cue-induced relapse in abstinent cocaine addicts.<sup>226–228</sup>

Cocaine also produces a switch of NMDAR subunit composition at excitatory synapses on dopaminergic neurons of the VTA, provoking the insertion of GluN3A subunits which reduces NMDAR function and are necessary for cocaine-evoked plasticity of AMPAR in these synapses. mGlu<sub>1</sub> potentiates NMDA transmission and restores subunit composition via a protein synthesis-dependent mechanism.<sup>229</sup>



Besides reversing the effects in adults, it has been observed that mGlu<sub>1</sub> activation can attenuate developmental deficits caused by *in utero* exposure to cocaine. Prenatal cocaine exposure uncouples mGlu<sub>1</sub> from its anchoring protein Homer and signal transducer G<sub>q/11</sub>, reducing phosphoinositide hydrolysis in the hippocampus and brain cortex.<sup>230</sup> It also causes delayed postsynaptic maturation of glutamatergic transmission in the VTA, and this effect is blunted by mGlu<sub>1</sub> positive modulation.<sup>231</sup>

#### *Role of the mGlu<sub>1</sub> receptor in schizophrenia*

The hypofunction of the NMDA receptor has been highlighted as an etiological factor for schizophrenia. The NMDA receptor function can be modulated by group I mGlu<sub>s</sub> and it has been proposed that these receptors could also contribute to the disease.

In postmortem studies of schizophrenic patients, an increase in protein expression of mGlu<sub>1a</sub> in the prefrontal cortex has been observed, but not in the striatum or the thalamus.<sup>232,233</sup> Higher postmortem mGlu<sub>1a</sub> mRNA levels have also been found in the prefrontal cortex. These changes were not attributed to the use of antipsychotic medications, and the patient samples presented no difference when they were stratified by sex, tendency for suicide or history of substance abuse.<sup>234</sup> However, the involvement of the receptor is hard to elucidate as these events could be the cause or a compensatory reaction to neurotransmitter dysregulation in schizophrenia.

The mGlu<sub>1</sub> knockout mice displayed deficits in prepulse inhibition (PPI) and the sensorimotor gating.<sup>235</sup> But the application of mGlu<sub>1</sub> antagonists EMQMCM and BAY 36-7620 in normal animals did not disturb PPI.<sup>236,237</sup> While mGlu<sub>1</sub> deletion in mice caused amphetamine to induce a higher motor response compared to wild type, studies using the amphetamine-induced hyperlocomotion have shown that mGlu<sub>1</sub> antagonists AIDA and MCPG did not affect the amphetamine related behavior.<sup>238,239</sup>

Additionally, mGlu<sub>1</sub> function has been reported to be affected by the action of other molecules related to schizophrenia, like dysbindin-1 encoded by schizophrenia risk gene *dtmbp1*.

This protein is reduced in the brain of schizophrenics and a loss of function mutation in *dtbpl* caused cognitive and social behavior impairment, accompanied by great reduction in DHPG-induced phosphorylation of ERK1/2, with no effect in group I mGlu expression. The mutation also affected plasticity related to group I mGlu receptor, reducing DHPG-induced LTD at CA1 excitatory synapses. Application of an mGlu<sub>5</sub> PAM rescued this phenotype, and the authors of the study indicated that the role of mGlu<sub>1</sub> should be explored.<sup>240</sup>

Multigenic clustered coding variants analysis of glutamatergic “hub genes” in the genome of schizophrenic and bipolar patients identified two exons encoding for the cysteine rich domain and the first TMD helix of *GRM1*, as a risk locus with five highly enriched mutations. Even though these mutations were not studied in *in vitro* or *in vivo*, *in silico* exploration identified them as polymorphisms that would probably affect protein folding, trafficking or activation of the receptor.<sup>241</sup>

More recently, deleterious mutations of *GRM1* were found in an Australian population of schizophrenics. These mutations were hereditary and they also were predicted to be deleterious. Four of these mutations were found in family members, and their diseases were not limited to schizophrenia (depression, anxiety, drug and alcohol dependence, and epilepsy). The *in vitro* analysis showed that these genetic changes decreased mGlu<sub>1</sub> induced inositol phosphate production and one of them reduced membrane expression.<sup>242,243</sup> The finding of appropriate activators of the mGlu<sub>1</sub> receptor could provide therapeutic benefit for patients carrying these mutations.

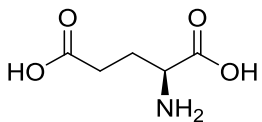
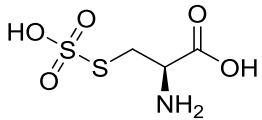
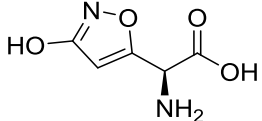
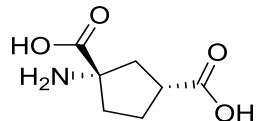
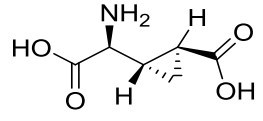
### **Ligands for the metabotropic glutamate receptor subtype 1**

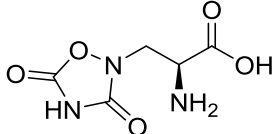
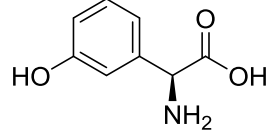
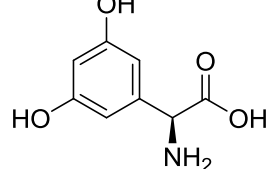
#### *Orthosteric Agonists*

mGlu<sub>1</sub> endogenous ligand, glutamate **3.1**, can potentiate both mGlu<sub>1</sub> and mGlu<sub>5</sub> with comparable EC<sub>50</sub>s.<sup>244</sup> The orthosteric mGlu<sub>1</sub> agonists available are characterized for being amino

acid derivatives that bind in the same *N*-terminal site as glutamate (Table 3.1). Products of oxidation of cysteine, such as *S*-sulfo-L-cysteine **3.2**, have demonstrated to activate the receptor weakly.<sup>245</sup> Ibotenic acid **3.3** is a natural product identified in the *Amanita muscaria* mushroom, this molecule can activate the group I and II of the metabotropic receptors, along with NMDA and has shown weak agonism in the AMPA and kainate receptors.<sup>244</sup> The first synthetic agonists discovered were ring-constrained amino acids, such as ACPD **3.4** and L-CCG-I **3.5**, which despite of activating the receptor lack selectivity with respect to the other forms of mGlu.<sup>244,246</sup> Quisqualate **3.6**, an oxadiazolidine analog, is one of the most potent mGlu<sub>1</sub> agonists and is selective for group I mGlu; although, it also activates AMPA and kainite receptor. The most selective agonists for group I orthosteric agonist are based on the structure of (*S*)-3-hydroxyphenylglycine **3.7**. In this group, (*S*)-DHPG **3.8** stands out as the most potent and employed chemical tool in the study of the effects of activation of mGlu<sub>1</sub> and mGlu<sub>5</sub>.<sup>244</sup>

**Table 3.1.** Representative orthosteric agonists for the mGlu<sub>1</sub> receptor.

Structure	Cpd #	Name	EC <sub>50</sub>	Ref
	<b>3.1</b>	Glutamate	1.0 μM <sup>b</sup>	244
	<b>3.2</b>	<i>S</i> -Sulfo-L-cysteine	>1000 μM <sup>a</sup>	245
	<b>3.3</b>	Ibotenic acid	2.3 μM <sup>b</sup>	244
	<b>3.4</b>	1 <i>S</i> ,3 <i>R</i> -ACPD	36.1 μM <sup>a</sup> 8 μM <sup>b</sup>	246
	<b>3.5</b>	L-CCG-I	2 μM <sup>b</sup>	244

	<b>3.6</b>	Quisqualic acid	0.045 $\mu\text{M}^{\text{b}}$	244
	<b>3.7</b>	(S)-HPG	52 $\mu\text{M}^{\text{b}}$	244
	<b>3.8</b>	(S)-DHPG	10 $\mu\text{M}^{\text{a}}$ 3.25 $\mu\text{M}^{\text{b}}$	246

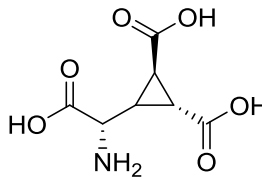
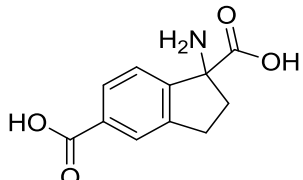
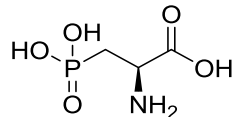
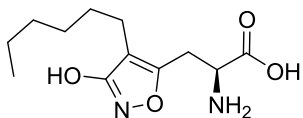
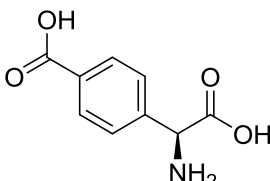
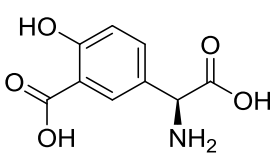
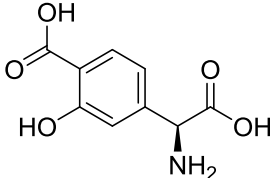
<sup>a</sup>Based on PI hydrolysis. <sup>b</sup>Calcium mobilization assay.

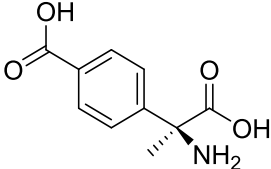
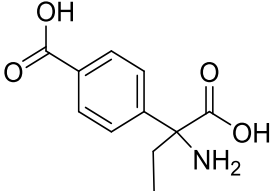
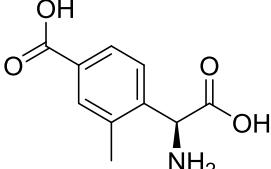
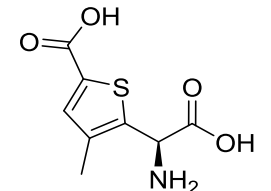
### Orthosteric Antagonists

Similarly to the agonists, orthosteric antagonists are also amino acid based molecules that exert their function competing for the extracellular glutamate binding site and stabilizing a resting/inactive conformation of the receptor (Table 3.2). DCG-IV **3.9** and AIDA **3.10** are ring-constrained amino acids, of which the former has cross activity between group I and II, while the latter selectively inhibits mGlu<sub>1</sub> but with low potency ( $K_i = 124 \mu\text{M}$ ).<sup>244,247</sup> Similarly, the phosphonic acid L-AP3 **3.11** inhibits phosphatidylinositol hydrolysis caused by group I mGlu but only at high concentrations.<sup>248</sup> In a campaign to find an mGlu<sub>1</sub> antagonist, structure-activity relationship studies were carried on using the agonist ibotenic acid **3.3** as a starting point. (S)-HexylHIBO **3.12** was obtained from this efforts, where homologation and *n*-hexyl substitution caused the switch in its pharmacological profile and also rendered the molecule preferential for group I mGlu receptors.<sup>249</sup> Studying similar structures to (S)-DHPG **3.8**, it was found that carboxyphenylglycines **3.13-3.19** can act as group I mGlu antagonists. The aromatic carboxylic acid function together with the introduction of an alkyl group in the  $\alpha$ -carbon are important features to develop antagonist activity.<sup>250,251</sup> From this scaffold, the most potent and selective molecules are LY367385 **3.18** and 3-MATIDA **3.19**, which share an *ortho*-methyl substitution

with respect to the amino acid; in **3.19**, the phenyl ring has been replaced for the thiophene bioisostere.<sup>252,253</sup>

**Table 3.2.** Representative orthosteric antagonists for the mGlu<sub>1</sub> receptor.

Structure	Cpd #	Name	K <sub>i</sub> /IC <sub>50</sub>	Ref.
	<b>3.9</b>	DCG-IV	IC <sub>50</sub> : 389 μM	247
	<b>3.10</b>	AIDA	K <sub>i</sub> : 124 μM <sup>a</sup>	244
	<b>3.11</b>	L-AP3	IC <sub>50</sub> : 2.1 mM <sup>b</sup>	248
	<b>3.12</b>	(S)-HexylHIBO	K <sub>b</sub> : 140 μM <sup>c</sup>	249
	<b>3.13</b>	(S)-4CPG	K <sub>i</sub> : 18 μM <sup>a</sup> IC <sub>50</sub> : 40 μM <sup>c</sup>	244,250,251
	<b>3.14</b>	(S)-3C4HPG	IC <sub>50</sub> : 400 μM <sup>c</sup>	250,251
	<b>3.15</b>	(S)-4C3HPG	K <sub>i</sub> : 11 μM <sup>a</sup> IC <sub>50</sub> : 30 μM <sup>c</sup>	244,250

	<b>3.16</b>	(S)-MCPG	IC <sub>50</sub> : 70 μM <sup>c</sup>	250,251
	<b>3.17</b>	E4CPG	K <sub>b</sub> : 367 μM <sup>c</sup>	254
	<b>3.18</b>	LY 367385	IC <sub>50</sub> : 8.8 μM <sup>c</sup>	253
	<b>3.19</b>	3-MATIDA	IC <sub>50</sub> : 6.3 μM <sup>c</sup>	252

<sup>a</sup>Calcium mobilization assay. <sup>b</sup>Evoke inward currents in voltage clamped. <sup>c</sup>Inhibition of phosphatidylinositol hydrolysis.

### *Allosteric ligands*

The allosteric modulators differentiate from the orthosteric ligands functionally and structurally. From a topographic stand point, the allosteric modulators bind to a site distinct from the orthosteric site; hence, ideally, they are not competitive with the endogenous agonist. The difference in binding site comes accompanied by a difference in chemical structure and properties with respect to the endogenous ligand. For example, in the class C of the GPCR family, the allosteric sites are usually found in the transmembrane domain and its allosteric modulators are in overall more lipophilic than the orthosteric ligands. In the case of central nervous system application, the design of allosteric modulators favors bioavailability, brain penetration and exposure to target.

Allosteric modulators act by causing or stabilizing conformational changes in the receptor which in turn will affect the sensitivity and the efficacy of the orthosteric ligand. A pure allosteric modulator would not cause an observable effect on its own, but only when the agonist is present. Then, allosteric modulation possess the advantage of a more fine tuning with better spatial and temporal control, which is especially important in the nervous system, where the signaling events are highly compartmentalized and synchronized. This feature will anticipate better efficacy and lower adverse event potential. In the case of positive allosteric modulators, these will additionally cause less desensitization and down-regulation of the receptor than an orthosteric agonist by not being permanently activating the receptor.

Besides, allosteric modulation has the intrinsic strategy of targeting a less evolutionary conserved site. When developing agonists compounds, the orthosteric binding site usually shares a higher homology in a family of receptors, as it has evolved to accommodate the same endogenous ligand; however, the allosteric sites are more divergent in its sequence, facilitating the discovery of isoform-selective allosteric modulators.

#### *Negative allosteric modulators*

The role of mGlu<sub>1</sub> in pain perception led to extensive studies for the production of non-competitive antagonists for the receptor. Several institutions have worked in the development of mGlu<sub>1</sub> negative allosteric modulators around different scaffolds (Table 3.3). The first molecule discovered in this group was (-)-CPCCOEt **3.20**. This oxime interacts with amino acids distant from the orthosteric site in the extracellular surface of TM7 (T815 and A818).<sup>255,256</sup> **3.20** demonstrated to be a selective and potent enough chemical probe to explore the target *in vitro*; however, it lacked good characteristics for *in vivo* use. Its analog, PHCCC **3.21**, inhibits the receptor with higher potency, but it is also active in mGlu<sub>4</sub>.

BAY36-7620 **3.22** was the first potent and selective mGlu<sub>1</sub> NAM with IC<sub>50</sub> below 160 nM, and behaving as an inverse agonist.<sup>257</sup> After that, several NAMs with high potencies have been obtained, and some of these compounds have been used in their tritiated form as radioligands, including EM-TBPC **3.23**, YM-298198 **3.38**, R214127 **3.25**, to study the distribution of mGlu<sub>1</sub> in the rat brain and quantify the affinity of other glutamate non-competitive ligands.<sup>258</sup> EM-TBPC **3.23**, despite being highly potent, shows significant cross-species difference, as this NAM is active in the rat form of the receptor but it has low affinity for the human one.<sup>258</sup> NPS2390 **3.24** is a quinoxaline analog with preferential mGlu<sub>1</sub> NAM activity and residual mGlu<sub>5</sub> inhibition.<sup>259</sup> Additional compounds in this series have improved selectivity for mGlu<sub>1</sub>, such as NPS2407, a 2-quinoxaline carboxamide, and NPS3018, a quinoxaline ester.

R214127 **3.25** is a non-competitive and selective mGlu<sub>1</sub> negative allosteric modulator with high affinity for the receptor. **3.20**, **3.22**, **3.23**, **3.24** and **3.38** can displace [<sup>3</sup>H]-R214127 *ex vivo* and *in vivo* slices, arguing for a common allosteric binding site for these different compounds. This radioligand facilitated the discovery of JNJ16259685 **3.26**, a potent mGlu<sub>1</sub> NAM with good receptor occupancy and long lasting coverage after systemic administration.<sup>260</sup>

Abbott has also developed different series of mGlu<sub>1</sub> NAMs, of which the most optimized is A841720 **3.27**. This compound has good pharmacodynamic properties and brain penetration, and it proved to have analgesic activity in models of neuropathic pain; although, it showed disruption of cognitive function.<sup>261</sup> Even when other series were explored to increase solubility, such as **3.28**, the SAR in the core was flat and **3.27** remained the more potent compound.<sup>262</sup> This scaffold was also explored by Schering-Plough with similar results.<sup>263</sup>

Pfizer also disclosed two different scaffolds for non-competitive antagonists of mGlu<sub>1</sub>, the first being **3.29** which showed to be potent, selective and stable in human liver microsomes.<sup>264</sup> The second scaffold **3.30** contains an indanamine and morpholine substituent, features that



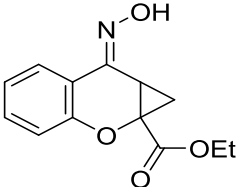
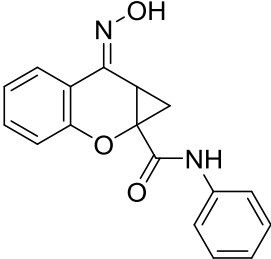
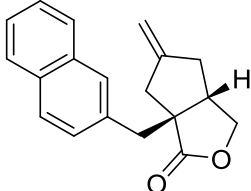
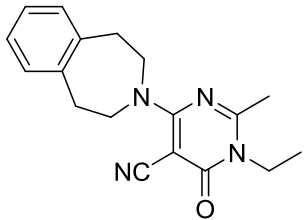
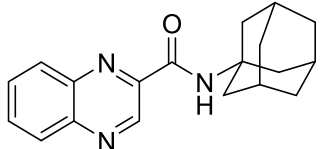
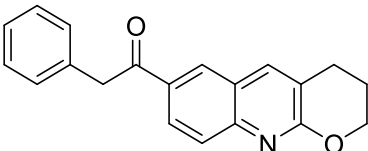
balance potency along with CNS penetration (50% in CSF). This molecule also possesses a relatively short half-life, but with good oral bioavailability, and its analgesic effects are comparable with morphine when concentration on target is ten-times its  $K_i$ .<sup>265</sup> A compound **3.31** with this pyrido[3,4-d]pyrimidine core has also been reported by Lilly as a selective mGlu<sub>1</sub> NAM with anticonvulsant, antinociceptive and anxiolytic effects.<sup>237,266</sup>

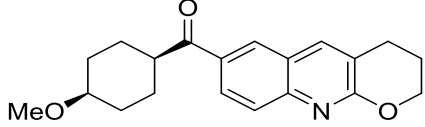
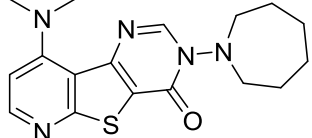
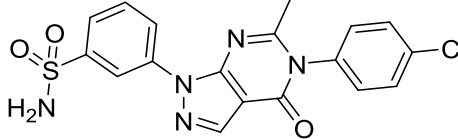
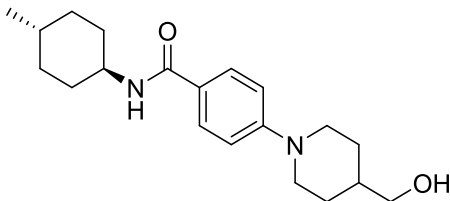
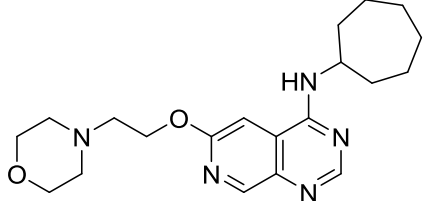
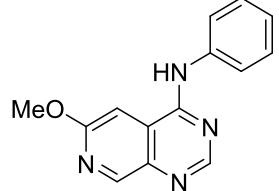
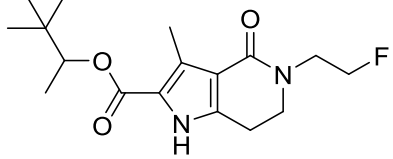
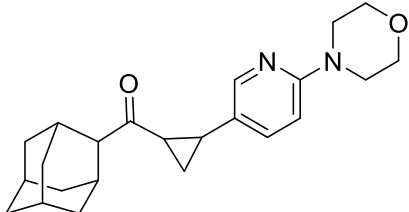
FTIDC **3.35** and FITM **3.34** are compounds developed by Merck-Banyu. FITDC **3.35** features in its structure a pyridine ring to decrease the log D with respect to previous molecules, a 2-fluoro substitution to decrease the basicity of the molecule, and a methyl group in the triazole that demonstrated to be important for potency and selectivity.<sup>267,268</sup> These characteristics allowed the study and confirmation of the analgesic profile of the compound; however, the compound has a short half-life due to oxidative dealkylation of the urea. FITM **3.34** was developed to improve P450 metabolism and water solubility.<sup>269</sup> The introduction of an *N*-isopropylpyrimidin-4-amine demonstrated to be useful to achieve these goals. FITM **3.34** demonstrated to be active as antipsychotic and to enable positive emission tomography (PET) studies through its <sup>11</sup>C-methyl and <sup>18</sup>F radiolabeled analogs.<sup>270</sup>

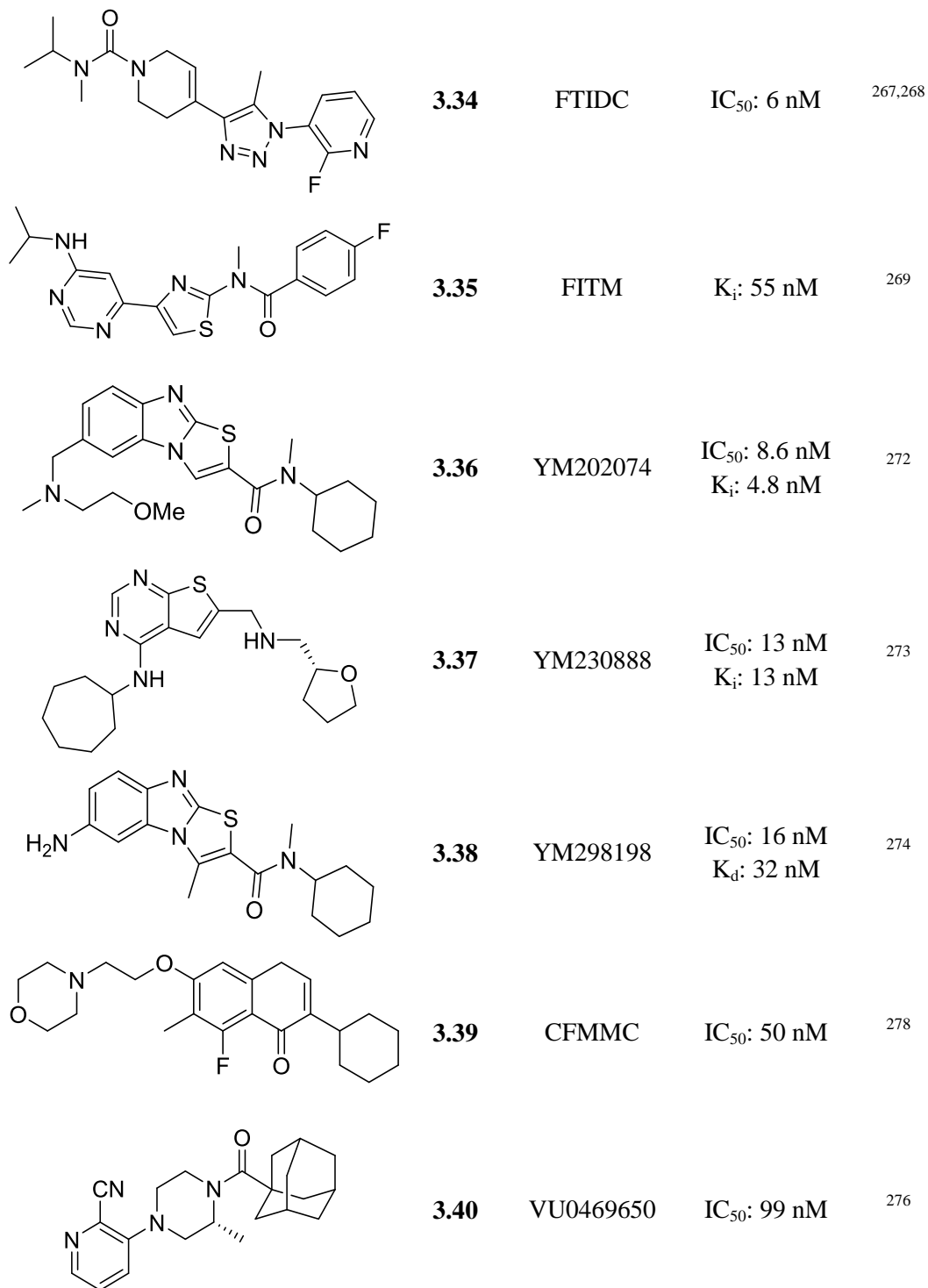
GlaxoSmithKline has reported different potent compounds, like **3.32**, obtained through a tied-back ring strategy on a pyrrole high-throughput screening hit.<sup>271</sup> Astellas has also disclosed various mGlu<sub>1</sub> NAMs (**3.36**, **3.37**, **3.38**) with high potency and selectivity that were efficacious in inhibiting nociception and as neuroprotective agents in stroke;<sup>272–274</sup> as well as the Banyu's Tsukuba Research Institute with CFMMC **3.39**. Merz also attempted to develop mGlu<sub>1</sub> NAMs through a virtual screening effort, using a template based on JNJ16259685, NPS2390, EM-TBPC, and even though antagonists with good potency were obtained (e.g. **3.33**) the compounds generated were very lipophilic.<sup>275</sup>

Finally, at Vanderbilt University our research group discovered potent and selective mGlu<sub>1</sub> NAM VU0469650 **3.40**.<sup>276</sup> This chemical probe is brain penetrant, has good free fraction in plasma (7%), but it suffers from high clearance.

**Table 3.3.** Representative negative allosteric modulators for the mGlu<sub>1</sub> receptor.

Structure	Cpd #	Name	K <sub>i</sub> /IC <sub>50</sub>	Ref.
	<b>3.20</b>	CPCCOEt	IC <sub>50</sub> : 6.5 μM <sup>a</sup>	255,256
	<b>3.21</b>	PHCCC	IC <sub>50</sub> : 3.0 μM <sup>a</sup>	277
	<b>3.22</b>	BAY 36-7620	IC <sub>50</sub> : 160 nM	257
	<b>3.23</b>	EM-TBPC	IC <sub>50</sub> : 15 nM K <sub>d</sub> : 6.6 nM	258
	<b>3.24</b>	NPS2390	K <sub>i</sub> : 1.36 nM	259
	<b>3.25</b>	R214127	K <sub>d</sub> : 0.9 nM	259

	<b>3.26</b>	JNJ16259685	IC <sub>50</sub> : 3.2 nM	260
	<b>3.27</b>	A841720	IC <sub>50</sub> : 11 nM K <sub>i</sub> : 10 nM	261
	<b>3.28</b>	---	K <sub>i</sub> : 127 nM	262
	<b>3.29</b>	---	K <sub>i</sub> : 9 nM	264
	<b>3.30</b>	---	K <sub>i</sub> : 6 nM	265
	<b>3.31</b>	LY456236	K <sub>i</sub> : 143 nM	266
	<b>3.32</b>	---	IC <sub>50</sub> : 19 nM	271
	<b>3.33</b>	---	K <sub>i</sub> : 24 nM	275

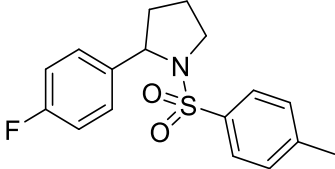
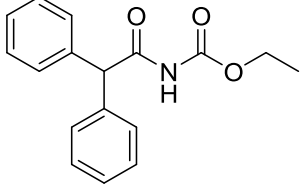
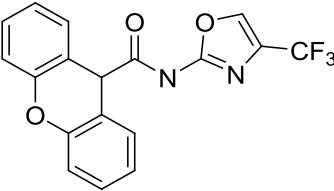


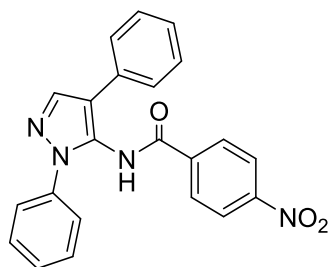
<sup>a</sup>Calcium mobilization assay. <sup>b</sup>Evoke inward currents in voltage clamped. <sup>c</sup>Inhibition of phosphatidylinositol hydrolysis.

### Positive allosteric modulators

In the mGlu<sub>1</sub> allosteric modulator realm, the negative allosteric modulators have been explored vastly in comparison with the positive allosteric modulator. The scaffolds available are mainly a contribution from Hoffman-La Roche (Table 3.4). Ro 67-7476 **3.41** and Ro 01-6128 **3.42** were obtained directly as hits from a high-throughput screening campaign, and while they were active at the rat form of the receptor, they do not potentiate the response in the human receptor; similar to what happened with VU-71 **3.44**. Both compounds, increased the binding of radiolabeled mGlu<sub>1</sub> agonist [<sup>3</sup>H]-quisqualate.<sup>279</sup> It is remarkable that none of these compounds can displace [<sup>3</sup>H]-R214127, indicating a different binding site with respect to the one observed for many negative allosteric modulators.<sup>280</sup> The only compound that has cross species activity is Ro 07-11401 **3.43** and its development will be described in the next section.

**Table 3.4.** Representative positive allosteric modulators for the mGlu<sub>1</sub> receptor.

Structure	Cpd #	Name	EC <sub>50</sub>	Ref
	<b>3.41</b>	Ro 67-7476	174 nM	279
	<b>3.42</b>	Ro 01-6128	200 nM	279
	<b>3.43</b>	Ro 07-11401	56 nM	281



3.44

VU-71

2.4  $\mu\text{M}$

280

---

### Study of the structure-activity relationship around Ro 07-11401

#### *Development of Ro 07-11401*

After finding Ro 67-7476 **3.41** and Ro 01-6128 **3.42** during a high throughput screening effort, the compounds were studied in kinetic fluorescence-based calcium mobilization assays and in electrophysiology models, where they demonstrated to potentiate the rat mGlu<sub>1</sub> receptor and selectivity with respect to other members of the mGlu family. These compounds bind in the transmembrane domain and different activity in the rat and human form of the receptor arises from a single amino acid change in position 757 in TM5 (leucine in human, valine in rat).<sup>279</sup>

In order to improve activity in the human receptor, SAR studies were carried on using Ro 01-6128 **3.42** as parent compound, employing different alkyl substituents in the oxygen of the carbamate and a cyclization strategy to produce xanthene and thioxanthene analogs. Here, the *n*-alkyl *9H*-xanthene-carbonyl carbamates were slightly more active than their diphenylacetyl congeners, while analogs with a *9H*-thioxanthene core were considerably less active. In the *9H*-xanthene scaffold, replacement of the carbamate with a thiocarbamate or an urea led to decrease the potency. A linear chain is preferred as the substituent in the carbamate, with bulkier substituents (*i*-Pr, *t*-Bu) being not well tolerated. The optimized length for the alkyl chain is four carbons in both series. Compound Ro 67-4853 **3.45** was obtained from this task, a highly potent

mGlu<sub>1</sub> PAM with cross species activity, but less selectivity than its predecessor and a small potentiating effect in mGlu<sub>5</sub> at 10 µM (Fig. 3.3).<sup>282</sup>

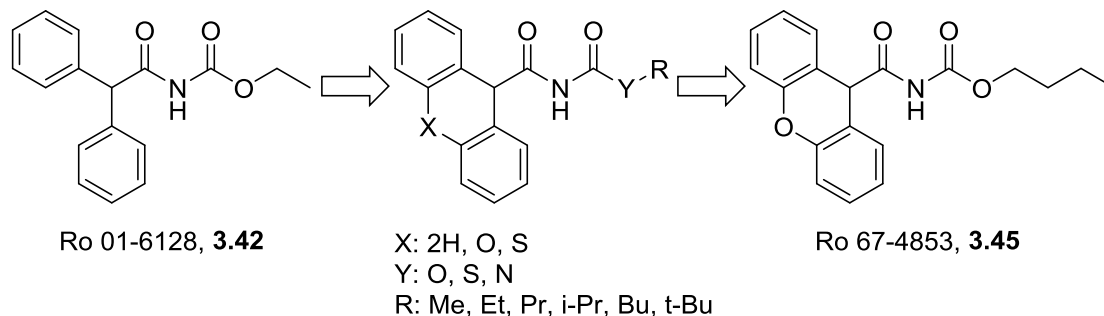


**Figure 3.3.** Discovery of compound Ro 67-4853 **3.45**.

However the improvements, Ro 67-4853 **3.45** demonstrated to be a highly labile compound, as the carbamate moiety is quickly hydrolyzed by esterases in blood plasma to generate inactive amides. A replacement of the carbamate for bioisosteric five-membered heteroaromatic rings, such as oxadiazoles and tetrazoles was performed. In this series, small alkyl and cycloalkyl substituents in the newly introduced rings were beneficial for mGlu<sub>1</sub> PAM activity (Fig. 3.4). Overall, **3.46** and **3.47** provided the best balance in potency, *in vitro* rat liver microsomal metabolism and solubility; but, when employed *in vivo*, IV administration showed that compounds metabolized quickly with half-lives of less than 30 minutes, they possess good bioavailability after *per oral* administration, but their brain penetration was poor ( $K_p$ : 0.16), even after IV infusion administration. Studies demonstrated that low access to CNS was not caused by the P-glycoprotein efflux transporter.<sup>283</sup>

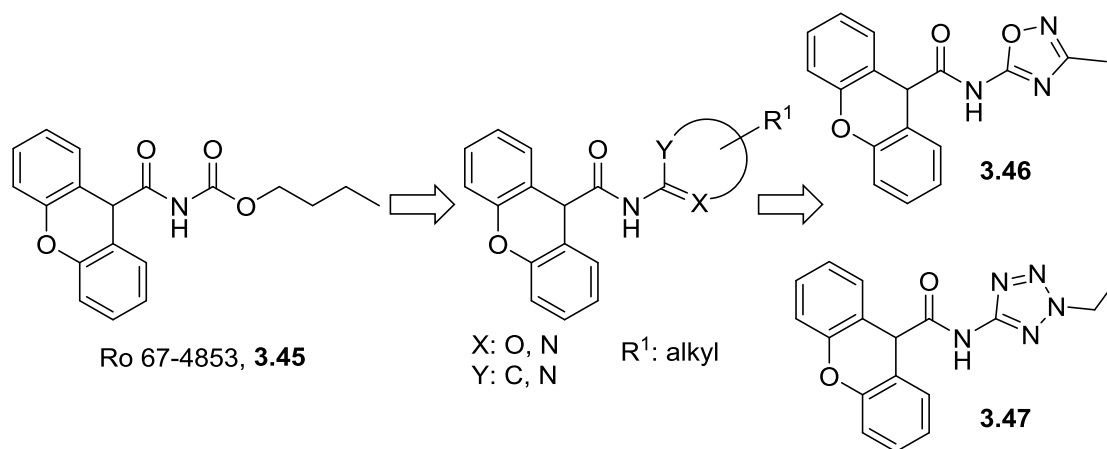


**Figure 3.4.** Bioisosteric replacement of the carbamate in the Ro 67-4853 **3.45** series.

In an effort to improve the pharmacokinetic profiles of newly generated mGlu<sub>1</sub> PAMs, SAR studies were performed employing an oxazole molecule. The 4-methyloxazole analog was found to have similar activity to the previously tried five-member rings. Biotransformation of this compound, as well as the 3-methyloxazole, revealed that oxidation occurred in the methyl and on positions C2 and C7 in the xanthene. Different fluorinated compounds around this scaffold were prepared to increase their metabolic stability. It was found that fluorine substitution in the xanthene decrease the mGlu<sub>1</sub> activity, affecting mostly the efficacy of the compounds. Also, replacing the methyl substituent for trifluoromethyl resulted in active compounds with decreased clearance with respect to the parent compound (Fig. 3.5). Ro 07-11401 **3.43** was obtained, a potent mGlu<sub>1</sub> PAM with a half-life of 54 minutes and K<sub>p</sub> of 0.8.<sup>281</sup> However, when Ro 07-11401 **3.43** was tested in our laboratories its properties differed considerably, especially its pharmacokinetics properties. Our measurements determined and *in vitro* rat intrinsic clearance of 661 mL/min/kg (63.3 mL/min/kg adjusted for hepatic blood flow), brain-plasma partition coefficient of 0.28 in mouse and rat, and inhibition of P450 1A2 (IC<sub>50</sub> = 13 μM) and 2C9 (IC<sub>50</sub> = 0.62 μM). Our studies also showed low fraction unbound in human (0.3%) and rat plasma (1.4%), and in rat brain homogenate (1.4%).



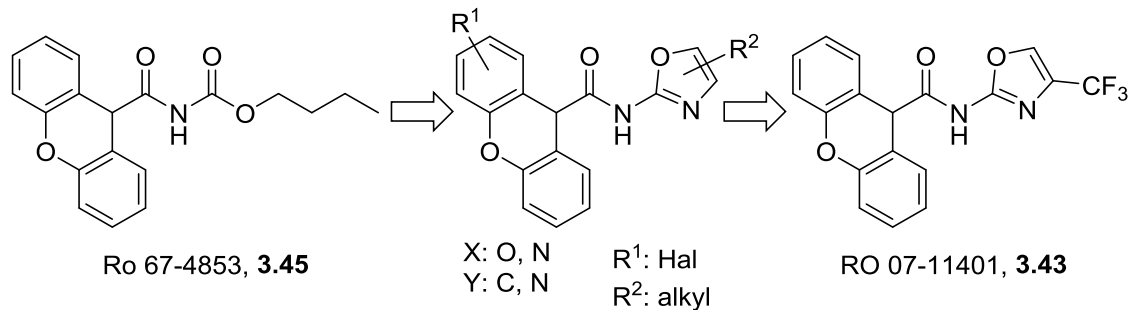


**Figure 3.5.** Discovery of compound Ro 07-11401 **3.43**.

#### *Modifications to the Ro 07-11401 scaffold*

The lack of good pharmacokinetic properties for Ro 07-11401 **1.43** motivated us to explore its SAR and develop an optimized chemical probe that could be used in target validation studies to determine the role that mGlu<sub>1</sub> activation can have in schizophrenia and other neuropsychiatric conditions.

The compound is an amide, and a vast chemical space can be explored by using different amines and carboxylic acids. In the amine side, the published SAR showed that only few rings were tried when replacing the carbamate from the previous series; therefore, we could survey different aromatic and saturated rings, as well as different substituents in those rings. As the xanthene had remained unchanged since the obtention of the high-throughput screening hit, chemical modifications on this ring system have not been explored; the xanthene moiety can be modified by eliminating rings, opening the tricyclic core, or introducing heteroatoms. Also, we could try to modify the linker that brings together both rings, such as the alkylation or performing the reverse amide (Fig. 3.6).

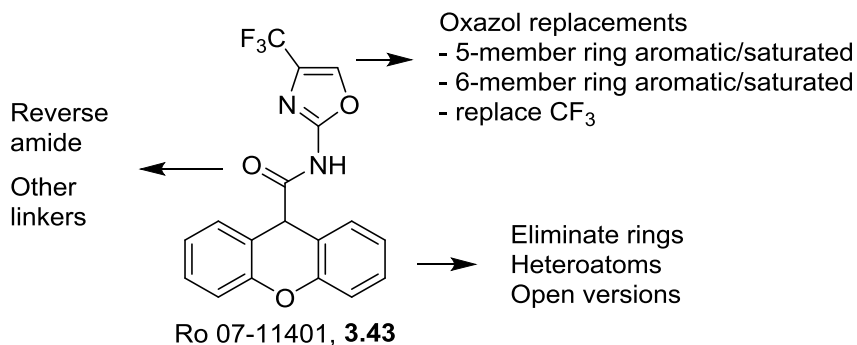
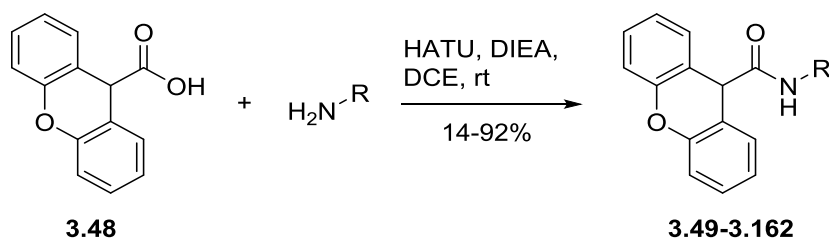


**Figure 3.6.** Possible chemical modifications to study the SAR around Ro 07-11401.

The first SAR iteration was directed towards probing the amine region. The synthesis of these molecules was carried out by performing the amide coupling between xanthene-9-carboxylic acid **3.48** and the respective amines, using 1-[Bis(dimethylamino)methylene]-1*H*-1,2,3-triazolo[4,5-*b*]pyridinium 3-oxide hexafluorophosphate (HATU) as amide coupling reagent and *N,N*-diisopropylethylamine as base, to generate analogs **3.49-3.160** (Scheme 3.1).



**Scheme 3.1.** Synthesis of diverse amines library, analogs **3.49-3.162**.

Acyclic saturated amines **3.49-3.67** were tried first and their propensity to enhance the mGlu<sub>1</sub> response towards glutamate was assayed at a single point concentration of 10 μM. From this set, no amine potentiated an EC<sub>20</sub> of glutamate (Fig. 3.7). A second subset of amides, synthesized using cyclic amines **3.68-3.113** derived from azetidine, pyrrolidine, piperidine, piperazine and morpholine, gave similar results with complete loss of activity at a 10 μM concentration in calcium mobilization assays (Fig. 3.8).

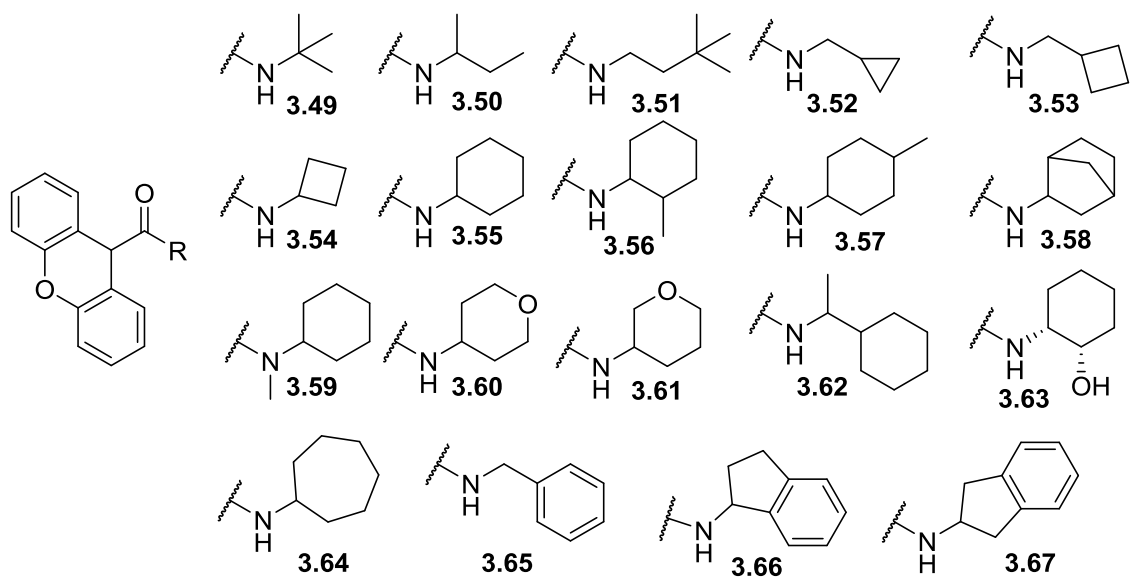


**Figure 3.7.** Saturated acyclic amines that yield inactive compounds for mGlu<sub>1</sub> PAM activity, analogs **3.49-3.67**.

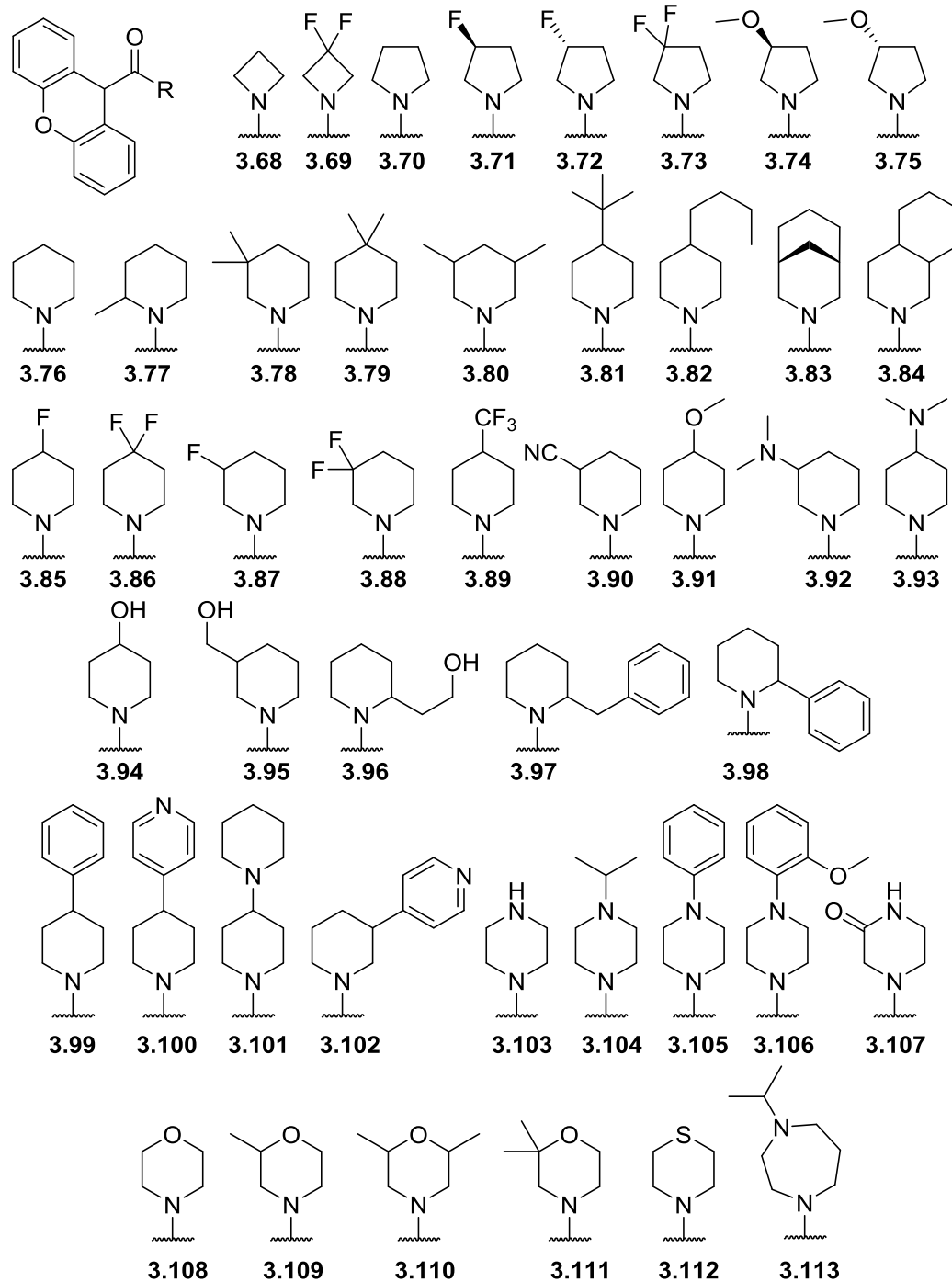


**Figure 3.8.** Saturated cyclic amines that yield inactive compounds for mGlu<sub>1</sub> PAM activity, analogs **3.68-3.113**.

A third subset consisting of aromatic amines **3.114-3.162** was employed. The single point screening at 10  $\mu$ M of these compounds was performed using the human form of mGlu<sub>1</sub> and

revealed the presence of active compounds in this set (Fig. 3.9 and Table 3.5). The naked and *ortho*, *meta* or *para*-substituted anilines (**3.114-3.123**) showed no PAM activity, as well as the pyridines (**3.124-3.126**), with the exception of the *ortho*-aminopyridine **3.124** which potentiated weakly the glutamate response to 48% of Glu<sub>Max</sub>. Five-membered aromatic rings were also tried, from this set the pyrazole (**3.129-3.139**), imidazole (**3.140-3.142**), isoxazole (**3.128**), 1,2,3-triazole (**3.143**), 1,2,4-triazole (**3.144-3.146**) and thiophenes (**3.147-3.149**) variants tested did not achieve potentiation of the EC<sub>20</sub>. Meanwhile, the 2-aminooxazole analog **3.127** caused an enhancement in glutamate response close to 79% of Glu<sub>Max</sub>, and several thiazole containing compounds were found to be active. In this family, it was observed that the 2-aminothiazole (**3.151**) achieved a higher level of %Glu<sub>Max</sub>, than the 5-aminothiazole (**3.152**) (88% vs 54%, respectively). Also, it was found that small groups were tolerated in the 4-position of the 2-aminothiazole, such as the cyano (**3.157**) and the *iso*-propyl (**3.153**), but bigger groups like *tert*-butyl (**3.154**) and phenyl (**3.158**) yield inactive compounds. Doubly substituted aminothiazole appeared to maintain part of the mGlu<sub>1</sub> activity, like the 4,5-dimethyl version **3.155** and the 2-aminobenzothiazole **3.160**, but when large groups were employed a complete loss of activity was observed, like in **3.156**. It was interesting that in the case of **3.156** a complete inhibition of the EC<sub>20</sub> was observed, a feature that could be associated with mGlu<sub>1</sub> NAM activity. Also, the 5-amino-1,2,4-thiadiazole **3.162** demonstrated to be active with a %Glu<sub>Max</sub> of 103%.

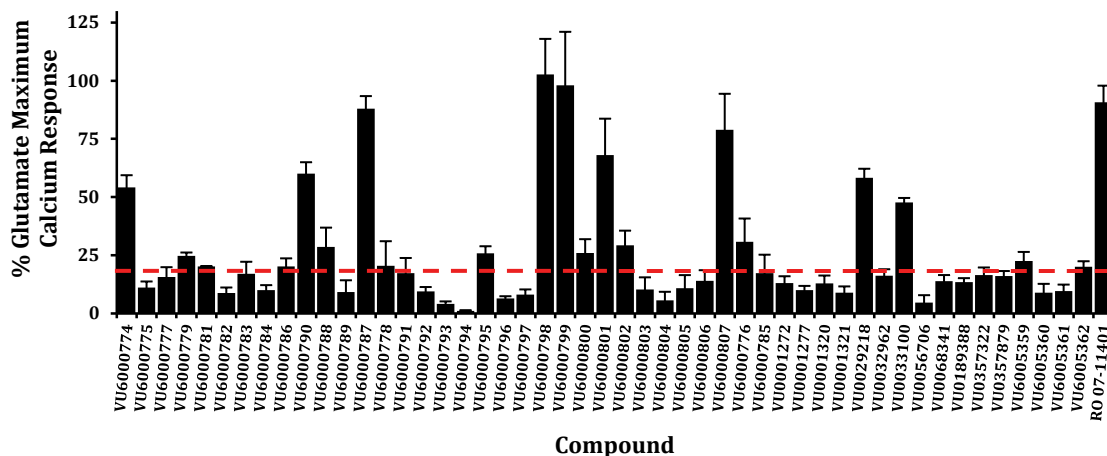
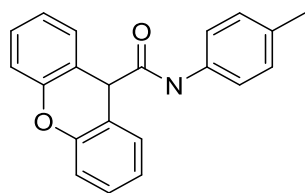


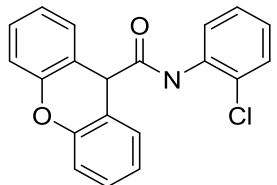
**Figure 3.9.** Comparison of the single point screening result for PAM activity in human mGlu<sub>1</sub> at 10  $\mu$ M for the aromatic amine library, analogs **3.114-3.162**. Calcium mobilization was used to obtain %Glu<sub>Max</sub> values for each compound in the presence of a submaximal concentration of glutamate (EC<sub>20</sub>) in cell lines expressing human mGlu<sub>1</sub>. Data represent the mean  $\pm$  S.E.M. of at least three replicate experiments with similar results.

**Table 3.5.** Structures of the aromatic amine library analogs **3.114-3.162** and associated PAM activity from the single point screening at 10  $\mu$ M in human mGlu<sub>1</sub>. Calcium mobilization responses for each compound are reported as a percentage of the maximum glutamate response. VU number denotes the compound identifier assigned by Vanderbilt University. Data represent the mean  $\pm$  S.E.M. of at least three replicate experiments with similar results.

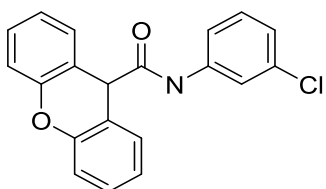
Structure	Cpd #	VU #	hmGlu <sub>1</sub> %Glu <sub>Max</sub>
	<b>3.114</b>	VU6005359	22.5 $\pm$ 3.9
	<b>3.115</b>	VU0056706	4.6 $\pm$ 3.2
	<b>3.116</b>	VU0001272	13.0 $\pm$ 2.9



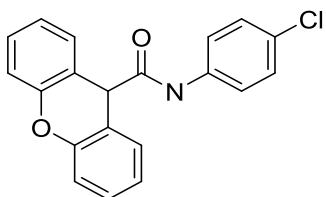
**3.117** VU0357322 16.4±3.3



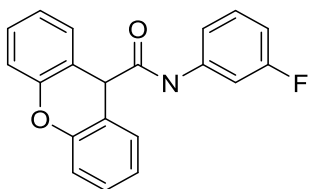
**3.118** VU0001277 10.0±1.8



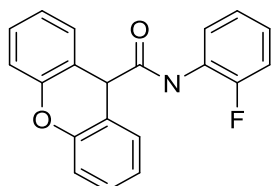
**3.119** VU0001321 8.9±2.7



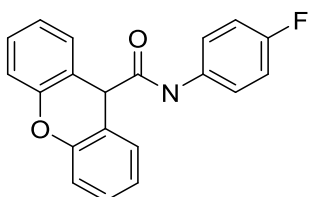
**3.120** VU6005360 8.9±3.8



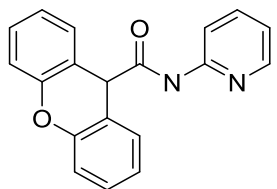
**3.121** VU0357879 16.0±2.2



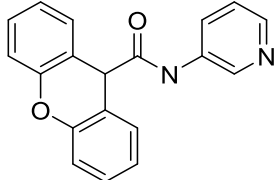
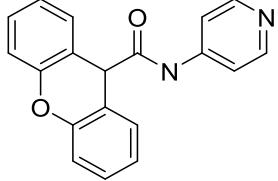
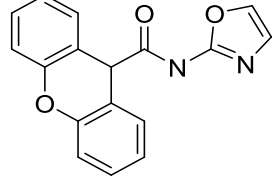
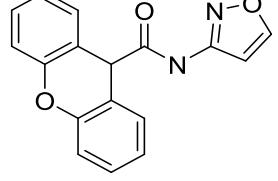
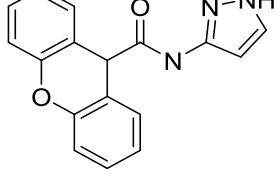
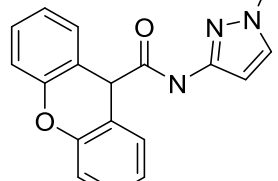
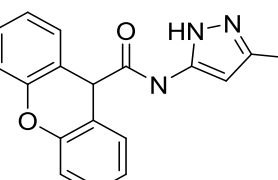
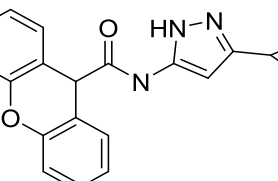
**3.122** VU6005361 9.6±2.8



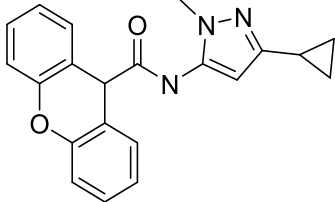
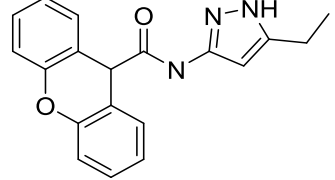
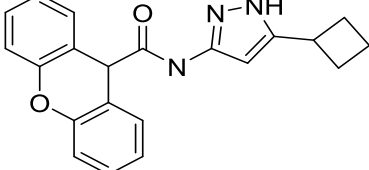
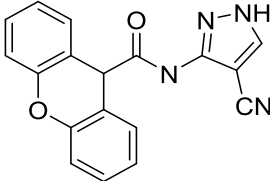
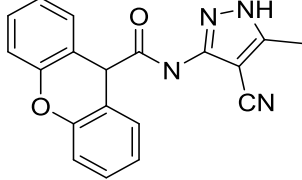
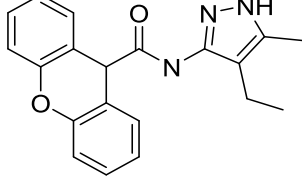
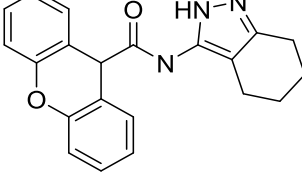
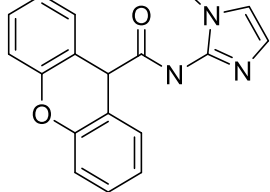
**3.123** VU0001320 12.8±3.4

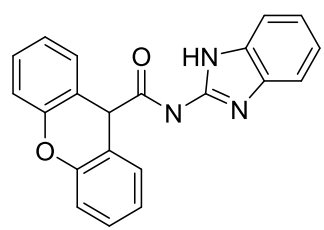
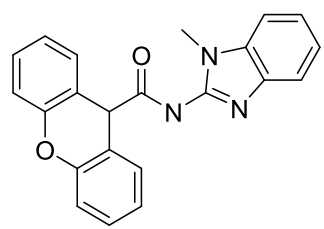
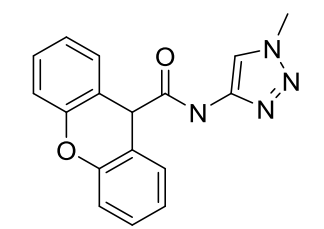
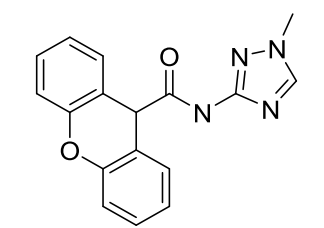
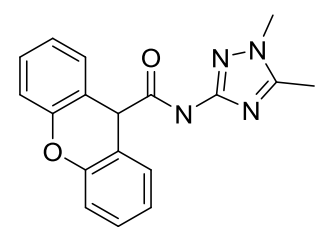
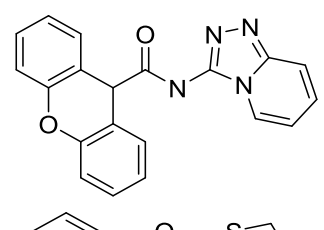
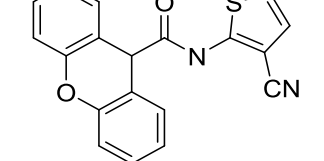


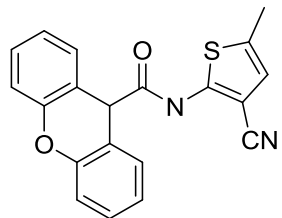
**3.124** VU0033100 47.7±1.9

	<b>3.125</b>	VU0032962	16.1±2.8
	<b>3.126</b>	VU0189388	13.5±1.6
	<b>3.127</b>	VU6000807	78.9±15.5
	<b>3.128</b>	VU6000802	29.2±6.3
	<b>3.129</b>	VU6000776	30.8±10.0
	<b>3.130</b>	VU6000800	25.9±5.9
	<b>3.131</b>	VU6000783	17.0±5.2
	<b>3.132</b>	VU6000782	8.8±2.3

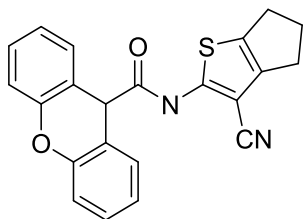


	<b>3.133</b>	VU6000781	20.1±0.1
	<b>3.134</b>	VU6000792	9.4±1.9
	<b>3.135</b>	VU6000793	4.1±1.0
	<b>3.136</b>	VU6000777	15.6±4.3
	<b>3.137</b>	VU6000784	9.9±2.2
	<b>3.138</b>	VU6000791	17.2±6.6
	<b>3.139</b>	VU6000785	17.3±7.9
	<b>3.140</b>	VU6000797	8.0±2.3

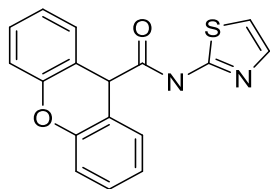
	<b>3.141</b>	VU6000786	20.1±3.5
	<b>3.142</b>	VU6000803	10.2±5.3
	<b>3.143</b>	VU6000806	13.9±4.6
	<b>3.144</b>	VU6000795	25.7±3.1
	<b>3.145</b>	VU6000796	6.4±1.0
	<b>3.146</b>	VU6000778	20.5±10.5
	<b>3.147</b>	VU6000805	10.8±5.7



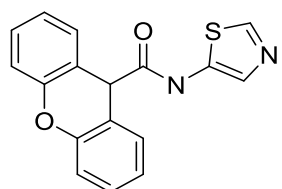
**3.148** VU6000804 5.5±3.7



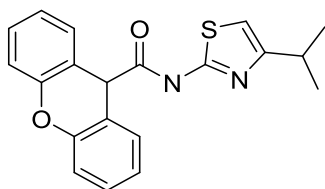
**3.149** VU6000789 9.2±5.1



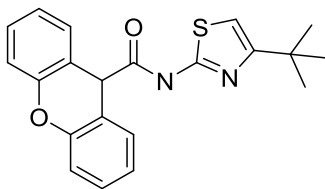
**3.150** VU6000787 88.0±5.4



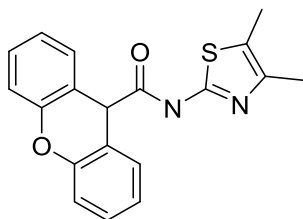
**3.151** VU6000774 54.2±5.2



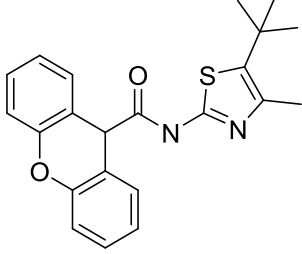
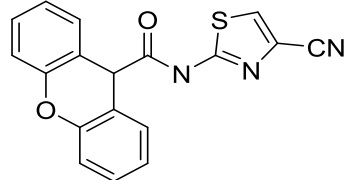
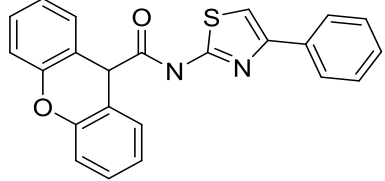
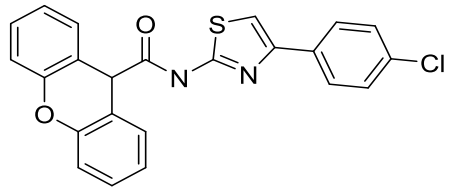
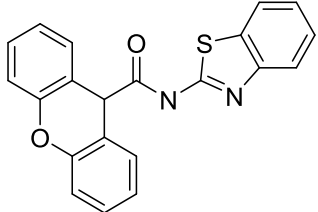
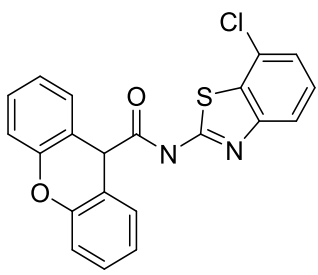
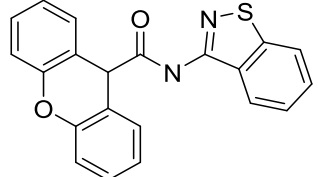
**3.152** VU6000790 60.0±4.9

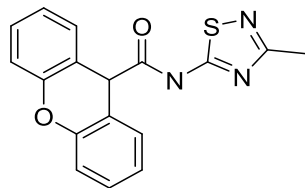


**3.153** VU6000788 28.5±8.3

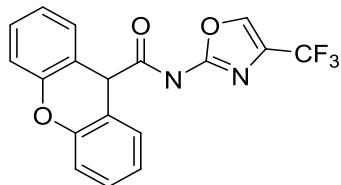


**3.154** VU6000801 68.0±15.7

	<b>3.155</b>	VU6000794	1.1±0.3
	<b>3.156</b>	VU6000799	98.0±23.0
	<b>3.157</b>	VU6005362	20.0±2.4
	<b>3.158</b>	VU0068341	13.9±2.6
	<b>3.159</b>	VU0029218	58.2±3.9
	<b>3.160</b>	VU6000775	11.1±2.6
	<b>3.161</b>	VU6000779	24.7±1.4



**3.162** VU6000798 102.7±15.3

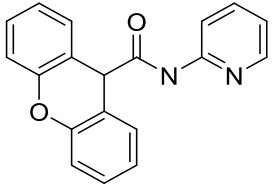
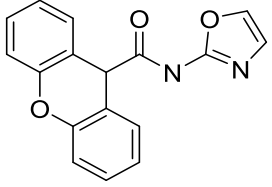
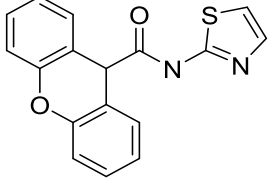
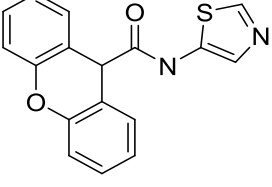
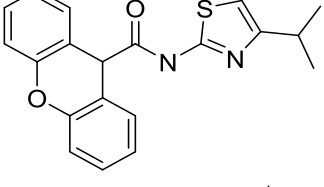
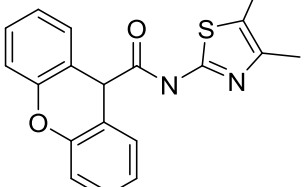


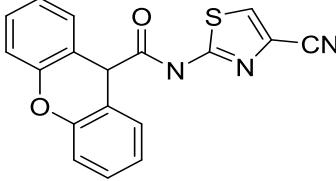
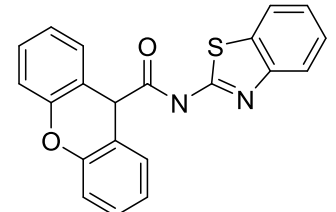
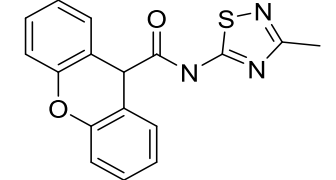
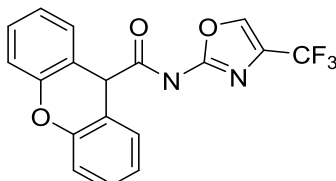
**3.43** RO 07-11401 90.7±7.2

---

The compounds that potentiate the glutamate response were assayed to obtain a concentration-response curve (CRC) and to determine their EC<sub>50</sub> in human and rat mGlu<sub>1</sub> (Table 3.6). Here, the 2-aminopyridine **3.124** demonstrated to have relatively good potency but with low efficacy. In this screening mode, the 2-aminothiazole **3.150** differentiated well from the 2-aminooxazole **3.127** and the 5-aminothiazole **3.151**, showing an EC<sub>50</sub> close to 1 μM and the latter two being only weak activators with potencies above 10 μM. The double substitution of the thiazole was confirmed to be detrimental for mGlu<sub>1</sub> activity even with small substituents (**3.154**) or in the case of fused aminobenzothiazole (**3.159**). The introduction of the additional nitrogen in the aminothiadiazole (**3.162**) produced a decrease of almost 2-fold in potency with respect to the aminothiazole. From this series, the most active compounds proved to be the 4-substituted 2-aminothiazole analogs **3.152** and **3.156**, with both compounds possessing an mGlu<sub>1</sub> EC<sub>50</sub> below 1 μM. In our screening, Ro 07-11401 **3.43** proved to be far less potent than the reported values; however, the compound is still close to 3-fold more potent than our most potent hits.

**Table 3.6.** Potencies in human and rat mGlu<sub>1</sub> for the active compounds obtained from the aromatic amine libraries single point screen. Calcium mobilization responses for each compound are reported as a percentage of the maximum glutamate response. VU number denotes the compound identifier assigned by Vanderbilt University. Data represent the mean  $\pm$  S.E.M. of at least three independent experiments with similar results. ND, not determined.

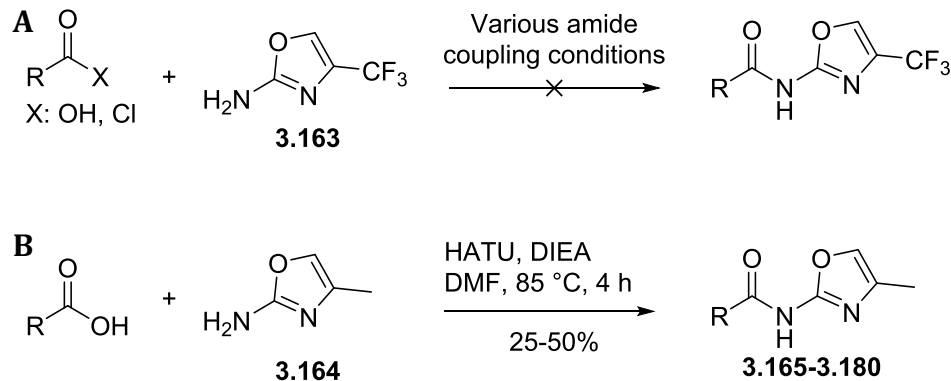
Structure	Cpd #	VU #	hmGlu <sub>1</sub>		rmGlu <sub>1</sub>	
			EC <sub>50</sub> ( $\mu$ M)	%Glu Max	EC <sub>50</sub> ( $\mu$ M)	%Glu Max
	<b>3.124</b>	VU0033100	1.68	59	ND	ND
	<b>3.127</b>	VU6000807	>10.0	79	ND	ND
	<b>3.150</b>	VU6000787	1.41	75.0	3.67	82
	<b>3.151</b>	VU6000774	>10.0	54	ND	ND
	<b>3.152</b>	VU6000790	0.901	90	2.39	111
	<b>3.154</b>	VU6000801	>10.0	68	---	---

	<b>3.156</b>	VU6000799	0.711	110	1.84	124
	<b>3.159</b>	VU0029218	4.77	97	---	---
	<b>3.162</b>	VU6000798	2.69	101	3.62	82
	<b>3.43</b>	RO 07-11401	0.246	96	0.277	109

Compounds **3.152** and **3.156** demonstrated to be active across species as they can potentiate the glutamate response of the rat form of the receptor; however, their  $EC_{50}$ s showed a close to 2-fold decrease with respect to human  $mGlu_1$  potency. It is worth mentioning that these PAMs showed an important increase in efficacy when screened in the rat receptor and this causes an apparent shift to the right in the concentration-response curve and its inflexion point, increasing the  $EC_{50}$ .

To explore the SAR around the xanthene moiety, we attempted to prepare new amides keeping constant the 2-amino-4-trifluoromethyloxazole moiety from Ro 07-11401 **3.43**. After the use of different amide coupling conditions, using carboxylic acid and coupling reagents or using acyclic chlorides, we were able to obtain only one product, the fluorencarboxylic acid analog using PyClU as amide coupling reagent and heating in the microwave for 20 minutes at 120 °C (Scheme 3.2A). This molecule demonstrated to be a weak activator with potency over 10  $\mu$ M and

efficacy of 56% of Glu<sub>Max</sub>. This reaction did not allow us to obtain more analogues, probably due to the poor nucleophilicity of the 2-amino-4-trifluoromethyl **3.163**.



**Scheme 3.2.** Synthesis of xanthene replacements library, analogs **3.165-3.180**.

In the report from the discovery of Ro 07-11401 **3.43**, the authors claimed that the 4-methylaminooxazole variant had similar mGlu<sub>1</sub> PAM activity;<sup>281</sup> thinking this could be beneficial for our chemistry, we proceeded to prepare the library of xanthene replacements using this amine piece (Scheme 3.2B). The 2-amino-4-methyloxazole **3.164** allowed us to obtain products for this reaction (**3.165-3.180**); although, yields were generally low. In this library, we assayed different strategies to replace the xanthene, such as elimination of rings (**3.165** and **3.166**), different fused rings (**3.167-3.177**) and ring opening (**3.178-3.180**). The compounds obtained from this library were screened in calcium mobilization assay in single point concentration mode at 10  $\mu$ M and we found that none of the replacement strategies was successful to produce an active mGlu<sub>1</sub> PAM (Fig. 3.10).



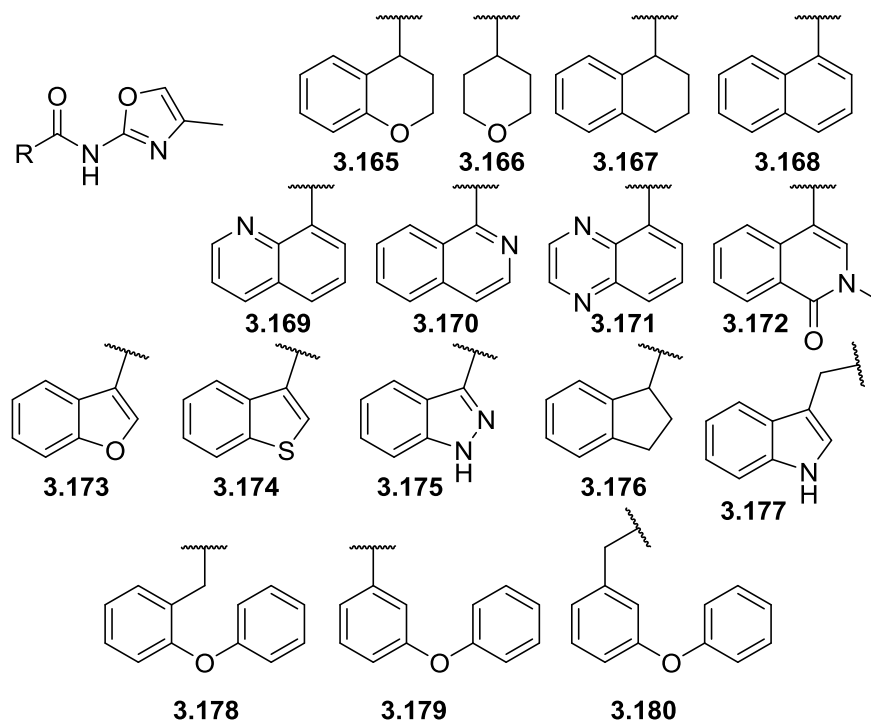


**Figure 3.10.** Xanthene replacements that yield inactive compounds for mGlu<sub>1</sub> PAM activity, analogs **3.165-3.180**.

After finding a very steep SAR in the xanthene moiety of the scaffold, it was decided to move forward with the characterization of VU6000790 **3.152** and VU6000799 **3.156**. The biological activity of these two compounds was analyzed in a fold-shift paradigm, using a fixed single concentration of the mGlu<sub>1</sub> PAMs and a full concentration-response curve of glutamate. This method allowed us understanding how the compounds affected the sensitivity and efficacy of the receptor towards glutamate. From this study, it was observed that the PAMs potentiate the glutamate response, increasing the potency of glutamate for the receptor and also the maximal response obtained (Fig. 3.11). The increase in fold-shift is correlated to the potency of the compounds, being Ro 07-11401 the one that induced the largest leftward shift of the CRC (6.6-fold decrease in EC<sub>50</sub>), while for VU6000790 **3.152** and VU6000799 **3.156** the fold-shift was 4.5 and 5.7, respectively. In contrast, the efficacy of the receptor was enhanced more with

compounds **3.152** and **3.156** than with Ro 07-11401, increasing the efficacy of the receptor signal to almost 115%  $\text{Glu}_{\text{Max}}$  (Table 3.7).

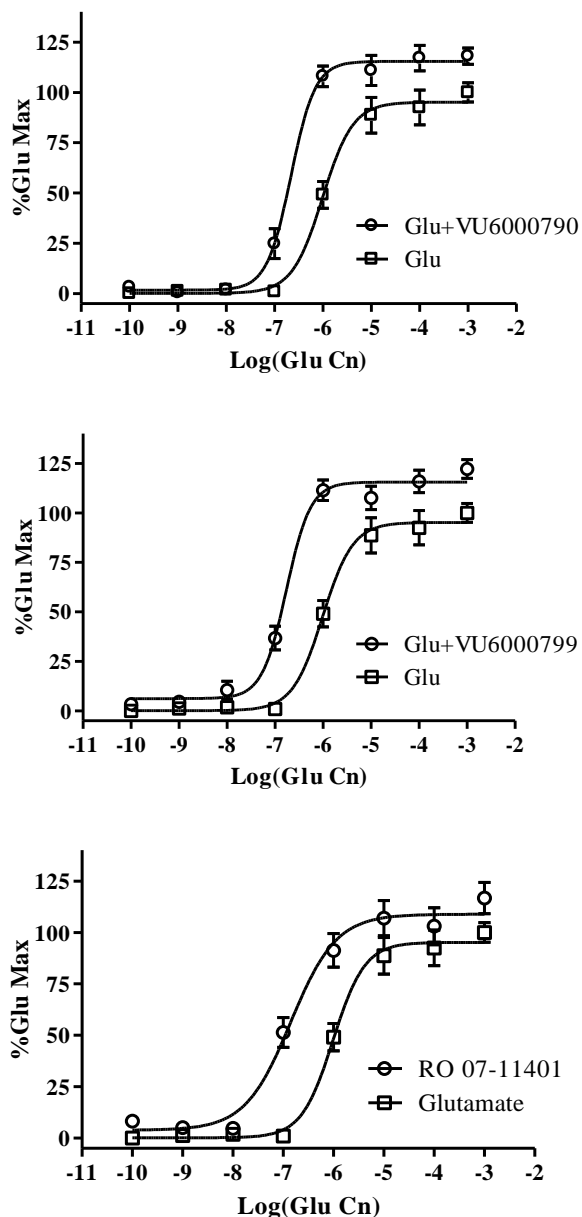


**Figure 3.11.** Glutamate concentration-response curve fold-shift experiments for compound VU6000790 **3.152**, VU6000799 **3.156** and Ro 07-11401 **3.43**. TR-Ex 293 cells expressing human  $\text{mGlu}_1$  were employed in calcium mobilization studies to obtain glutamate CRC in the presence of vehicle or 10  $\mu\text{M}$  concentration of compound. Data represent the mean  $\pm$  S.E.M. of at least three independent experiments with similar results.

**Table 3.7.** Effect of the VU6000790 **3.152**, VU6000799 **3.156** and Ro 07-11401 **3.43** at 10  $\mu$ M in the potency and efficacy of glutamate in the human mGlu<sub>1</sub> receptor in a fold-shift experiment. Data represent the mean  $\pm$  S.E.M. of at least three independent experiments with similar results.

	Glutamate	VU6000790	VU6000799	Ro 07-11401
Top	95.2	115	116	109
EC <sub>50</sub> (nM)	983	219	172	141
Fold-shift	---	4.48	5.72	6.59

The introduction of the thiazole in these molecules might be beneficial to their pharmacokinetic properties, as it is observed that the thiazole is more soluble in water and can increase free fraction unbound and decreased clearance with respect to the oxazole version (Table 3.8). Compounds VU6000790 **3.152** and VU6000799 **3.156** displayed an improvement in the human microsomal stability with respect to Ro 07-11401 **3.43**; however, this did not translate to a slower predicted rat hepatic clearance, which was our main driver for the development of a chemical probe for target validation studies. With respect to P450 inhibition, **3.152** and **3.156** caused inhibition of CYP2C9, but in less extent compared with Ro 07-11401 **3.43**, and **3.156** showed strong inhibition also in CYP1A2.

VU6000799 **3.156**, showed a slight increase in free fraction in rat and human plasma, as well as in rat brain homogenate, while a considerable decrease was observed for VU6000790 **3.152**. This is related to the polarity of the molecule, and it can be associated to a higher logP due to the presence of the isopropyl group in VU6000790 **3.152** (clogP = 4.53; TPSA: 51.2), with respect to VU6000799 **3.156** (clogP = 3.25; TPSA = 75.0).

Finally, the property that was affected dramatically with **3.152** and **3.156** was the brain:plasma concentration coefficient ( $K_p$ ). After intravenous administration of the PAMs, the CNS penetration was evaluated and it was found that **3.152** and **3.156** diffused freely into the brain with  $K_p$  close to the unity. The unbound concentrated partition coefficient was also

calculated. The  $K_{p,uu}$  values confirmed the superiority of **3.15** and **3.16** with respect to the Roche analog, in terms of exposure of the probes to the target in the brain. The unbound coefficient is also a differentiating factor between **3.15** and **3.16**, as  $K_{p,uu}$  is almost 8-fold higher in the case of the latter. This represents a significant improvement for this scaffold and it could pave the way to better analogs in this class.

**Table 3.8.** *In vitro* pharmacokinetic characterization and brain penetrance evaluation of VU6000790 **3.152**, VU6000799 **3.156** and Ro 07-11401 **3.43**.

Parameter	VU6000790	VU6000799	Ro 07-11401
clogP	4.53 (TPSA: 51.2)	3.25 (TPSA: 75.0)	3.75 (TPSA: 64.4)
Hum $Cl_{int}$ (mL/min/kg)	59.0	18.6	262
Hum $Cl_{hep}$ (mL/min/kg)	15.5	9.85	19.4
Rat $Cl_{int}$ (mL/min/kg)	753	560	661
Rat $Cl_{hep}$ (mL/min/kg)	64.0	62.2	63.3
Hum $F_u$ plasma	0.001	0.027	0.014
Rat $F_u$ plasma	0.002	0.005	0.003
Rat $F_u$ brain	0.001	0.017	0.001
P450 $IC_{50}$ ( $\mu$ M)			
1A2 2C9	19.3 2.0	2.9 2.9	13 0.6
2D6 3A4	26.5 >30	10.3 >30	>30 >30
$K_p$ (0.25 mg/kg IV , 0.25 h)	1.01	1.19	0.29
$K_{p,uu}$	0.51	4.05	0.10

#### *Computational efforts to optimize Ro 07-11401*

In order to find an improved replacement to the xanthene group in Ro 07-11401 and to develop an mGlu<sub>1</sub> PAM with good potency and pharmacokinetic characteristics, we started a

virtual screening campaign in collaboration with Alexander Geanes, a member from the Jens Meiler laboratory.

Some amino acid residues that interact with the PAMs produced by Roche have been identified and an X-ray crystal structure of the transmembrane domain of human mGlu<sub>1</sub> has been obtained. These data provided preliminary information that could aid an attempt at a structure-based design strategy, though it does not provide information of the binding pose of the ligand in the receptor, or the actual conformation of the protein when the ligand is bound. Furthermore, the published mGlu<sub>1</sub> structure was crystallized in the presence of a negative allosteric modulator, and it probably reflects an inactive conformation of the receptor which would be different from the one that would be produced upon binding of a PAM. Therefore, we decided to carry on a ligand-base design effort.

We envisioned a ligand-centric approach with different filters that could provide reasonable structures that allow getting a handle of compounds with mGlu<sub>1</sub> PAM activity and without the xanthene ring system (Fig. 3.12). In this approach we planned to start with a large library of compounds, submit them to a first screening round based on neural network models trained to identify mGlu<sub>1</sub> PAMs versus inactive compounds generated using available mGlu<sub>1</sub> PAM activity data, submit the top hits from this model into a second round of screening using a SurflexSim model, and finally evaluate the synthetic feasibility to obtain the top hit compounds. After every screening round, we performed visual inspection of the hits to avoid duplicates and to also remove structures with undesired features that we were not able to filter out with automated curation of the data sets.



**Figure 3.12.** Flow diagram of the ligand-based approach to improve the properties of Ro 07-11401.

We prepared our screening library by performing an *in silico* amide coupling between 2-amino-4-trifluoromethyloxazole and the carboxylic acids available in eMolecules (approx. 83000). This would allow for the exploration of chemical diversity on the xanthene side, while the oxazole would facilitate finding mGlu<sub>1</sub> PAM active compounds. The library was then curated with a pan-assay interference compound (PAINS) and rapid elimination of swill (REOS) filters to remove structures with undesired reactive features, to afford a set of 44109 compounds.

The neural network models were built with mGlu<sub>1</sub> PAM activity data taken from Roche papers (all compounds sharing a similar scaffold with Ro 07-11401) and the analogs from our libraries. Overall the data set presents 55 actives ( $EC_{50} < 10 \mu\text{M}$ ) and 220 inactives ( $EC_{50} > 10 \mu\text{M}$ ) compounds. For this model, the two-dimensional chemical structure is converted into a set of numerical descriptors that act as a fingerprint for each molecule. The neural network models are trained to recognize features of fingerprints that indicate a compound is mGlu<sub>1</sub> PAM active versus one that is inactive. Model performance was evaluated using a cross-validation procedure where the model predicts biological activities on a portion of the data that was not used for training. This approach provided a way of approximating how well the model will recognize the active from inactive compounds on new data. Our model demonstrated the ability to differentiate active mGlu<sub>1</sub> PAMs over inactive ones at a rate substantially higher than random chance, as the calculated area under the receiver-operator characteristic (ROC) curve was 0.92 (perfect model=1.0, random chance=0.5) (Fig. 3.13).

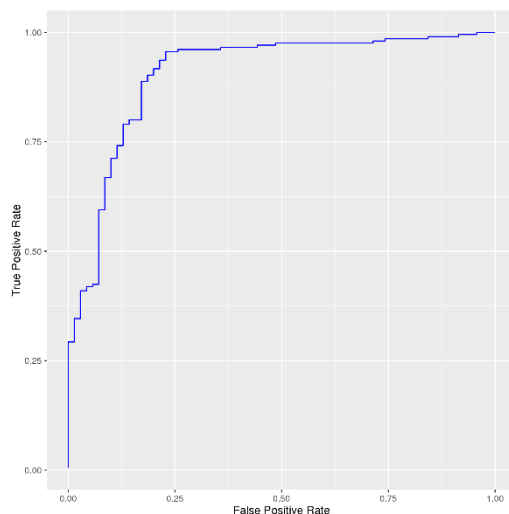


**Figure 3.13.** Machine-learning neural network model performance. Area under the curve: 0.92 (perfect model=1.0, random chance=0.5), average enrichment (up to 0.10 FPR): 2.26 (random chance=1.0).

Our *in silico* compound library was analyzed using the machine-learning neural network model, and the fit of the compounds was scored. The results for the screening were clustered by structure similarity and representative examples of each class were selected. From this, the top 100 hits were visually inspected and we chose the 85 hits to advance to the next filter step with a three dimensional model. The Surfex-Sim model<sup>284</sup> was produced employing the most active mGlu<sub>1</sub> PAMs in the literature, compound Ro 07-11401 **3.43** and Ro 67-4853 **3.45**. Using this template, the hits from the previous model were screened. The molecules were scored based on the similarity of the query molecules to the template molecules. Using these results, we chose 15 compounds from this set based on their score and synthetic feasibility. We proceeded to synthesize these compounds, but again the 2-amino-4-trifluoromethyloxazole presented problems for the amide coupling. Instead, we decided to use the 4-methyl version **3.164** as we did previously, and were able to obtain the desired amide products **3.181-3.195** (Fig. 3.14). These compounds were analyzed in a calcium mobilization assay at a concentration of 10  $\mu$ M, but none of them potentiated an EC<sub>20</sub> of glutamate in the mGlu<sub>1</sub> receptor.

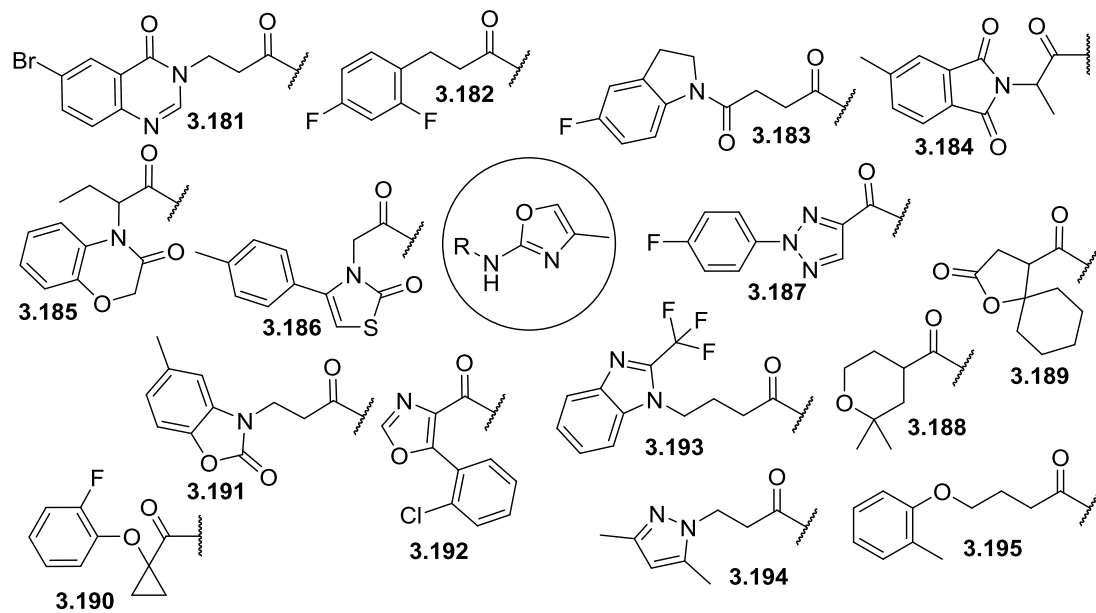


**Figure 3.14.** Synthesized virtual screening hits, analogs 3.181-3.195.



## Summary and future directions

We have tried to optimize Ro 07-11401, a potent and selective mGlu<sub>1</sub> PAM with a poor pharmacokinetic profile for a chemical probe to be used in target validation studies in neurosciences. We explored the amine region and the acid region of this amide and generated several libraries. The SAR around this scaffold proved to be steep, and it was shown that only thiazole analogs maintain some activity, being the most relevant VU6000790 **3.152** and VU6000799 **3.156** (Fig. 3.15). These compounds have submicromolar potency, and even when they showed a decrease in potency with respect to Ro 07-11401, they increased approximately 5-fold the sensitivity of mGlu<sub>1</sub> towards glutamate, along with raising considerably its maximal response.

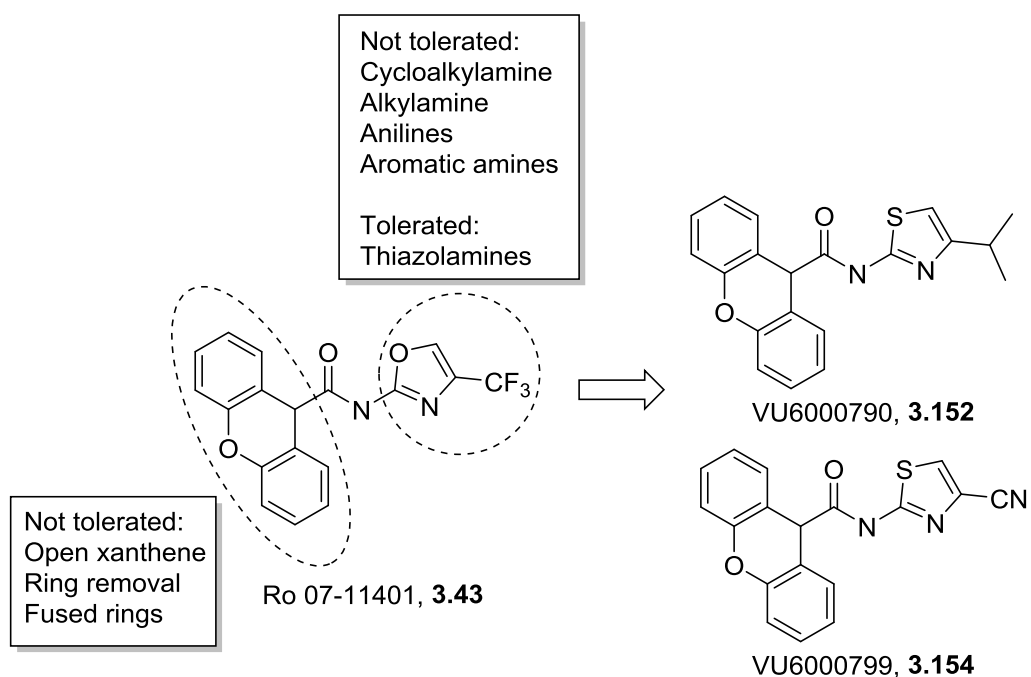


**Figure 3.15.** Summary of the results of the structure-activity relationship study around Ro 07-11401 **3.43**.

The study of the pharmacokinetic properties of these compounds showed that despite still having a high clearance, they can diffuse freely into the CNS with a brain to plasma partition

coefficient close to one. This is the most relevant feature denoted from our SAR studies, as the use of the thiazole might prove useful if it can be introduced in a molecule with improved potency.

Our computational efforts to provide a better compound, in terms of stability, were hindered by the production of only inactive analogs. At this point, it is clear that the model needs further improvement. The introduction of the new generated data to retrain the model and a successful synthesis methodology that allows obtaining the trifluoromethyl analogs of the compounds tested, are potential actions that could improve our results.

## EXPERIMENTAL METHODS

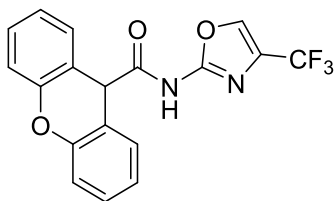
### *General chemical synthesis and characterization*

All reactions were carried out employing standard chemical techniques under inert atmosphere. All reagents and solvents were commercial grade and purified prior to use when necessary. Solvents used for extraction, washing, and chromatography were HPLC grade. Analytical thin layer chromatography was performed on 250  $\mu\text{m}$  silica gel glass backed plates from Sorbent Technologies. Visualization was accomplished with UV light and/or the use of iodine or ninhydrin solution followed by heating. Analytical HPLC was performed on an Agilent 1200 LCMS with UV detection at 215 and 254 nm along with ELSD detection and electrospray ionization, with all final compounds showing >95% purity and a parent mass ion consistent with the desired structure. Low resolution mass spectra were obtained on an Agilent 6130 mass spectrometer with electrospray ionization source. MS parameters were as follows: fragmentor: 100, capillary voltage: 3000 V, nebulizer pressure: 40 psig, drying gas flow: 11 L/min, drying gas temperature: 350 °C. Samples were introduced via an Agilent 1200 HPLC comprised of a degasser, G1312A binary pump, G1367B HP-ALS, G1316A TCC, G1315D DAD, and a Varian 380 ELSD. UV absorption was generally observed at 215 nm and 254 nm with a 4 nm bandwidth. Column: Thermo Accucore C18, 2.1 x 30 mm, 2.6  $\mu\text{m}$ . Gradient conditions: 7% to 95%  $\text{CH}_3\text{CN}$  in  $\text{H}_2\text{O}$  (0.1% TFA) over 1.6 min, hold at 95%  $\text{CH}_3\text{CN}$  for 0.35 min, 1.5 mL/min, 45 °C. Flash column chromatography was performed on a Teledyne ISCO Combiflash Rf system. Preparative purification of library compounds was performed on a Gilson 215 preparative LC system. Column: Thermo Accucore C18, 2.1 x 30 mm, 2.6  $\mu\text{m}$ . Gradients condition: variable,  $\text{CH}_3\text{CN}$  in  $\text{H}_2\text{O}$  (0.1% TFA) over 4 minutes, hold at 95%  $\text{CH}_3\text{CN}$  for 0.35 min, 50 mL/min. Purity for all final compounds was >95%, and each showed a parent mass ion consistent with the desired structure in low resolution LC-MS.  $^1\text{H}$  and  $^{13}\text{C}$  NMR spectra were recorded on Bruker DRX-400 (400 MHz) instrument. Chemical shifts are reported in ppm relative to residual solvent

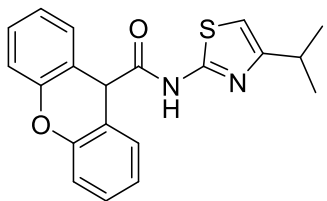
peaks as an internal standard at the following chemical shifts ( $^1\text{H}$  and  $^{13}\text{C}$  respectively): 7.26 and 77.0 ppm for  $\text{CDCl}_3$ ; 2.50 and 39.52 ppm for  $\text{DMSO}-d_6$ , 3.31 and 49.2 ppm for  $\text{CD}_3\text{OD}$ . Data are reported as follows: chemical shift, integration, multiplicity (s = singlet, d = doublet, t = triplet, q = quartet, dd = doublet of doublets, br = broad, m = multiplet), coupling constant (Hz).

*General procedure for the synthesis of amine library analogs 3.49-3.162*

In a vial, 9*H*-xanthene-9-carboxylic acid (**3.48**, 25 mg, 0.111 mmol) was added and dissolved in 1 mL of a mixture of dichloroethane (DCE) and *N,N*-diisopropylethylamine (DIEA) (9:1). 1-[Bis(dimethylamino)methylene]-1*H*-1,2,3-triazolo[4,5-*b*]pyridinium 3-oxide hexafluorophosphate (HATU) (46 mg, 0.122 mmol, 1.1 equivalents) was added to the vial and the reaction was stirred for five minutes. Then, the amine (0.122 mmol, 1.1 equivalents) was added. The reaction was stirred for 2 hours at room temperature; completion and formation of the desired product were confirmed by LC-MS monitoring. The reaction was worked up by addition of water and extractions with DCM (thrice). The organic phases were combined, filter through a phase separator and the volatiles were evaporated. The crude was dissolved in DMSO and purified by HPLC prep (C18 column, ACN in Water-TFA 0.1% gradient).

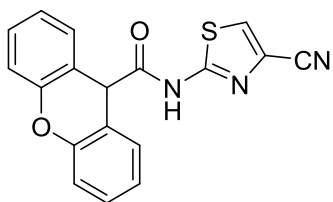


**Ro 07-11401, N-methyl-N-(4-(trifluoromethyl)oxazol-2-yl)-9*H*-xanthene-9-carboxamide (3.43).** Cream solid.  $^1\text{H-NMR}$  (400.1 MHz,  $\text{CDCl}_3$ )  $\delta$  (ppm): 7.89 (1H, s), 7.74 (1H, m), 7.35-7.47 (4H, m), 7.22 (2H, dd,  $J = 8.2$  Hz,  $J = 1.0$  Hz), 7.18 (2H, td,  $J = 7.5$  Hz,  $J = 1.1$  Hz), 5.20 (1H, s).  $^{13}\text{CNMR}$  (100.6 MHz,  $\text{CDCl}_3$ )  $\delta$  (ppm): 153.6, 150.8, 134.8, 130.2, 129.3, 124.2, 117.6, 116.5, 47.5.



**VU6000790, N-(4-isopropylthiazol-2-yl)-N-methyl-9H-xanthene-9-carboxamide**

**(3.152).** Pale yellow solid.  $^1\text{H-NMR}$  (400.1 MHz,  $\text{CDCl}_3$ )  $\delta$  (ppm): 7.44 (2H, d,  $J= 7.7$  Hz), 7.37 (2H, dd,  $J= 7.0$  Hz,  $J= 1.4$  Hz), 7.21 (2H, dd,  $J= 8.1$  Hz,  $J= 0.8$  Hz), 7.14 (2H, td,  $J= 7.5$  Hz,  $J= 1.1$  Hz), 6.51 (1H, s), 5.23 (1H, s), 2.91 (1H, heptet,  $J= 6.8$  Hz), 1.23 (6H, d,  $J= 6.8$  Hz).  $^{13}\text{CNMR}$  (100.6 MHz,  $\text{CDCl}_3$ )  $\delta$  (ppm): 169.6, 157.8, 151.1, 129.7, 129.3, 127.0, 123.9, 117.4, 117.2, 105.9, 46.7, 30.2, 21.9.



**VU6000799, N-(4-cyanothiazol-2-yl)-N-methyl-9H-xanthene-9-carboxamide (3.156).**

Pale yellow solid.  $^1\text{H-NMR}$  (400.1 MHz,  $\text{CDCl}_3$ )  $\delta$  (ppm): 7.62 (1H, s), 7.37-7.44 (4H, m), 7.24 (2H, d,  $J= 7.9$  Hz), 7.18 (2H, td,  $J= 7.5$  Hz,  $J= 1.1$  Hz), 5.23 (1H, s).  $^{13}\text{CNMR}$  (100.6 MHz,  $\text{CDCl}_3$ )  $\delta$  (ppm): 169.8, 158.1, 151.0, 130.2, 129.3, 125.5, 124.2, 121.8, 117.6, 116.5, 113.9, 46.6.

*General procedure for the synthesis of carboxylic acid library analogs 3.165-3.180 and hit compounds from virtual screening 3.181-3.195.*

In a vial, the carboxylic acid (0.1 mmol) was added and dissolved in 1 mL of a mixture of *N,N*-dimethylformamide (DMF) and DIEA (9:1). HATU (54.8 mg, 0.144 mmol, 1.2 equivalents) was added to the vial and the reaction was stirred for five minutes. Then, 2-amino-4-methyloxazole **3.164** (11.8 mg, 0.122 mmol, 1.2 equivalents) was added. The vial was closed and the reaction was stirred for 2 hours at 85 °C; completion and formation of the desired product

were confirmed by LC-MS monitoring. The reaction was worked up by the addition of water and extractions with DCM (thrice). The organic phases were combined, filter through a phase separator and the volatiles were evaporated. The crude was dissolved in DMSO and purified by HPLC prep (C18 column, ACN in Water-TFA 0.1% gradient).

### *Molecular pharmacology*

Tetracycline-tested fetal bovine serum (FBS) was purchased from Atlanta Biologicals (Lawrenceville, GA), and all other tissue culture reagents and Fluo-4-acetoxymethylester (Fluo-4-AM) were purchased from Life Technologies (Carlsbad, CA). Tetracycline hydrochloride (Sigma), L-glutamic acid (Tocris, Minneapolis, MN).

**Cell Culture.** Tetracycline-inducible rat and human mGlu<sub>1</sub> WT T-REx<sup>TM</sup>-293 cells<sup>112</sup> were cultured at 37 °C in Dulbecco's Modified Eagle Medium (DMEM) growth medium containing 10% Tet-tested FBS, 2 mM L-glutamine, 20 mM HEPES, 0.1 mM non-essential amino acids, 1 mM sodium pyruvate, antibiotic/antimycotic, 100 µg/mL hygromycin and 5 µg/mL blasticidin in the presence of 5% CO<sub>2</sub>.

**Poly-D-lysine plate coating.** A stock solution of poly-D-lysine hydrobromide (Sigma P7886) at a concentration of 1 mg/mL was prepared using sterile deionized water, and filtering through a 0.22 µm in the cell culture hood. The solution was aliquoted and stored at -20 °C, and on the day of use the solution was thawed and diluted with sterile water to 100 µg/mL. 96-well black wall, clear bottom plate, sterile (Costar 3603) were coated using 50 µL of the poly-D-lysine work solution. The plate was placed in the cell incubator for 3 hours at 37 °C. After this time, the poly-D-lysine solution excess was removed, and the plates were gently washed twice with 100 µL/well of sterile water. The plates were stored at 2-8 °C.

**Calcium Mobilization Assay.** To determine the potency of the mGlu<sub>1</sub> PAMs in calcium assays, Ca flux was measured as previously described.<sup>112</sup> Briefly, the day before the assay, human or rat mGlu<sub>1</sub> T-REx<sup>TM</sup>-293 cells were plated in black-walled, clear-bottomed, poly-D-lysine coated 96-well plates at 80,000 cells/100  $\mu$ L assay medium (DMEM supplemented with 10% dialyzed FBS, 20 mM HEPES, and 1 mM sodium pyruvate) containing 50 ng/mL (human mGlu<sub>1</sub>) or 10 ng/mL (rat mGlu<sub>1</sub>) of tetracycline to induce mGlu<sub>1</sub> expression. The next day, media was removed and the cells were incubated with 50  $\mu$ L of 1.15  $\mu$ M Fluo-4 AM dye solution prepared in assay buffer (Hank's balanced salt solution, 20 mM HEPES, and 2.5 mM probenecid) for 45 min at 37 °C, the dye was removed and replaced with 45  $\mu$ L of assay buffer. Then, calcium flux was measured using Flexstation II (Molecular Devices, Sunnyvale, CA). The compounds or DMSO vehicle were added to cells and incubated for 2.5 min and an EC<sub>20</sub> concentration of glutamate was added and incubated for 1 min. An EC<sub>max</sub> concentration of glutamate was also added to cells that were incubated with DMSO vehicle to accurately calculate the EC<sub>20</sub> calcium response. Data were normalized by subtracting the basal florescent peak before EC<sub>20</sub> agonist addition from the maximal peak elicited by EC<sub>20</sub> agonist and PAMs. For the single point concentration screening, a single concentration of 10  $\mu$ M of compound in assay buffer was employed. For EC<sub>50</sub> determinations compounds were serially diluted at half log concentrations in DMSO and further diluted in assay buffer. Using GraphPad Prism 5.0, the concentration response curves were generated and the potencies of the mGlu<sub>1</sub> PAMs were determined using a four-parameter non-linear regression model. In the case of fold-shift assays, a 10  $\mu$ M solution of the compound in assay buffer was used, and instead of a fix concentration of glutamate, a serial dilution of glutamate was performed to generate concentration-response curves that were analyzed with GraphPad Prism 5.0 to obtain the EC<sub>50</sub> values for glutamate.

### Pharmacokinetic characterization

The *in vitro* DMPK assays, including those assessing hepatic microsomal intrinsic clearance ( $Cl_{int}$ ), cytochrome P450 inhibition, plasma protein binding (PPB) and brain homogenate binding (BHB) were performed as described previously.<sup>285</sup>

**Intrinsic clearance:** Human or rat hepatic liver microsomes (0.5 mg/mL) and 1  $\mu$ M test compound were incubated in 100 mM potassium phosphate pH 7.4 buffer with 3 mM  $MgCl_2$  at 37 °C with constant shaking. After a 5 min preincubation, the reaction was initiated by addition of NADPH (1 mM). The incubations, performed in 96-well plates, were continued at 37 °C under ambient oxygenation and aliquots (80  $\mu$ L) were removed at selected time intervals (0, 3, 7, 15, 25, and 45 min). Aliquots were taken and subsequently placed into a 96-well plate containing cold acetonitrile with internal standard (50 ng/mL carbamazepine), to promote protein precipitation. Plates were then centrifuged at 3000 rcf (4 °C) for 10 min, and the supernatant was transferred to a separate 96-well plate and diluted 1:1 with water for LC/MS/MS analysis. The *in vitro* half-life ( $t_{1/2}$ , min, Eq. 1), intrinsic clearance ( $Cl_{int}$ , mL/min/kg, Eq. 2) and subsequent predicted hepatic clearance ( $Cl_{hep}$ , mL/min/kg, Eq. 3) were determined employing the following equations:

$$t_{1/2} = \frac{\ln(2)}{k} \quad [3.1]$$

**Equation 3.1.** Determination of half-life.  $k$  represents the slope from linear regression analysis (% test compound remaining) in function of incubation time.

$$Cl_{int} = \frac{0.693}{t_{1/2}} \times \frac{mL \text{ incubation}}{mg \text{ microsomes}} \times \frac{45 \text{ mg microsomes}}{g \text{ liver}} \times \frac{20^a \text{ g liver}}{kg \text{ body weight}} \quad [3.2]$$

**Equation 3.2.** Determination of intrinsic clearance. <sup>a</sup>scale-up factor: 20 (human) or 45 (rat).



$$Cl_{hep} = \frac{Q_h \times Cl_{int}}{Q_h + Cl_{int}} \quad [3.3]$$

**Equation 3.3.** Determination of predicted hepatic clearance.  $Q_h$  represents hepatic blood flow: 21 mL/min/kg (human) and 70 mL/min/kg (rat).

**Plasma protein binding and homogenate brain binding.** Protein binding was determined in rat or human plasma via equilibrium dialysis employing single-use rapid equilibrium dialysis (RED) plates with inserts (ThermoFisher Scientific, Rochester, NY). Briefly, plasma (220  $\mu$ L) was added to the 96 well plate containing test compound and mixed thoroughly to a final compound concentration of 5  $\mu$ M. Subsequently, 200  $\mu$ L of the plasma-test compound mixture was transferred to the *cis* chamber (red) of the RED plate, with an accompanying 350  $\mu$ L of phosphate buffer (25 mM, pH 7.4) in the *trans* chamber. The RED plate was sealed and incubated 4 h at 37  $^{\circ}$ C with shaking. At completion, 50  $\mu$ L aliquots from each chamber were diluted 1:1 (50  $\mu$ L) with either plasma (*cis*) or buffer (*trans*) and transferred to a new 96 well plate, at which time ice-cold acetonitrile containing 50 ng/mL carbamazepine as internal standard (2 volumes) was added to extract the matrices. The plate was centrifuged (3000 rcf, 10 min) and supernatants transferred to a new 96 well plate. The sealed plate was stored at  $-20$   $^{\circ}$ C until LC/MS/MS analysis. Each compound was assayed in triplicate within the same 96-well plate. Fraction unbound in plasma was determined using the following equation:

$$f_u = \frac{Cn_{buffer}}{Cn_{plasma}} \quad [3.4]$$

**Equation 3.4.** Determination of fraction unbound in plasma.

Rat brain homogenate binding was determined through a similar methodology using RED plates, using brain homogenate instead of plasma. In this experiment, the compound was tested at a final concentration of 1  $\mu$ M. The brain preparation was obtained from naïve rat brains homogenized in Dulbecco's Phosphate Buffered Saline (DPBS) (1:3 brain:DPBS, w/w) using a

Mini-Bead Beater™ machine. Fraction unbound was determined using equation 3.4, but replacing the concentration in plasma for concentration in homogenate.

**LC/MS/MS Bioanalysis of Samples from Plasma Protein Binding and Intrinsic Clearance Assays.** Samples were analyzed on a Thermo Electron TSQ Quantum Ultra triple quad mass spectrometer (San Jose, CA) via electrospray ionization (ESI) with two Thermo Electron Accella pumps (San Jose, CA), and a Leap Technologies CTC PAL autosampler (Carrboro, NC). Analyses were separated by gradient elution on a dual column system with two Thermo Hypersil Gold (2.1 x 30 mm, 1.9 µm) columns (San Jose, CA) thermostated at 40°C. HPLC mobile phase A was 0.1% formic acid in water and mobile phase B was 0.1% formic acid in acetonitrile. The gradient started at 10% B after a 0.2 min hold and was linearly increased to 95% B over 0.8 min; hold at 95% B for 0.2 min; returned to 10% B in 0.1 min. The total run time was 1.3 min and the HPLC flow rate was 0.8 mL/min. While pump 1 ran the gradient method, pump 2 equilibrated the alternate column isocratically at 10% B. Compound optimization, data collection and processing was performed using Thermo Electron's QuickQuan software (v2.3) and Xcalibur (v2.0.7 SP1).

**Inhibition of P450 enzymes.** A cocktail of substrates for cytochrome P450 enzymes (1A2: Phenacetin, 10 µM; 2C9: Diclofenac, 5 µM; 2D6: Dextromethorphan, 5 µM; 3A4: Midazolam, 2 µM) were mixed for cocktail analysis. The positive control for pan-P450 inhibition (miconazole) was included alongside each test compound in analysis. A reaction mixture of 100 mM potassium phosphate buffer, pH 7.4, 0.1 mg/mL human liver microsomes (HLM) and substrate mix is prepared and aliquoted into a 96-deepwell block. Test compound and positive control (in duplicate) were then added such that the final concentration of test compound ranged from 0.1 – 30 µM. The plate was vortexed briefly and then pre-incubated at 37 °C while shaking for 15 minutes. The reaction was initiated with the addition of NADPH (1 mM final

concentration). The incubation continued for 8 min and the reaction was quenched by adding cold acetonitrile containing internal standard (50 nM carbamazepine) (2 volumes). The plate was centrifuged for 10 minutes (4000 rcf, 4°C) and the resulting supernatant diluted 1:1 with water for LC/MS/MS analysis. A 12 point standard curve of substrate metabolites over the range of 0.98 nM to 2000 nM was employed.

Samples were analyzed via electrospray ionization (ESI) on an AB Sciex API-4000 (Foster City, CA) triple-quadrupole instrument that was coupled with Shimadzu LC-10AD pumps (Columbia, MD) and a Leap Technologies CTC PAL auto-sampler (Carrboro, NC). Analytes were separated by gradient elution using a Fortis C18 3.0 x 50 mm, 3 µm column (Fortis Technologies Ltd, Cheshire, UK) thermostated at 40 °C. HPLC mobile phase A was 0.1% formic acid in water (pH unadjusted), mobile phase B was 0.1% formic acid in acetonitrile (pH unadjusted). The gradient started at 10% B after a 0.2 min hold and was linearly increased to 90% B over 1.2 min; held at 90% B for 0.1 min and returned to 10% B in 0.1 min followed by a re-equilibration (0.9 min). The total run time was 2.5 min and the HPLC flow rate was 0.5 mL/min. The source temperature was set at 500°C and mass spectral analyses were performed using multiple reaction monitoring (MRM), with transitions specific for each compound utilizing a Turbo-Ionspray® source in positive ionization mode (5.0 kV spray voltage).

The IC<sub>50</sub> values for each compound were obtained for the individual P450 enzymes by quantitating the inhibition of metabolite formation for each probe substrate. A 0 µM compound condition (or control) was set to 100% enzymatic activity and the effect of increasing test compound concentrations on enzymatic activity could then be calculated from the % of control activity. Curves were fitted using XLfit 5.2.2 (four-parameter logistic model, equation 201) to determine the concentration that produces half-maximal inhibition (IC<sub>50</sub>).

**Animal care and use** All animal study procedures were approved by the Institutional Animal Care and Use Committee and were conducted in accordance with the National Institutes

of Health regulations of animal care covered in Principles of Laboratory Animal Care (National Institutes of Health). All animals were group housed under a 12-hour light/dark cycle with food and water available *ad libitum*.

***In vivo* plasma and brain drug concentration measurements in rodents.** Compounds were formulated as 10% tween 80 micro suspensions in sterile water at the concentration of 1 mg/ml and administered intraperitoneally to male Sprague-Dawley rats weighing 225 to 250 g (Harlan, Inc., Indianapolis, IN) at the dose of 0.25 mg/kg. The rat blood and brain were collected at 0.25 hr. Animals were euthanized and decapitated, and the brains were removed, thoroughly washed in cold phosphate buffered saline and immediately frozen on dry ice. Trunk blood was collected in EDTA Vacutainer tubes, and plasma was separated by centrifugation and stored at -80 °C until analysis. Plasma was separated by centrifugation (4000 rcf, 4°C) and stored at -80 °C until analysis. On the day of analysis, frozen whole-rat brains were weighed and diluted with 1:3 (w/w) parts of 70:30 isopropanol:water. The mixture was then subjected to mechanical homogenation employing a Mini-Beadbeater™ and 1.0 mm Zirconia/Silica Beads (BioSpec Products) followed by centrifugation. The sample extraction of plasma (20 µL) or brain homogenate (20 µL) was performed by a method based on protein precipitation using three volumes of ice-cold acetonitrile containing an internal standard (50 ng/mL carbamazepine). The samples were centrifuged (3000 rcf, 5 min) and supernatants transferred and diluted 1:1 (supernatant:water) into a new 96 well plate, which was then sealed in preparation for LC/MS/MS analysis.

*In vivo* samples were analyzed via electrospray ionization (ESI) on an AB Sciex API-5500 QTrap (Foster City, CA) instrument that was coupled with Shimadzu LC-20AD pumps (Columbia, MD) and a Leap Technologies CTC PAL auto-sampler (Carrboro, NC). Analytes were separated by gradient elution using a Fortis C18 3.0 x 50 mm, 3 µm column (Fortis Technologies Ltd, Cheshire, UK) thermostated at 40 °C. HPLC mobile phase A was 0.1% formic

acid in water (pH unadjusted), mobile phase B was 0.1% formic acid in acetonitrile (pH unadjusted). The gradient started at 30% B after a 0.2 min hold and was linearly increased to 90% B over 0.8 min; held at 90% B for 0.5 min and returned to 30% B in 0.1 min followed by a re-equilibration (0.9 min). The total run time was 2.5 min and the HPLC flow rate was 0.5 mL/min. The source temperature was set at 500°C and mass spectral analyses were performed using multiple reaction monitoring (MRM), with transitions specific for each compound utilizing a Turbo-Ionspray® source in positive ionization mode (5.0 kV spray voltage). The calibration curves were constructed in blank plasma. All data were analyzed using AB Sciex Analyst software v1.5.1.

#### *Computational methods*

**QSAR models.** Artificial neural network (ANN) models were built to classify mGlu<sub>1</sub> PAMs over inactives using data available from in-house medicinal chemistry projects and from literature (gathered via the ChEMBL database).<sup>286</sup> Preprocessing the mGlu<sub>1</sub> PAM dataset involved associating the pEC<sub>50</sub> value with each structure, ensuring that only unique structures were present, and generating a single 3-dimensional conformation for each compound using CORINA version 3.60.<sup>287</sup> These structures were then encoded into a feature vector using the BioChemical Library which resulted in 1315 floating point values and encoded information such as the 2- and 3-dimensional distribution of charge, steric bulk, and polarizability.<sup>288</sup> The architecture of the ANNs consisted of a single hidden of 32 nodes, and a single-valued output layer, and used sigmoid transition functions. These models were trained using a binary-valued dataset in which the compounds were labeled as either mGlu<sub>1</sub> PAMs (pEC<sub>50</sub> > 5) or inactive (pEC<sub>50</sub> < 5). A five-fold cross-validation procedure using both monitoring and validation dataset and dropout were used to prevent overtraining. The cross-validation procedure also provided an unbiased way to evaluate model performance in the absence of additional data. This procedure

resulted in a total of 20 ANN models whose scores were averaged to provide a consensus score for each input for virtual screening.

**Compound generation.** An *in-silico* reaction-based approach was used to select possible replacements for the xanthene moiety. The eMolecules database was filtered for compounds containing single carboxylic acid or acyl chloride groups, and were converted to the corresponding trifluoromethyl oxazole-containing mGlu<sub>1</sub> PAM analogs through an *in-silico* amide coupling reaction using the BioChemical Library (BCL). This resulted in a total of 4250 candidate compounds which were then subjected to virtual screening.

**Initial compound selection.** The *in-silico* candidate compounds were prioritized using the ANN QSAR models described previously and the top compounds were visually inspected. The top compounds initially contained a substantial number of artifacts such as multiple fluorine atoms or other highly charged groups which were likely picked out as a result of an insufficient number of training examples to circumvent this problem. A comparison of histogram of scores between the generated compounds and the known mGlu<sub>1</sub> PAMs (Fig. 1.16) revealed that these compounds had artificially high scores relative to the training data. Therefore, only the compounds that had scores between 1.09 (lowest active score) and 4.42 (highest active score) were used. The top 10 percent of highest scoring compounds that fit these criteria were selected for further analysis.

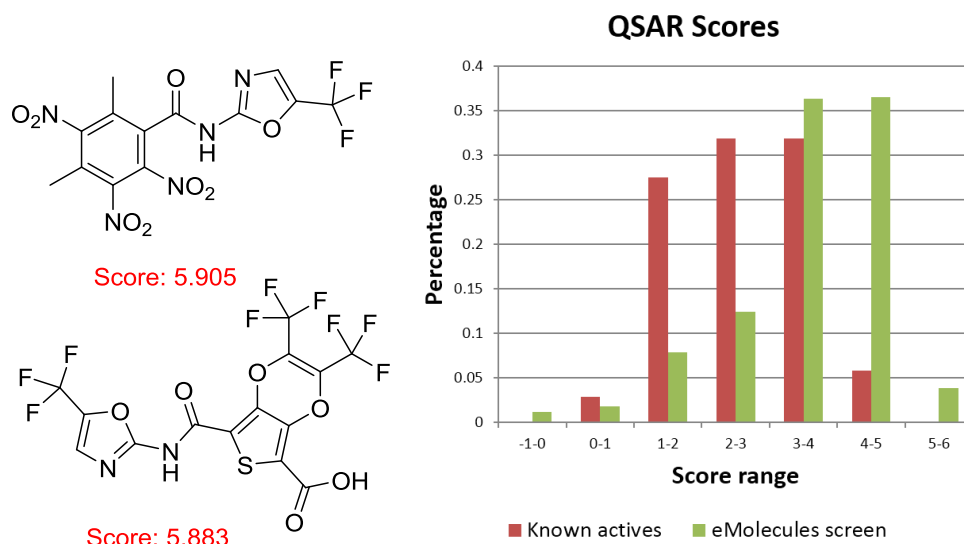


**Figure 3.16.** Initial compound selection from the virtual screening by the artificial neural network. Left, examples of compounds containing artifacts picked up by the ANN models. Right, a comparison of QSAR scores for known mGluR1 PAMs (red) and in-silico designed compounds (green).

**Clustering.** Clustering was performed using an in-house clustering algorithm to select a diverse set of compounds within the set of prioritized compounds. First, a random portion of the prioritized molecule data set is sampled. Murcko scaffolds are generated for each selected compound, and the maximum common substructure between each pair of Murcko scaffolds is calculated.<sup>289</sup> Ring and chain fragments from each scaffold are also added to supplement the fragment list. Fingerprint vectors of each compound of interest were computed by searching for the presence of each fragment in the query structure. A distance metric between pairs of compounds was calculated as the Tanimoto coefficient between fingerprint vectors and hierarchical agglomerative clustering was applied to the molecule data set using this distance metric.<sup>290</sup> Application of this clustering approach to the top 10 percent of the highest-scoring in-silico generated compounds resulted in 658 clusters at a Tanimoto similarity cutoff of 0.3. The top two compounds (or a single compound if the cluster was a singleton) were selected from each cluster, and the top 100 highest-scoring compounds from this set were visually inspected. Of

these compounds, 15 contained undesirable structures and were discarded. The remaining 85 compounds were used in further processing steps.

**SurflexSim model.** The Surflex-Sim program<sup>284</sup> was used to generate binding hypotheses and perform shape-based virtual screening for prioritizing mGlu<sub>1</sub> PAM compounds in a ligand-based manner. Two compounds were chosen to model the xanthene-containing compounds, namely Ro 67-4853 **3.45** and Ro 07-11401 **3.43**. Both compounds contained a xanthene ring, but differed at the terminal end and contained a propylcarbamate or a 4-trifluoro-2-oxazole, respectively. These compounds were aligned with the Surflex-Sim mutual alignment algorithm using default parameters with the exception of allowing ring flexibility. The highest-scoring hypothesis (Fig. 1.17) was used to align desired compounds picked using machine learning QSAR models and further reduce the 85 selected compounds from the machine learning models to 15 through a combination of score consideration and visual inspection. The corresponding carboxylic acids from these compounds were then identified and purchased to enable synthesis and experimental testing of the resulting compounds.

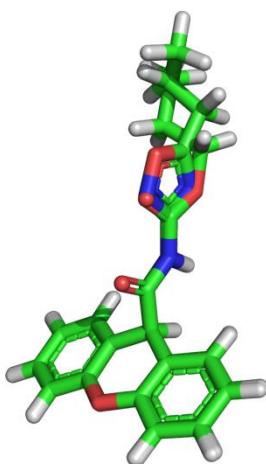


**Figure 3.17.** The highest-scoring Surflex-Sim binding hypothesis using Ro 07-11401 **3.43** and Ro 67-4853 **3.45**.



## CHAPTER IV

### DISCOVERY OF POSITIVE ALLOSTERIC MODULATORS FOR THE METABOTROPIC GLUTAMATE RECEPTOR SUBTYPE 1 AROUND A NEW CHEMOTYPE

#### **Identification of a starting point for a campaign to develop an mGlu<sub>1</sub> positive allosteric modulator**

##### *Medicinal chemistry around CDPBB and VU-71 structure*

The first steps for developing an mGlu<sub>1</sub> PAM, around a different scaffold from Ro 07-11401 **3.43**, within the Vanderbilt Center for Neuroscience Drug Discovery (VCNDD) led to the discovery of VU-71.<sup>280</sup> This new class of mGlu<sub>1</sub> PAMs was discovered when doing analogs around the mGlu<sub>5</sub> PAM CDPBB **4.1** to explore the structural requisites for activation of this receptor.<sup>291</sup> Through this exercise, it was found that different benzamide replacements could generate a compound with dual mGlu<sub>1</sub>/mGlu<sub>5</sub> activity in the rat form of these receptors, such as **4.2-4.6** (Fig. 4.1).

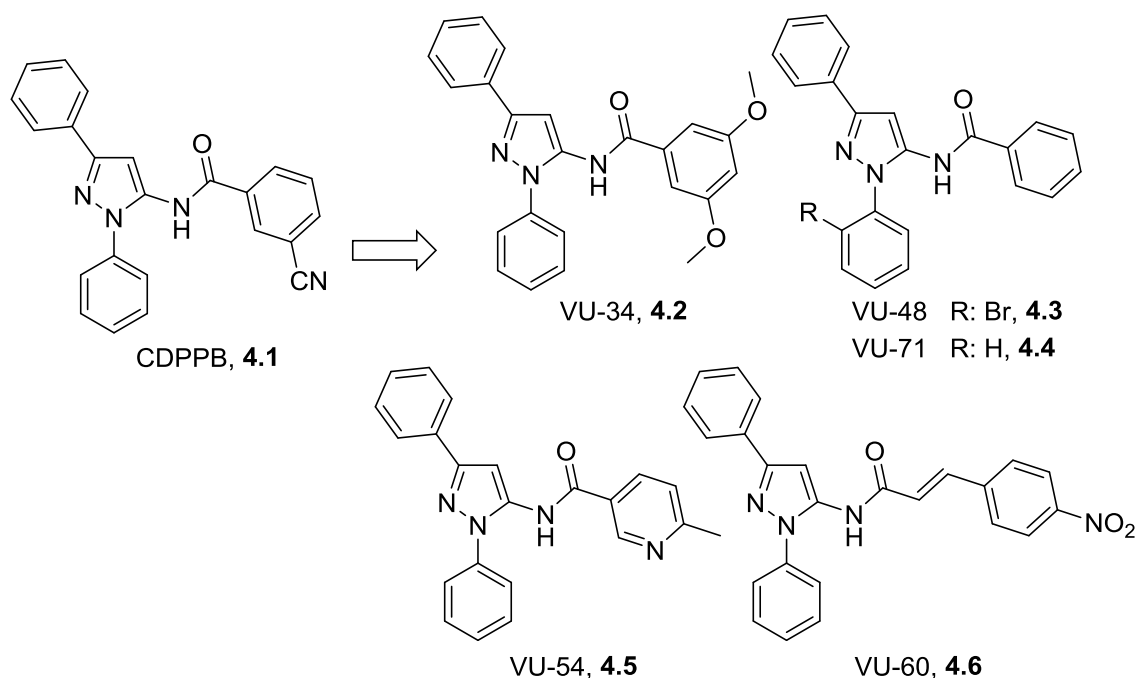


**Figure 4.1.** CDPPB analogs that potentiate the rat mGlu<sub>1</sub> receptor.

These analogs were further analyzed and showed leftward fold-shift in a glutamate response curve from 2 to 3, EC<sub>50</sub>s between 0.5 and 3.9 μM (Fig 4.2) and no displacement of [<sup>3</sup>H]-R214127 in radioligand binding studies.<sup>280</sup> From this subset, the most selective compound was VU-71 **4.4**, which differentiates from CPDBB only by a 4-nitro substituent in the benzamide region. **4.4** demonstrated to be only active in the rat form of the receptor and to lose activity when the mutation V757L was introduced. The importance of this mutation relies in that this is the only change observed between that rat (V757) and human (L757) mGlu<sub>1</sub> transmembrane domain.

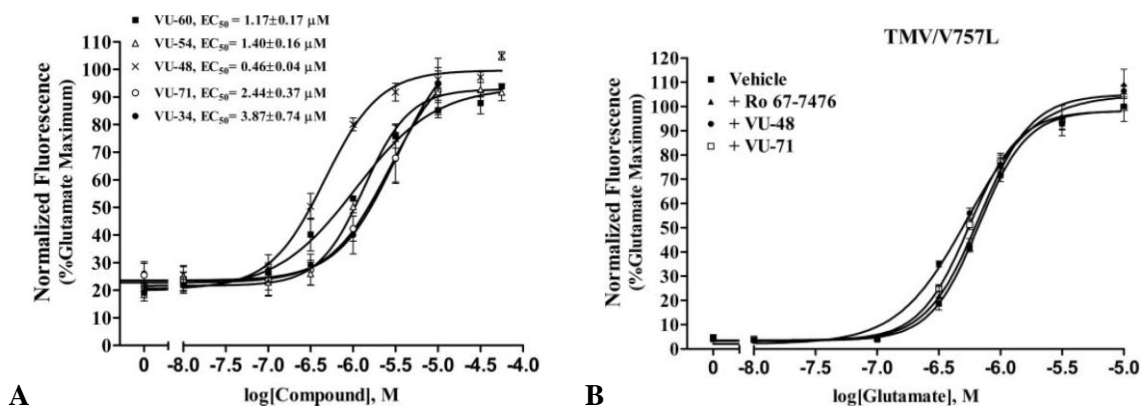


**Figure 4.2.** VU-71 **4.4** activity in the rat mGlu<sub>1</sub> receptor. A) Concentration-response curve and rat mGlu<sub>1</sub> EC<sub>50</sub> for CDPBB analogs **4.2-4.6**. B) Fold-shift analysis of **4.4** in rat mGlu<sub>1</sub> V757L.<sup>280</sup>

At the VCND, a medicinal chemistry campaign was started with **4.4** to improve its suboptimal potency and cross-species difference in activity. Analogs with different benzamides, altering the position of the phenyl ring in the core and various *N*-substituents in the pyrazole were synthesized and screened but these chemical modifications did not yield any active compound. Furthermore, when they resynthesized VU-48, the most potent compound in the family, it showed a potency of 2.35 μM, more than 5-fold less its reported value.<sup>280</sup> These results led to stop the exploration of further SAR around this scaffold.

#### *Dual mGlu<sub>1</sub>/mGlu<sub>4</sub> PAMs as a starting point for the development of selective mGlu<sub>1</sub> PAMs*

Interested in their possible antiparkinsonian effects, a program for the discovery and development of mGlu<sub>4</sub> positive allosteric modulators initiated at the VCND. In this effort, thousands of compounds have been synthesized around several chemotypes and when a compound demonstrates good potency for the mGlu<sub>4</sub> receptor they are tested in other members of the mGlu family. During these selectivity screenings, some picolinamide derivatives showed cross-activity on the human mGlu<sub>1</sub> receptor (Fig. 4.3). Based on its potency, we chose to explore VU0405622 **4.8** further and we were pleased to observe that it also activated the rat mGlu<sub>1</sub> receptor with a similar potency. **4.8** represents a novel scaffold for mGlu<sub>1</sub> PAM activity.

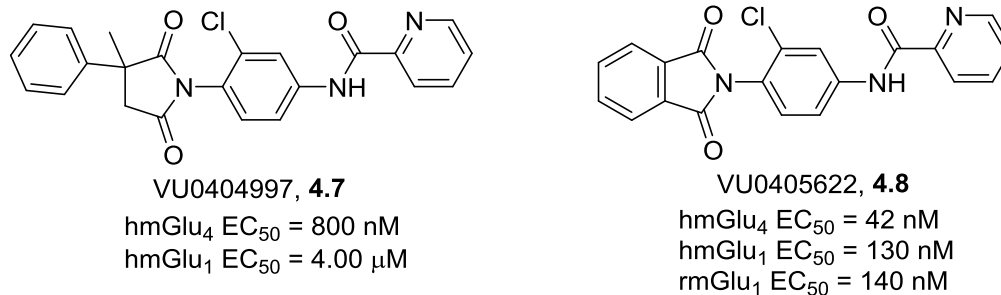


**Figure 4.3.** Dual mGlu<sub>1</sub>/mGlu<sub>4</sub> PAMs derived from mGlu<sub>4</sub> PAM drug discovery program at the VCNDD.

### Exploration of the structure-activity relationship around VU0405622

#### *Medicinal chemistry strategy for the exploration of VU0405622 4.8*

Being a cross-species active potentiator of mGlu<sub>1</sub>, we decided to use the scaffold of **4.8** as the starting point for our medicinal chemistry campaign to develop novel positive allosteric modulators for this receptor. The scaffold is synthetically accessible, facilitating the production of libraries of analogs with changes in different parts of the molecule. The structure can be divided in three main regions: the western phthalimide, the central phenyl ring and the eastern picolinamide. Analogs with different substituents or replacements of these groups can be synthesized to evaluate the impact of these modifications in the potency and selectivity for mGlu<sub>1</sub> (Fig. 4.4).

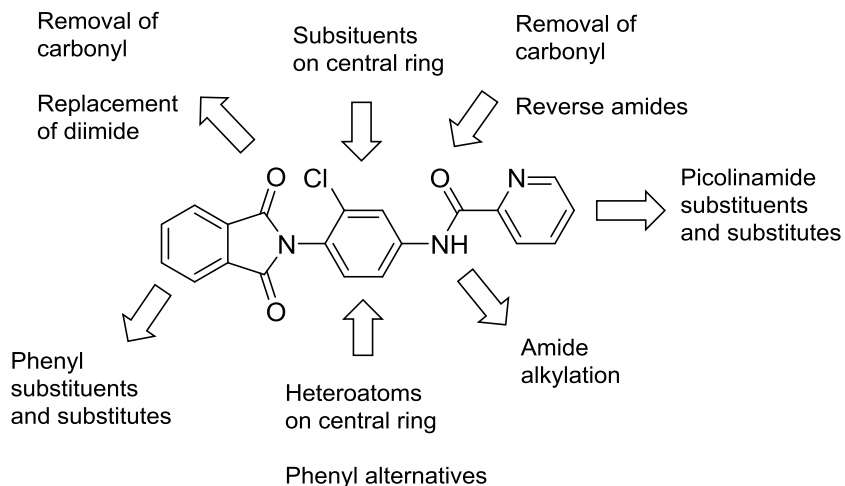


**Figure 4.4.** Possible chemical modifications to explore the SAR around VU0405622 **4.8** scaffold.

So, a multidimensional, iterative, parallel synthesis approach to develop analogs of **4.8** was initiated. This methodology consisted of the synthesis of focused chemical libraries based around a specific region of the molecule while the rest of the pharmacophore is held constant. Following this, the new compounds will be screened for biological activity in cell-based calcium mobilization assays. The bioactivity of the compounds guided subsequent design, so beneficial structural characteristics for mGlu<sub>1</sub> PAM activity could be discovered and held constant in additional rounds of chemical modification. In this way, the molecule would be improved iteratively as we expanded and developed valuable SAR knowledge. In our initial efforts, the primary goal was to make the compounds more selective for mGlu<sub>1</sub>, but our overall goal was to obtain a compound that satisfied the pharmacodynamic and pharmacokinetic properties needed for *in vivo* target validation studies; and these characteristics described our optimization workflow (Fig. 4.5).

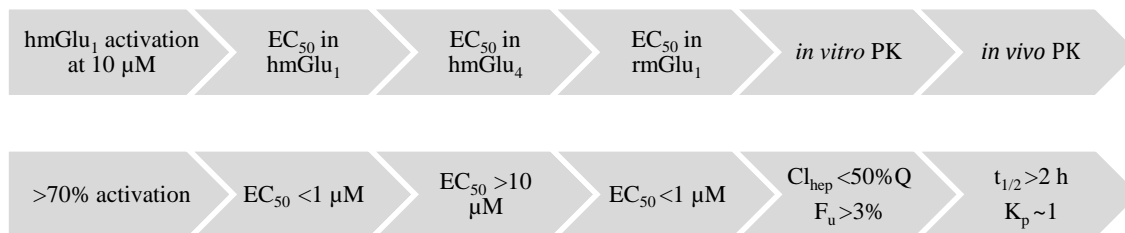
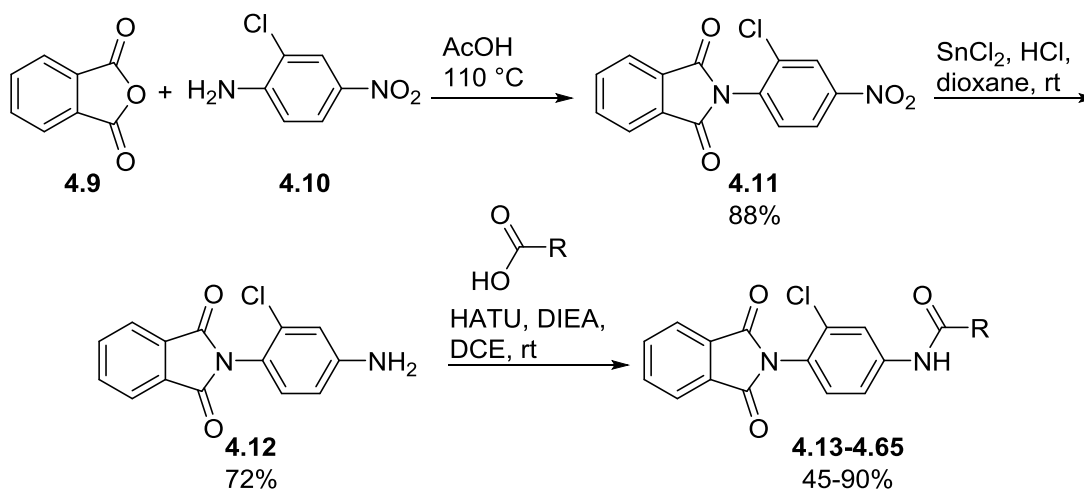


**Figure 4.5.** Optimization work flow for the development of adequate mGlu<sub>1</sub> PAMs for *in vivo* target validation studies. Cl<sub>hep</sub>: predicted hepatic clearance from studies with liver microsomes. Q: hepatic blood flow. F<sub>u</sub>: fraction unbound in plasma. K<sub>p</sub>: brain to plasma partition coefficient.

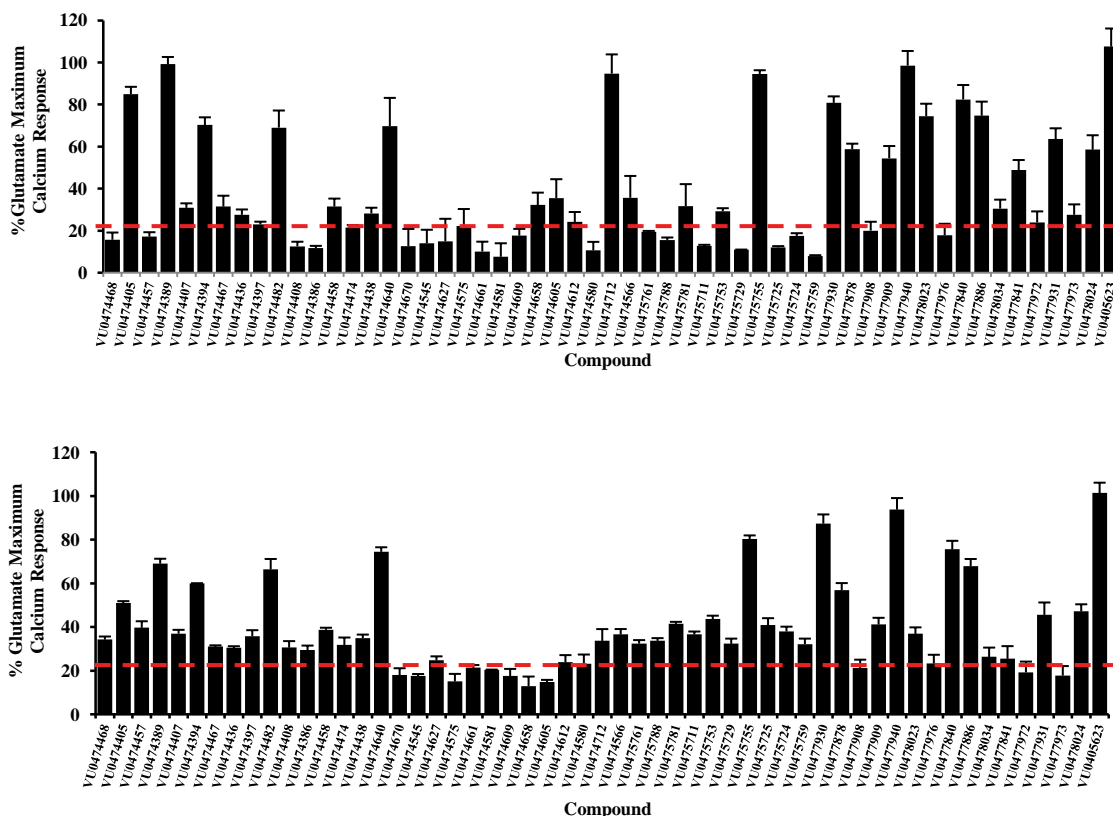
#### Modification on the eastern picolinamide of VU0405622 4.8

We initiated our SAR study by exploring different amides in the picolinamide side. A 3-step synthetic route using simple starting materials was developed to access analogs with diversity in this side of the molecule. Our synthesis started condensing phthalic anhydride **4.9** and 2-chloro-4-nitroaniline **4.10** in refluxing acetic acid to provide phthalimide **4.11** in 88% yield. The nitroaromatic intermediate **4.11** was reduced to the aniline **4.12** using tin(II) chloride (72% yield). The library step was an amide coupling performed under standard HATU conditions, where different carboxylic acids were employed along with intermediate **4.12**. For this library, pyridine carboxylic acid derivatives as well as some alkyl acid examples were used.



**Scheme 4.1.** Synthesis of picolinamide analogs **4.13-4.65**.

The library was screened in both human and rat mGlu<sub>1</sub> receptors at a single concentration of 10 μM. From this set, several compounds showed an enhancement of the submaximal EC<sub>20</sub> concentration of glutamate (Figure 4.6 and Table 4.1); however, this potentiating effect was lower with respect to VU0405622 **4.8**. The few aliphatic analogs (**4.40**, **4.41**, **4.45** and **4.48**) assayed did not show any activity and most of the active compounds are picolinamide or pyrazine analogs. It was observed that derivatives of nicotinic acid (**4.23**, **4.29**, **4.30**, **4.35**, **4.37-4.39**, **4.44**, and **4.50**) and isonicotinic acid (**4.24**, **4.49**) were inactive, indicating the importance of the position of the nitrogen in the eastern ring; also, oxidation of the nitrogen of the picolinamide (**4.64**) render the compound inactive. Moreover, the use of 2-quinoline and 2-quinoxalinecarboxylic acid generated inactive compounds (**4.32**, **4.62**), indicating limitations for steric bulk in this position. In the picolinamide analogs, 3- and 4-substitutions generally maintained mGlu<sub>1</sub> PAM activity, while substituents in the 5 and 6 position were detrimental. Positions 3 and 4 in the picolinamide tolerated small substituents, but when the group was bigger the activity decreased considerably, such as the 4-cyano **4.19**, 4-methoxy **4.54** and the 4-phenyl **4.26**.

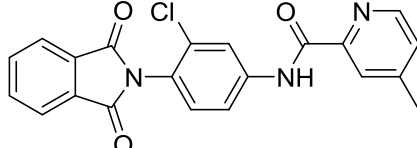
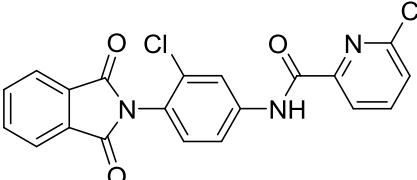
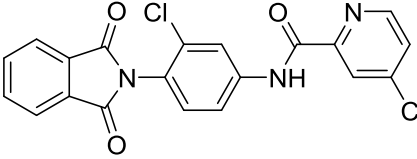
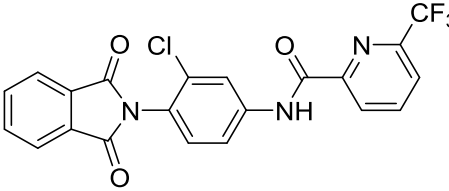
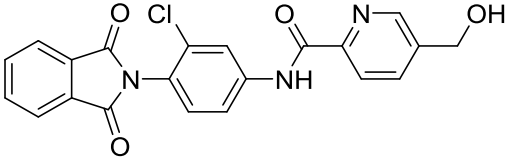
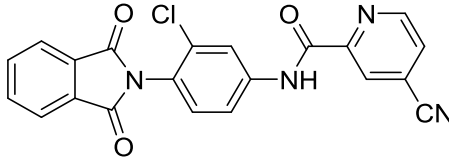
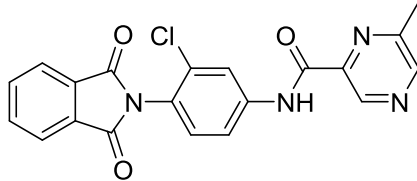
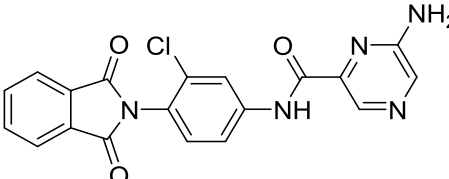


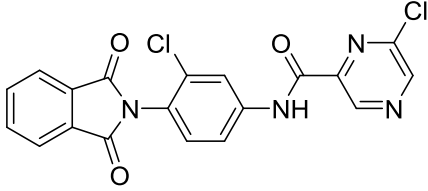
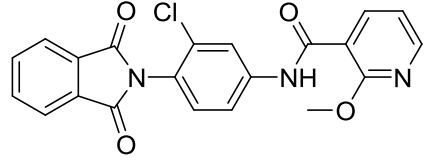
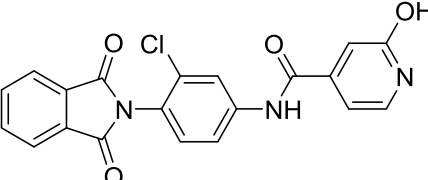
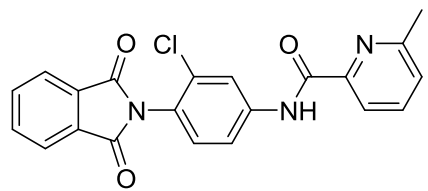
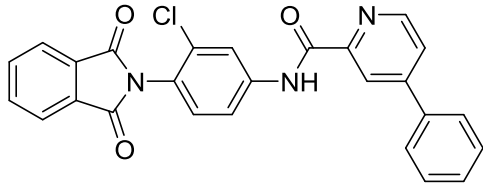
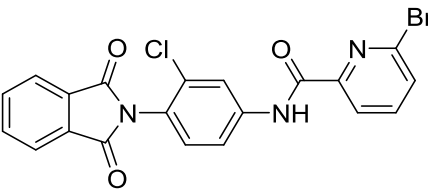
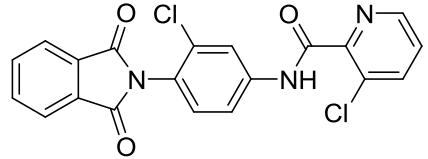
**Figure 4.6.** Comparison of the single point screen result for PAM activity in rat (top) and human (bottom) mGlu<sub>1</sub> at 10 μM for the amide library, analogs **4.13-4.65**. Calcium mobilization was used to obtain %Glu<sub>Max</sub> values for each compound in the presence of a submaximal concentration of glutamate (EC<sub>20</sub>) in cell lines expressing human mGlu<sub>1</sub>. Data represent the mean ± S.E.M. of at least three experiments with similar results.

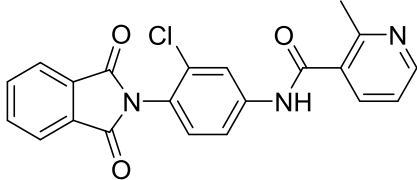
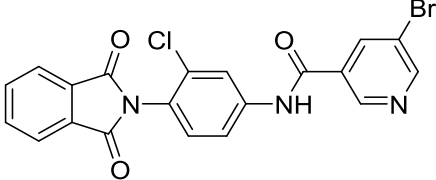
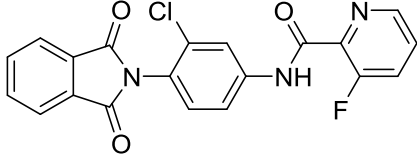
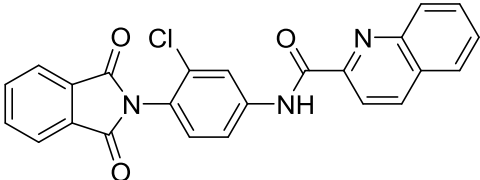
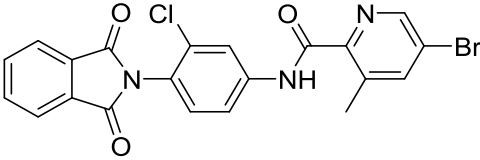
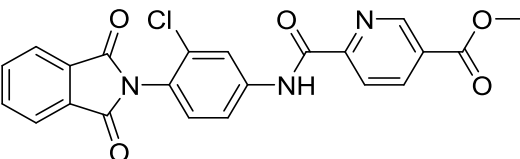
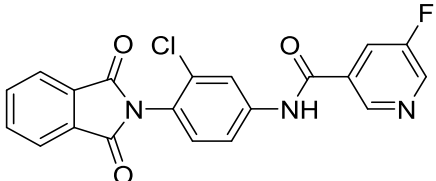
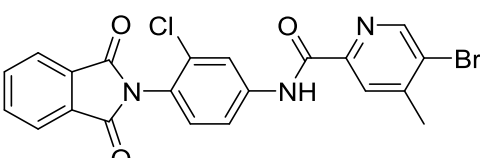
**Table 4.1.** Structures of the amide library analogs **4.13-4.65** and associated PAM activity from the single point screening at 10 μM in human mGlu<sub>1</sub>. Calcium mobilization responses for each compound are reported as a percentage of the maximum glutamate response. VU number denotes the compound identifier assigned by Vanderbilt University. Data represent the mean ± S.E.M. of at least three replicate experiments with similar results.

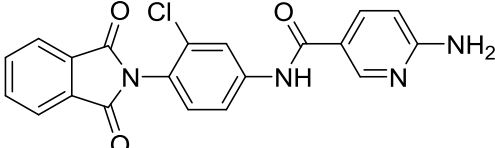
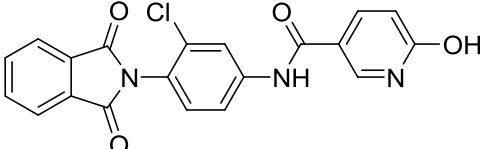
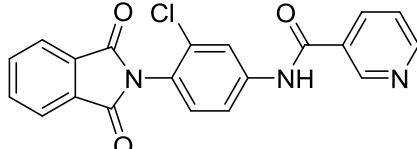
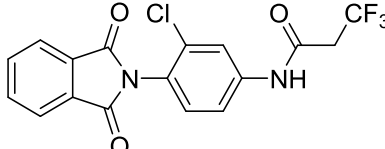
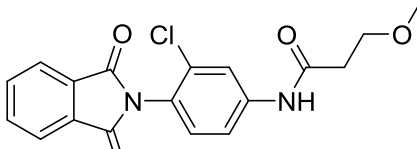
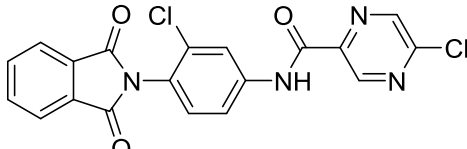
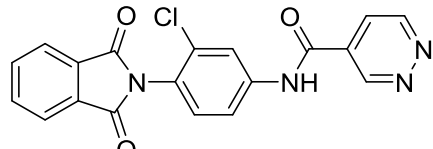
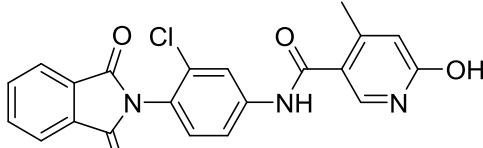
Structure	Cpd #	VU #	hmGlu <sub>1</sub> %Glu <sub>Max</sub>
	<b>4.13</b>	VU0474468	34.3±1.4

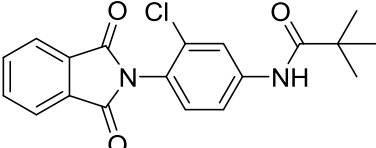
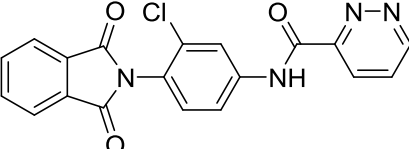
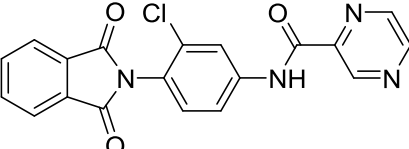
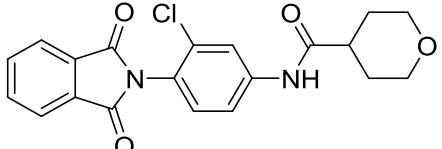
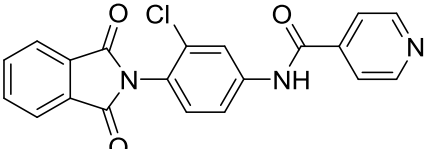
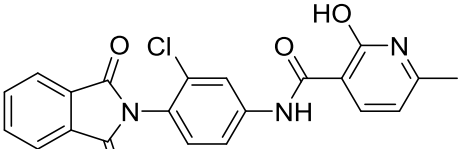
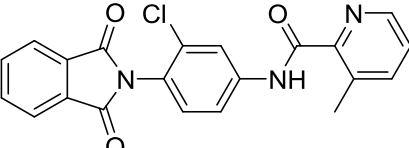
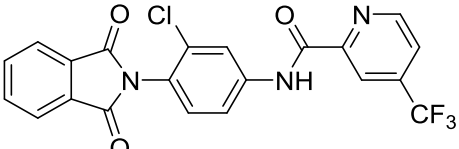


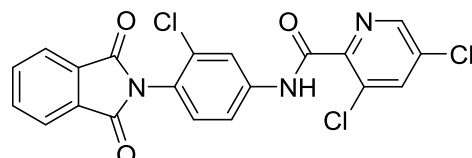
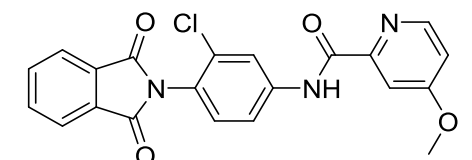
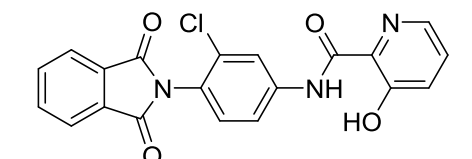
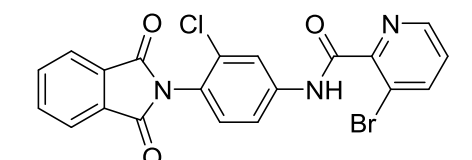
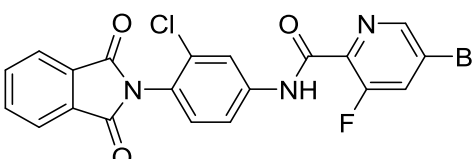
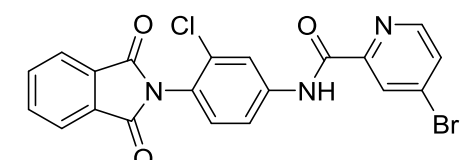
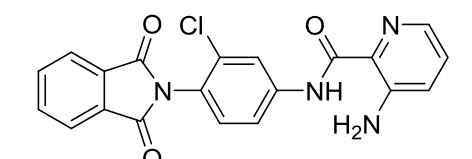
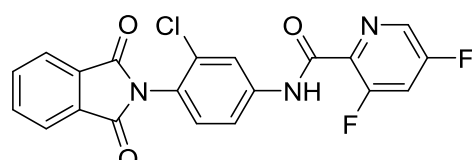
	<b>4.14</b>	VU0474405	51.0±1.0
	<b>4.15</b>	VU0474457	39.7±3.0
	<b>4.16</b>	VU0474389	69.1±2.3
	<b>4.17</b>	VU0474407	37.0±1.8
	<b>4.18</b>	VU0474394	60.0±0.2
	<b>4.19</b>	VU0474467	31.0±0.6
	<b>4.20</b>	VU0474436	30.5±0.7
	<b>4.21</b>	VU0474397	35.8±2.8

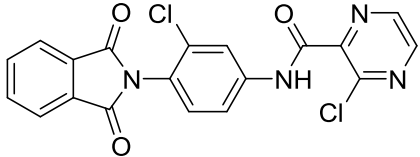
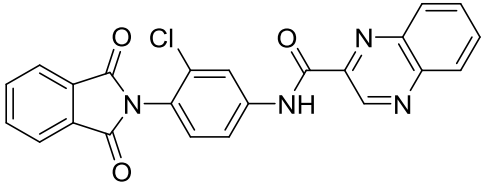
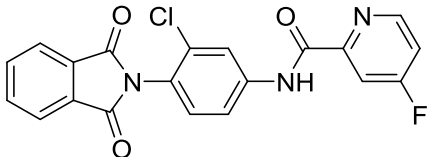
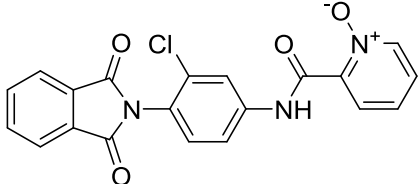
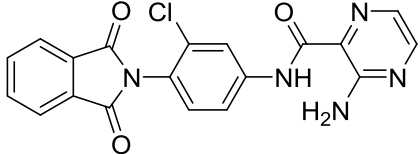
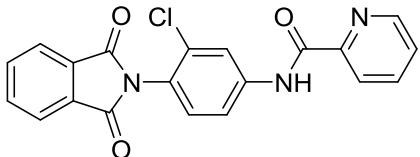
	<b>4.22</b>	VU0474482	66.4±4.8
	<b>4.23</b>	VU0474408	30.6±3.0
	<b>4.24</b>	VU0474386	29.4±2.1
	<b>4.25</b>	VU0474458	38.8±1.0
	<b>4.26</b>	VU0474474	31.9±3.4
	<b>4.27</b>	VU0474438	34.9±1.7
	<b>4.28</b>	VU0474640	74.5±2.1

	<b>4.29</b>	VU0474670	18.1±3.1
	<b>4.30</b>	VU0474627	24.8±1.9
	<b>4.31</b>	VU0474575	15.1±3.5
	<b>4.32</b>	VU0474661	21.4±1.3
	<b>4.33</b>	VU0474581	20.4±0.2
	<b>4.34</b>	VU0474609	17.7±3.2
	<b>4.35</b>	VU0474658	12.9±4.4
	<b>4.36</b>	VU0474605	14.8±1.0

	<b>4.37</b>	VU0474612	23.9±3.3
	<b>4.38</b>	VU0474580	23.1±4.4
	<b>4.39</b>	VU0474566	36.6±2.5
	<b>4.40</b>	VU0475761	32.5±1.6
	<b>4.41</b>	VU0475788	33.7±1.3
	<b>4.42</b>	VU0475781	41.5±0.9
	<b>4.43</b>	VU0475711	36.6±1.4
	<b>4.44</b>	VU0475715	45.7±1.8

	<b>4.45</b>	VU0475753	43.7±1.6
	<b>4.46</b>	VU0475729	32.4±2.4
	<b>4.47</b>	VU0475755	80.4±1.6
	<b>4.48</b>	VU0475725	41.0±3.2
	<b>4.49</b>	VU0475724	38.0±2.2
	<b>4.50</b>	VU0475759	32.2±2.6
	<b>4.51</b>	VU0477930	87.4±4.2
	<b>4.52</b>	VU0477878	56.9±3.3

	<b>4.53</b>	VU0477908	21.4±3.8
	<b>4.54</b>	VU0477909	41.2±3.1
	<b>4.55</b>	VU0477940	93.8±5.3
	<b>4.56</b>	VU0478023	36.9±3.0
	<b>4.57</b>	VU0477976	23.3±4.1
	<b>4.58</b>	VU0477840	75.6±3.9
	<b>4.59</b>	VU0477886	67.9±3.3
	<b>4.60</b>	VU0478034	26.4±4.3

	<b>4.61</b>	VU0477841	25.5±5.8
	<b>4.62</b>	VU0477972	19.3±4.9
	<b>4.63</b>	VU0477931	45.6±5.7
	<b>4.64</b>	VU0477973	17.8±4.4
	<b>4.65</b>	VU0478024	47.2±3.3
	<b>4.8</b>	VU0405622	101.4±4.7

---

To assess the differences between the active compounds obtained from our first library, we proceed to determine the EC<sub>50</sub> of the analogs that display over 50% mGlu<sub>1</sub> potentiation during the single point screening (Table 4.2). Besides, compounds were screened in hmGlu<sub>4</sub> to evaluate their selectivity. Pyridazine **4.47** showed submicromolar potency in hmGlu<sub>1</sub> and an EC<sub>50</sub> close to 1 μM in rmGlu<sub>1</sub> keeping good efficacy in both cases; however, it presents low efficacy and very

high potency in hmGlu<sub>4</sub> (EC<sub>50</sub> = 70 nM). The introduction of a 6-chloro substitution **4.22**, maintain similar potency in mGlu<sub>1</sub> and provide a significant improvement in selectivity.

**Table 4.2.** Potencies in human and rat forms of mGlu<sub>1</sub> and human mGlu<sub>4</sub> for the active compounds obtained from the amide library single point screening. Calcium mobilization responses for each compound are reported as a percentage of the maximum glutamate response. VU number denotes the compound identifier assigned by Vanderbilt University. Data represent the mean ± S.E.M. of at least three independent experiments with similar results. ---, no potentiation. ND, not determined.

Cpd #	VU #	hmGlu <sub>1</sub>		ratmGlu <sub>1</sub>		hmGlu <sub>4</sub>	
		EC <sub>50</sub> (μM)	%Glu Max	EC <sub>50</sub> (μM)	%Glu Max	EC <sub>50</sub> (μM)	%Glu Max
<b>4.8</b>	VU0405622	0.13	108	0.14	101	0.042	130
<b>4.14</b>	VU0474405	1.02	92	0.378	64	>10	---
<b>4.16</b>	VU0474389	0.64	105	1.09	85	>10	---
<b>4.18</b>	VU0474394	4.08	90	5.49	91	ND	ND
<b>4.22</b>	VU0474482	1.246	100	0.748	53	>10	---
<b>4.28</b>	VU0474640	1.29	102	0.57	77	>10	---
<b>4.47</b>	VU0475755	0.73	105	1.09	85	0.070	52
<b>4.51</b>	VU0477930	0.87	95	1.41	109	>10	---
<b>4.52</b>	VU0477878	2.20	85	>10	80	>10	---
<b>4.55</b>	VU0477940	0.43	103	0.032	105	0.13	115
<b>4.58</b>	VU0477840	0.96	90	0.49	95	>10	60
<b>4.59</b>	VU0477886	1.87	83	ND	ND	0.095	89

The 3-substituted picolinamides present an interesting SAR. Although fluoro (**4.31**) and bromo (**4.56**) were not tolerated, other small groups (**4.28**, **4.51**, **4.55**, and **4.59**) allowed retaining



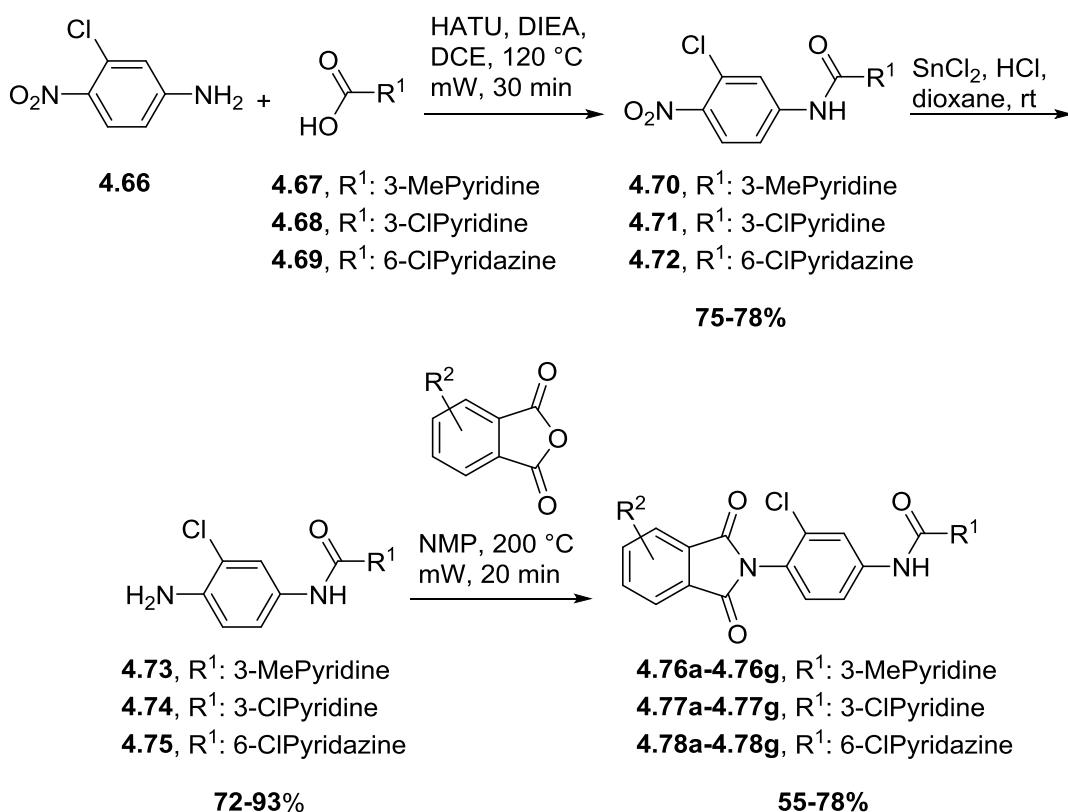
cross-species mGlu<sub>1</sub> activity. The 3-methyl (**4.51**) and the 3-chloro (**4.28**) substitution gained significant selectivity, showing no potentiation of mGlu<sub>4</sub> even at 30 μM. Hydrogen bond donating groups in the 3-position (**4.55**, **4.59**) had a singular effect. The 3-amino substituted **4.59** showed a human mGlu<sub>1</sub> EC<sub>50</sub> close to 2 μM, but was potent for mGlu<sub>4</sub>; while the 3-hydroxy analog **4.55** was potent in both mGlu<sub>1</sub> (especially the rat form) and mGlu<sub>4</sub>. These findings caught the attention of the mGlu<sub>4</sub> PAM drug discovery program and they selected the 3-aminopicolinamide **4.59** for further studies and optimization. **4.59** demonstrated to be brain penetrant ( $K_p = 1.3$ ), possessing low clearance ( $Cl_p = 4.0$  mL/min/kg,  $t_{1/2} = 3.7$  h) and robust efficacy in haloperidol-induced catalepsy, a preclinical model for Parkinson.

As mentioned, the 4-position tolerates little steric bulk, this was reiterated with the 4-trifluoromethyl analog **4.52** which maintains moderate potency in human mGlu<sub>1</sub> but is very weak enhancing glutamate responses in the rat receptor. The 4-methyl **4.14**, 4-chloro **4.16** and 4-bromo **4.58** were active in both human and rat mGlu<sub>1</sub>, with potencies between 400 nM and 1.1 μM. **4.14** and **4.16** were inactive in mGlu<sub>4</sub>, while **4.58** was a weak activator. As in the 3-picolinamide, the 4-fluoro analog **4.63** was inactive in both mGlu<sub>1</sub> and mGlu<sub>4</sub>.

#### *Exploration of the SAR in the phthalimide in the context of **4.51**, **4.28** and **4.22***

These first iteration represented a great advancement in terms of differentiation between mGlu<sub>1</sub> and mGlu<sub>4</sub> activity; however, all selective compounds showed significantly lower potency for mGlu<sub>1</sub> activation with respect to its parent, VU0405622. We decided to take analogs **4.51**, **4.28** and **4.22**, and develop focused matrix libraries around them, varying the phthalimide region. The synthesis of these compounds was based on our prior route from scheme 4.1, but inverting the order of steps so the diversity step could be performed last (Scheme 4.2). In this case, we started with the amide coupling between the nitroaniline **4.66** and carboxylic acids **4.67-4.69** to obtain amides **4.70-4.72**. The regular conditions used in Scheme 4.1 that were useful to obtain final library compounds did not result in good yields when using nitroaniline **4.66**. After trying

several amide coupling reagents, yields did not improve, but it was found that carrying the reaction in the microwave gave robust amounts of product in good yields (75-78%). Then, the nitroaromatic intermediates **4.70-4.72** were reduced with tin(II) chloride under acidic conditions (72-93% yield). Finally, anilines **4.73-4.75** were condensed with different phthalic anhydrides by heating the reaction in NMP in the microwave, to yield compounds **4.76a-4.78g** in moderate yields (55-78%).



**Scheme 4.2.** Synthesis of the matrix library with variations on the picolinamide and phthalimide region, analogs **4.76a-4.78g**.

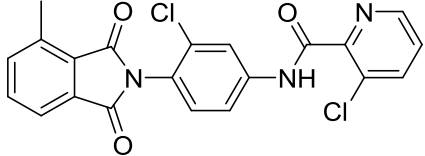
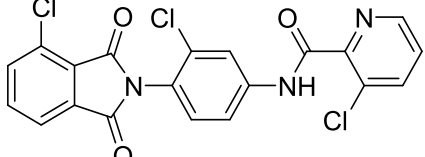
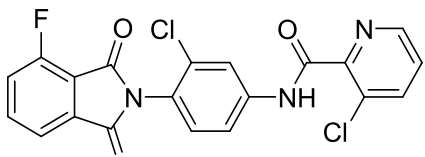
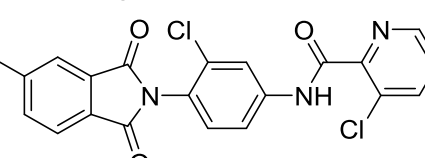
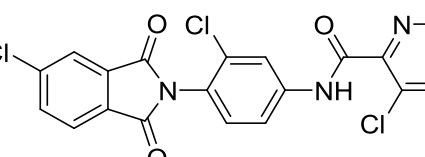
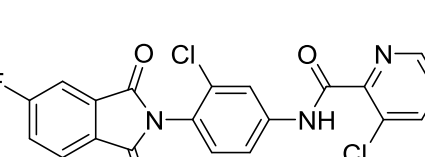
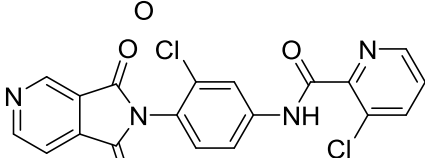
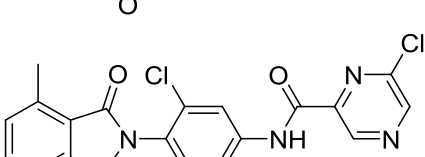
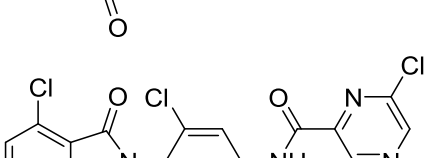
Analogues with methyl, chloro and fluoro substituents in the phthalimide, as well as the introduction of a nitrogen atom in the position 4 of the phthalimide ring were obtained. The potencies of these analogues were evaluated in human mGlu<sub>1</sub> and mGlu<sub>4</sub> in calcium mobilization assays (Table 4.3). The introduction of a nitrogen in the ring and 4-substitutions generated less

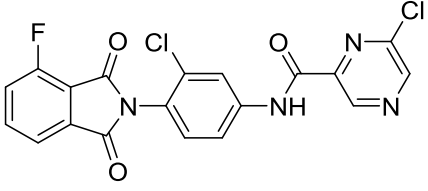
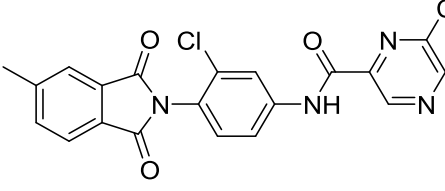
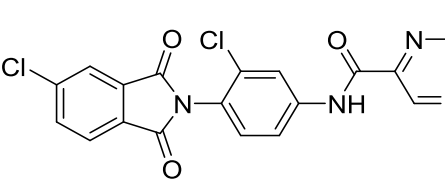
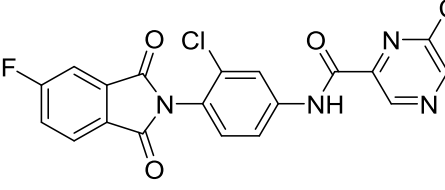
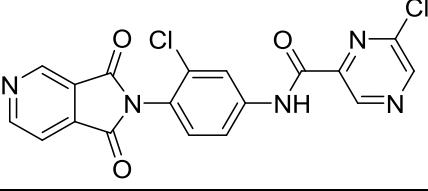
potent compounds (**4.76d-4.76g**, **4.77d-4.77g** and **4.78d**, **4.78e**,**4.78g**), with the exception of **4.78f** (VU6002183) that had an hmGlu<sub>1</sub> EC<sub>50</sub> of 360 nM. Despite the improvement in potency, **4.78f** lacked of adequate selectivity as is only 3-fold more potent in hmGlu<sub>1</sub> with respect to hmGlu<sub>4</sub>.

The 3-substituted phthalimide analogs demonstrated to be more potent than their naked phthalimide versions. All 3-substituted compounds **4.78a-4.78c** from the 6-chloropyridazine library, were potent for mGlu<sub>1</sub> but they still exhibited considerable mGlu<sub>4</sub> PAM activity, except for **4.78b**, that is a weak activator. In the case of the series derived from 3-methylpicolinamide **4.51** and 3-chloropicolinamide **4.28**, the most potent members are the 3-methylphthalimide analogs (**4.76a** and **4.77a**), but again with little selectivity over mGlu<sub>4</sub> activation. The 3-chloro analogs **4.76b** and **4.77b** displayed good potency for mGlu<sub>1</sub> (EC<sub>50</sub> = 250 nM and 360 nM, respectively) with weak activation of mGlu<sub>4</sub> (EC<sub>50</sub>>10μM), allowing for 40-fold and 28-fold differences in potencies between the receptors. Finally, the 3-fluoroanalog **4.76c** and **4.77c** showed a divergent behavior with respect to mGlu<sub>1</sub> activity; while **4.77c** was less active than its unsubstituted phthalimide parent **4.28**, **4.76c** represents an improvements in potency of 2-fold with respect to the original compound **4.51**, but recover some mGlu<sub>4</sub> potentiation.

**Table 4.3.** Potencies in human mGlu<sub>1</sub> and mGlu<sub>4</sub> of compounds derived from the matrix library **4.76a-4.78g**. Calcium mobilization responses for each compound are reported as a percentage of the maximum glutamate response. VU number denotes the compound identifier assigned by Vanderbilt University. Data represent the mean ± S.E.M. of at least three independent experiments with similar results. ---, no potentiation. ND, not determined.

Structure	Cpd #	VU #	hmGlu <sub>1</sub>		hmGlu <sub>4</sub>	
			EC50 (μM)	%Glu <sub>Max</sub>	EC50 (μM)	%GI <sub>uMax</sub>
	<b>4.76a</b>	VU0483657	0.19	99	2.20	186
	<b>4.76b</b>	VU0483737	0.25	90	>10	170
	<b>4.76c</b>	VU0483635	0.40	87	0.37	45
	<b>4.76d</b>	VU0486392	9.27	88	ND	ND
	<b>4.76e</b>	VU0483681	2.00	92	ND	ND
	<b>4.76f</b>	VU0483604	>10	87	ND	ND
	<b>4.76g</b>	VU0483621	>10	86	ND	ND

	<b>4.77a</b>	VU0483710	0.23	104	0.47	89
	<b>4.77b</b>	VU0483605	0.36	102	>10	51
	<b>4.77c</b>	VU0483709	1.15	119	ND	ND
	<b>4.77d</b>	VU0486324	3.14	107	ND	ND
	<b>4.77e</b>	VU0483712	1.83	85	ND	ND
	<b>4.77f</b>	VU0483537	3.89	101	ND	ND
	<b>4.77g</b>	VU0483653	>10	88	ND	ND
	<b>4.78a</b>	VU6002199	0.18	93	1.35	94
	<b>4.78b</b>	VU6002180	0.15	93	>10	80

	<b>4.78c</b>	VU6002200	0.14	99	0.70	41
	<b>4.78d</b>	VU6002181	>10	82	ND	ND
	<b>4.78e</b>	VU6002182	>10	91	ND	ND
	<b>4.78f</b>	VU6002183	0.36	93	1.04	31
	<b>4.78g</b>	VU6002184	>10	96	ND	ND

Due to their good potency and selectivity, it was decided to evaluate **4.76b** (VU0483737) and **4.77b** (VU0483605) further and determine their activity in the rat mGlu<sub>1</sub> receptor (Fig. 4.7). In this assay, the compounds displayed robust efficacy and EC<sub>50</sub>s comparable to the human mGlu<sub>1</sub> potencies (VU0483737 EC<sub>50</sub>: 327.0 nM, 116.7% Glu<sub>Max</sub>; VU0483605 EC<sub>50</sub>: 290 nM, 111.6% Glu<sub>Max</sub>).

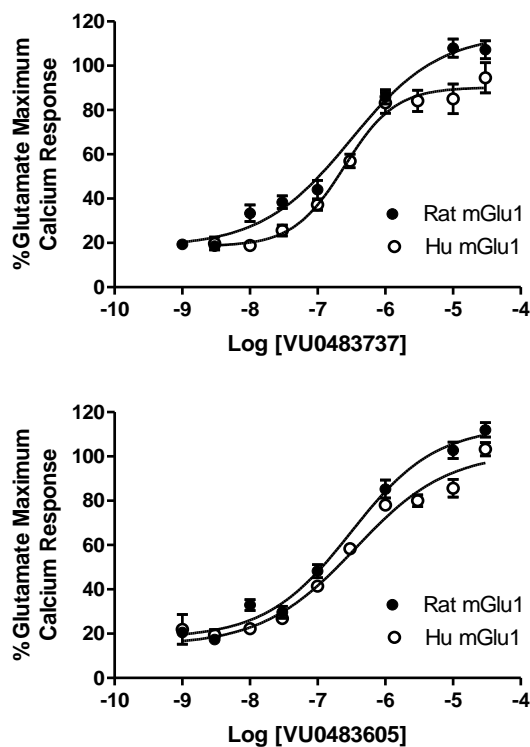


**Figure 4.7.** Potency of analogs **4.76b** (VU0483737, up) and **4.77b** (VU0483605, down) in the rat and human mGlu<sub>1</sub> receptor. Calcium mobilization assays were used to obtain CRCs in the presence of a fixed submaximal concentration of glutamate (EC<sub>20</sub>). Data represent the mean ± S.E.M. of at least three independent experiments with similar results.

Besides mGlu<sub>4</sub>, the selectivity of VU0483605 **4.77b** was evaluated against the other members of mGlu family using a calcium mobilization assay in the case of mGlu<sub>5</sub> and thallium flux/GIRK assays for the other mGlus that couple to G<sub>i/o</sub>. **4.77b** was assayed in fold-shift format and no potentiation of the mGlu receptors was observed, granting good selectivity against all members in the family (Fig. 4.8).

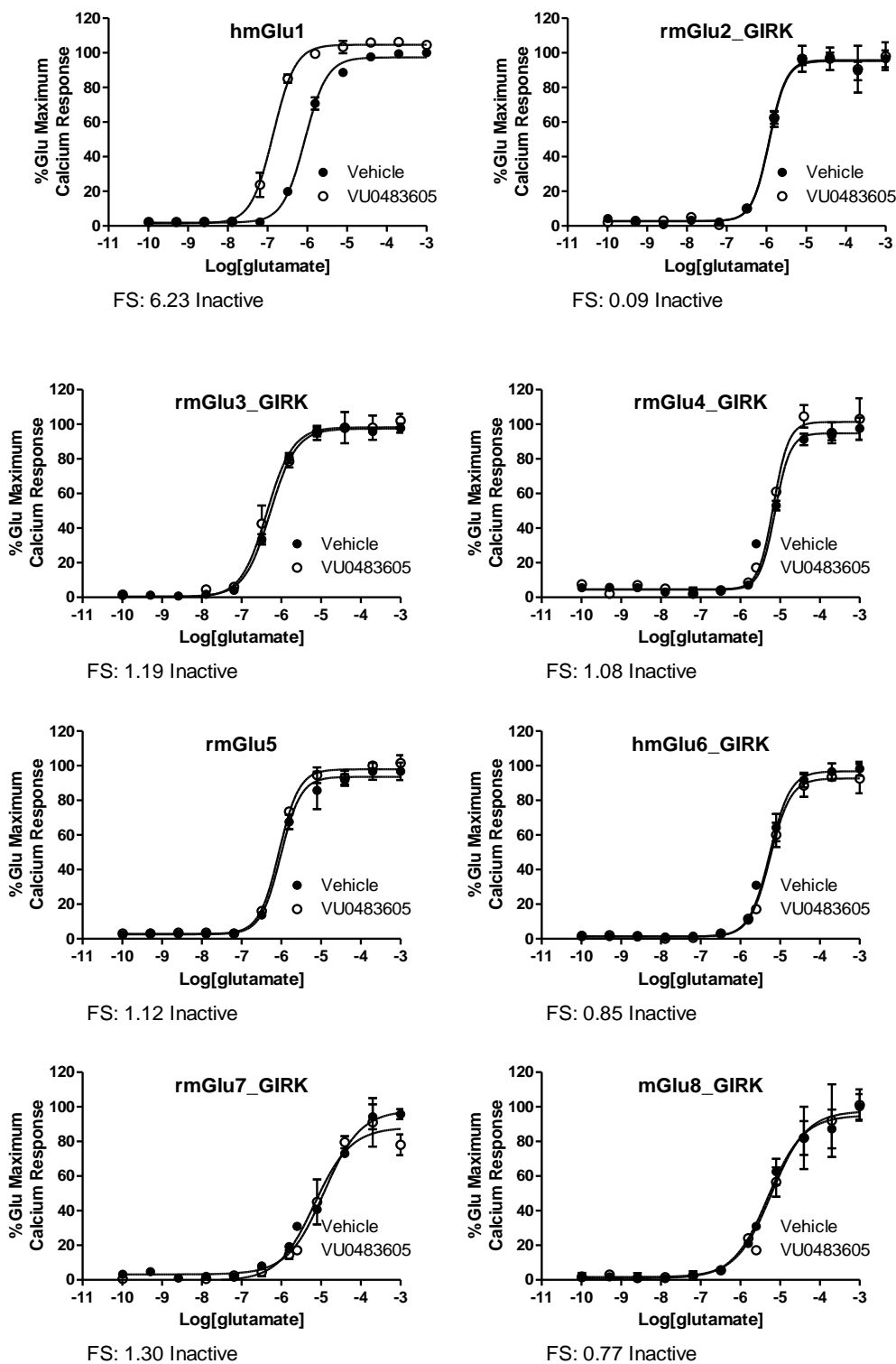
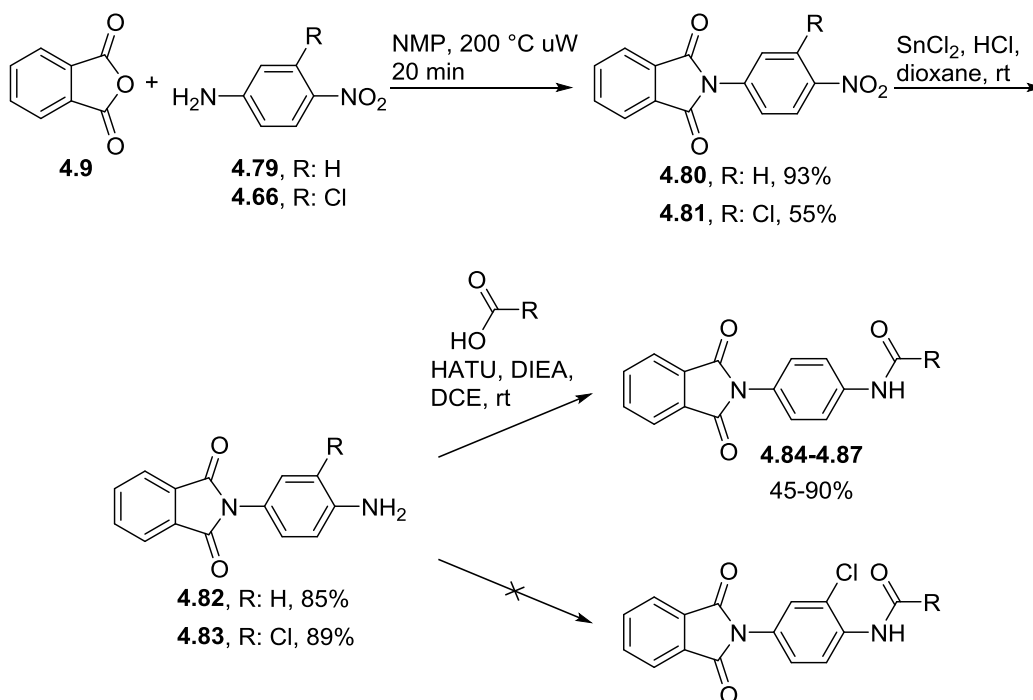


**Figure 4.8.** Selectivity of VU0483605 **4.77b** against the mGlu<sub>s</sub> determined in fold-shift mode. Calcium mobilization assays with hmGlu<sub>1</sub> and rmGlu<sub>5</sub> were used to obtain CRCs in the presence of 10  $\mu$ M of **4.77b**. The analysis of mGlu<sub>2,3,4,6,7,8</sub> selectivity was performed with thallium flux assays. Data represent the mean  $\pm$  S.E.M. of at least three independent experiments with similar results.



*Additional SAR around scaffold VU0405622 and its picolinamide derivatives*

Besides modification to the phthalimide and picolinamide region, a few changes in the central phenyl ring were explored. Here, we explore analogs with the naked central phenyl ring and also walking the chlorine substituent to the position adjacent to the picolinamide region. For this, compounds were synthesized in a similar fashion to our first amide library but changing the nitroaniline core (Scheme 4.3). Derivatives with the naked phenyl ring **4.84-4.87** were readily synthesized in overall good yields for the 3-step sequence, while compounds with the chloro substituent close to the picolinamide were harder to obtain. After trying several methodologies for the amide coupling unsuccessfully, we decide to invert the sequence of steps similarly to Scheme 4.2; however, this approach did not allow us to obtain the compounds with naked phthalimide. In order to be able to test this substitution pattern in the central ring, we decided to switch to the more electrophilic 3-fluorophthalic anhydride during our condensation reaction and we were able to obtain **4.88** and **4.89** in low yields.



**Scheme 4.3.** Synthesis of phenyl ring modified analogs **4.84-4.87**.

When the evaluation of these compounds was performed, it was found that both modifications, the removal and shifting of the chlorine in the central ring were detrimental for mGlu<sub>1</sub> activity (Fig. 4.9 and Table 4.4). Only **4.86** (VU0484059) still enhanced the response of glutamate in mGlu<sub>1</sub>, therefore this compound was evaluated further to determine its potency. **4.86** hmGlu<sub>1</sub> EC<sub>50</sub> was 905 nM, which represented a 2-fold loss in potency with respect to the parent compound **4.55** and a reason to halt the exploration of its properties.

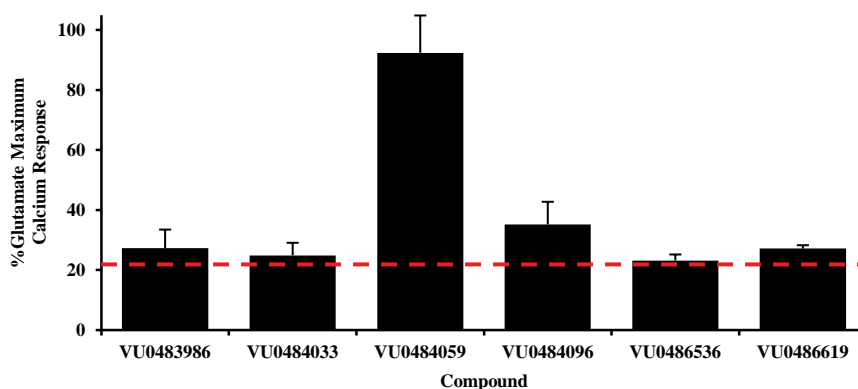


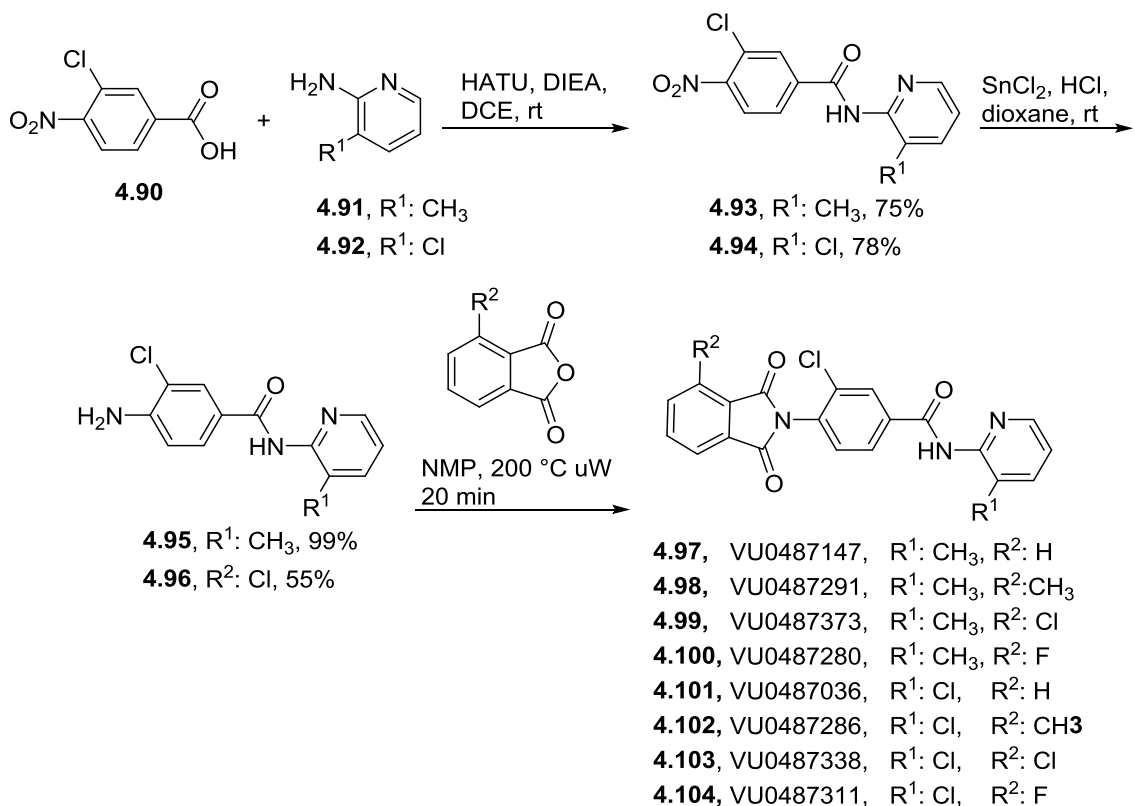
**Figure 4.9.** Comparison of the single point screen result for PAM activity in human mGlu<sub>1</sub> at 3  $\mu$ M for the phenyl ring modified analogs **4.84-4.89**. Calcium mobilization was used to obtain %Glu<sub>Max</sub> values for each compound in the presence of a submaximal concentration of glutamate (EC<sub>20</sub>) in cell lines expressing human mGlu<sub>1</sub>. Data represent the mean  $\pm$  S.E.M. of at least three replicate experiments with similar results.

**Table 4.4.** Structures of phenyl ring modified analogs **4.84-4.89** and associated PAM activity from the single point screening at 3  $\mu$ M in rat mGlu<sub>1</sub>. Calcium mobilization responses for each compound are reported as a percentage of the maximum glutamate response. VU number denotes the compound identifier assigned by Vanderbilt University. Data represent the mean  $\pm$  S.E.M. of at least three replicate experiments with similar results.

Structure	Cpd #	VU #	hmGlu <sub>1</sub> %Glu <sub>Max</sub>
	<b>4.84</b>	VU0483986	27.3
	<b>4.85</b>	VU0484033	24.9
	<b>4.86</b>	VU0484059	92.4
	<b>4.87</b>	VU0484096	35.2
	<b>4.88</b>	VU0486536	23.2
	<b>4.89</b>	VU0486619	27.2

Modifications in the linker between the picolinamide and the central phenyl ring were also assessed. Here, a reverse amide strategy was attempted first. The analogs to evaluate this change were synthesized in a 3-step process (Scheme 4.4). Starting from *p*-nitrobenzoic acid **4.90**, the amide coupling with anilines **4.91** and **4.92** was performed to obtain derivatives **4.93** and **4.94** in 75% and 78% yield respectively. These intermediates were reduced with tin(II)

chloride to obtain anilines **4.95** and **4.96** in 55% to quantitative yields. For the library step, condensation of the anilines with phthalic anhydrides was performed to obtain analogs **4.97-4.104**.



**Scheme 4.4.** Synthesis of reverse amide analogs **4.97-4.104**.

The synthesized compounds **4.97-4.104** were evaluated in the human mGlu<sub>1</sub> receptor in a single point concentrations study; however, none of them showed potentiation of the glutamate response at a concentration of 10 μM (Fig. 4.10). This indicates that the disposition of the amide is critical for mGlu<sub>1</sub> activity.

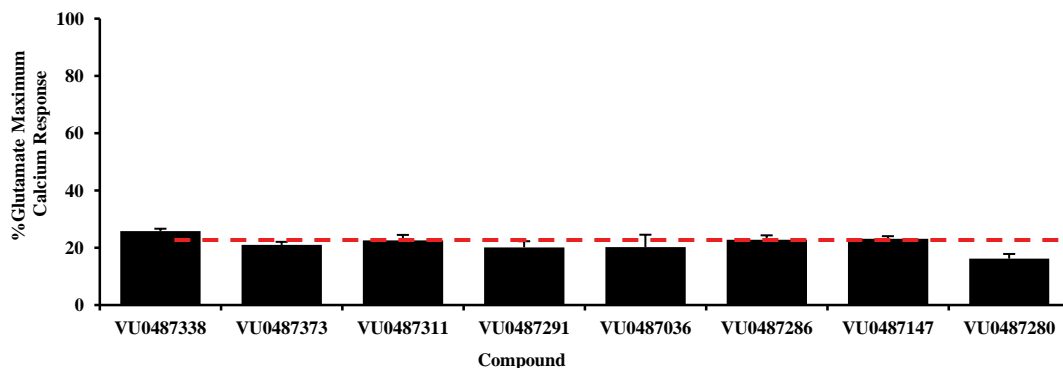
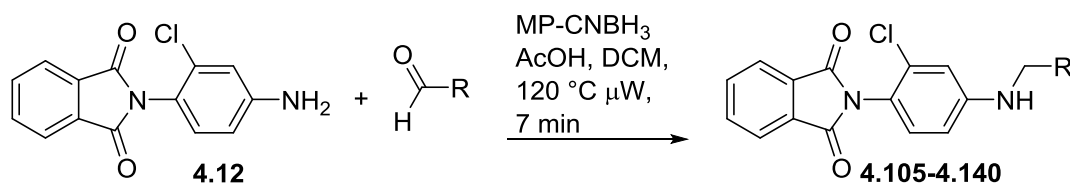


**Figure 4.10.** Comparison of the single point screen result for PAM activity in human mGlu<sub>1</sub> at 10  $\mu$ M for the phenyl ring modified analogs **4.97-4.104**. Calcium mobilization was used to obtain %Glu<sub>Max</sub> values for each compound in the presence of a submaximal concentration of glutamate (EC<sub>20</sub>) in cell lines expressing human mGlu<sub>1</sub>. Data represent the mean  $\pm$  S.E.M. of at least three replicate experiments with similar results.

The removal of the carbonyl group in the picolinamide was also studied by swapping the amide for the alkylamine. These compounds were synthesized employing intermediate **4.12** and subjected to reductive amination conditions with different aldehydes (Scheme 4.5). In this set, we assayed some of the pyridine substitutions that engender mGlu<sub>1</sub> PAM activity, as well as a couple of aliphatic substituents and multiple benzyl derivatives with different substitution patterns (Fig. 4.11).



**Scheme 4.5.** Synthesis of analogs **4.105-4.140** to assess the effect of the removal of the carbonyl group in the picolinamide side of VU0405622.

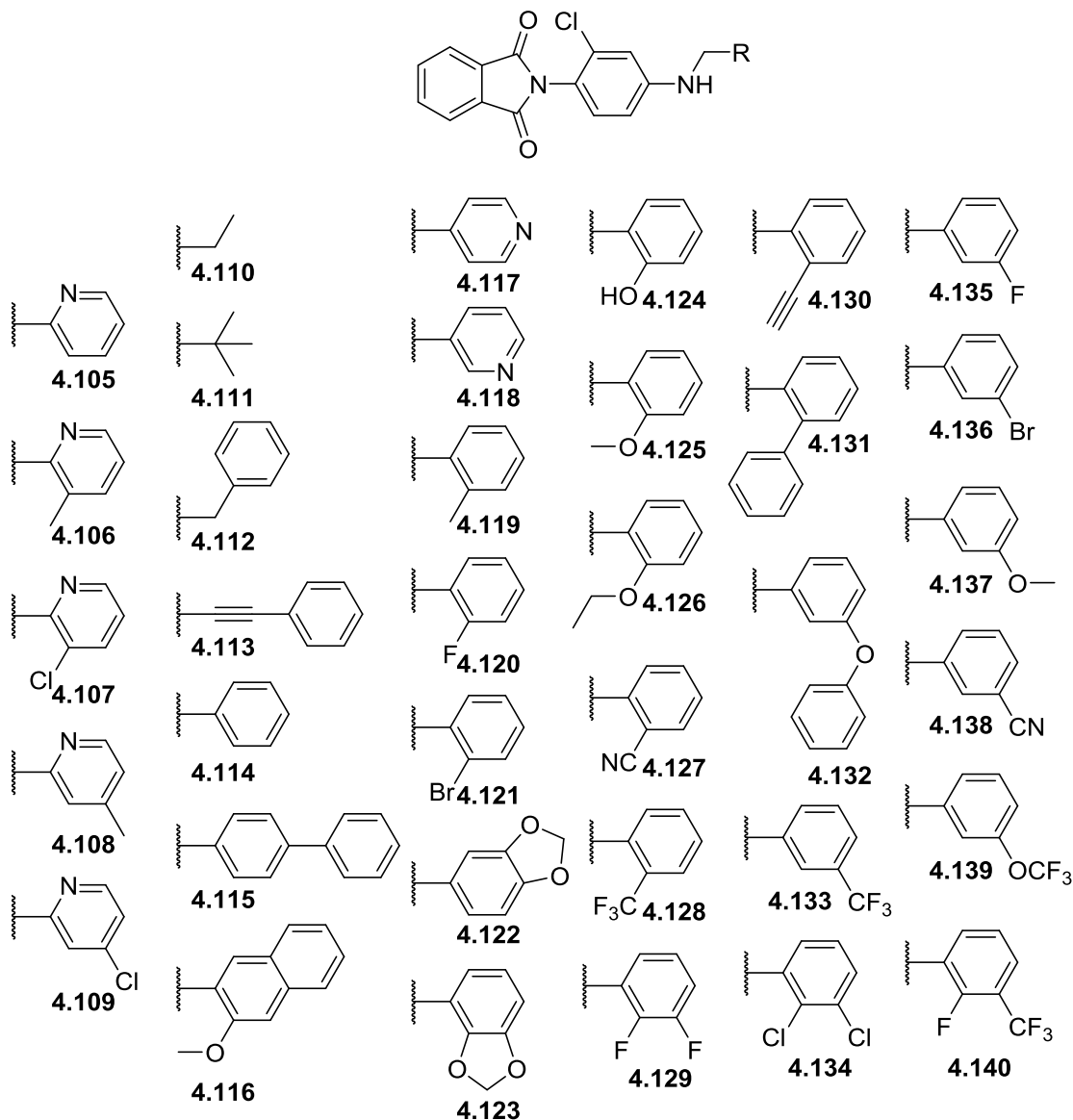


**Figure 4.11.** Analogs to assess the effect of the removal of the carbonyl group in the picolinamide side of VU0405622.

Compounds **4.105-4.140** were tested in our single point calcium mobilization assay for mGlu<sub>1</sub> potentiation and overall, the change in the linker from the carbonyl to the methylene had detrimental effects in hmGlu<sub>1</sub> potency. The only compound from this subset that displayed discernible activity was **4.106** (VU6000839), with an EC<sub>50</sub> of 1.00 μM, which is a close value to the activity of the parent amide.

## Evaluation of the new mGlu<sub>1</sub> PAMs in the wild type and mutated receptors

There is evidence of a higher density of non-synonymous single nucleotide polymorphisms in the *GRM1* gene in the schizophrenic and bipolar population.<sup>241</sup> Part of these mutations have reported to cause a decrease in phosphoinositide hydrolysis,<sup>242</sup> and showed how powerful a change in a single amino acid can be for receptor's function. These mutations are not confined to a single region of the protein; they are widespread from the Venus fly-trap domain to the intracellular C-terminus (Fig. 4.12).

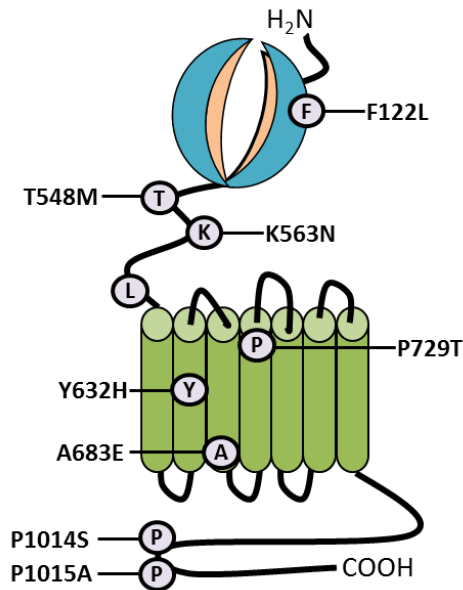


**Figure 4.12.** Distribution of mutations in the hmGlu<sub>1</sub> gene that are enriched in schizophrenic and bipolar patients.

We decided to confirm in our laboratory the effects of these mutations in the output of the receptor. The mutant receptors were tested by Ayoub and collaborators in an end point assay after incubation with 10  $\mu$ M of glutamate after for 45 minutes.<sup>242</sup> We believed that this set up is not the most adequate for this system, as the events that generate the phosphatidylinositol hydrolysis occur rapidly in the cell and other biochemical processes might affect the outcome of experiment

after long incubation times, such as receptor desensitization. We selected to study the activation of the receptor using a calcium mobilization kinetic protocol, a procedure that monitors continuously the intracellular calcium concentration, allowing for better tracking of receptor's activity.

Nine of the reported mutations were introduced into human mGlu<sub>1</sub> constructs and expressed in TR-Ex<sup>TM</sup> 293. The effect of glutamate and the group I selective agonist DHPG was evaluated in these constructs in our kinetic calcium mobilization assay (Fig. 4.13). The mutations affected considerably the effect of glutamate on the receptors (Fig. 4.13A, C, and E). The main change was observed in the maximum achievable signal, a reflection of the efficacy of the receptor towards glutamate activation; while the EC<sub>50</sub> for glutamate is relatively similar across the wild type and mutant constructs. Most of the mutants showed an efficacy between 48 and 64% of the maximum response obtained with the wild type receptor, with the exception of K563N (90%) and P1015A (86%) that were less affected (Table 4.5). The responses exerted by DHPG in these receptors were higher than the ones observed by glutamate, but overall they show the same tendency (Fig. 4.13B, D, and F). The different mutations did not affect much the EC<sub>50</sub> but they decrease the amplitude of the signal (Table 4.5). However, using DHPG as agonist demonstrated to have a considerably different effect in K563N with respect to glutamate, as the response was even higher than in the wild-type mGlu<sub>1</sub> in this mutant construct.



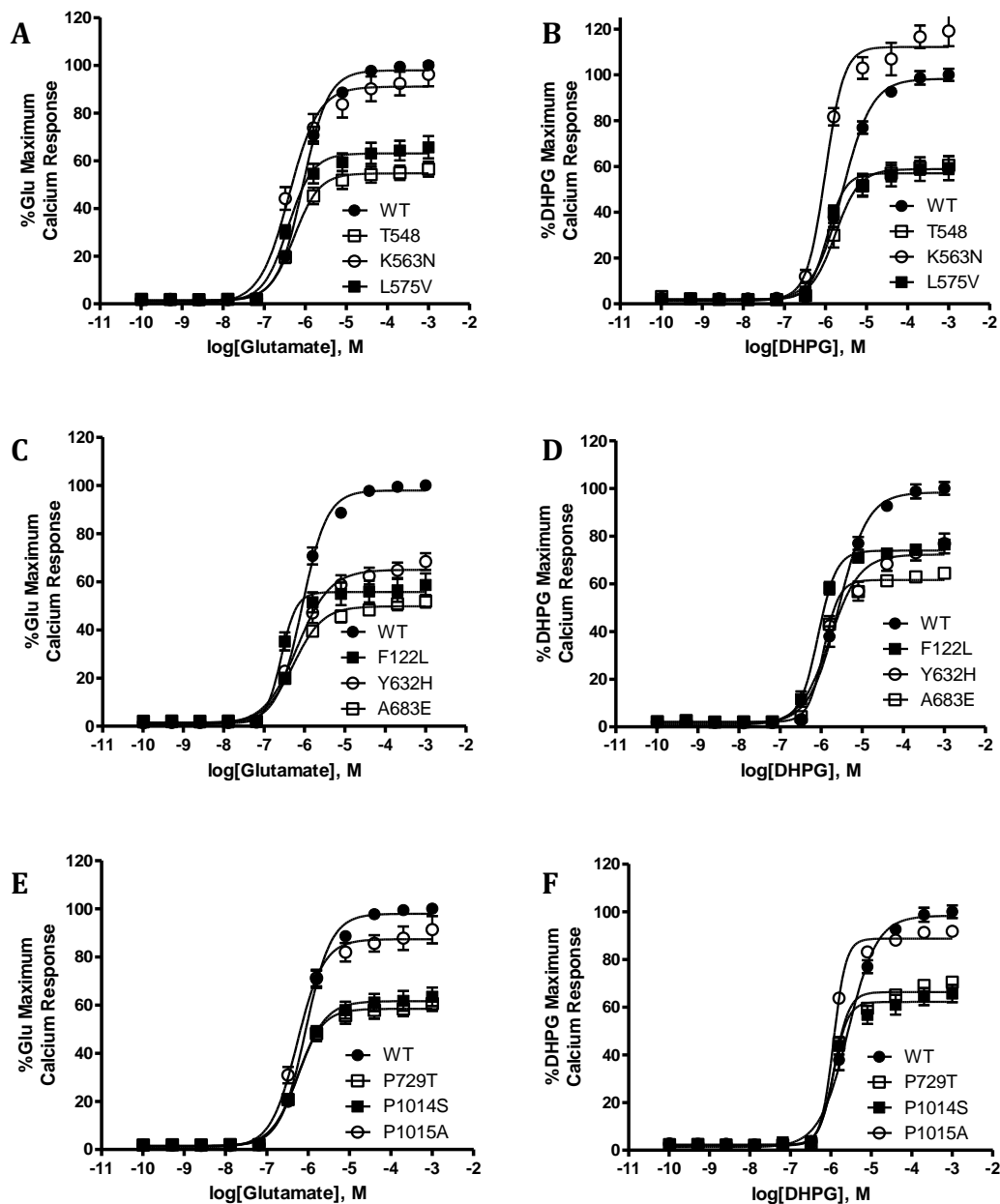


**Figure 4.13.** Effect of mutations in the mGlu<sub>1</sub> response of glutamate (A, C, E) and DHPG (B, D, F), with respect to wild type in fold shift experiments. Calcium mobilization assays were used to obtain CRCs in the different mGlu<sub>1</sub> constructs. Data represent the mean  $\pm$  S.E.M. of at least three independent experiments with similar results.

**Table 4.5.** Maximal efficacy of agonists glutamate and DHPG in wild type and mutant mGlu<sub>1</sub> receptors obtained in kinetic calcium mobilization assays. Data represent the mean  $\pm$  S.E.M. of at least three independent experiments with similar results.

Receptor	%Maximal glutamate response	%Maximal DHPG response
Wild type	96.4	97.0
T548	53.3	57.0
K563N	90.8	110.3
L575V	62.0	55.0
F122L	54.5	71.9
Y632H	64.4	71.5
A683E	48.4	59.5
P729T	57.0	64.4
P1014S	60.2	59.9
P1015A	86.4	86.4

After confirming the decrease in function of the mutant mGlu<sub>1</sub> constructs, we proceeded to evaluate the effect of various mGlu<sub>1</sub> PAMs in these receptors. For these experiments we select two of our PAMs, VU0483737 **4.76b**, VU0483605 **4.77b**, and Ro 07-11401 **3.43**. The selection of **4.76b** and **4.77b** responds to their good potency, efficacy in mGlu<sub>1</sub> and selectivity against human mGlu<sub>4</sub>. In preparation for these experiments, we started by characterizing the effect of the compounds in the wild-type receptor using a fold-shift assay. Using glutamate as agonist, Ro 07-11401 and VU0483605 **4.77b** displayed similar increase in potency for glutamate and efficacy; while with VU0483737 **4.76b**, despite having similar potency to VU0483605 **4.77b**, the enhancement was weaker and the fold-shift smaller (Fig. 4.14A).

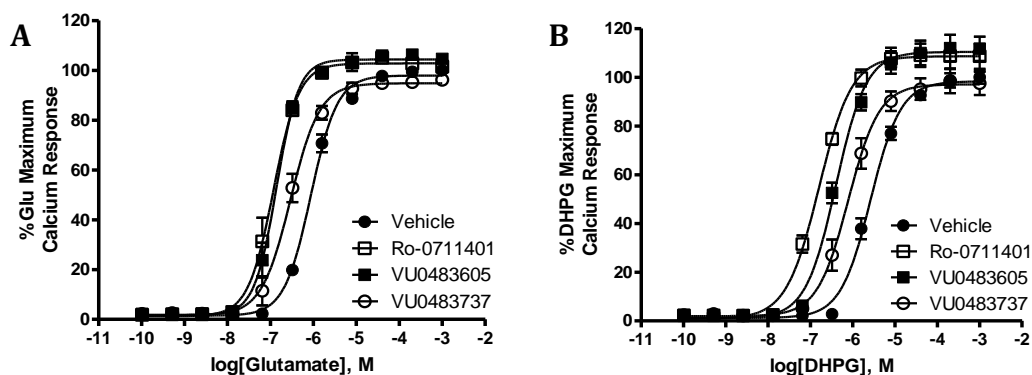


**Figure 4.14.** Effect of PAMs on the concentration-response curve of glutamate (A) and DHPG (B) in hmGlu<sub>1</sub>. Calcium mobilization fold-shift assays with hmGlu<sub>1</sub> were used to obtain glutamate CRCs in the absence and presence of 10  $\mu$ M concentration of VU0483737 **4.76b**, VU0483605 **4.77b** and Ro 07-11401 **3.43**. Data represent the mean  $\pm$  S.E.M. of at least three independent experiments with similar results.

**Table 4.6.** Effect of PAMs on the parameters of concentration-response curve of glutamate and DHPG in hmGlu<sub>1</sub>. Calcium mobilization fold-shift assays with hmGlu<sub>1</sub> were used to obtain glutamate CRCs in the absence and presence of 10  $\mu$ M concentration of VU0483737 **4.76b**, VU0483605 **4.77b** and Ro 07-11401 **3.43**. Data represent the mean  $\pm$  S.E.M. of at least three independent experiments with similar results.

Cpd	Glutamate			DHPG		
	EC <sub>50</sub> ( $\mu$ M)	Fold-Shift	Efficacy (%)	EC <sub>50</sub> ( $\mu$ M)	Fold-Shift	Efficacy (%)
Glutamate	0.871	1.00	97.9	---	---	---
DHPG	---	---	---	2.65	1.00	98.3
Ro 07-11401 <b>3.43</b>	0.118	7.38	102.8	0.159	16.7	108.6
VU0483605 <b>4.77b</b>	0.139	6.27	104.4	0.402	6.59	110.4
VU0483737 <b>4.76b</b>	0.294	2.96	94.80	0.783	3.38	97.1

When the experiments were run with DHPG as agonist, a larger differentiation between the PAMs was observed (Fig 4.14B). This time Ro 07-11041 **3.43** and VU0483605 **4.77b** did not show equivalent responses, being Ro 07-11401 the one that displayed the largest leftward shift in the concentration response curve, and increasing the potency of glutamate around 2 times more

than VU0483605 **4.77b**. Although, these compounds had similar effect increasing of efficacy of the receptor, achieving an increment of close to 10% the original value. Meanwhile, VU0483737 **4.76b** achieve the smallest fold-shift with no increment in the efficacy with respect to control.

After this, we evaluated the effect of the mGlu<sub>1</sub> PAMs in the nine mutant constructs that we analyzed previously. A concentration of 10 μM of every compound demonstrates to potentiate the activity of glutamate in all mutants, although this increase was smaller than in the wild type receptor (Fig. 4.15). Ro 07-11401 induced the largest increase in potency with variable fold-shift depending on the mutant (3.6-7.4). The mutants that display the largest enhancement were T548M, K563, P729 and P1014S, increasing the potency for glutamate close to 6-fold and more than 7-fold in the case of P729. In terms of efficacy, Ro 07-11401 did not show major improvement with respect to vehicle, in most instances it actually decrease the maximum glutamate activity (Table 4.7).

From our compounds, VU0483605 **4.77b** is the one that induced the largest change in potency (2.3-4.4), potentiating more the responses of mutations in the transmembrane domain (Y632H, A683E, P729T). VU0483605 **4.77b** is also the compound that provoked the largest increase in efficacy of the glutamate response, while VU0483737 **4.76b** showed decreased efficacy with respect to vehicle. VU0483605 **4.77b** increments in efficacy are between 10 to 25% of the original response of the mutants, except for Y632H and P729T were it increased only a 5%. Moreover, in the case of the P1015S, it showed full recovery from the decrease in efficacy caused by the mutation (Fig. 4.15).

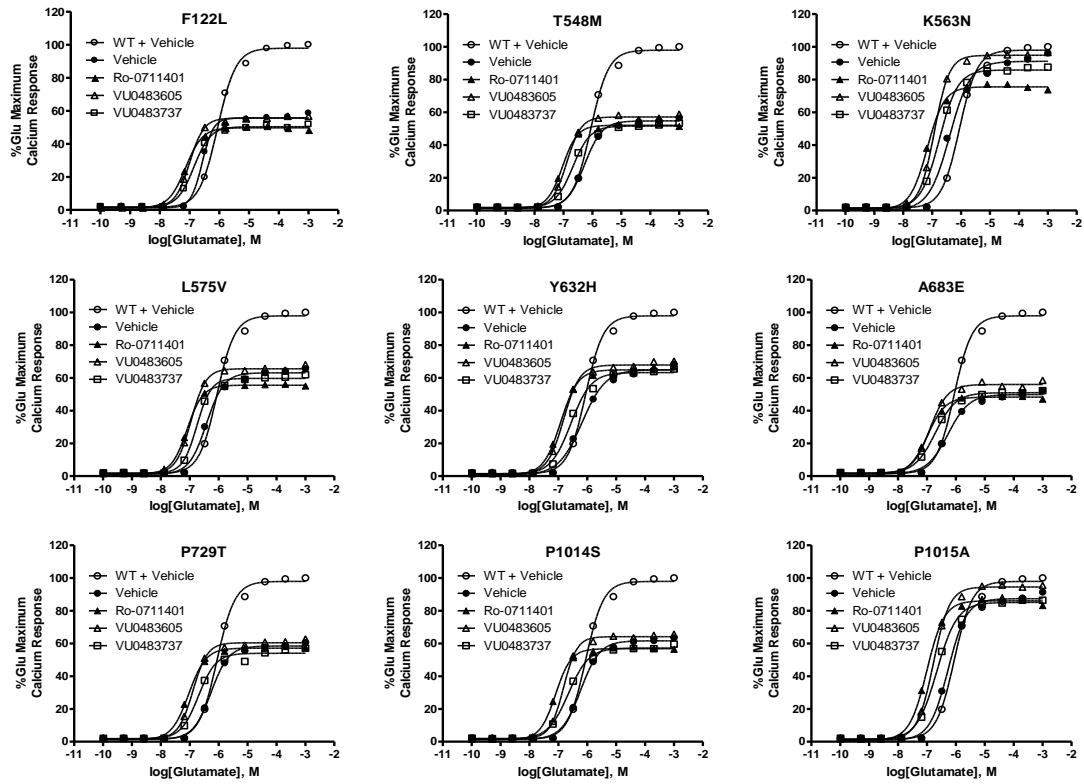


**Figure 4.15.** Effect of the application of mGlu<sub>1</sub> PAMs on the concentration response curve of glutamate in hmGlu<sub>1</sub> mutant constructs. Calcium mobilization fold-shift assays with different mGlu<sub>1</sub> constructs were used to obtain glutamate CRCs in the absence and presence of 10  $\mu$ M concentration of VU0483737 **4.76b**, VU0483605 **4.77b** and Ro 07-11401 **3.43**. Data represent the mean  $\pm$  S.E.M. of at least three independent experiments with similar results different mGlu<sub>1</sub> constructs.

**Table 4.7.** Effect of PAMs on the parameters of concentration-response curve of glutamate in hmGlu<sub>1</sub> mutant constructs. Calcium mobilization fold-shift assays with different mGlu<sub>1</sub> constructs were used to obtain glutamate CRCs in the absence and presence of 10 μM concentration of VU0483737 **4.76b**, VU0483605 **4.77b** and Ro 07-11401 **3.43**. Data represent the mean ± S.E.M. of at least three independent experiments with similar results.

Cpd		Mutant								
		F122L	T548M	K563N	L575V	Y632H	A683E	P729T	P1014S	P1015A
Vehicle	EC <sub>50</sub> (nM)	264	533	404	378	661	532	539	591	538
	Efficacy (%)	55.7	54.7	91.1	63.1	65.0	49.8	58.4	61.6	87.3
Ro 07-11401	EC <sub>50</sub> (nM)	72.8	92.0	67.5	80.6	120	104	92.0	80.2	99
	Fold-shift	3.63	5.79	5.98	4.68	5.50	5.11	5.85	7.37	5.44
	Efficacy (%)	49.7	52.0	75.5	55.5	64.9	48.2	57.1	56.8	86.0
VU0483605	EC <sub>50</sub> (nM)	99.9	130	119	110	152	127	129	151	167
	Fold-shift	2.64	4.10	3.39	3.44	4.35	4.19	4.18	3.91	3.23
	Efficacy (%)	55.6	57.1	94.8	65.6	67.8	55.9	60.4	64.1	94.5
VU0483737	EC <sub>50</sub> (nM)	139	210	178	176	271	194	199	222	220
	Fold-shift	1.90	2.54	2.27	2.12	2.44	2.74	2.71	2.66	2.44
	Efficacy (%)	50.4	51.6	84.5	59.7	63.2	50.9	53.4	57.2	85.0

We repeated this experiments using DHPG as agonist to activate the mGlu<sub>1</sub> mutants and with a 10 μM concentration of the PAMs. The results showed that the compounds potentiated the DHPG response in all the mutated receptors (Fig. 4.16). In contrast to glutamate, the potentiating effect match better what was observed in the wild-type with DHPG for the three PAMs. Ro 07-11401 was the compound that achieved the largest fold-shift, and in most cases this is even larger than the shift observed in wild type (16.7), like in T548M (29.3) and P1014S (22.0) (Table 4.8). However, the compound effect in efficacy was minimal, maintaining or slightly decreasing the

maximum response obtained in the mutants with vehicle alone. The only exception for this was mutant Y632H where an increase in efficacy of around 8% was observed, an interesting effect as this receptor was also the one that present the smallest shift in the EC<sub>50</sub> of DHPG.

Between our compounds, VU0483605 **4.77b** perform better than VU0483737 **4.76b**, similarly to what was observed with glutamate. VU0483605 **4.77b** showed fold-shift between 4.6 and 8.0 in the mutant constructs, being higher than in wild-type for K563N (7.5) and L575V (8.0). Also, only this PAM increased the efficacy of the DHPG response with respect to vehicle uniformly across the different mutant receptors; this increase ranges between 4 and 15%, and is larger for Y632H (12%) and A683E (15%).

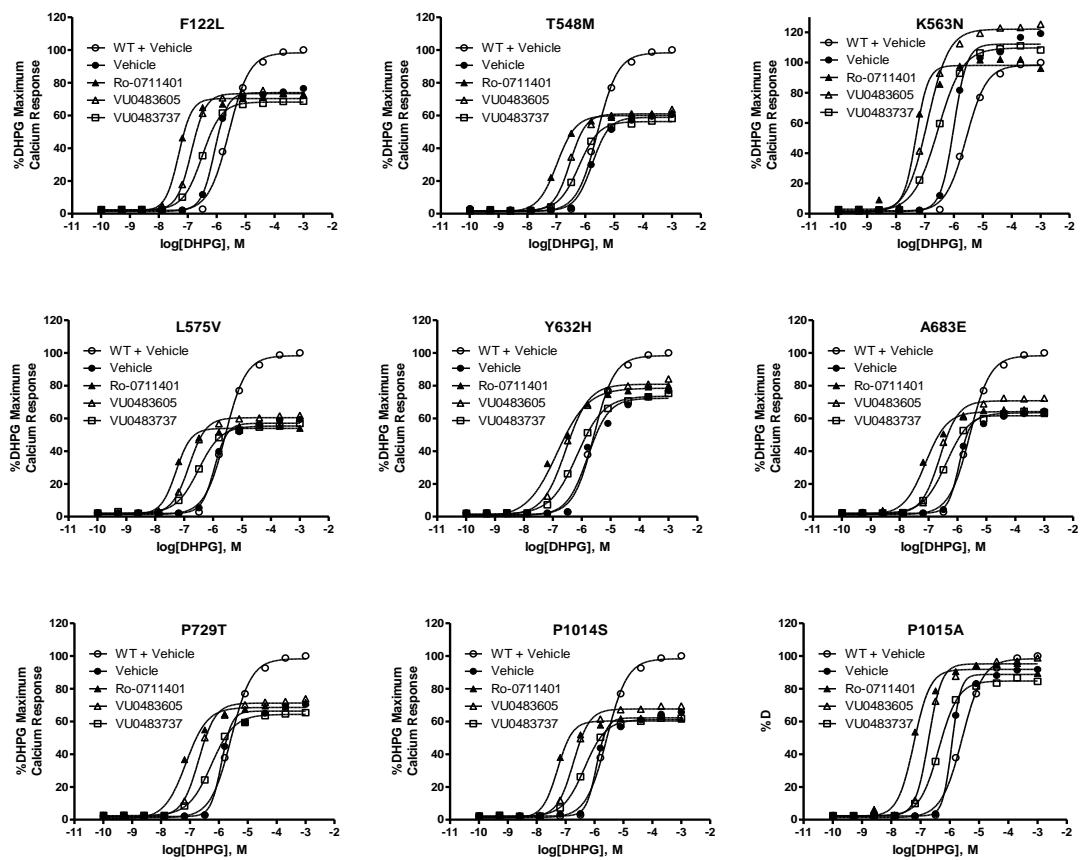


**Figure 4.16.** Effect of the application of mGlu<sub>1</sub> PAMs on the concentration response curve of DHPG in hmGlu<sub>1</sub> mutant constructs. Calcium mobilization fold-shift assays with different mGlu<sub>1</sub> constructs were used to obtain glutamate CRCs in the absence and presence of 10  $\mu$ M concentration of VU0483737 **4.76b**, VU0483605 **4.77b** and Ro 07-11401 **3.43**. Data represent the mean  $\pm$  S.E.M. of at least three independent experiments with similar results different mGlu<sub>1</sub> constructs



**Table 4.8.** Effect of PAMs on the parameters of concentration-response curve of DHPG in hmGlu<sub>1</sub> mutant constructs. Calcium mobilization fold-shift assays with different mGlu<sub>1</sub> constructs were used to obtain glutamate CRCs in the absence and presence of 10 μM concentration of VU0483737 **4.76b**, VU0483605 **4.77b** and Ro 07-11401 **3.43**. Data represent the mean ± S.E.M. of at least three independent experiments with similar results.

Cpd		Mutant								
		F122L	T548 M	K563 N	L575V	Y632 H	A683E	P729T	P1014 S	P1015 A
Vehicle	EC <sub>50</sub> (nM)	834	1725	990	1099	1606	1139	1210	1150	1158
	Efficacy (%)	73.9	58.8	112.2	57.0	72.3	61.6	66.3	62.2	88.7
Ro 07- 11401	EC <sub>50</sub> (nM)	48.2	105	48.5	52.3	141	77.7	72.5	52.3	59.3
	Fold- shift	17.3	29.3	20.4	21.0	11.3	14.7	16.7	22.0	19.5
	Efficacy (%)	70.3	60.0	98.1	53.9	78.4	64.11	68.6	60.3	91.8
VU048 3605	EC <sub>50</sub> (nM)	133	296	123	147	282	245	201	184	187
	Fold- shift	6.3	5.8	8.0	7.5	5.7	4.6	6.0	6.3	6.2
	Efficacy (%)	73.3	60.9	122	60.4	80.8	70.7	71.2	67.6	95.2
VU048 3737	EC <sub>50</sub> (nM)	316	600	282	314	686	407	543	449	425
	Fold- shift	2.6	2.9	3.5	3.5	2.3	2.8	2.2	2.6	2.7
	Efficacy (%)	68.2	56.2	109.7	55.4	73.6	63.4	64.3	61.2	84.7

### Pharmacokinetic characterization of the new mGlu<sub>1</sub> PAMs

#### *In vitro* pharmacokinetic properties and brain penetrance of novel mGlu<sub>1</sub> PAMs

To execute target validation studies in animals and elucidate the role of mGlu<sub>1</sub> in neuropsychiatric disorders, it is necessary to have adequate chemical probes. For these experiments, these chemical tools should have good pharmacodynamic properties so the receptor

can be activated selectively but also they should have good pharmacokinetic properties, so it can be guaranteed that the compound reach its target in enough concentration and at an adequate time to have the desired effect. We chose to analyze the pharmacokinetic properties of a few compounds from our libraries that showed good potency, including the PAMs tested in the hmGlu<sub>1</sub> mutants, VU0483605 **4.77b** and VU0483737 **4.76b**. The compounds were subjected first to *in vitro* pharmacokinetic experiments, including determination of intrinsic clearance in liver microsomes, cytochrome P450 inhibition and plasma protein binding.

The intrinsic clearance measurements were performed incubating the compounds with preparations of rat and liver microsomes. In these experiments the analyzed compounds presented half-life of roughly one hour. After calculations to obtain the intrinsic and predicted hepatic clearance, it was observed that the compounds had moderate hepatic clearance in both species. In the human liver microsomes, compounds behave similarly, with predicted hepatic clearance ranging from 31 to 52% of the hepatic blood flow; while in rat VU0483605 **4.77b** stand out with predicted clearance of 35% of the hepatic blood flow, while the other compounds showed values close to 60% (Table 4.9).

**Table 4.9.** Intrinsic clearance and predicted hepatic clearance for the new mGlu<sub>1</sub> PAMs. Intrinsic clearance was determined using rat and human liver microsomes.

Cpd #	VU #	Human		Rat	
		Cl <sub>int</sub> mL/min/kg	Cl <sub>hep</sub> mL/min/kg	Cl <sub>int</sub> mL/min/kg	Cl <sub>hep</sub> mL/min/kg
<b>4.76a</b>	VU0483657	9.66	6.62	77.0	36.7
<b>4.76b</b>	VU0483737	16.1	9.10	95.9	40.5
<b>4.76c</b>	VU0483635	22.5	10.9	108	42.5
<b>4.77b</b>	VU0483605	17.2	9.46	39.9	25.4

Using a cocktail strategy, the inhibition of different isoforms of P450 enzymes by the PAMs was tested. All of them showed a clean CYP profile with no inhibition of 1A2, 2C9, 2D6 and 3A4 at a concentration of 30  $\mu$ M.

For the probes to interact properly with the receptor they need to be free in solution. We proceed to quantify the fraction unbound in human and rat plasma. Unfortunately, it was not possible to determine this parameter in the plasma protein binding studies, as the compounds quickly degraded during the incubation with the plasma preparations.

Brain penetrance in rats was assessed for VU0483605 **4.77b** and VU0483737 **4.76b**. The PAMs were administered intraperitoneally and after 1.25 hours, the concentrations in brain and plasma were measured. The brain to plasma partition coefficient of VU0483737 **4.76b** was 0.64, which is not optimal but is more than three times higher the  $K_p$  of Ro 07-11401. In the case of VU0483605 **4.77b**, the coefficient was 0.85, a more desirable value indicating greater brain penetrance. However, it was observed with both compounds that the actual concentrations achieved in plasma and in the brain were low. Even at 56.6 mg/kg (IP), poor exposure is observed and concentration in plasma for these compounds was lower than their  $EC_{50}$  in mGlu<sub>1</sub> (1.25 h, 51 nM and 152 nM for VU0483737 **4.76b** and VU0483605 **4.77b**, respectively). Also, plasma instability of the compounds did not allow the calculation of a  $K_{p,uu}$  value.

#### *Plasma biotransformation analysis of a compound around VU0405622 4.8 scaffold*

As the compounds have moderate hepatic clearance and demonstrated to partition between brain and plasma with relative ease, the cause of the low concentrations of compounds achieved *in vivo* seems to be due to the plasma instability. Therefore, it was decided to study the biotransformation in plasma of compounds around this scaffold, in order to identify the metabolites generated and the decomposition process that was taking place. This would favor the confirmation of the specific region in the molecule that is labile to metabolism and the use of this information could guide the design of more stable compounds.

At the time, due to availability of the compounds, we selected VU0405623 **4.141** to perform this biotransformation study. This is an mGlu<sub>1</sub>/mGlu<sub>4</sub> dual PAM closely related to VU0405622 **4.8** and VU0483605. The compound was incubated with rat and human plasma and monitored for two hours (Fig. 4.17).

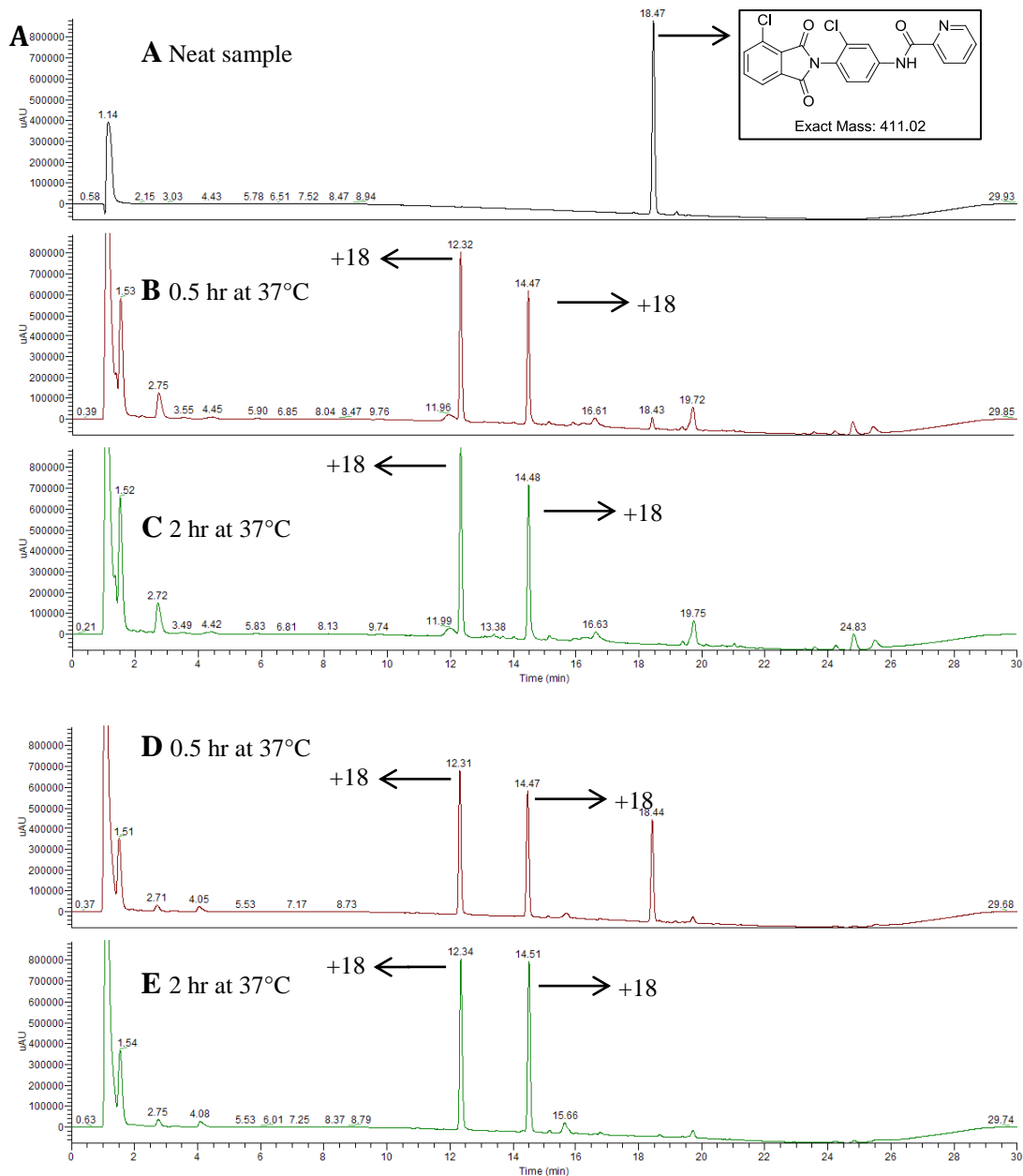


**Figure 4.17.** Biotransformation analysis of VU0405623 **4.141** in rat (B and C) and human (D and E) plasma. Analysis of samples incubated for 30 minutes and 2 hours was made by LC-MS.

In rat plasma, the compound is completely metabolized in less than 30 minutes, while in human plasma it took around 1 hour to consume PAM **4.141**. As the plasma preparation could have a supraphysiological amount of proteins and enzymes, the analysis was also performed in whole rat blood, to evaluate if the compound could be more stable in the presence of erythrocytes. In rat whole blood, the test article showed slower degradation, but it still degrades rapidly at a rate comparable to the observed in human plasma. From these experiments, it was observed that the **4.141** was mainly transformed into two more polar metabolites that have 18 more atomic mass units. After analyzing the fragmentation patterns with LC/MS<sup>n</sup>, the transformation was narrowed down to opening of the phthalimide to generate the regioisomeric phthalamic acids (Fig. 4.18).

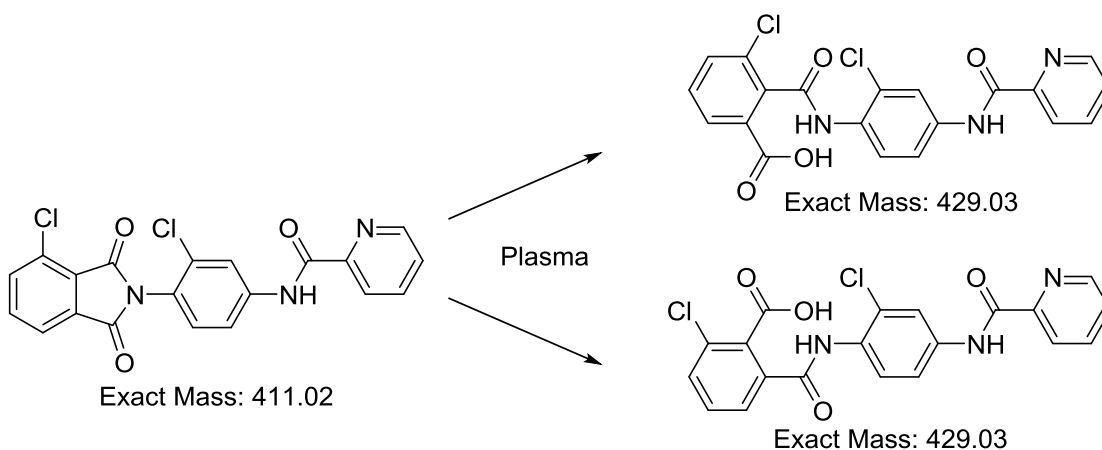


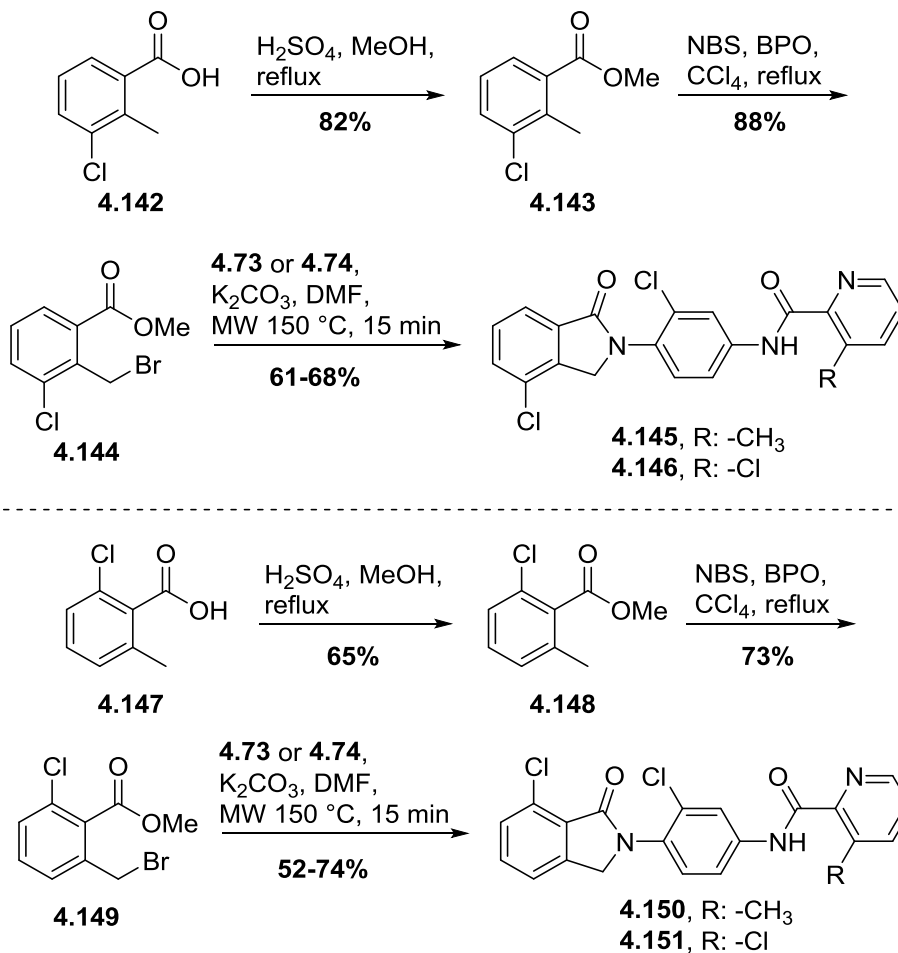
**Figure 4.18.** Identification of metabolites for plasma degradation of VU0405623 **4.141**. Analysis of samples incubated for 2 hours was made by LC-MS<sup>n</sup>.

#### *Designing of mGlu<sub>1</sub> PAMs with better plasma stability*

Due to plasma instability of the phthalimide moiety, we started to contemplate alternatives to this group. One approach assessed was the replacement of one of the carbonyls in the phthalimide for a methylene, engendering an isoindolinone. The use of the lactam poses the advantage that its carbonyl will be less electrophilic than the carbonyls in the imide. In the case of

the imide, the possibility of more resonance forms will cause the distribution of the electrons from the nitrogen into a larger system, while in the amide from the lactam ring this will be confined into a smaller region. This will make the carbon in the carbonyl less electropositive and less susceptible to nucleophilic attack. Hence, it would be expected that the rate of hydrolysis in plasma for the phthalimide diminish.

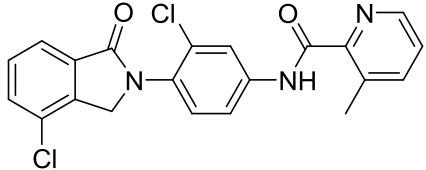
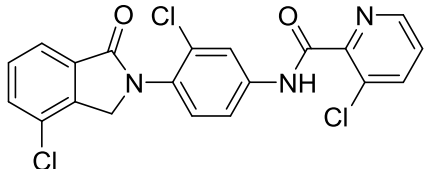
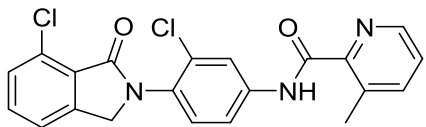
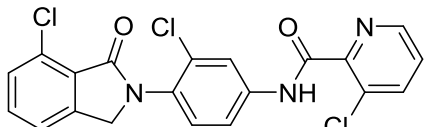
In order to test our hypothesis, isoindolinone analogs of VU0483737 **4.76b** and VU0483605 **4.77b** were envisioned. As these parent compounds have a substituent in the phenyl ring of the phthalimide the carbonyls are not equivalent and it was needed to synthesize both isoindolinone regioisomers, the 4-chloro and 7-chloro substituted analogs, as they may possess different biological activity. Several methods to access the isoindolinone compounds were tried. Isobenzofuranone opening with the aniline using different Lewis and Brønsted acids did not yield the intermediate acyclic precursor needed for the formation of the lactam. As well, copper and palladium amidation procedures using the preformed isoindolinone and the corresponding aryl bromide or the aryl iodide did not provide satisfactory results. Finally, we tried the synthesis of these compounds through tandem nucleophilic substitution-cyclization employing *ortho*-bromomethylbenzoate esters (Scheme 4.6). Our synthetic route started with the formation of the methyl ester **4.143** and **4.148** with the chloro-substituted *ortho*-methylbenzoic acids **4.142** and **4.147** through a classical Fischer esterification procedure. Then, a Wohl-Ziegler radical bromination allowed the obtention of **4.144** and **4.149** in good yields. The final step to afford analogs **4.145-4.146** and **4.150-4.151** was the nucleophilic substitution with anilines **4.73** and **4.74** followed by the formation of the lactam; a reaction carried in the microwave with potassium carbonate as base that produced the desired isoindolinones in moderate yields.



**Scheme 4.6.** Synthesis of isoindolinone analogs **4.145-4.146** and **4.150-4.151**.

Screening of the compounds showed that the position of the chlorine was relevant for mGlu<sub>1</sub> activity, as the 4-chloroisoindolinone analogs **4.145-4.146** maintain activity while its 7-chloro regioisomers **4.150-4.151** were only weak potentiators (Table 4.10). It was also learned from this experiment that the carbonyls in the phthalimide are important for mGlu<sub>1</sub> activity, as the EC<sub>50</sub>s of the active regioisomers **4.145-4.146** are 3 to 5 times larger with respect to their parent compounds.

**Table 4.10.** Potencies in human mGlu<sub>1</sub> and mGlu<sub>4</sub> of isoindolinone analogs **4.145-4.146** and **4.150-4.151**. Calcium mobilization responses for each compound are reported as a percentage of the maximum glutamate response. VU number denotes the compound identifier assigned by Vanderbilt University. Data represent the mean ± S.E.M. of at least three independent experiments with similar results. ---, no potentiation. ND, not determined.

Structure	Cpd #	VU #	hmGlu <sub>1</sub>	
			EC <sub>50</sub> (μM)	%Glu <sub>Max</sub>
	<b>4.145</b>	VU0487229	1.36	89
	<b>4.146</b>	VU0487312	1.82	97
	<b>4.150</b>	VU0487011	>10.0	117
	<b>4.151</b>	VU0487028	>10.0	75

Despite the decrease in activity, these new analogs showed half-lives of over four hours in rat and human plasma, demonstrating that the removal of one of the carbonyls was beneficial for plasma stability. This allowed us to hypothesize that if we find a phthalimide parent compound of adequate potency, we could introduce this chemical modification and afford for the loss in potency, gaining remarkable plasma stability.



## Summary and future directions

After trying to optimize with little success the properties of Ro 07-11401, we focused our efforts in the VU0405622 **4.8** scaffold. This starting point displayed the advantage of submicromolar potency for mGlu<sub>1</sub> but with the caveat of no selectivity, being an mGlu<sub>1</sub>/mGlu<sub>4</sub> dual PAM.

We started the exploration of the SAR of this scaffold by making modifications on the picolinamide side of the molecule (Fig. 4.19). It was found that small substituents in the 3 and 4 position of the pyridine allowed differentiation between mGlu<sub>1</sub> and mGlu<sub>4</sub>, maintaining the effect on mGlu<sub>1</sub> and losing activity for mGlu<sub>4</sub>; however, this was accompanied by loss in potency. A second iteration of chemical modifications this time in the phthalimide region led us to find that substituents in the 3 position of the phthalimide can enhance the potency for the mGlu<sub>1</sub> receptor and allowed us to obtain VU0483605 **4.77b** and VU0483737 **4.76b**. Further SAR exploration showed that the presence and orientation of the amide in the picolinamide side was essential for mGlu<sub>1</sub> activity, and also that the chlorine in the phenyl ring was beneficial for mGlu<sub>1</sub> potentiation.

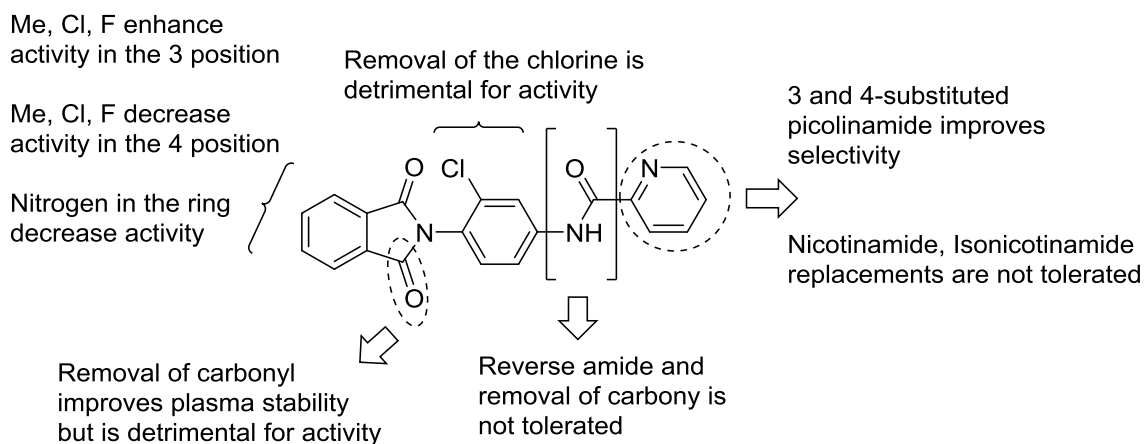


**Figure 4.19.** Exploration of SAR in the VU0405622 **4.8** scaffold.

VU0483605 **4.77b** and VU0483737 **4.76b** showed good potency and activity across human and rat mGlu<sub>1</sub>. Both compounds are selective against mGlu<sub>4</sub>, and VU0483605 **4.77b** demonstrated to be selective against all other mGlu receptors. These PAMs decreased the EC<sub>50</sub> of glutamate and DHPG in wild type and schizophrenia related mutants. In the majority of mutant constructs, VU0483605 **4.77b** increased the efficacy of the glutamate response, an effect that was not observed as robustly with VU0483737 **4.76b** and Ro 07-11401 **3.43**. The relevance of this enhancement of EC<sub>50</sub> and efficacy of glutamate caused by the PAMs is a question that would require additional *in vivo* testing in mutant mice strains.

In preparation for *in vivo* tests, we started the pharmacokinetic characterization of these mGlu<sub>1</sub> PAMs. These analogs demonstrated to have moderate intrinsic clearance in rat and human liver microsomes and no inhibition of main P450 drug-metabolizing enzymes, but their fraction unbound in plasma could not be obtained due to plasma instability. Analysis of the biotransformation of a close analog in plasma and whole blood identified the phthalimide as the site of metabolism.

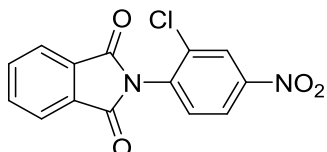
In an effort to generate more stable compounds, we develop isoindolinone analogs **4.145-4.146** that demonstrated good plasma stability but with decrease mGlu<sub>1</sub> activity. Because of the remarkable improvement in plasma stability, it was thought that if the removal of one of the carbonyls is applied to a more potent parent compound, the loss in potency might be afforded and it will generate a compound with acceptable pharmacokinetic properties. Our next steps were focused in finding a more potent compound for mGlu<sub>1</sub> activity and these are detailed in the next chapter of this document.

## EXPERIMENTAL METHODS

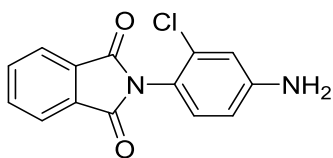
### *General chemical synthesis and characterization*

All reactions were carried out employing standard chemical techniques under inert atmosphere. All reagents and solvents were commercial grade and purified prior to use when necessary. Solvents used for extraction, washing, and chromatography were HPLC grade. Analytical thin layer chromatography was performed on 250  $\mu\text{m}$  silica gel glass backed plates from Sorbent Technologies. Visualization was accomplished with UV light and/or the use of iodine or ninhydrin solution followed by heating. Analytical HPLC was performed on an Agilent 1200 LCMS with UV detection at 215 and 254 nm along with ELSD detection and electrospray ionization, with all final compounds showing >95% purity and a parent mass ion consistent with the desired structure. Low resolution mass spectra were obtained on an Agilent 6130 mass spectrometer with electrospray ionization source. MS parameters were as follows: fragmentor: 100, capillary voltage: 3000 V, nebulizer pressure: 40 psig, drying gas flow: 11 L/min, drying gas temperature: 350° C. Samples were introduced via an Agilent 1200 HPLC comprised of a degasser, G1312A binary pump, G1367B HP-ALS, G1316A TCC, G1315D DAD, and a Varian 380 ELSD. UV absorption was generally observed at 215 nm and 254 nm with a 4 nm bandwidth. Column: Thermo Accucore C18, 2.1 x 30 mm, 2.6  $\mu\text{m}$ . Gradient conditions: 7% to 95%  $\text{CH}_3\text{CN}$  in  $\text{H}_2\text{O}$  (0.1% TFA) over 1.6 min, hold at 95%  $\text{CH}_3\text{CN}$  for 0.35 min, 1.5 mL/min, 45 °C. Flash column chromatography was performed on a Teledyne ISCO Combiflash Rf system. Preparative purification of library compounds was performed on a Gilson 215 preparative LC system. Column: Thermo Accucore C18, 2.1 x 30 mm, 2.6  $\mu\text{m}$ . Gradients condition: variable,  $\text{CH}_3\text{CN}$  in  $\text{H}_2\text{O}$  (0.1% TFA) over 4 minutes, hold at 95%  $\text{CH}_3\text{CN}$  for 0.35 min, 50 mL/min. Purity for all final compounds was >95%, and each showed a parent mass ion consistent with the desired structure in low resolution LC-MS.  $^1\text{H}$  and  $^{13}\text{C}$  NMR spectra were recorded on Bruker DRX-400 (400 MHz) instrument. Chemical shifts are reported in ppm relative to residual solvent

peaks as an internal standard at the following chemical shifts ( $^1\text{H}$  and  $^{13}\text{C}$  respectively): 7.26 and 77.0 ppm for  $\text{CDCl}_3$ ; 2.50 and 39.52 ppm for  $\text{DMSO}-d_6$ , 3.31 and 49.2 ppm for  $\text{CD}_3\text{OD}$ . Data are reported as follows: chemical shift, integration, multiplicity (s = singlet, d = doublet, t = triplet, q = quartet, dd = doublet of doublets, br = broad, m = multiplet), coupling constant (Hz).



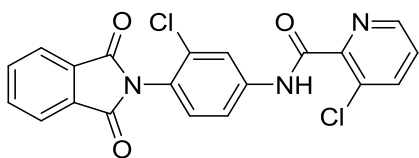
**2-(2-chloro-4-nitrophenyl)isoindoline-1,3-dione (4.11).** In a flask, 200 mg (1.622 mmol, 1.2 equiv.) of 2-chloro-4-nitroaniline and 280 mg (1.350 mmol, 1.0 equiv.) of phthalic anhydride were added and dissolved in 5 mL of acetic acid. The mixture was refluxed for 24 hours. After cooling the solution a precipitate is formed. The solid was filtered and carefully triturated with cold methanol to obtain a light yellow powder (359 mg, 88%).  $^1\text{H-NMR}$  (400.1 MHz,  $\text{CDCl}_3$ )  $\delta$  (ppm): 8.45 (1H, d,  $J=2.4$  Hz), 8.28 (1H, dd,  $J=8.7$  Hz,  $J=2.5$  Hz), 8.00 (2H, m), 7.86 (2H, m), 7.58 (1H, d,  $J=8.6$  Hz).  $^{13}\text{CNMR}$  (100.6 MHz,  $\text{CDCl}_3$ )  $\delta$  (ppm): 165.6, 148.2, 135.6, 134.9, 134.6, 131.6, 131.4, 125.7, 124.2, 122.6.



**2-(4-amino-2-chlorophenyl)isoindoline-1,3-dione (4.12).** In a vial, 300 mg (0.993 mmol, 1.0 equiv.) of **4.11** were suspended in dioxane. The suspension was cold in an ice bath and purged with argon. A previously prepared solution of tin(II) chloride (847 mg, 4.469 mmol, 4.5 equiv.) in concentrated hydrochloric acid (5M concentration of  $\text{SnCl}_2$ ) was added dropwise to the suspension. After 2 hours of stirring at room temperature, the reaction was neutralized carefully with aqueous potassium carbonate 20%, filtered and extracted with diethyl ether. The organic

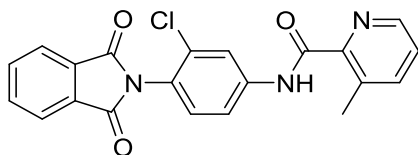
phase was dried with magnesium sulphate, filtered and the volatiles eliminated *in vacuo* to yield a yellow powder (196 mg, 72%). <sup>1</sup>H-NMR (400.1 MHz, DMSO-*d*<sub>6</sub>) δ (ppm): 7.97 (2H, m), 7.90 (2H, m), 7.14 (1H, d, *J*=8.5 Hz), 6.76 (1H, d, *J*=2.4 Hz), 6.60 (1H, dd, *J*=8.6 Hz, *J*=2.4 Hz), 5.74 (2H, s, -NH<sub>2</sub>). <sup>13</sup>CNMR (100.6 MHz, DMSO-*d*<sub>6</sub>) δ (ppm): 167.5, 151.5, 135.3, 132.7, 131.78, 131.76, 123.9, 116.5, 113.6, 113.0.

**General synthesis of *N*-(3-chloro-4-(1,3-dioxisoindolin-2-yl)phenyl)amides (4.13-4.65).** In a vial, 0.088 mmol (1.2 equiv.) of the carboxylic acid were added and dissolved in 0.5 mL mixture of DCM:DIEA (9:1), then 41 mg (0.110 mmol, 1.5 equiv.) of HATU were added. The mixture was stirred for 10 minutes, and 20 mg (0.073 mmol, 1.0 equiv.) of **4.12** dissolved in 0.5 mL of DCM:DIEA (9:1) were added, followed by 3 drops of DMF. The reaction was stirred for 24 hours at room temperature. After this time, the reaction was quenched with the addition of water, and was worked up by extraction with DCM. The organic phases was filtered through a phase separator, volatiles were evaporated, the crude was dissolved in DMSO and purified by preparative HPLC.

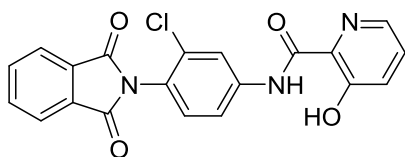


***N*-(3-chloro-4-(1,3-dioxisoindolin-2-yl)phenyl)-3-chloropicolinamide (4.28).** White powder. <sup>1</sup>H-NMR (400.1 MHz, CDCl<sub>3</sub>) δ (ppm): 10.19 (1H, s), 8.55 (1H, dd, *J*=4.5 Hz, *J*=1.0 Hz), 8.19 (1H, d, *J*=2.3 Hz), 7.98 (2H, m), 7.92 (1H, dd, *J*=8.1 Hz, *J*=1.0 Hz), 7.82 (2H, m), 7.76 (1H, dd, *J*=8.6 Hz, *J*=2.3 Hz), 7.48 (1H, dd, *J*=8.2 Hz, *J*=4.5 Hz), 7.35 (1H, d, *J*=8.6 Hz). <sup>13</sup>CNMR (100.6 MHz, CDCl<sub>3</sub>) δ (ppm): 166.7, 160.7, 145.8, 144.5, 141.1, 139.5, 134.4, 133.8,

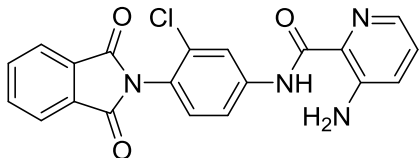
132.9, 131.8, 130.8, 127.2, 125.0, 123.9, 120.8, 118.4. HRMS (TOF, ES+)  $C_{20}H_{12}Cl_2N_3O_3$  [M+H]<sup>+</sup> calc. mass 412.0256, found 412.0253.



***N*-(3-chloro-4-(1,3-dioxoisindolin-2-yl)phenyl)-3-methylpicolinamide (4.51).** White powder. <sup>1</sup>H-NMR (400.1 MHz, CDCl<sub>3</sub>) δ (ppm): 10.47 (1H, s), 8.47 (1H, d, *J*=3.7 Hz), 8.18 (1H, d, *J*=2.3 Hz), 7.97 (2H, m), 7.81 (2H, m), 7.74 (1H, dd, *J*=8.6 Hz, *J*=2.3 Hz), 7.67 (1H, d, *J*=7.3 Hz), 7.40 (1H, dd, *J*=7.8 Hz, *J*=4.6 Hz), 7.33 (1H, d, *J*=8.6 Hz), 2.83 (3H, s). <sup>13</sup>CNMR (100.6 MHz, CDCl<sub>3</sub>) δ (ppm): 166.8, 163.6, 146.0, 145.4, 141.4, 140.0, 136.5, 134.4, 133.7, 131.9, 130.7, 126.4, 124.6, 123.9, 120.7, 118.3, 20.7. HRMS (TOF, ES+)  $C_{21}H_{15}ClN_3O_3$  [M+H]<sup>+</sup> calc. mass 392.0802, found 392.0799.

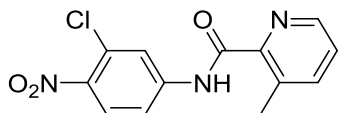


***N*-(3-chloro-4-(1,3-dioxoisindolin-2-yl)phenyl)-3-hydroxypicolinamide (4.55).** Cream powder. <sup>1</sup>H-NMR (400.1 MHz, CDCl<sub>3</sub>) δ (ppm): 10.09 (1H, s), 8.16 (1H, d, *J*=3.1 Hz), 8.10 (1H, d, *J*=2.2 Hz), 7.97 (2H, m), 7.81 (2H, m), 7.74 (1H, dd, *J*=8.6 Hz, *J*=2.3 Hz), 7.44 (1H, dd, *J*=8.5 Hz, *J*=4.2 Hz), 7.37 (2H, m). <sup>13</sup>CNMR (100.6 MHz, CDCl<sub>3</sub>) δ (ppm): 166.7, 158.3, 139.6, 138.7, 138.1, 134.5, 133.9, 131.8, 131.0, 130.7, 129.4, 126.7, 124.0, 121.3, 119.1, 118.8. HRMS (TOF, ES+)  $C_{20}H_{13}ClN_3O_4$  [M+H]<sup>+</sup> calc. mass 394.0595, found 394.0598.



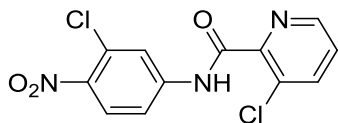
**3-amino-N-(3-chloro-4-(1,3-dioxisoindolin-2-yl)phenyl)picolinamide (4.59).** Cream powder.  $^1\text{H-NMR}$  (400.1 MHz,  $\text{CDCl}_3$ )  $\delta$  (ppm): 10.33 (1H, s), 8.16 (1H, d,  $J = 2.3$  Hz), 8.01 (2H, m), 7.95 (1H, dd,  $J = 4.2$  Hz,  $J = 1.1$  Hz), 7.83 (2H, m), 7.74 (1H, dd,  $J = 8.6$  Hz,  $J = 2.3$  Hz), 7.35 (1H, d,  $J = 8.6$  Hz), 7.25 (1H, dd,  $J = 8.4$  Hz,  $J = 4.3$  Hz), 7.09 (1H, dd,  $J = 8.4$  Hz,  $J = 1.2$  Hz).  $^{13}\text{CNMR}$  (100.6 MHz,  $\text{CDCl}_3$ )  $\delta$  (ppm): 166.8, 165.6, 146.3, 139.9, 136.6, 134.4, 133.6, 131.9, 130.7, 128.6, 27.9, 125.4, 124.4, 120.6, 118.3. HRMS(TOF, ES+)  $\text{C}_{20}\text{H}_{14}\text{ClN}_4\text{O}_3$   $[\text{M}+\text{H}]^+$  calcd mass 393.0754, found 394.0753.

**General synthesis of N-(2-chloro-4-nitrophenyl)picolinamides (4.70-4.72).** In a microwave vial, 2.20 mmol (1.0 equiv.) of the 3-substituted picolinic acid were added and dissolved in 5 mL of DCE:DIEA (9:1), then 1254 mg (3.30 mmol, 1.5 equiv.) of HATU were added. The mixture was stirred for five minutes, and 2.64 mmol (1.2 equiv.) of 3-chloro-4-nitroaniline dissolved in 5 mL of DCE:DIEA (9:1) were added, followed by 3 drops of DMF. The reaction was heated in the microwave at 120 °C for 30 minutes. The reaction was cooled to room temperature and water was added, causing the precipitation of the product. The crude was filtrated *in vacuo* and carefully triturated with cold methanol.

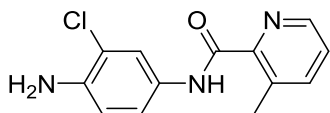


**N-(2-chloro-4-nitrophenyl)-3-methylpicolinamide (4.70).** White powder. 500 mg (78%).  $^1\text{H-NMR}$  (400.1 MHz,  $\text{DMSO}-d_6$ )  $\delta$  (ppm): 11.21 (1H, s, -NH), 8.58 (1H, br), 8.34 (1H, s), 8.14 (1H, d,  $J=8.8$  Hz), 8.04 (1H, d,  $J=9.3$  Hz), 7.84 (1H, d,  $J=7.3$  Hz), 7.57 (1H, m), 2.65

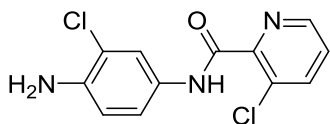
(3H, s).  $^{13}\text{C}$ -NMR (100.6 MHz,  $\text{DMSO-}d_6$ )  $\delta$  (ppm): 165.7, 148.3, 146.4, 144.2, 142.2, 141.1, 134.9, 127.7, 127.0, 126.8, 121.7, 119.0, 19.8.



***N*-(2-chloro-4-nitrophenyl)-3-chloropicolinamide (4.71).** Pale yellow powder. 517 mg (75%).  $^1\text{H}$ -NMR (400.1 MHz,  $\text{DMSO-}d_6$ )  $\delta$  (ppm): 11.36 (1H, s, -NH), 8.69 (1H, dd,  $J=4.6$  Hz,  $J=1.3$  Hz), 8.23 (1H, d,  $J=2.1$  Hz), 8.17 (2H, m), 7.92 (1H, dd,  $J=9.0$  Hz,  $J=2.1$  Hz), 7.68 (1H, 1H, dd,  $J=8.2$  Hz,  $J=4.6$  Hz).  $^{13}\text{C}$ -NMR (100.6 MHz,  $\text{DMSO-}d_6$ )  $\delta$  (ppm): 164.1, 149.7, 147.8, 143.7, 142.5, 139.6, 129.4, 128.0, 127.6, 127.1, 121.5, 118.9.



***N*-(4-amino-2-chlorophenyl)-3-methylpicolinamide (4.73).** Compound was obtained similarly to **4.12**. 500 mg (1.714 mmol) of **4.70** were employed to yield 329 mg (74%) of a pale yellow powder.  $^1\text{H}$ -NMR (400.1 MHz,  $\text{DMSO-}d_6$ )  $\delta$  (ppm): 10.31 (1H, s, -NH), 8.51 (1H, d,  $J=4.0$  Hz), 7.87 (1H, d,  $J=2.1$  Hz), 7.79 (1H, d,  $J=7.6$  Hz), 7.49 (1H, dd,  $J=7.7$  Hz,  $J=4.7$  Hz), 7.42 (1H, dd,  $J=8.7$  Hz,  $J=2.2$  Hz), 6.78 (1H, d,  $J=8.7$  Hz), 5.19 (2H, s, -NH<sub>2</sub>), 2.56 (3H, s).  $^{13}\text{C}$ -NMR (100.6 MHz,  $\text{DMSO-}d_6$ )  $\delta$  (ppm): 164.5, 150.0, 146.2, 141.5, 140.7, 133.7, 129.1, 125.9, 121.2, 120.6, 116.9, 115.6, 19.6.

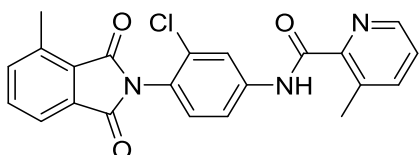


***N*-(4-amino-2-chlorophenyl)-3-chloropicolinamide (4.74).** Compound was obtained similarly to **4.12**. 500 mg (1.714 mmol) of **4.71** were employed to yield 428 mg (92%) of a pale



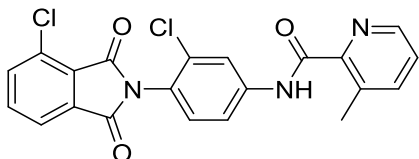
yellow powder.  $^1\text{H-NMR}$  (400.1 MHz,  $\text{DMSO-}d_6$ )  $\delta$  (ppm): 10.42 (1H, s, -NH), 8.61 (1H, dd,  $J=4.6$  Hz,  $J=1.2$  Hz), 8.09 (1H, dd,  $J=8.2$  Hz,  $J=1.2$  Hz), 7.74 (1H, d,  $J=2.1$  Hz), 7.59 (1H, dd,  $J=8.2$  Hz,  $J=4.7$  Hz), 7.33 (1H, dd,  $J=8.7$  Hz,  $J=2.2$  Hz), 6.79 (1H, d,  $J=8.7$  Hz), 5.24 (2H, s, - $\text{NH}_2$ ).  $^{13}\text{C-NMR}$  (100.6 MHz,  $\text{DMSO-}d_6$ )  $\delta$  (ppm): 162.9, 151.6, 147.6, 141.8, 139.0, 128.8, 126.7, 121.0, 120.4, 116.9, 115.7.

**General synthesis of substituted *N*-(3-chloro-4-(1,3-dioxoisindolin-2-yl)phenyl)picolinamides (4.76a-g, 4.77a-g, 4.78a-g).** In a microwave vial, 0.0709 mmol (1.0 equiv.) of the aniline (4.73, 4.74 or 4.75) and 0.106 mmol (1.5 equiv.) of the substituted phthalic anhydride were added and dissolved in 1 mL of NMP. The vial was sealed and the mixture was heated at 200 °C for 20 minutes. After this time, the reaction was quenched with the addition of water, and was worked up by extraction with DCM (2 mL, thrice). The organic phase was filtered through a phase separator, volatiles were evaporated; the crude was dissolved in DMSO and purified by preparative HPLC.



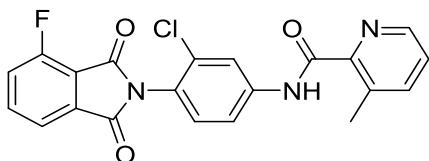
***N*-(3-chloro-4-(4-methyl-1,3-dioxoisindolin-2-yl)phenyl)-3-methylpicolinamide (4.76a).** Cream powder.  $^1\text{H-NMR}$  (400.1 MHz,  $\text{CDCl}_3$ )  $\delta$  (ppm): 10.63 (1H, s), 8.40 (1H, d,  $J=4.3$  Hz), 8.16 (1H, d,  $J=2.3$  Hz), 7.80 (1H, d,  $J=7.3$ ), 7.76 (1H, dd,  $J=8.6$  Hz,  $J=2.3$  Hz), 7.73 (1H, d,  $J=7.7$  Hz), 7.66 (1H, t,  $J=7.5$  Hz), 7.55 (1H, d,  $J=7.8$  Hz), 7.45 (1H, dd,  $J=7.8$  Hz,  $J=4.7$  Hz), 7.33 (1H, d,  $J=8.6$  Hz), 2.83 (3H, s), 2.75 (3H, s).  $^{13}\text{CNMR}$  (100.6 MHz,  $\text{CDCl}_3$ )  $\delta$  (ppm): 167.5, 166.8, 163.1, 145.9, 144.7, 141.9, 139.9, 138.6, 136.7, 136.6, 133.9, 133.7, 132.3, 130.8, 128.6,

126.4, 124.9, 121.5, 120.8, 118.4, 20.6, 17.7. HRMS (TOF, ES+)  $C_{22}H_{17}ClN_3O_3$   $[M+H]^+$  calc. mass 406.0958, found 406.0956.



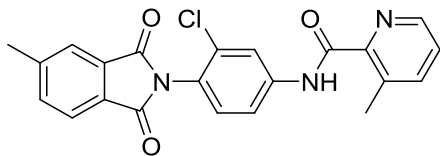
***N*-(3-chloro-4-(4-chloro-1,3-dioxisoindolin-2-yl)phenyl)-3-methylpicolinamide**

**(4.76b).** Cream powder.  $^1H$ -NMR (500 MHz,  $CDCl_3$ )  $\delta$  (ppm): 10.49 (1H, s), 8.47 (1H, d,  $J=4.3$  Hz,  $J=1.1$  Hz), 8.18 (1H,  $J=2.3$  Hz), 7.90 (1H, m), 7.74 (3H, m), 7.67 (1H, d,  $J=7.8$  Hz), 7.40 (1H, dd,  $J=7.8$  Hz,  $J=4.6$  Hz), 7.32 (1H, d,  $J=8.6$  Hz), 2.83 (3H, s).  $^{13}C$ NMR (100.6 MHz,  $CDCl_3$ )  $\delta$  (ppm): 165.3, 164.3, 162.8, 145.7, 144.2, 142.3, 140.0, 136.7, 136.1, 135.3, 133.9, 133.6, 132.0, 130.7, 127.6, 126.5, 124.4, 122.3, 120.9, 118.6, 20.4. HRMS (TOF, ES+)  $C_{21}H_{14}Cl_2N_3O_3$   $[M+H]^+$  calc. mass 426.0412, found 426.0414.



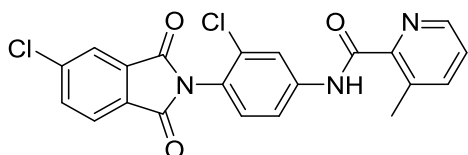
***N*-(3-chloro-4-(4-fluoro-1,3-dioxisoindolin-2-yl)phenyl)-3-methylpicolinamide**

**(4.76c).** Brown powder.  $^1H$ -NMR (400.1 MHz,  $CDCl_3$ )  $\delta$  (ppm): 10.48 (1H, s), 8.46 (1H, dd,  $J=4.5$  Hz,  $J=1.0$  Hz), 8.18 (1H, d,  $J=2.3$  Hz), 7.81 (2H, m), 7.74 (1H, dd,  $J=8.6$  Hz,  $J=2.4$  Hz), 7.67 (1H, d,  $J=7.8$  Hz,  $J=0.8$  Hz), 7.47 (1H, m), 7.40 (1H, dd,  $J=7.8$  Hz,  $J=4.6$  Hz), 7.33 (1H, d,  $J=8.6$  Hz), 2.83 (3H, s).  $^{13}C$ NMR (125.7 MHz,  $CDCl_3$ )  $\delta$  (ppm): 165.6, 163.7, 163.4, 157.9 ( $^1J_{CF}$ , d,  $J=266$  Hz), 146.0, 145.4, 141.44, 141.39, 140.2, 137.0 ( $^3J_{CF}=7.5$  Hz), 136.6, 134.0, 133.7, 130.7, 126.4, 124.2, 122.8 ( $^2J_{CF}=19.7$  Hz), 120.7, 120.1 ( $^4J_{CF}=3.2$  Hz), 118.4, 20.8. HRMS (TOF, ES+)  $C_{21}H_{14}ClFN_3O_3$   $[M+H]^+$  calc. mass 410.0708, found 410.0706.



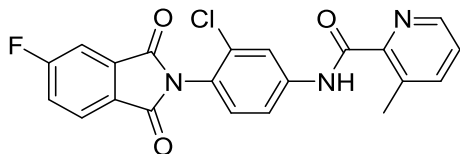
***N*-(3-chloro-4-(5-methyl-1,3-dioxisoindolin-2-yl)phenyl)-3-methylpicolinamide**

**(4.76d).** Cream powder.  $^1\text{H-NMR}$  (400.1 MHz,  $\text{CDCl}_3$ )  $\delta$  (ppm): 10.51 (1H, s), 8.45 (1H, d,  $J=3.9$  Hz), 8.17 (1H, d,  $J=2.3$  Hz), 7.85 (1H, d,  $J=7.6$  Hz), 7.78 (1H, s), 7.74 (1H, dd,  $J=8.6$  Hz,  $J=2.3$  Hz), 7.68 (1H, d,  $J=7.7$  Hz), 7.59 (1H, d,  $J=7.6$  Hz), 7.41 (1H, dd,  $J=7.8$  Hz,  $J=4.6$  Hz), 7.33 (1H, d,  $J=8.6$  Hz), 2.83 (3H, s), 2.57 (3H, s).  $^{13}\text{CNMR}$  (100.6 MHz,  $\text{CDCl}_3$ )  $\delta$  (ppm): 167.0, 166.9, 163.2, 145.9, 145.8, 144.8, 141.8, 139.9, 136.6, 134.9, 133.7, 132.2, 130.8, 129.3, 126.4, 124.8, 124.4, 123.8, 120.8, 118.4, 22.0, 20.6. HRMS (TOF, ES+)  $\text{C}_{22}\text{H}_{17}\text{ClN}_3\text{O}_3$   $[\text{M}+\text{H}]^+$  calc. mass 406.0958, found 406.0956.



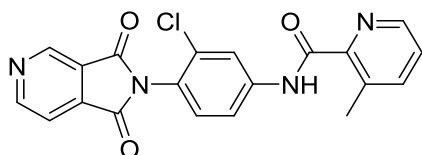
***N*-(3-chloro-4-(5-chloro-1,3-dioxisoindolin-2-yl)phenyl)-3-methylpicolinamide**

**(4.76e).** Cream powder.  $^1\text{H-NMR}$  (400.1 MHz,  $\text{CDCl}_3$ )  $\delta$  (ppm): 10.54 (1H, s), 8.45 (1H, d,  $J=4.0$  Hz), 8.18 (1H, d,  $J=2.3$  Hz), 7.94 (1H, d,  $J=1.6$  Hz), 7.90 (1H, d,  $J=8.0$  Hz), 7.76 (2H, m), 7.69 (1H, d,  $J=7.6$  Hz), 7.42 (1H, dd,  $J=7.8$  Hz,  $J=4.6$  Hz), 7.32 (1H, d,  $J=8.6$  Hz), 2.83 (3H, s).  $^{13}\text{CNMR}$  (100.6 MHz,  $\text{CDCl}_3$ )  $\delta$  (ppm): 165.8, 165.5, 163.0, 145.8, 144.6, 142.0, 141.2, 140.1, 136.7, 134.5, 133.6, 133.5, 130.7, 129.9, 126.5, 125.1, 124.4, 124.3, 120.8, 118.5, 20.5. HRMS (TOF, ES+)  $\text{C}_{21}\text{H}_{14}\text{Cl}_2\text{N}_3\text{O}_3$   $[\text{M}+\text{H}]^+$  calc. mass 426.0412, found 426.0416.



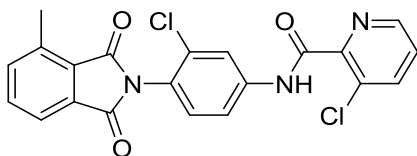
***N*-(3-chloro-4-(5-fluoro-1,3-dioxisoindolin-2-yl)phenyl)-3-methylpicolinamide**

**(4.76f).** Cream powder.  $^1\text{H-NMR}$  (400.1 MHz,  $\text{CDCl}_3$ )  $\delta$  (ppm): 10.53 (1H, s), 8.46 (1H, d,  $J=4.2$  Hz), 8.18 (1H, d,  $J=2.3$  Hz), 7.98 (1H, dd,  $J=8.2$  Hz,  $J=4.5$  Hz), 7.76 (1H, dd,  $J=8.6$  Hz,  $J=2.3$  Hz), 7.70 (1H, d,  $J=7.7$  Hz), 7.64 (1H, dd,  $J=7.0$  Hz,  $J=2.2$  Hz), 7.48 (1H, dt,  $J=8.5$  Hz,  $J=8.5$  Hz,  $J=2.3$  Hz), 7.42 (1H, dd,  $J=7.8$  Hz,  $J=4.6$  Hz), 7.32 (1H, d,  $J=8.6$  Hz), 2.82 (3H, s).  $^{13}\text{CNMR}$  (100.6 MHz,  $\text{CDCl}_3$ )  $\delta$  (ppm): 166.6 ( $^1J_{\text{CF}}=258$  Hz), 165.7, 165.4, 163.2, 145.8, 144.8, 141.9, 140.1, 136.6, 134.7 ( $^3J_{\text{CF}}=9.5$  Hz), 133.6, 130.7, 127.6 ( $^4J_{\text{CF}}=3.2$  Hz), 126.5, 126.3 ( $^3J_{\text{CF}}=9.5$  Hz), 124.4, 121.5 ( $^2J_{\text{CF}}=19.6$  Hz), 120.8, 118.5, 111.6 ( $^2J_{\text{CF}}=24.6$  Hz), 20.6. HRMS (TOF, ES+)  $\text{C}_{21}\text{H}_{14}\text{ClFN}_3\text{O}_3$  [M+H]<sup>+</sup> calc. mass 410.0708, found 410.0707.



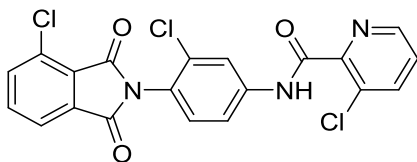
***N*-(3-chloro-4-(1,3-dioxo-1,3-dihydro-2H-pyrrolo[3,4-c]pyridin-2-yl)phenyl)-3-**

**methylpicolinamide (4.76g).** Pale orange solid.  $^1\text{H-NMR}$  (400.1 MHz,  $\text{CDCl}_3$ )  $\delta$  (ppm): 10.57 (1H, s), 9.29 (1H, s), 9.17 (1H, d,  $J=4.8$  Hz), 8.47 (1H, d,  $J=4.2$  Hz), 8.21 (1H, d,  $J=2.3$  Hz), 7.89 (1H, d,  $J=4.8$  Hz), 7.78 (1H, dd,  $J=8.6$  Hz,  $J=2.3$  Hz), 7.71 (1H, d,  $J=7.7$  Hz), 7.44 (1H, dd,  $J=7.8$  Hz,  $J=4.6$  Hz), 7.34 (1H, d,  $J=8.6$  Hz), 2.83 (3H, s).  $^{13}\text{CNMR}$  (100.6 MHz,  $\text{CDCl}_3$ )  $\delta$  (ppm): 165.5, 165.2, 163.4, 155.8, 145.3, 145.1, 141.7, 140.4, 139.2, 136.7, 133.5, 130.6, 126.5, 125.7, 123.8, 120.8, 118.5, 117.3, 20.7. HRMS (TOF, ES+)  $\text{C}_{20}\text{H}_{14}\text{ClN}_4\text{O}_3$  [M+H]<sup>+</sup> calc. mass 393.0754, found 393.0755.



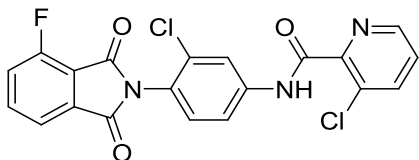
***N*-(3-chloro-4-(4-methyl-1,3-dioxisoindolin-2-yl)phenyl)-3-chloropicolinamide**

**(4.77a).** Cream powder.  $^1\text{H-NMR}$  (400.1 MHz,  $\text{CDCl}_3$ )  $\delta$  (ppm): 10.17 (1H, s), 8.55 (1H, dd,  $J=4.5$  Hz,  $J=1.4$  Hz), 8.18 (1H, d,  $J=2.3$  Hz), 7.92 (1H, dd,  $J=8.1$  Hz,  $J=1.4$  Hz), 7.80 (2H, d,  $J=7.3$  Hz), 7.75 (1H, dd,  $J=8.6$  Hz,  $J=2.4$  Hz), 7.66 (1H, t,  $J=7.5$  Hz), 7.55 (1H, d,  $J=7.7$  Hz), 7.47 (1H, dd,  $J=8.2$  Hz,  $J=4.5$  Hz), 7.34 (1H, d,  $J=8.6$  Hz), 2.76 (3H, m).  $^{13}\text{CNMR}$  (100.6 MHz,  $\text{CDCl}_3$ )  $\delta$  (ppm): 167.5, 166.8, 160.7, 145.8, 144.6, 141.1, 139.4, 138.7, 136.7, 133.9, 133.8, 132.9, 132.3, 130.9, 128.6, 127.1, 125.2, 121.5, 120.8, 118.3, 17.7. HRMS (TOF, ES+)  $\text{C}_{21}\text{H}_{14}\text{Cl}_2\text{N}_3\text{O}_3$   $[\text{M}+\text{H}]^+$  calc. mass 426.0412, found 426.0411.



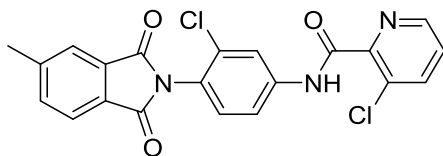
***N*-(3-chloro-4-(4-chloro-1,3-dioxisoindolin-2-yl)phenyl)-3-chloropicolinamide**

**(4.77b).** Cream powder.  $^1\text{H-NMR}$  (400.1 MHz,  $\text{CDCl}_3$ )  $\delta$  (ppm): 10.18 (1H, s), 8.55 (1H, dd,  $J=4.5$  Hz,  $J=1.4$  Hz), 8.19 (1H, d,  $J=2.3$  Hz), 7.91 (2H, m), 7.75 (3H, m), 7.48 (1H, dd,  $J=8.2$  Hz,  $J=4.5$  Hz), 7.33 (1H, d,  $J=8.6$  Hz).  $^{13}\text{CNMR}$  (100.6 MHz,  $\text{CDCl}_3$ )  $\delta$  (ppm): 165.2, 164.2, 160.7, 145.8, 144.5, 141.1, 139.7, 136.1, 135.3, 133.9, 133.7, 132.9, 132.0, 130.8, 127.6, 127.2, 124.7, 122.4, 120.8, 118.4. HRMS (TOF, ES+)  $\text{C}_{20}\text{H}_{11}\text{Cl}_3\text{N}_3\text{O}_3$   $[\text{M}+\text{H}]^+$  calc. mass 445.9866, found 445.9869.



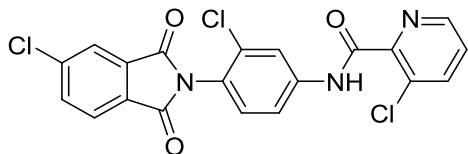
***N*-(3-chloro-4-(4-fluoro-1,3-dioxoisindolin-2-yl)phenyl)-3-chloropicolinamide**

**(4.77c).** Cream powder.  $^1\text{H-NMR}$  (400.1 MHz,  $\text{CDCl}_3$ )  $\delta$  (ppm): 10.18 (1H, s), 8.55 (1H, dd,  $J=4.5$  Hz,  $J=1.3$  Hz), 8.19 (1H, d,  $J=2.3$  Hz), 7.91 (1H, dd,  $J=8.18$  Hz,  $J=1.4$  Hz), 7.81 (2H, m), 7.75 (1H, dd,  $J=8.6$  Hz,  $J=2.4$  Hz), 7.47 (2H, m), 7.34 (1H, d,  $J=8.6$  Hz).  $^{13}\text{CNMR}$  (100.6 MHz,  $\text{CDCl}_3$ )  $\delta$  (ppm): 165.5, 163.3, 160.7, 157.9 (d,  $^1J_{\text{CF}}=267$  Hz), 145.8, 144.5, 141.1, 139.7, 136.96 (d,  $^3J_{\text{CF}}=7.6$  Hz), 133.9, 133.8, 132.9, 130.8, 127.2, 127.0, 124.6, 122.8 ( $^2J_{\text{CF}}=19.7$  Hz), 121.7, 120.8, 120.1, 118.4. HRMS (TOF, ES+)  $\text{C}_{20}\text{H}_{11}\text{Cl}_2\text{FN}_3\text{O}_3$   $[\text{M}+\text{H}]^+$  calc. mass 430.0162, found 430.0163.



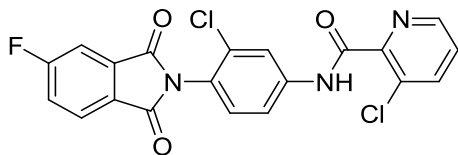
***N*-(3-chloro-4-(5-methyl-1,3-dioxoisindolin-2-yl)phenyl)-3-chloropicolinamide**

**(4.77d).** Cream powder.  $^1\text{H-NMR}$  (400.1 MHz,  $\text{CDCl}_3$ )  $\delta$  (ppm): 10.16 (1H, s), 8.55 (1H, dd,  $J=4.5$  Hz,  $J=1.3$  Hz), 8.17 (1H, d,  $J=2.3$  Hz), 7.91 (1H, dd,  $J=8.2$  Hz,  $J=1.3$  Hz), 7.85 (1H, d,  $J=7.6$  Hz), 7.78 (1H, s), 7.74 (1H, dd,  $J=8.6$  Hz,  $J=2.4$  Hz), 7.60 (1H, d,  $J=7.7$  Hz), 7.47 (1H, dd,  $J=8.2$  Hz,  $J=4.5$  Hz), 7.34 (1H, d,  $J=8.6$  Hz), 2.56 (3H, s).  $^{13}\text{CNMR}$  (100.6 MHz,  $\text{CDCl}_3$ )  $\delta$  (ppm): 166.9, 166.8, 160.7, 145.8, 145.8, 144.6, 141.1, 139.5, 135.0, 133.8, 132.9, 132.2, 130.9, 129.2, 127.1, 125.2, 124.4, 123.8, 120.8, 118.3, 22.0. HRMS (TOF, ES+)  $\text{C}_{21}\text{H}_{14}\text{Cl}_2\text{N}_3\text{O}_3$   $[\text{M}+\text{H}]^+$  calc. mass 426.0412, found 426.0413.



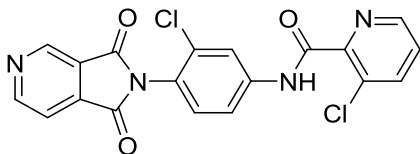
***N*-(3-chloro-4-(5-chloro-1,3-dioxisoindolin-2-yl)phenyl)-3-chloropicolinamide**

**(4.77e).** Cream powder.  $^1\text{H-NMR}$  (400.1 MHz,  $\text{CDCl}_3$ )  $\delta$  (ppm): 10.19 (1H, s), 8.55 (1H, dd,  $J=4.5$  Hz,  $J=1.3$  Hz), 8.19 (1H, d,  $J=2.3$  Hz), 7.95 (1H, d,  $J=1.5$  Hz), 7.92 (2H, m), 7.77 (2H, m), 7.48 (1H, dd,  $J=8.2$  Hz,  $J=4.5$  Hz), 7.34 (1H, d,  $J=8.6$  Hz).  $^{13}\text{CNMR}$  (100.6 MHz,  $\text{DMSO-}d_6$ )  $\delta$  (ppm): 170.8, 170.4, 168.7, 155.3, 152.5, 145.8, 145.1, 144.2, 140.0, 138.5, 137.5, 136.8, 135.1, 133.9, 132.1, 130.7, 129.7, 129.1, 125.3, 124.3. HRMS (TOF, ES+)  $\text{C}_{20}\text{H}_{11}\text{Cl}_3\text{N}_3\text{O}_3$   $[\text{M}+\text{H}]^+$  calc. mass 445.9866, found 445.9869.

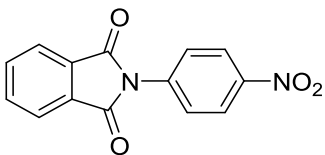


***N*-(3-chloro-4-(5-fluoro-1,3-dioxisoindolin-2-yl)phenyl)-3-chloropicolinamide**

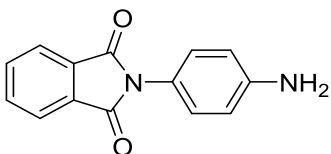
**(4.77f).** Brown powder.  $^1\text{H-NMR}$  (400.1 MHz,  $\text{CDCl}_3$ )  $\delta$  (ppm): 10.19 (1H, s), 8.55 (1H, dd,  $J=4.5$  Hz,  $J=1.2$  Hz), 8.19 (1H,  $J=2.3$  Hz), 7.98 (1H,  $J=8.2$  Hz,  $J=4.5$  Hz), 7.92 (1H, dd,  $J=8.2$  Hz,  $J=1.3$  Hz), 7.77 (1H, dd,  $J=8.6$  Hz,  $J=2.4$  Hz), 7.65 (1H, dd,  $J=7.0$  Hz,  $J=2.2$  Hz), 7.48 (2H, m), 7.34 (1H, d,  $J=8.6$  Hz).  $^{13}\text{CNMR}$  (100.6 MHz,  $\text{CDCl}_3$ )  $\delta$  (ppm): 166.7 ( $^1J_{\text{CF}}=258$  Hz), 165.7, 165.4, 160.8, 145.9, 144.6, 141.2, 139.8, 134.7 ( $^3J_{\text{CF}}=10.0$  Hz), 133.8, 133.0, 130.8, 127.7 ( $^4J_{\text{CF}}=3.2$  Hz), 127.3, 126.4 ( $^3J_{\text{CF}}=9.3$  Hz), 124.8, 121.6 ( $^2J_{\text{CF}}=23.3$  Hz), 120.9, 118.5, 111.7 ( $^2J_{\text{CF}}=24.5$  Hz). HRMS (TOF, ES+)  $\text{C}_{20}\text{H}_{11}\text{Cl}_2\text{FN}_3\text{O}_3$   $[\text{M}+\text{H}]^+$  calc. mass 430.0162, found 430.0163.



***N*-(3-chloro-4-(1,3-dioxo-1,3-dihydro-2H-pyrrolo[3,4-c]pyridin-2-yl)phenyl)-3-methylpicolinamide (4.77g)**. Orange solid.  $^1\text{H-NMR}$  (400.1 MHz,  $\text{CDCl}_3$ )  $\delta$  (ppm): 10.20 (1H, s), 9.30 (1H, s), 9.17 (1H, d,  $J=4.8$  Hz), 8.56 (1H, dd,  $J=4.5$  Hz,  $J=1.3$  Hz), 8.22 (1H, d,  $J=2.3$  Hz), 7.93 (1H, dd,  $J=8.2$  Hz,  $J=1.3$  Hz), 7.89 (1H, d,  $J=4.8$  Hz), 7.78 (1H, dd,  $J=8.6$  Hz,  $J=2.4$  Hz), 7.49 (1H, dd,  $J=8.2$  Hz,  $J=4.5$  Hz), 7.35 (1H, d,  $J=8.6$  Hz).  $^{13}\text{CNMR}$  (100.6 MHz,  $\text{CDCl}_3$ )  $\delta$  (ppm): 165.5, 165.1, 160.8, 155.8, 145.9, 145.3, 144.5, 141.2, 139.9, 139.2, 133.6, 133.0, 130.6, 127.2, 125.7, 124.2, 120.9, 118.5, 117.3. HRMS (TOF, ES+)  $\text{C}_{19}\text{H}_{11}\text{Cl}_2\text{N}_4\text{O}_3$   $[\text{M}+\text{H}]^+$  calc. mass 413.0208, found 430.0207.



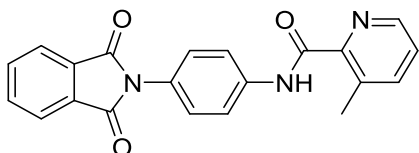
**2-(4-nitrophenyl)isoindoline-1,3-dione (4.80)**. Procedure from the synthesis and purification of **4.11** was followed using 4-nitroaniline (336 mg, 2.43 mmol, 1.2 equiv.). A cream solid was obtained (507 mg, 93%).  $^1\text{H-NMR}$  (400.1 MHz,  $\text{DMSO-}d_6$ )  $\delta$  (ppm): 8.42 (2H, d,  $J=8.9$  Hz), 8.03 (2H, m), 7.95 (2H, m), 7.81 (2H, d,  $J=8.9$  Hz).  $^{13}\text{CNMR}$  (100.6 MHz,  $\text{DMSO-}d_6$ )  $\delta$  (ppm): 166.8, 146.5, 138.2, 135.4, 131.9, 128.1, 124.6, 124.1.



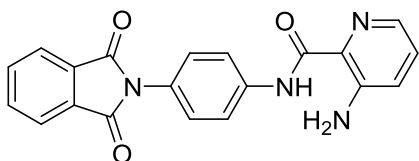
**2-(4-aminophenyl)isoindoline-1,3-dione (4.82)**. Procedure from the synthesis and purification of **4.12** was followed using 4-nitroaniline (268 mg, 1.00 mmol). An orange solid was



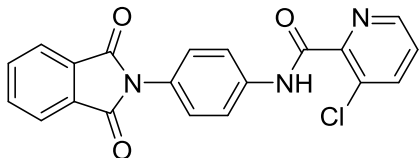
obtained (203 mg, 85%).  $^1\text{H-NMR}$  (400.1 MHz,  $\text{CDCl}_3$ )  $\delta$  (ppm): 7.95 (2H, m), 7.79 (2H, m), 7.19 (2H, d,  $J=8.6$  Hz), 6.79 (2H, d,  $J=8.6$  Hz).  $^{13}\text{CNMR}$  (100.6 MHz,  $\text{CDCl}_3$ )  $\delta$  (ppm): 167.7, 146.4, 134.1, 131.8, 127.8, 123.5, 115.2, 112.7.



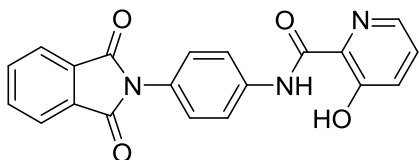
***N*-(4-(1,3-dioxoisindolin-2-yl)phenyl)-3-methylpicolinamide (4.87)**. This compound was synthesized using the general procedure to obtain library **4.13-4.65**, but using **4.82** as starting material.  $^1\text{H-NMR}$  (400.1 MHz,  $\text{CDCl}_3$ )  $\delta$  (ppm): 10.41 (1H, s), 8.49 (1H, d,  $J=3.9$  Hz), 7.98 (2H, m), 7.94 (2H, d,  $J=8.8$  Hz), 7.81 (2H, m), 7.68 (1H, d,  $J=7.8$  Hz), 7.48 (2H, d,  $J=8.8$  Hz), 7.41 (1H, dd,  $J=7.8$  Hz,  $J=4.7$  Hz), 2.85 (3H, s).  $^{13}\text{CNMR}$  (100.6 MHz,  $\text{CDCl}_3$ )  $\delta$  (ppm): 167.3, 163.5, 146.5, 145.3, 141.3, 137.8, 136.3, 134.3, 131.7, 127.14, 127.10, 126.1, 123.6, 119.9, 20.8.



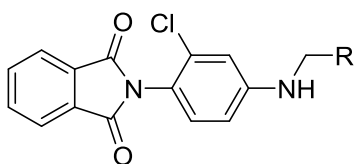
**3-amino-*N*-(4-(1,3-dioxoisindolin-2-yl)phenyl)picolinamide (4.84)**. This compound was synthesized using the general procedure to obtain library **4.13-4.65**, but using **4.82** as starting material.  $^1\text{H-NMR}$  (400.1 MHz,  $\text{CDCl}_3$ )  $\delta$  (ppm): 10.27 (1H, s), 7.98 (3H, m), 7.91 (2H, d,  $J=9.0$  Hz), 7.82 (2H, m), 7.47 (2H,  $J=8.7$  Hz), 7.25 (2H,  $J=8.4$  Hz,  $J=4.4$  Hz), 7.25 (2H,  $J=8.4$  Hz,  $J=1.3$  Hz).



**3-chloro-*N*-(4-(1,3-dioxisoindolin-2-yl)phenyl)picolinamide (4.85).** This compound was synthesized using the general procedure to obtain library **4.13-4.65**, but using **4.82** as starting material.  $^1\text{H-NMR}$  (400.1 MHz,  $\text{CDCl}_3$ )  $\delta$  (ppm): 10.1 (1H, s), 8.57 (1H, d,  $J=3.9$  Hz), 7.95 (5H, m), 7.82 (2H, m), 7.49 (3H, m).

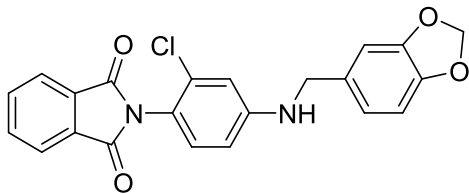


***N*-(4-(1,3-dioxisoindolin-2-yl)phenyl)-3-hydroxypicolinamide (4.86).** This compound was synthesized using the general procedure to obtain library **4.13-4.65**, but using **4.82** as starting material.  $^1\text{H-NMR}$  (400.1 MHz,  $\text{CDCl}_3$ )  $\delta$  (ppm): 10.07 (1H, s), 8.17 (1H, dd,  $J=4.2$  Hz,  $J=1.4$ Hz), 7.99 (2H, m), 7.91 (2H, d,  $J=8.8$  Hz), 7.83 (2H, m), 7.53 (2H, d,  $J=8.8$  Hz), 7.48 (2H, d,  $J=8.8$  Hz), 7.45 (1H, dd,  $J=8.4$  Hz,  $J=4.2$  Hz), 7.40 (1H, dd,  $J=8.4$  Hz,  $J=1.4$  Hz).



***N*-(3-chloro-4-(1,3-dioxisoindolin-2-yl)phenyl)amines (4.105-4.140).** In a microwave vial, **4.12** (20 mg, 0.073 mmol, 1.0 equiv.), the corresponding aldehyde (1.2 equiv.) and polymer bound cyanoborohydride (1.5 equiv.) were added. The mixture was suspended in 600  $\mu\text{L}$  of DCM and 50  $\mu\text{L}$  of glacial acetic acid were added. The vial was sealed and heated in the microwave for seven minutes at 110  $^\circ\text{C}$ . The reactions were monitored by LC-MS to confirm the presence of

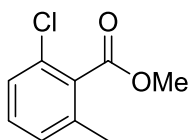
product. The matrix was filtered, and volatiles evaporated *in vacuo*. The crude product was dissolved in DMSO and purified by preparative HPLC.



**2-(4-((benzo[d][1,3]dioxol-5-ylmethyl)amino)-2-chlorophenyl)isoindoline-1,3-dione**

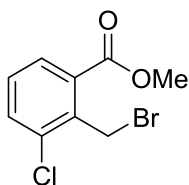
**(4.122).** White solid.  $^1\text{H-NMR}$  (400.1 MHz,  $\text{CDCl}_3$ )  $\delta$  (ppm): 7.96 (2H, m), 7.81 (2H, m), 7.2 (1H, d,  $J=8.3$  Hz), 6.83 (4H, m), 6.68 (1H, d,  $J=7.9$  Hz), 5.99 (2H, s), 4.28 (2H, s).

**General procedure for the esterification of *ortho*-methylbenzoic acids.** In a flask, the carboxylic acid (11.72 mmol, 1.0 equiv.) was dissolved in 6 mL of methanol. Then, 0.5 mL of concentrated sulfuric acid were added dropwise. The reaction was heated at reflux and monitored by LC-MS until there was no starting material in the chromatogram. At this point, the reaction was stopped and cooled to room temperature. For the workup, water was added to the mixture and successive extractions with ethyl ether were performed. The organic phases were combined and washed with  $\text{NaHCO}_3$  5% and brine. The organic phase was dried with anhydrous  $\text{MgSO}_4$ , filtered and concentrated *in vacuo*. The crude product was purified by silica gel flash chromatography (Teledyne ISCO) using a gradient of hexanes to 10% EtOAc in hexanes.



**Methyl 2-chloro-6-methylbenzoate (4.148).** Clear oil.  $^1\text{H-NMR}$  (400.1 MHz,  $\text{CDCl}_3$ )  $\delta$  (ppm): 7.08 (2H, m), 6.96 (1H, m), 3.81 (3H, s), 2.19 (3H, s).  $^{13}\text{CNMR}$  (100.6 MHz,  $\text{CDCl}_3$ )  $\delta$  (ppm): 167.7, 136.80, 133.61, 130.51, 130.10, 128.51, 126.86, 52.26, 19.33.

**General procedure for the bromination of *ortho*-methylbenzoate esters.** The ester (9.60 mmol, 1.0 equiv.) was dissolved in 60 mL of CCl<sub>4</sub>. Then, *N*-bromosuccinimide (10.56 mmol, 1.2 equiv.) was added, followed by benzoyl peroxide (0.192 mmol, 0.02 equiv.). The reaction was heated at reflux and monitored by LC-MS until there was no starting material in the chromatogram. At this point, the reaction was stopped and cooled to room temperature. For the workup, the mixture was filtered and concentrated *in vacuo*. The crude product was purified by silica gel flash chromatography (Teledyne ISCO) using a gradient of hexanes to 5% EtOAc in hexanes.

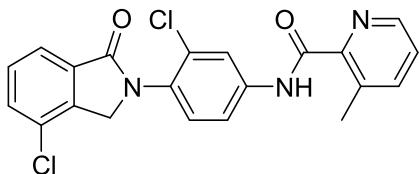


**Methyl 2-(bromomethyl)-3-chlorobenzoate (4.144).** Clear light orange oil. <sup>1</sup>H-NMR (400.1 MHz, CDCl<sub>3</sub>) δ (ppm): 7.75 (1H, dd, *J*=7.9 Hz, *J*=1.3 Hz), 7.47 (1H, dd, *J*=8.0 Hz, *J*=1.3 Hz), 7.21 (1H, t, *J*=8.0 Hz), 5.01 (2H, s), 3.86 (3H, s). <sup>13</sup>CNMR (100.6 MHz, CDCl<sub>3</sub>) δ (ppm): 166.4, 136.4, 136.3, 133.6, 131.4, 129.7, 129.1, 52.6, 26.7.

**General procedure for the synthesis of isoindolinones 4.145-4.146 and 4.150-4.151.** In a microwave vial, the corresponding methyl bromomethylbenzoate (0.085 mmol, 1.2 equiv.) and aniline (0.0709, 1.0 equiv.) were added and dissolved in 1 mL of DMF. Then, K<sub>2</sub>CO<sub>3</sub> (0.141 mmol, 2.0 equiv.) was added and the vial was sealed. The reaction was heated in the microwave at 150 °C for 15 minutes. The reaction was monitored by LC-MS and a second round of heating was applied if there was presence of starting material or the acyclic ester intermediate. The reaction was worked up by addition of water and successive extractions with DCM. The organic

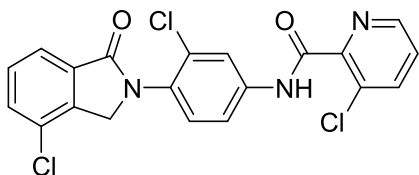
phases were filtered through a phase separator, combined and volatiles were evaporated *in vacuo*.

Crude products were dissolved in DMSO and purified by preparative HPLC.



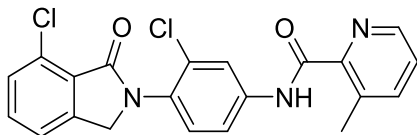
***N*-(3-chloro-4-(4-chloro-1-oxoisindolin-2-yl)phenyl)-3-methylpicolinamide (4.145).**

Cream powder.  $^1\text{H-NMR}$  (400.1 MHz,  $\text{CDCl}_3$ )  $\delta$  (ppm): 10.13 (1H, s), 8.54 (1H, dd,  $J= 4.5$  Hz,  $J= 1.3$  Hz), 8.15 (1H, d,  $J= 2.4$  Hz), 7.92 (1H, dd,  $J= 8.2$  Hz,  $J= 1.3$  Hz), 7.87 (1H, d,  $J=7.4$  Hz), 7.71 (1H, dd,  $J= 8.6$  Hz,  $J= 2.4$  Hz), 7.59 (1H, d,  $J= 7.9$  Hz), 7.49 (2H, m), 7.42 (1H, d,  $J= 8.6$  Hz), 4.80 (2H, s).  $^{13}\text{CNMR}$  (100.6 MHz,  $\text{CDCl}_3$ )  $\delta$  (ppm): 167.3, 160.7, 145.8, 144.6, 141.1, 139.8, 138.6, 133.9, 133.1, 132.9, 131.9, 130.9, 130.2, 129.9, 129.2, 127.1, 122.8, 121.1, 118.7, 51.4



**3-chloro-*N*-(3-chloro-4-(4-chloro-1-oxoisindolin-2-yl)phenyl)picolinamide (4.146).**

Cream powder.  $^1\text{H-NMR}$  (400.1 MHz,  $\text{CDCl}_3$ )  $\delta$  (ppm): 10.13 (1H, s), 8.54 (1H, dd,  $J= 4.5$  Hz,  $J= 1.3$  Hz), 8.15 (1H, d,  $J= 2.4$  Hz), 7.92 (1H, dd,  $J= 8.2$  Hz,  $J= 1.3$  Hz), 7.87 (1H, d,  $J=7.4$  Hz), 7.71 (1H, dd,  $J= 8.6$  Hz,  $J= 2.4$  Hz), 7.59 (1H, d,  $J= 7.9$  Hz), 7.49 (2H, m), 7.42 (1H, d,  $J= 8.6$  Hz), 4.80 (2H, s).  $^{13}\text{CNMR}$  (100.6 MHz,  $\text{CDCl}_3$ )  $\delta$  (ppm): 167.3, 160.7, 145.8, 144.6, 141.1, 139.8, 138.6, 133.9, 133.1, 132.9, 131.9, 130.9, 130.2, 129.9, 129.2, 127.1, 122.8, 121.1, 118.7, 51.4.



***N*-(3-chloro-4-(7-chloro-1-oxoisindolin-2-yl)phenyl)-3- (4.150)**. Cream powder.  $^1\text{H-NMR}$  (400.1 MHz,  $\text{CDCl}_3$ )  $\delta$  (ppm): 10.56 (1H, s), 8.40 (1H, d,  $J= 4.2$  Hz), 8.12 (1H,  $J= 2.3$  Hz), 7.70 (2H, m), 7.46 (5H, m), 4.76 (2H, s), 2.80 (3H, s).  $^{13}\text{CNMR}$  (100.6 MHz,  $\text{CDCl}_3$ )  $\delta$  (ppm): 165.9, 163.0, 145.9, 144.6, 144.0, 142.0, 138.8, 136.5, 133.0, 132.7, 132.2, 130.8, 130.3, 129.9, 127.9, 126.5, 121.3, 121.1, 118.8, 51.1, 20.5.

#### *Molecular pharmacology*

Tetracycline-tested fetal bovine serum (FBS) was purchased from Atlanta Biologicals (Lawrenceville, GA), and all other cell culture reagents and Fluo-4-acetoxymethylester (Fluo-4-AM) were purchased from Life Technologies (Carlsbad, CA). Tetracycline hydrochloride (Sigma), L-glutamic acid (Tocris, Minneapolis, MN).

**Cell Culture and mutagenesis.** Tetracycline-inducible rat and human mGlu<sub>1</sub> WT-T-REx<sup>TM</sup>-293 cells<sup>112</sup> were cultured at 37 °C in Dulbecco's Modified Eagle Medium (DMEM) growth medium containing 10% Tet-tested FBS, 2 mM L-glutamine, 20 mM HEPES, 0.1 mM non-essential amino acids, 1 mM sodium pyruvate, antibiotic/antimycotic, 100  $\mu\text{g}/\text{mL}$  hygromycin and 5  $\mu\text{g}/\text{mL}$  blasticidin in the presence of 5%  $\text{CO}_2$ . To generate a collection of stable cell lines carrying tetracycline-inducible hmGlu<sub>1</sub> schizophrenic mutants,<sup>241,242</sup> site-directed mutagenesis of human mGlu<sub>1</sub> WT in pcDNA5/TO was performed using Quikchange II XL kit (Agilent Technologies, Santa Clara, CA), and all point-mutations were confirmed by sequencing. The mutant stable cell lines were generated in the same manner as the WT as previously described and cultured in the growth medium described above.

Human mGlu<sub>4</sub> CHO cells stably transfected expressing the chimeric G protein G<sub>qi5</sub> in pIRESneo3 (Invitrogen, Carlsbad, CA) were cultured in 90% Dulbecco's Modified Eagle Media (DMEM), 10% dialyzed fetal bovine serum (FBS), 100 units/ml penicillin/streptomycin, 20 mM HEPES (pH 7.3), 1 mM sodium pyruvate, 2 mM glutamine, 400 µg/ml G418 sulfate (Mediatech, Inc., Herndon, VA) and 5 nM methotrexate (Calbiochem, EMD Chemicals, Gibbstown, NJ).

**Biotinylation of cell surface expression of mGlu<sub>1</sub> receptor.** To determine the receptor expression level on the cell surface among the mGlu<sub>1</sub> WT and schizophrenia (Sz) mutant cell lines, cells were plated in a 10 cm dish at 8x10<sup>6</sup> cells/8mL density in the assay medium containing either 20 ng/mL (WT) or 1µg/mL (mutants) TET to induce the receptor expression. The next morning, dishes were placed on ice and gently washed with ice cold PBS. Immediately, cells were scraped in cold PBS into a 1.5 mL tube, and spun down at 500xg for 4 min at 4 °C. All steps were carried at 4 °C unless otherwise noted. Cells were gently resuspended in 1 mL of cold PBS containing 2 mg of EZ-Link Sulfo-NHS-SS-Biotin and gently rocked for 30 min. Biotinylation was quenched by adding 500 µL of 150 mM Tris (pH 8.0) and cells were spun down and resuspended in 1 mL of 50 mM Tris (pH 8.0) to completely quench the reaction. Cells were spun down and resuspended in 1 mL of lysis buffer (25 mM Tris, pH 7.4, 150 mM NaCl, 1% NP-40, 0.5% sodium deoxycholate containing protease inhibitors) and incubated for 30 min. The lysates were spun at 16,000xg for 15 min, and the resulting supernatants were gently transferred to a new 1.5 mL tube to incubate with 60 µL of 50% slurry of NeutrAvidin beads by nutating at room temperature for 1 h. The beads were washed three times with lysis buffer and the biotinylated proteins bound to the beads were extracted by heating the beads at 65 °C for 5 min in SDS sample buffer containing 150 mM DTT. The proteins were resolved by 8% SDS-PAGE and the mGlu<sub>1</sub> expression level was determined by Western blotting using the mGlu<sub>1</sub>-specific antibody (Clone 20, BD Transduction Lab). The density of the mGlu<sub>1</sub> protein bands was measured using Quantity One software (Bio-Rad, Hercules, CA).

**Poly-D-lysine plate coating.** See *Molecular Pharmacology* in the experimental methods in chapter 3.

**Calcium Mobilization Assay.** Single point screening and determination of potency for human and rat mGlu<sub>1</sub> PAM activity was performed following the experimental procedure stated in chapter 3.

To examine the functional activity of all hmGlu<sub>1</sub>-mutants compared to the WT, calcium flux was measured using the Functional Drug Screening System (FDSS7000, Hamamatsu, Japan) as previously described.<sup>39</sup> Briefly, the day before the assay, the mGlu<sub>1</sub>-T-REx<sup>TM</sup>-293 cells were plated in black-walled, clear-bottomed, poly-D-lysine coated 384-well plates (BD Biosciences, San Jose, CA) at 20,000 cells/ well in 20  $\mu$ L of assay medium (DMEM supplemented with 10% dialyzed FBS, 20 mM HEPES, and 1 mM sodium pyruvate) that contains tetracycline (TET) to induce mGlu<sub>1</sub> expression; 20 ng/mL TET was used for WT and 1  $\mu$ g/mL TET for all mutants. The next day, cells were washed with assay buffer (Hank's balanced salt solution, 20 mM HEPES, and 2.5 mM probenecid) using ELx microplate washer (BioTek Instruments, Winooski, VT), and immediately incubated with 20  $\mu$ L of 1.15  $\mu$ M Fluo-4 AM dye solution prepared in assay buffer for 45 min at 37 °C. The dye was removed and washed with assay buffer before measuring the fluorescent calcium traces in FDSS. Agonists, glutamate or DHPG, were 1:5 serially diluted into 11 point concentrations, added to the cells, and incubated for 2 min. The agonist-mediated calcium response was calculated by subtracting the basal fluorescent peak before agonist addition from the maximal peak elicited by agonist. When testing the effect of the mGlu<sub>1</sub> PAMs, cells were first incubated with the PAMs (10  $\mu$ M final concentration) or DMSO vehicle diluted in assay buffer for 2.2 min and then stimulated with glutamate or DHPG. Concentration response curves were generated using GraphPad Prism 5.0 (GraphPad Software, Inc., La Jolla, CA).

To determine the PAM potency of the compounds on human mGlu<sub>4</sub> PAMs in calcium assays, Ca flux was measured as previously described.<sup>285</sup> Human mGlu<sub>4</sub>/G<sub>q15</sub>/CHO cells (30,000



cells/20  $\mu$ l/well) were plated in blackwalled, clear-bottomed, TC treated, 384 well plates (Greiner Bio-One, Monroe, North Carolina) in DMEM containing 10% dialyzed FBS, 20 mM HEPES, 100 units/ml penicillin/streptomycin, and 1 mM sodium pyruvate (Plating Medium). The cells were grown overnight at 37 °C in the presence of 5% CO<sub>2</sub>. During the day of assay, the medium was replaced with 20  $\mu$ L of 1  $\mu$ M Fluo-4 AM (Invitrogen, Carlsbad, CA) prepared as a 2.3 mM stock in DMSO and mixed in a 1:1 ratio with 10% (w/v) pluronic acid F-127 and diluted in Assay Buffer (Hank's balanced salt solution, 20 mM HEPES and 2.5 mM Probenecid (Sigma-Aldrich, St. Louis, MO)) for 45 minutes at 37 °C. The dye was removed and replaced with 20  $\mu$ L of Assay Buffer. Test compounds were transferred to daughter plates using an Echo acoustic plate reformatter (Labcyte, Sunnyvale, CA) and then diluted into Assay Buffer. Ca<sup>2+</sup> flux was measured using the Functional Drug Screening System 7000 (FDSS7000, Hamamatsu, Japan). Baseline readings were taken (10 images at 1 Hz, excitation, 470  $\pm$  20 nm, emission, 540  $\pm$  30 nm) and then 20  $\mu$ l/well test compounds at 2X their final concentration were added using the FDSS's integrated pipettor. Cells were incubated with compounds for approximately 2.5 minutes and then an EC<sub>20</sub> concentration of glutamate was applied; 2 min. later an EC<sub>80</sub> concentration of glutamate was added. Data was collected at 1/2 Hz until 10 seconds prior to agonist addition, when the rate was increased to 1 Hz for the remainder of the assay. For concentration-response curve experiments, compounds were serially diluted 1:3 into 10 point concentration response curves and were transferred to daughter plates using the Echo. Test compounds were again applied and followed by EC<sub>20</sub> and EC<sub>80</sub> concentrations of glutamate. Curves were fitted using a four point logistical equation using Microsoft XLfit (IDBS, Bridgewater, NJ). Subsequent confirmations of concentration response parameters were performed using independent serial dilutions of source compounds and data from multiple days experiments were integrated and fitted using a four point logistical equation in GraphPad Prism (GraphPad Software, Inc., La Jolla, CA).

### *Pharmacokinetic characterization*

The *in vitro* DMPK assays, including those assessing hepatic microsomal intrinsic clearance ( $Cl_{int}$ ), cytochrome P450 inhibition, plasma protein binding (PPB) and brain homogenate binding (BHB) were performed as described previously.<sup>285</sup> The experimental procedures for the pharmacokinetic characterization of the compounds are described in chapter 3.

## CHAPTER V

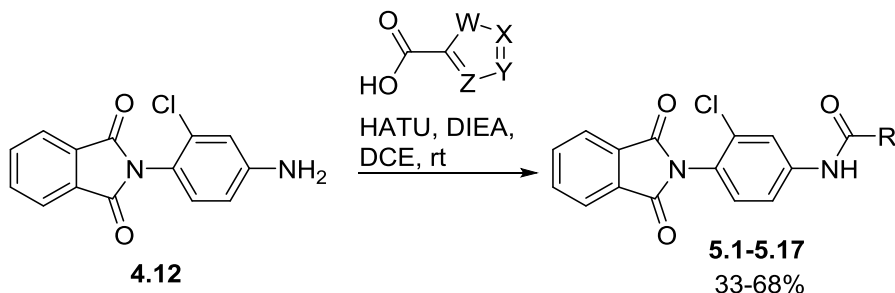
### DISCOVERY OF VU0486321, A POTENT, PREFERENTIAL AND BRAIN PENETRANT MGLU1 PAM

#### **Finding a more potent eastern piece as a replacement of the VU0405622's picolinamide**

##### *Bioisostere replacements for the picolinamide*

After finding that the removal of one of the carbonyls in the scaffold of VU0483605 **4.77b** renders the molecule plasma stable but accompanied with a decrease in mGlu<sub>1</sub> activity of 3 to 5-fold, we thought that this could be a reasonable modification if applied to a more potent parent compound. In order to assess this, we embarked in finding a compound with a higher potency.

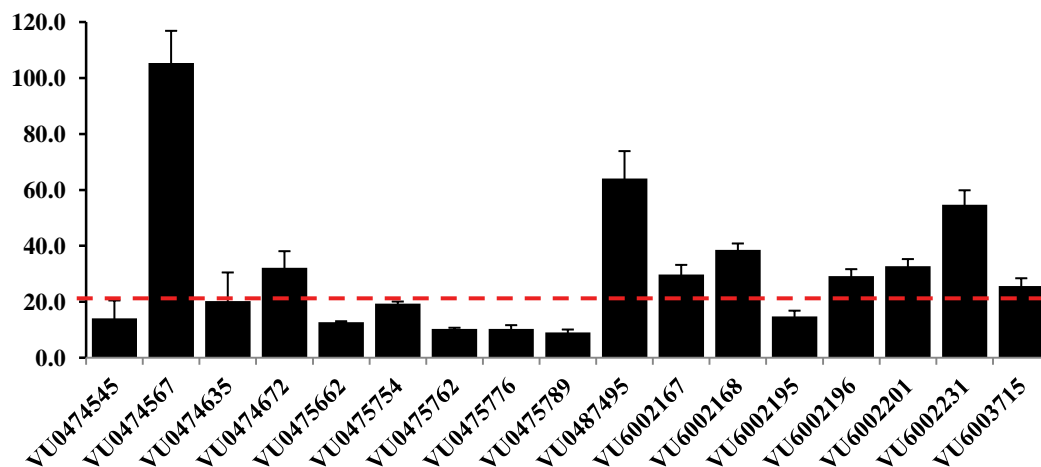
We chose to continue exploring the picolinamide region of the VU0405622 scaffold, as our previous iterations have shown that the structure-activity in this part of the molecule presented more texture, while the chemical modification on the central phenyl ring and the linker showed steep changes in mGlu<sub>1</sub> activity. As multiple heteroaromatic six-membered rings were already explored as a replacement for the pyridine, we chose to analyze the effect of five-membered heterocyclic rings. These analogs were prepared in one step, performing an amide coupling with the different heterocyclic carboxylic acids and the previously synthesized aniline **4.12** (Scheme 5.1); only **5.4** required an additional deprotection step as the protected *tert*-(butoxycarbonyl)proline was employed for the formation of the amide.



**Scheme 5.1.** Synthesis of pyridine bioisostere analogs **5.1-5.17**.

The compounds were evaluated in a TR-Ex<sup>TM</sup> 293 human mGlu<sub>1</sub> expressing cell line to determine its capacity of enhancing the glutamate response of the receptor. The test at 10 μM concentration showed that only three compounds potentiate mGlu<sub>1</sub> PAM activity above 50% Glu<sub>Max</sub> (Fig. 5.1 and Table 5.1). Here, the pyrrole **5.1**, thiophene **5.3** and pyrrolidine **5.4** were inactive, while the furan analog **5.2** the mGlu<sub>1</sub> response to 64% Glu<sub>Max</sub>, an example of how subtle changes in the structure can have a strong effect in mGlu<sub>1</sub> PAM activity.

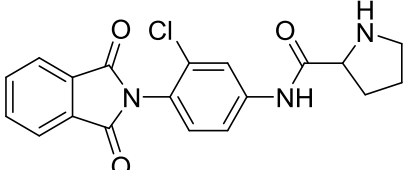
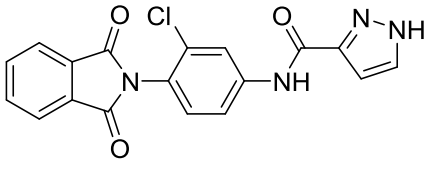
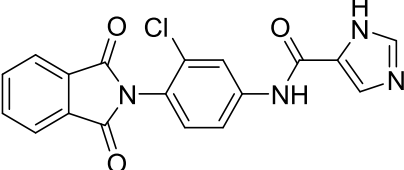
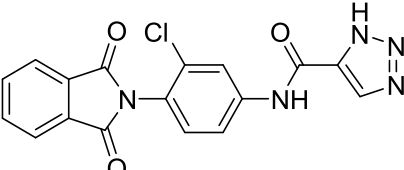
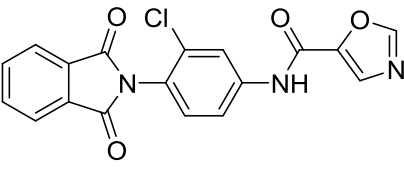
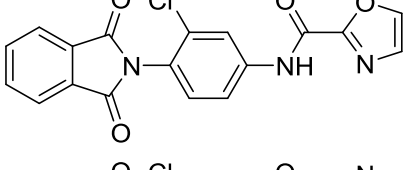
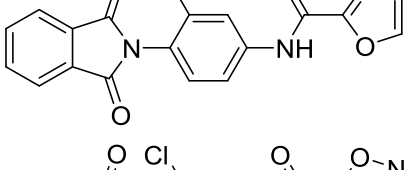
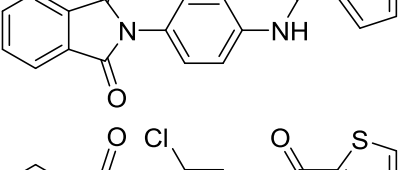
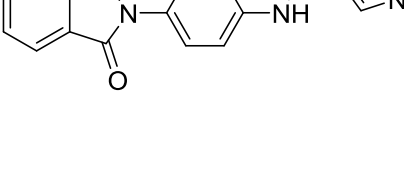
Similar observations were made in the case of the azole compounds. In the nitrogen-only azoles, it was observed that pyrazole **5.5** and triazole **5.7** were not active in mGlu<sub>1</sub> but the close relative imidazole **5.6** potentiated the receptor's response (55% Glu<sub>Max</sub>). Nitrogenated fused-rings also proved to generate inactive analogs (**5.15-5.17**). The different oxazole and isoxazole compounds **5.8-5.11** did not show any activity as mGlu<sub>1</sub> PAMs, while in the thiazoles, only **5.13** display enhancement of mGlu<sub>1</sub> signal. The other members in this family demonstrated that rearrangement of the nitrogen and sulfur atoms **5.12** or introduction of an additional nitrogen **5.14** decrease mGlu<sub>1</sub> PAM activity. **5.13** showed the highest response from this set of bioisosteres (105% Glu<sub>Max</sub>); this thiazole can be described as the “thiophene” version of the picolinamide in VU0405622 and has the same disposition of heteroatoms as the active imidazole **5.6**.

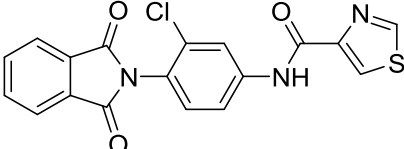
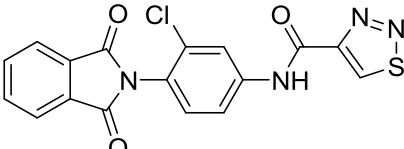
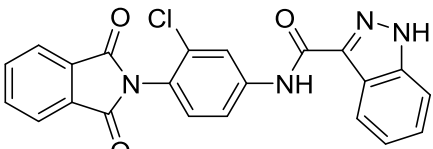
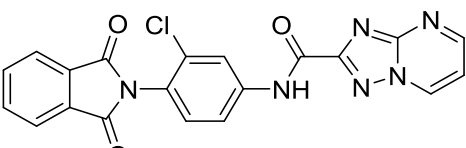
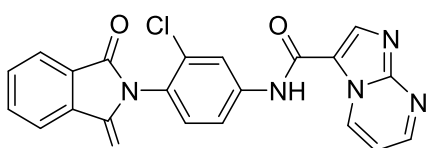


**Figure 5.1.** Comparison of the single point screen result for PAM activity in human mGlu<sub>1</sub> at 10  $\mu$ M for the pyridine bioisostere library, analogs **5.1-5.17**. Calcium mobilization was used to obtain %Glu<sub>Max</sub> values for each compound in the presence of a submaximal concentration of glutamate (EC<sub>20</sub>) in cell lines expressing human mGlu<sub>1</sub>. Data represent the mean  $\pm$  S.E.M. of at least three experiments with similar results.

**Table 5.1.** Structures of the pyridine bioisostere library, analogs **5.1-5.17** and associated PAM activity from the single point screening at 10  $\mu$ M in human mGlu<sub>1</sub>. Calcium mobilization responses for each compound are reported as a percentage of the maximum glutamate response. VU number denotes the compound identifier assigned by Vanderbilt University. Data represent the mean  $\pm$  S.E.M. of at least three replicate experiments with similar results.

Structure	Cpd #	VU #	hmGlu <sub>1</sub> %Glu <sub>Max</sub>
	<b>5.1</b>	VU0474672	32.2 $\pm$ 5.9
	<b>5.2</b>	VU0487495	64.1 $\pm$ 9.8
	<b>5.3</b>	VU0474635	20.3 $\pm$ 10.2

	<b>5.4</b>	VU6003715	25.6±2.8
	<b>5.5</b>	VU0475789	9.1±1.0
	<b>5.6</b>	VU6002231	54.7±5.2
	<b>5.7</b>	VU0475662	12.7±0.3
	<b>5.8</b>	VU6002201	32.7±2.6
	<b>5.9</b>	VU6002196	29.2±2.5
	<b>5.10</b>	VU6002195	14.8±2.0
	<b>5.11</b>	VU0474545	14.0±6.4
	<b>5.12</b>	VU6002167	29.8±3.4

	<b>5.13</b>	VU0474567	105.4±11.5
	<b>5.14</b>	VU6002168	38.5±2.3
	<b>5.15</b>	VU0475754	19.3±0.8
	<b>5.16</b>	VU0475762	10.3±0.4
	<b>5.17</b>	VU0475776	10.3±1.3

We decided to further analyze analogs **5.2** (VU0487495), **5.6** (VU6002231) and **5.13** (VU0474567) and to determine their mGlu<sub>1</sub> EC<sub>50</sub>. The results from this experiment identified marked differences between these PAMs (Fig. 5.2). The imidazole **5.6** was a very weak mGlu<sub>1</sub> PAM with potency above 10 μM. The thiazole **5.13** despite presenting great efficacy levels at 10 μM, showed a borderline activity with an EC<sub>50</sub> of 4.5 μM. The most active compound from this panel was the furan **5.2**, the compound presented partial PAM activity with maximum response of 74% Glu<sub>Max</sub> and a submicromolar potency of 484 nM.

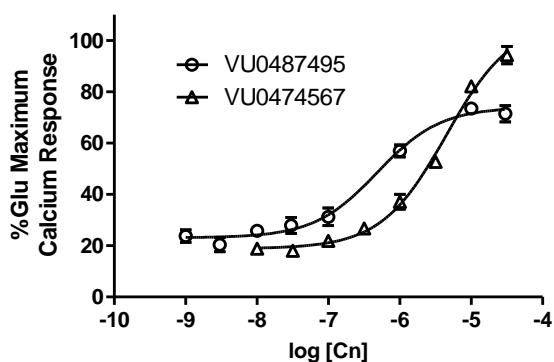


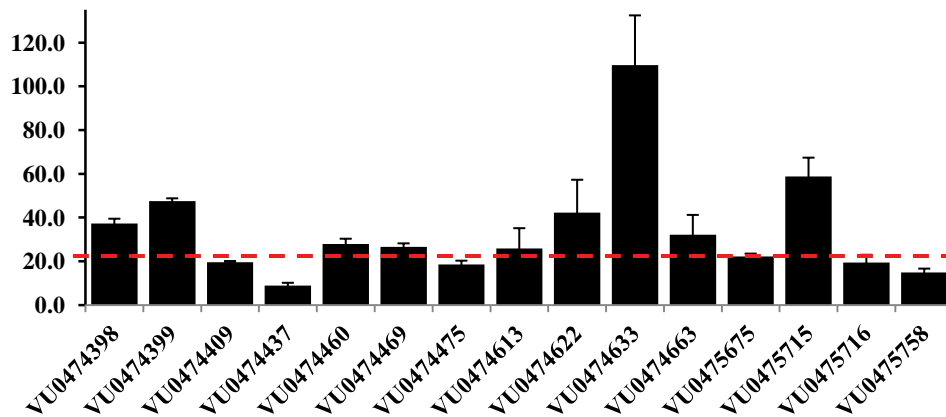
**Figure 5.2.** Comparison of the concentration-response of curve for PAM activity of **5.2** (VU0487495) and **5.13** (VU0474567) in human mGlu<sub>1</sub>. Calcium mobilization was used to obtain %Glu<sub>Max</sub> values for each compound at different concentrations in the presence of a submaximal concentration of glutamate (EC<sub>20</sub>) in cell lines expressing human mGlu<sub>1</sub>. Data represent the mean ± S.E.M. of at least three experiments with similar results.

#### *Exploration of the SAR around the furan*

Due to its high potency, we decided to take analog **5.2** and explore the effect of different substitutions on the furan ring for mGlu<sub>1</sub> PAM activity. In this case, compounds were synthesized in a similar manner as shown in Scheme 5.1 and were screened in a 10 μM single point assay (Fig. 5.3 and Table 5.2).

The substitution on the furan ring demonstrated a very steep SAR, as most modifications were detrimental for activity. All substituents in position 5 caused a loss in mGlu<sub>1</sub> potentiation with respect to the parent compound, and only the smallest substituents, like the methyl **5.18** (59% Glu<sub>Max</sub>), chlorine **5.21** (48% Glu<sub>Max</sub>), bromine **5.22** (42% Glu<sub>Max</sub>) and trifluoromethyl **5.23** (37% Glu<sub>Max</sub>) maintain some activity. Substitutions in position 3 of the furan showed a similar pattern where the phenyl analog **5.28** was inactive, while a gain in activity was observed with the small methyl substituent **5.27**, that allowed potentiation of the receptor response to 110% Glu<sub>Max</sub>. Doubly substituted 3,5-dimethyl **5.29**, the reduced tetrahydrofuran **5.32** and benzofuran variants **5.30** and **5.31**, did not display enhancement of mGlu<sub>1</sub> activity.

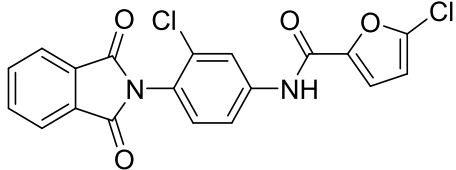
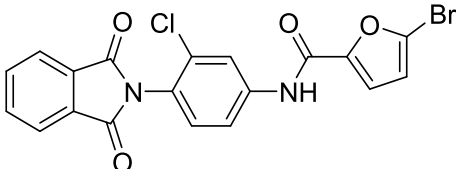
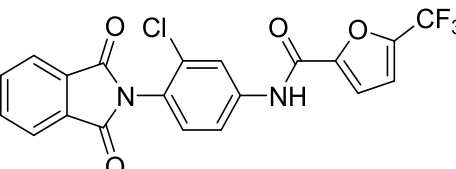
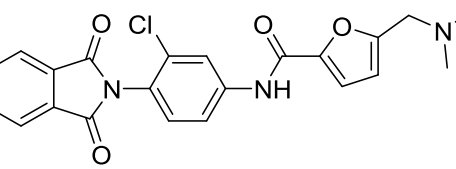
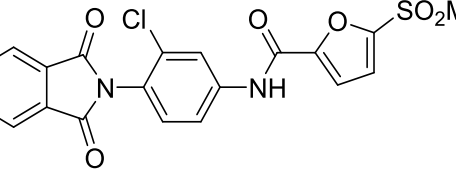
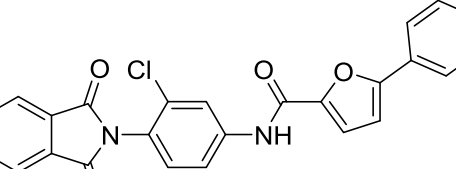
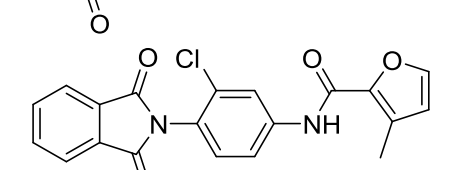
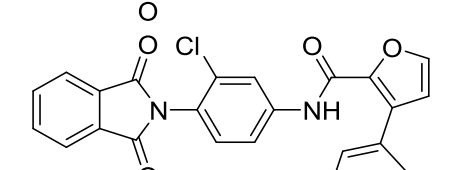
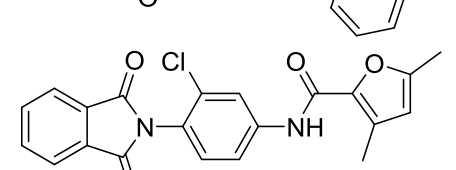


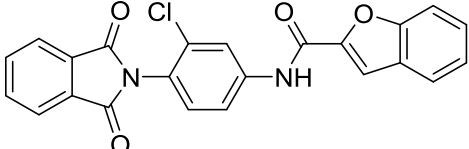
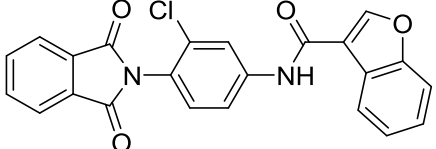
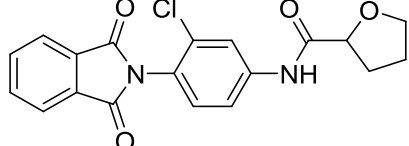


**Figure 5.3.** Comparison of the single point screening results for PAM activity in human mGlu<sub>1</sub> at 10  $\mu$ M for the pyridine bioisostere library, analogs **5.18-5.32**. Calcium mobilization was used to obtain %Glu<sub>Max</sub> values for each compound in the presence of a submaximal concentration of glutamate (EC<sub>20</sub>) in cell lines expressing human mGlu<sub>1</sub>. Data represent the mean  $\pm$  S.E.M. of at least three experiments with similar results.

**Table 5.2.** Structures of the pyridine bioisostere library, analogs **5.18-5.32** and associated PAM activity from the single point screening at 10  $\mu$ M in human mGlu<sub>1</sub>. Calcium mobilization responses for each compound are reported as a percentage of the maximum glutamate response. VU number denotes the compound identifier assigned by Vanderbilt University. Data represent the mean  $\pm$  S.E.M. of at least three replicate experiments with similar results.

Structure	Cpd #	VU #	hmGlu <sub>1</sub> %Glu <sub>Max</sub>
	<b>5.18</b>	VU0475715	58.9 $\pm$ 8.6
	<b>5.19</b>	VU0474663	32.2 $\pm$ 9.0
	<b>5.20</b>	VU0474437	8.9 $\pm$ 1.2

	<b>5.21</b>	VU0474399	47.5±1.3
	<b>5.22</b>	VU0474622	42.3±15.0
	<b>5.23</b>	VU0474398	37.3±2.2
	<b>5.24</b>	VU0474475	18.6±1.7
	<b>5.25</b>	VU0474460	27.9±2.4
	<b>5.26</b>	VU0474469	26.5±1.7
	<b>5.27</b>	VU0474633	109.7±22.8
	<b>5.28</b>	VU0474409	19.6±0.5
	<b>5.29</b>	VU0474613	25.8±9.4

	<b>5.30</b>	VU0475758	14.9±1.7
	<b>5.31</b>	VU0475716	19.4±3.6
	<b>5.32</b>	VU0475675	22.3±1.3

The potencies of compounds **5.18** (5-methyl) and **5.27** (3-methyl) were analyzed in a concentration-response assay. It was determined that **5.18** was a weak potentiator with an  $EC_{50}$  above 10  $\mu$ M. Meanwhile, **5.27** (VU0474633) showed good potency (hu mGlu<sub>1</sub>  $EC_{50}$  = 96 nM) and high efficacy (119%  $Glu_{Max}$ ) for mGlu<sub>1</sub>, being the most potent PAM with an unsubstituted phthalimide at the time. It was decided to evaluate this PAM in the rat mGlu<sub>1</sub> receptor, where the compound demonstrated to be potent (rat mGlu<sub>1</sub>  $EC_{50}$  = 238 nM) and highly efficacious (126%  $Glu_{Max}$ ). **5.27** was also evaluated for its mGlu<sub>4</sub> potency where it showed 12-fold preference for mGlu<sub>1</sub> (hu mGlu<sub>4</sub>  $EC_{50}$  = 1.2  $\mu$ M, 117%  $PHCCC_{Max}$ ).

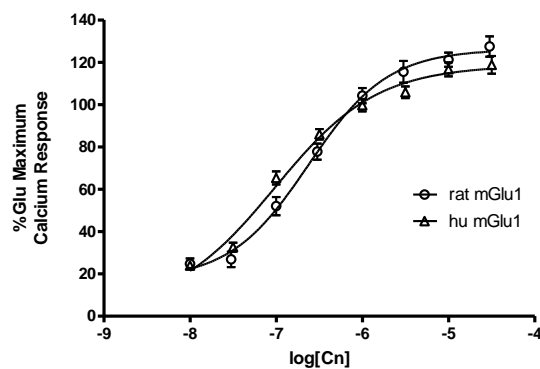
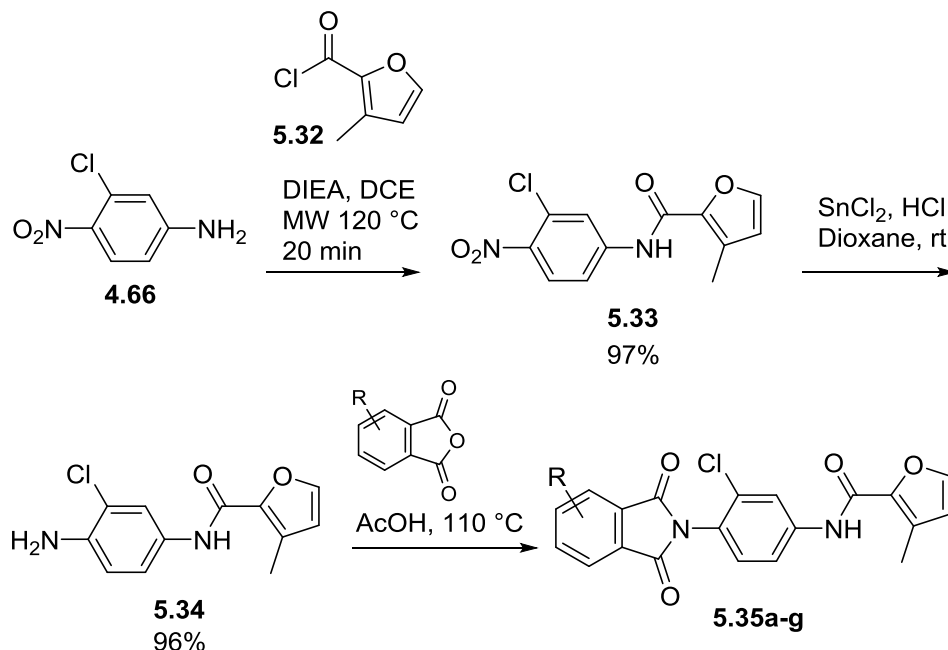


**Figure 5.4.** Concentration-response of curve for PAM activity of VU0474633 **5.27** in human and rat mGlu<sub>1</sub>. Calcium mobilization was used to obtain %Glu<sub>Max</sub> values for each compound at different concentrations in the presence of a submaximal concentration of glutamate (EC<sub>20</sub>) in cell lines expressing human mGlu<sub>1</sub>. Data represent the mean ± S.E.M. of at least three experiments with similar results.

### Discovery and characterization of VU0486321

#### *Phthalimide modifications of VU0474633 5.27*

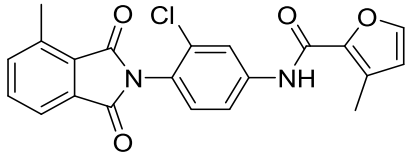
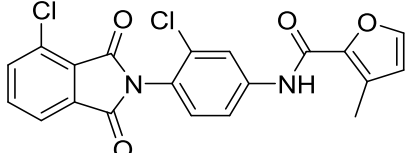
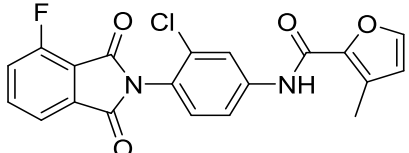
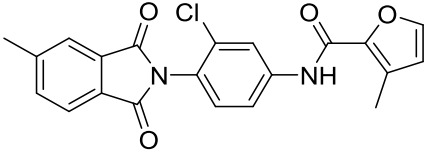
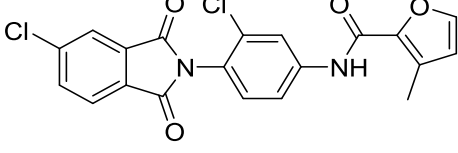
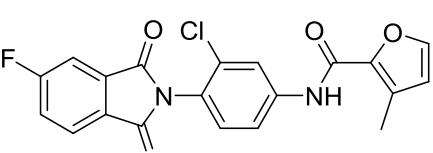
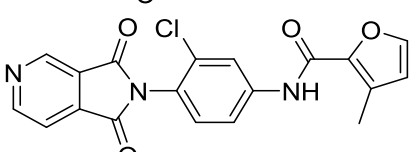
The potency and selectivity characteristics of **5.27** prompted us to evaluate the impact of the different substituents of the phthalimide on mGlu<sub>1</sub> potency. For this effort, analogs with the substituents used in previous scaffolds (VU0477930 **4.51** and VU0474640 **4.28**) were synthesized, allowing a more direct comparison between these analogs and those reported in chapter 4. We envisioned accessing these compounds through a similar 3-step approach as in scheme 4.2; however, after using EDCI, HATU and PyCIU at room temperature and with microwave heating, only little amounts of product were obtained. Using the acyl chloride **5.32** with the aniline **4.66** at room temperature was not a viable approach, but the reaction was considerably more productive when heating in the microwave at 120 °C for 20 minutes, allowing **5.33** to be obtained in excellent yields. Then, this nitro aromatic intermediate **5.33** was reduced almost quantitatively with tin(II) chloride to obtain aniline **5.34**, which in turn was condensed with the phthalic anhydrides in refluxing acetic acid to yield analogs **5.35a-g** (Scheme 5.2).



**Scheme 5.2.** Synthesis of analogs **5.35a-g** derived from VU0474633 **5.27** with modifications on the phthalimide.

These analogs were tested in human mGlu<sub>1</sub> and mGlu<sub>4</sub> to assess their potency and selectivity (Table 5.3). It was observed that the 3-substituted phthalimide analogs **5.35a-5.35c** decrease the EC<sub>50</sub> for mGlu<sub>1</sub> by 3 to 4-fold compared to VU0474633 **5.27**. The 4-substituted **5.35d-5.35f** also increased their potency with respect to the parent compound, but this effect was more variable and more important for the 4-fluoro analog **5.35f**. While the introduction of a nitrogen in the phthalimide (**5.35g**) maintained the original activity of VU0474633 **5.27**. These results showed a substantial improvement in potency compared with the compounds derived from VU0474640 **4.28** and VU0477930 **4.51**, as an example, in both these cases the direct comparators of **4.77g** and **4.76g** were weak PAMs with over 10 μM potencies.

**Table 5.3.** Potencies in human mGlu<sub>1</sub> and mGlu<sub>4</sub> of VU0474633 analogs **5.35a-5.35g**. Calcium mobilization responses for each compound are reported as a percentage of the maximum glutamate response. VU number denotes the compound identifier assigned by Vanderbilt University. Data represent the mean ± S.E.M. of at least three independent experiments with similar results. ---, no potentiation. ND, not determined.

Structure	Cpd #	VU #	hmGlu <sub>1</sub>		hmGlu <sub>4</sub>	
			EC <sub>50</sub> (nM)	%Glu <sub>Max</sub>	EC <sub>50</sub> (μM)	%Glu <sub>Max</sub>
	<b>5.35a</b>	VU0486286	24.3	86	0.62	153
	<b>5.35b</b>	VU0486388	33.0	91	1.14	163
	<b>5.35c</b>	VU0486321	31.8	98	1.11	122
	<b>5.35d</b>	VU0486322	54.4	86	0.32	69
	<b>5.35e</b>	VU0486320	80.9	94	2.25	89
	<b>5.35f</b>	VU0486323	24.1	88	0.71	97
	<b>5.35g</b>	VU0486287	98.8	94	>10	18

In terms of selectivity, these new set of compounds proved to activate the human mGlu<sub>4</sub> receptor (Table 5.3). The higher efficacies were observed in the 3-substituted phthalimides **5.35a-**

**5.35c**, while the lower EC<sub>50</sub>s were observed with analogs **5.35b**, **5.35e** and **5.35g**. Balancing these two factors, we chose analogs **5.35c**, **5.35e** and **5.35g** for further analysis. Compounds **5.35c** and **5.35e** are 35-fold and 28-fold selective for mGlu<sub>1</sub> with respect to mGlu<sub>4</sub>, and **5.35g** display full selectivity for mGlu<sub>1</sub>, being inactive at mGlu<sub>4</sub> (EC<sub>50</sub>>10 μM, >101 fold selective).

*Pharmacodynamic characterization of VU0474633 analogs*

Analogs VU0486321 **5.35c**, VU0486320 **5.35e** and VU0486287 **5.35g** were advanced for further characterization. First, the cross species activity of the compounds was confirmed by determining their EC<sub>50</sub> in the rat mGlu<sub>1</sub>. **5.35e** (rat mGlu<sub>1</sub> EC<sub>50</sub> = 160 nM, 107%) and **5.35g** (rat mGlu<sub>1</sub> EC<sub>50</sub> = 177 nM, 107%) are slightly less potent in the rat than in the human receptor, but this difference is associated to higher efficacy for the rat receptor as the concentration response curve are fairly similar. In the case of **5.35c**, the EC<sub>50</sub> and efficacy similar in both receptors (rat mGlu<sub>1</sub> EC<sub>50</sub> = 37 nM, 102%).

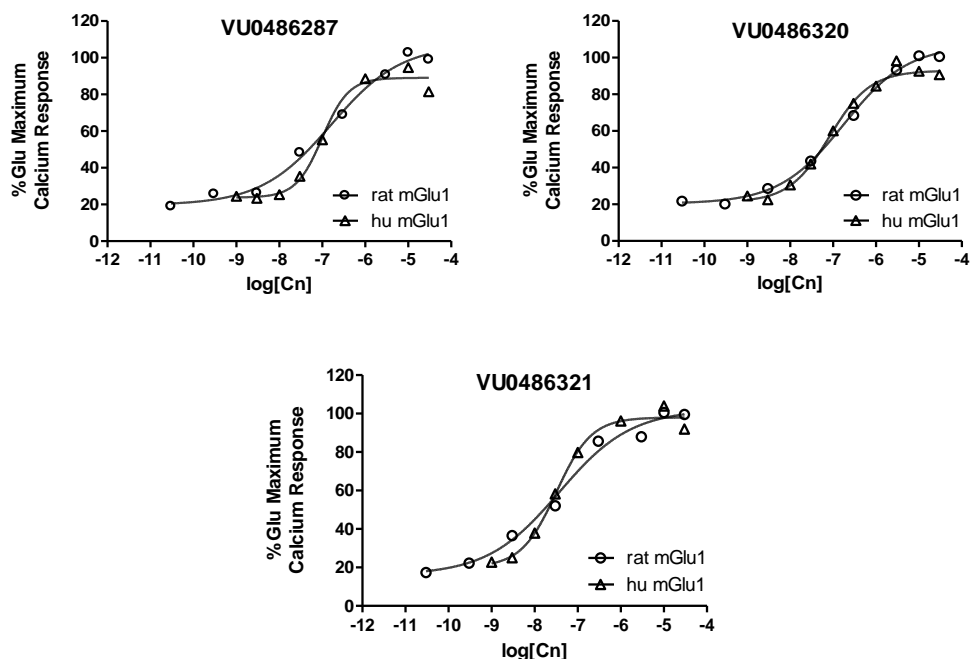


**Figure 5.5.** Concentration-response of curve for PAM activity of VU0486321 **5.35c**, VU0486320 **5.35e** and VU0486287 **5.35g** in human and rat mGlu<sub>1</sub>. Calcium mobilization was used to obtain %Glu<sub>Max</sub> values for each compound at different concentrations in the presence of a submaximal concentration of glutamate (EC<sub>20</sub>) in cell lines expressing human or rat mGlu<sub>1</sub>. Data represent the mean ± S.E.M. of at least three experiments with similar results.

The selectivity of these analogs in other mGlu receptors was evaluated in fold-shift experiments (Fig. 5.6). None of the compounds potentiated the mGlu<sub>2</sub> and mGlu<sub>3</sub> receptors. In the mGlu<sub>5</sub> receptor, the compounds presented weak fold-shift, with VU0486321 **5.35c** presenting the largest shift at 2.7. When selectivity against mGlu<sub>6</sub> and mGlu<sub>7</sub> was assessed a decrease in the EC<sub>50</sub> of glutamate was observed for VU0486321 **5.35c** (6.7 and 7.0 fold-shift, respectively), but no potentiation was observed with VU0486320 **5.35e** and VU0486287 **5.35g**. Finally, the analogs did not potentiate mGlu<sub>8</sub>, with the exception of VU0486321 **5.35c** that presented a small fold-shift of 2.3.



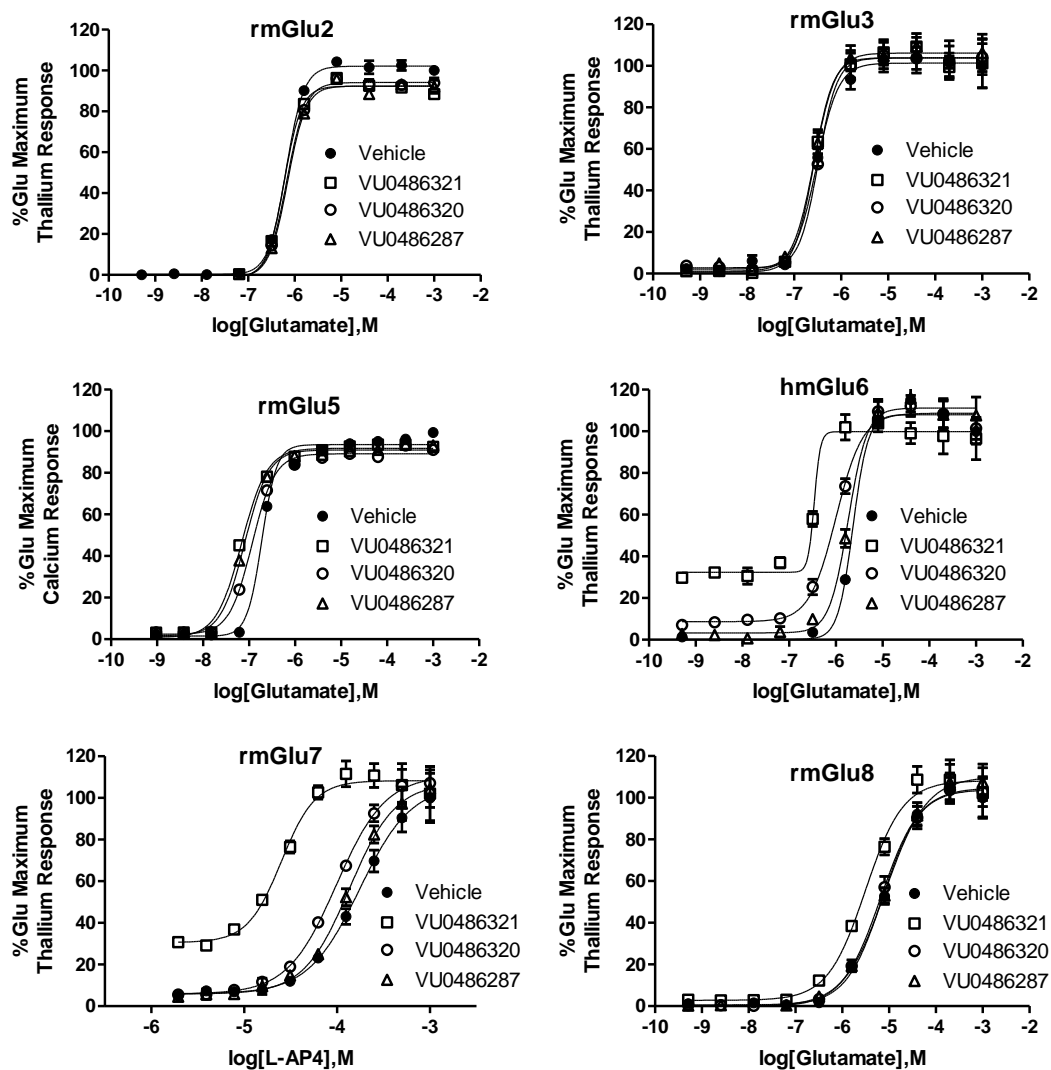


**Figure 5.6.** Selectivity of VU0486321 **5.35c**, VU0486320 **5.35e** and VU0486287 **5.35g** against the mGlu receptors determined in fold-shift mode. Calcium mobilization assays with rmGlu<sub>5</sub> were used to obtain CRCs in the presence of a fixed concentration of 10  $\mu$ M of the PAMs. The analysis of rmGlu<sub>2,3,4,7,8</sub> and rmGlu<sub>6</sub> selectivity was performed with thallium flux assays. Data represent the mean  $\pm$  S.E.M. of at least three independent experiments with similar results.

Continuing the pharmacological characterization of these mGlu<sub>1</sub> PAMs, fold-shift experiments were performed with different concentrations of the compounds to evaluate their effect in the concentration-response curve of glutamate (Fig. 5.7). It was observed that these analogs behave as PAMs with different degrees of agonism at 10  $\mu$ M. VU0486321 **5.35c** presents the higher agonism with 34% Glu<sub>Max</sub>, followed by VU0486320 **5.35e** with 15% Glu<sub>Max</sub> and

VU0486287 **5.35g** with 12% Glu<sub>Max</sub>; in the three compounds, this agonist response is completely lost when using concentration of 1  $\mu$ M or lower.

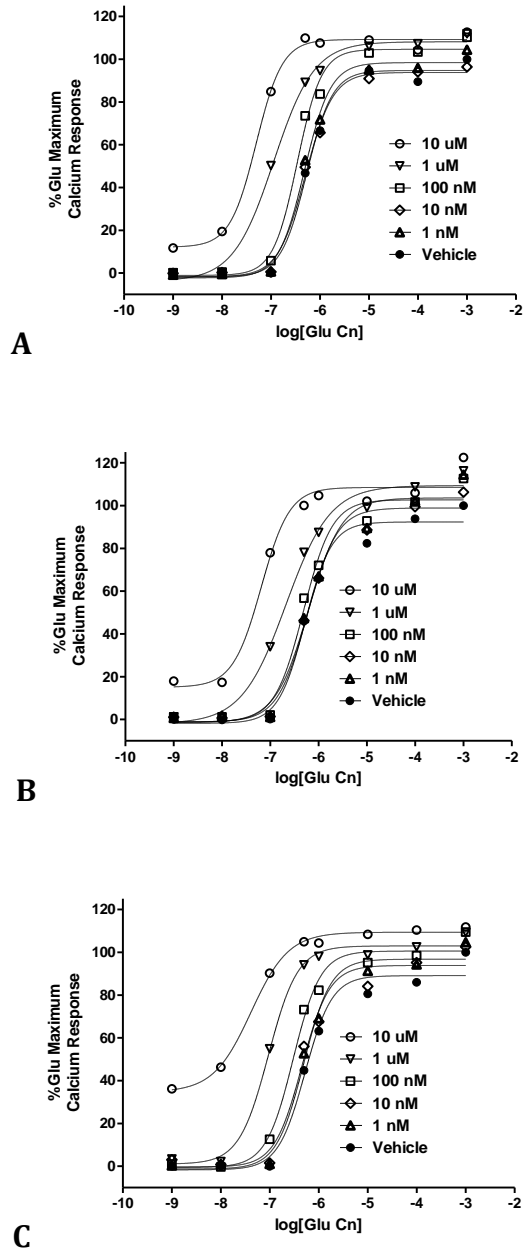


**Figure 5.7.** Effect of VU0486287 **5.35g**, VU0486320 **5.35e** and VU0486321 **5.35c** on the concentration-response curve of glutamate in hmGlu<sub>1</sub>. Calcium mobilization fold-shift assays with hmGlu<sub>1</sub> were used to obtain glutamate CRCs in the absence and presence of 10  $\mu$ M concentration of the PAMs. Data represent the mean  $\pm$  S.E.M. of at least three independent experiments with similar results.

After the analysis of the fold-shift data using the compounds at 10  $\mu\text{M}$ , we found that these PAMs provoked the largest fold-shift in the human mGlu<sub>1</sub> (Table 5.4), being even higher than the one recorded for Ro 07-11401 (Table 4.6). VU0486321 **5.35c** increased the sensitivity of the receptor for glutamate almost 13-fold. Also, analogs **5.35c**, **5.35e** and **5.35g** increased the efficacy of the receptor to 109%, a change of almost 15% with respect to the fitted value for the top of the concentration-response curve of glutamate alone.

**Table 5.4.** Effect of VU0486287 **5.35g**, VU0486320 **5.35e** and VU0486321 **5.35c** on the parameters of concentration-response curve of glutamate in hmGlu<sub>1</sub>. Calcium mobilization fold-shift assays with hmGlu<sub>1</sub> were used to obtain glutamate CRCs in the absence and presence of 10  $\mu\text{M}$  concentration of the PAMs. Data represent the mean  $\pm$  S.E.M. of at least three independent experiments with similar results.

Cpd	EC <sub>50</sub> (nM)	Fold-Shift	Efficacy (%)
Glutamate	535	1.0	94.7
VU0486287 <b>5.35g</b>	49.9	10.7	109
VU0486320 <b>5.35e</b>	65.0	8.2	109
VU0486321 <b>5.35c</b>	41.4	12.9	109

We next evaluated the effect of these PAMs in representative schizophrenia related mutant constructs of mGlu<sub>1</sub> (Fig. 5.8). The mutations Y632H, A683, P729T, and P1014S were selected for this analysis as these represent the most functionally affected receptors from the previously tested constructs. In this assay, VU0486320 **5.35e** and VU0486287 **5.35g** potentiated the mutant receptors, and at a concentration of 10  $\mu\text{M}$  they show larger fold-shifts than Ro 07-11401. VU0486321 **5.35c** showed more of a mixed profile, performing better than the Roche compound in Y632H, similar in P729T, and causing a smaller shift in the EC<sub>50</sub> in A683E and P1014S; these intriguing discrepancies can be rationalized as an artifact caused by the agonistic

effect of VU0486321 **5.35c**, as raising the efficacy in the left part of the curve cause a right-shift in the inflexion point of concentration response curve.

The efficacies of the compounds are also affected by the agonistic effect. The efficacies in Table 5.5 show how only VU0486320 **5.35e** manages to increase the efficacy of the mutant receptor in 15 to 25% of its original response. However, if the curves at lower concentration are analyzed it is possible to find that the 1  $\mu$ M concentration gives consistently the highest efficacies for VU0486321 **5.35c** and VU0486287 **5.35g**, which are comparable to the values obtained for VU0486320 **5.35e**. The importance of this *in vitro* effect in the EC<sub>50</sub> and efficacy of the glutamate response of mutant receptor can only be determined in *in vivo* studies.

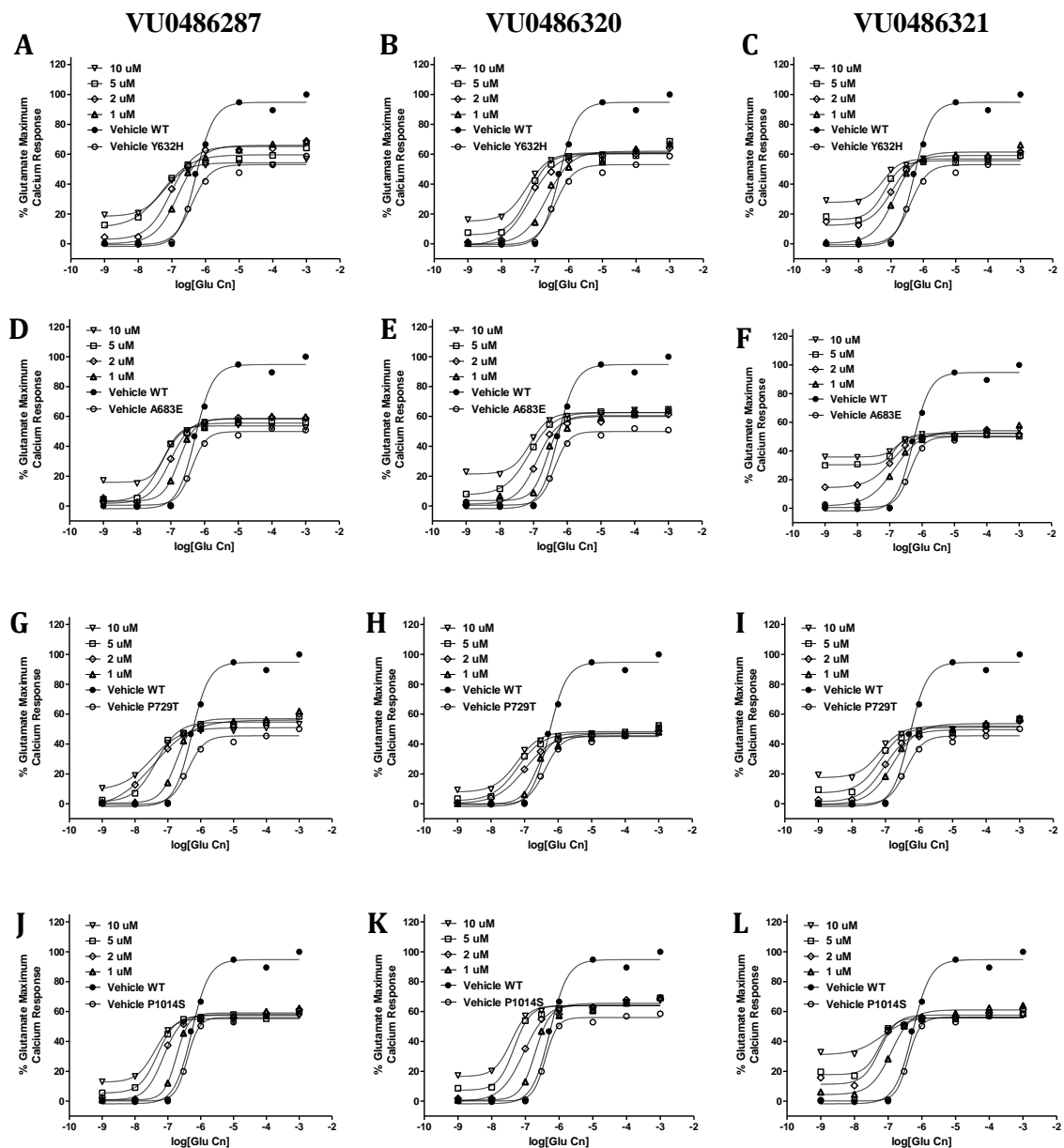


**Figure 5.8.** Effect of the application of mGlu<sub>1</sub> PAMs VU0486287 **5.35g** (panel A, D, G, J), VU0486320 **5.35e** (panel B, E, H, K) and VU0486321 **5.35c** (panel C, F, I, L) on the concentration response curve of glutamate in hmGlu<sub>1</sub> mutant constructs. Calcium mobilization fold-shift assays with different mGlu<sub>1</sub> constructs were used to obtain glutamate CRCs in the absence and presence of 10  $\mu$ M concentration of the PAMs. Data represent the mean  $\pm$  S.E.M. of at least three independent experiments with similar results different mGlu<sub>1</sub> constructs

**Table 5.5.** Effect of VU0486287 **5.35g**, VU0486320 **5.35e** and VU0486321 **5.35c** on the parameters of concentration-response curve of glutamate in hmGlu<sub>1</sub> mutant constructs. Calcium mobilization fold-shift assays with different mGlu<sub>1</sub> constructs were used to obtain glutamate CRCs in the absence and presence of 10  $\mu$ M concentration of the PAMs. Data represent the mean  $\pm$  S.E.M. of at least three independent experiments with similar results.

Cpd		Mutant			
		Y632H	A683E	P729T	P1014S
Vehicle	EC <sub>50</sub> (nM)	389	417	404	390
	Efficacy (%)	53.0	49.9	45.5	56.0
VU0486287	EC <sub>50</sub> (nM)	60.9	70.5	32.1	40.8
	Fold-shift	6.39	5.91	12.6	9.56
	Efficacy (%)	54.2	53.6	50.9	55.2
VU0486320	EC <sub>50</sub> (nM)	58.2	81.1	60.5	38.5
	Fold-shift	6.68	5.14	6.68	10.12
	Efficacy (%)	61.0	62.5	47.3	64.0
VU0486321	EC <sub>50</sub> (nM)	58.0	178	70.1	66.4
	Fold-shift	6.71	2.34	5.76	5.87
	Efficacy (%)	56.8	52.2	52.0	56.3

*Pharmacokinetic characterization of VU0474633 analogs*

The *in vitro* pharmacokinetic properties of the three pharmacologically characterized analogs were studied (Table 5.6). In this set VU0486287 **5.35g** showed high intrinsic clearance in human and rat liver microsomes, with the predicted hepatic clearance approximating 85% of the hepatic blood flow in both species. VU0486320 **5.35e** and VU0486321 **5.35c** displayed low intrinsic clearance in human liver microsomes, but they behaved differently in the rat microsomal

preparation, where VU0486320 **5.35e** showed low clearance and an improvement from VU0483605 **4.77b**, while VU0486321 **5.35c** displayed a hepatic clearance of close to 75% of rat hepatic blood flow.

**Table 5.6.** *In vitro* pharmacokinetic properties of analogs VU0486287 **5.35g**, VU0486320 **5.35e** and VU0486321 **5.35c**.

Parameter	RO 07-11401	VU0483605	VU0486320	VU0486321	VU0486287
Hu Cl <sub>int</sub> (mL/min/kg)	262	17.2	2.90	3.10	167
Hu Cl <sub>hep</sub> (mL/min/kg)	19.4	9.46	2.54	2.70	18.6
Rat Cl <sub>int</sub> (mL/min/kg)	661	39.9	22.8	207	405
Rat Cl <sub>hep</sub> (mL/min/kg)	63.3	25.4	17.2	52.3	59.7
P450 IC <sub>50</sub> (μM)					
1A2	13	>30	>30	25.2	>30
2C9	0.6	>30	>30	6.45	>30
2D6	>30	>30	>30	>30	>30
3A4	>30	>30	>30	>30	>30
Hu f <sub>u</sub> plasma	0.014	unstable	unstable	0.051	unstable
Rat f <sub>u</sub> plasma	0.003	unstable	unstable	0.030	0.030
Rat f <sub>u</sub> brain	0.001	ND	0.001	0.005	0.346

The compounds also displayed a different inhibition profile of P450 enzymes (Table 5.6). Similarly to picolinamide VU0483605 **4.77b**, VU0486287 **5.35g** and VU0486320 **5.35e** did not show inhibition of the evaluated cytochromes at a concentration of 30 μM. However, the introduction of the furan ring in the context of the 4-fluorophthalimide caused VU0486321 **5.35c** to gain inhibition for 1A2 and 2C9. While the 1A2 inhibition is weak, the effect on 2C9 inhibition is considerable and we would like to decrease it; the replacement of the furan ring would probably ameliorate this parameter.

The fraction unbound in plasma was evaluated for these analogs using rat and human plasma (Table 5.6). As it was observed previously with VU0483605 analogs, we found that VU0486320 **5.35e** was unstable in the plasma preparations, while VU0486287 **5.35g** was labile in human plasma but it allowed the determination of fraction unbound in rat plasma ( $f_u = 0.03$ ). Interestingly, VU0486321 **5.35c** was stable enough in both human and rat plasma, and had a fraction unbound of 0.05 and 0.03, respectively. These values are encouraging for a chemical probe designed to access the central nervous system; though, it was found that VU0486321 **5.35c** was still highly unstable after 4 hours incubations in plasma. Biotransformation analysis confirmed analogous metabolism to the analyzed picolinamide VU0405623 **4.141**, with hydrolysis of the phthalimide to generate the phthalamic acid regioisomers (Fig. 5.9).

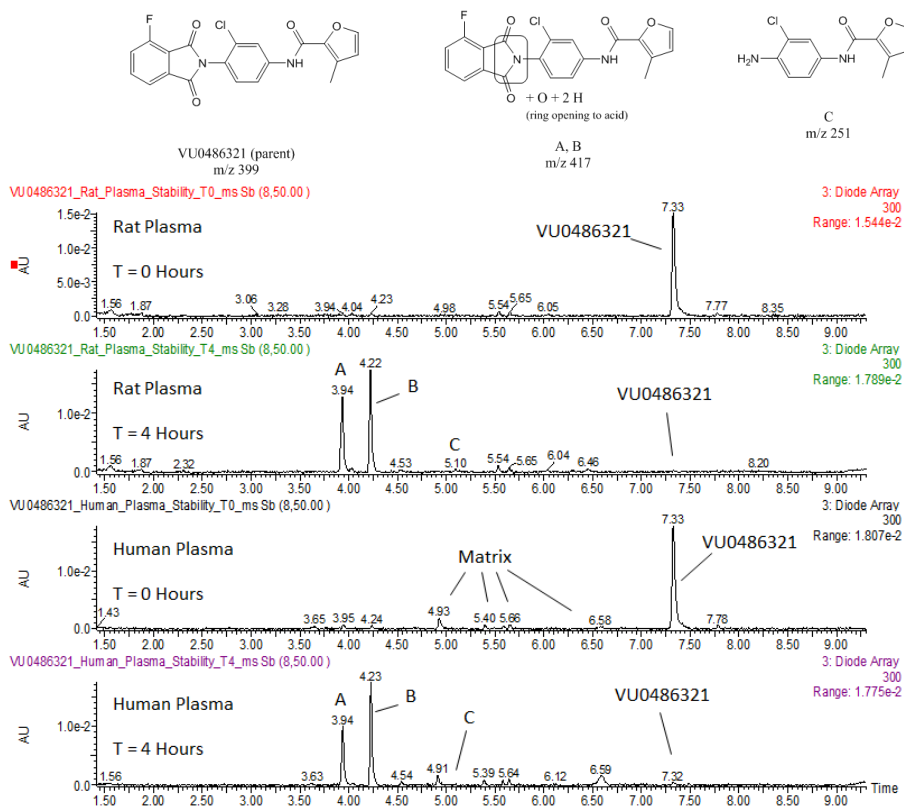


**Figure 5.9.** Biotransformation analysis of VU0486321 **5.35c** in rat and human plasma. Analysis of samples incubated for 4 hours in plasma was made by LC-MS<sup>n</sup>.



Exploration of the *in vivo* pharmacokinetic properties was performed in rats administering the compounds intravenously at a dose of 0.2 mg/kg (Table 5.7). The highest clearance was observed with VU0486287 **5.35g** which had a half-life of five minutes. VU0486320 **5.35e** was the analog with the longest half-life (~1.5 hours), however its calculated plasma clearance is similar to Ro 07-11401. VU0486321 **5.35c** has a 54 minute half-life, but its clearance is considerably slower with respect to VU0486320 **5.35e** and Ro 07-11401. Also, when the concentrations are analyzed, it was observed that VU0486321 **5.35c** reach plasma concentrations more than two times higher than VU0486320 **5.35e**, and more than four times higher than VU0486287 **5.35g**.

**Table 5.6.** *In vivo* rat pharmacokinetic properties of analogs VU0486287 **5.35g**, VU0486320 **5.35e** and VU0486321 **5.35c**.

Parameter	RO 07-11401	VU0486320	VU0486321	VU0486287
Rat IV PK (0.2 mg/kg)				
$t_{1/2}$ (min)	54	91.1	53.6	5.38
MRT (min)	50	53.5	64.1	7.85
$Cl_p$ (mL/min/kg)	35	33.0	13.3	382
$V_{ss}$ (L/kg)	1.34	1.76	0.85	3.00
Rat IV PBL (0.25 h, 0.2 mg/kg)				
Cn plasma (ng/mL)	276	173	200	12.5
Cn brain (ng/mL)	81	108	204	35.2
$K_p$	0.29	0.63	1.02	2.81
$K_{p,uu}$	0.10	ND	0.17	ND

Concerning brain penetrance, VU0486321 **5.35c** demonstrated to be the best PAM in this set, reaching a brain to plasma coefficient of approximately 1, with concentrations in brain and in plasma of 200 ng/mL (~500 nM), more than 15-fold its mGlu<sub>1</sub> EC<sub>50</sub>. Compound VU0486287 **5.35g** achieved a high  $K_p$  but with very low concentrations of the PAM. Finally, VU0486320 **5.35e** reached lower concentrations in the brain than VU0486321 **5.35c**, but higher than Ro 07-11401 with a  $K_p$  close to 0.6. When the unbound partition coefficient is calculated,

compound VU0486321 still represents the best from this batch, although there is considerable room for improvement for this parameter.

*Adverse event propensity of VU0474633 analogs*

The orthosteric, amino acid agonists of group I mGlu<sub>1</sub> allowed early efforts directed to understand the physiological role of these receptors; though their excitotoxicity and seizure liability has limited their utility.<sup>292–297</sup> For example, DHPG, the dual mGlu<sub>1/5</sub> agonist, induces severe epileptiform activity, and this liability was important in early mGlu<sub>5</sub> PAM programs, as it was not clear if this was due to mGlu<sub>1</sub>, mGlu<sub>5</sub> or both. Moreover, it was not clear if a pure mGlu<sub>5</sub> modulator would avoid this behavior. Over the years, multiple mGlu<sub>5</sub> PAMs, across diverse chemotypes, that possessed even modest ago-PAM, or pure PAMs that *in vivo* generated ago-PAM metabolites, have induced epileptiform activity in slice electrophysiology as well as Racine scale (4+) seizures in rodents.<sup>298–300</sup> This severe adverse effect has hindered the development of positive allosteric modulators for mGlu<sub>5</sub>.

Thus, with analogs **5.35c**, **5.35e** and **5.35g**, we were poised to assess the adverse effect liability of mGlu<sub>1</sub> PAM with various levels of agonism and that can penetrate the blood brain barrier reaching the CNS. We decided to explore VU0486321 **5.35c** as we believed that if there was a propensity to induce an adverse event, it would be more discernible after the administration of the compound with higher agonism.

*In vitro* extracellular electrophysiology recordings of epileptiform activity in the CA3 region of the hippocampus were performed with either vehicle control, 10 μM VU0486321 **5.35c** or the group I agonist DHPG. In this experiment, DHPG induced significant epileptiform activity in the CA3 region in the hippocampus, as it has been observed in the literature. In contrast, VU0486321 **5.35c** does not cause this form of activity in slices, despite possessing ~35% agonism at this concentration (Fig. 5.10).

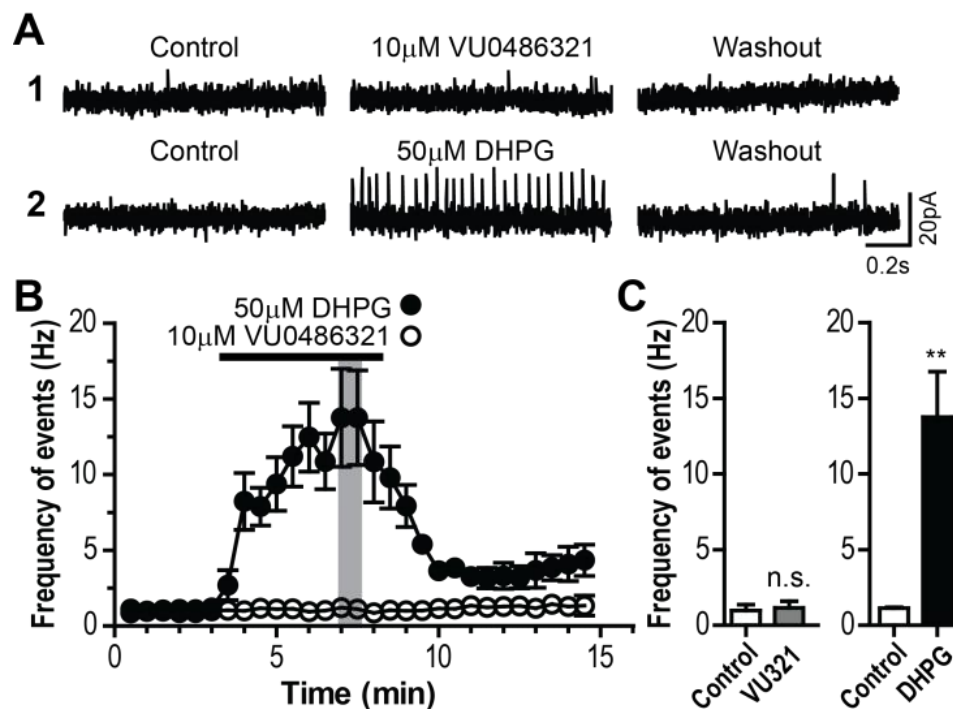


**Figure 5.10.** mGlu<sub>1</sub> ago-PAM VU0486321 **5.35c** did not induce epileptiform activity in CA3 region of the hippocampus. **A.** Traces of extracellular recordings from CA3 pyramidal cell body layer in hippocampal slices treated with 10  $\mu$ M **5.35c** (A1) and 50  $\mu$ M DHPG (A2). **B.** Average time courses of frequency of spontaneous activity during application of **5.35c** ( $n = 6$ ) and DHPG ( $n = 6$ ), respectively. Gray bar indicates the time point at which the data were taken to make statistical comparison to the control. **C.** Bar graphs summarizing the effects of 10  $\mu$ M **17e** (left) and 50  $\mu$ M DHPG (right) on the frequency of spontaneous activity in hippocampal CA3 region. n.s.  $p = 0.36$ ; \*\*  $p = 0.0084$ ; paired t-test.

To corroborate this effect *in vivo*, the tendency of producing seizures by VU0486321 **5.35c** was evaluated in C57bl/6 mice (Fig. 5.11). After administering the compound intraperitoneally at 100 mg/kg, the animals presented no seizures. Using satellite animals the total concentration in the brain was quantified, observing an exposure of 9.2  $\mu$ M, a value over 280-fold larger than the mGlu<sub>1</sub> PAM EC<sub>50</sub>, and over 8-fold when taking into account fraction unbound ( $f_u = 0.03$ ). VU0486320 **5.35e** and VU0486287 **5.35g** were also administered at 100 mg/kg i.p. in C57bl/6 mice, and no seizures were observed; although, total brain levels of 1.4  $\mu$ M and 2.52  $\mu$ M were achieved.

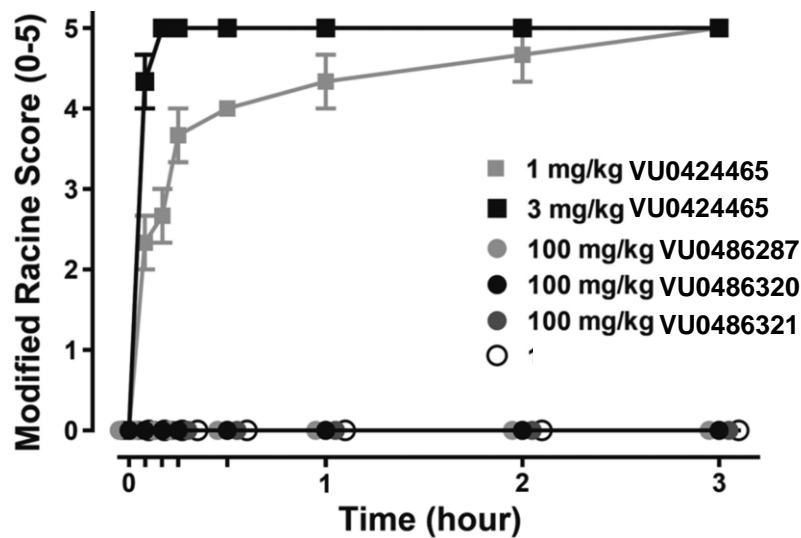


**Figure 5.11.** mGlu<sub>1</sub> PAMs do not induce behavioral convulsions in mice. Animals were dose intraperitoneally mGlu<sub>5</sub> ago-PAM VU0424465 (1 and 3 mg/kg), VU0486287 **5.35g**, VU0486320 **5.35e** or VU0486321 **5.35c** at 100 mg/kg. Data represent the mean ± SEM, n = 3.

As a comparison, the mGlu<sub>5</sub> ago-PAM VU0424465 and a pure mGlu<sub>5</sub> PAM were administered to mice. Historically, drug levels within 2-fold of the mGlu<sub>5</sub> EC<sub>50</sub> of the ago-PAM induced seizures in this test.<sup>301</sup> For the first time, these data suggest that the epileptiform activity induced by the group I dual mGlu<sub>1/5</sub> agonist is mediated by agonism at mGlu<sub>5</sub>. This data set provided the basis to speculate that mGlu<sub>1</sub> ago-PAMs will have a larger therapeutic window than mGlu<sub>5</sub> ago-PAMs, and could avoid excitotoxicity and seizures.

## Summary and future directions

In order to find a mGlu<sub>1</sub> PAM with better potency and pharmacokinetic properties than compound VU0483605 **4.77b**, further SAR exploration on this scaffold was made (Figure 5.12). First, different analogs carrying bioisosteres of the picolinamide were synthesized. From this library, the 5-thiazolecarboxamide **5.13** and the 2-furancarboxamide **5.2** analogs show good efficacy for potentiating the effect of glutamate in mGlu<sub>1</sub>, the latter the most potent of the pair with an EC<sub>50</sub> of 484 nM. After the development of analogs of **5.18-5.32** with different substituents in the furan, it was shown that small changes in this region had a big impact in activity and steep SAR. This iteration led to only one active compound, the 3-methylfuran carboxamide **5.27** which showed a 5-fold improved potency in mGlu<sub>1</sub>, but only 12-fold selectivity against mGlu<sub>4</sub>. Subsequent modifications of the phthalimide proved beneficial for mGlu<sub>1</sub> potency and allowed the discovery of analogs **5.35c**, **5.35e**, and **5.35g** which have decreased activity for mGlu<sub>4</sub> in comparison to VU0474633 **5.27** (Fig. 5.12).

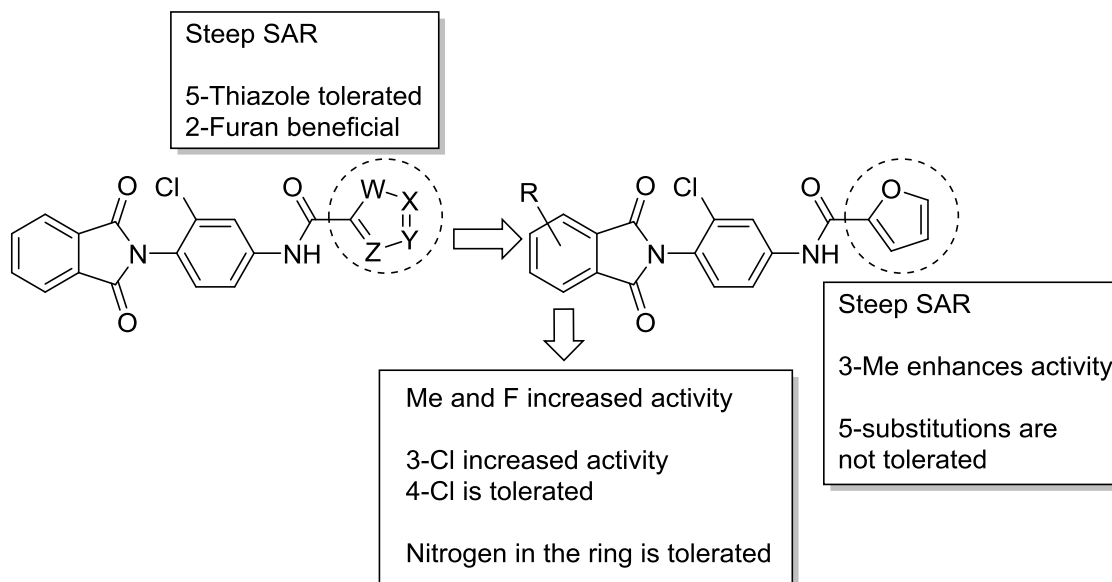


**Figure 5.12.** SAR summary for the obtention of analogs **5.35c**, **5.35e** and **5.35g**.

Further pharmacological characterization of PAMs VU0486321 **5.35c**, VU0486320 **5.35e**, and VU0486287 **5.35g** let us to confirm that the compounds had similar EC<sub>50</sub> in the rat mGlu<sub>1</sub>, establishing cross-species activity. These compounds were screened against the other members of the mGlu family where they show good selectivity, with only VU0486321 **5.35c** showing some potentiation in mGlu<sub>6</sub> and mGlu<sub>7</sub>.

These analogs displayed a larger fold-shift in the glutamate concentration response curve for mGlu<sub>1</sub>, compared to Ro 0711401; probably due to their higher potency. The compounds also showed different degrees of agonism, with VU0486321 **5.35c** giving the strongest agonistic response (35% at 10 μM). In mutants, **5.35e** and **5.35g** enhanced more the glutamate response than Ro 07-11401, but this was not the case for **5.35c**, which was probably due to its agonistic effect. Also the compounds induced an increase in the maximum efficacy achieved by the mutants, being more robust with **5.35e** at 10 μM which enhances the original mutant response 15 to 25%.

In terms of pharmacokinetic properties, *in vitro* intrinsic clearance was high for VU0486287 **5.35g**, while it was moderate for VU0486321 **5.35c** and low for VU0486320 **5.35e**. Only VU0486321 **5.35c** showed moderate inhibition of CYP2C9, while the others showed no effect in the main P450 drug enzymes. These compounds suffered also from plasma instability as VU0483605 **4.77b**, but in the case of VU0486321 **5.35c**, we were able to measure plasma fraction unbound which was between 3 to 5%. Despite this, a disconnect was observed when clearance was evaluated *in vivo* after intravenous administration as VU0486320 **5.35e** and VU0486321 **5.35c** were more stable than expected, with half-lives of close to one hour. In terms of brain penetrance, VU0486321 **5.35c** performed better, achieving good brain exposure and brain to plasma concentration coefficient close to 1 (Fig. 5.13).

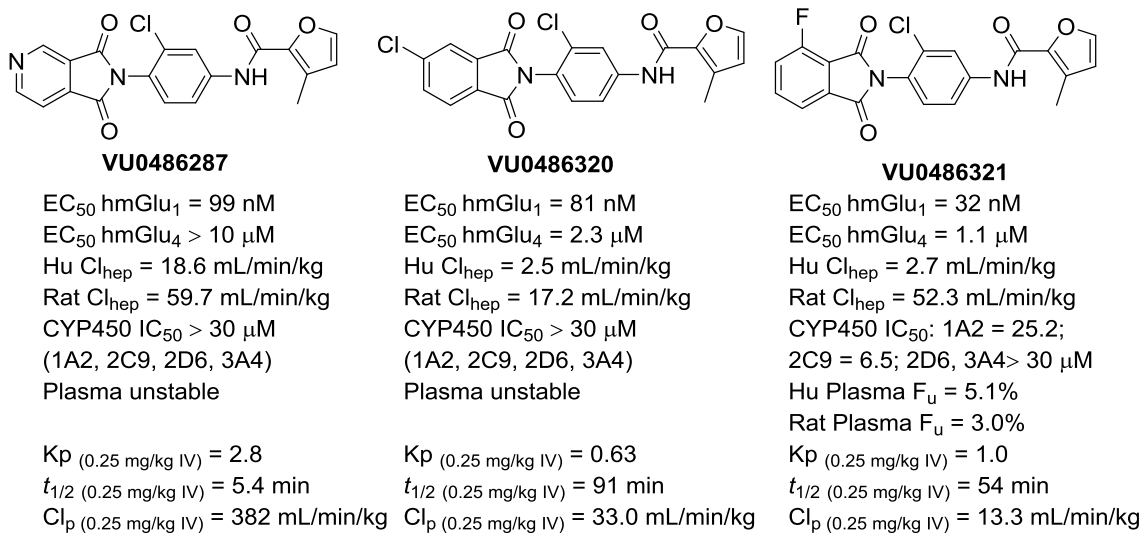


**Figure 5.13.** Summary of VU0486287 **5.35g**, VU0486320 **5.35e** and VU0486321 **5.35c** properties.

The propensity to cause seizures and epileptiform activity in the CA3 region of mice brain was evaluated for these compounds, as non-selective group I agonists and mGlu<sub>5</sub> ago-PAMs have been shown to cause this adverse events and excitotoxicity. Our mGlu<sub>1</sub> ago-PAMs did not exhibited these features, arguing for a possible advantage in safety for the enhancement of mGlu<sub>1</sub> compared to mGlu<sub>5</sub> activation.

Characterization of these compounds showed that the scaffold can generate potent and brain penetrant compounds but there is still room for improvement in their selectivity and pharmacokinetic properties, especially in their plasma stability and *in vivo* half-life. Further SAR exploration in an attempt to improve these compounds and produce a better *in vivo* chemical probe is outlined in the next chapter.

## EXPERIMENTAL METHODS

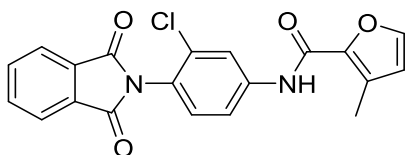
### *General chemical synthesis and characterization*

All reactions were carried out employing standard chemical techniques under inert atmosphere. All reagents and solvents were commercial grade and purified prior to use when necessary. Solvents used for extraction, washing, and chromatography were HPLC grade. Analytical thin layer chromatography was performed on 250  $\mu\text{m}$  silica gel glass backed plates from Sorbent Technologies. Visualization was accomplished with UV light, and/or the use of iodine or ninhydrin solution followed by heating. Analytical HPLC was performed on an Agilent 1200 LCMS with UV detection at 215 and 254 nm along with ELSD detection and electrospray ionization, with all final compounds showing >95% purity and a parent mass ion consistent with the desired structure. Low resolution mass spectra were obtained on an Agilent 6130 mass spectrometer with electrospray ionization source. MS parameters were as follows: fragmentor: 100, capillary voltage: 3000 V, nebulizer pressure: 40 psig, drying gas flow: 11 L/min, drying gas temperature: 350° C. Samples were introduced via an Agilent 1200 HPLC comprised of a degasser, G1312A binary pump, G1367B HP-ALS, G1316A TCC, G1315D DAD, and a Varian 380 ELSD. UV absorption was generally observed at 215 nm and 254 nm with a 4 nm bandwidth. Column: Thermo Accucore C18, 2.1 x 30 mm, 2.6  $\mu\text{m}$ . Gradient conditions: 7% to 95%  $\text{CH}_3\text{CN}$  in  $\text{H}_2\text{O}$  (0.1% TFA) over 1.6 min, hold at 95%  $\text{CH}_3\text{CN}$  for 0.35 min, 1.5 mL/min, 45° C. Flash column chromatography was performed on a Teledyne ISCO Combiflash Rf system. Preparative purification of library compounds was performed on a Gilson 215 preparative LC system. Column: Thermo Accucore C18, 2.1 x 30 mm, 2.6  $\mu\text{m}$ . Gradients condition: variable,  $\text{CH}_3\text{CN}$  in  $\text{H}_2\text{O}$  (0.1% TFA) over 4 minutes, hold at 95%  $\text{CH}_3\text{CN}$  for 0.35 min, 50 mL/min. Purity for all final compounds was >95%, and each showed a parent mass ion consistent with the desired structure in low resolution LC-MS.  $^1\text{H}$  and  $^{13}\text{C}$  NMR spectra were recorded on Bruker DRX-400 (400 MHz) instrument. Chemical shifts are reported in ppm relative to residual solvent



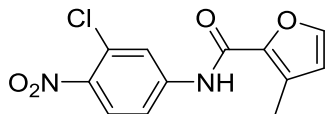
peaks as an internal standard at the following chemical shifts ( $^1\text{H}$  and  $^{13}\text{C}$  respectively): 7.26 and 77.0 ppm for  $\text{CDCl}_3$ ; 2.50 and 39.52 ppm for  $\text{DMSO}-d_6$ , 3.31 and 49.2 ppm for  $\text{CD}_3\text{OD}$ . Data are reported as follows: chemical shift, integration, multiplicity (s = singlet, d = doublet, t = triplet, q = quartet, dd = doublet of doublets, br = broad, m = multiplet), coupling constant (Hz).

**General synthesis of *N*-(3-chloro-4-(1,3-dioxisoindolin-2-yl)phenyl)amides (5.1-5.32).** In a vial, 0.088 mmol (1.2 equiv.) of the carboxylic acid were added and dissolved in 0.5 mL mixture of DCM:DIEA (9:1), then 41 mg (0.110 mmol, 1.5 equiv.) of HATU were added. The mixture was stirred for 10 minutes, and 20 mg (0.073 mmol, 1.0 equiv.) of **4.12** dissolved in 0.5 mL of DCM:DIEA (9:1) were added, followed by 3 drops of DMF. The reaction was stirred for 24 hours at room temperature. After this time, the reaction was quenched with the addition of water, and was worked up by extraction with DCM (2 mL, thrice). The organic phase was filtered through a phase separator, volatiles were evaporated, the crude product was dissolved in DMSO and purified by preparative HPLC.

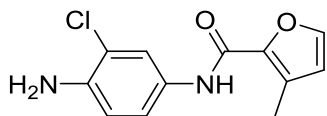


***N*-(3-Chloro-4-(1,3-dioxisoindolin-2-yl)phenyl)-3-methylfuran-2-carboxamide**

**(5.27).** Cream powder.  $^1\text{H}$ -NMR (400.1 MHz,  $\text{CDCl}_3$ )  $\delta$  (ppm): 8.14 (1H, s), 8.06 (1H, d,  $J=2.4$  Hz), 7.97 (2H, m), 7.81 (2H, m), 7.64 (1H, dd,  $J=8.6$  Hz,  $J=2.4$  Hz), 7.40 (1H, d,  $J=1.5$  Hz), 7.32 (1H, d,  $J=8.6$  Hz), 6.43 (1H, d,  $J=1.5$  Hz), 2.47 (3H, s).  $^{13}\text{C}$ NMR (100.6 MHz,  $\text{CDCl}_3$ )  $\delta$  (ppm): 166.7, 157.1, 142.8, 141.4, 139.6, 134.4, 133.7, 131.8, 130.8, 129.9, 124.8, 123.9, 120.8, 118.3, 116.0, 11.2. HRMS (TOF,  $\text{ES}^+$ )  $\text{C}_{20}\text{H}_{14}\text{ClN}_2\text{O}_4$   $[\text{M}+\text{H}]^+$  calc. mass 381.0642, found 381.0644.



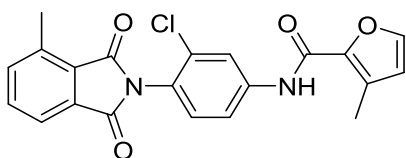
***N*-(2-Chloro-4-nitrophenyl)-3-methylfuran-2-carboxamide (5.33).** In a microwave vial, 912 mg (5.28 mmol, 1.2 equiv.) 2-chloro-4-nitroaniline were added and dissolved in 20 mL of DCE:DIEA (9:1), followed by addition of 500  $\mu$ L (4.40 mmol, 1.0 equiv.) of the 3-methylfuran-carbonyl chloride. The reaction was heated in the microwave at 120  $^{\circ}$ C for 30 minutes. The reaction was cooled to room temperature and water was added, causing the precipitation of the product. The crude was filtered *in vacuo* and titrated with methanol to give a cream colored solid (1195 mg, 97% yield).  $^1\text{H-NMR}$  (400.1 MHz, DMSO- $d^6$ )  $\delta$  (ppm): 10.71 (1H, s), 8.27 (1H, d,  $J=2.2$  Hz), 8.14 (1H, d,  $J=9.1$  Hz), 7.99 (1H, dd,  $J=9.1$  Hz,  $J=2.2$  Hz), 7.88 (1H, d,  $J=1.5$  Hz), 6.66 (1H, d,  $J=1.5$  Hz), 2.37 (3H, s).  $^{13}\text{CNMR}$  (100.6 MHz, DMSO- $d^6$ )  $\delta$  (ppm): 158.1, 144.9, 144.3, 141.9, 141.4, 130.3, 127.7, 126.9, 121.7, 119.0, 116.4, 11.5. HRMS (TOF, ES+)  $\text{C}_{12}\text{H}_9\text{ClN}_2\text{O}_4$  [ $\text{M}^+$ ] calc. mass 280.0251, found 280.0254.



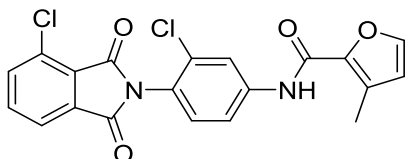
***N*-(4-Amino-2-chlorophenyl)-3-methylfuran-2-carboxamide (5.34).** In a flask, 480 mg (1.71 mmol, 1.0 equiv.) of **5.33** were suspended in dioxane. The suspension was cold in an ice bath and purged with argon. A previously prepared solution of tin(II) chloride (1.45 g, 7.70 mmol, 4.5 equiv.) in concentrated hydrochloric acid (5M concentration of  $\text{SnCl}_2$ ) was added dropwise to the suspension. After 2 hour of stirring at room temperature, the reaction was neutralized carefully with aqueous potassium carbonate 20%, filtered and extracted with diethyl ether. The organic phase was dried with magnesium sulfate, filtered and the volatiles eliminated *in vacuo* to yield a cream solid (410 mg, 96% yield).  $^1\text{H-NMR}$  (400.1 MHz, DMSO- $d^6$ )  $\delta$  (ppm): 9.87 (1H, s), 7.76 (1H, d,  $J=1.6$  Hz), 7.74 (1H, d,  $J=2.3$  Hz), 7.41 (1H, dd,  $J=8.7$  Hz,  $J=2.3$  Hz),

6.82 (1H, d,  $J=8.7$  Hz), 6.58 (1H, d,  $J=1.6$  Hz), 5.51 (2H, br), 2.32 (3H, s).  $^{13}\text{C}$ NMR (100.6 MHz, DMSO- $d^6$ )  $\delta$  (ppm): 157.5, 143.8, 142.3, 139.8, 129.9, 127.7, 121.8, 121.2, 117.8, 116.4, 116.0, 11.4. HRMS (TOF, ES+)  $\text{C}_{12}\text{H}_{11}\text{ClN}_2\text{O}_2$  [M $^+$ ] calc. mass 250.0509, found 250.0513.

**General synthesis of substituted *N*-acyl *N*-(4-aminophenyl)-3-methylfuran-2-carboxamides (5.35a-g).** In a vial, (30 mg, 0.12 mmol, 1.0 equiv.) of the aniline **5.34** and (0.18 mmol, 1.5 equiv.) of the phthalic anhydride were added and dissolved in 1 mL of acetic acid. The mixture was heated at 110 °C while stirring for 4 hours. After this time, volatiles were evaporated, the crude product was dissolved in DMSO and resolved by preparative HPLC.

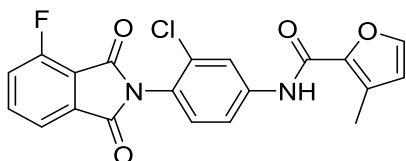


***N*-(3-Chloro-4-(4-methyl-1,3-dioxoisindolin-2-yl)phenyl)-3-methylfuran-2-carboxamide (5.35a).** Cream powder.  $^1\text{H}$ -NMR (400.1 MHz,  $\text{CDCl}_3$ )  $\delta$  (ppm): 8.15 (1H, s), 8.05 (1H, d,  $J=2.4$  Hz), 7.79 (1H, d,  $J=7.4$  Hz), 7.65 (2H, m), 7.55 (1H, d,  $J=7.7$  Hz), 7.39 (1H, d,  $J=1.5$  Hz), 7.29 (1H, d,  $J=8.6$  Hz), 6.43 (1H, d,  $J=1.6$  Hz), 2.47 (3H, s), 2.46 (3H, s).  $^{13}\text{C}$ NMR (100.6 MHz,  $\text{CDCl}_3$ )  $\delta$  (ppm): 167.5, 166.8, 157.1, 142.8, 141.4, 139.5, 138.6, 136.7, 133.9, 133.8, 132.3, 130.8, 129.9, 128.6, 125.0, 121.5, 120.8, 118.2, 116.0, 17.7, 11.2. HRMS (TOF, ES+)  $\text{C}_{21}\text{H}_{16}\text{ClN}_2\text{O}_4$  [M+H] $^+$  calc. mass 395.0799, found 395.0798.



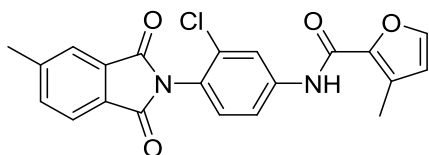
***N*-(3-Chloro-4-(4-chloro-1,3-dioxoisindolin-2-yl)phenyl)-3-methylfuran-2-carboxamide (5.35b).** Cream powder  $^1\text{H}$ -NMR (400.1 MHz,  $\text{CDCl}_3$ )  $\delta$  (ppm): 8.16 (1H, s), 8.06

(1H, d,  $J=2.3$  Hz), 7.88 (1H, m) 7.74 (2H, m), 7.63 (1H, dd,  $J=8.6$  Hz,  $J=2.3$  Hz), 7.39 (1H, d,  $J=1.2$  Hz), 7.29 (1H, d,  $J=8.6$  Hz), 6.42 (1H, d,  $J=1.2$  Hz), 2.46 (3H, s).  $^{13}\text{C}$ NMR (100.6 MHz,  $\text{CDCl}_3$ )  $\delta$  (ppm): 165.2, 164.3, 157.2, 142.9, 141.4, 139.8, 136.1, 135.2, 133.9, 133.7, 132.0, 130.7, 130.0, 127.6, 124.4, 122.3, 120.8, 118.3, 116.1, 11.2. HRMS (TOF, ES+)  $\text{C}_{20}\text{H}_{13}\text{Cl}_2\text{N}_2\text{O}_4$   $[\text{M}+\text{H}]^+$  calc. mass 415.0252, found 415.0254.



***N*-(3-Chloro-4-(4-fluoro-1,3-dioxoisindolin-2-yl)phenyl)-3-methylfuran-2-**

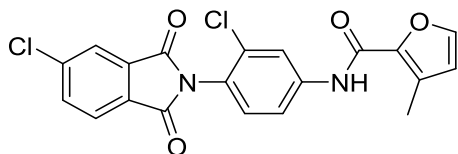
**carboxamide (5.35c).** Cream powder.  $^1\text{H}$ -NMR (400.1 MHz,  $\text{CDCl}_3$ )  $\delta$  (ppm): 8.16 (1H, s), 8.06 (1H, d,  $J=2.3$  Hz), 7.80 (2H, m), 7.65 (1H, dd,  $J=8.6$  Hz,  $J=2.4$  Hz), 7.49 (1H, m), 7.39 (1H, d,  $J=1.4$  Hz), 7.30 (1H, d,  $J=8.6$  Hz), 6.42 (1H, d,  $J=1.4$  Hz), 2.46 (3H, s).  $^{13}\text{C}$ NMR (100.6 MHz,  $\text{CDCl}_3$ )  $\delta$  (ppm): 165.5, 163.3, 157.9 ( $^1J_{\text{CF}}$ , d,  $J=266$  Hz), 157.2, 142.9, 142.7, 141.4, 139.8, 137.0 ( $^3J_{\text{CF}}$ , d,  $J=7.6$  Hz), 133.8 ( $^2J_{\text{CF}}$ , d,  $J=22.6$  Hz), 130.8, 130.0, 124.3, 122.7 ( $^2J_{\text{CF}}$ , d,  $J=19.6$  Hz), 120.8, 120.1 ( $^4J_{\text{CF}}$ , d,  $J=3.2$  Hz), 118.7, 118.3, 116.1, 11.2. HRMS (TOF, ES+)  $\text{C}_{20}\text{H}_{13}\text{ClFN}_2\text{O}_4$   $[\text{M}+\text{H}]^+$  calc. mass 399.0548, found 399.0547.



***N*-(3-Chloro-4-(5-methyl-1,3-dioxoisindolin-2-yl)phenyl)-3-methylfuran-2-**

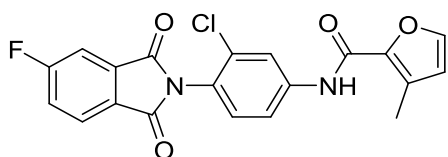
**carboxamide (5.35d).** Cream powder.  $^1\text{H}$ -NMR (400.1 MHz,  $\text{CDCl}_3$ )  $\delta$  (ppm): 8.15 (1H, s), 8.05 (1H, d,  $J=2.3$  Hz), 7.84 (1H, d,  $J=7.7$  Hz), 7.77 (1H, d,  $J=7.4$  Hz), 7.62 (1H, dd,  $J=8.6$  Hz,  $J=2.4$  Hz), 7.59 (1H, d,  $J=7.7$  Hz), 7.38 (1H, d,  $J=1.5$  Hz), 7.30 (1H, d,  $J=8.6$  Hz), 6.42 (1H, d,  $J=1.5$  Hz), 2.56 (3H, s), 2.46 (3H, s).  $^{13}\text{C}$ NMR (100.6 MHz,  $\text{CDCl}_3$ )  $\delta$  (ppm): 166.9, 166.8, 157.1,

145.8, 142.8, 141.4, 139.6, 135.0, 133.8, 132.2, 130.8, 129.9, 129.2, 124.9, 124.4, 123.8, 120.8, 118.3, 116.0, 22.0, 11.2. HRMS (TOF, ES+) C<sub>21</sub>H<sub>16</sub>ClN<sub>2</sub>O<sub>4</sub> [M+H]<sup>+</sup> calc. mass 395.0799, found 395.0798.



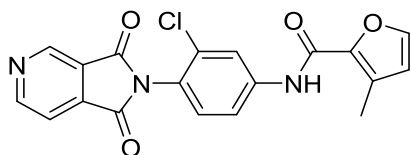
***N*-(3-Chloro-4-(5-chloro-1,3-dioxisoindolin-2-yl)phenyl)-3-methylfuran-2-**

**carboxamide (5.35e).** Cream powder. <sup>1</sup>H-NMR (400.1 MHz, CDCl<sub>3</sub>) δ (ppm): 8.16 (1H, s), 8.06 (1H, d, *J*=2.3 Hz), 7.94 (1H, d, *J*=1.7 Hz), 7.90 (1H, d, *J*=8.0 Hz), 7.77 (1H, dd, *J*=8.0 Hz, *J*=1.7 Hz), 7.63 (1H, dd, *J*=8.6 Hz, *J*=2.3 Hz), 7.40 (1H, d, *J*=1.4 Hz), 7.30 (1H, d, *J*=8.6 Hz), 6.43 (1H, d, *J*=1.4 Hz), 2.46 (3H, s). <sup>13</sup>CNMR (100.6 MHz, CDCl<sub>3</sub>) δ (ppm): 165.8, 165.4, 157.1, 142.9, 141.4, 141.2, 139.8, 134.5, 133.6, 133.5, 130.7, 130.0, 129.8, 125.1, 124.4, 124.3, 120.8, 118.3, 116.1, 11.2. HRMS (TOF, ES+) C<sub>20</sub>H<sub>13</sub>Cl<sub>2</sub>N<sub>2</sub>O<sub>4</sub> [M+H]<sup>+</sup> calc. mass 415.0252, found 415.0251.



***N*-(3-Chloro-4-(5-fluoro-1,3-dioxisoindolin-2-yl)phenyl)-3-methylfuran-2-**

**carboxamide (5.35f).** Cream powder. <sup>1</sup>H-NMR (400.1 MHz, CDCl<sub>3</sub>) δ (ppm): 8.16 (1H, s), 8.06 (1H, d, *J*=2.3 Hz), 7.97 (1H, dd, *J*=8.2 Hz, *J*=4.5 Hz), 7.64 (2H, m), 7.47 (1H, td, *J*=8.5 Hz, *J*=2.2 Hz), 7.40 (1H, d, *J*=1.5 Hz), 7.30 (1H, d, *J*=8.6 Hz), 6.43 (1H, d, *J*=1.5 Hz), 2.47 (3H, s). <sup>13</sup>CNMR (100.6 MHz, CDCl<sub>3</sub>) δ (ppm): 165.6, 165.3, 157.1, 142.9, 141.4, 139.8, 134.6 (<sup>3</sup>J<sub>CF</sub>, d, *J*=9.7 Hz), 133.7, 130.7, 130.0, 127.6 (<sup>4</sup>J<sub>CF</sub>, d, *J*=2.9 Hz), 126.3 (<sup>3</sup>J<sub>CF</sub>, d, *J*=9.1 Hz), 124.5, 121.5 (<sup>2</sup>J<sub>CF</sub>, d, *J*=22.9 Hz), 120.8, 118.3, 116.1, 111.6 (<sup>2</sup>J<sub>CF</sub>, d, *J*=25.0 Hz), 11.2. HRMS (TOF, ES+) C<sub>20</sub>H<sub>13</sub>ClFN<sub>2</sub>O<sub>4</sub> [M+H]<sup>+</sup> calc. mass 399.0548, found 399.0546.



***N*-(3-chloro-4-(1,3-dioxo-1,3-dihydro-2H-pyrrolo[3,4-c]pyridin-2-yl)phenyl)-3-methylfuran-2-carboxamide (5.35 g).** Cream powder.  $^1\text{H-NMR}$  (400.1 MHz,  $\text{DMSO-}d^6$ )  $\delta$  (ppm): 10.47 (1H, s), 9.31 (1H, s), 9.21 (1H, d,  $J=4.8$  Hz), 8.21 (1H, d,  $J=2.2$  Hz), 8.06 (1H, d,  $J=4.8$  Hz), 7.92 (1H, dd,  $J=8.7$  Hz,  $J=2.2$  Hz), 7.86 (1H, d,  $J=1.4$  Hz), 7.56 (1H, d,  $J=8.7$  Hz), 6.65 (1H, d,  $J=1.4$  Hz), 2.37 (1H, s).  $^{13}\text{CNMR}$  (100.6 MHz,  $\text{DMSO-}d^6$ )  $\delta$  (ppm): 166.2, 165.9, 158.0, 156.8, 145.1, 144.5, 141.7, 141.4, 139.3, 132.3, 131.5, 129.4, 125.9, 124.1, 121.1, 120.0, 117.8, 116.3, 11.5. HRMS (TOF, ES+)  $\text{C}_{19}\text{H}_{12}\text{ClN}_3\text{O}_4$   $[\text{M}]^+$  calc. mass 381.0516, found 381.0519.

#### *Molecular pharmacology*

Molecular pharmacology experiments to characterize the  $\text{mGlu}_1$  PAMs were performed following the procedures described in chapter 3 and 4.

#### *Pharmacokinetic characterization*

The *in vitro* DMPK assays, including those assessing hepatic microsomal intrinsic clearance ( $\text{Cl}_{\text{int}}$ ), cytochrome P450 inhibition, plasma protein binding (PPB) and brain homogenate binding (BHB) were performed as described previously.<sup>285</sup> The experimental procedures for the pharmacokinetic characterization of the compounds are described in chapter 3.

*Evaluation for propensity for seizures*

**Extracellular recordings of epileptiform activity from CA3 region of the hippocampus *in vitro*.** Male C57BL/6 mice (69–75 days old, JAX) were deeply anaesthetized with isoflurane and decapitated. The brains were quickly removed from the skull and submerged in oxygenated (95% O<sub>2</sub>/5% CO<sub>2</sub>), ice-cold cutting solution composed of (in mM): 220 glucose, 2.5 KCl, 8 MgSO<sub>4</sub>, 0.5 CaCl<sub>2</sub>, 1.25 NaH<sub>2</sub>PO<sub>4</sub>, 26 NaHCO<sub>3</sub>, and 10 D-glucose. Coronal brain slices (400 µm) containing the hippocampus were cut using a Leica VT1200S microtome (Leica Microsystems Inc.), incubated in artificial cerebrospinal fluid (ACSF) at 32°C for 30 minutes, and then maintained at room temperature for at least 30 minutes until transferred to a recording chamber. The chamber was continuously perfused with oxygenated ACSF at 32°C. The ACSF contained (in mM): 126 NaCl, 2.5 KCl, 2.0 CaCl<sub>2</sub>, 1.3 MgSO<sub>4</sub>, 1.25 NaH<sub>2</sub>PO<sub>4</sub>, 26 NaHCO<sub>3</sub>, and 10 D-glucose. Spontaneous field epileptiform activity was recorded from hippocampal CA3 regions using a grass patch pipette filled with ACSF and placed in the CA3 pyramidal cell body layer. The electrophysiological signal was acquired using a MultiClamp 700B amplifier coupled with pClamp10 software (Molecular Devices). Data were analyzed offline using MiniAnalysis (Synaptosoft Inc.). Compound stock solutions were made using DMSO and diluted to the appropriate concentration in ACSF with the final DMSO concentration of 0.1%. All compounds were bath applied.

**Behavioral manifestations of seizure activity.** Mice received a single intraperitoneal (i.p.) administration of either mGlu5 ago-PAM VU0424465 (1 or 3 mg/kg) or mGlu1 ago-PAMs **5.35c**, **5.35e**, or **5.35g** (100 mg/kg) at a volume of 10 ml/kg. Compounds were formulated in 10% Tween 80 (pH 7.0). Animals were monitored continuously and scored for behavioral manifestations of seizure activity at 5, 10, 15, 30, 60, 120 and 180 minutes. Behavioral manifestations of seizures were scored using a modified Racine scoring system.<sup>301,302</sup> Briefly, a score of 0 represents no behavior alterations; score 1, immobility, mouth and facial movements, or facial clonus; score 2, head nodding, tail extension; score 3, forelimb clonus, repetitive

movements; score 4, rearing, and tonic clonic seizures; and score 5, continuous rearing and falling, climbing, running, severe generalized tonic clonic seizure. Mice were then euthanized and brains removed and processed to measure compound exposure levels.



## CHAPTER VI

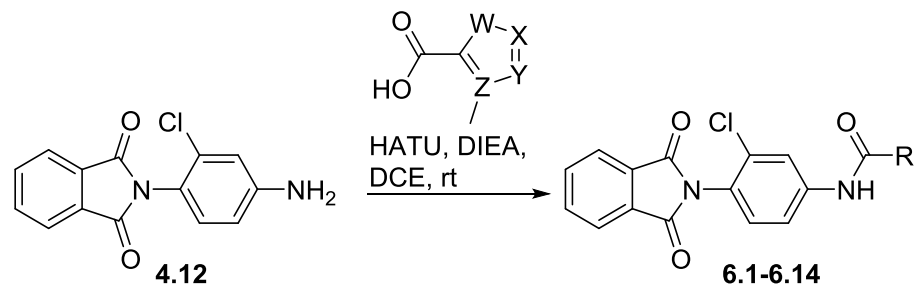
### LEAD OPTIMIZATION OF VU0486321 SERIES: DISCOVERY OF VU0487351 AND VU6004909, MGLU1 PAMS WITH AN IMPROVED PHARMACOKINETIC PROFILE

Upon the discovery and characterization of VU0486321 **5.35c**, it was found that the compound fulfills our requisites of potency for a chemical probe and displays enhanced plasma stability compared to VU0483605 **4.77b**, with a half-life in rat close to one hour; however, this mGlu<sub>1</sub> PAM still showed activity in human mGlu<sub>4</sub> and can be improved in terms of selectivity and *in vivo* plasmatic clearance. Therefore, in order to improve these properties, we decided to further explore the SAR around this scaffold making chemical modifications in the following three regions of the molecule: the phthalimide, the central phenyl ring and the furan ring.

#### **SAR exploration for the replacement of the furan ring**

##### *Screening of different methyl substituted rings as replacements of the furan*

We started by exploring replacements of the furan, this time employing rings with a methyl substitution analogous to the one in VU0486321 **5.35c**. We wanted to explore different pyrrole and thiophene regioisomers, as well as members of the azole family. Synthetically, these compounds were accessed by amide coupling of intermediate **4.12** and different methyl substituted heteroaromatic carboxylic acids (Scheme 6.1)

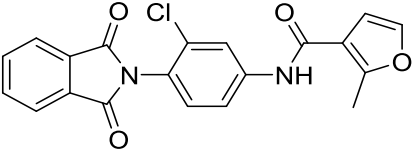
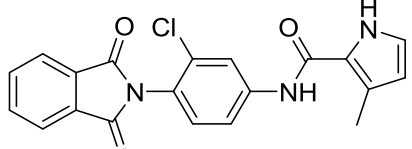
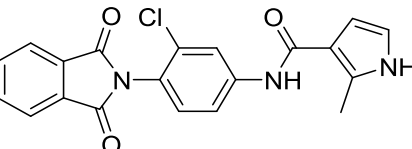
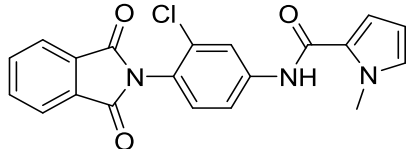
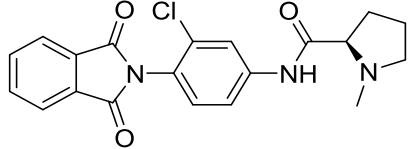
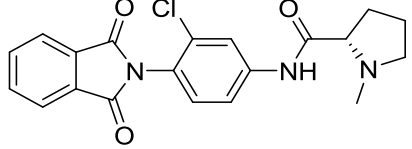
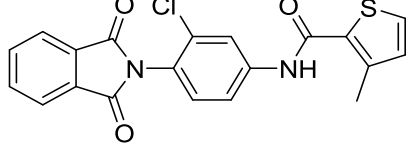
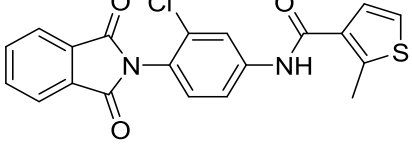


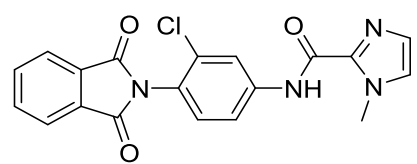
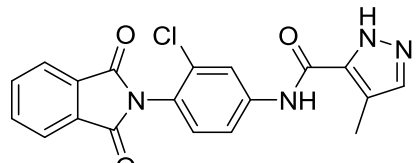
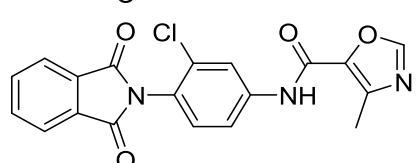
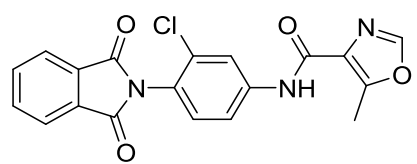
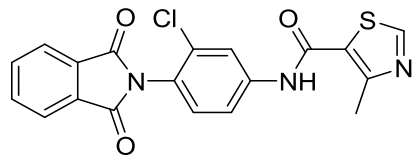
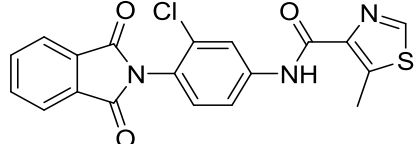
**Scheme 6.1.** Synthesis of analogs **6.1-6.14**.

The compounds were evaluated in our human mGlu<sub>1</sub> expressing cell line in a concentration-response study to obtain their EC<sub>50</sub> for PAM activity. From this batch, we observed that the different pyrroles **6.2-6.4** had weak activity as PAMs. The most active pyrrole **6.2** was the direct comparator to VU0474633 **5.27**, with potency around 3.4 μM and good efficacy of 86% Glu<sub>Max</sub>; while the *N*-methylpyrrole **6.4** EC<sub>50</sub> was 5.2 μM and **6.3** showed over 10 μM potency. Alkyl derivatives, *N*-methyl proline analogs **6.5** and **6.6** were not active. In the case of the thiophenes, the regioisomers tested showed similar potency for mGlu<sub>1</sub> potentiation, with the 3-thiophenecarboxamide **6.8** being more active than the 2-thiophene analog **6.7**, displaying the inverse tendency from the pyrrole data.

In the azole family, the nitrogenated rings **6.9-6.10** maintained mGlu<sub>1</sub> PAM activity. The *N*-methylimidazole **6.9** was potent (EC<sub>50</sub> = 297 nM) but it showed only partial PAM efficacy, while the pyrazole **6.10** was completely efficacious but with a potency of 1.2 μM. In the case of the oxazoles **6.11-6.12** and thiazoles **6.13-6.14**, an important difference in activity was observed for the assessed regioisomers. In both groups the most active compounds were the constitutional isomers **6.12** and **6.14** with the amide in position 4, while 5-carboxamide analogs **6.11** and **6.13** were inactive. The oxazole **6.12** was a full PAM with EC<sub>50</sub> of 1.30 μM, while the thiazole **6.14** was found to be the most active replacement, with better potency than the original furan compound VU0474633 **5.27**.

**Table 6.1.** Structures of the amide library analogs **6.1-6.14** and associated PAM activity from the single point screening at 10  $\mu\text{M}$  in human  $\text{mGlu}_1$ . Calcium mobilization responses for each compound are reported as a percentage of the maximum glutamate response. VU number denotes the compound identifier assigned by Vanderbilt University. Data represent the mean  $\pm$  S.E.M. of at least three replicate experiments with similar results.

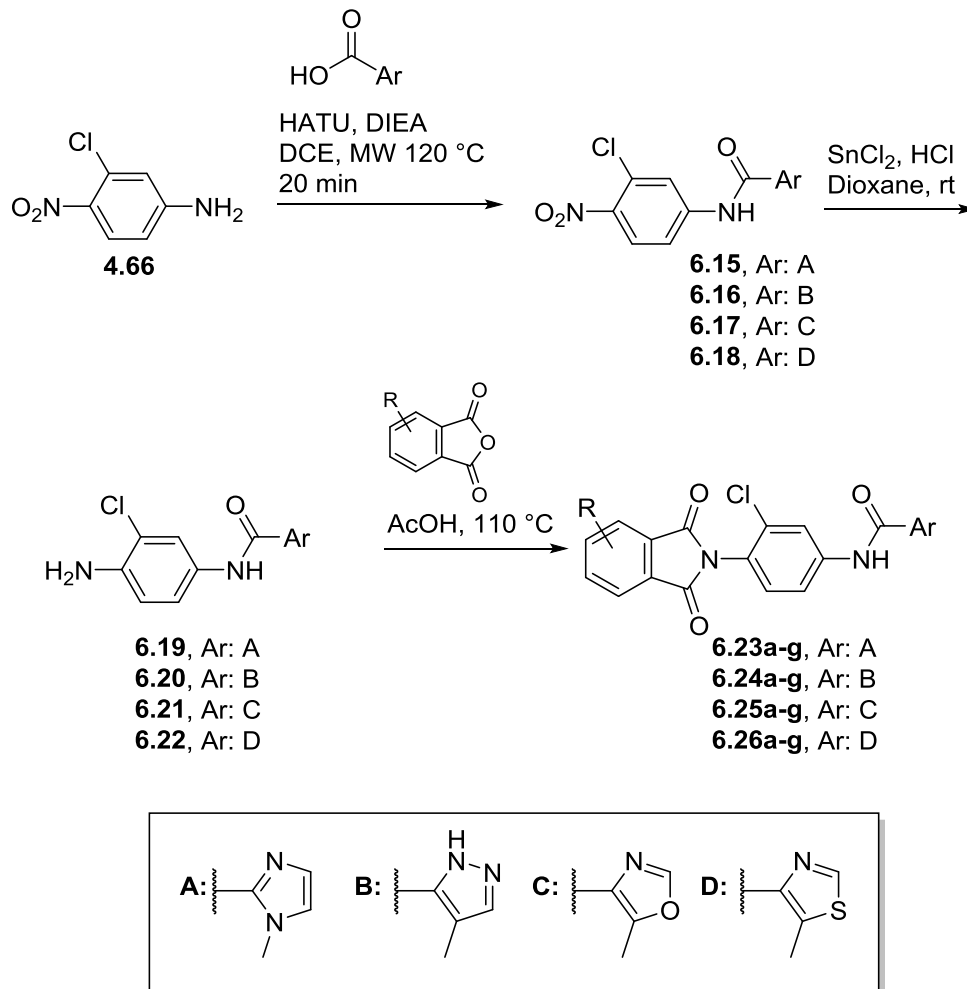
Structure	Cpd #	VU #	hmGlu <sub>1</sub>	
			EC <sub>50</sub> ( $\mu\text{M}$ )	%Glu <sub>Max</sub>
	<b>6.1</b>	VU6003723	3.64	71
	<b>6.2</b>	VU6002198	3.42	86
	<b>6.3</b>	VU0487504	>10	59
	<b>6.4</b>	VU0487386	5.26	95
	<b>6.5</b>	VU517519	>10	31
	<b>6.6</b>	VU0487622	>10	26
	<b>6.7</b>	VU6002203	2.71	96
	<b>6.8</b>	VU6002202	1.51	105

	<b>6.9</b>	VU0487384	0.30	63
	<b>6.10</b>	VU6002197	1.24	107
	<b>6.11</b>	VU0487564	>10	44
	<b>6.12</b>	VU0517529	1.30	99
	<b>6.13</b>	VU0487388	>10	40
	<b>6.14</b>	VU0487563	0.063	97

*Modification of the phthalimide in the context of methyl-substituted furan replacements in **6.9**, **6.10**, **6.12** and **6.14***

From this group of compounds, the rings in **6.9**, **6.10**, **6.12** and **6.14** were selected for further study, as they have shown to have potencies below 1.5  $\mu\text{M}$  and they would likely engender molecules with less propensity for P450 inhibition with respect to the furan. Thus, a matrix library with two points of diversity was planned, to explore the effect of phthalimide substitutions in the context of these heteroaromatic rings. These compounds were prepared using a three-step process similarly to the synthesis of VU0483605 **4.77b** (Scheme 6.2). Starting with the nitroaniline **4.66**, an amide coupling reaction with the selected acids was carried under

microwave heating and using HATU. Anilines **6.19-6.22** were obtained through reduction of **6.15-6.18** with tin(II) chloride, and then condensed with different phthalic anhydrides to prepare the final analogs **6.23a-6.26g**.

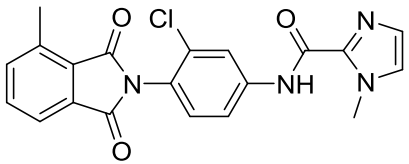
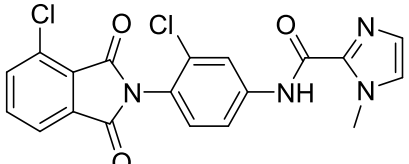
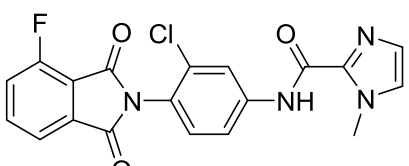
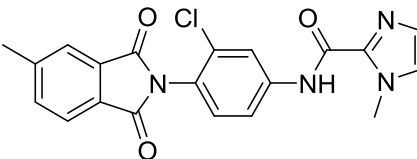
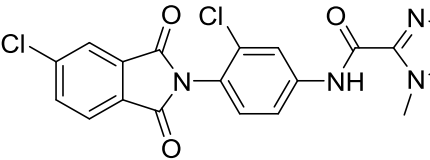


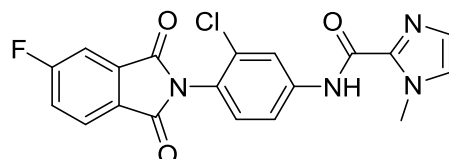
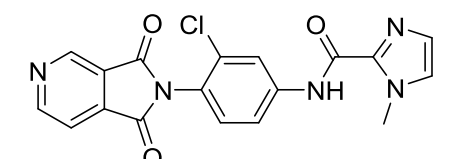
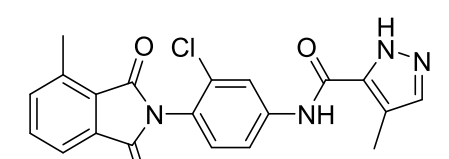
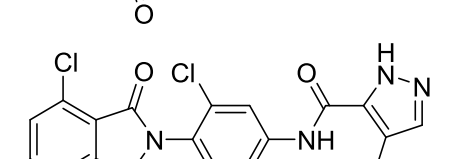
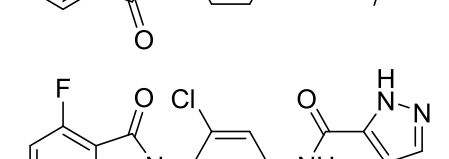
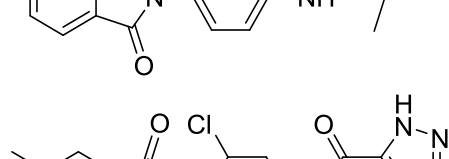
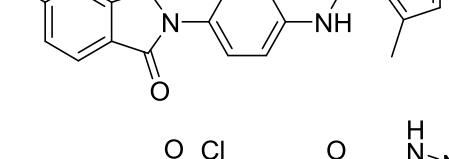
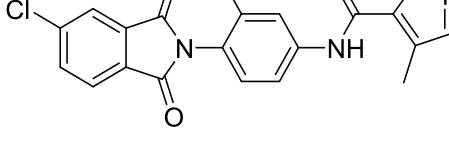
**Scheme 6.2.** Synthesis of matrix library analogs **6.23a-6.26g** to assess alternatives to the 3-methylfuran carboxamide in VU0486321 **5.35c**.

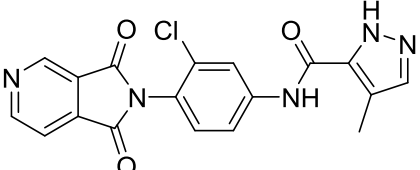
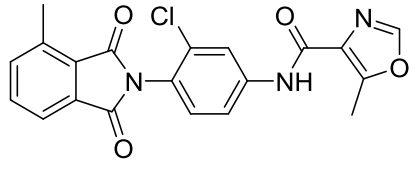
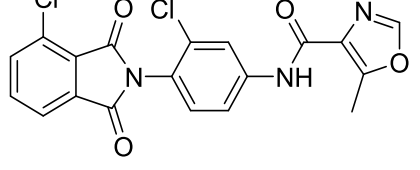
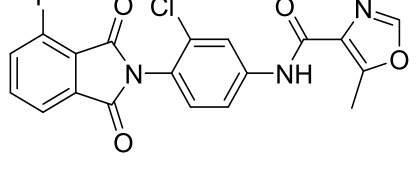
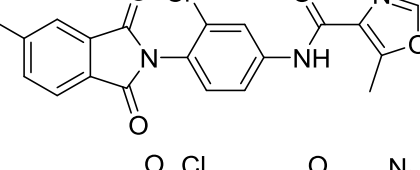
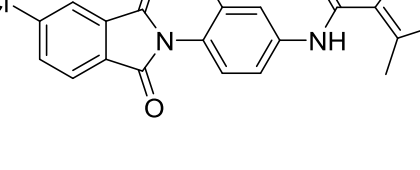
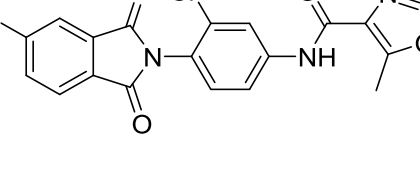
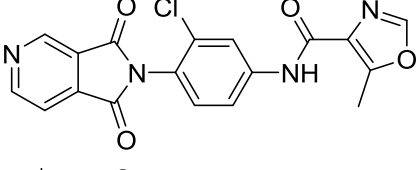
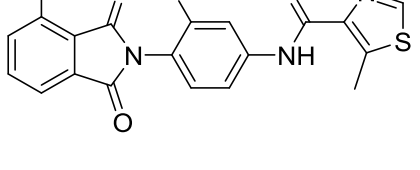
The compounds were evaluated for mGlu<sub>1</sub> and mGlu<sub>4</sub> PAM activity in calcium mobilization assays. Phthalimide substitution in the *N*-methylimidazole analogs **6.23a-6.23g** showed a beneficial effect when it occurred at the 3 position, **6.23a-6.23c**, maintaining good potency and increasing significantly the efficacy of the glutamate response in the case of the 3-methyl (**6.23a**) and 3-chloro (**6.23b**) substitution. The 3-fluoro compound (**6.23c**) showed better

efficacy, but a 2-fold decrease in potency. In sharp contrast, the 4-substituted **6.23d-6.23f** and the 4-aza **6.23g** phthalimides render very weak PAMs. Despite the increase in efficacy and relative good standing potency of compounds around this scaffold, the imidazole moiety did not demonstrate improved selectivity over mGlu<sub>4</sub>, as these compounds were less selective than VU0486321 **5.35c** with fold-selectivities between 1.6 and 5.8.

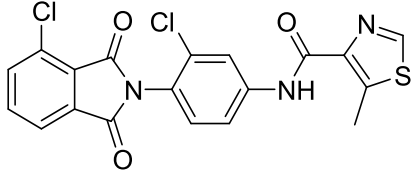
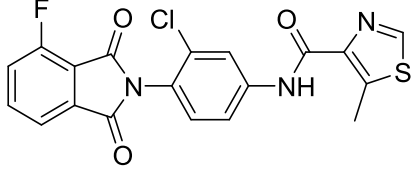
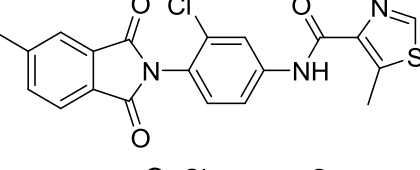
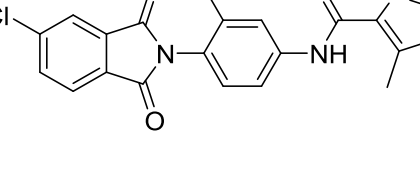
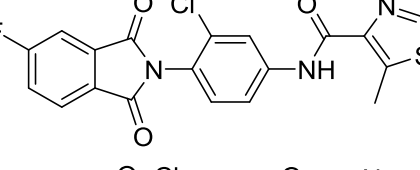
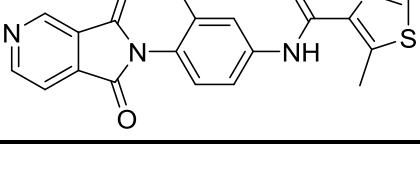
**Table 6.2.** Potencies in human mGlu<sub>1</sub> and mGlu<sub>4</sub> of compounds derived from the matrix library **6.23a-6.26g**. Calcium mobilization responses for each compound are reported as a percentage of the maximum glutamate response. VU number denotes the compound identifier assigned by Vanderbilt University. Data represent the mean ± S.E.M. of at least three independent experiments with similar results. ---, no potentiation. ND, not determined.

Structure	Cpd #	VU #	hmGlu <sub>1</sub>		hmGlu <sub>4</sub>	
			EC <sub>50</sub> (μM)	%Glu Max	EC <sub>50</sub> (μM)	%Glu Max
	<b>6.23a</b>	VU6002211	0.25	108	0.60	124
	<b>6.23b</b>	VU6002212	0.27	103	1.57	145
	<b>6.23c</b>	VU6002213	0.67	87	1.07	63
	<b>6.23d</b>	VU6002214	>10	30	0.51	32
	<b>6.23e</b>	VU6002215	>10	30	>10	30

	<b>6.23f</b>	VU6002216	>10	43	1.09	42
	<b>6.23g</b>	VU6002217	>10	44	>10	-
	<b>6.24a</b>	VU6002218	0.56	106	2.75	133
	<b>6.24b</b>	VU6002219	0.86	113	3.38	117
	<b>6.24c</b>	VU6002220	0.63	106	6.20	59
	<b>6.24d</b>	VU6002221	4.94	110	>10	-
	<b>6.24e</b>	VU6002222	>10	94	>10	-
	<b>6.24f</b>	VU6002223	0.60	106	>10	-

	<b>6.24g</b>	VU6002232	>10	37	>10	27
	<b>6.25a</b>	VU6001777	0.041	98	0.198	75
	<b>6.25b</b>	VU6001778	0.054	104	0.41	67
	<b>6.25c</b>	VU6001779	0.14	93	0.64	36
	<b>6.25d</b>	VU6001780	0.47	91	0.519	39
	<b>6.25e</b>	VU6001781	1.29	112	0.983	24
	<b>6.25f</b>	VU6001782	0.24	98	0.397	39
	<b>6.25g</b>	VU6001783	1.70	91	2.53	45
	<b>6.26a</b>	VU517592	0.022	86	1.12	161



	<b>6.26b</b>	VU517526	0.051	91	1.98	169
	<b>6.26c</b>	VU517527	0.063	98	0.31	52
	<b>6.26d</b>	VU517621	0.23	104	1.41	75
	<b>6.26e</b>	VU517472	1.37	121	>10	59
	<b>6.26f</b>	VU517463	0.19	111	0.47	52
	<b>6.26g</b>	VU517622	0.19	98	>10	-

In the context of the pyrazole, a similar effect to the imidazole library was observed, where 3-substituted phthalimides **6.24a-6.24c** managed to increase the potency and maintain efficacy for the target, with the 3-methyl substituent (**6.24a**) engendering the most active molecule in the family ( $EC_{50} = 560$  nM). A decrease in activity was observed for the 4-substituted analogs **6.24d-6.24g**, except for **6.24f**, where the 4-fluoro phthalimide was actually beneficial ( $EC_{50} = 600$  nM) and increased mGlu<sub>1</sub> activity with respect to the parent compound. When compounds were evaluated against mGlu<sub>4</sub>, they demonstrated to be preferential for mGlu<sub>1</sub>; however, their selectivity was not as high as desired. In the 3-substituted phthalimide group

**6.24a-6.24c**, it was found that the analogs were between 4.9 and 9.8 times more potent in mGlu<sub>1</sub> than mGlu<sub>4</sub>, and in the case of the 4-fluoro **6.24f** selectivity was over 16-fold. So, despite the pyrazole ring demonstrated to impart more selectivity than the imidazole towards mGlu<sub>1</sub>, it still does not represent a good replacement for the furan.

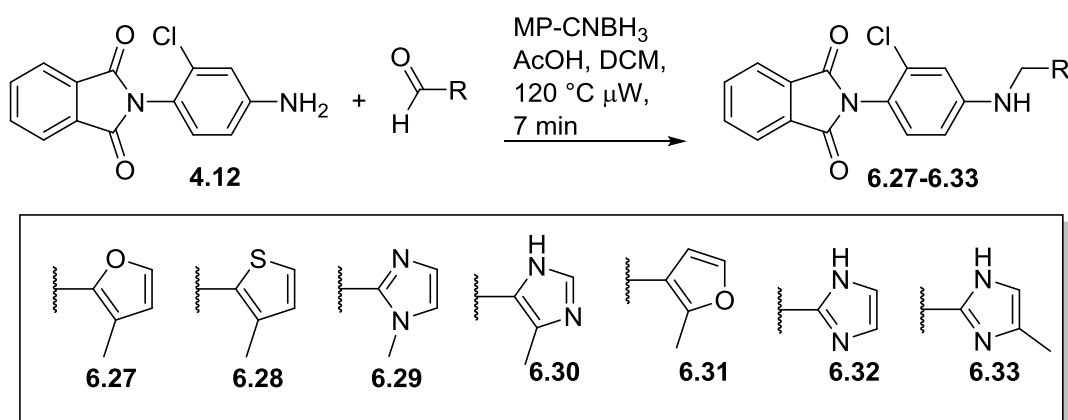
The oxazole analogs **6.25a-6.25g** showed a similar tendency to the one observed in the pyrazole and the imidazole, where 3-substitutions (**6.25a-6.25c**) increased mGlu<sub>1</sub> activity. But in this case, the improvement in potency was dramatic, achieving EC<sub>50</sub> values even 30-fold smaller with respect to the parent compound in the case of 3-methyl **6.25a** (EC<sub>50</sub> = 41 nM vs. **6.12** EC<sub>50</sub> = 1.3 μM), 24-fold for 3-chloro **6.25b** and 9-fold for 3-fluoro **6.25c**. In contrast to the other rings, the 4-methyl **6.25d** and 4-fluoro **6.25f** also showed an improvement in potency (2.8 and 5.4-folds, respectively) but it was less than what was observed in the 3-substituted phthalimides; the other 4-substituted analogs, **6.25e** and **6.25g** maintained potency values close to the parent compound EC<sub>50</sub>. Despite the improvement in mGlu<sub>1</sub> activity, none of these compounds showed a significant improvement in terms of selectivity. Most analogs showed preferential activity for mGlu<sub>1</sub> with fold-selectivities between 4.6 and 7.4, where the more potent 3-substituted analogs **6.25a-6.25c** had the lower relative activity in mGlu<sub>4</sub>.

The thiazole ring generated the most potent compound in the previous iteration and, as in the SAR described above, the 3-substitutions (**6.26a-6.26c**) in the phthalimide were beneficial for mGlu<sub>1</sub> activity. Similar to the other five-member rings, the 3-methyl **6.26a** was the more potent analog in this family, being slightly more potent than VU0486321 **5.35c**. 4-substituted analogs **6.26d-6.26f** showed a variable decrease in mGlu<sub>1</sub> PAM activity. While the 4-chloro **6.26e** showed a substantial loss in potency (22 fold) with respect to the parent compound **6.14**, the other analogs maintained considerable potency with EC<sub>50</sub>s values around 200 nM. All compounds in the family showed preferential activity for mGlu<sub>1</sub>. The 4-substituted analogs **6.26d-6.26f** showed little selectivity being only 2.5-6.1 times preferent for mGlu<sub>1</sub>. The 3-substituted phthalimides **6.26a-6.26c** showed different degrees of mGlu<sub>4</sub> activity, 3-fluoro **6.26c** was the less selective with only

a 5-fold preference for mGlu<sub>1</sub>. Analogs **6.26a** and **6.26b** demonstrated 51 and 39-fold selectivity for mGlu<sub>1</sub>, a difference driven by their high potency in mGlu<sub>1</sub> as these analogs also activated the mGlu<sub>4</sub> receptor with EC<sub>50</sub>s between 1 and 2 μM. These compounds represented an improvement in selectivity in terms of potency with respect to VU0486321 **5.35c** that is 35-fold selective for mGlu<sub>1</sub>; however, **6.26a** and **6.26b** displayed very high efficacy for mGlu<sub>4</sub> activation, being close to 170% of the maximal glutamate response, a factor that halted further study of this compounds. Analog 4-aza **6.26g** showed good selectivity; but, despite a relatively good potency of 190 nM, this analog is almost 6-fold less potent than VU0486321 **5.35c**.

*Exploration of different heteroaromatic rings in the context of a methylene linker*

To evaluate the importance of the carbonyl linker in the furan carboxamide, a small library of compounds with a methylene linker was synthesized. These analogs were accessed by using aniline intermediate **4.12** and different aldehydes in a reductive amination reaction with polymer supported cyanoborohydride (Scheme 6.3).



**Scheme 6.3.** Synthesis of analogs **6.27-6.33** to assess the effect of the removal of the carbonyl group in the furancarboxamide side of VU0486321 scaffold.

Different five member ring aldehydes were used to obtain this library, including direct comparators of active compounds, such as **6.27** which is the reduced version of VU0474633 **5.27**.

Evaluation of this library at a single concentration of 10  $\mu\text{M}$  showed that the amide is essential for activity as none of the synthesized compounds could enhance the glutamate's  $\text{mGlu}_1$  response.

### SAR exploration in the central phenyl ring

#### *Study of substituents in the central phenyl ring.*

As most of the previous work exploring VU0483605 **4.77b** and VU0486321 **5.35c** scaffolds focused in the eastern amide and modifications of the phthalimide, it was decided to explore the structure-activity relationships in the central phenyl ring (Fig. 6.1). We proposed to study the effect of different substituents on the phenyl ring, as well as replacing it with naphthalene, pyridine and pyrimidine moieties.

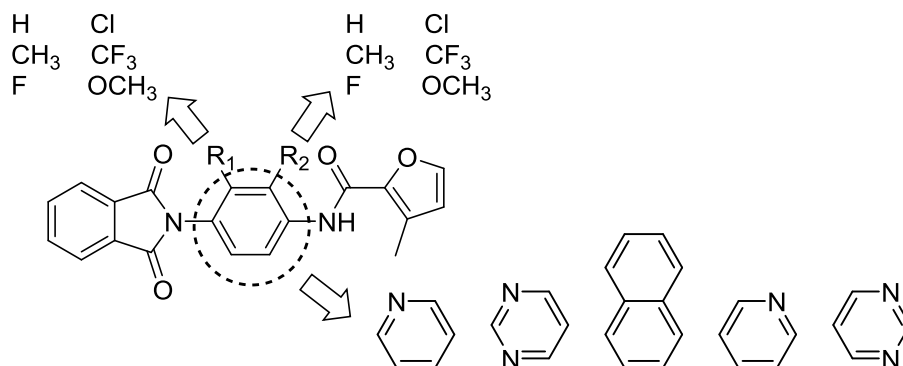
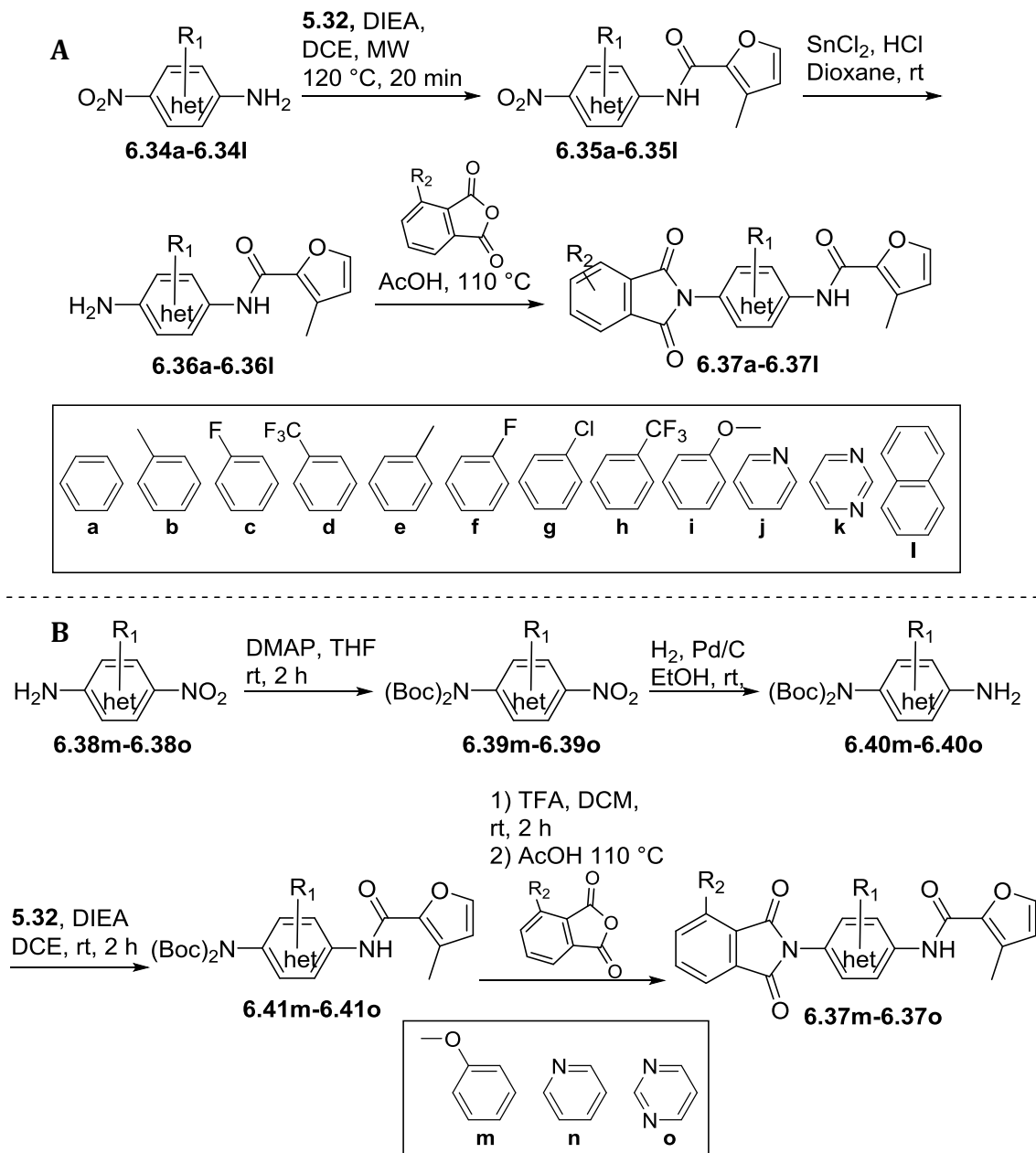


**Figure 6.1.** SAR exploration around the central phenyl ring of the VU0486321 scaffold.

The obtention of the necessary compounds to assess the effect of the modifications of the phenyl ring was performed in a three-step synthetic route. Similarly to the previously described in scheme 5.3, the route involves the amide coupling of nitroanilines **6.34a-6.34l** with acyl chloride **5.32**, reduction of the nitro group **6.35a-6.35l** and condensation with phthalic anhydrides in refluxing acetic acid (Scheme 6.4A). For this matrix library, only the unsubstituted and 3-substituted phthalimides were prepared, as these are the patterns that usually presented better

mGlu<sub>1</sub> activity. It was possible to synthesize most of the examples this way, with the exception of the methoxy analogs **6.37m1-6.37m4**, pyridines **6.37n1-6.37n4** and pyrimidines **6.37o1-6.37o4** where a different approach deemed necessary. For these latter analogs, the process started with the DMAP catalyzed Boc protection of the corresponding 4-nitroaniline **6.38m-6.38o** and then the reduction of nitro **6.39m-6.39o** group with hydrogen and palladium on carbon to produce intermediates **6.40m-6.40o** (Scheme 6.4B). The bis Boc protected 4-aminoanilines **6.40m-6.40o** had the advantage that the unprotected amino group now became more nucleophilic than its counterpart in the 4-nitroanilines; this change in reactivity allowed the amide coupling with the acyl chloride **5.32** to obtain intermediates **6.41m-6.41o** without heating in the microwave. Then, furancarboxamides **6.41m-6.41o** were Boc deprotected with TFA at room temperature, and the obtained anilines were condensed with phthalic anhydrides in acetic acid at reflux.

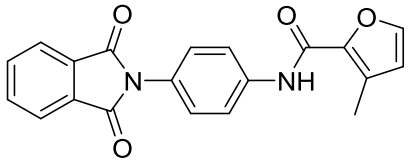
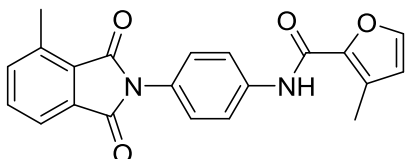
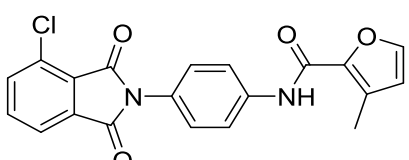
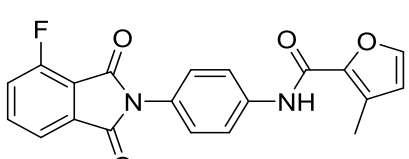


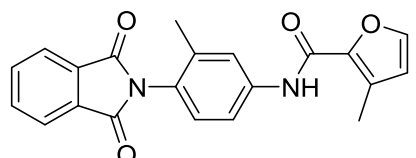
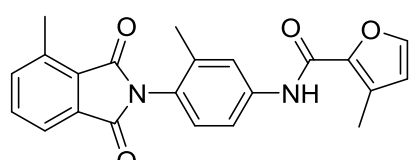
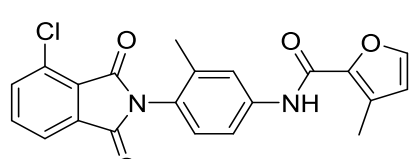
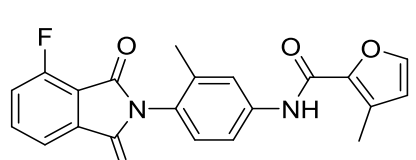
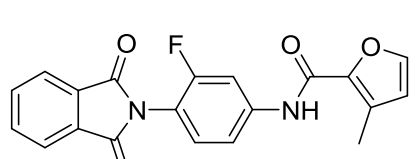
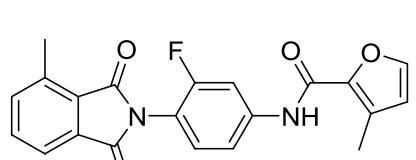
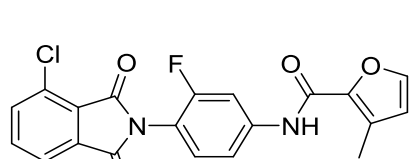
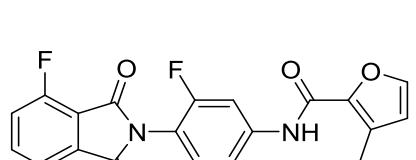
**Scheme 6.4.** Synthesis of analogs **6.37a-6.37o** to assess the effect of modifications on the central phenyl ring of VU0486321 scaffold. For each example of modification on the central phenyl ring phthalic anhydride, 3-methylphthalic anhydride, 3-chlorophthalic anhydride and 3-fluorophthalic anhydride were used.

The activity of the compounds was evaluated in the human mGlu<sub>1</sub> and human mGlu<sub>4</sub> receptors to assess the effect of the modifications in potency on target and selectivity (Table 6.3). The removal of the chlorines (**6.37a1-6.37a4**) from the central ring was beneficial or maintained

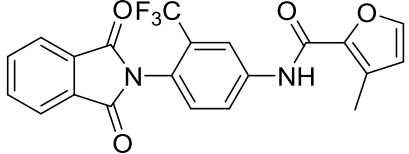
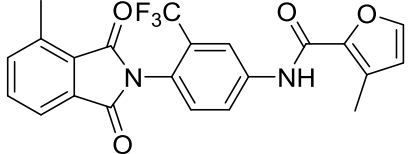
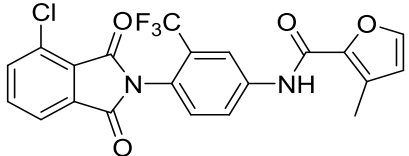
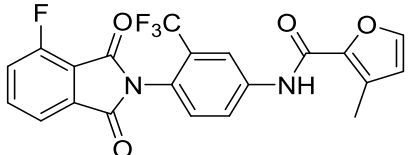
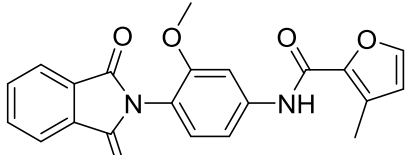
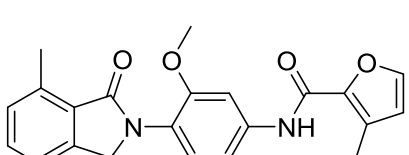
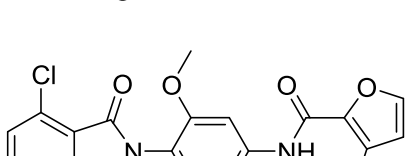
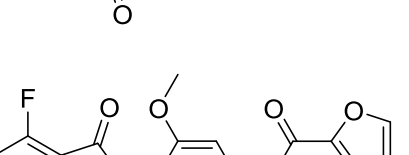
mGlu<sub>1</sub> PAM activity. The naked phthalimide **6.37a1** displayed excellent selectivity with no observable activity in mGlu<sub>4</sub>; however, further exploration of the product was halted due to its low solubility in water and in our common solvent systems. The other analogs **6.37a2-6.37a4** showed moderate selectivity, being 8.6 to 21.7 times more active in mGlu<sub>1</sub> than mGlu<sub>4</sub>, where they presented low efficacy values (34%-62% PHCCC<sub>Max</sub>).

**Table 6.3.** Potencies in human mGlu<sub>1</sub> and mGlu<sub>4</sub> of compounds derived from the matrix library with modifications in the central phenyl ring, **6.37a**, **6.37b**, **6.37c**, **6.37d** and **6.37m**. Calcium mobilization responses for each compound are reported as a percentage of the maximum glutamate response. VU number denotes the compound identifier assigned by Vanderbilt University. Data represent the mean  $\pm$  S.E.M. of at least three independent experiments with similar results. ---, no potentiation. ND, not determined.

Structure	Cpd #	VU #	hmGlu <sub>1</sub>		hmGlu <sub>4</sub>	
			EC <sub>50</sub> ( $\mu$ M)	%Glu Max	EC <sub>50</sub> ( $\mu$ M)	%Glu Max
	<b>6.37a1</b>	VU0484010	0.0430	81	>10.0	---
	<b>6.37a2</b>	VU0487230	0.0161	108	0.349	62
	<b>6.37a3</b>	VU0487372	0.0300	101	0.483	35
	<b>6.37a4</b>	VU0487251	0.0442	96	0.382	34

	<b>6.37b1</b>	VU6001769	0.0888	105	0.885	75
	<b>6.37b2</b>	VU6001770	0.0213	100	0.422	122
	<b>6.37b3</b>	VU6001771	0.0493	117	1.01	127
	<b>6.37b4</b>	VU6001772	0.0490	95	1.10	86
	<b>6.37c1</b>	VU6001773	0.0223	101	0.265	65
	<b>6.37c2</b>	VU6001774	0.0261	107	0.287	102
	<b>6.37c3</b>	VU6001775	0.0277	100	0.264	93
	<b>6.37c4</b>	VU601776	0.0350	104	0.674	78



	<b>6.37d1</b>	VU0604490	0.130	108	6.66	86
	<b>6.37d2</b>	VU0604389	0.533	117	5.76	109
	<b>6.37d3</b>	VU0604390	0.106	105	2.47	120
	<b>6.37d4</b>	VU0604641	0.155	110	2.87	80
	<b>6.37m1</b>	VU6002224	0.0461	96	1.18	50
	<b>6.37m2</b>	VU6002225	0.0490	94	0.882	107
	<b>6.37m3</b>	VU6002226	0.0179	93	0.647	103
	<b>6.37m4</b>	VU6002224	0.144	103	1.93	73

The exchange of the chlorine for a methyl or a fluorine in the 2-position of the central ring proved to be beneficial, as analogs **6.37b1-6.37c4** maintained excellent potencies in mGlu<sub>1</sub> with efficacies around 100% of Glu<sub>Max</sub>. In terms of selectivity, both replacements generated preferential compounds for mGlu<sub>1</sub>; however, these were more efficacious than the deschloro analogs **6.37a1-6.37a4**. Reduced selectivity was obtained with the fluoro analogs **6.37c1-6.37c4** as most of them had only 10-fold selectivity versus mGlu<sub>4</sub>, with **6.37c4** displaying 19 times better potency in mGlu<sub>1</sub> with respect to mGlu<sub>4</sub>. The methyl group **6.37b** engendered more selective compounds with fold-selectivities around 20, except for the naked phthalimide **6.37b1** where difference was only 10-fold.

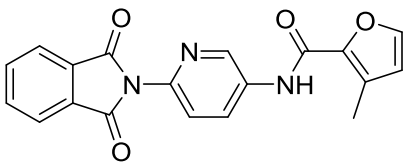
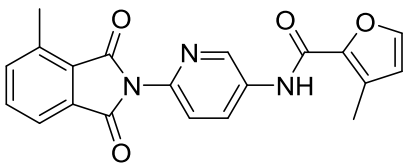
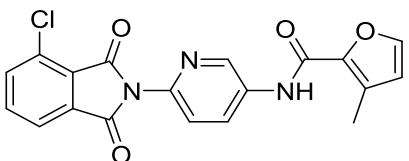
The use of the trifluoromethyl substituent (**6.37d1-6.37d4**) led to a decrease in mGlu<sub>1</sub> activity. In contrast to what has been observed in our previous SAR, the 3-methyl substituent in **6.37d2** caused a substantial decrease in potency (around 20-fold) with respect to the direct comparator derived from the VU0486321 scaffold (**5.35a**), in the other cases the decrease in potency was of only 2-3 times and in the naked phthalimide **6.37d1** the EC<sub>50</sub> value was comparable to the parent compounds. These PAMs are also preferential for the mGlu<sub>1</sub> receptor and they present different degrees of modulation of the glutamate response in mGlu<sub>4</sub>. Here, the most selective compound was the naked phthalimide **6.37d1** which is 54 times more potent in mGlu<sub>1</sub> than in mGlu<sub>4</sub>.

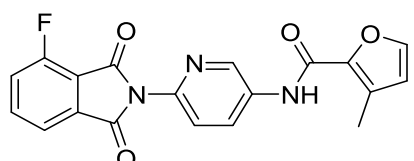
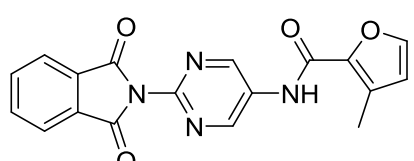
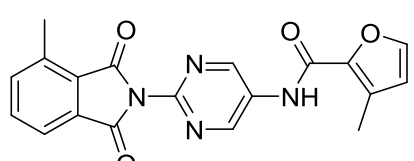
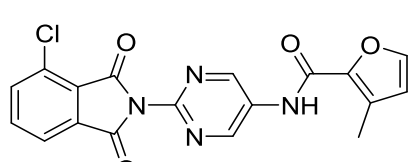
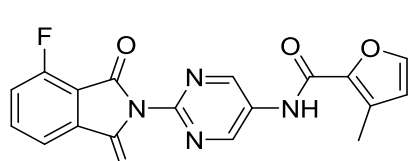
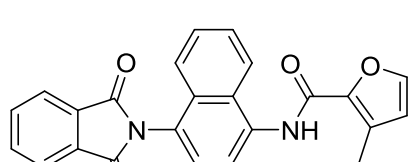
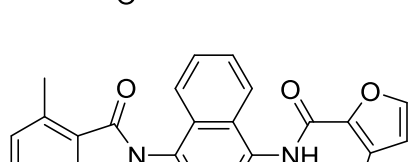
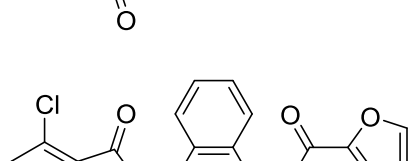
The bulkier methoxy substituent was tolerated and still provided potent mGlu<sub>1</sub> PAMs (**6.37m1-6.37m4**). The only case where it showed a decrease in activity was in the 3-fluoro analog **6.37m4**, causing a 4-fold decrease in potency with respect to VU0486321 **5.35c**. The other substituted phthalimides analogs **6.37m1-6.37m3** displayed EC<sub>50</sub>s between 18 and 49 nM. However, none of these analogs (**6.37m1-6.37m4**) presented an improvement in selectivity with respect to VU0486321 **5.35c**, as they are only 13 to 36 times preferent for mGlu<sub>1</sub> versus mGlu<sub>4</sub>.

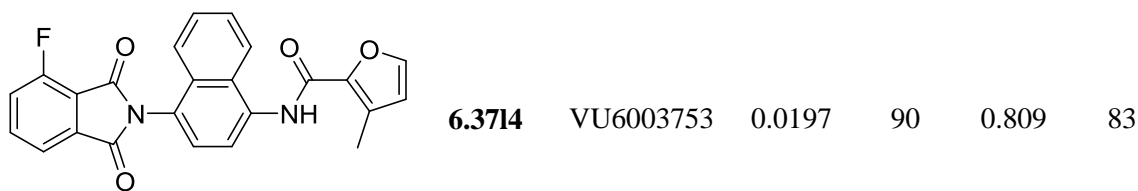
The replacement of the phenyl ring with pyridine, pyrimidine and naphthalene was also evaluated (Table 6.4). The introduction of a pyridine (**6.37n1-6.37n4**), having the nitrogen in the

position where the chlorine is in VU0486321 **5.35c**, led to a variable effect in mGlu<sub>1</sub> PAM potency depending on the substituents on the phthalimide. While the 3-chloro phthalimide **6.37n3** retain the original mGlu<sub>1</sub> potency, all the other analogs (**6.37n1**, **6.37n2** and **6.37n4**) suffered from a decrease in PAM activity from 3 to 6 times. The decrease in mGlu<sub>1</sub> activity was accompanied also by a decrease in mGlu<sub>4</sub> potentiation, and the compounds showed preference for mGlu<sub>1</sub>. The 3-chloro **6.37n3** was the most selective from this batch (53-fold selective versus mGlu<sub>4</sub>), which was driven by its good potency in mGlu<sub>1</sub>, while the other compounds (**6.37n1**, **6.37n2** and **6.37n4**) had micromolar potencies in mGlu<sub>4</sub> and fold-selectivities between 18 and 32.

**Table 6.4.** Potencies in human mGlu<sub>1</sub> and mGlu<sub>4</sub> of compounds derived from the matrix library with modifications in the central phenyl ring, **6.37n**, **6.37o** and **6.37l**. Calcium mobilization responses for each compound are reported as a percentage of the maximum glutamate response. VU number denotes the compound identifier assigned by Vanderbilt University. Data represent the mean ± S.E.M. of at least three independent experiments with similar results. ---, no potentiation. ND, not determined.

Structure	Cpd #	VU #	hmGlu <sub>1</sub>		hmGlu <sub>4</sub>	
			EC <sub>50</sub> (μM)	%Glu Max	EC <sub>50</sub> (μM)	%Glu Max
	<b>6.37n1</b>	VU6002166	0.387	80	>10.0	---
	<b>6.37n2</b>	VU6002228	0.0947	105	5.00	100
	<b>6.37n3</b>	VU6002229	0.0348	91	1.11	44

	<b>6.37n4</b>	VU6002230	0.198	93	3.55	19
	<b>6.37o1</b>	VU6003724	4.61	89	4.67	23
	<b>6.37o2</b>	VU6003725	0.751	111	4.47	104
	<b>6.37o3</b>	VU6003726	0.208	84	2.53	45
	<b>6.37o4</b>	VU6003727	5.33	99	>10.0	24
	<b>6.37i1</b>	VU6003750	0.0203	99	0.353	54
	<b>6.37i2</b>	VU6003751	0.0157	88	0.429	103
	<b>6.37i3</b>	VU6003752	0.0225	92	0.513	102



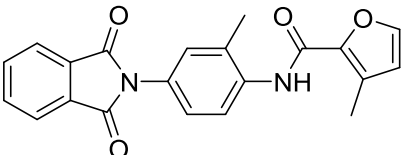
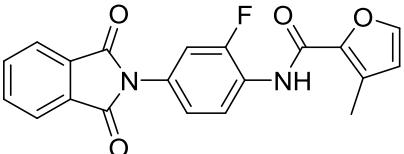
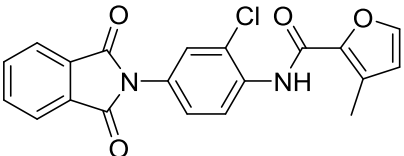
The introduction of one additional nitrogen (**6.37o1-6.37o4**) to obtain a pyrimidine in the central ring caused a significant decrease in activity with respect to VU0486321 **5.35c** and to the pyridine analogs **6.37n1-6.37n4**, showing that increasing the polar surface area in the central ring beyond the addition of one nitrogen is detrimental for activity. The most potent compound in this set was the 3-chloro **6.37o3**, similarly to what occurred with pyridine **6.37n3**, but with an 8-fold loss in potency with respect to the 3-chloro version of VU0486321 **5.35b**. With the other substituents, the decrease in potency was more marked, being 30-fold for 3-methyl **6.37o2** and up to 160 times for the 3-fluoro **6.37o4**. These compounds showed micromolar potencies in the mGlu<sub>4</sub> receptor; however, due to their lower potencies in mGlu<sub>1</sub> they do not differentiate well between the two receptors.

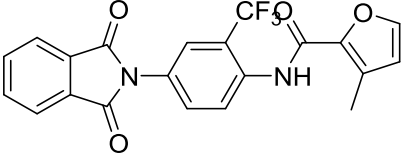
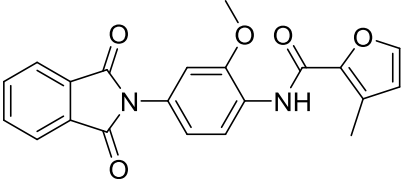
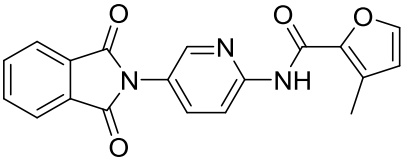
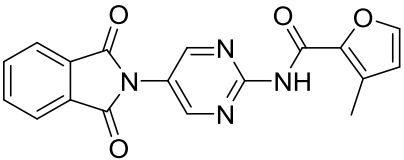
The larger naphthalene group showed that the binding site of this PAMs can tolerate more bulk around the central phenyl ring, as analogs **6.37i1-6.37i4** exhibited excellent potency between 15 and 20 nM in all cases for mGlu<sub>1</sub> potentiation. Yet, these analogs are active and have submicromolar activities in human mGlu<sub>4</sub>, which caused these compounds to be moderately selective with 17 to 41 higher potencies for mGlu<sub>1</sub>.

Overall, the replacement of the chlorine in VU0486321 **5.35c**, with the different substituents shown in Table 6.3 and Table 6.4, did not provide a considerable increase in selectivity against mGlu<sub>4</sub>. The next attempt to improve the selectivity was to switch the position of the substituents in the central ring, from adjacent to the phthalimide to next to the furan carboxamide. The same group of substituents was prepared in the context of the naked phthalimide (Scheme 6.4) and the potency in mGlu<sub>1</sub> and mGlu<sub>4</sub> was evaluated in our fluorescence

calcium mobilization assay (Table 6.5). It was found that analogs **6.37e**, **6.37f** and **6.37g** achieved excellent potency in human mGlu<sub>1</sub>, improving around 5-fold the potency with respect to its direct comparator VU0474633 **5.27**. Meanwhile, the introduction of a methoxy group (**6.37i**) led to a three-fold decrease in mGlu<sub>1</sub> and to the complete loss of activity in the case of trifluoromethyl **6.37h**; showing that smaller substituents such as fluoro, methyl and chloro are desirable in this position. Also, the replacement of the phenyl group by the pyridine (**6.37j**) and the pyrimidine (**6.37k**) abolished entirely the mGlu<sub>1</sub> PAM activity of the compounds. While the **6.37e** methyl and the **6.37i** methoxy analogs achieved a moderate preference for mGlu<sub>1</sub> (40 and 30-fold respectively), **6.37f** and **6.37g** stood out from this collection for its excellent selectivity against mGlu<sub>4</sub>, being over 793 and 384 times more potent for mGlu<sub>1</sub>.

**Table 6.5.** Potencies in human mGlu<sub>1</sub> and mGlu<sub>4</sub> of compounds derived from modifications in the central phenyl ring, **6.37e-k**. Calcium mobilization responses for each compound are reported as a percentage of the maximum glutamate response. VU number denotes the compound identifier assigned by Vanderbilt University. Data represent the mean ± S.E.M. of at least three independent experiments with similar results. ---, no potentiation. ND, not determined.

Structure	Cpd #	VU #	hmGlu <sub>1</sub>		hmGlu <sub>4</sub>	
			EC <sub>50</sub> (μM)	%Glu Max	EC <sub>50</sub> (μM)	%Glu Max
	<b>6.37e</b>	VU6002193	0.015	90±2	0.609	52
	<b>6.37f</b>	VU6002194	0.013	84±2	>10.0	---
	<b>6.37g</b>	VU0487104	0.029	68±5	>10.0	---

	<b>6.37h</b>	VU6003728	>10.0	-	>10.0	---
	<b>6.37i</b>	VU6003729	330	80±6	>10.0	---
	<b>6.37j</b>	VU6003730	>10.0	-	>10.0	---
	<b>6.37k</b>	VU6003768	>10.0	-	>10.0	---

Considering the selectivity of analogs **6.37f** (VU6002194) and **6.37g** (VU0487104), these were also explored in the mGlu<sub>5</sub> receptor, where they demonstrated selectivity with potencies of over 10 μM. The *in vitro* pharmacokinetic properties of these compounds were also studied (Fig. 6.2). Incubations with preparations of liver microsomes showed that the two compounds had a similar predicted hepatic clearance, being moderate in human (44% of hepatic blood flow) and high in rat (70% hepatic blood flow). Interestingly, the compounds were stable enough in plasma to determine their fraction unbound in plasma; although, the observed free fraction was very small in rat and human plasma. A similar behavior was observed when the fraction unbound in rat brain homogenate binding was evaluated, as free fractions under 1% were obtained. Therefore, these analogs displayed comparable *in vitro* pharmacokinetic characteristics.

The main differentiator for these PAMs was noticed when CNS penetration was assessed. Intravenous administration of a dosage of 0.2 mg/kg of the compounds proved that the fluoro

analog VU6002194 **6.37f** is substantially more brain penetrant than its chloro counterpart VU0487104 **6.37g**, having a  $K_p$  of 1.57 compared to 0.12. This behavior is hard to explain as both analogs have the same value of calculated topological polar surface area ( $81.3 \text{ \AA}^2$ ) and the same number of rotatable bonds. Furthermore, the calculated logP of the chloro analog **6.37g** is higher (4.14) compared to the fluoro analog **6.37f** (clogP = 3.63), a relationship that is in disagreement with the  $K_p$ s observed. To explain this effect, it could be hypothesized that the fluoro decreased the magnitude of the dipolar moment of the molecule or that there may be a considerable change in the conformational equilibrium that makes fluoro **6.37f** more rigid and less flexible than the chloro **6.37g**, such as the consequence for an electrostatic interaction between the C-F  $\delta^-$  in the aryl and N-H  $\delta^+$  in the furancarboxamide.<sup>303</sup>

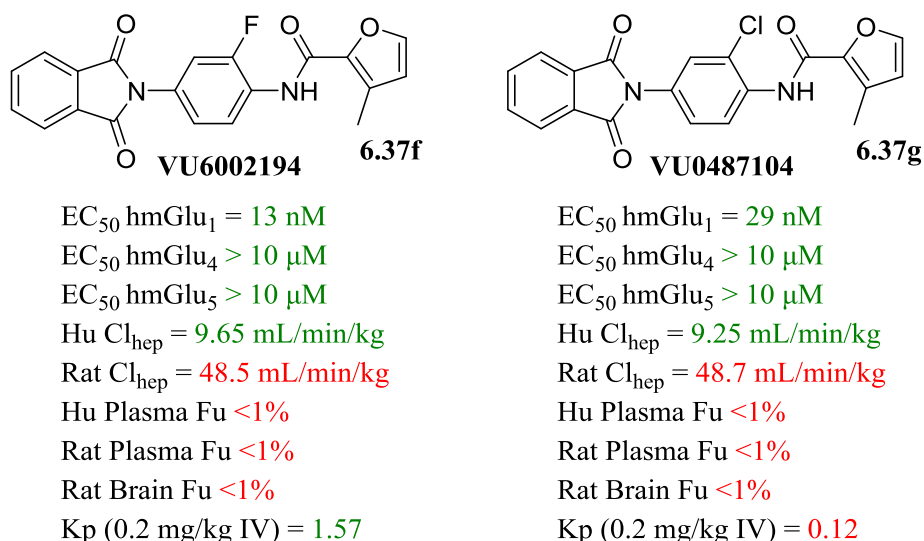
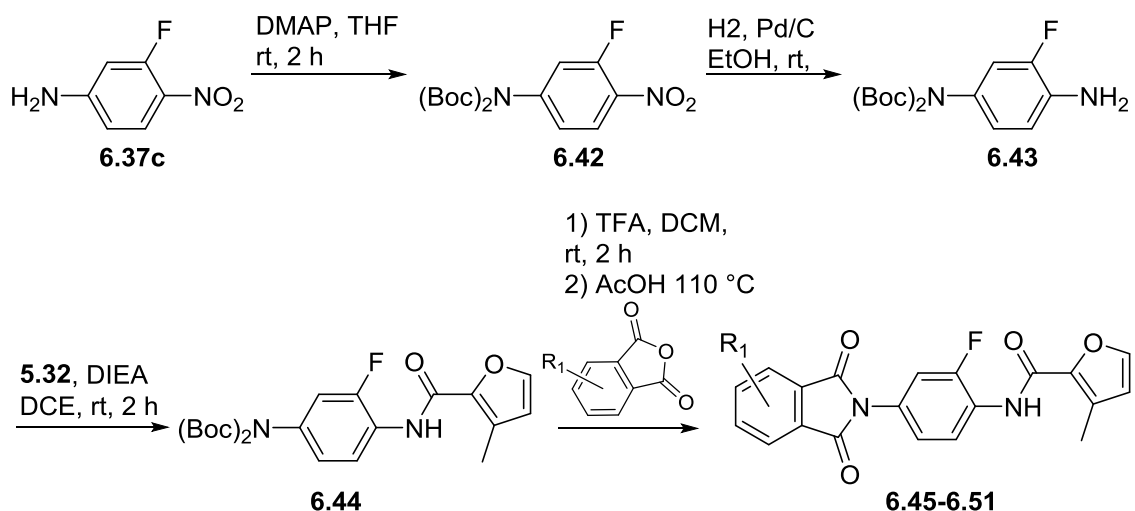


**Figure 6.2.** Comparison of the pharmacodynamic and pharmacokinetic properties of analogs VU6002194 **6.37f** and VU0487104 **6.37g**.

As the fluorine substitution in VU6002194 **6.37f** represented a great improvement in selectivity for the scaffold while maintaining brain penetrance, we proceeded to develop a library with different substituents in the phthalimide. The compounds were prepared similar to the analogs with the modified central phenyl ring and starting with the Boc protection of 3-fluoro-4-



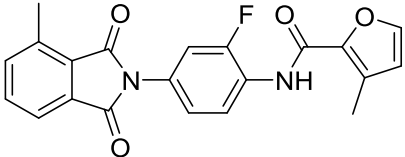
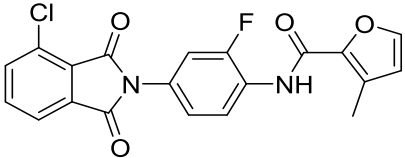
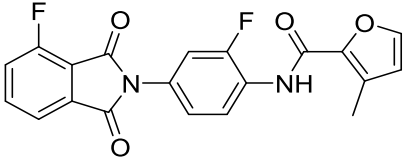
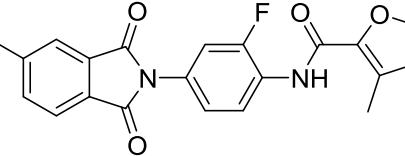
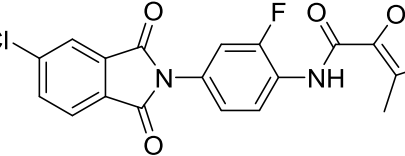
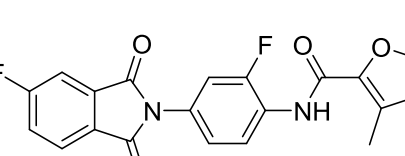
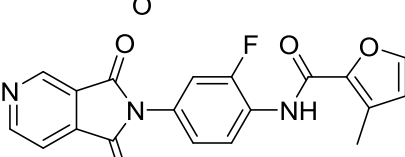
nitroaniline **6.37c**, followed by the reduction of the nitro group **6.42**, the amide coupling between aniline **6.43** and acyl chloride **5.32**, deprotection of the bis Boc protected aniline **6.44** and finally condensation of the unmasked aniline with the phthalic anhydrides to afford the desired analogs **6.45-6.51** (Scheme 6.5).



**Scheme 6.5.** Synthesis of analogs of VU6002194 **6.37f** with modifications in the phthalimide, **6.45-6.51**.

The analogs of VU6002194, **6.45-6.51**, were evaluated in calcium mobilization assays to obtain their potencies in human mGlu<sub>1</sub> and mGlu<sub>4</sub> (Table 6.6). All analogs except for the 4-chloro **6.49** and 4-aza phthalimide **6.51** displayed excellent potencies between 5 and 26 nM and behaved as partial mGlu<sub>1</sub> PAMs with efficacies between 60 and 81%. When analyzed in the mGlu<sub>4</sub> receptor, all analogs were inactive or weak potentiators with EC<sub>50</sub>s above 10 μM, which gives several hundred fold-selectivity for the mGlu<sub>1</sub> receptor. The compounds were also tested in the mGlu<sub>5</sub> receptor where they also displayed potencies above 10 μM.

**Table 6.6.** Potencies in human mGlu<sub>1</sub> and mGlu<sub>4</sub> of compounds derived from modifications of the phthalimide in VU6002194, **6.45-6.51**. Calcium mobilization responses for each compound are reported as a percentage of the maximum glutamate response. VU number denotes the compound identifier assigned by Vanderbilt University. Data represent the mean ± S.E.M. of at least three independent experiments with similar results. ---, no potentiation. ND, not determined.

Structure	Cpd #	VU #	hmGlu <sub>1</sub>		hmGlu <sub>4</sub>	
			EC <sub>50</sub> (μM)	%Glu Max	EC <sub>50</sub> (μM)	%Glu Max
	<b>6.45</b>	VU6004907	0.011	81	>10.0	37
	<b>6.46</b>	VU6004910	0.0053	60	>10.0	28
	<b>6.47</b>	VU6004911	0.019	81	>10.0	49
	<b>6.48</b>	VU6004909	0.026	70	>10.0	34
	<b>6.49</b>	VU6005703	>10.0	60	ND	ND
	<b>6.50</b>	VU6004912	0.022	67	>10.0	31
	<b>6.51</b>	VU6005704	2.04	104	ND	ND

The pharmacokinetic properties of these compounds were analyzed *in vitro*, and it was observed that in general they are less metabolically labile in comparison to VU6002194 **6.37f**. The predicted hepatic clearance with human liver microsomes was lower with all compounds except for the 3-chloro analog **6.46**, while in the case of the rat microsomes this improvement was observed in three analogs from the set: 3-methyl **6.45** (50% hepatic blood flow), 4-methyl **6.48** (41% hepatic blood flow) and 4-fluoro **6.50** (51% hepatic blood flow). The P450 inhibition of drug metabolizing enzymes was also ameliorated with respect to VU0486321 **5.35c**, as now the compounds did not inhibit CYP2C9 and only slight inhibition of CYP1A2 is observed with **6.45** and **6.46**.

**Table 6.7.** *In vitro* pharmacokinetic properties of analogs **6.45-6.48** and **6.50**.

Parameter	<b>6.45</b>	<b>6.46</b>	<b>6.47</b>	<b>6.48</b>	<b>6.50</b>
Hum CL <sub>hep</sub> (ml/min/kg)	4.40	11.9	6.72	6.64	4.48
Rat CL <sub>hep</sub> (ml/min/kg)	35.0	46.7	52.0	28.9	35.8
P450 IC <sub>50</sub> (μM)					
1A2 2C9	10 >30	6.3 >30	>30 >30	>30 >30	>30 >30
2D6 3A4	>30 >30	>30 >30	>30 >30	>30 >30	>30 >30
Hum F <sub>u</sub> plasma	0.002	<0.001	0.030	0.009	0.027
Rat F <sub>u</sub> plasma	0.009	0.001	0.011	0.038	0.011
Rat F <sub>u</sub> brain	0.193	0.272	0.170	0.298	0.034

We were pleased to find that these compounds were stable enough in plasma to estimate their unbound fraction. In the plasma protein binding assays, the best free fractions in rat plasma were observed with 4-methyl **6.48** with 3.8% free drug, while in the case of human plasma the 3-fluoro **6.47** provided the higher fraction unbound with 3.0% free drug; while the lowest free fractions in both preparations were observed with 3-chloro **6.46**. Additionally, this set of

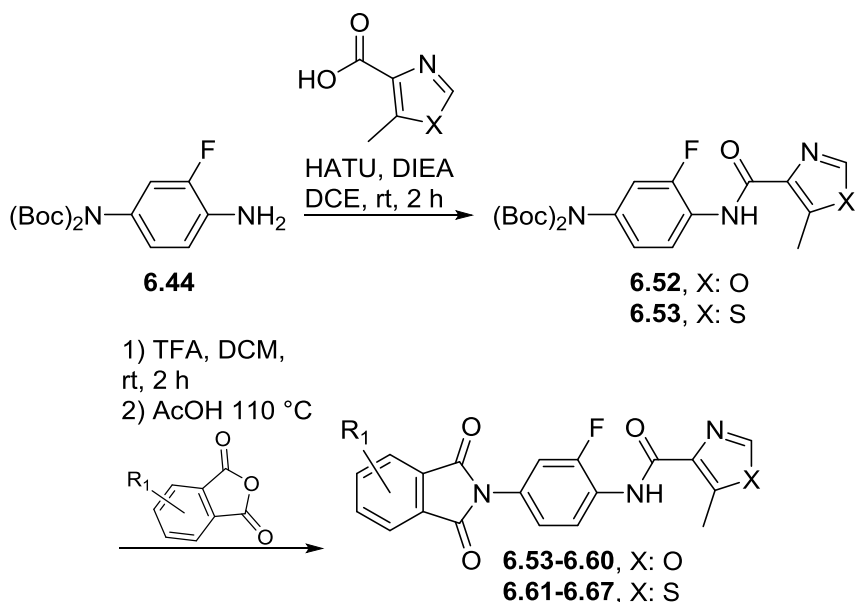
compounds (**6.45-6.48** and **6.50**) showed high free fraction in brain homogenate with the majority of them presenting between 17% and 30% of fraction unbound.

Then, the brain penetrance and *in vivo* clearance of these PAMs was determined in rats (Table 6.8). It was found that 3-methyl **6.45** had the lowest brain to plasma partition coefficient, while the highest  $K_{ps}$  were observed with 4-methyl **6.48** and 3fluoro **6.47**, being in both cases close to 1. In terms of the unbound partition coefficient, all these analogs displayed values superior to the unity. In terms of clearance, the analogs ranked similarly as in the *in vitro* microsomal experiment; however, clearance differed considerably in magnitude. While clearance was underestimated for the highly metabolized 3-chloro **6.46** and 3-fluoro **6.47**, it was overestimated for the other three analogs. The 4-fluoro **6.50** had a half-life of 77 minutes, but the most impressive improvement was observed with the methyl-substituted analogs **6.45** and **6.48**, which displayed half-lives close to five hours. All data combined points to the superiority of VU6004909 (**6.48**), an analog that achieved excellent potency and selectivity, and combines good fraction unbound and brain penetrance with an adequate half-life for *in vivo* target validation studies.

**Table 6.8.** *In vivo* pharmacokinetic properties of analogs **6.45-6.48** and **6.50**.

Parameter	<b>6.45</b>	<b>6.46</b>	<b>6.47</b>	<b>6.48</b>	<b>6.50</b>
Rat IV PBL (0.25 mg/kg)					
Cn plasma (ng/mL)	699	217	151	191	151
Cn brain (ng/g)	177	120	147	182	97.2
$K_p$ (at 0.25 h)	0.25	0.55	0.97	0.95	0.64
$K_{p,uu}$	5.36	150	15.0	7.45	1.98
Rat IV PK (0.25 mg/kg)					
$t_{1/2}$ (min)	296	51.5	38.9	285	76.6
MRT (min)	330	45.4	30.7	186	80.4
$Cl_p$ (mL/min/kg)	4.61	65.5	62.6	6.94	16.7
$V_{ss}$ (L/kg)	1.52	2.97	1.92	1.29	1.34

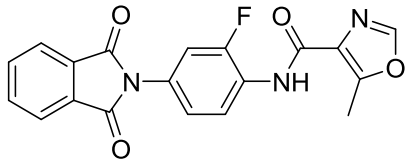
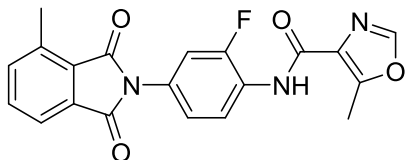
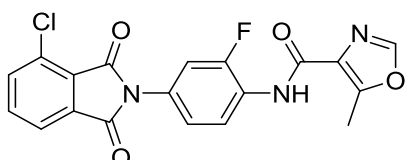
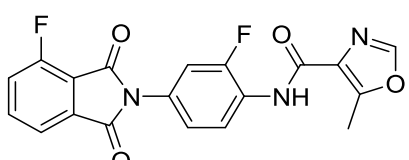
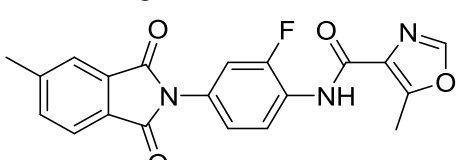
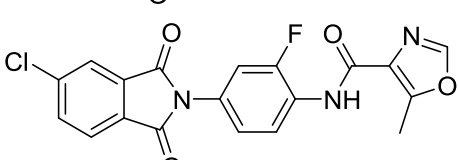
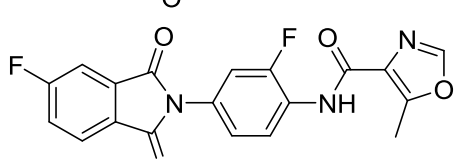
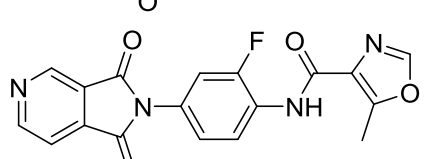
Due to the interesting possibilities that offer the use of the fluorine in the central phenyl ring along with the substituted phthalimides, the implementation of these functionalities was assessed in the context of the oxazole and thiazole amides. These compounds, in theory, would have the advantage of possessing selectivity but eliminating the potentially undesirable furan. The analogs were synthesized using a similar strategy as for the fluoro PAMs **6.45-6.51**, using as key intermediate the bis Boc protected 4-aminoanilines **6.43**.

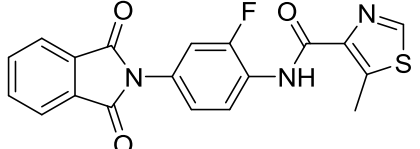
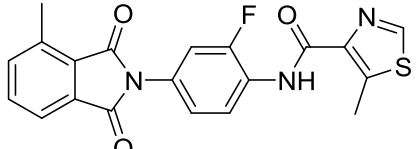
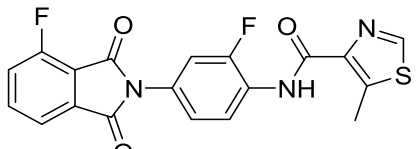
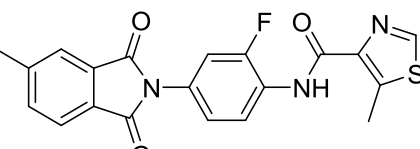
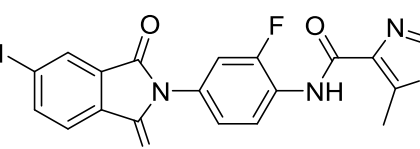
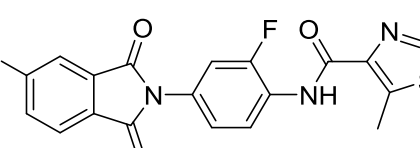
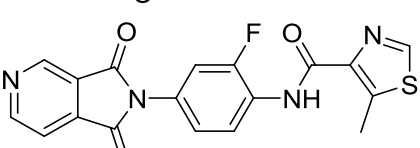


**Scheme 6.6.** Synthesis of analogs of VU6002194 **6.37f** with modifications in the furan, **6.53-6.67**.

The compounds were screened using a 10  $\mu\text{M}$  concentration in our calcium mobilization assay to assess mGlu<sub>1</sub> activation, and it was found that none of them exert an important enhancement of the glutamate response in the receptor (Table 6.9). While the oxazoles **6.53-6.60** did not potentiate glutamate's EC<sub>20</sub>, only a few from the thiazole examples (**6.61-6.67**) managed to increase the observed signal, and to small values around 45% Glu<sub>Max</sub> in the best cases. This demonstrated how the effect of substitutions in the central ring is context dependent and varied with the substituent in the amide, an example that illustrates the intricacies of allosteric modulation SAR.

**Table 6.9.** Comparison of the single point screen result for PAM activity in human mGlu<sub>1</sub> at 10  $\mu$ M for compounds derived from modifications in the furan region of VU6002194, analogs **6.53-6.67**. Calcium mobilization was used to obtain %Glu<sub>Max</sub> values for each compound in the presence of a submaximal concentration of glutamate (EC<sub>20</sub>) in cell lines expressing human mGlu<sub>1</sub>. Data represent the mean  $\pm$  S.E.M. of at least three experiments with similar results.

Structure	Cpd #	VU #	hmGlu <sub>1</sub> %Glu <sub>Max</sub>
	<b>6.53</b>	VU6005712	18
	<b>6.54</b>	VU6005717	14
	<b>6.55</b>	VU6005713	25
	<b>6.56</b>	VU6005715	16
	<b>6.57</b>	VU6005718	20
	<b>6.58</b>	VU6005714	27
	<b>6.59</b>	VU6005716	36
	<b>6.60</b>	VU6005719	9

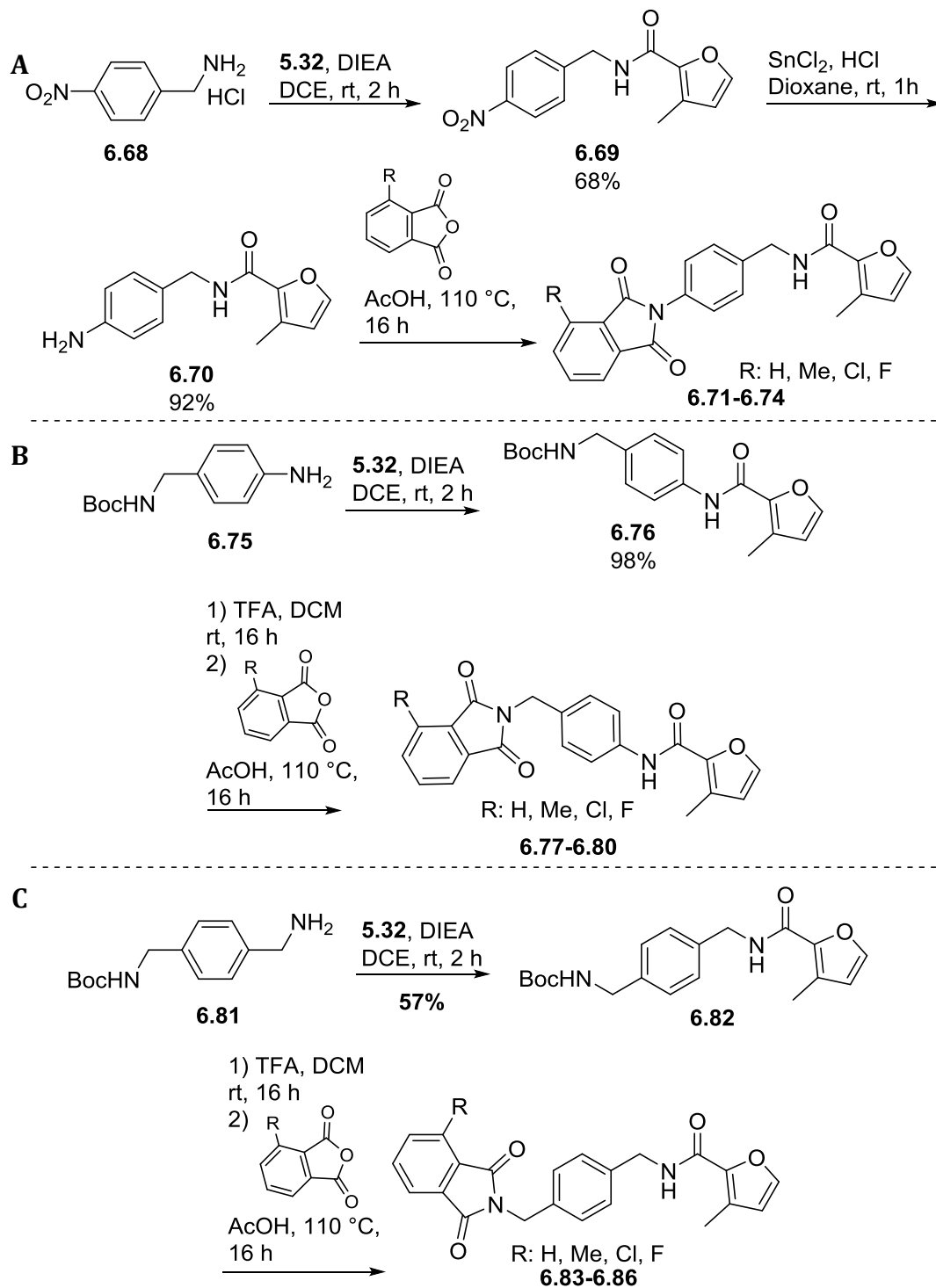
	<b>6.61</b>	VU6005705	49
	<b>6.62</b>	VU6005709	36
	<b>6.63</b>	VU6005707	22
	<b>6.64</b>	VU6005710	17
	<b>6.65</b>	VU6005706	40
	<b>6.66</b>	VU6005708	45
	<b>6.67</b>	VU6005711	42

#### *Homologation of the anilines in the central phenyl ring*

In an effort to explore the appropriate distance between the phthalimide and the furancarboxamide of the central phenyl ring of the scaffold of VU0486321 **5.35c**, we prepared compounds where methylene groups were introduced in between the ring and the nitrogen. For these analogs, we eliminated the chlorine in the central phenyl ring as it had shown to have little impact in the activity of compounds in the VU0486321 scaffold. This also allowed a simpler synthetic route to quickly access the desired analogs. The synthesis of these compounds

proceeded with a sequence of three steps (Scheme 6.7). Analogs **6.71-6.74** were synthesized starting with 4-nitrobenzylamine **6.68** and performing the amide coupling with acyl chloride **5.32** to obtain intermediate **6.69** in 68% yield. This nitroaromatic compound was reduced with tin(II) chloride to the aniline **6.70** in good yield (92%) and then the aniline was condensed with the selected phthalic anhydrides to provide the desired final compounds **6.71-6.74**. Analogs **6.77-6.80** were prepared using 4-(Boc-aminomethyl)aniline **6.75** as the starting material to perform the amide coupling with acyl chloride **5.32** and obtain intermediate **6.76** in excellent yields. Then, this intermediate was Boc deprotected with TFA, and the amine was condensed with the selected phthalic anhydrides. A similar procedure was performed to obtain analogs **6.83-6.86**, with methylenes on both sides of the phenyl ring, but this time employing the Boc-protected amine **6.81** as starting material.



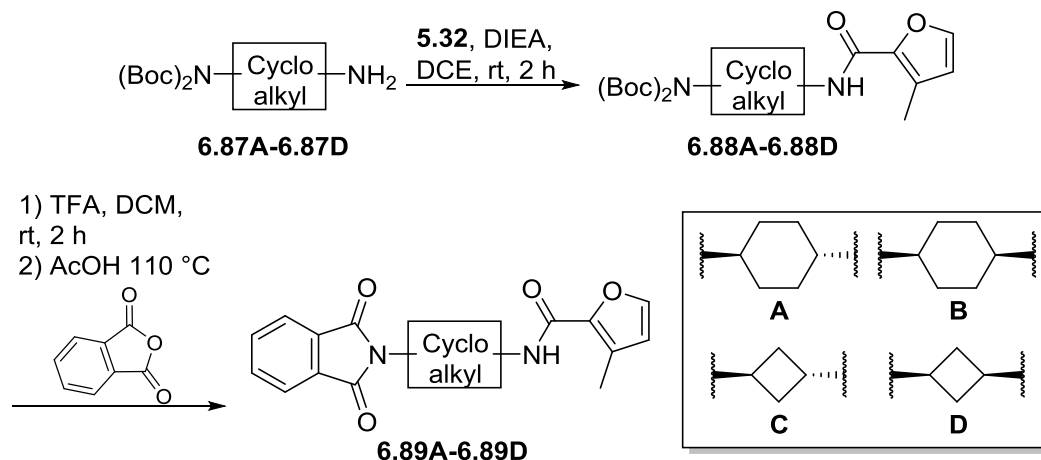


**Scheme 6.7.** Synthesis of homologues of VU0486321 **5.35c**, analogs **6.71-6.74**, **6.77-6.80** and **6.83-6.86**.

The preparation of these compounds was followed by the evaluation of their mGlu<sub>1</sub> PAM activity at a single concentration of 10 μM in a calcium mobilization assay. The addition of one extra carbon on either side of the phenyl ring (distance between nitrogens: 6.2 Å), or addition of a methylene in both ends (distance between nitrogens: 7.3 Å) led to complete loss of activity in the prepared analogs, demonstrating that the separation between the nitrogens is important for mGlu<sub>1</sub> PAM activity and that the phenyl ring spacer gives an optimal distance (around 5.3 Å).

#### *Cycloalkanes replacement for the central phenyl ring*

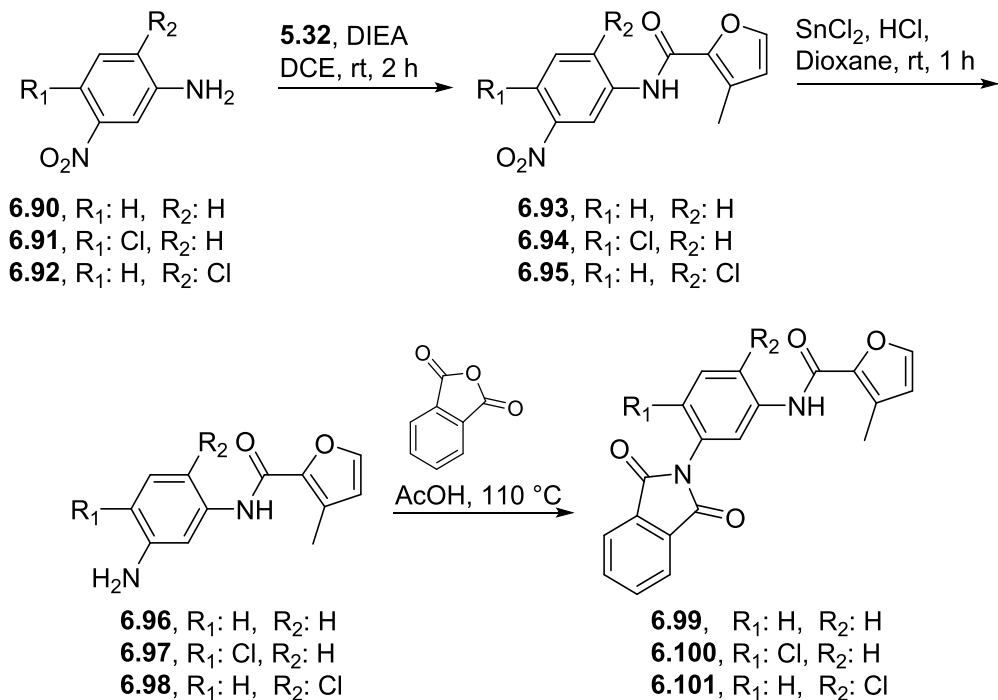
As only aromatic versions had been tested in the central phenyl ring, compounds with a saturated hydrocarbon core were synthesized as replacements of the phenyl ring. For this purpose, the cyclohexyl and the cyclobutyl were selected in order to not vary considerably the distance and orientation of substituents in the ring. In these cases, the *trans* isomers of the cyclohexyl and cyclobutyl diamines was our main focus of interest, but the *cis* were also prepared to explore their biological activity. The analogs were synthesized using the mono Boc protected diamines **6.87A-6.87D** to perform the amide couplings with acyl chloride **5.32**. Then, the intermediates **6.88A-6.88D** were Boc deprotected to generate the amines, which in turn were condensed using phthalic anhydride to obtain the final compounds **6.89A-6.89D** (Scheme 6.8). After evaluation for mGlu<sub>1</sub> PAM activity in a single point concentration calcium mobilization assay, it was discovered that none of the produced analogs exert potentiation in the glutamate's receptor response, highlighting the importance of the aromaticity and planarity of the central ring of VU0486321 scaffold.



**Scheme 6.8.** Synthesis of analogs of VU0486321 **5.35c** with a cycloalkyl central ring, analogs **6.89A-6.89D**.

*Substitution pattern in the central phenyl ring*

All analogs synthesized showed a 1,4-diamino phenyl ring in the central portion of the molecule, or a close relative with the same *para* distribution. In an effort to assess the importance of this substitution pattern, *meta*-substituted analogs were synthesized (Scheme 6.9). Chlorinated and non-chlorinated nitroanilines were employed to also assess the effect of the presence of halogen in these compounds. Similar to the 1,4-substituted analogs, the synthesis began with 3-nitroanilines **6.90-6.92** and an amide coupling with acyl chloride **5.32** in the microwave, followed by reduction of a nitro group **6.93-6.95** and condensation with phthalic anhydride. The synthesized compounds **6.99-6.101** did not enhance the mGlu<sub>1</sub> response towards glutamate in our calcium mobilization assay, indicating the importance of the 1,4-substitution pattern in the central phenyl ring, which likely provides a more rod-like overall structure than the 1,3 arrangement which produced a more ramified shape.

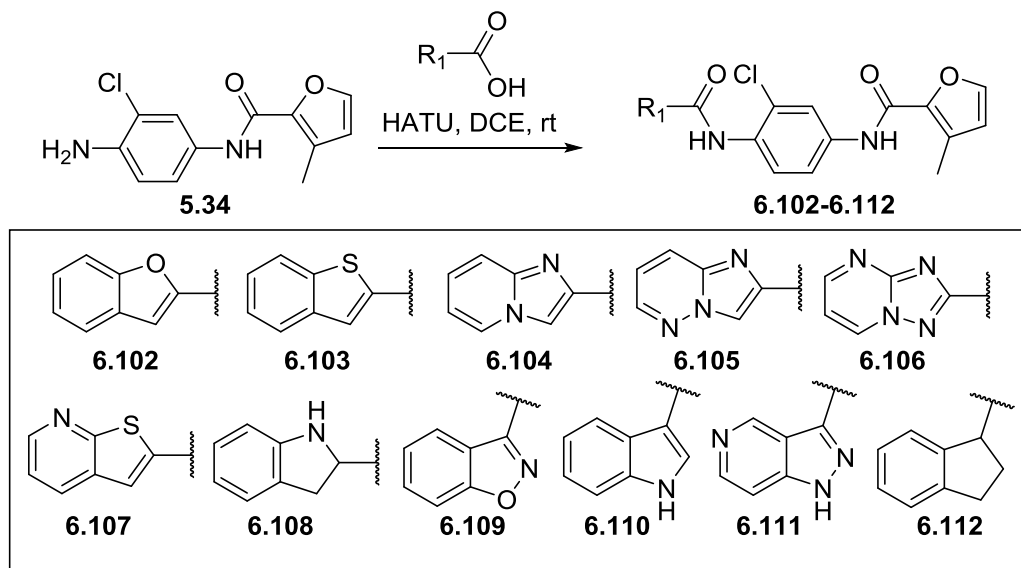


**Scheme 6.9.** Synthesis of analogs of VU0486321 **5.35c** with *meta* distribution in the central phenyl ring, analogs **6.99-6.101**.

### SAR exploration for the replacement of the phthalimide

#### *Fused rings as substitutes of the phthalimide ring*

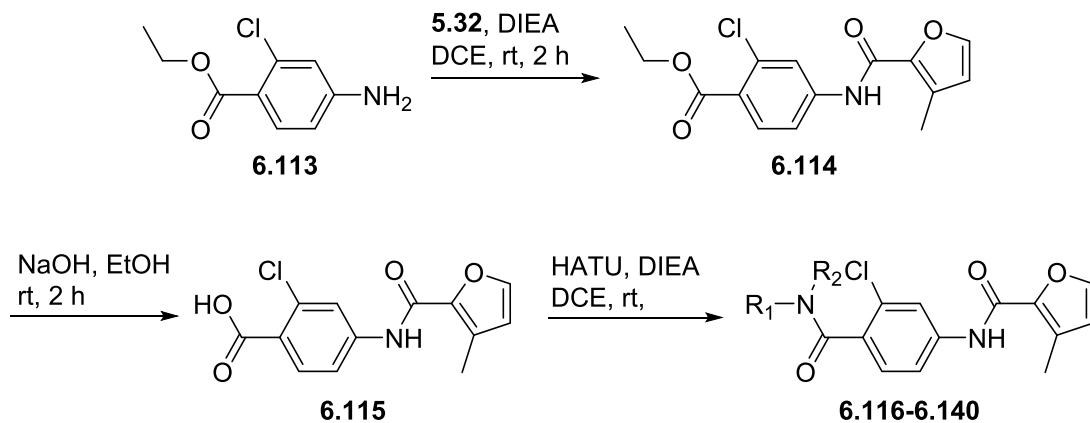
As the phthalimide in VU0486321 **5.35c** causes the molecule to be plasma unstable, we surveyed different approaches to remove this moiety. One of the first attempts consisted of the introduction of different fused rings carboxamides instead of the phthalimide. Here, the analogs were prepared through a HATU mediated amide coupling using intermediate **5.34** along with the desired carboxylic acids to afford final compounds (Scheme 6.10). In this case, no potentiation of glutamate's mGlu<sub>1</sub> response was observed at a concentration of 10 μM of test article. Therefore, the evaluated fused ring systems were not suitable alternatives to the phthalimide for mGlu<sub>1</sub> PAM activity.



**Scheme 6.10.** Synthesis of analogs of VU0486321 **5.35c** to replace the phthalimide with fused ring amides, analogs **6.102-6.112**.

*Reverse amides as replacements of the phthalimide*

Another strategy to find an appropriate substitute to the phthalimide moiety was the introduction of reverse amides. To assess this idea, a library was created with different amines in which the location of the carbonyl was switched with respect to the phthalimide in VU0486321 **5.35c**. These compounds were synthesized in three steps, starting with the amide coupling between 4-aminobenzoate ester **6.113** and acyl chloride **5.32** at room temperature, followed by the basic hydrolysis of the ethyl ester **6.114** (Scheme 6.11). The library step consisted of a HATU mediated amide coupling with the different amines to generate analogs **6.116-6.140**.



**Scheme 6.11.** Synthesis of analogs of VU0486321 **5.35c** to replace the phthalimide with reverse amides, analogs **6.116-6.140**.

After evaluation of analogs **6.116-6.140** for their capacity to potentiate glutamate's mGlu<sub>1</sub> response, it was observed that only a few examples presented observable PAM activity (Fig. 6.3 and Table 6.10). From the aniline examples, only the *o*-anisidine analog **6.117**, showed potentiation of the receptor activity, but further studies showed that it was a weak potentiator with an EC<sub>50</sub> over 10 μM. Examples of benzylamines, cyclohexylamines, aminoindanes and substituted pyrrolidines did not engender mGlu<sub>1</sub> PAM activity. The compounds showing the highest efficacies were isoindoline **6.122** (90%), indoline **6.123** (90%) and tetrahydroisoquinoline **6.124** (78%). When the analogs were tested to obtain their concentration-response curves for PAM activity, a similar tendency was observed in the ranking for their potencies. **6.124** proved to be the least potent of the set with an EC<sub>50</sub> of 3.60 μM (86% Glu<sub>Max</sub>), while **6.122** and **6.123** were the most active (EC<sub>50</sub> = 0.90 μM, 110% Glu<sub>Max</sub> and EC<sub>50</sub> = 1.23 μM, 105% Glu<sub>Max</sub>, respectively). So, this strategy was not pursued further as it was observed that in the best scenario these modifications caused around a nine-fold loss in potency versus their direct comparator VU0474633 **5.27**.

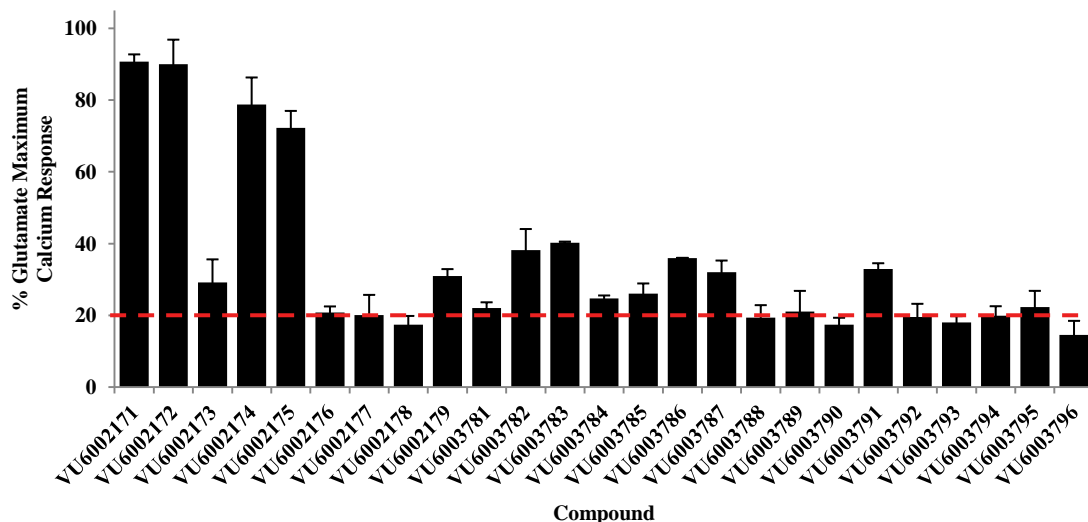


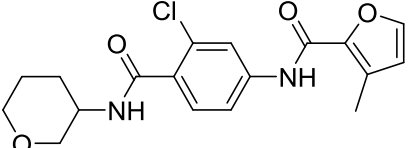
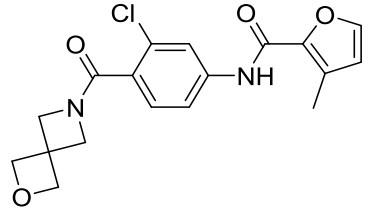
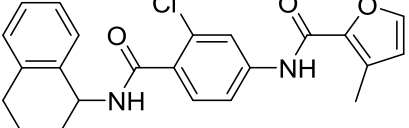
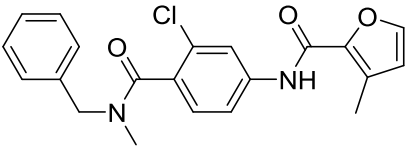
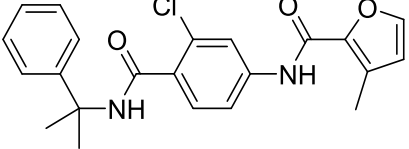
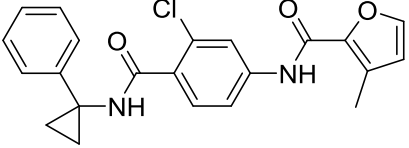
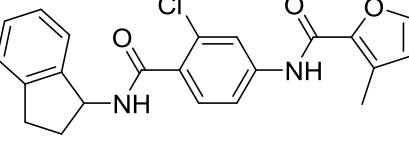
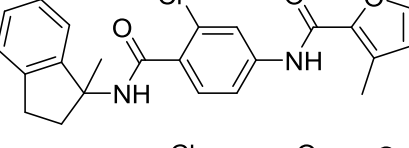
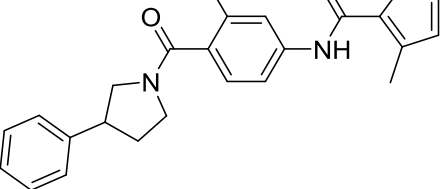
**Figure 6.3.** Comparison of the single point screen result for PAM activity in human mGlu<sub>1</sub> at 10  $\mu$ M for reverse amide analogs **6.116-6.140**. Calcium mobilization was used to obtain %Glu<sub>Max</sub> values for each compound in the presence of a submaximal concentration of glutamate (EC<sub>20</sub>) in cell lines expressing human mGlu<sub>1</sub>. Data represent the mean  $\pm$  S.E.M. of at least three experiments with similar results.

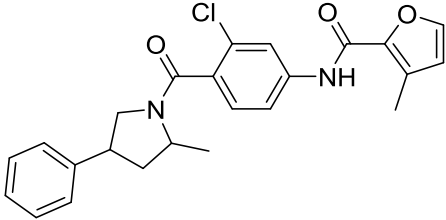
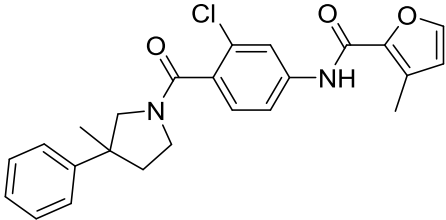
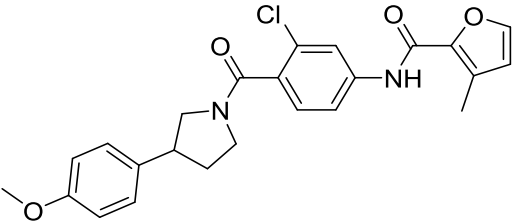
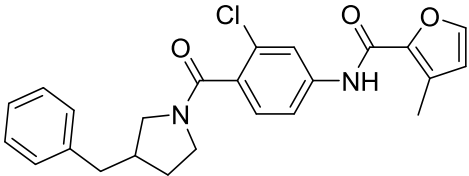
**Table 6.10.** Structures of the reverse amide analogs **6.116-6.140** and associated PAM activity from the single point screening at 10  $\mu$ M in human mGlu<sub>1</sub>. Calcium mobilization responses for each compound are reported as a percentage of the maximum glutamate response. VU number denotes the compound identifier assigned by Vanderbilt University. Data represent the mean  $\pm$  S.E.M. of at least three replicate experiments with similar results.

Structure	Cpd #	VU #	hmGlu <sub>1</sub> %Glu <sub>Max</sub>
	<b>6.116</b>	VU6002173	29.2 $\pm$ 6.4
	<b>6.117</b>	VU6002175	72.3 $\pm$ 4.7
	<b>6.118</b>	VU6002176	20.8 $\pm$ 1.7

	<b>6.119</b>	VU6002177	20.1±5.6
	<b>6.120</b>	VU6002179	31.0±1.9
	<b>6.121</b>	VU6002178	17.4±2.4
	<b>6.122</b>	VU6002171	90.7±2.0
	<b>6.123</b>	VU6002172	90.0±6.8
	<b>6.124</b>	VU6002174	78.8±7.5
	<b>6.125</b>	VU6003781	22.0±1.6
	<b>6.126</b>	VU6003787	32.0±3.3
	<b>6.127</b>	VU6003792	19.6±3.6



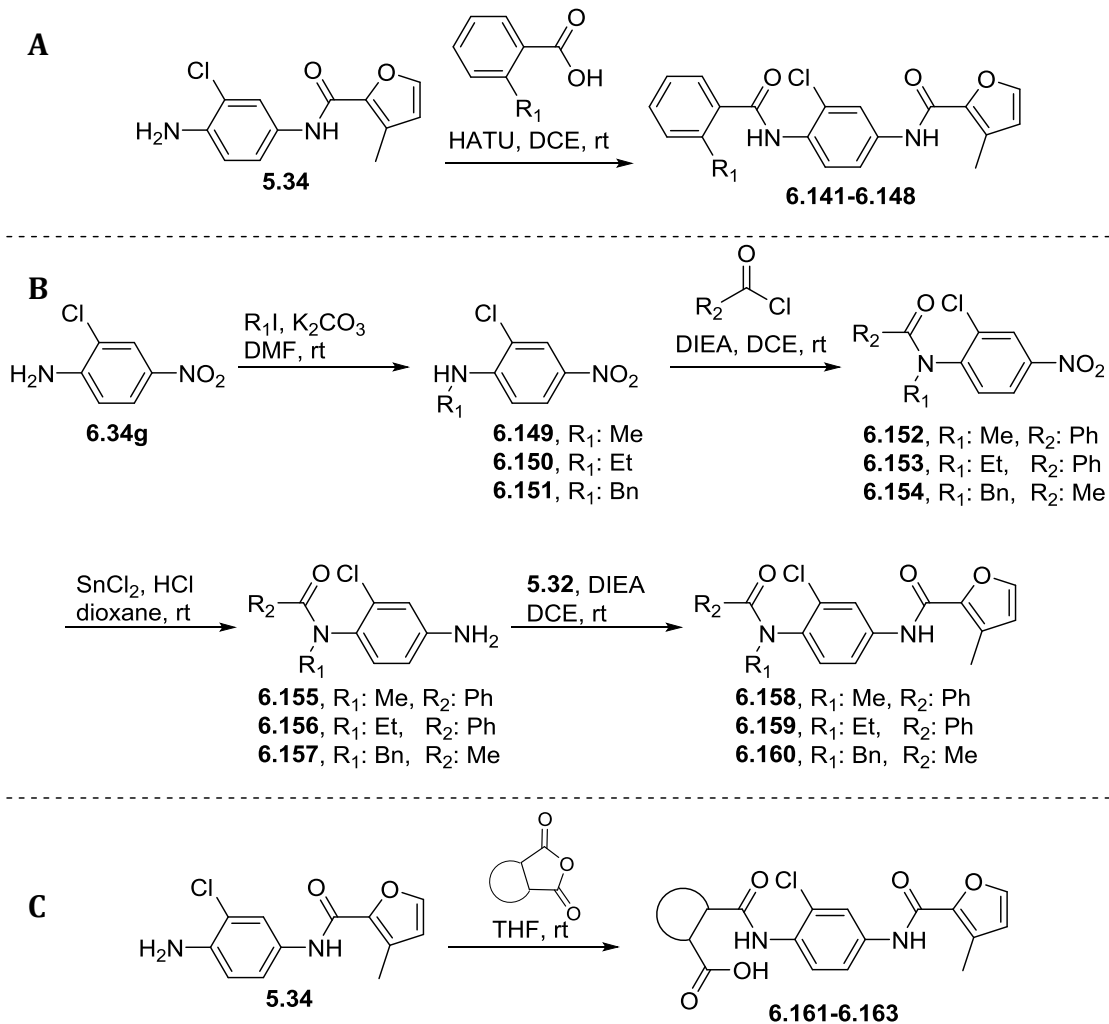
	<b>6.128</b>	VU6003793	18.1±1.7
	<b>6.129</b>	VU6003796	14.6±3.9
	<b>6.130</b>	VU6003788	19.4±3.5
	<b>6.131</b>	VU6003782	38.2±5.9
	<b>6.132</b>	VU6003794	19.9±2.7
	<b>6.133</b>	VU6003790	17.4±1.9
	<b>6.134</b>	VU6003795	22.3±4.5
	<b>6.135</b>	VU6003789	21.1±5.8
	<b>6.136</b>	VU6003783	40.3±0.3

	<b>6.137</b>	VU6003784	24.7±0.8
	<b>6.138</b>	VU6003791	33.0±1.6
	<b>6.139</b>	VU6003785	26.1±2.8
	<b>6.140</b>	VU6003786	36.00±0.04

#### Ring opening of the phthalimide

We also explored the effect of analogs that mimicked the ring opening or fragmentation of the phthalimide. In this case, different *ortho*-benzoic acids were used to generate analogs **6.141-6.148** following similar procedures to those described in scheme 6.10 (Scheme 6.12A). Analogs representing fragmented versions of the phthalimide rings **6.158-6.160** were synthesized in four-steps (Scheme 6.12B), starting with the alkylation of nitroaniline **6.34g** with alkyl iodides to produce intermediates **6.149-6.151**, followed by acylation and reduction to obtain anilines **6.155-6.157**. Then, the final step involved the amide coupling between **6.155-6.157** and **5.32**. Additionally, phthalamic acid related compounds **6.161-6.163** were synthesized by the opening of cyclic anhydride with aniline **5.34** in THF at room temperature (Scheme 6.12C); these analogs

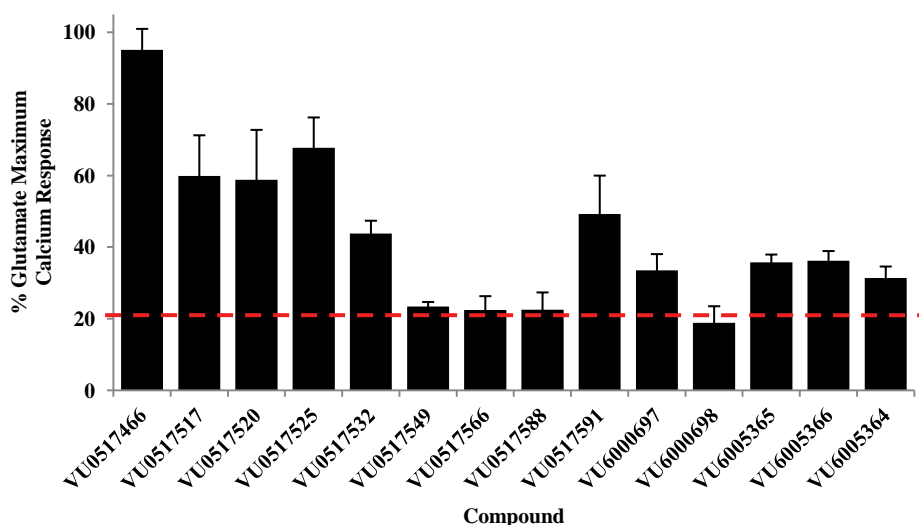
represent the structures generated during the incubations in plasma which allowed the testing of these metabolites for mGlu<sub>1</sub> PAM activity.



**Scheme 6.12.** Synthesis of analogs of VU0486321 **5.35c** to replace the phthalimide with open ring variants, analogs **6.141-6.148** and **6.158-6.163**.

Evaluation of the compounds at 10  $\mu$ M demonstrated the importance of the phthalimide in the VU0486321 scaffold for mGlu<sub>1</sub> PAM activity, as most compounds displayed significantly reduced or completely absent mGlu<sub>1</sub> potentiation (Fig. 6.4 and Table 6.11). Between the synthesized benzamides **6.141-6.148**, only the naked benzamide **6.141**, the *o*-methyl **6.142**, the *o*-

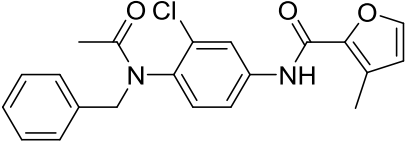
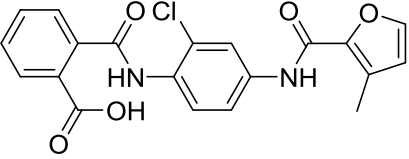
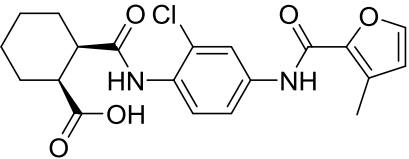
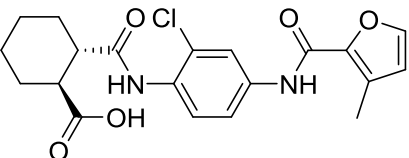
ethyl **6.143**, the 2,3-dimethyl **6.146** and the *o*-ethoxy **6.145** showed some weak PAM activity, with the latter been the most efficacious achieving 68%  $\text{Glu}_{\text{Max}}$ . The fragmented versions of the phthalimide **6.158-6.160** with the alkylated amide did not show an enhanced glutamate response. The best results were observed with phthalamic acid **6.161** that achieved the highest calcium mobilization signal in our assay, with a potency in human  $\text{mGlu}_1$  of 0.93  $\mu\text{M}$  (108%  $\% \text{Glu}_{\text{Max}}$ ). This shows that the metabolites generated in plasma, despite maintaining  $\text{mGlu}_1$  PAM activity, are likely to be less potent. For example, **6.161** is 9-fold less active than its direct phthalimide comparator VU0474633 **5.27**; while the cyclohexyl analogs **6.162** and **6.163** were completely inactive.



**Figure 6.4.** Comparison of the single point screen result for PAM activity in human  $\text{mGlu}_1$  at 10  $\mu\text{M}$  for open ring analogs **6.141-6.148** and **6.158-6.163**. Calcium mobilization was used to obtain  $\% \text{Glu}_{\text{Max}}$  values for each compound in the presence of a submaximal concentration of glutamate ( $\text{EC}_{20}$ ) in cell lines expressing human  $\text{mGlu}_1$ . Data represent the mean  $\pm$  S.E.M. of at least three experiments with similar results.

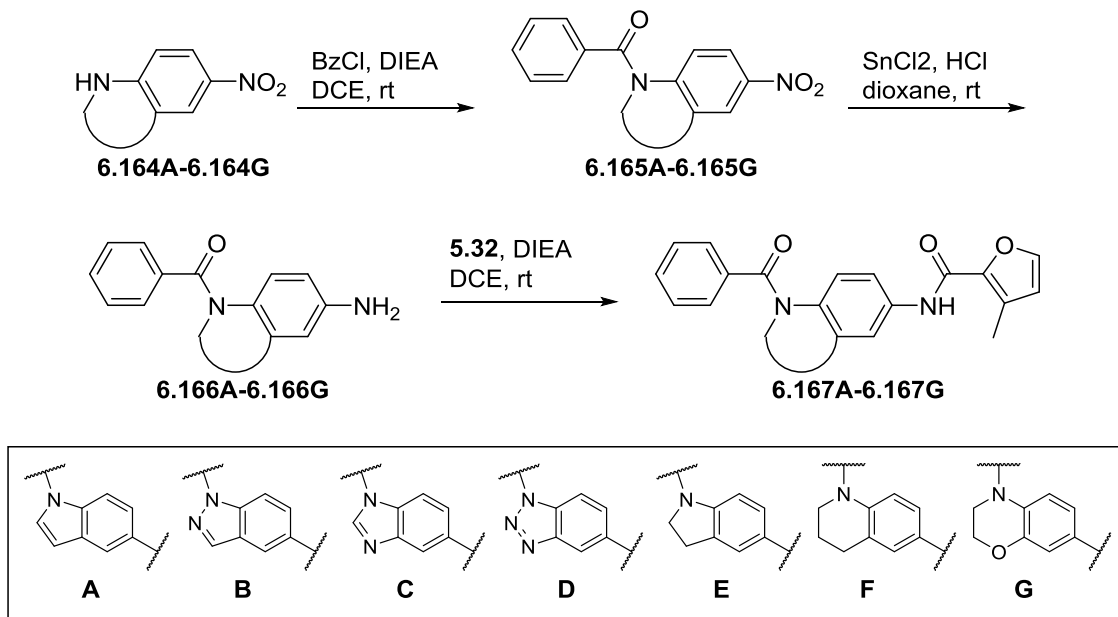
**Table 6.11.** Structures of the open ring analogs **6.141-6.148** and **6.158-6.163**, and associated PAM activity from the single point screening at 10  $\mu$ M in human mGlu<sub>1</sub>. Calcium mobilization responses for each compound are reported as a percentage of the maximum glutamate response. VU number denotes the compound identifier assigned by Vanderbilt University. Data represent the mean  $\pm$  S.E.M. of at least three replicate experiments with similar results.

Structure	Cpd #	VU #	hmGlu <sub>1</sub> %Glu <sub>Max</sub>
	<b>6.141</b>	VU0517591	49.2 $\pm$ 10.7
	<b>6.142</b>	VU0517517	59.9 $\pm$ 11.3
	<b>6.143</b>	VU0517520	58.8 $\pm$ 13.9
	<b>6.143</b>	VU0517549	23.4 $\pm$ 1.3
	<b>6.145</b>	VU0517525	67.7 $\pm$ 8.4
	<b>6.146</b>	VU0517532	43.8 $\pm$ 3.5
	<b>6.147</b>	VU0517566	22.5 $\pm$ 3.8
	<b>6.148</b>	VU0517588	22.6 $\pm$ 4.8
	<b>6.158</b>	VU6005365	35.7 $\pm$ 2.2
	<b>6.159</b>	VU6005366	36.2 $\pm$ 2.7

	<b>6.160</b>	VU6005364	31.4±3.2
	<b>6.161</b>	VU0517466	95.0±5.8
	<b>6.162</b>	VU6000697	33.5±4.5
	<b>6.163</b>	VU6000698	18.8±4.6

#### *Tied-back rings as replacements of the phthalimide*

Another effort to attempt to remove the phthalimide group from the scaffold was the development of different tied back rings. In these examples, one of the carbonyl groups from the phthalimide will still remain in the molecule forming a more plasma stable amide, while the other one will be removed and the nitrogen would be connected to the ring through a linker to form a bicyclic fused ring. Analogs to evaluate this idea were synthesized starting with different nitro substituted bicyclic heterocycles **6.164A-6.164G**, which were acylated using benzoyl chloride to form intermediates **6.165A-6.165G**. Then, the nitro group was reduced with tin(II) chloride and the generated anilines **6.166A-6.166G** were used in an amide coupling with acyl chloride **5.32** to provide the final compounds **6.167A-6.167G** (Scheme 6.13).



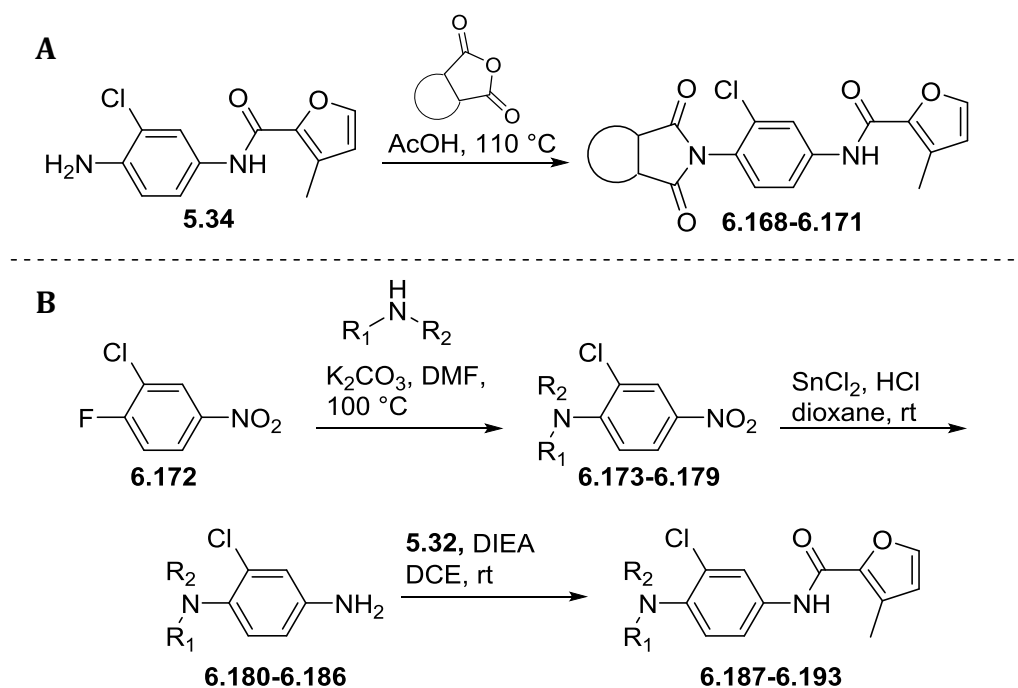
**Scheme 6.13.** Synthesis of analogs of VU0486321 **5.35c** to replace the phthalimide with a tied back ring strategy, analogs **6.167A-6.167G**.

These analogs were tested in our calcium mobilization assay, and only **6.167A** displayed enhancement of mGlu<sub>1</sub> activity at 10  $\mu$ M. The mGlu<sub>1</sub> PAM potency for this compound was 2.64  $\mu$ M (74% Glu<sub>Max</sub>). As the best compound in this set represented nearly a 26-fold decrease in potency with respect to the parent compound, this effort was abandoned.

#### *Other replacements of the phthalimide*

To replace the phthalimide moiety, analogs maintaining the imide functional group but in an aliphatic scaffold or with a methylene linker were prepared; these compounds would virtually have a more stable imide compared to the aromatic imide. Analogs **6.168-6.171** were prepared by condensation of cyclic anhydrides with intermediate **5.34** in refluxing acetic acid (Scheme 6.14A). Moreover, analogs where the phthalimide was replaced with other fused rings, maintaining the nitrogen directly connected to the central phenyl ring, were synthesized. In this case, a three-step procedure was employed starting with a nucleophilic aromatic substitution using fluoronitrobenzene **6.172** and different cyclic amines. Then, intermediates **6.173-6.179**

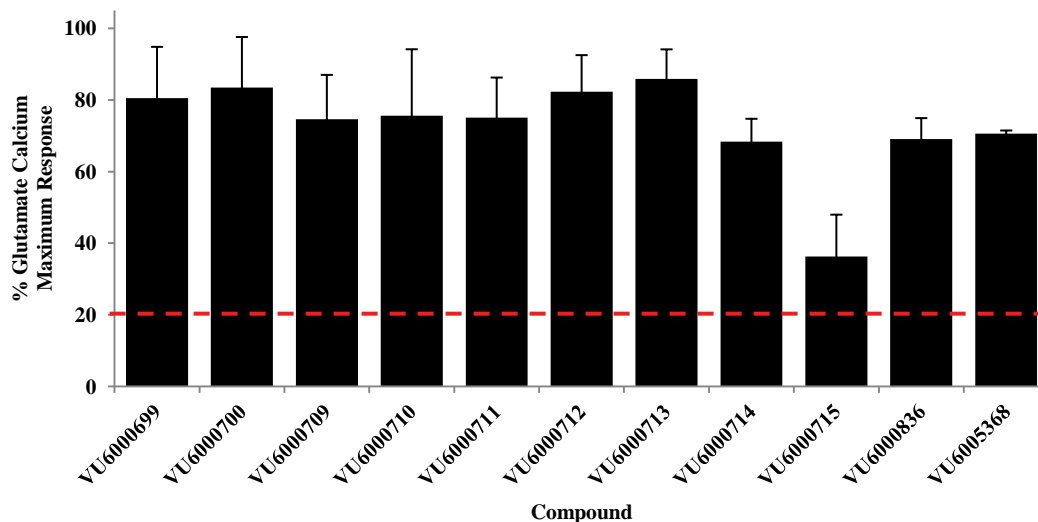
where reduced with tin(II) chloride, and a HATU-mediated amide coupling with the anilines **6.180-6.186** and acyl chloride **5.32** was performed to produce final compounds **6.187-6.193** (Scheme 6.14B).



**Scheme 6.14.** Synthesis of analogs of VU0486321 **5.35c** with different phthalimide replacements, analogs **6.168-6.171** and **6.187-6.193**.

Analogs **6.168-6.171** and **6.187-6.193** were screened at a 10  $\mu\text{M}$  concentration to assess their effect in mGlu<sub>1</sub> response. It was encouraging that very different structures provided potentiation of the EC<sub>20</sub>, as active compounds were found in the imide and the non-imide replacement analogs with %Glu<sub>Max</sub> between 68 and 86%, with only quinazoline **6.179** giving low levels of potentiation.

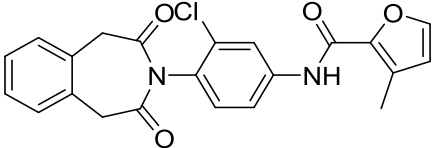
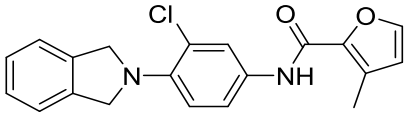
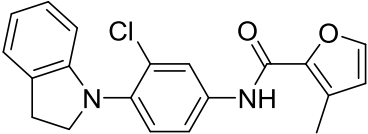
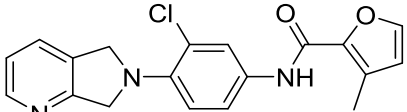
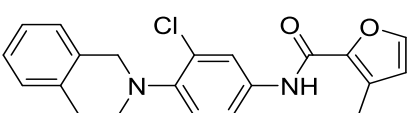
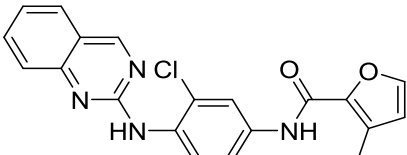
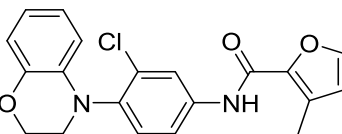
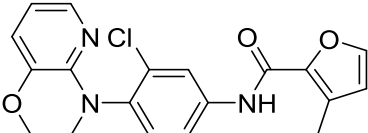




**Figure 6.5.** Comparison of the single point screen result for PAM activity in human mGlu<sub>1</sub> at 10  $\mu$ M for different phthalimide replacements, analogs **6.168-6.171** and **6.187-6.193**. Calcium mobilization was used to obtain %Glu<sub>Max</sub> values for each compound in the presence of a submaximal concentration of glutamate (EC<sub>20</sub>) in cell lines expressing human mGlu<sub>1</sub>. Data represent the mean  $\pm$  S.E.M. of at least three experiments with similar results.

**Table 6.12.** Structures of the phthalimide replacement analogs **6.168-6.171** and **6.187-6.193**, and associated PAM activity from the single point screening at 10  $\mu$ M in human mGlu<sub>1</sub>. Calcium mobilization responses for each compound are reported as a percentage of the maximum glutamate response. VU number denotes the compound identifier assigned by Vanderbilt University. Data represent the mean  $\pm$  S.E.M. of at least three replicate experiments with similar results.

Structure	Cpd #	VU #	hmGlu <sub>1</sub> %Glu <sub>Max</sub>
	<b>6.168</b>	VU6000699	80.5 $\pm$ 14.3
	<b>6.169</b>	VU6000700	83.5 $\pm$ 14.0
	<b>6.170</b>	VU6000713	85.9 $\pm$ 8.2

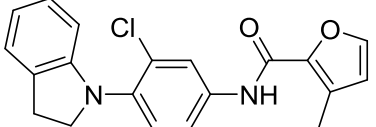
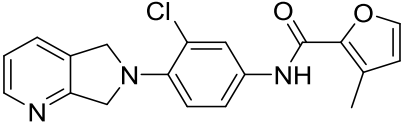
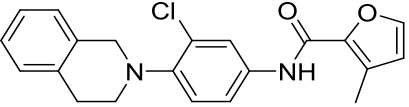
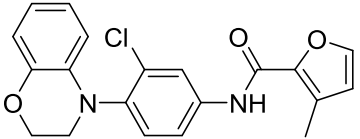
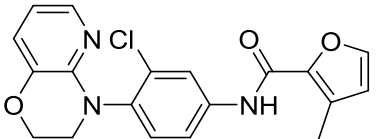
	<b>6.171</b>	VU6005368	70.6±0.9
	<b>6.187</b>	VU6000709	74.6±12.4
	<b>6.188</b>	VU6000710	75.6±18.9
	<b>6.189</b>	VU6000711	75.0±11.2
	<b>6.190</b>	VU6000836	69.1±5.8
	<b>6.191</b>	VU6000715	36.3±11.7
	<b>6.192</b>	VU6000714	68.3±6.4
	<b>6.193</b>	VU6000712	82.3±10.2

These compounds were further screened at different concentrations to obtain their EC<sub>50</sub> for mGlu<sub>1</sub> PAM activity. The set of imides revealed different potencies, where the cyclohexyl congeners **6.168** and **6.169** were the weakest PAMs in the group with over 10 μM EC<sub>50</sub>s, followed by the seven-ring member **6.171** with 3.6 μM potency (95% Glu<sub>Max</sub>); the most potent was the homophthalimide analog **6.170** (human mGlu<sub>1</sub> EC<sub>50</sub> = 0.22 μM, 104% Glu<sub>Max</sub>). As **6.170** represented only a two-fold loss in potency from its comparator phthalimide **5.27**, the PAM was analyzed further. The compound was found to be equally potent in the rat mGlu<sub>1</sub> (EC<sub>50</sub> = 0.24

$\mu\text{M}$ , 105%  $\text{Glu}_{\text{Max}}$ ); however, its pharmacokinetic characteristics were not stellar. *In vitro* evaluation of intrinsic clearance showed moderate clearance in human liver microsomes ( $\text{Cl}_{\text{hep}} = 13.5 \text{ mL/min/kg}$ ) and high clearance in rat liver microsomes ( $\text{Cl}_{\text{hep}} = 54.0 \text{ mL/min/kg}$ ), along with moderate inhibition of CYP2C9 ( $\text{IC}_{50} = 5.18 \mu\text{M}$ ). These properties along with their instability, made it impossible to measure fraction unbound in plasma and made us not explore further this series of compounds.

**Table 6.13.** Potencies in human  $\text{mGlu}_1$  of VU0486321phthalimide replacements analogs **6.168-6.171** and **6.187-6.193**. Calcium mobilization responses for each compound are reported as a percentage of the maximum glutamate response. VU number denotes the compound identifier assigned by Vanderbilt University. Data represent the mean  $\pm$  S.E.M. of at least three independent experiments with similar results. ---, no potentiation. ND, not determined.

Structure	Cpd #	VU #	hmGlu <sub>1</sub>	
			EC <sub>50</sub> ( $\mu\text{M}$ )	%Glu <sub>Max</sub>
	<b>6.168</b>	VU6000699	>10	80.5
	<b>6.169</b>	VU6000700	>10	83.5
	<b>6.170</b>	VU6000713	0.22	104.3
	<b>6.171</b>	VU6005368	3.57	94.9
	<b>6.187</b>	VU6000709	1.77	95.3

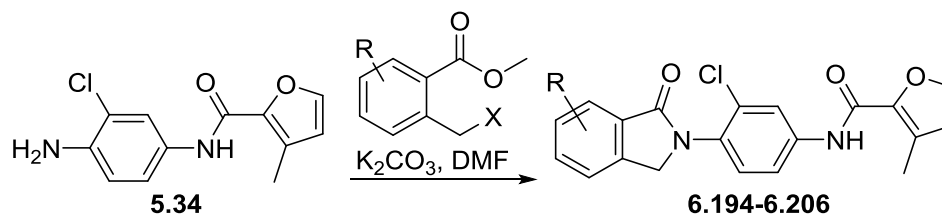
	<b>6.188</b>	VU6000710	5.71	82.6
	<b>6.189</b>	VU6000711	9.55	78.7
	<b>6.190</b>	VU6000836	2.47	93.8
	<b>6.192</b>	VU6000714	3.62	100.0
	<b>6.193</b>	VU6000712	2.61	93.4

In the non-imide replacement assays, the isoindoline **6.187** was the most potent of the set with an EC<sub>50</sub> of 1.8 μM. Switching the nitrogen location to the indoline **6.188** or introduction of an additional nitrogens in position 4 (**6.189**) led to a decrease in activity of up to 5-fold. Homologation of the isoindoline to the tetrahydroisoquinoline (**6.190**) showed a less harmful effect, increasing the potency only to 2.47 μM. However, when an attempt was performed to measure the intrinsic clearance and plasma fraction unbound of isoindoline **6.187**, it was observed that the DMSO stock solution of this compound decompose rapidly after exposure to air, making hard to accurately measure its concentration. LC-MS<sup>n</sup> analysis narrowed down the decomposition process to the electron rich isoindolines, where oxidation of one of the methylenes of the rings was found to generate a lactam (+14 m/z). Meanwhile, the benzoxazines analog **6.192** and **6.193** displayed modest activity with an opposite trend as the isoindolines, as the azabenzoxazine is the most potent of the pair. So, from these analogs, despite achieving good glutamate responses at 10 μM, it was not possible to find a suitable replacement for the phthalimide that engendered good potency for mGlu<sub>1</sub> PAM activity.

### *Isoindolinones as replacements of the phthalimide*

At the end of chapter 4, the generation of isoindolinone analogs (**4.145-4.146**) was presented. These compounds while having decrease potency represented an improvement in plasma stability, as they are not metabolized significantly in plasma preparations for four hours. These results led us to hypothesize that if a phthalimide with enough potency was generated, it would be possible to accommodate for the decrease in potency after the removal of a carbonyl and generate a potent and plasma stable isoindolinone.

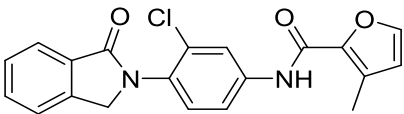
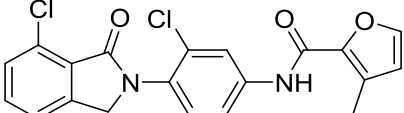
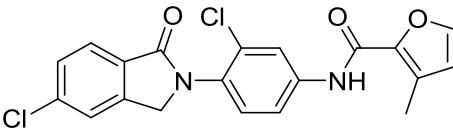
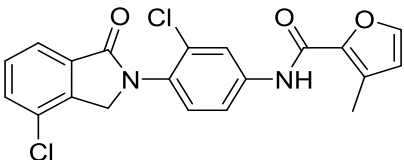
Several analogues that achieved two-digit nanomolar potencies have been presented. From this, it was believed that the VU0486321 **5.35c** had enough potency to start developing isoindolinone analogs and test our hypothesis. These compounds were synthesized following a similar procedure to the one presented in chapter 4, where aniline **5.34** was reacted with different bromomethylbenzoates in a tandem nucleophilic substitution-cyclization reaction to produce analogs **6.194-6.206**. To produce these analogs, most bromomethylbenzoates were produced by radical bromination of *o*-methylbenzoate esters while others were commercially available. In addition to substituted isoindolinones, other analogs that represented changes in the isoindolinone core such as the homologues **6.207-6.212** were prepared. In this case, the route depicted in Scheme 6.14B was used, starting with nucleophilic aromatic substitution in a fluoronitroaniline **6.172** and the corresponding amides instead of the aromatic amines.

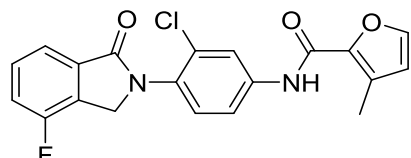
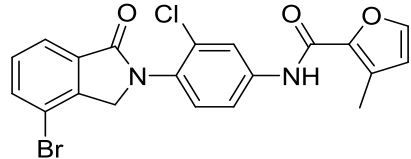
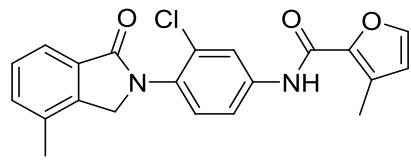
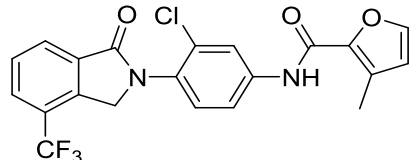
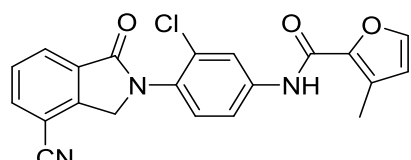
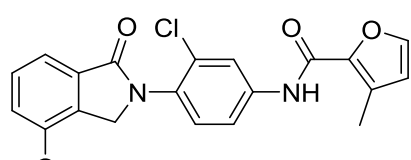
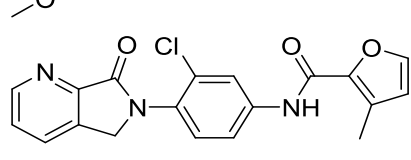
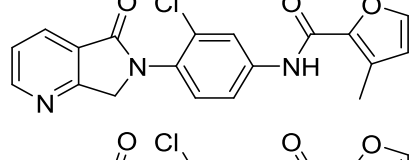
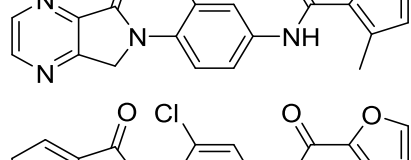
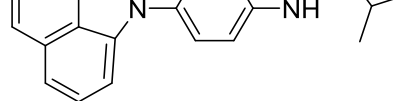


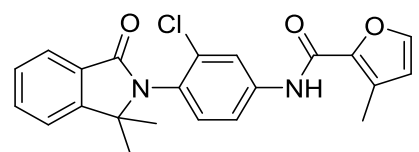
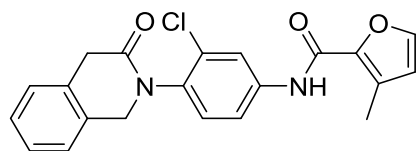
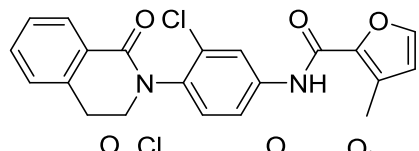
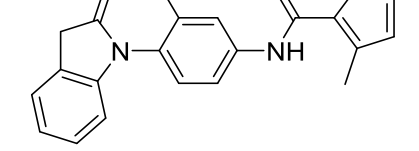
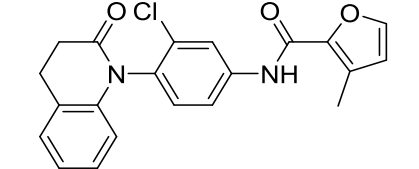
**Scheme 6.15.** Synthesis of analogs of VU0486321 **5.35c** to replace the phthalimide with an isoindolinone, analogs **6.194-6.206**.

These isoindolinone analogs were tested in calcium mobilization assays to determine their EC<sub>50</sub> for mGlu<sub>1</sub> PAM activity. The unsubstituted isoindolinone **6.194** showed weak activity, and it caused a decrease of more than 37-fold with respect to its direct phthalimide comparator **5.27**. Walking a chlorine around the phenyl ring showed that positions 4 (**6.197**) and 7 (**6.195**), gave active compounds while the 5-chloro **6.196** exert only weak PAM activity with 59% Glu<sub>Max</sub>. The most active isoindolinone from this effort was the 4-chloro **6.197**, having an EC<sub>50</sub> of 220 nM (88% Glu<sub>Max</sub>) and maintaining the same SAR tendency observed with the isoindolinones in the context of the picolinamides **4.145** and **4.146**.

**Table 6.14.** Potencies in human mGlu<sub>1</sub> of isoindolinone related analogs **6.194-6.212**. Calcium mobilization responses for each compound are reported as a percentage of the maximum glutamate response. VU number denotes the compound identifier assigned by Vanderbilt University. Data represent the mean ± S.E.M. of at least three independent experiments with similar results. ---, no potentiation. ND, not determined.

Structure	Cpd #	VU #	hmGlu <sub>1</sub>	
			EC <sub>50</sub> (μM)	%Glu <sub>Max</sub>
	<b>6.194</b>	VU6003731	3.72	91
	<b>6.195</b>	VU04867266	0.48	109
	<b>6.196</b>	VU6005374	>10	59
	<b>6.197</b>	VU0487351	0.22	88

	<b>6.198</b>	VU6005370	0.88	83
	<b>6.199</b>	VU6000821	0.39	100
	<b>6.200</b>	VU6005417	1.08	90
	<b>6.201</b>	VU6005367	1.13	105
	<b>6.202</b>	VU6005373	2.10	108
	<b>6.203</b>	VU0517648	>10	56
	<b>6.204</b>	VU6000704	>10	11
	<b>6.205</b>	VU6001123	>10	55
	<b>6.206</b>	VU6000705	>10	39
	<b>6.207</b>	VU6005371	1.76	76

	<b>6.208</b>	VU0517521	6.93	89
	<b>6.209</b>	VU6005415	3.38	105
	<b>6.210</b>	VU6005416	0.78	94
	<b>6.211</b>	VU6000823	>10	41
	<b>6.212</b>	VU6000822	1.29	108

As the 4-chloro analog **6.197** (VU0487351) showed good potency for mGlu<sub>1</sub>, several analogs with different substitutions were prepared and screened. From this set it was observed the halogen substituted analogs **6.198** and **6.199** gave the better potencies. The bromo compound **6.199** was found to be the most active of the pair and 2-fold less potent compared to **6.197**. It was observed that as the size of the substituent in the 4 position increased, the PAM potency subtly decreases. The 4-methyl **6.200** and 4-trifluoromethyl **6.201** have decreased activity with respect to **6.197** but comparable activity between each other (human mGlu<sub>1</sub> EC<sub>50</sub> = 1.08 μM and 1.13 μM, respectively). There was an extra drop in activity with the more extended cyano group (**6.202**, human mGlu<sub>1</sub> EC<sub>50</sub> = 2.10 μM) and the bulkier methoxy group (**6.203**) generated a very weak PAM with over 10 μM potency and 56% Glu<sub>Max</sub>. The benzimidazole analog **6.207** represented a tied back ring strategy between the position 4 and the methylene linker, and despite retaining activity, the modification was not beneficial in comparison to **6.197**. Additionally, the



introduction of nitrogens in the 4 and 7 positions were explored with analogs **6.204-6.206** as a way to introduced polar surface area in this ring: however, these compounds showed weak mGlu<sub>1</sub> PAM activity.

The attempted modifications in the isoindolinone scaffold demonstrated that there is room for change in the structure, especially when these compounds are compared with the naked isoindolinone **6.194**. The isoindolinone homologues **6.209** and **6.210** maintained mGlu<sub>1</sub> PAM activity, being the 3,4-dihydroisoquinolinone **6.210** the most active of these examples with a submicromolar EC<sub>50</sub> of 780 nM. The oxyindole **6.211** showed low PAM activity while its homologue dihydroquinolinone **6.212** was highly efficacious and had an mGlu<sub>1</sub> PAM potency close to 1 μM. These isoindolinone-related ring systems are interesting, and they could be starting points for more SAR directed to find if their substituted analogs can increase potency on target.

From this group, it was decided to explore further the 4-chloro analog **6.197** VU0487351, as it represented the most potent isoindolinone example. The activity of **6.197** VU0487351 in rat mGlu<sub>1</sub> was evaluated to determine its PAM activity cross-species, and it was found that the compound presented a 2-fold decrease in activity with respect to the human receptor, achieving a potency of 513 nM (93% Glu<sub>Max</sub>). The compound was also analyzed for mGlu selectivity against mGlu<sub>4</sub> and mGlu<sub>5</sub> where it demonstrated to be highly selective, showing over 10 μM potencies and efficacies below 40% in both cases.

The *in vitro* pharmacokinetic properties of **6.197** VU0487351 were analyzed to evaluate its intrinsic clearance and plasma fraction unbound (Table 6.15). VU0487351 displayed moderate clearance in human liver microsomes (40% of the hepatic blood flow) and high clearance in the rat microsomal preparation (77% of the hepatic blood flow) with a clean P450 inhibition profile (1A2, 2D6, 2C9, 3A4). The compound was remarkably stable in plasma, maintaining high concentrations of test article after incubations in this media for 4 hours. However, the main caveat of **6.197** is its small free fraction in plasma and brain homogenate, as it was found to be around 0.1%.

**Table 6.15.** *In vitro* pharmacokinetic properties of isoindolinone **6.197** VU0487351.

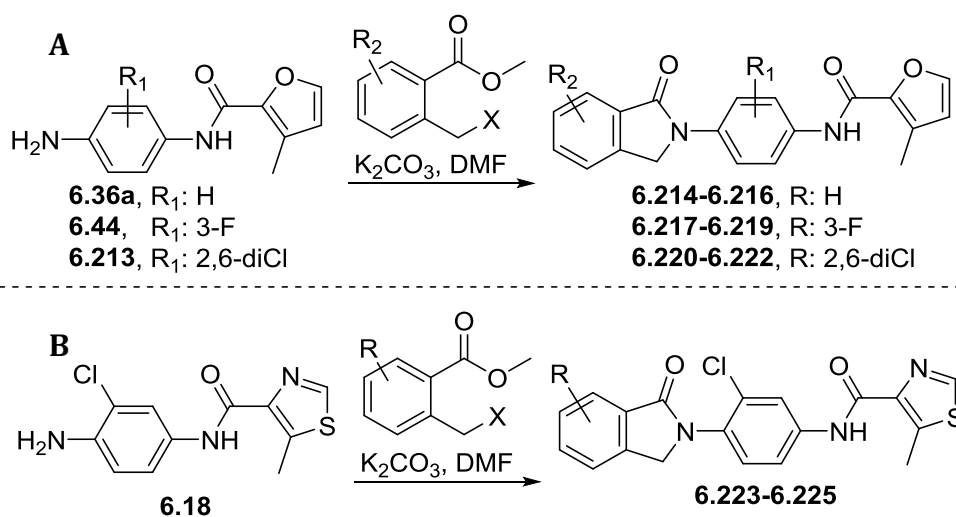
PK parameter	VU0487351
Human Cl <sub>int</sub> (mL/min/kg)	14.4
Human Cl <sub>hep</sub> (mL/min/kg)	8.53
Rat Cl <sub>int</sub> (mL/min/kg)	239
Rat Cl <sub>hep</sub> (mL/min/kg)	54.1
P450 IC <sub>50</sub> (μM) 1A2, 2C9, 2D6, 3A4	>30
Human Plasma Stability (4h)	91%
Rat Plasma Stability (4h)	78%
Human F <sub>u</sub> plasma	<0.001
Rat F <sub>u</sub> plasma	0.001
Rat F <sub>u</sub> Brain	0.001

*In vivo* pharmacokinetic analysis of **6.197** VU0487351 demonstrated that the compound is brain penetrant after IV administration, with a K<sub>p</sub> higher than 1 (Table 6.16). VU0487351 **6.197** displayed a disconnect from its *in vivo* metabolism, as after IV administration it was observed that the compound had low clearance and a half-life close to 90 minutes. The pharmacodynamic and pharmacokinetic properties of VU0487351 **6.197** make this compound the most attractive PAM after VU6004909 **6.48**.

**Table 6.16.** *In vivo* pharmacokinetic properties of isoindolinone **6.197** VU0487351.

PK parameter	VU0487351
$K_p$ (0.2 mg/kg IV, 0.25 h)	1.39
$K_{p,uu}$	1.39
Rat IV PK (0.2 mg/kg IV)	
$t_{1/2}$ (min)	93
$Cl_p$ (mL/min/kg)	11.1
$V_{ss}$ (L/Kg)	3.36

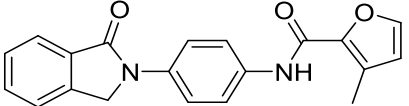
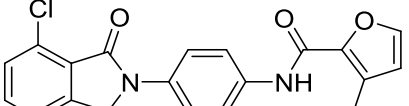
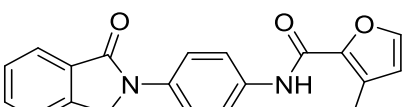
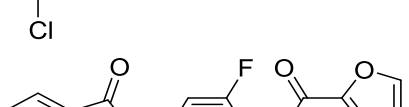
Finally, changes in the central phenyl ring were assessed in the context of the isoindolinones. For this purpose, the naked phenyl ring and the fluoro substituted one were selected as they demonstrated to maintain good potency in the context of the phthalimide. In addition, a dichlorophenyl central ring was employed to assess the effect of hindered rotation on the isoindolinone side, as well as the replacement of the furan of the VU0486321 **5.35c** for the thiazole moiety. The synthesis of analogs to explore different phenyl rings was made as described in scheme 6.15, but using different anilines **6.36a**, **6.44** and **6.213** (Scheme 6.16A). While for the thiazole analogs intermediate **6.18** was employed and reacted with the bromomethylbenzoates to produce isoindolinones **6.223-6.225** (Scheme 6.16B).

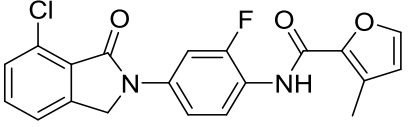
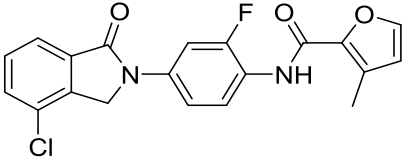
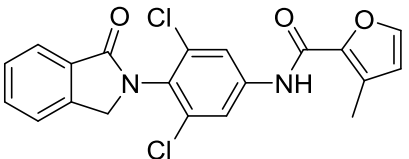
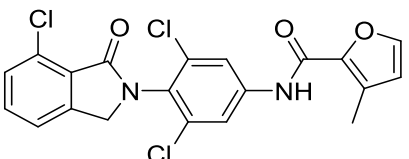
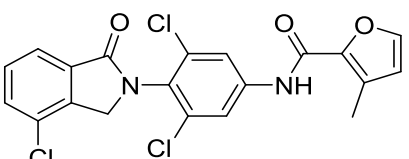
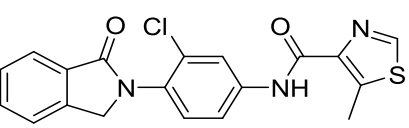
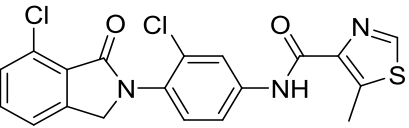
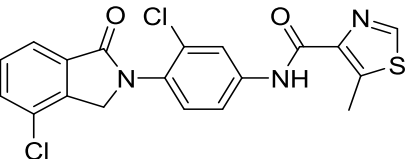


**Scheme 6.16.** Synthesis of isoindolinone analogs of VU0486321 **5.35c** with additional modifications in the central phenyl ring, analogs **6.223-6.225**.

When the analogs were tested in our calcium mobilization assay to obtain their mGlu<sub>1</sub> potencies, it was observed that unsubstituted phenyl ring analogs **6.214-6.216** had similar potencies compared to the chloro substituted phenyl analogs like VU0487351 **6.197**. The fluorophenyl isoindolinones **6.217-6.219** demonstrated that the changes in activity observed in the modified central phenyl ring analogs of the phthalimide cannot be directly extrapolated to the isoindolinone scaffold; as this fluoro substitution was beneficial in the phthalimide scaffold generating compounds with potencies under 25 nM, while in the case of the isoindolinones it induced an important decrease of mGlu<sub>1</sub> PAM activity. The introduction of two chlorines in the ring (**6.220-6.222**) was also detrimental for activity, identifying that hindering rotation around the isoindolinone side of the scaffold is not a good feature for PAM activity on the receptor.

**Table 6.17.** Potencies in human mGlu<sub>1</sub> of isoindolinone related analogs **6.214-6.225**. Calcium mobilization responses for each compound are reported as a percentage of the maximum glutamate response. VU number denotes the compound identifier assigned by Vanderbilt University. Data represent the mean  $\pm$  S.E.M. of at least three independent experiments with similar results. ---, no potentiation. ND, not determined.

Structure	Cpd #	VU #	hmGlu <sub>1</sub>	
			EC <sub>50</sub> ( $\mu$ M)	%Glu <sub>Max</sub>
	<b>6.214</b>	VU6005732	1.60	94
	<b>6.215</b>	VU0487916	0.35	101
	<b>6.216</b>	VU0487915	0.25	100
	<b>6.217</b>	VU6005728	>10	6

	<b>6.218</b>	VU6005686	1.26	86
	<b>6.219</b>	VU6005685	>10	9
	<b>6.220</b>	VU0517623	>10	28
	<b>6.221</b>	VU0517516	6.53	82
	<b>6.222</b>	VU0517528	>10	49
	<b>6.223</b>	VU6003733	>10	33
	<b>6.224</b>	VU6005687	2.67	71
	<b>6.225</b>	VU0517646	0.95	66

Another example of the non-additive behavior of the SAR allosteric modulators was observed with the introduction of the thiazole group (**6.223-6.225**). This ring that engendered potent compounds in the context of the phthalimide, decreased considerably the activity with respect to the furan in the isoindolinone analogs; but, it maintained a similar order in the potencies ( $EC_{50}$  unsubstituted **6.223** > 7-chloro **6.224** > 4-chloro **6.225**).

## Summary and future directions

In an effort to improve the pharmacodynamic and pharmacokinetic properties around the scaffold VU0486321 **5.35c**, its SAR was explored in the furancarboxamide, the central phenyl ring and the phthalimide region. Attempts to replace the 3-methylfuran with other methyl substituted five-member rings produced more tractable SAR compared to the unsubstituted versions tested in chapter 5. From this group, the pyrazole, imidazole, oxazole and thiazole delivered good potencies, and phthalimides focused libraries where synthesized containing these four pieces. Better mGlu<sub>1</sub> PAMs were obtained with the thiazole moiety in terms of potency and selectivity; however, they did not represent an important improvement with respect to VU0486321 **5.35c**. The removal of the carbonyl was also attempted on this side of the molecule, but it caused a complete loss in mGlu<sub>1</sub> PAM.

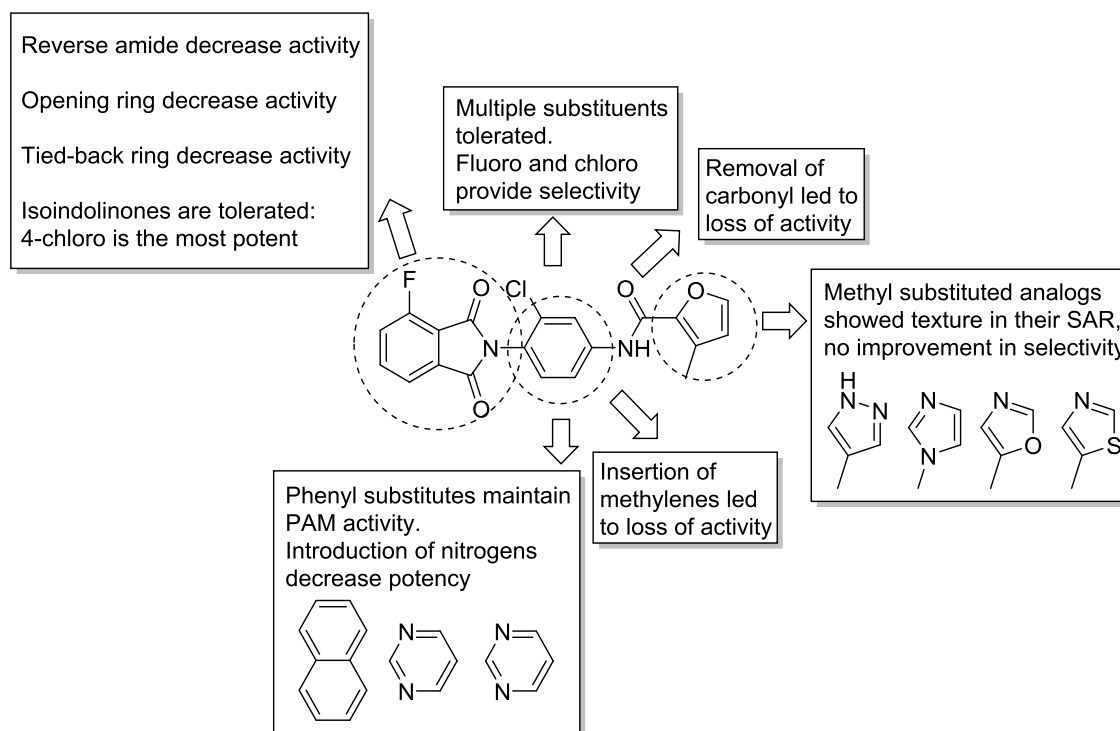


**Figure 6.6.** Structure activity relationship around VU0486321 **5.35c**.

In the central phenyl ring, the insertion of methylenes between the nitrogen and the aromatic ring in either side of the molecule was detrimental for mGlu<sub>1</sub> activity, as well as using saturated hydrocarbon rings such as the cyclohexyl and the cyclobutyl. Additionally, it was found that the ring could tolerate a vast array of small substituents to replace the chlorine, as well as swapping the ring for a pyridine or a naphthalene. In the adjacent position, SAR demonstrated to be tighter, only allowing fluoro, chlorine and methyl substituents; but increasing considerably the selectivity in the case of the fluoro and the chloro analogs. The fluoro **6.37f** was found to be the best of the pair due to its good brain penetration. Additional analogs of **6.37f** with different substitutions in the phthalimide also showed good potency and selectivity. From this group, VU6004909 (**6.48**) stood out due its low clearance and longer half-life of close to five hours. Because of its optimized pharmacodynamic and pharmacokinetic characteristics, VU6004909 **6.48** is the best mGlu<sub>1</sub> PAM that has been reported to date (Fig. 6.7).

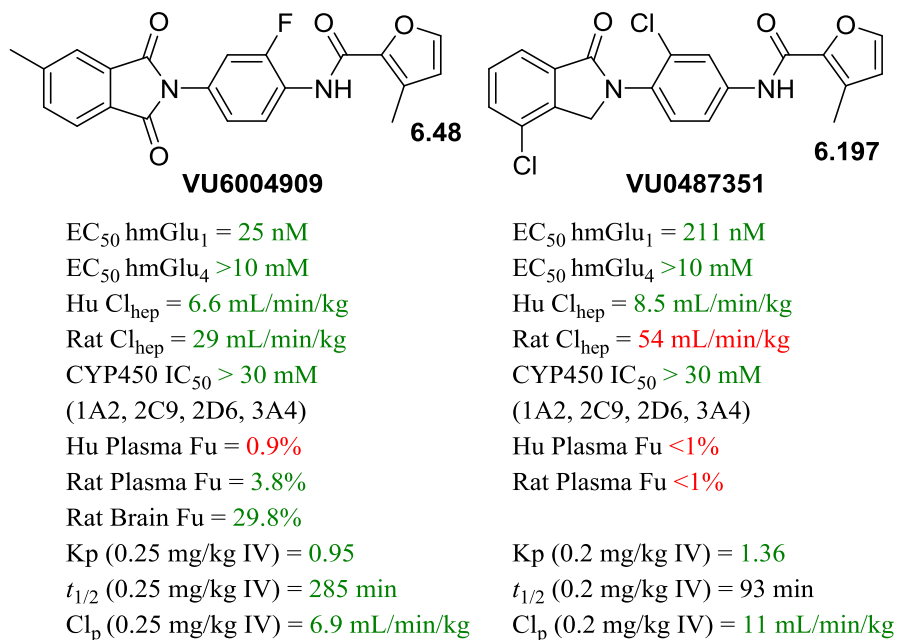


**Figure 6.7.** Pharmacodynamic and pharmacokinetic profile of VU6004909 **6.48** and VU0487351 **6.197**.

Different strategies to replace the phthalimide were also tested in this chapter to develop compounds with no plasma instability. From these efforts, it was observed that ring opening, tied-back ring analogs and reverse amides were not suitable alternatives to the phthalimide group due to a great decrease in potency against the mGlu<sub>1</sub> receptor. The production of isoindolinones was also assayed, as in chapter 4 with analogs of VU0483605 **4.77b**. In the context of the furan, a similar tendency was observed after walking the chlorine around the ring, with the 4-chloroisoindolinone **6.197** (VU0487351) being the most potent analog of this class. Different substituents, the introduction of nitrogens in the ring as well as the homologation of the isoindolinone, were attempted; however, none of these modifications generated a compound with better activity than **6.197**. Interestingly, when the selectivity and pharmacokinetic properties of VU0487351 **6.197** were evaluated, the compound demonstrated to not potentiate the mGlu<sub>4</sub> receptor and to possess relatively good pharmacokinetic properties with an *in vivo* half-life close to 90 minutes, good plasma stability and relatively small plasma fraction unbound (Fig. 6.7).

VU0487351 **6.197** and VU6004909 **6.48** were found to be the best compounds obtained from our efforts in the development of novel mGlu1 PAMS. In the future, we plan to analyze the pharmacokinetic properties of these compounds using different routes of administration besides intravenous, and to determine the best way to deliver the PAMs into animals. Once this is clarified, the effect of these modulators will be evaluated in *in vivo* behavioral assays such as amphetamine or MK-801 induced hyperlocomotion and prepulse inhibition, typical models that try to imitate relevant features of the schizophrenic phenotype. Additionally, an effort to characterize the consequences of *in vitro* mGlu<sub>1</sub> activation in neurons has recently been initiated in the laboratory of P. Jeffrey Conn. Preliminary electrophysiological studies have shown that the application of VU6004909 potentiates the decrease in dopamine release in the striatum, a desirable feature for antipsychotic activity.



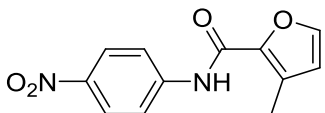
## EXPERIMENTAL METHODS

### *General chemical synthesis and characterization*

All reactions were carried out employing standard chemical techniques under inert atmosphere. All reagents and solvents were commercial grade and purified prior to use when necessary. Solvents used for extraction, washing, and chromatography were HPLC grade. Analytical thin layer chromatography was performed on 250  $\mu\text{m}$  silica gel glass backed plates from Sorbent Technologies. Visualization was accomplished with UV light, and/or the use of iodine or ninhydrin solution followed by heating. Analytical HPLC was performed on an Agilent 1200 LCMS with UV detection at 215 and 254 nm along with ELSD detection and electrospray ionization, with all final compounds showing >95% purity and a parent mass ion consistent with the desired structure. Low resolution mass spectra were obtained on an Agilent 6130 mass spectrometer with electrospray ionization source. MS parameters were as follows: fragmentor: 100, capillary voltage: 3000 V, nebulizer pressure: 40 psig, drying gas flow: 11 L/min, drying gas temperature: 350° C. Samples were introduced via an Agilent 1200 HPLC comprised of a degasser, G1312A binary pump, G1367B HP-ALS, G1316A TCC, G1315D DAD, and a Varian 380 ELSD. UV absorption was generally observed at 215 nm and 254 nm with a 4 nm bandwidth. Column: Thermo Accucore C18, 2.1 x 30 mm, 2.6  $\mu\text{m}$ . Gradient conditions: 7% to 95%  $\text{CH}_3\text{CN}$  in  $\text{H}_2\text{O}$  (0.1% TFA) over 1.6 min, hold at 95%  $\text{CH}_3\text{CN}$  for 0.35 min, 1.5 mL/min, 45° C. Flash column chromatography was performed on a Teledyne ISCO Combiflash Rf system. Preparative purification of library compounds was performed on a Gilson 215 preparative LC system. Column: Thermo Accucore C18, 2.1 x 30 mm, 2.6  $\mu\text{m}$ . Gradients condition: variable,  $\text{CH}_3\text{CN}$  in  $\text{H}_2\text{O}$  (0.1% TFA) over 4 minutes, hold at 95%  $\text{CH}_3\text{CN}$  for 0.35 min, 50 mL/min. Purity for all final compounds was >95%, and each showed a parent mass ion consistent with the desired structure in low resolution LC-MS.  $^1\text{H}$  and  $^{13}\text{C}$  NMR spectra were recorded on Bruker DRX-400 (400 MHz) instrument. Chemical shifts are reported in ppm relative to residual solvent

peaks as an internal standard at the following chemical shifts ( $^1\text{H}$  and  $^{13}\text{C}$  respectively): 7.26 and 77.0 ppm for  $\text{CDCl}_3$ ; 2.50 and 39.52 ppm for  $\text{DMSO}-d_6$ , 3.31 and 49.2 ppm for  $\text{CD}_3\text{OD}$ . Data are reported as follows: chemical shift, integration, multiplicity (s = singlet, d = doublet, t = triplet, q = quartet, dd = doublet of doublets, br = broad, m = multiplet), coupling constant (Hz).

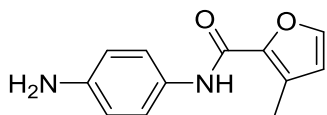
**General synthesis *N*-(nitroaryl)-3-methylfuran-2-carboxamide (6.35a-6.35l).** In a microwave vial, the aromatic amine (1.2 equiv.) was added and dissolved in a mixture DCE:DIEA (9:1) (concentration of the amine 0.15 M), followed by addition of 3-methylfuran-carbonyl chloride. The reaction was heated in the microwave at 120 °C for 30 minutes. The reaction was cooled to room temperature and water was added, causing the precipitation of the product. The crude product was filtrated *in vacuo* and titrated with cold methanol to give product.



**3-methyl-*N*-(4-nitrophenyl)furan-2-carboxamide (6.35a).** Cream solid.  $^1\text{H-NMR}$  (400.1 MHz,  $\text{DMSO}-d_6$ )  $\delta$  (ppm): 8.35 (1H, s), 8.26 (2H, d,  $J=9.2$  Hz), 7.85 (2H, d,  $J=9.1$  Hz), 7.43 (1H, d,  $J=1.3$  Hz), 6.46 (1H, d,  $J=1.3$  Hz), 2.48 (3H, s).  $^{13}\text{CNMR}$  (100.6 MHz,  $\text{DMSO}-d_6$ )  $\delta$  (ppm): 157.1, 143.5, 143.4, 143.1, 141.2, 130.6, 125.1, 118.9, 116.2, 11.3

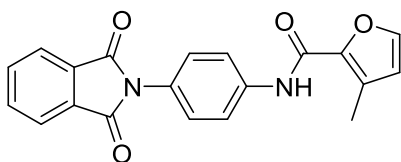
**General synthesis *N*-(aminoaryl)-3-methylfuran-2-carboxamide (6.36a-6.36l).** In a flask, the corresponding nitroaryl **6.35** (1.0 equiv.) was suspended in dioxane (0.1 M concentration of **6.35**). The suspension was cold in an ice bath and purged with argon. A previously prepared solution of tin(II) chloride (4.5 equiv.) in concentrated hydrochloric acid (5M concentration of  $\text{SnCl}_2$ ) was added dropwise to the suspension. After 2 hour of stirring at room temperature, the reaction was neutralized carefully with aqueous potassium carbonate 20%,

filtered and extracted with diethyl ether. The organic phase was dried with magnesium sulfate, filtered and the volatiles eliminated *in vacuo* to yield product.

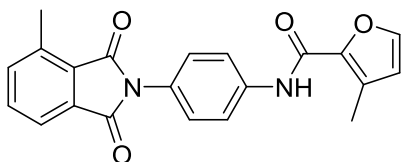


***N*-(4-aminophenyl)-3-methylfuran-2-carboxamide (6.36a).** Yellow solid.  $^1\text{H-NMR}$  (400.1 MHz,  $\text{CDCl}_3$ )  $\delta$  (ppm): 7.97 (1H, s), 7.39 (2H, d,  $J=8.4$  Hz), 7.31 (1H, s), 6.65 (2H, d,  $J=8.4$  Hz), 6.36 (1H, s), 3.59 (2H, s), 2.43 (3H, s).  $^{13}\text{CNMR}$  (100.6 MHz,  $\text{CDCl}_3$ )  $\delta$  (ppm): 157.3, 143.3, 142.2, 142.1, 128.8, 128.1, 121.8, 115.6, 115.4, 11.2.

**General synthesis *N*-(4-(1,3-dioxisoindolin-2-yl)aryl)-3-methylfuran-2-carboxamide (6.37a-6.37l).** In a vial, the corresponding aniline **6.36** (1.0 equiv.) and the corresponding phthalic anhydride (1.5 equiv.) were added and dissolved in acetic acid (0.12 M concentration of the aniline). The mixture was heated at 110 °C while stirring for 4 hours. After this time, volatiles were evaporated, the crude product was dissolved in DMSO and purified by preparative HPLC.

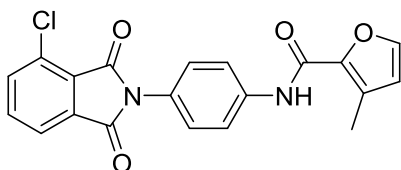


***N*-(4-(1,3-dioxisoindolin-2-yl)phenyl)-3-methylfuran-2-carboxamide (6.37a1).** Cream solid.  $^1\text{H-NMR}$  (400.1 MHz,  $\text{CDCl}_3$ )  $\delta$  (ppm): 8.13 (1H, s), 7.95 (2H, m), 7.80 (4H, m), 7.44 (2H, m), 7.39 (1H, d,  $J=1.5$  Hz), 6.41 (1H, d,  $J=1.5$  Hz), 2.47 (3H, s).  $^{13}\text{CNMR}$  (100.6 MHz,  $\text{CDCl}_3$ )  $\delta$  (ppm): 167.3, 157.2, 142.6, 141.7, 137.4, 134.3, 131.7, 129.3, 127.3, 127.2, 123.7, 120.0, 115.9, 11.2.



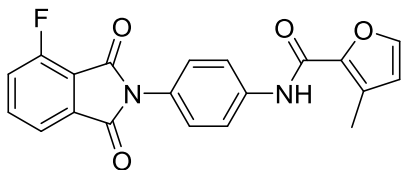
**3-methyl-N-(4-(4-methyl-1,3-dioxisoindolin-2-yl)phenyl)furan-2-carboxamide**

**(6.37a2).** Cream solid.  $^1\text{H-NMR}$  (400.1 MHz,  $\text{CDCl}_3$ )  $\delta$  (ppm): 8.14 (1H, s), 7.79 (3H, m), 7.64 (1H, t,  $J= 7.5$  Hz), 7.53 (1H, d,  $J= 7.8$  Hz), 7.43 (2H, d,  $J= 8.8$  Hz), 7.38 (1H, d,  $J= 1.5$  Hz), 6.41 (1H, d,  $J= 1.5$  Hz), 2.75 (3H, s), 2.47 (3H, s).  $^{13}\text{CNMR}$  (100.6 MHz,  $\text{CDCl}_3$ )  $\delta$  (ppm): 167.8, 167.3, 157.2, 142.5, 141.7, 138.4, 137.3, 136.7, 133.8, 132.1, 129.2, 128.3, 127.4, 127.2, 121.3, 119.9, 115.9, 17.7, 11.2.



**N-(4-(4-chloro-1,3-dioxisoindolin-2-yl)phenyl)-3-methylfuran-2-carboxamide**

**(6.37a3).** Cream solid.  $^1\text{H-NMR}$  (400.1 MHz,  $\text{CDCl}_3$ )  $\delta$  (ppm): 8.14 (1H, s), 7.88 (1H, t,  $J= 4.1$  Hz), 7.80 (2H, d,  $J= 8.8$  Hz), 7.71 (2H, m), 7.44 (2H, d,  $J= 8.8$  Hz), 7.38 (1H, d,  $J= 1.4$  Hz), 6.41 (1H, d,  $J= 1.4$  Hz), 2.46 (3H, s).  $^{13}\text{CNMR}$  (100.6 MHz,  $\text{CDCl}_3$ )  $\delta$  (ppm): 165.8, 164.8, 157.3, 142.6, 141.7, 137.6, 136.1, 135.2, 133.8, 131.8, 129.4, 127.3, 127.2, 126.9, 122.2, 120.0, 115.9, 11.2.

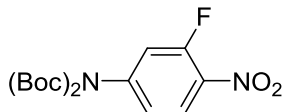


**N-(4-(4-fluoro-1,3-dioxisoindolin-2-yl)phenyl)-3-methylfuran-2-carboxamide**

**(6.37a4).** Cream solid.  $^1\text{H-NMR}$  (400.1 MHz,  $\text{CDCl}_3$ )  $\delta$  (ppm): 8.14 (1H, s), 7.80 (4H, m), 7.45

(3H, m), 7.39 (1H, d,  $J = 1.5$  Hz), 6.42 (1H, d,  $J = 1.5$  Hz), 2.46 (3H, s).  $^{13}\text{C}$ NMR (100.6 MHz, DMSO- $d_6$ )  $\delta$  (ppm): 166.5, 164.4, 157.9, 157.3 ( $^1J_{\text{CF}}=261.0$  Hz), 144.1, 142.1, 138.9, 138.0 ( $^3J_{\text{CF}}=7.8$  Hz), 134.3, 128.5, 128.1, 127.1, 123.0 ( $^2J_{\text{CF}}=19.8$  Hz), 121.0, 120.3 ( $^4J_{\text{CF}}=3.0$  Hz), 117.9 ( $^2J_{\text{CF}}=12.4$  Hz), 116.1, 11.5.

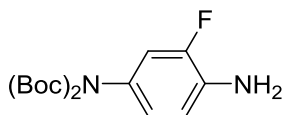
**General synthesis of bis Boc-protected nitroanilines (638m-6.38o and 6.42).** In a flask, the corresponding nitroaniline (1.0 equiv.) was added and dissolved in THF (0.2 M concentration of the aniline). Then, di-*tert*-butyl dicarbonate (2.2 equiv.) was added, followed by DMAP (0.2 equiv.). The mixture was stirred at room temperature and monitored by LC-MS. The reaction was stopped when full conversion to the bis Boc-protected nitroaniline was observed with no sign of the mono-Boc product. The reaction was worked up by the addition of water and performing successive extractions with DCM. The organic phases were combined, dried with anhydrous  $\text{MgSO}_4$ , filtered and concentrated *in vacuo*.



**Bis(tert-butyl)(3-fluoro-4-nitrophenyl)carbamate (6.42).** White solid.  $^1\text{H}$ -NMR (400.1 MHz,  $\text{CDCl}_3$ )  $\delta$  (ppm): 8.08 (1H, t,  $J=8.6$  Hz), 7.15 (1H, dd,  $J=11.4$ ,  $J=2.1$ ), 7.11 (1H, m), 1.46 (18H, s).  $^{13}\text{C}$ NMR (100.6 MHz,  $\text{CDCl}_3$ )  $\delta$  (ppm): 155.3 ( $^1J_{\text{CF}}=266$  Hz), 150.4, 145.5 ( $^2J_{\text{CF}}=10.0$  Hz), 135.7 ( $^3J_{\text{CF}}=7.2$  Hz), 126.1 ( $^4J_{\text{CF}}=1.5$  Hz), 123.8 ( $^3J_{\text{CF}}=3.9$  Hz), 117.7 ( $^2J_{\text{CF}}=22.5$  Hz), 84.2, 27.7.

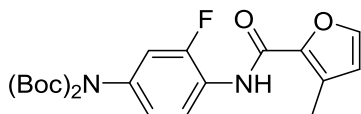
**General synthesis of bis Boc-protected aminoanilines (639m-6.39o and 6.43).** In a flask, the corresponding Boc-protected nitroaniline (1.0 equiv.) was added and dissolved in ethanol (0.1 M concentration of the aniline). Then 10% Pd/C was added (50 mg/mmol of nitroaniline). The flask was filled with argon and evacuated three times. This procedure was repeated with hydrogen, maintaining the system under hydrogen after last purge. The mixture was

stirred at room temperature and monitored by LC-MS. The reaction was stopped when full conversion to the bis Boc-protected aminoaniline was observed with no sign of starting material. The product was obtained by filtration of the reaction matrix through a celite pad, washing with DCM and evaporating the volatiles from the filtrate *in vacuo*.



**Bis(tert-butyl)(4-amino-3-fluorophenyl)carbamate (6.43).** Yellow oil.  $^1\text{H-NMR}$  (400.1 MHz,  $\text{CDCl}_3$ )  $\delta$  (ppm): 6.76 (1H, d,  $J=11.6$  Hz), 6.69 (2H, m), 3.77 (2H, br s), 1.40 (18H, s).  $^{13}\text{CNMR}$  (100.6 MHz,  $\text{CDCl}_3$ )  $\delta$  (ppm): 152.0, 150.6 ( $^1J_{\text{CF}}=239$  Hz), 134.0 ( $^2J_{\text{CF}}=12.68$  Hz), 129.5 ( $^3J_{\text{CF}}=9.0$  Hz), 124.0 ( $^4J_{\text{CF}}=3.0$  Hz), 116.0 ( $^3J_{\text{CF}}=4.3$  Hz), 115.1 ( $^2J_{\text{CF}}=20.0$  Hz), 84.5, 27.8.

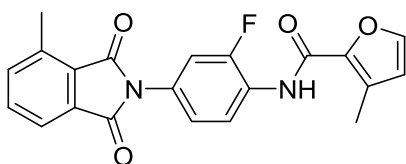
**General synthesis of bis Boc *N*-(aminoaryl)-3-methylfuran-2-carboxamides (6.40m-6.40o and 6.44).** In a flask, the corresponding bis Boc-protected aminoaniline (1.2 equiv.) was added and dissolved in a mixture DCE:DIEA (9:1) (concentration of the amine 0.15 M), followed by addition of 3-methylfuran-carbonyl chloride. The reaction was stirred at room temperature and monitored by LC-MS. The reaction was stopped when full conversion to the furancarboxamide was observed with no sign of starting material. The reaction was worked up by the addition of water and successive extractions with DCM. The organic phases were combined, dried with  $\text{MgSO}_4$ , filtered and the volatiles concentrated *in vacuo*. The crude product was purified by silica gel flash chromatography, using a gradient of hexanes:EtOAc.



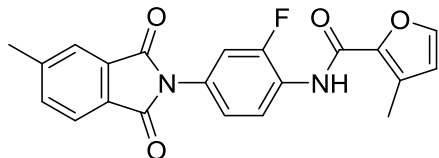
**Bis(tert-butyl)(3-fluoro-4-(3-methylfuran-2-carboxamido)phenyl)carbamate (6.44).** White solid.  $^1\text{H-NMR}$  (400.1 MHz,  $\text{CDCl}_3$ )  $\delta$  (ppm): 8.41 (1H, dd,  $J=9.0$  Hz,  $J=8.6$  Hz), 8.24 ( $J=2.8$  Hz), 7.32 ( $J=1.6$  Hz), 6.90 (1H, m), 6.87 (1H, m), 6.33 ( $J=1.6$  Hz), 2.38 (3H, s), 1.35

(18H, s).  $^{13}\text{C}$ NMR (100.6 MHz,  $\text{CDCl}_3$ )  $\delta$  (ppm): 157.1, 151.5 ( $^1J_{\text{CF}}=244.5$  Hz), 151.4, 142.9, 141.6, 134.7 ( $^3J_{\text{CF}}=9.7$  Hz), 129.5, 125.6 ( $^3J_{\text{CF}}=9.7$  Hz), 124.2 ( $^4J_{\text{CF}}=3.1$  Hz), 120.5, 115.9, 114.8 ( $^2J_{\text{CF}}=20.7$  Hz), 82.9, 27.8, 11.2.

**General synthesis *N*-(4-(1,3-dioxoisindolin-2-yl)aryl)-3-methylfuran-2-carboxamides (6.37m-6.37o and 6.45-6.51).** In a vial, the corresponding bis Boc-protected aniline (1.0 equiv.) was added and dissolved in DCM (0.1 M concentration of the bis Boc-protected aniline). TFA was added drop wise to a final concentration of 10% v/v. The reaction was stirred at room temperature for and monitored by LC-MS. The reaction was stopped when full deprotection of the starting material was observed. The reaction was worked up by evaporating the volatiles *in vacuo* and the product was use crude for the subsequent step. In a vial, the crude deprotected aniline (1.0 equiv.) and the corresponding phthalic anhydride (1.5 equiv.) were added and dissolved in acetic acid (0.12 M concentration of the aniline). The mixture was heated at 110 °C while stirring for 4 hours. After this time, volatiles were evaporated, the crude product was dissolved in DMSO and purified by preparative HPLC.



***N*-(2-fluoro-4-(4-methyl-1,3-dioxoisindolin-2-yl)phenyl)-3-methylfuran-2-carboxamide (6.45).** Pale yellow solid.  $^1\text{H}$ -NMR (400.1 MHz,  $\text{CDCl}_3$ )  $\delta$  (ppm): 8.64 (1H, dd,  $J=9.1$  Hz,  $J=8.6$  Hz), 8.39 (1H, br s), 7.80 (1H, d,  $J=7.3$  Hz), 7.66 (1H, t,  $J=7.3$  Hz), 7.56 (1H, d,  $J=7.7$  Hz), 7.43 ( $J=1.4$  Hz), 7.30-7.36 (m, 2H), 6.44 (1H, d,  $J=1.4$  Hz), 2.77 (3H, s), 2.49 (3H, s).  $^{13}\text{C}$ NMR (100.6 MHz,  $\text{CDCl}_3$ )  $\delta$  (ppm): 167.6, 166.9, 157.1, 151.8 ( $^1J_{\text{CF}}=244.2$  Hz), 143.0, 141.6, 138.6, 136.8, 134.0, 131.9, 129.7, 128.1, 127.1 ( $^3J_{\text{CF}}=10.0$  Hz), 126.0 ( $^3J_{\text{CF}}=10.0$  Hz), 122.6 ( $^4J_{\text{CF}}=3.3$  Hz), 121.4, 121.0, 115.9, 113.4 ( $^2J_{\text{CF}}=22.3$  Hz), 17.7, 11.2.

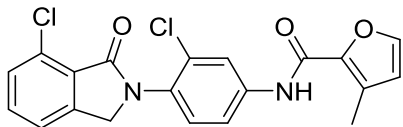


***N*-(2-fluoro-4-(5-methyl-1,3-dioxisoindolin-2-yl)phenyl)-3-methylfuran-2-**

**carboxamide (6.48).** Pale yellow solid.  $^1\text{H-NMR}$  (400.1 MHz,  $\text{CDCl}_3$ )  $\delta$  (ppm): 8.62 (1H, dd,  $J=9.2$  Hz,  $J=8.5$  Hz), 8.35 (1H, d,  $J=2.2$  Hz), 7.83 (1H, d,  $J=7.7$  Hz), 7.75 (1H, s), 7.58 (1H, d,  $J=7.6$  Hz), 7.41 (1H, d,  $J=1.6$  Hz), 7.34-7.28 (2H, m), 6.41 (1H, d,  $J=1.5$  Hz), 2.55 (3H, s), 2.46 (3H, s).  $^{13}\text{CNMR}$  (100.6 MHz,  $\text{CDCl}_3$ )  $\delta$  (ppm): 167.1, 166.9, 157.1, 151.7 ( $^1J_{\text{CF}}=245.0$  Hz), 145.9, 142.9, 141.6, 135.1, 131.9, 129.7, 128.9, 127.2 ( $^3J_{\text{CF}}=10.0$  Hz), 126.9 ( $^3J_{\text{CF}}=9.9$  Hz), 124.3, 123.7, 122.5 ( $^4J_{\text{CF}}=3.5$  Hz), 121.0, 115.9, 113.3 ( $^2J_{\text{CF}}=22.3$  Hz), 22.0, 11.2.

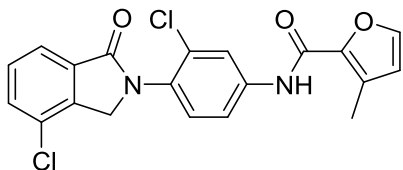
**General procedure for the synthesis of *N*-(3-chloro-4-(1-oxisoindolin-2-yl)phenyl)-3-methylfuran-2-carboxamide (6.194-6.206).** In a microwave vial, the corresponding methyl bromomethylbenzoate (0.085 mmol, 1.2 equiv.) and aniline (0.0709, 1.0 equiv.) were added and dissolved in 1 mL of DMF. Then,  $\text{K}_2\text{CO}_3$  (0.141 mmol, 2.0 equiv.) was added and the vial was sealed. The reaction was heated in the microwave at 150 °C for 15 minutes. The reaction was monitored by LC-MS and a second round of heating was applied if there was presence of starting material or the acyclic ester intermediate. The reaction was worked up by addition of water and successive extractions with DCM. The organic phases were filtered through a phase separator, combined and volatiles were evaporated *in vacuo*. Crude products were dissolved in DMSO and purified by preparative HPLC.





***N*-(3-chloro-4-(7-chloro-1-oxoisindolin-2-yl)phenyl)-3-methylfuran-2-carboxamide**

**(6.195).**  $^1\text{H-NMR}$  (400.1 MHz,  $\text{CDCl}_3$ )  $\delta$  (ppm): 8.22 (1H, s), 8.00 (1H, d,  $J= 2.4$  Hz), 7.56 (1H,  $J= 8.5$  Hz,  $J= 2.4$  Hz), 7.52 (1H, d,  $J= 7.5$  Hz), 7.47 (1H, d,  $J= 7.5$  Hz), 7.41 (1H, d,  $J= 7.4$  Hz), 7.36 (2H, m), 6.41 (1H, d,  $J= 1.5$  Hz), 4.75 (2H, s), 2.46 (3H, s).  $^{13}\text{CNMR}$  (100.6 MHz,  $\text{CDCl}_3$ )  $\delta$  (ppm): 165.9, 157.3, 144.0, 142.8, 141.5, 138.5, 132.9, 132.7, 132.2, 130.8, 130.2, 129.9, 129.7, 127.9, 121.3, 121.2, 118.7, 116.0, 51.1, 11.2.



***N*-(3-chloro-4-(4-chloro-1-oxoisindolin-2-yl)phenyl)-3-methylfuran-2-carboxamide**

**(6.197).**  $^1\text{H-NMR}$  (400.1 MHz,  $\text{CDCl}_3$ )  $\delta$  (ppm): 8.16 (1H, s), 8.02 (1H, d,  $J= 2.3$  Hz), 7.87 (1H,  $J= 7.4$  Hz), 7.59 (2H, m), 7.51 (1H, t,  $J= 7.7$  Hz), 7.38 (2H, m), 6.42 (1H), 4.78 (2H, s), 2.47 (3H, s).  $^{13}\text{CNMR}$  (100.6 MHz,  $\text{CDCl}_3$ )  $\delta$  (ppm): 167.3, 157.2, 142.8, 141.4, 139.8, 138.6, 133.9, 133.1, 131.9, 130.7, 130.1, 129.9, 129.8, 129.2, 129.8, 129.2, 122.8, 121.1, 118.7, 116.0, 51.4, 11.2.

*Molecular pharmacology*

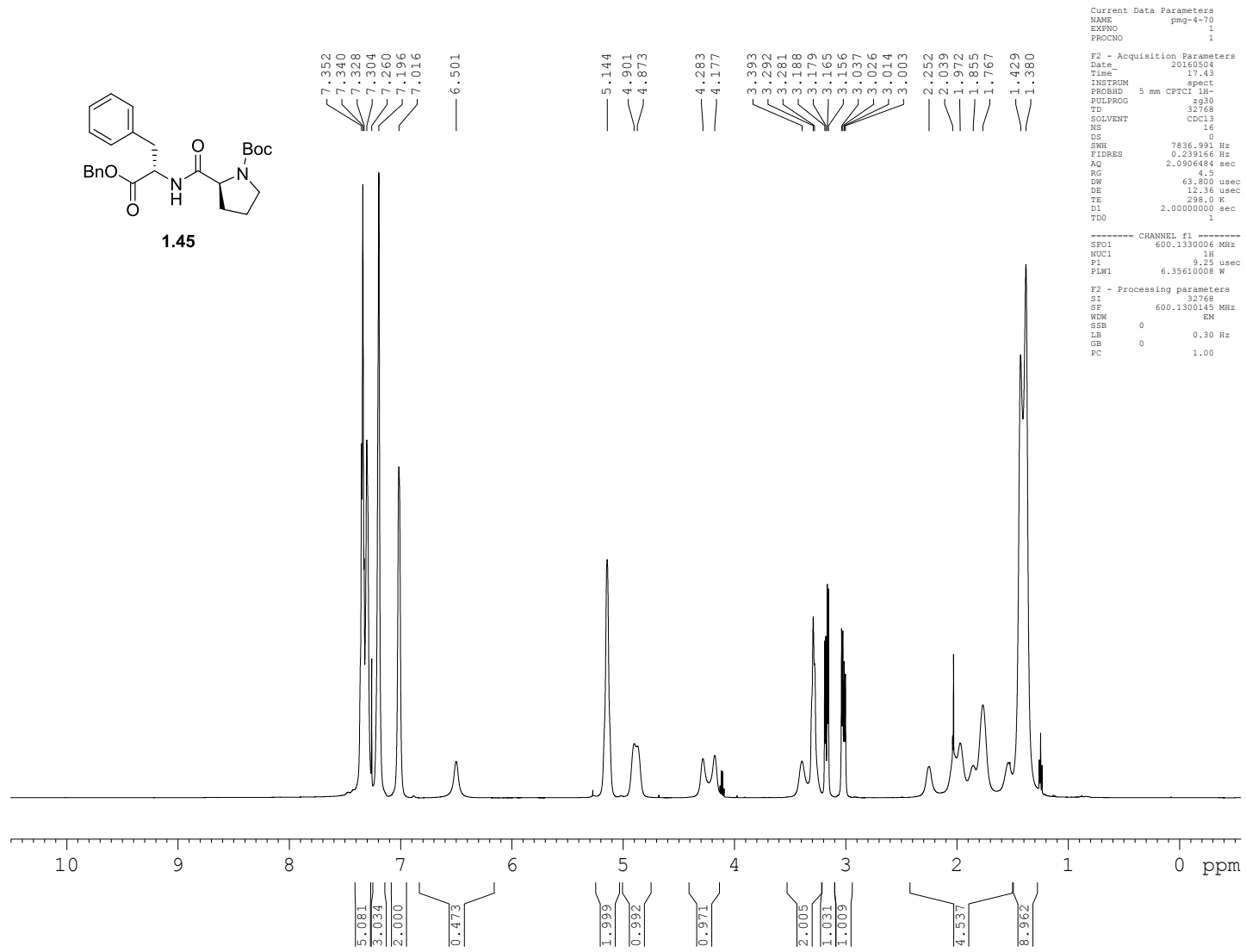
Molecular pharmacology experiments to characterize the mGlu<sub>1</sub> PAMs were performed following the procedures in chapter 3 and 4.

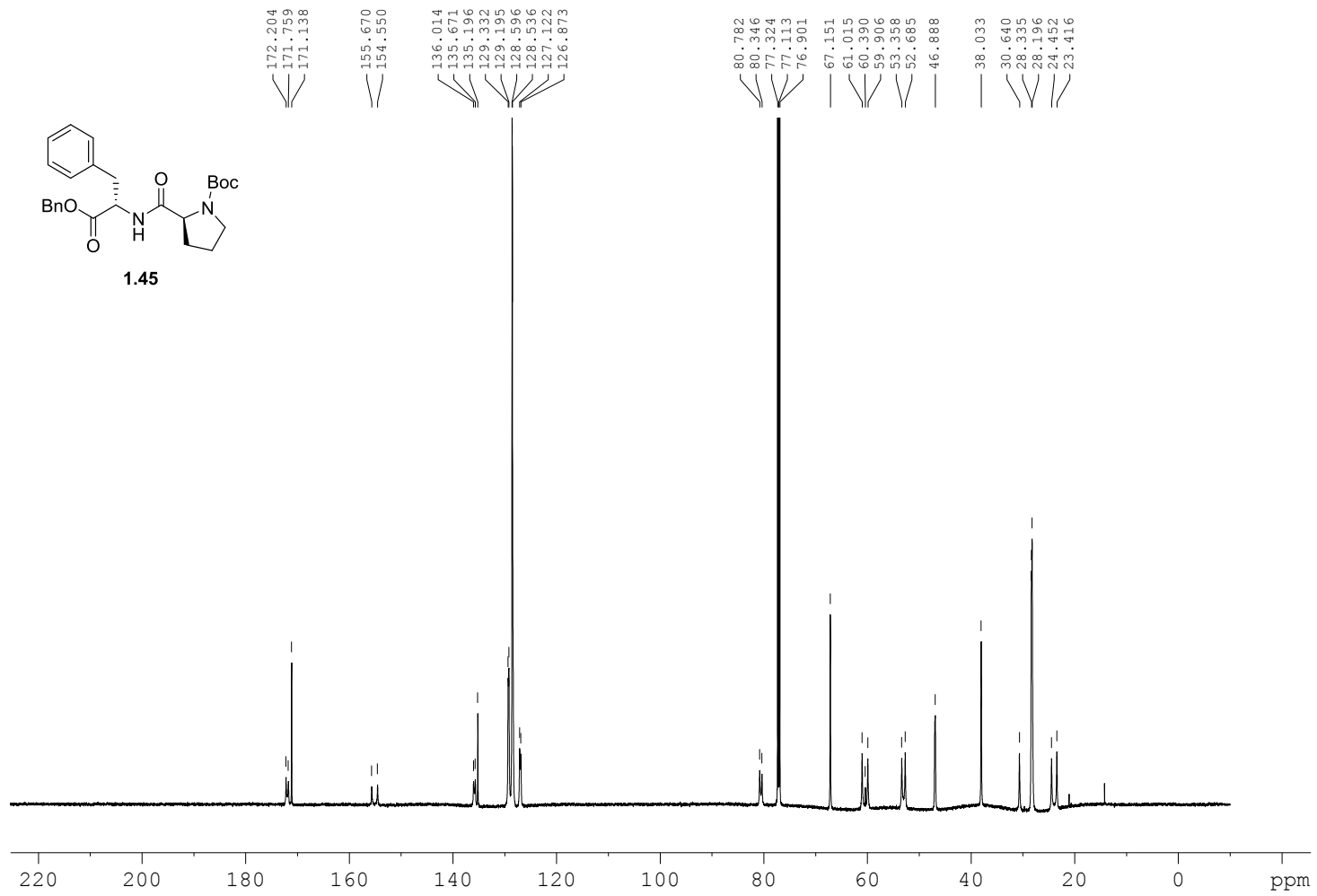
### *Pharmacokinetic characterization*

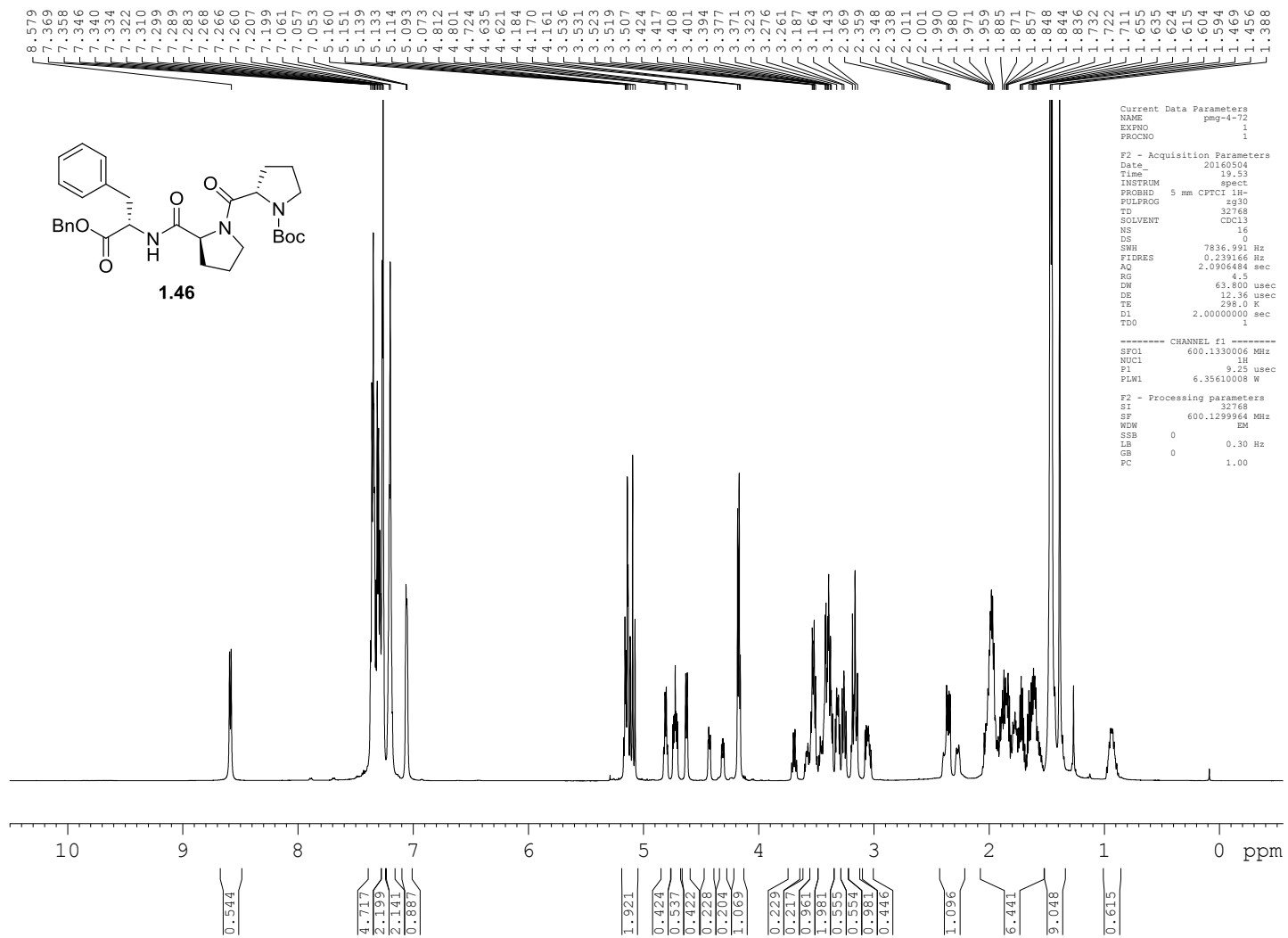
The *in vitro* DMPK assays, including those assessing hepatic microsomal intrinsic clearance ( $Cl_{int}$ ), cytochrome P450 inhibition, plasma protein binding (PPB) and brain homogenate binding (BHB) were performed as described previously.<sup>285</sup> The experimental procedures for the pharmacokinetic characterization of the compounds are described in chapter 3.

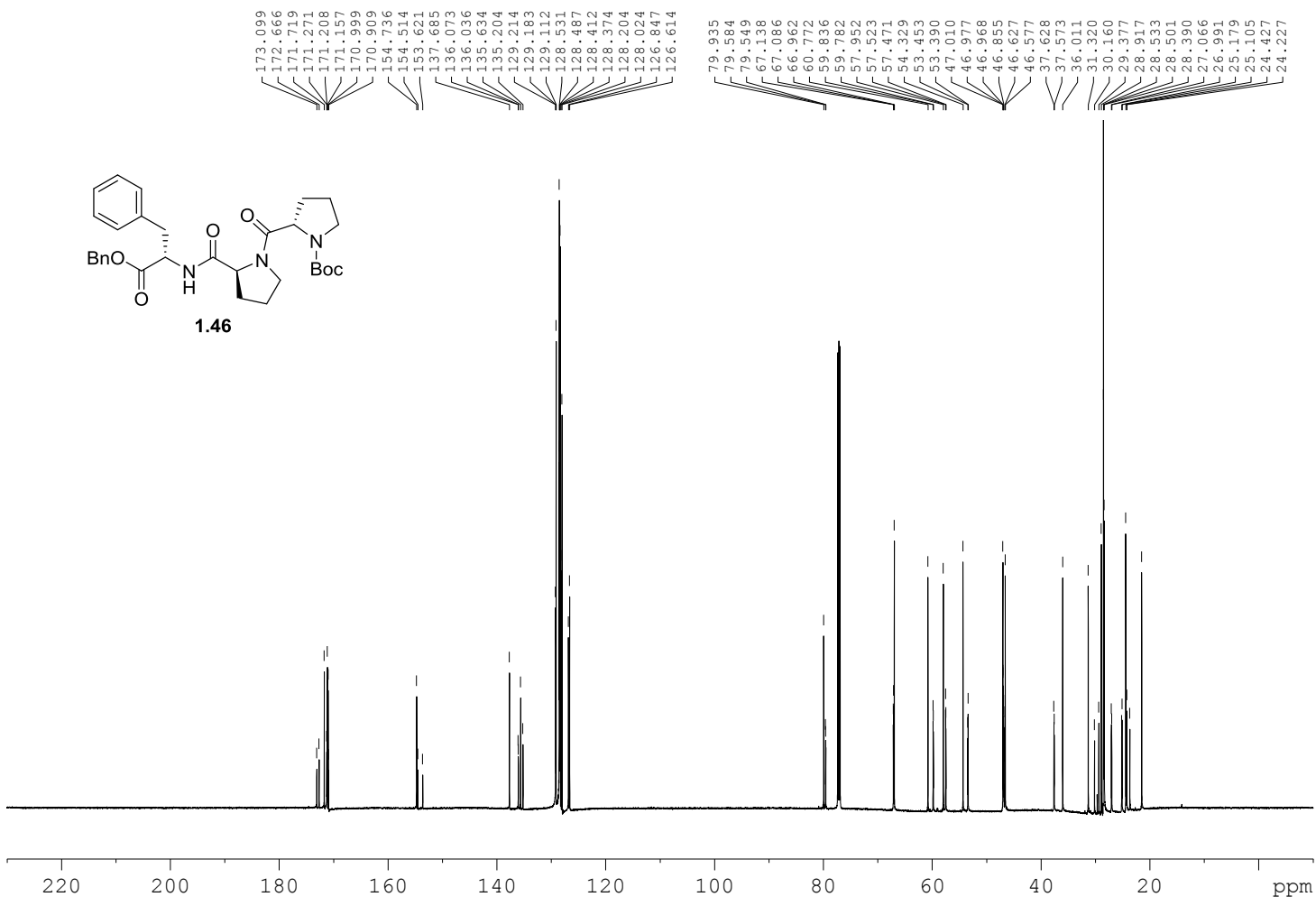
# Appendix A

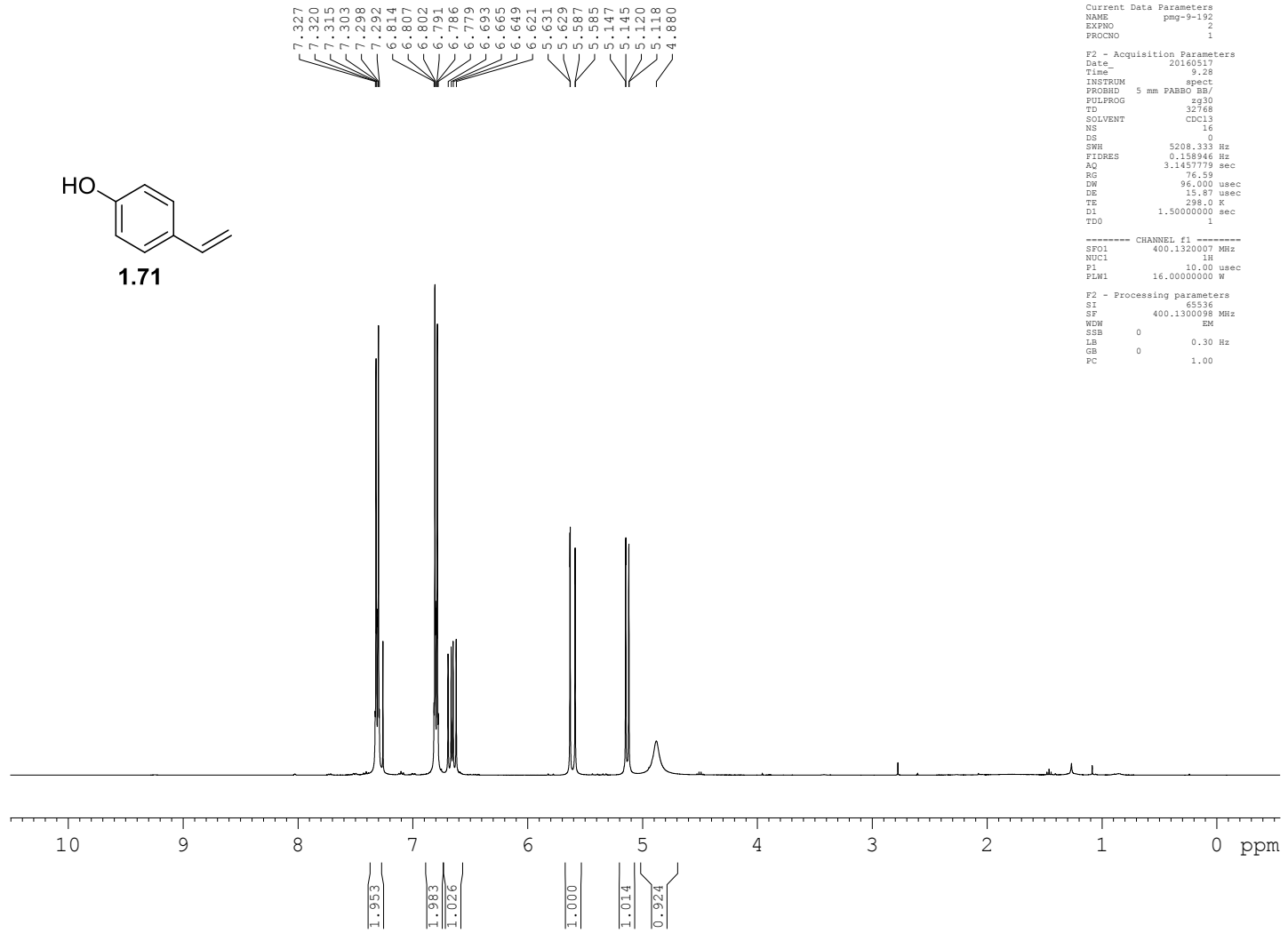
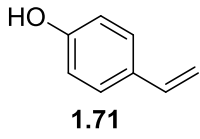
Relevant spectra for chapter I



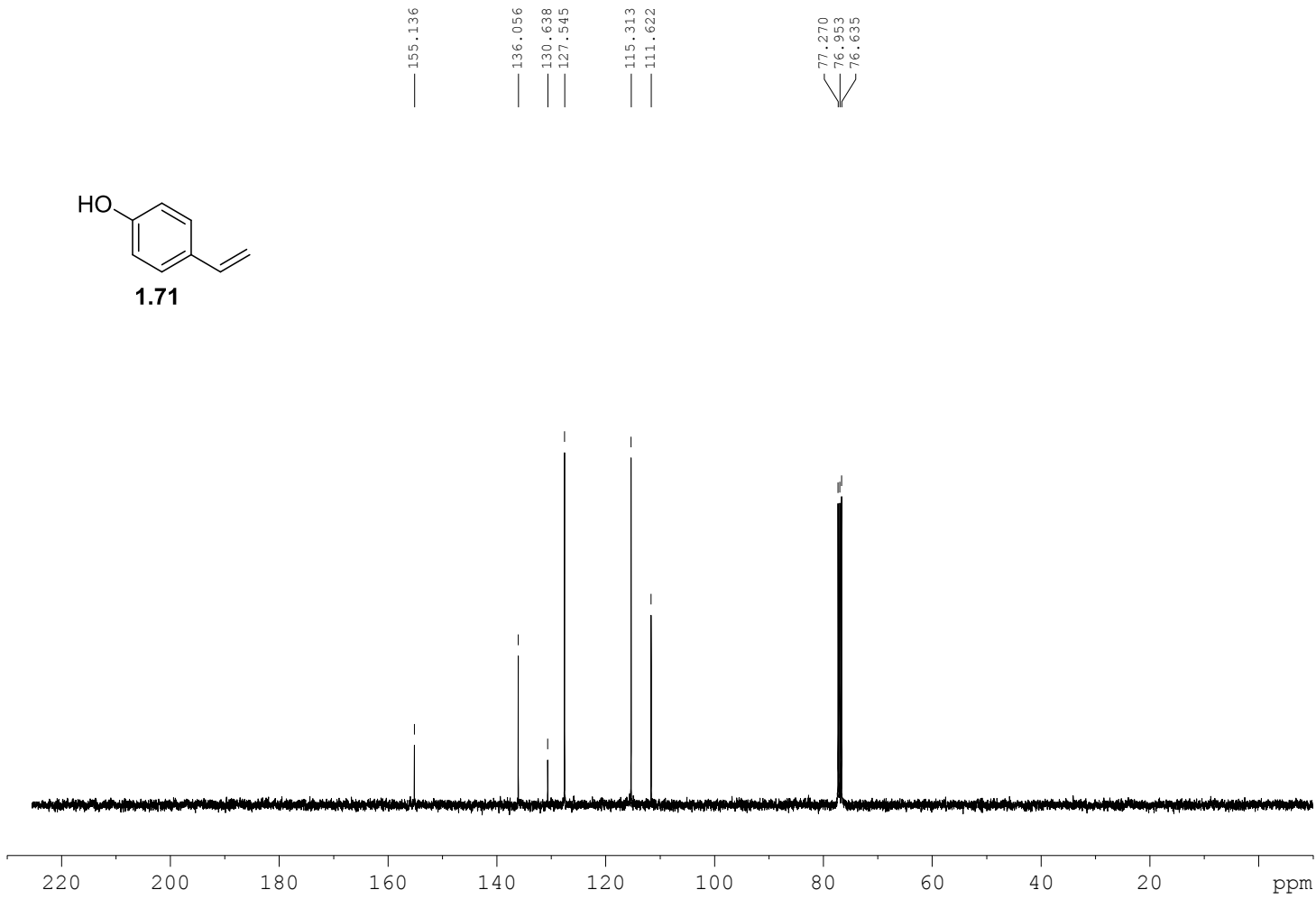
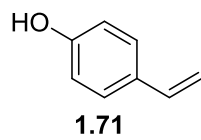


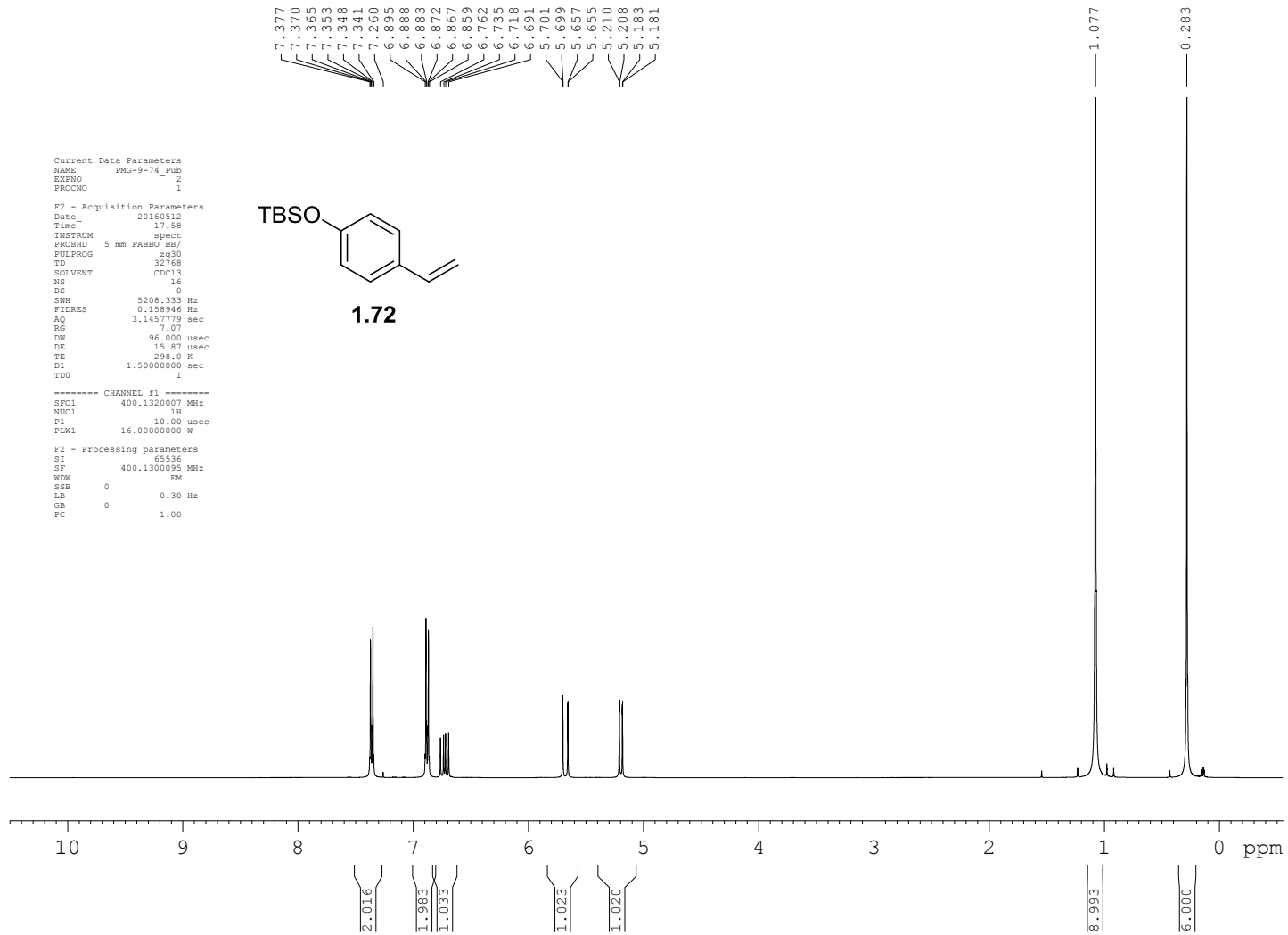


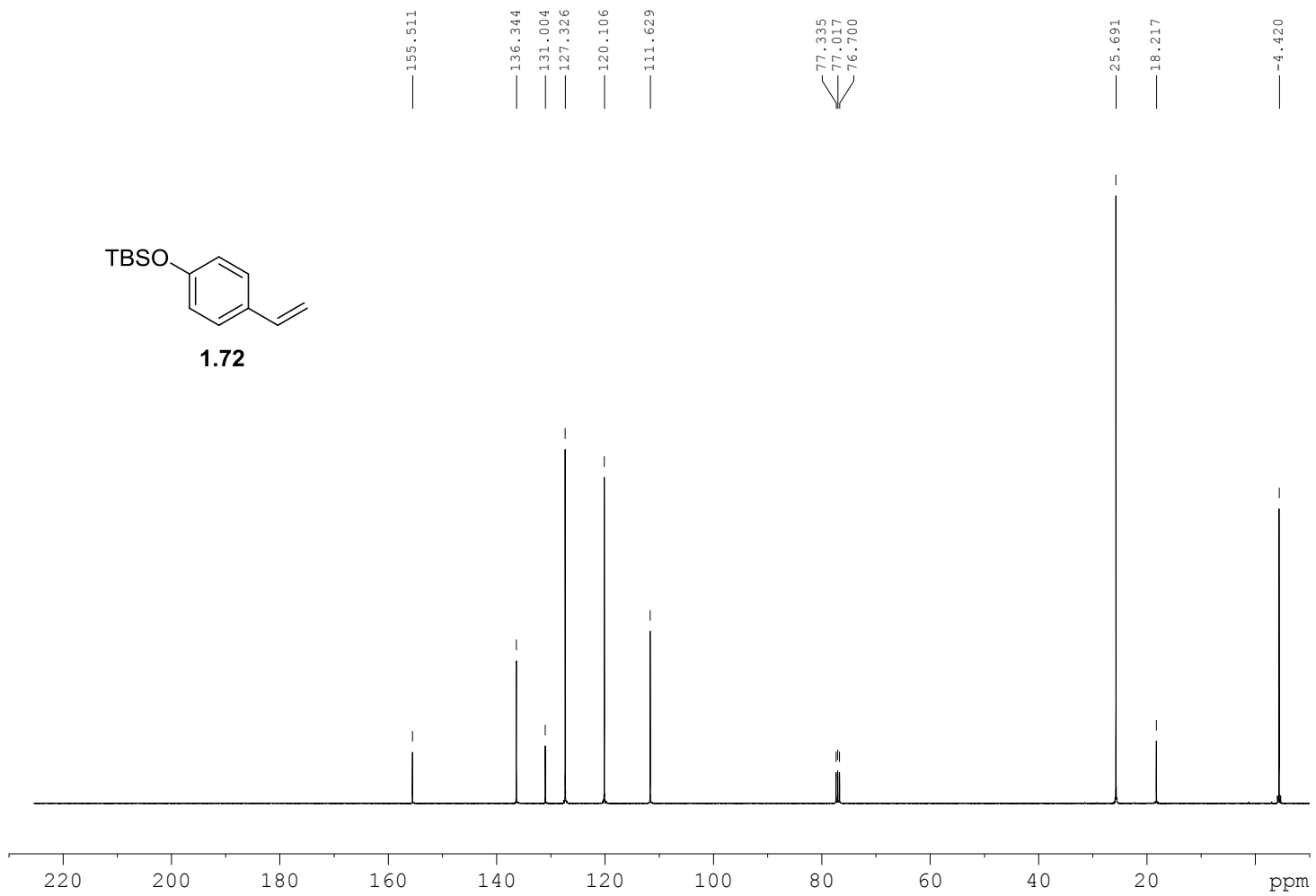
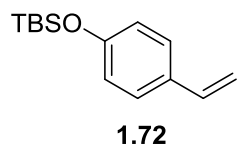


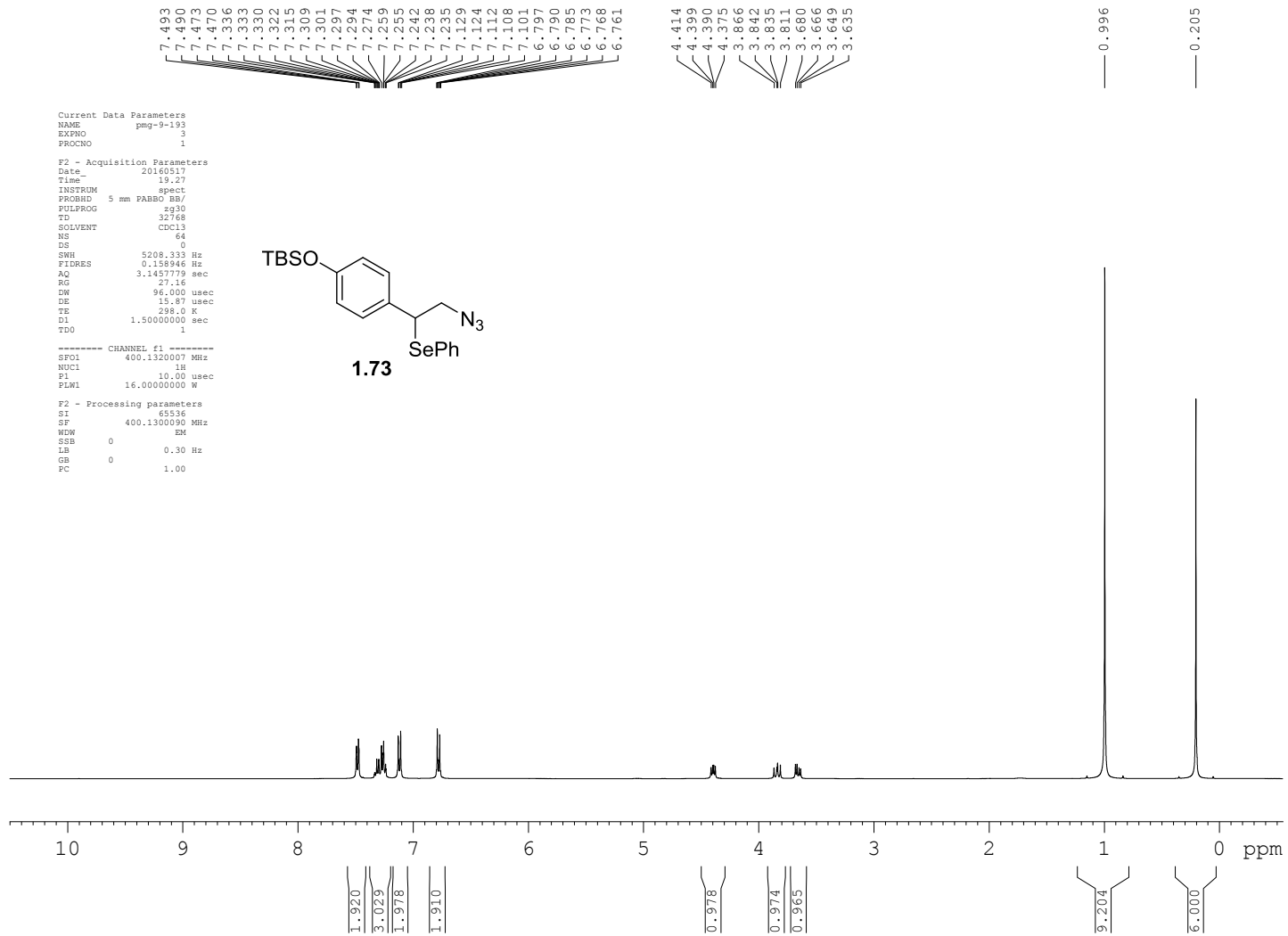


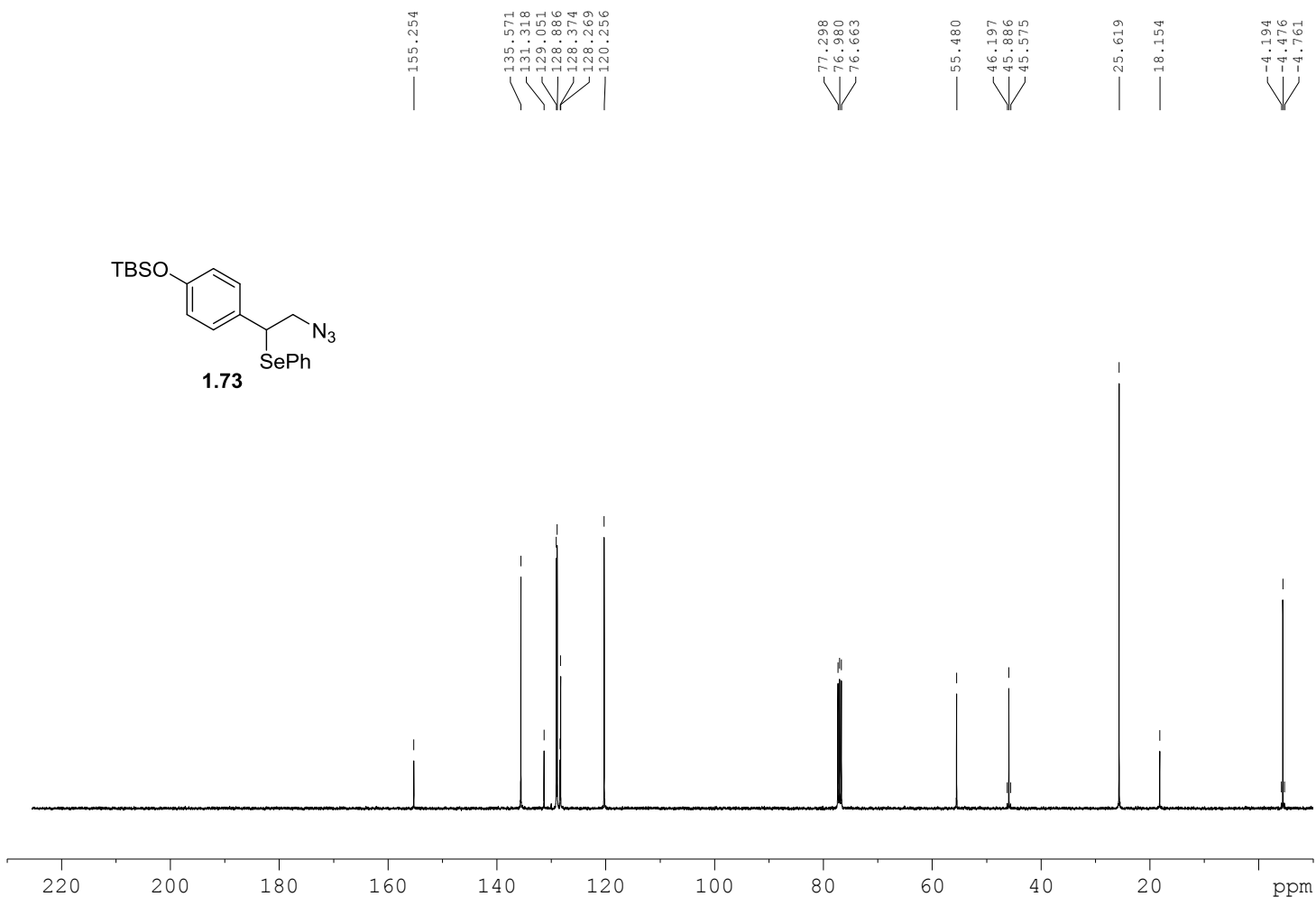
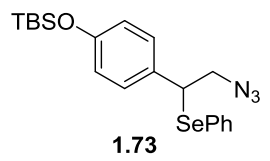


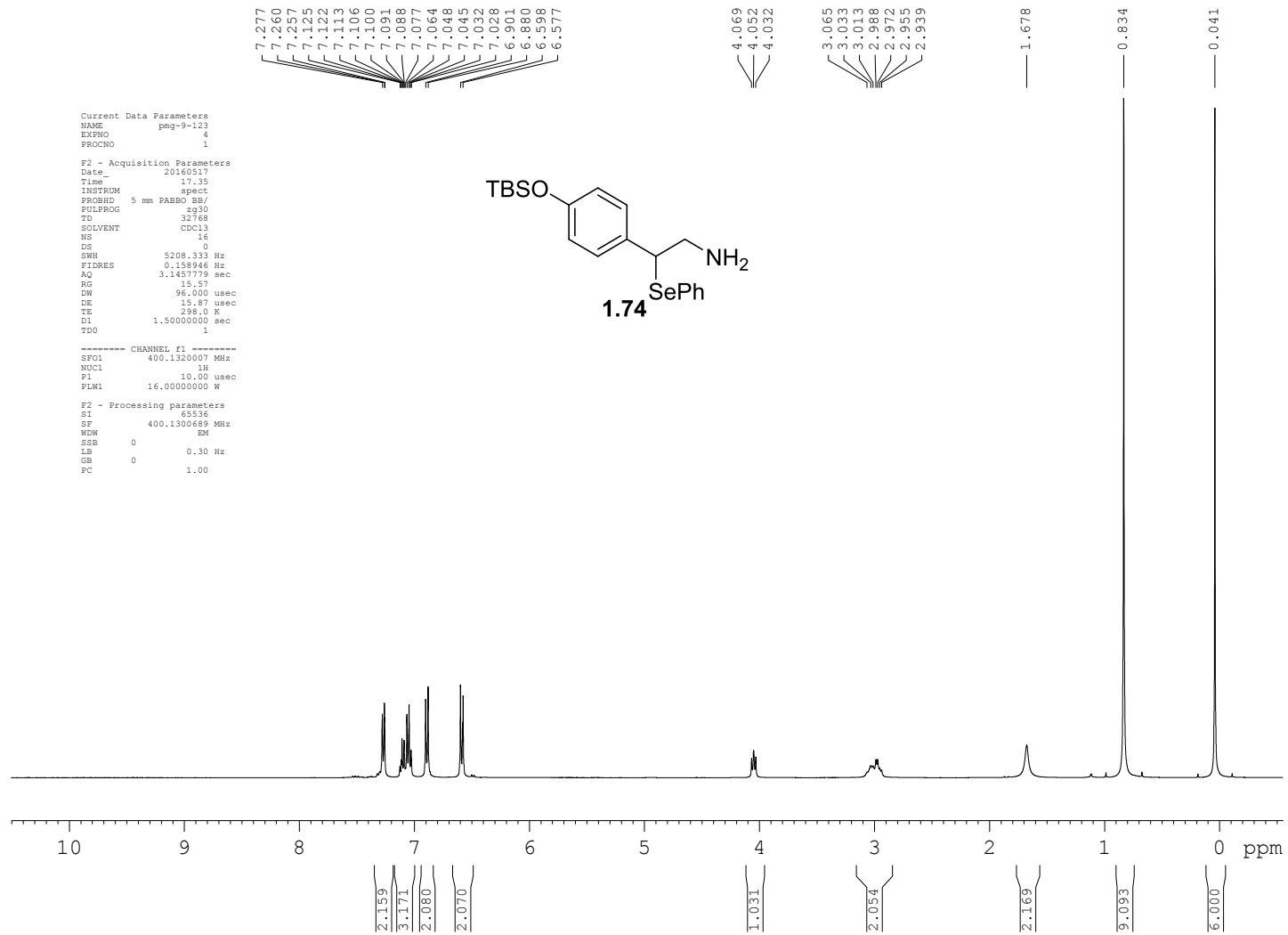




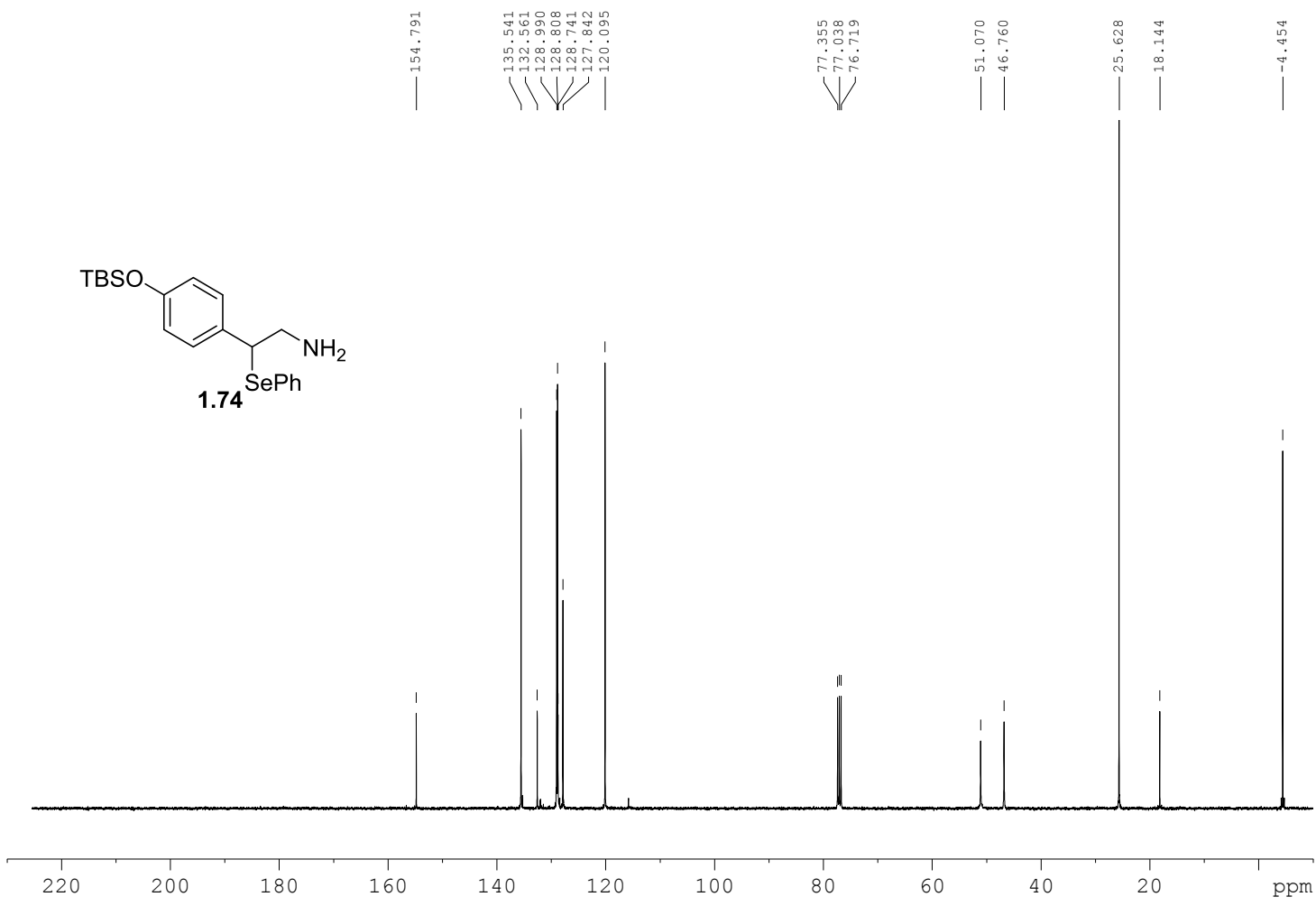


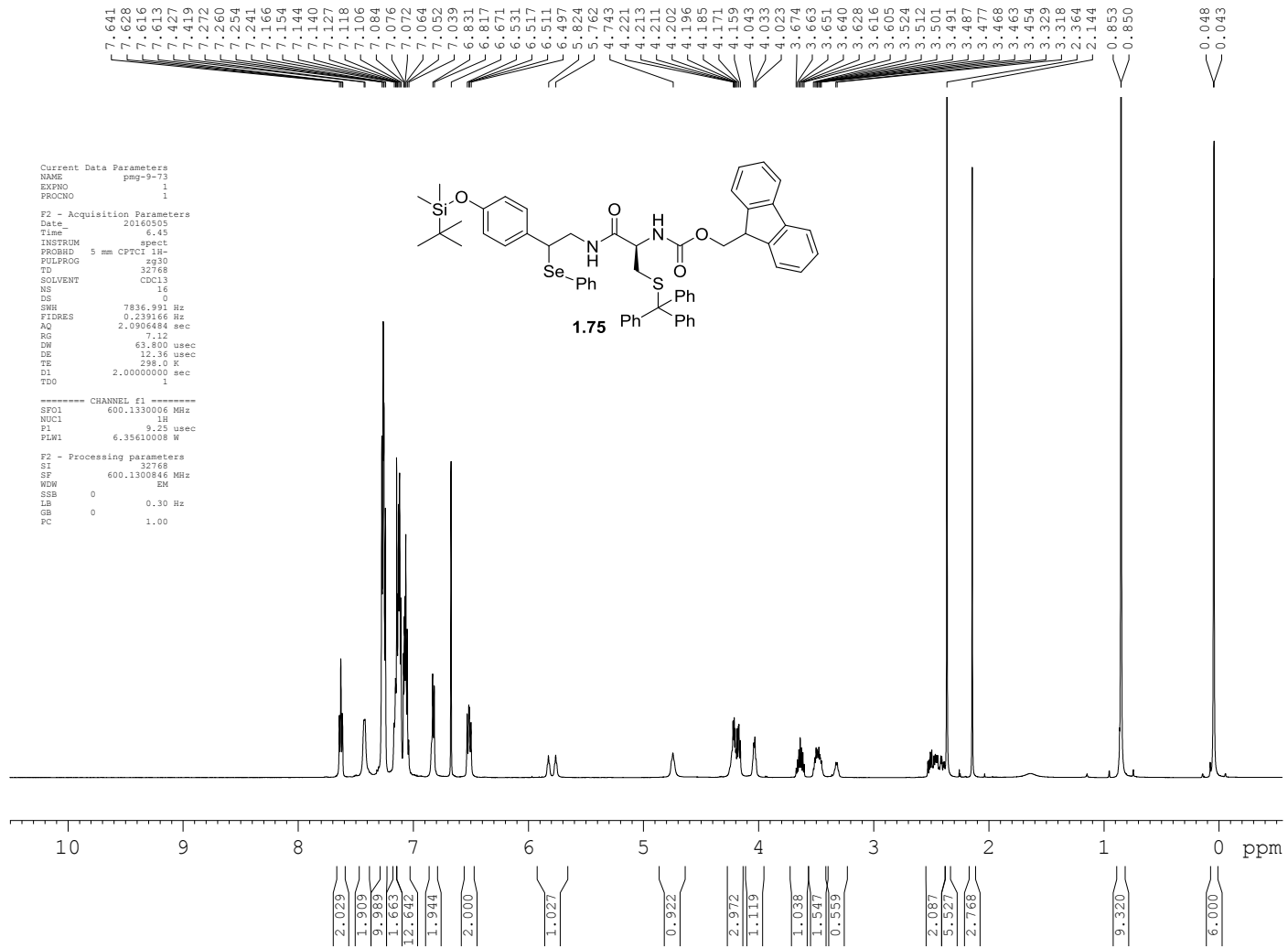




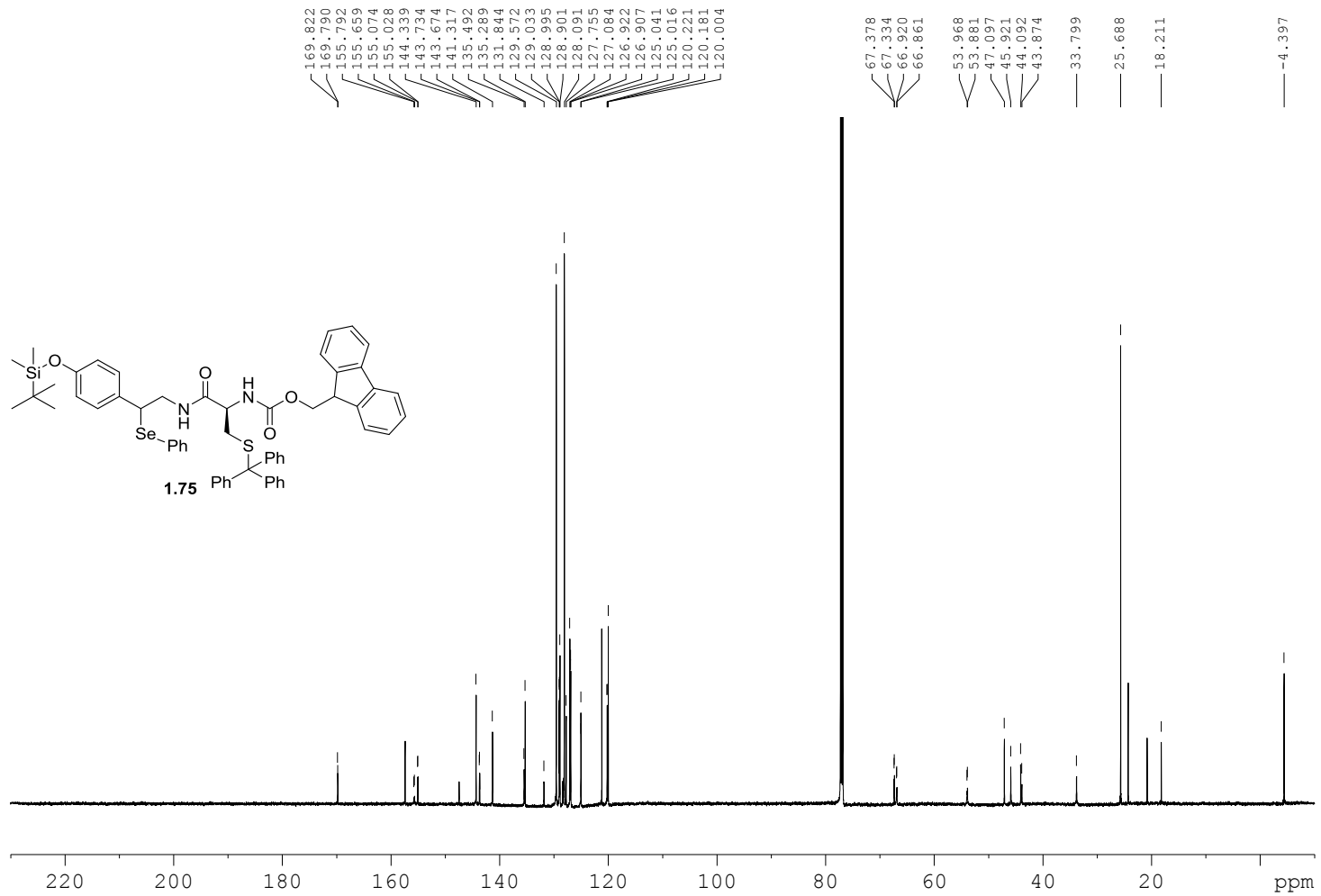


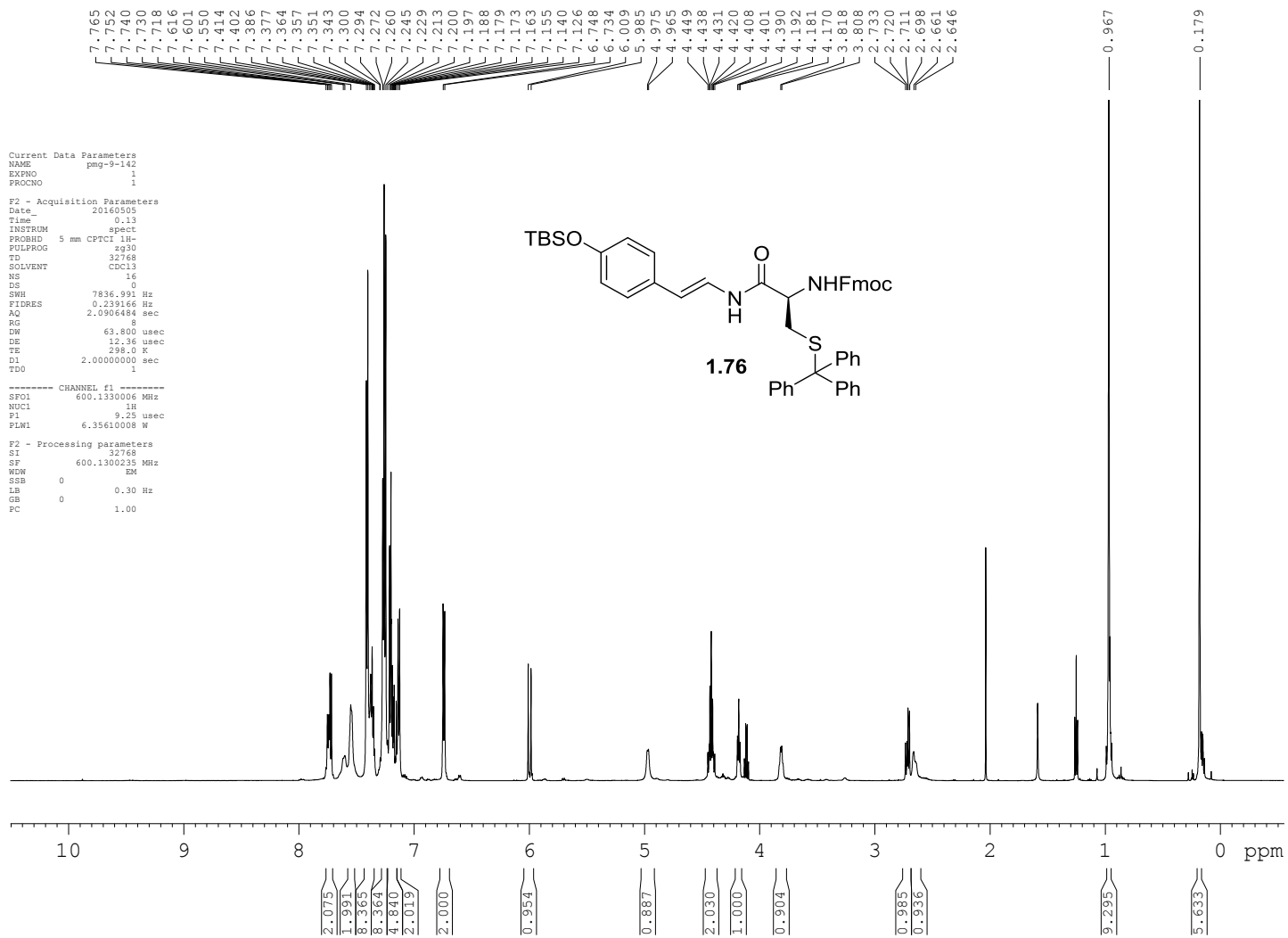
350



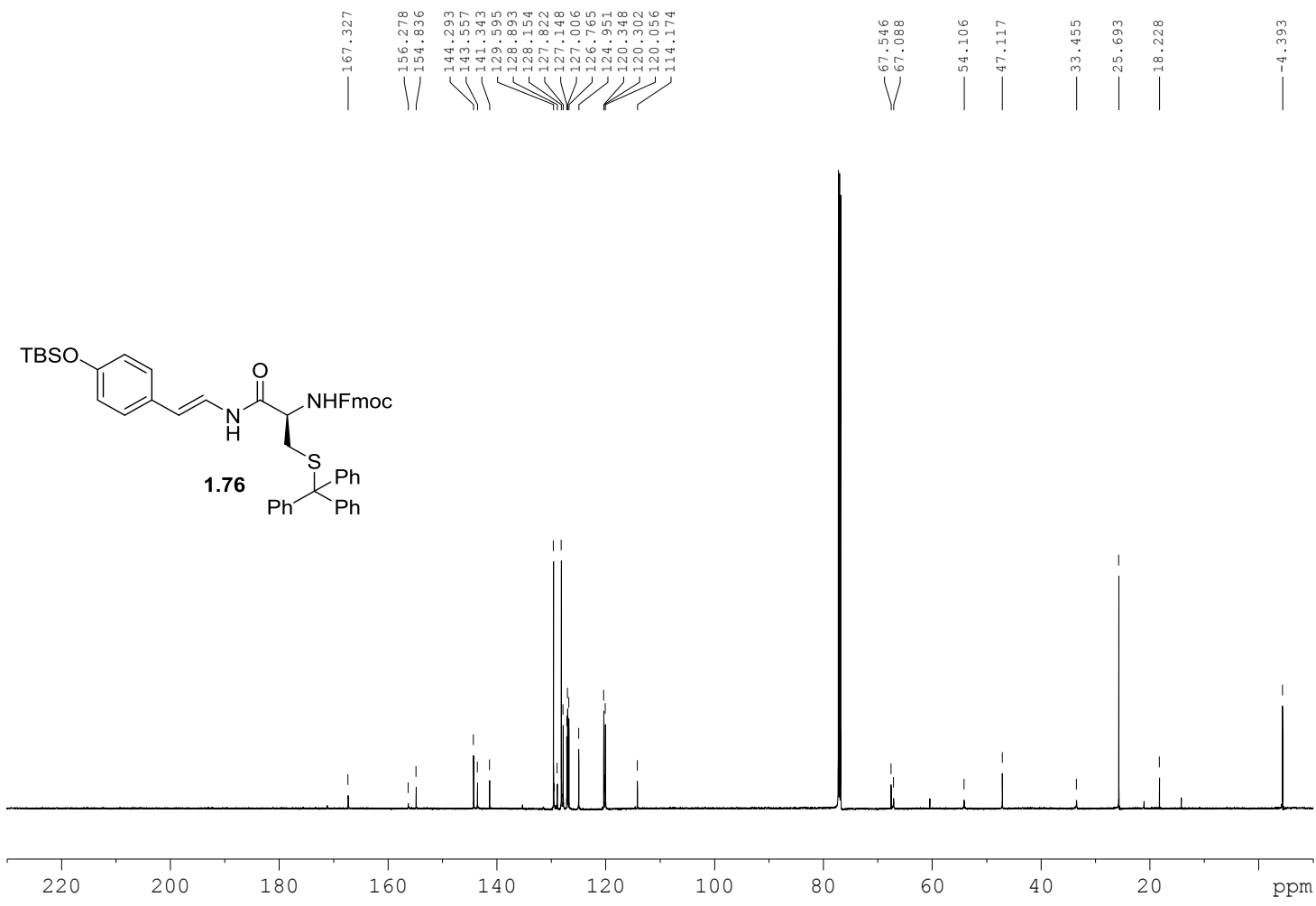


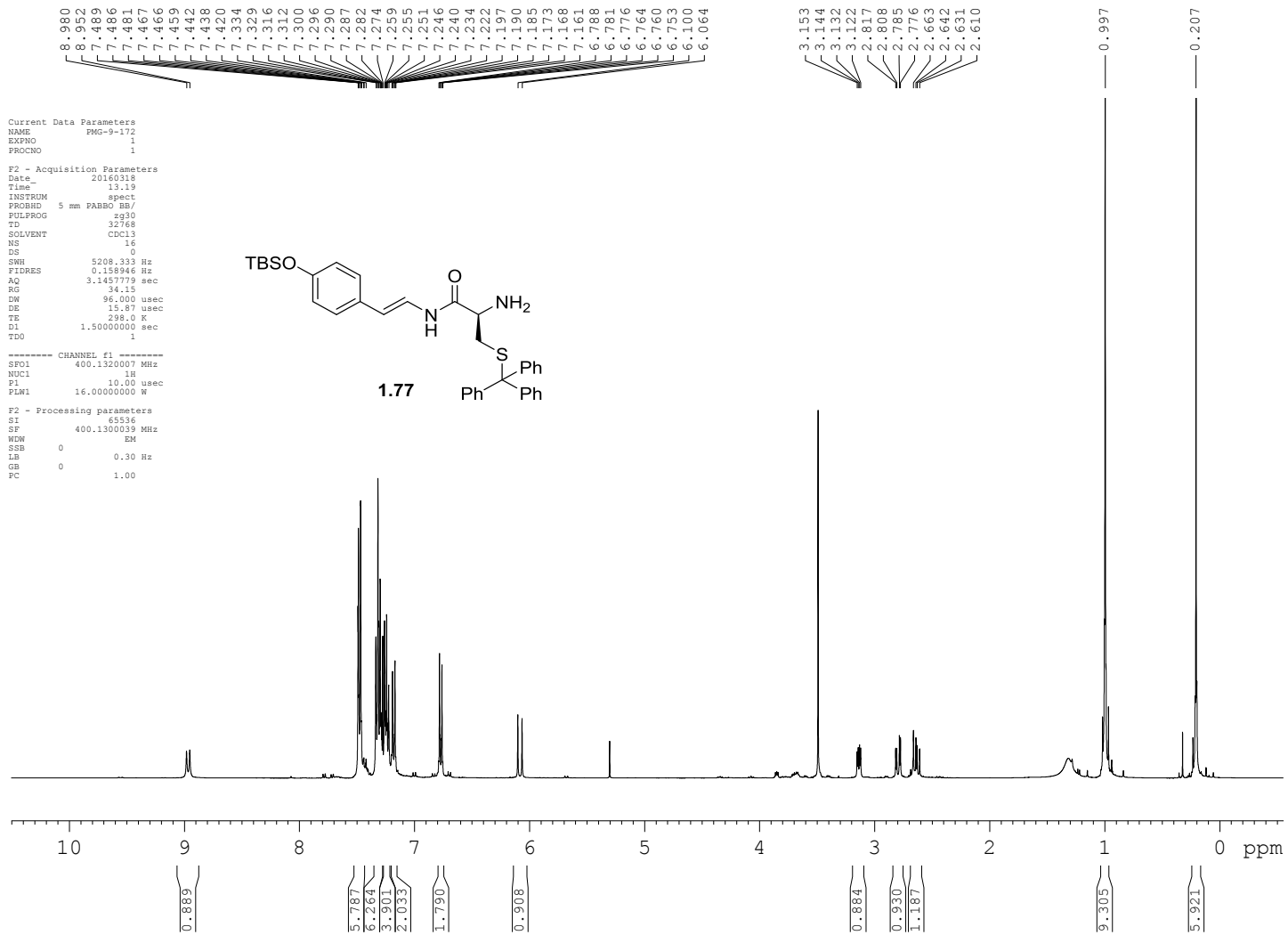


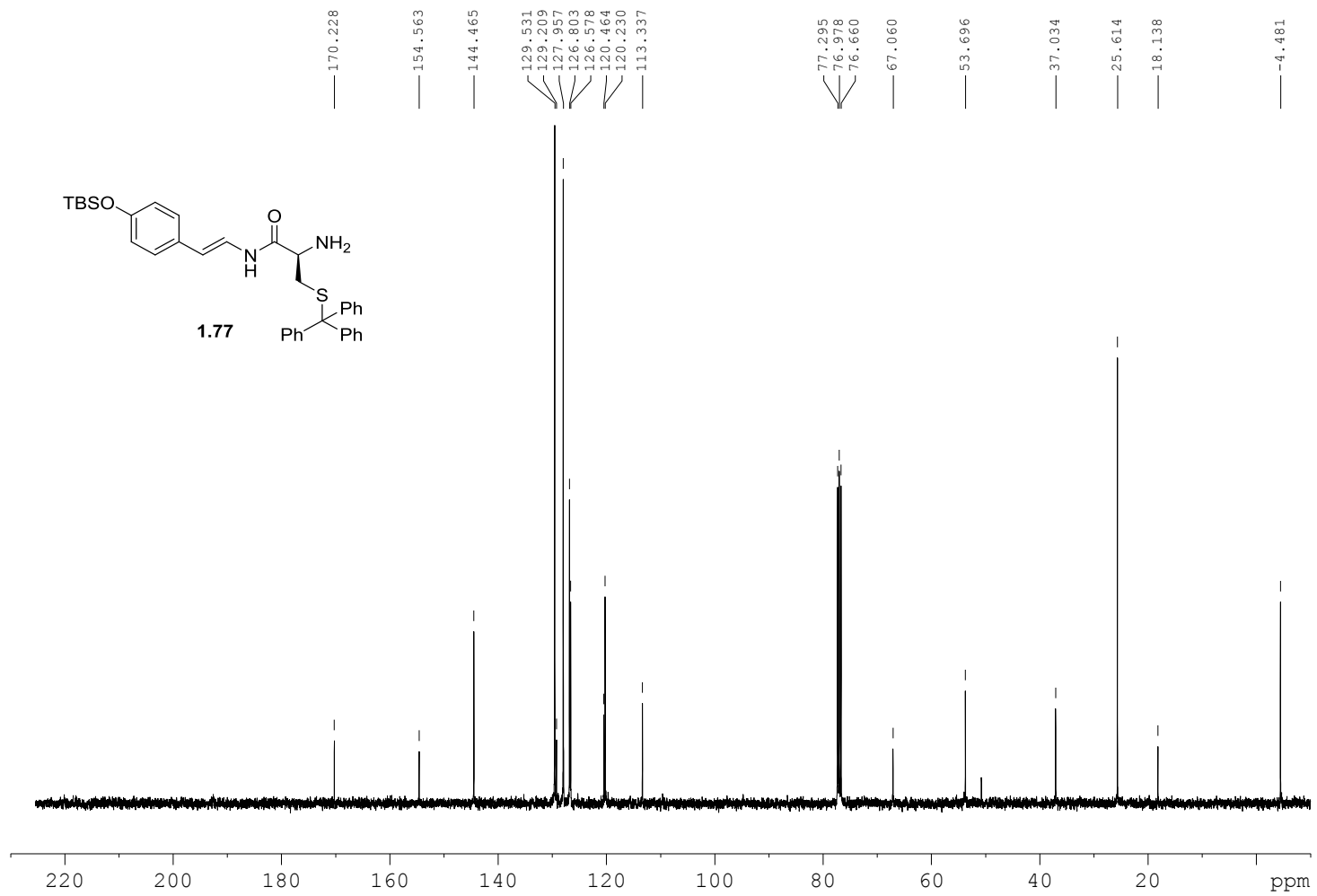


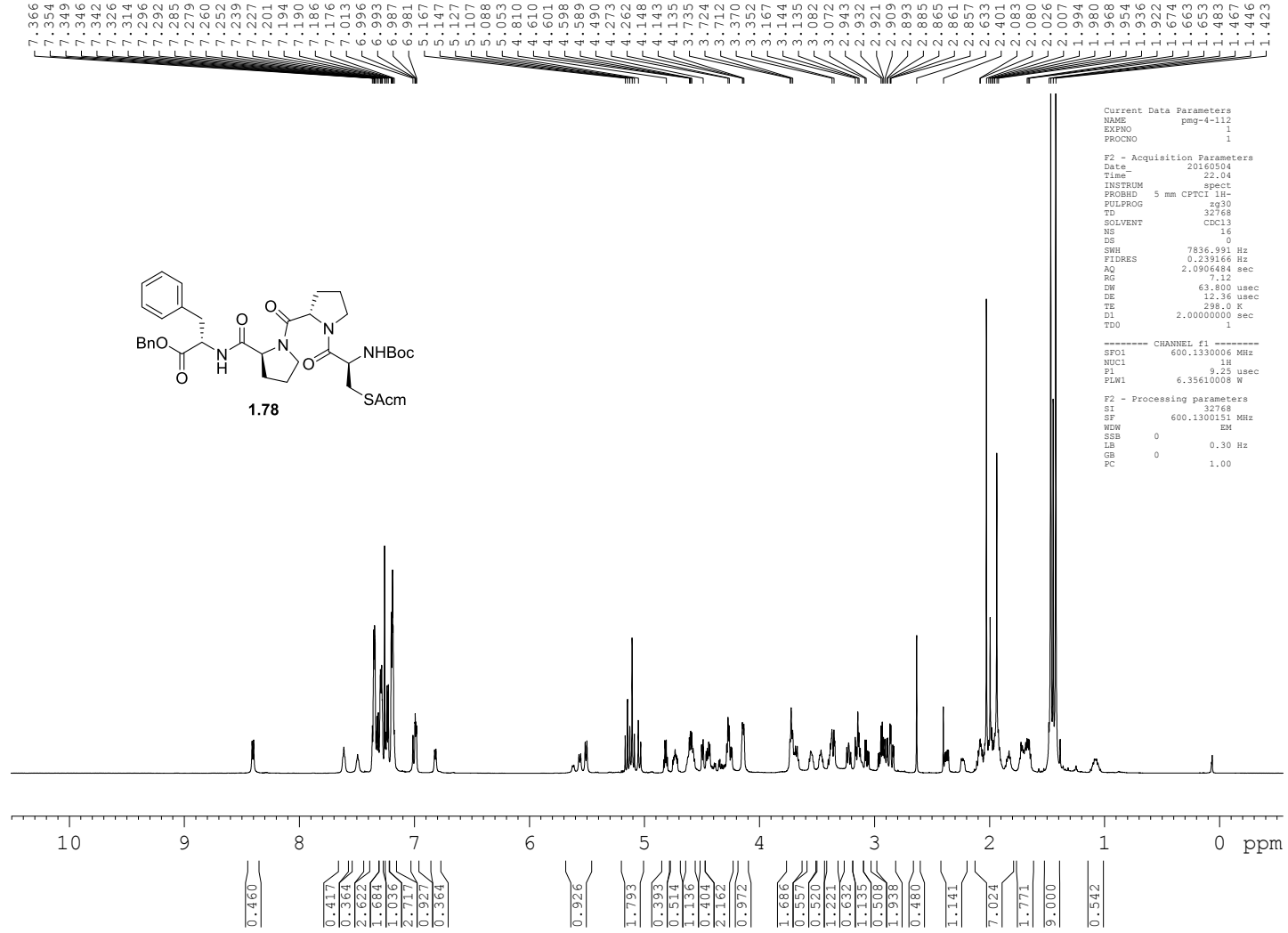


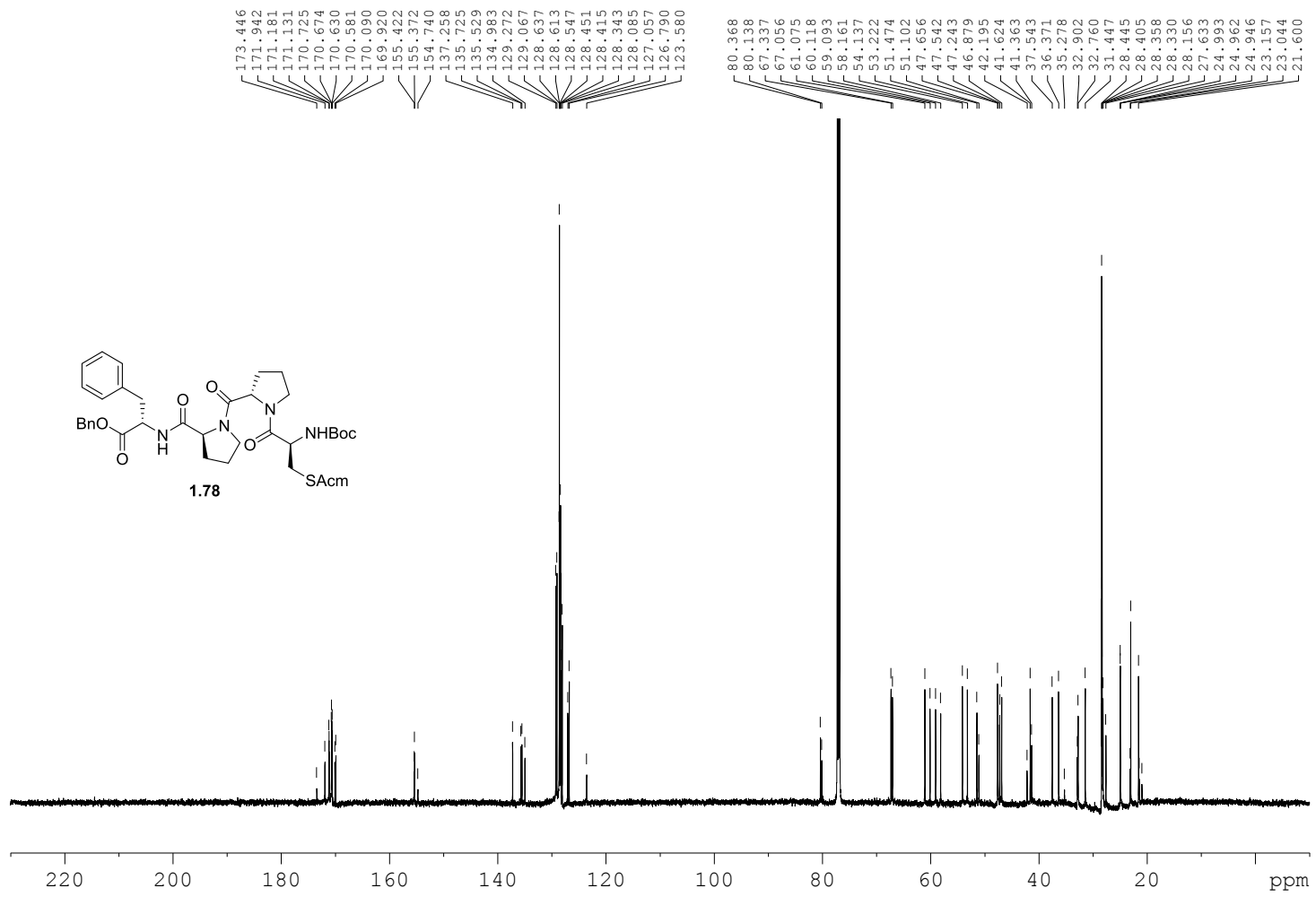
354

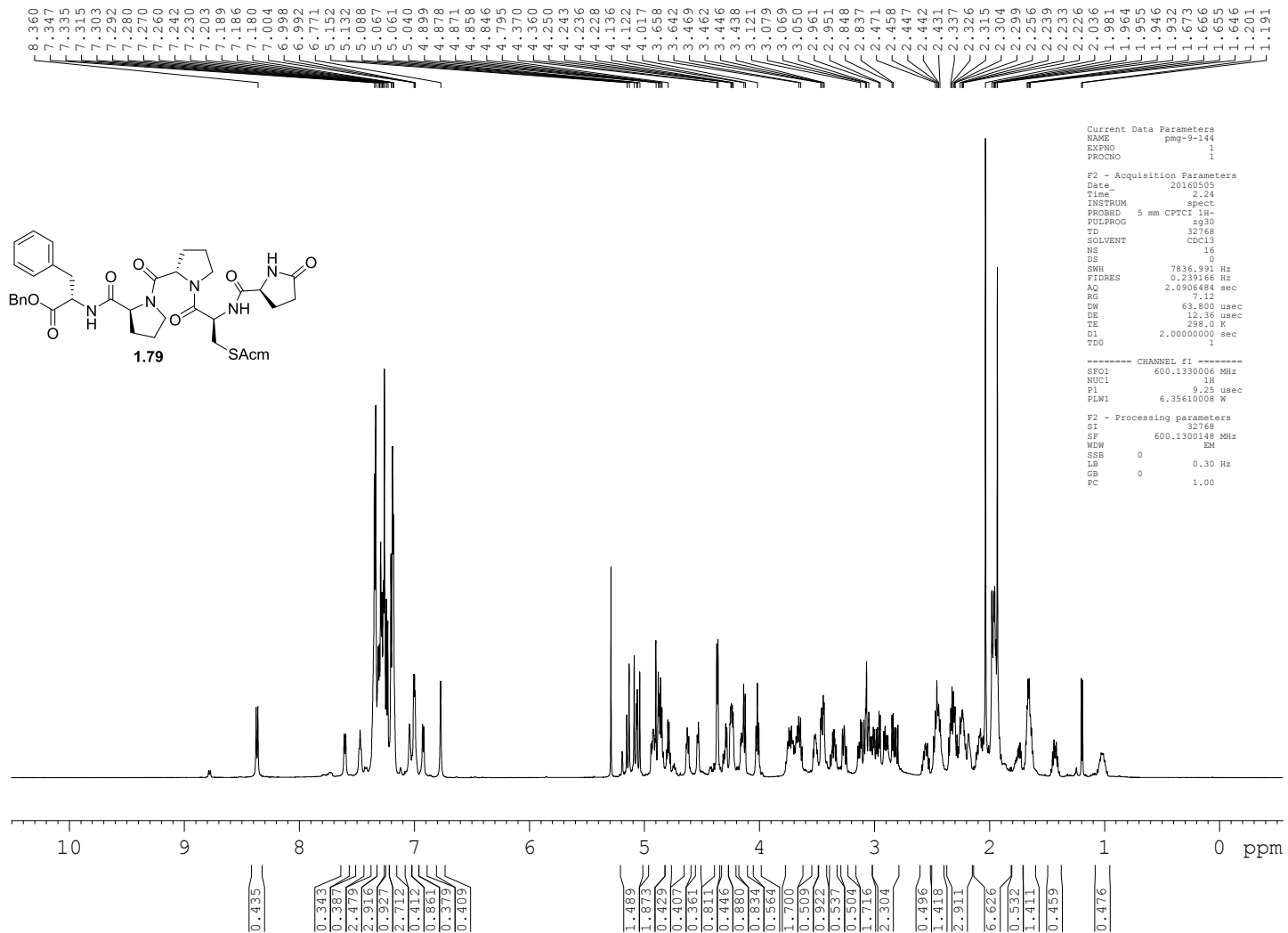




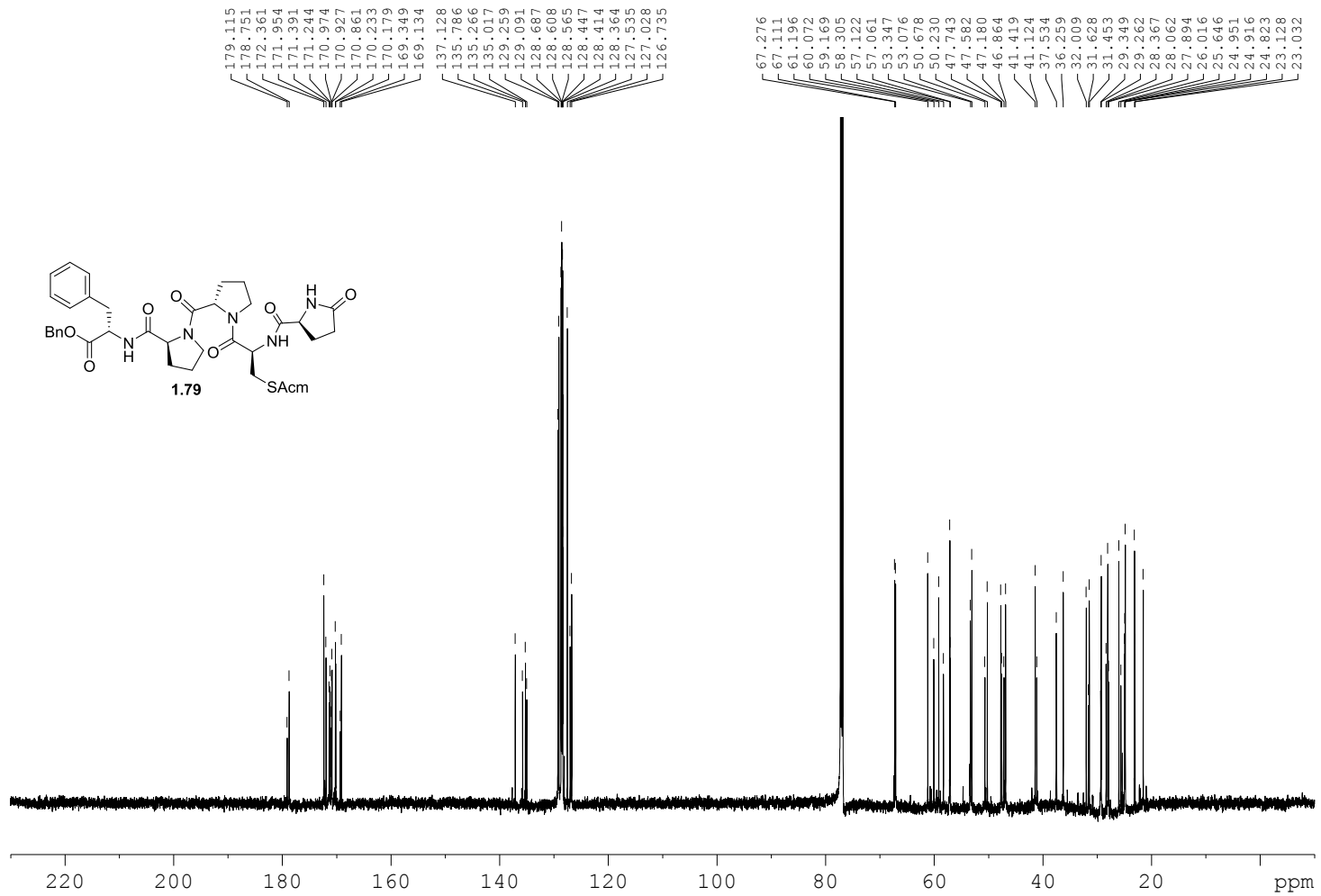


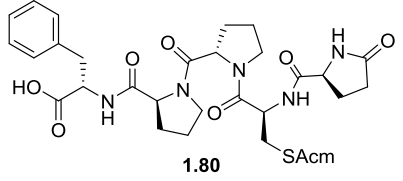
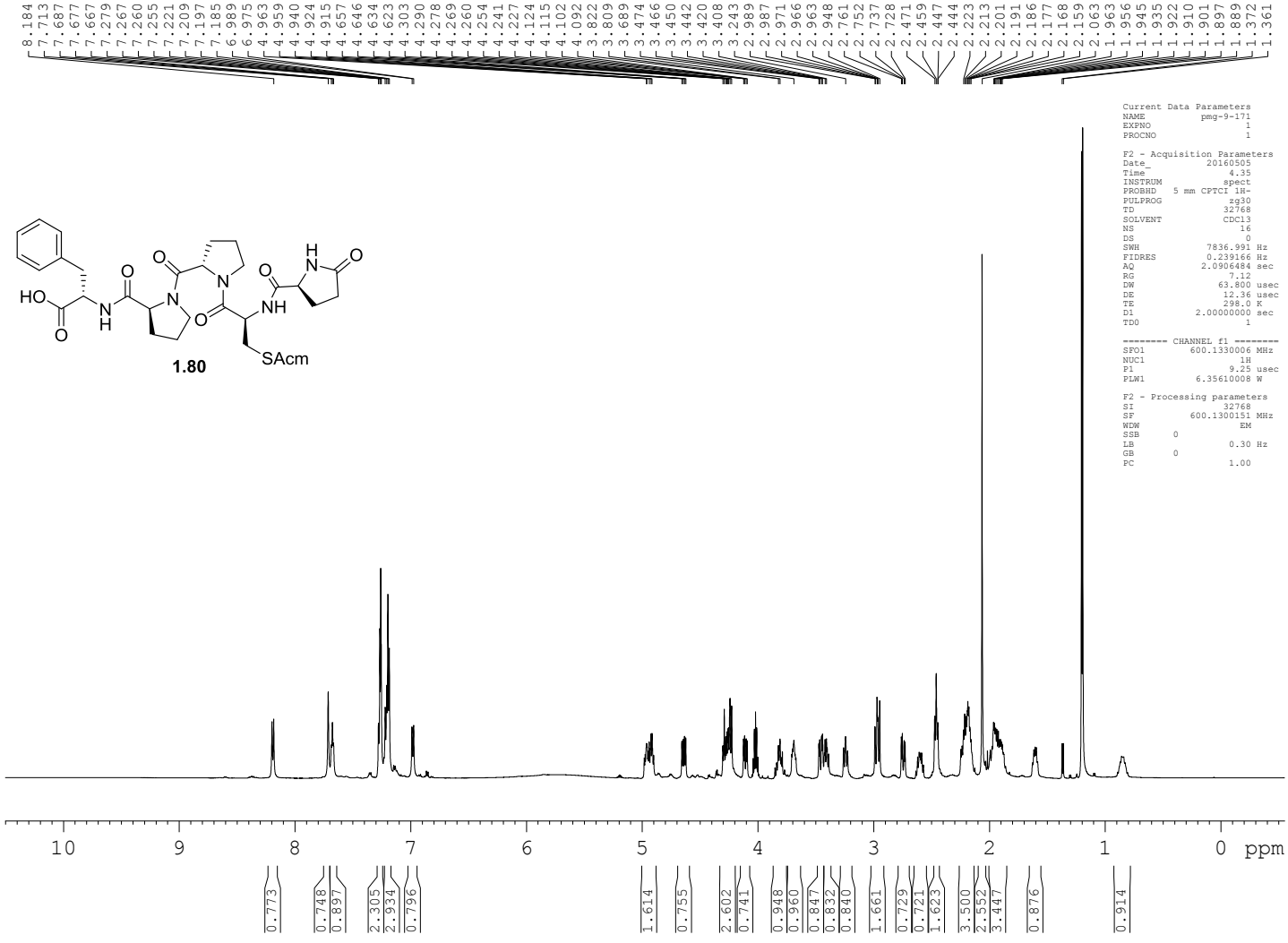


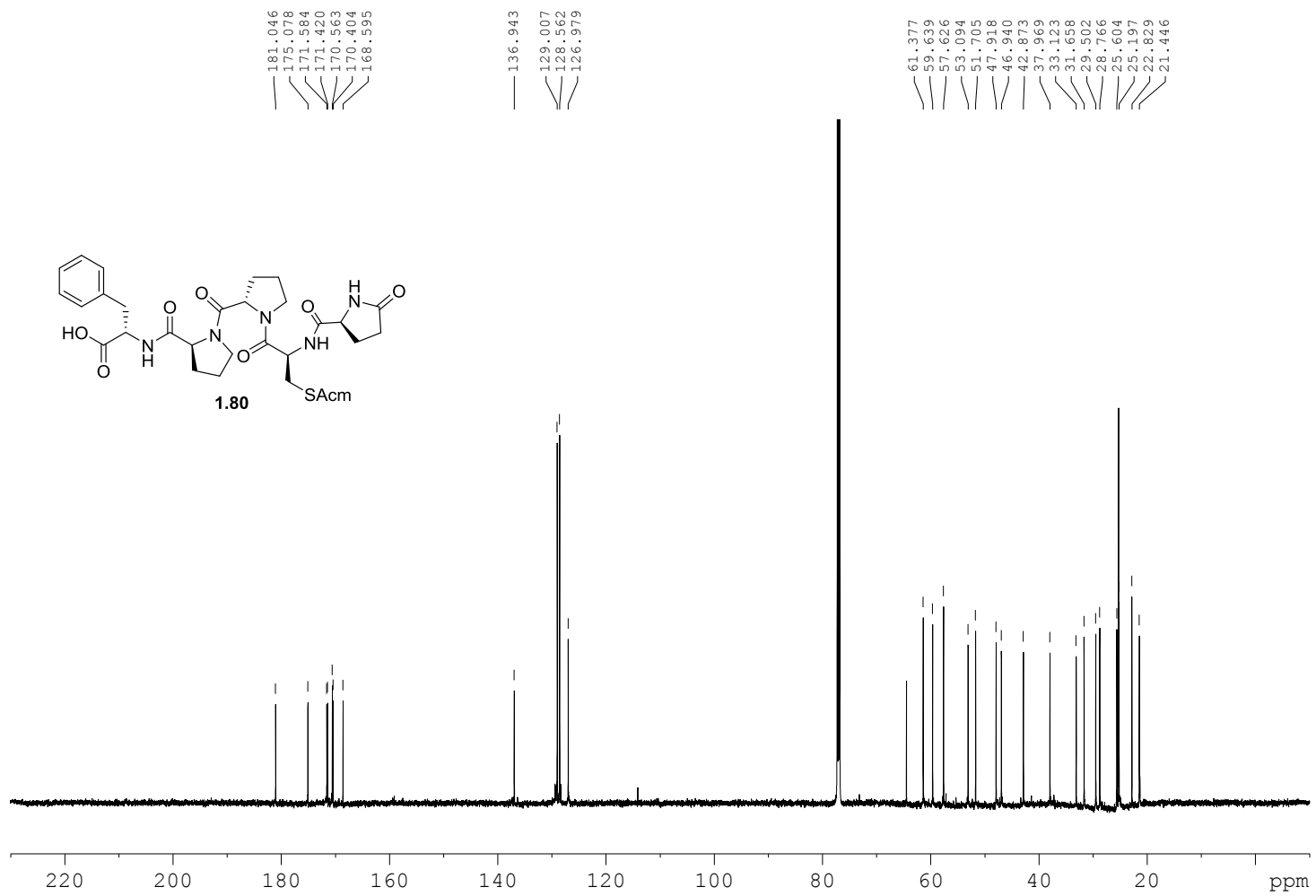


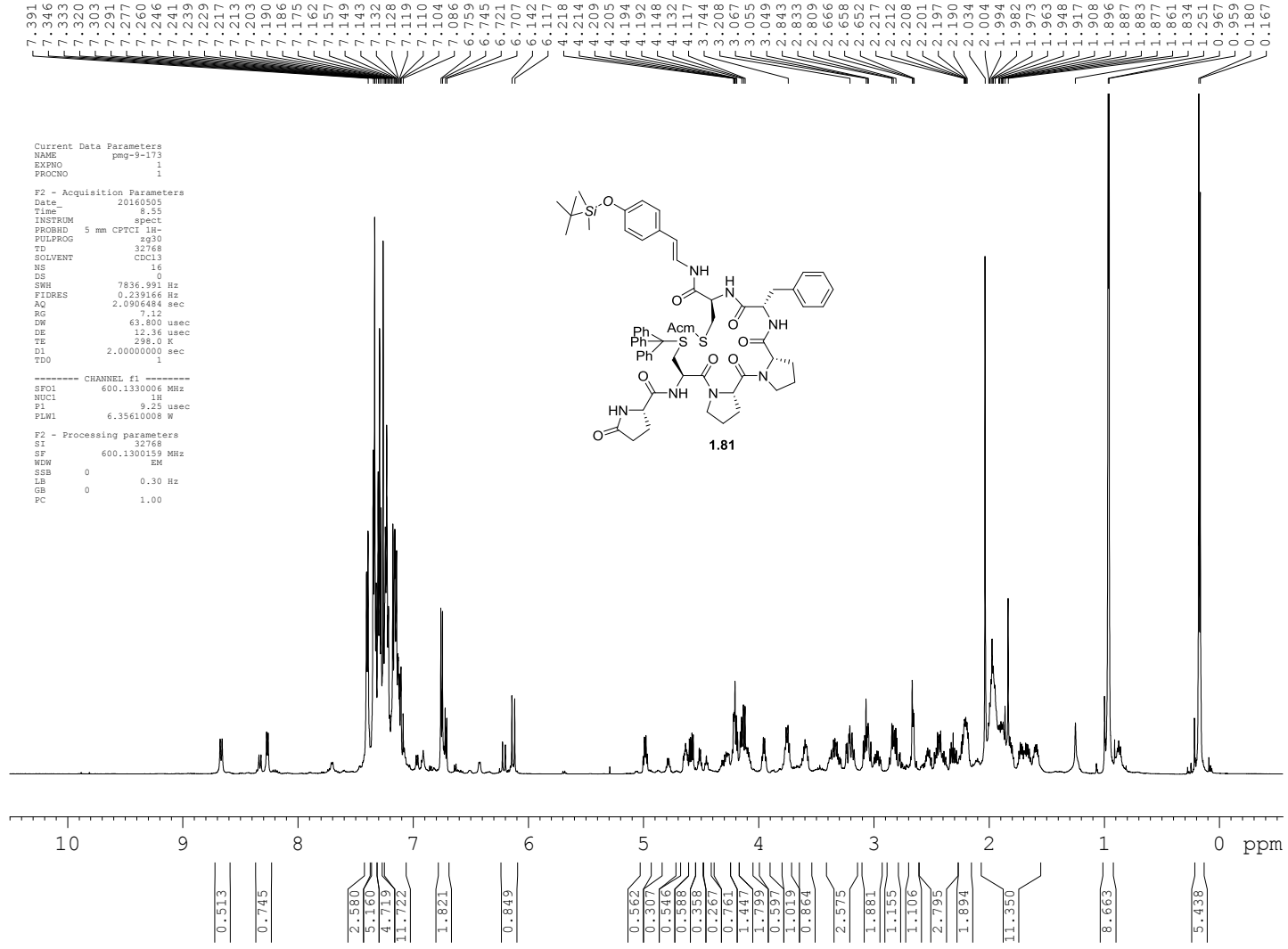


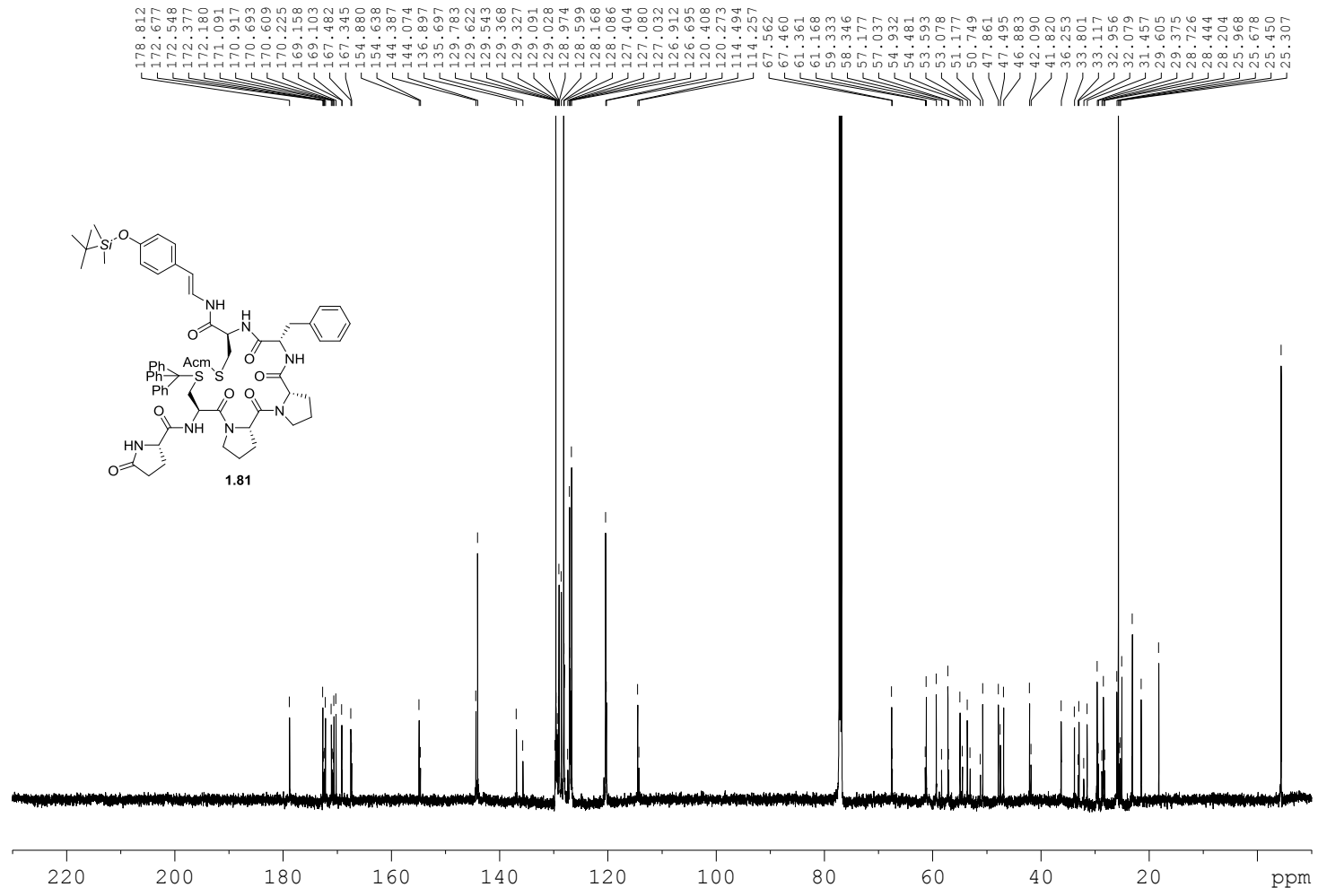


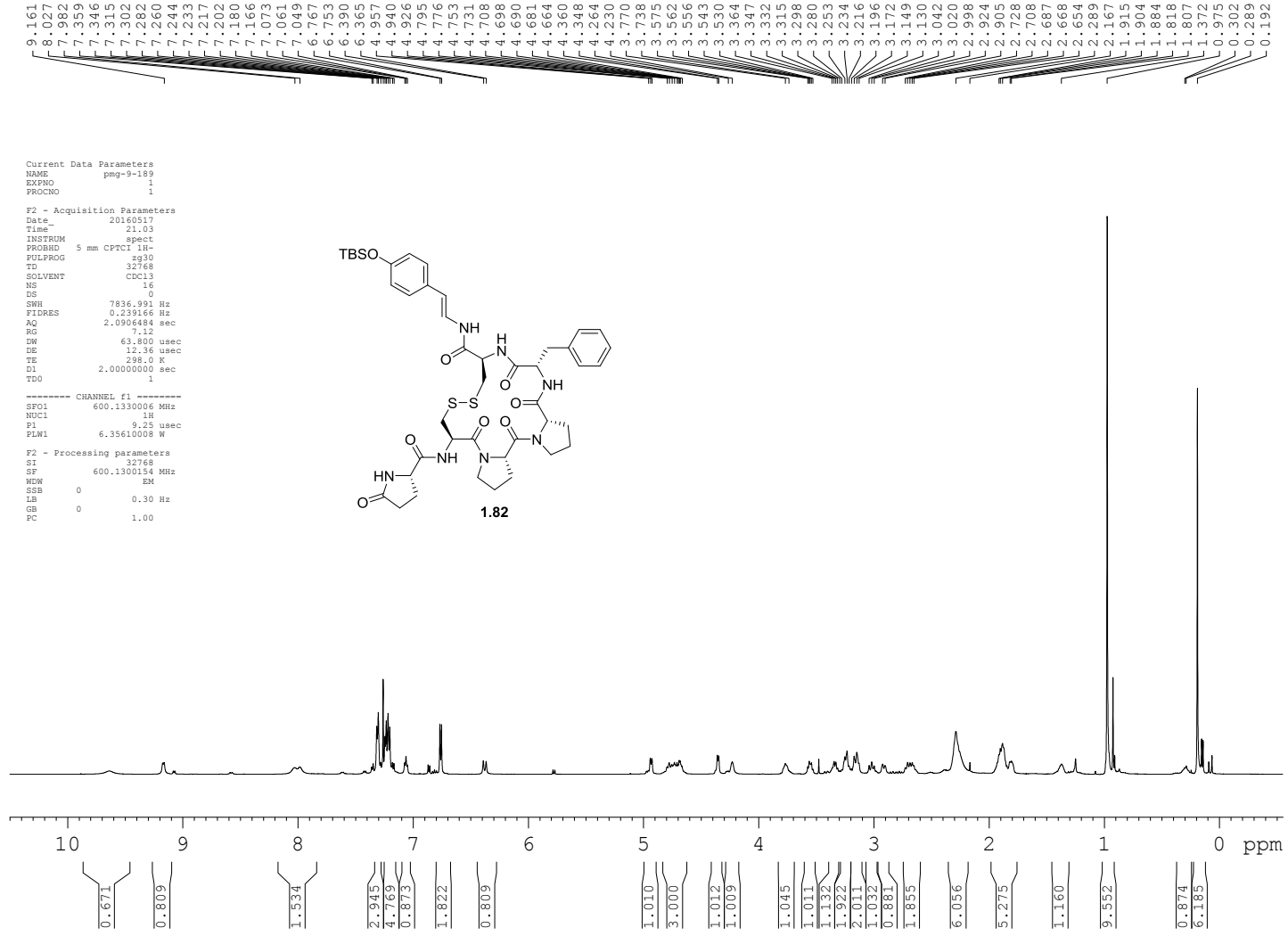


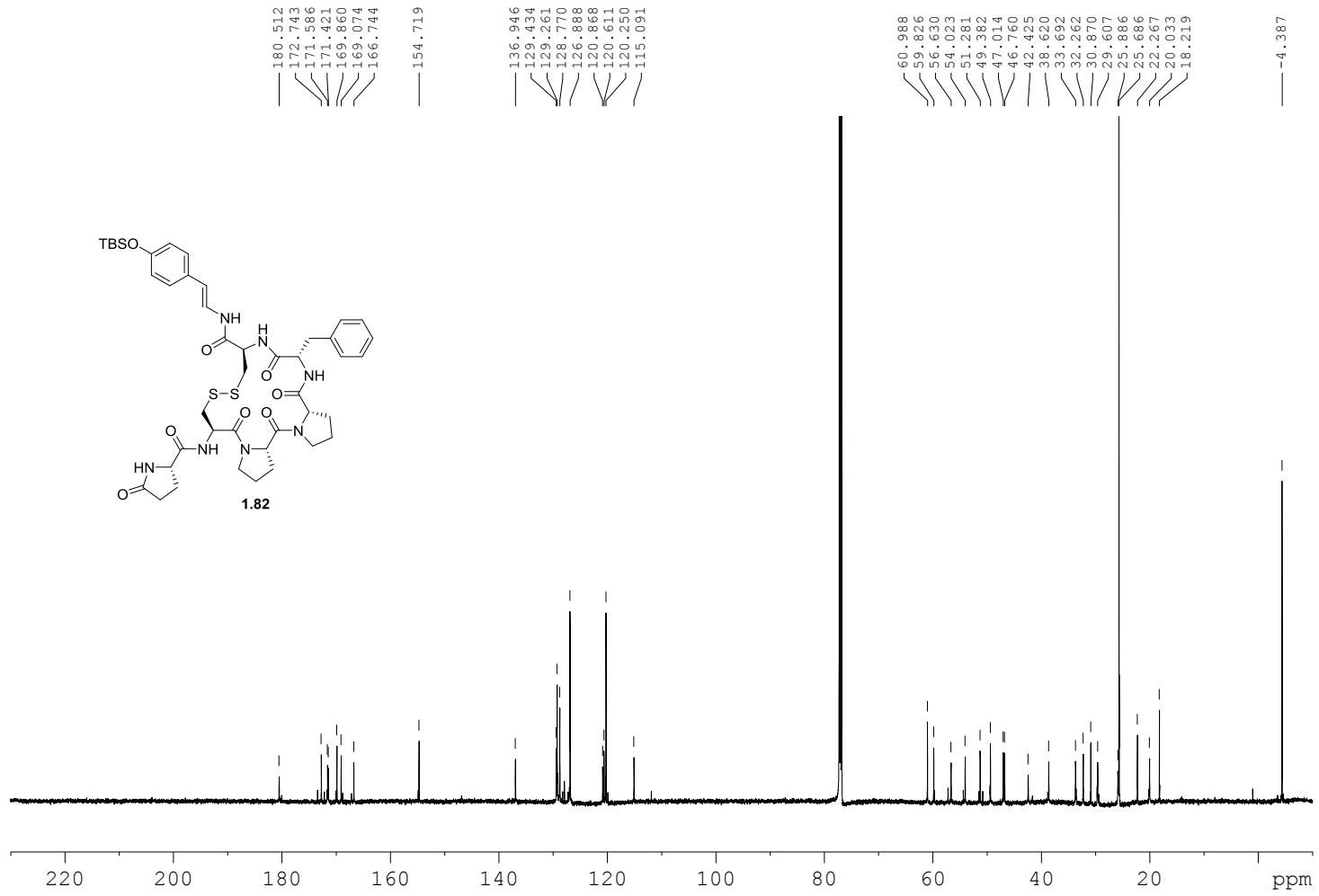


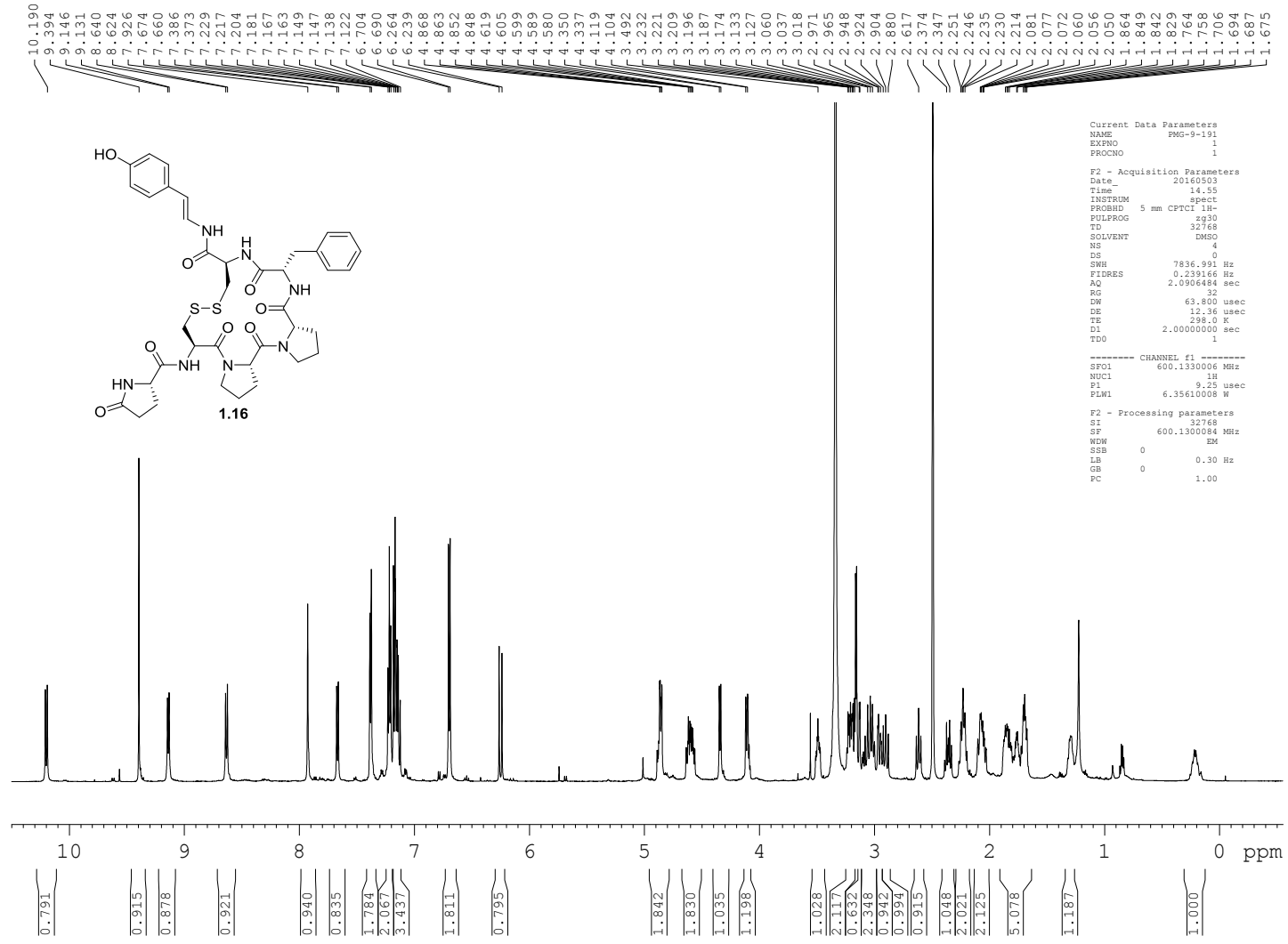




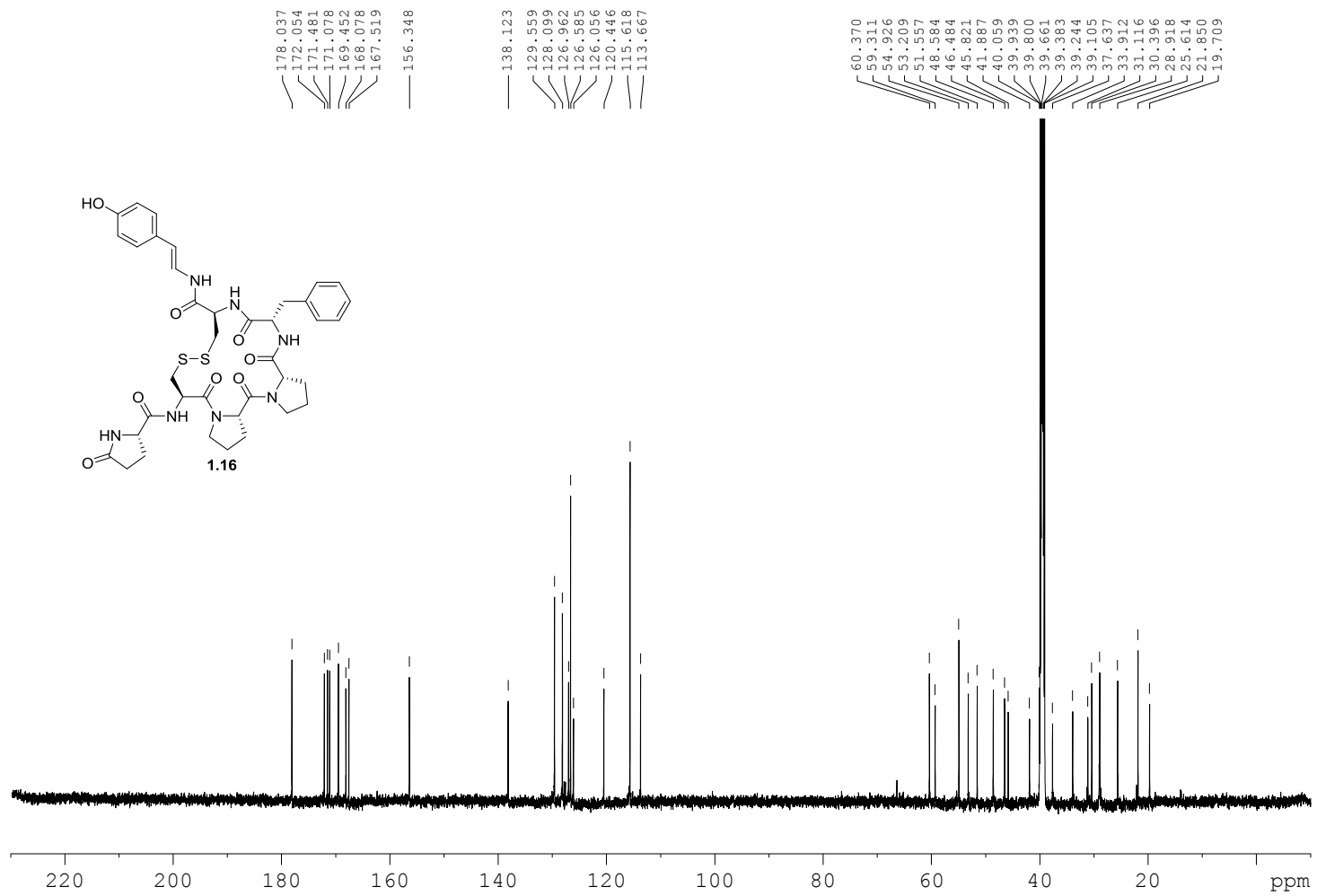






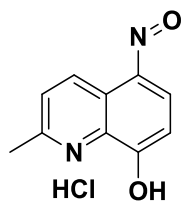






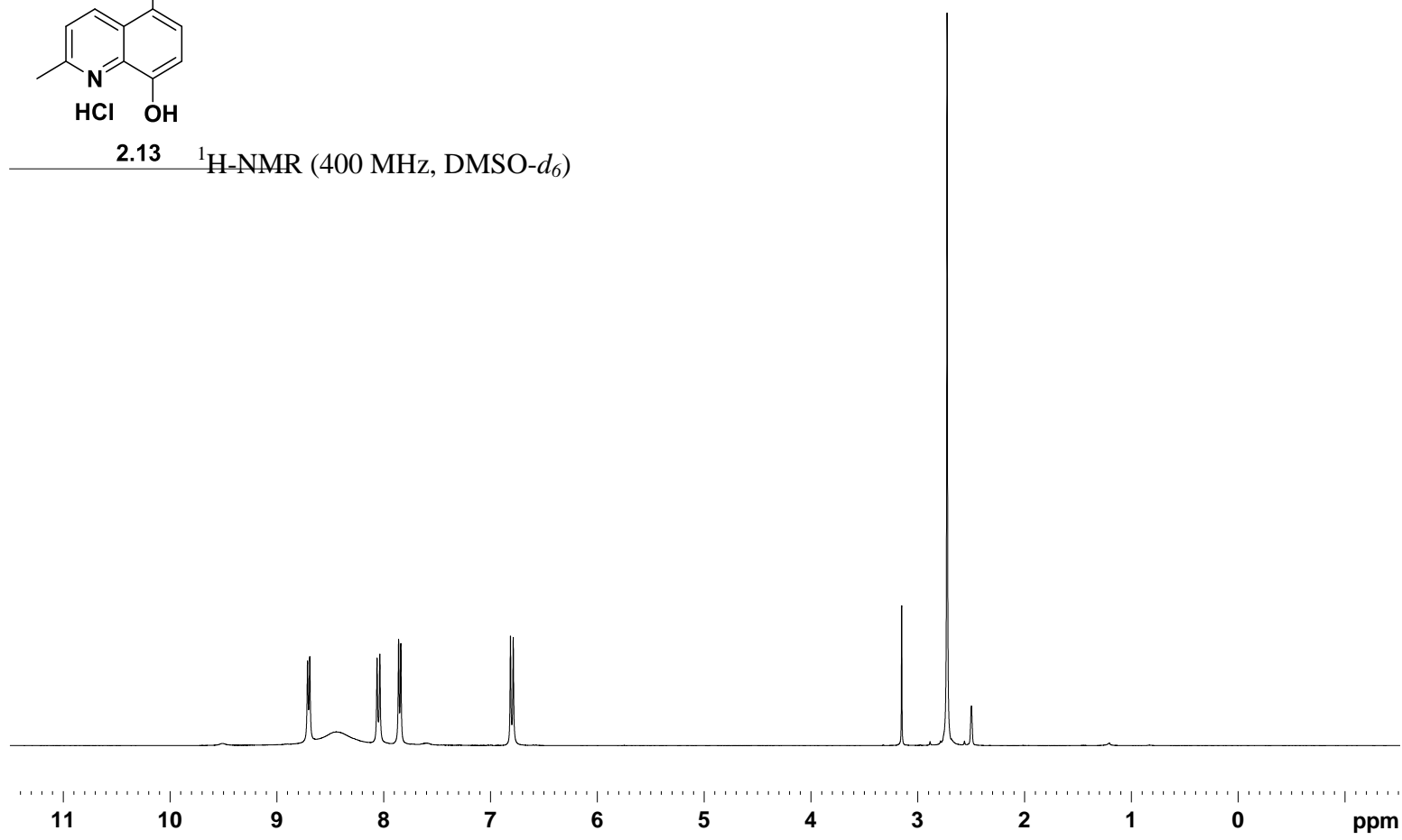
## **Appendix B**

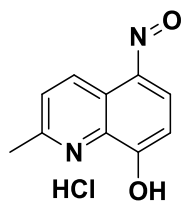
Relevant spectra for chapter II



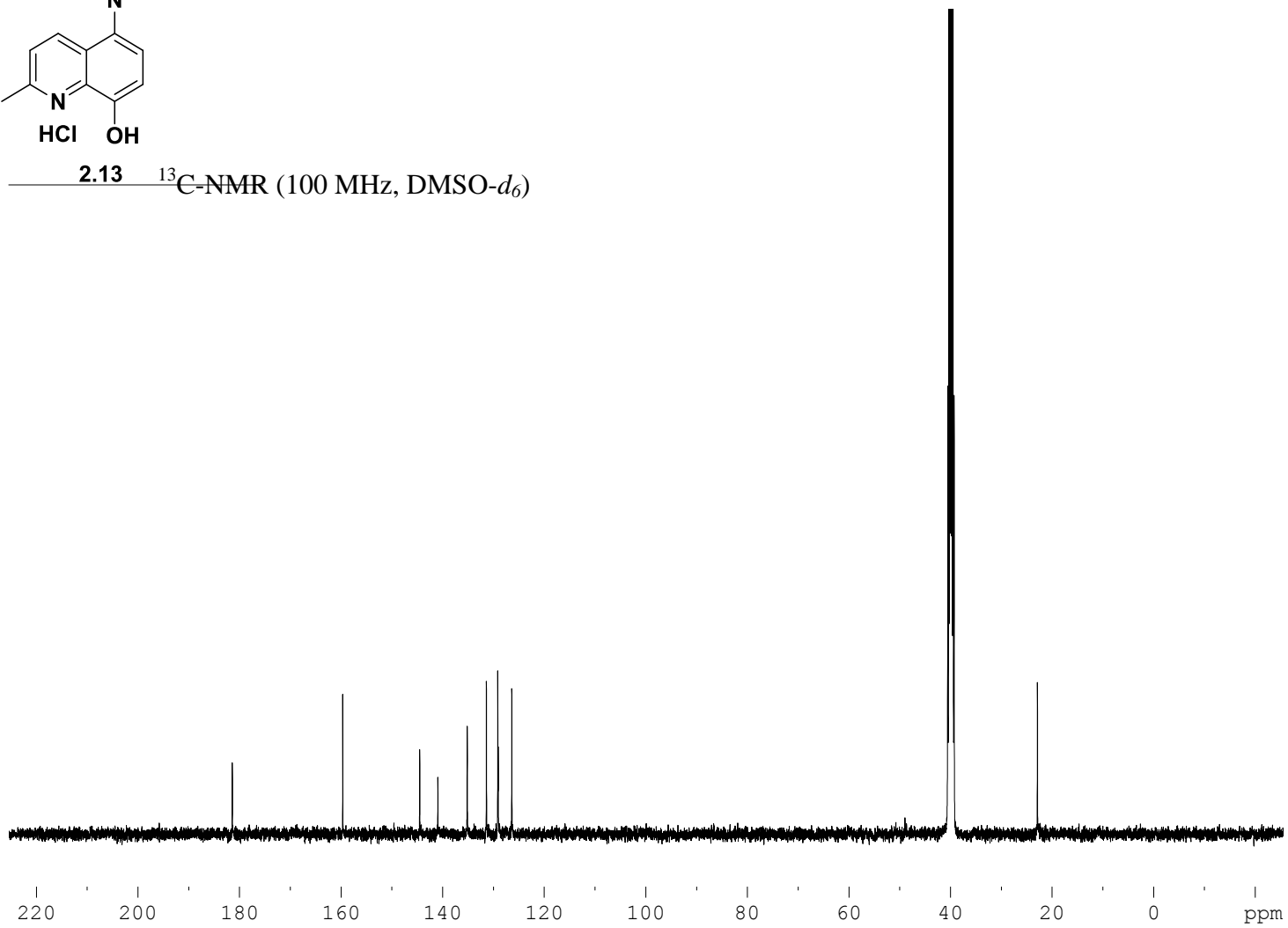
2.13 <sup>1</sup>H-NMR (400 MHz, DMSO-*d*<sub>6</sub>)

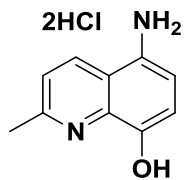
370



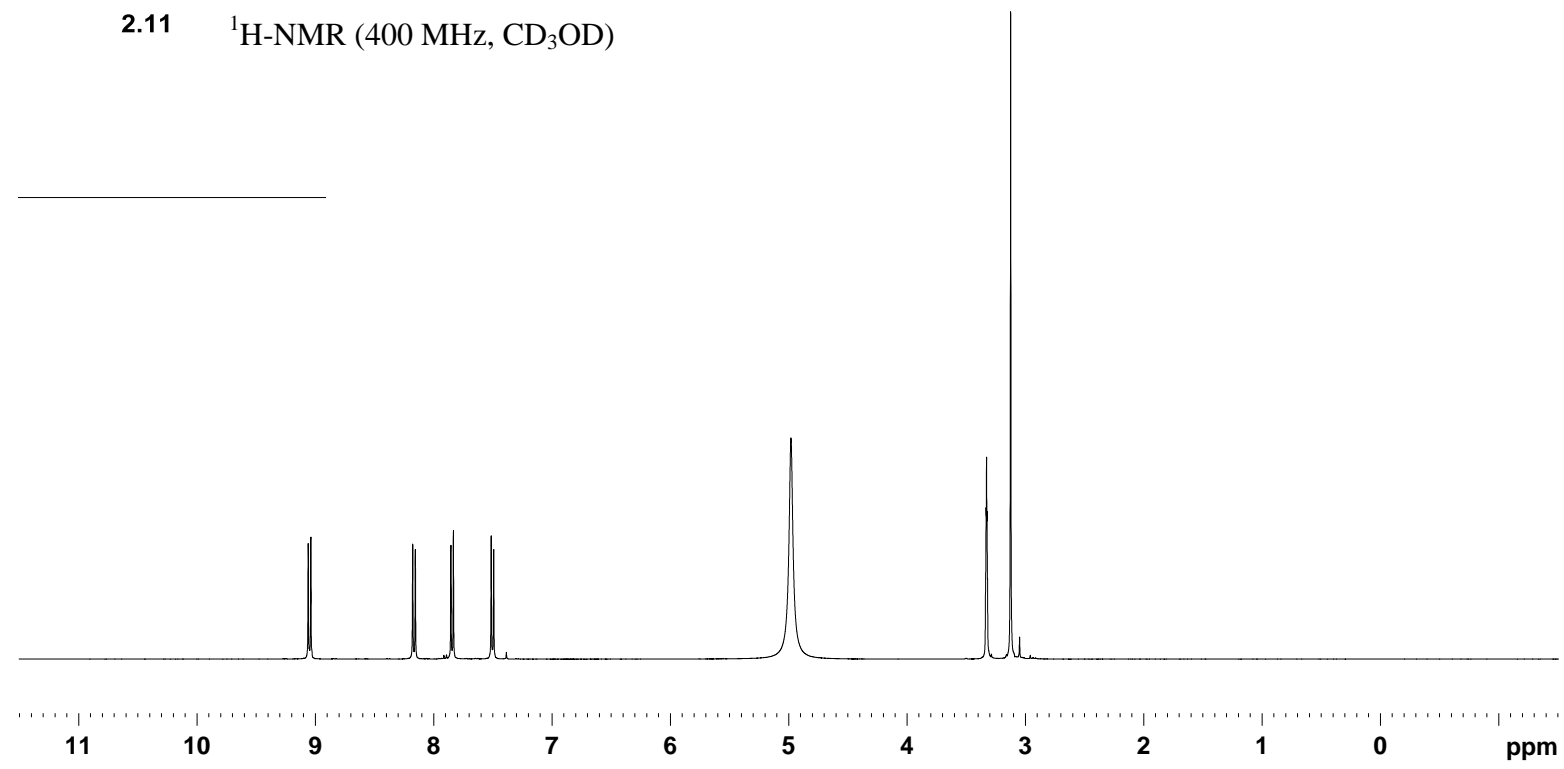


2.13 <sup>13</sup>C-NMR (100 MHz, DMSO-d<sub>6</sub>)

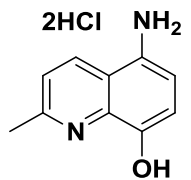




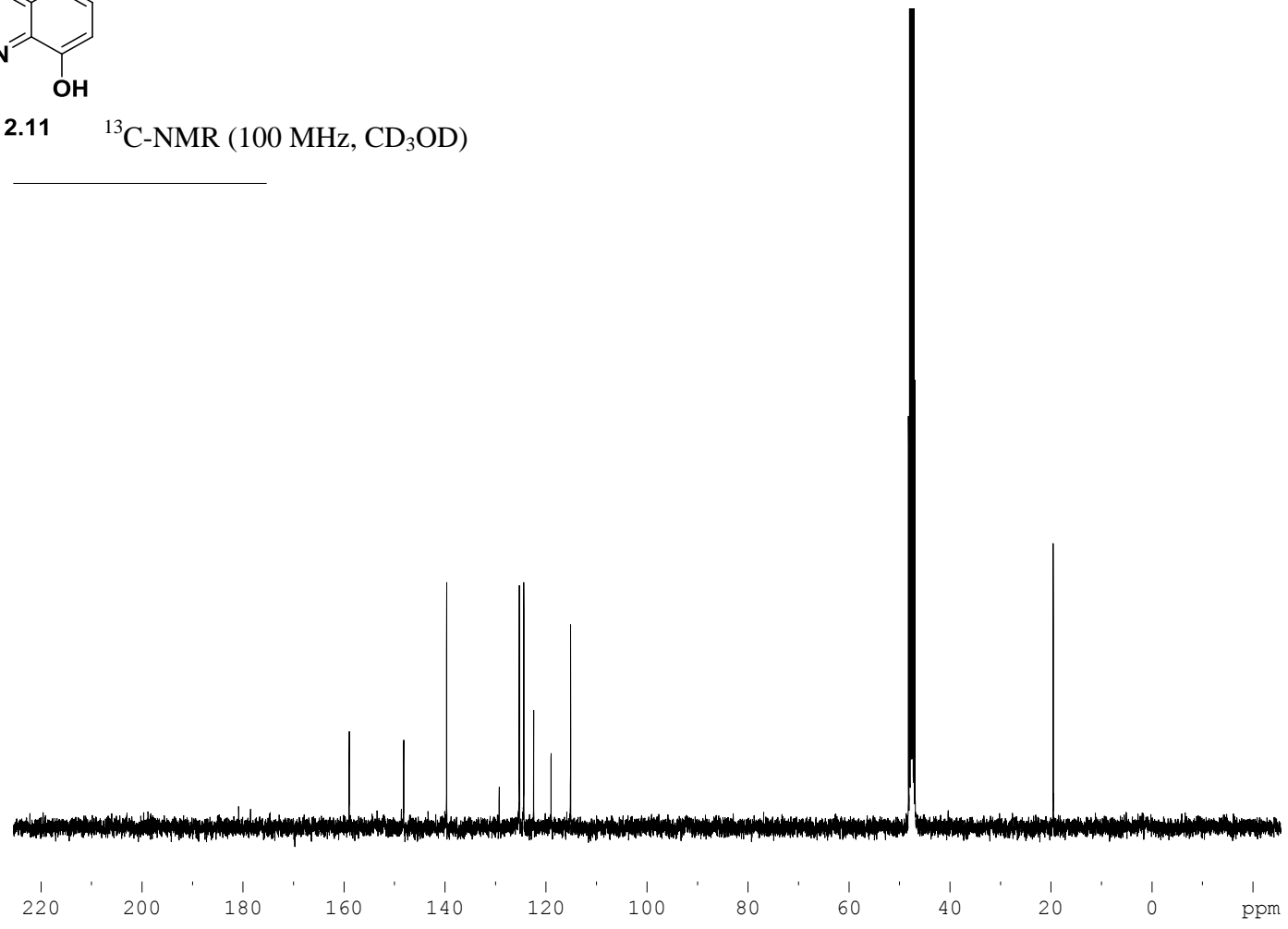
2.11 <sup>1</sup>H-NMR (400 MHz, CD<sub>3</sub>OD)

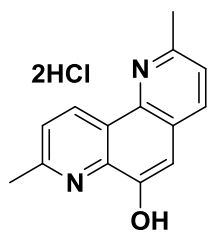


372



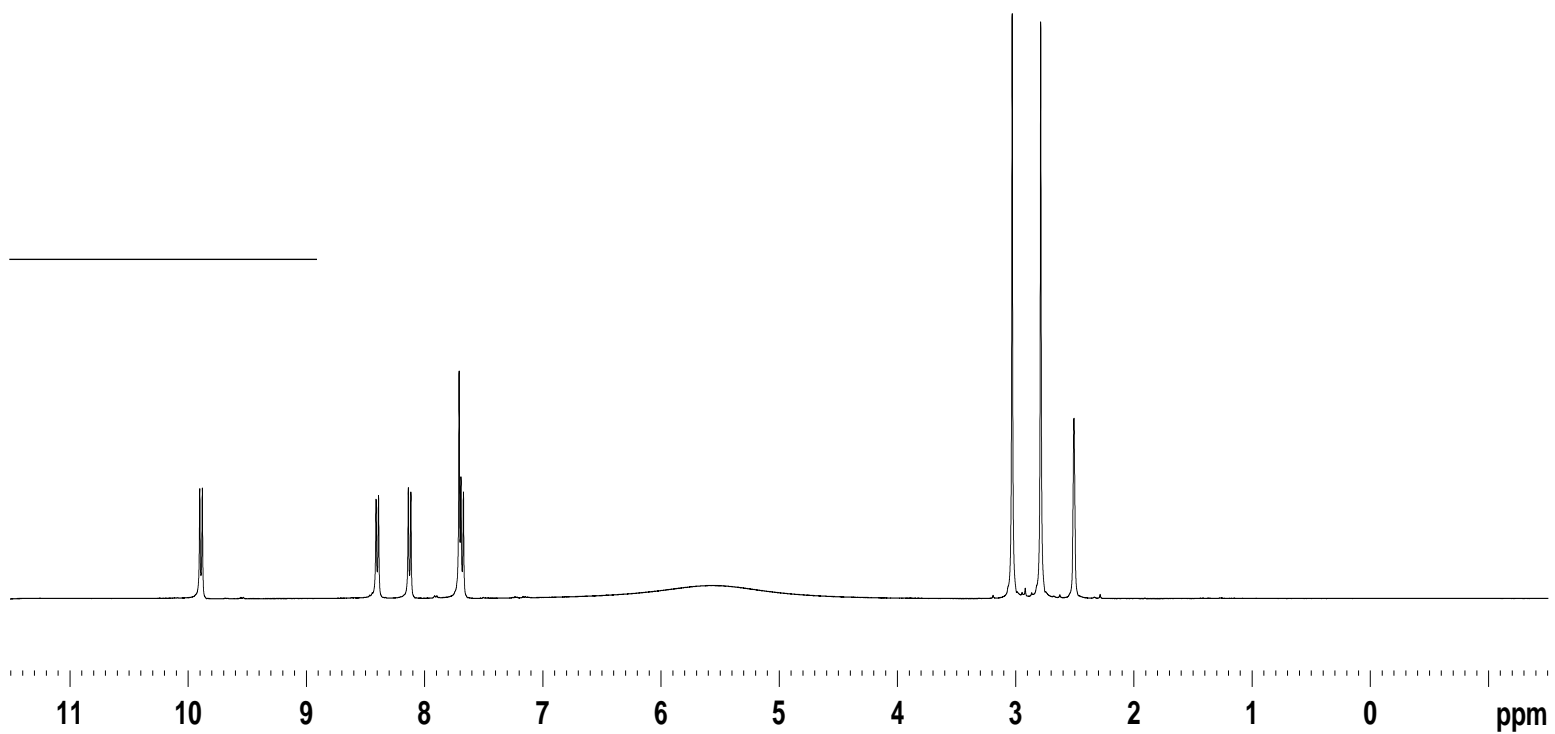
2.11  $^{13}\text{C}$ -NMR (100 MHz,  $\text{CD}_3\text{OD}$ )

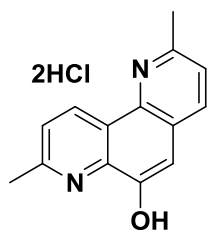




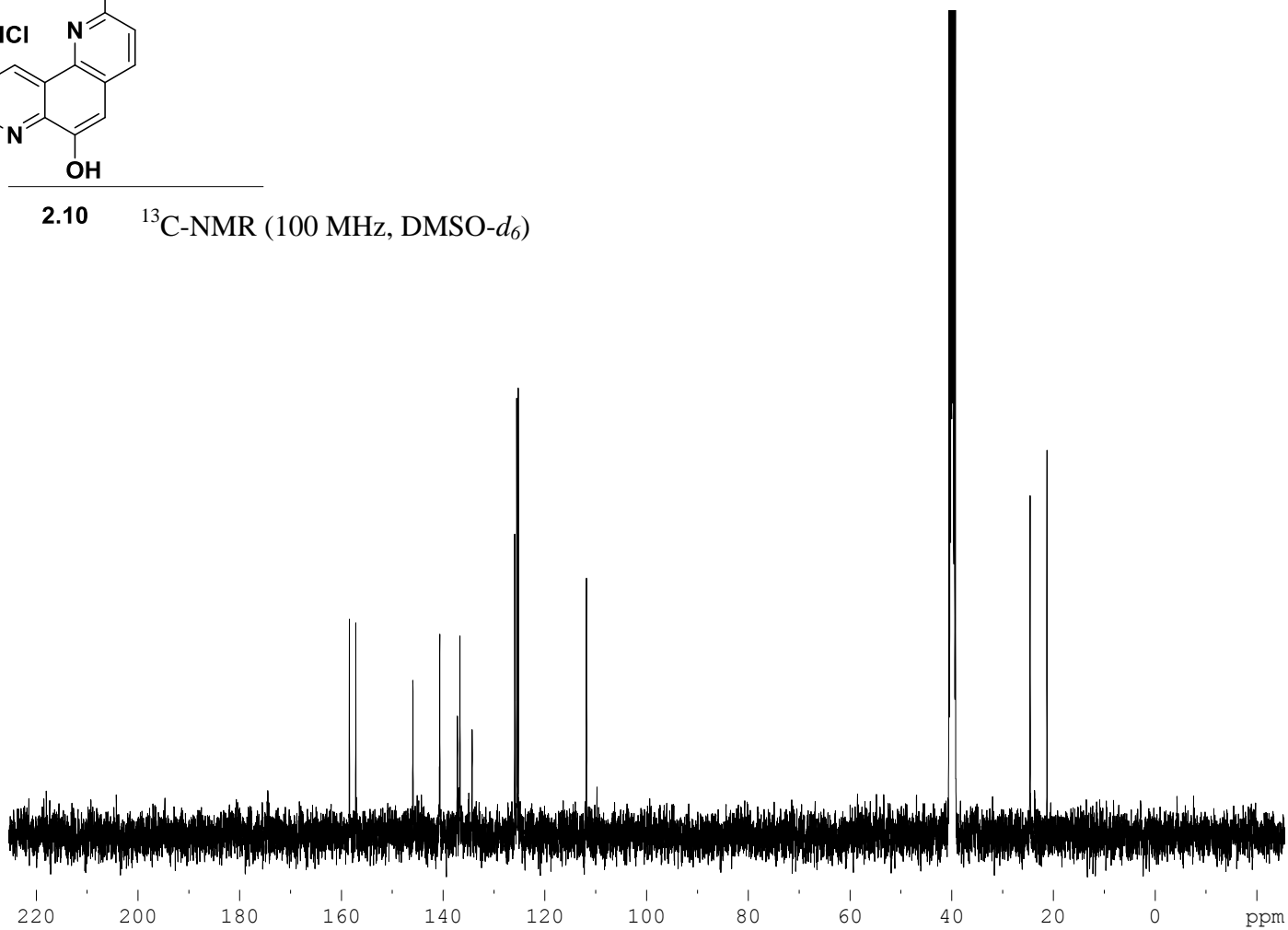
2.10  $^1\text{H-NMR}$  (400 MHz,  $\text{DMSO-}d_6$ )

374

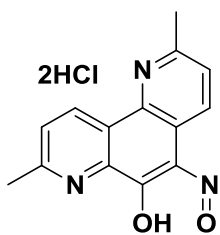




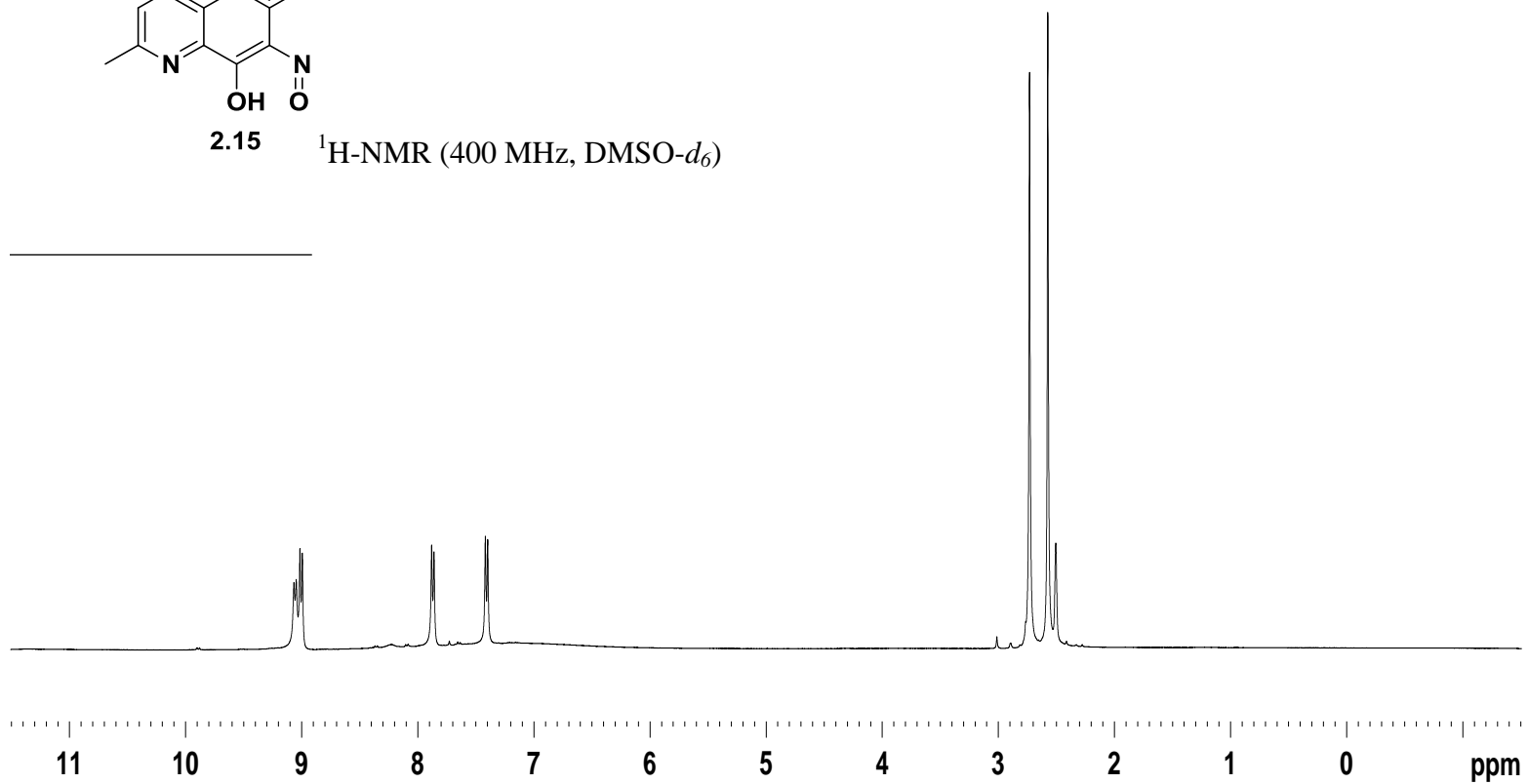
2.10  $^{13}\text{C}$ -NMR (100 MHz, DMSO- $d_6$ )

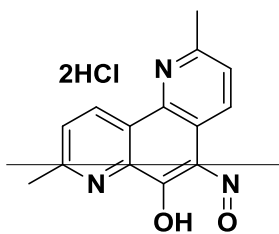




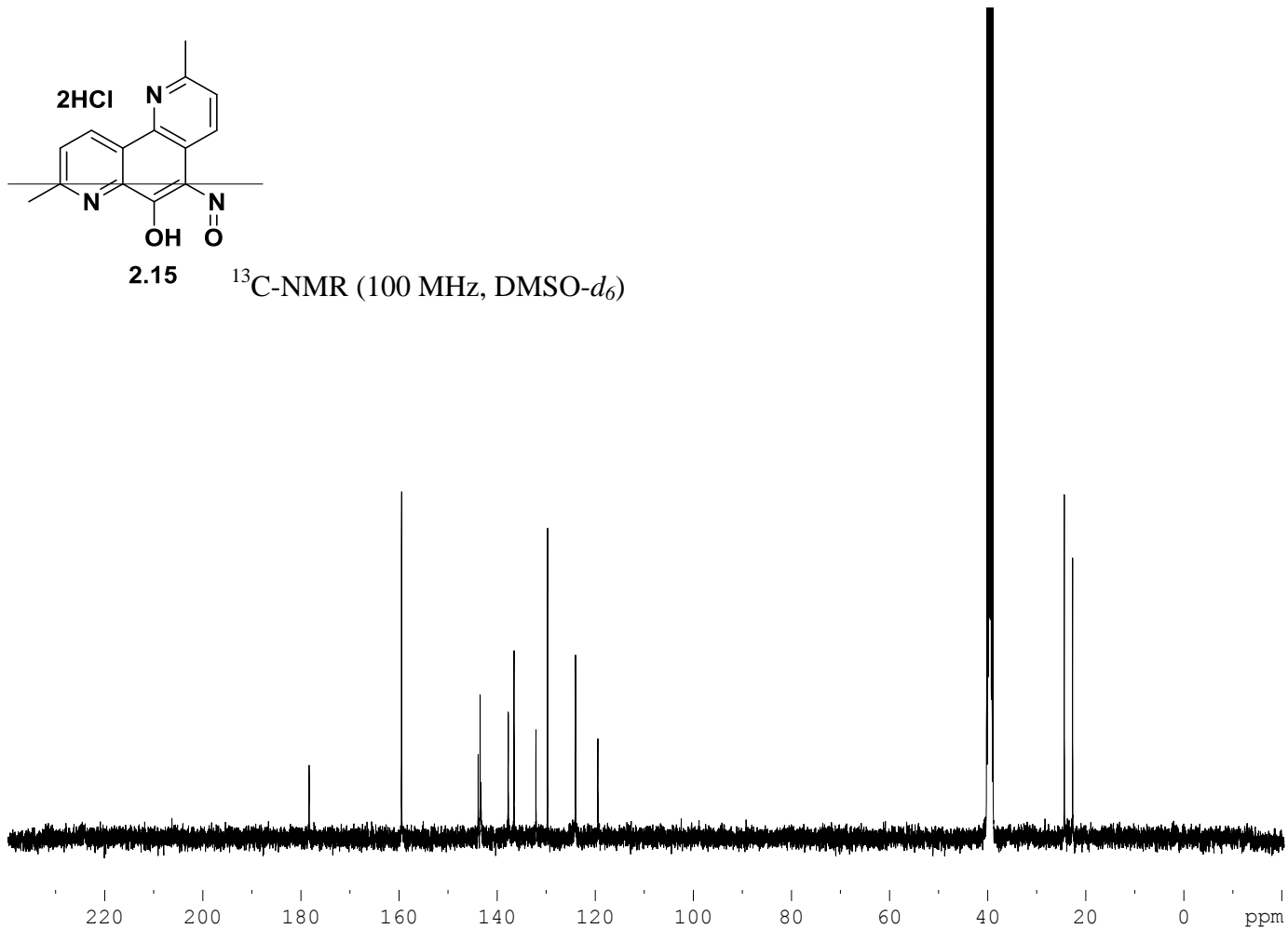


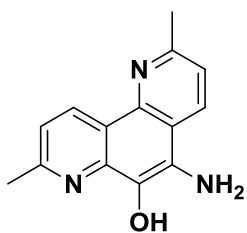
2.15 <sup>1</sup>H-NMR (400 MHz, DMSO-*d*<sub>6</sub>)





2.15  $^{13}\text{C}$ -NMR (100 MHz, DMSO- $d_6$ )

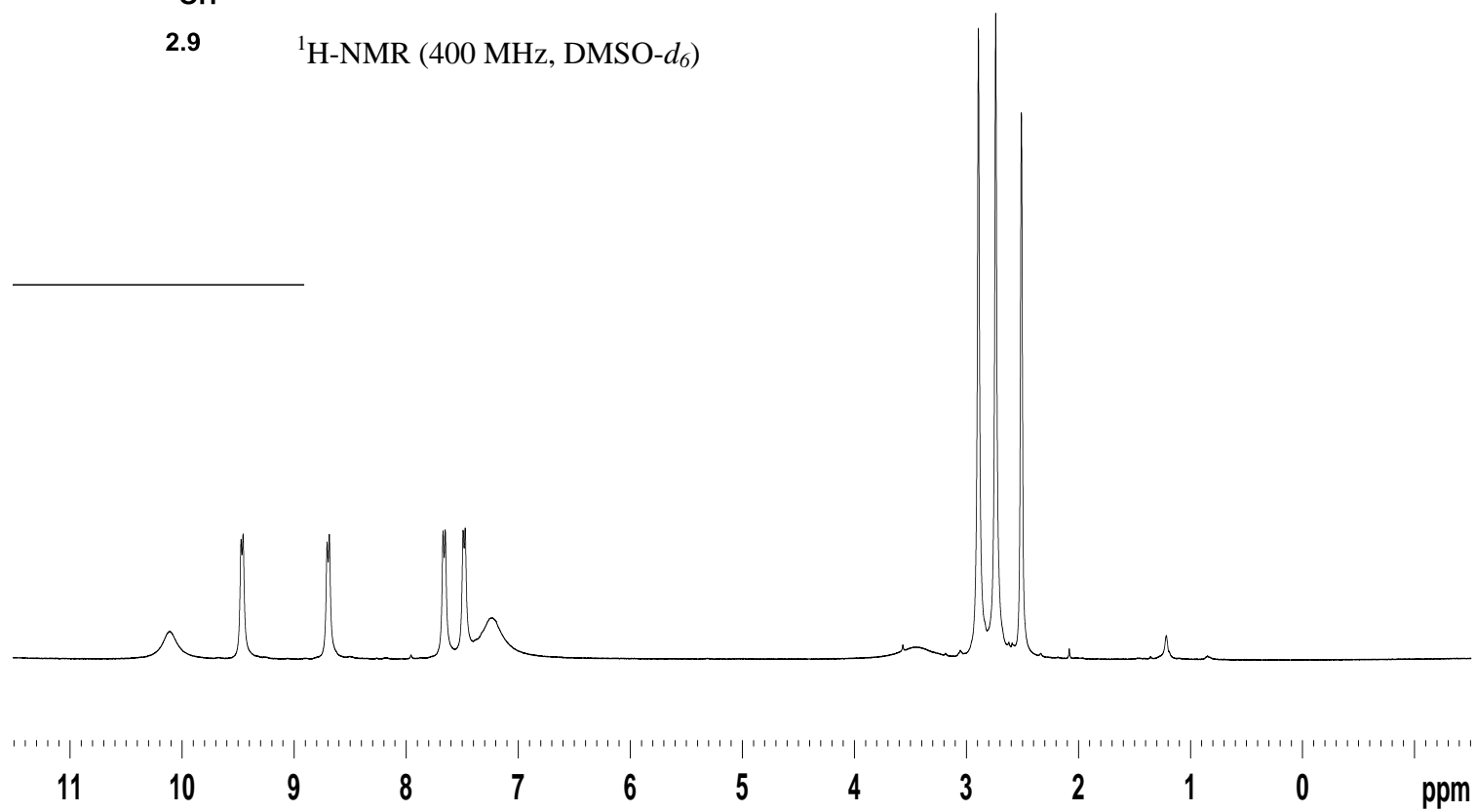


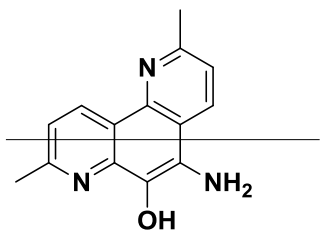


2.9

<sup>1</sup>H-NMR (400 MHz, DMSO-*d*<sub>6</sub>)

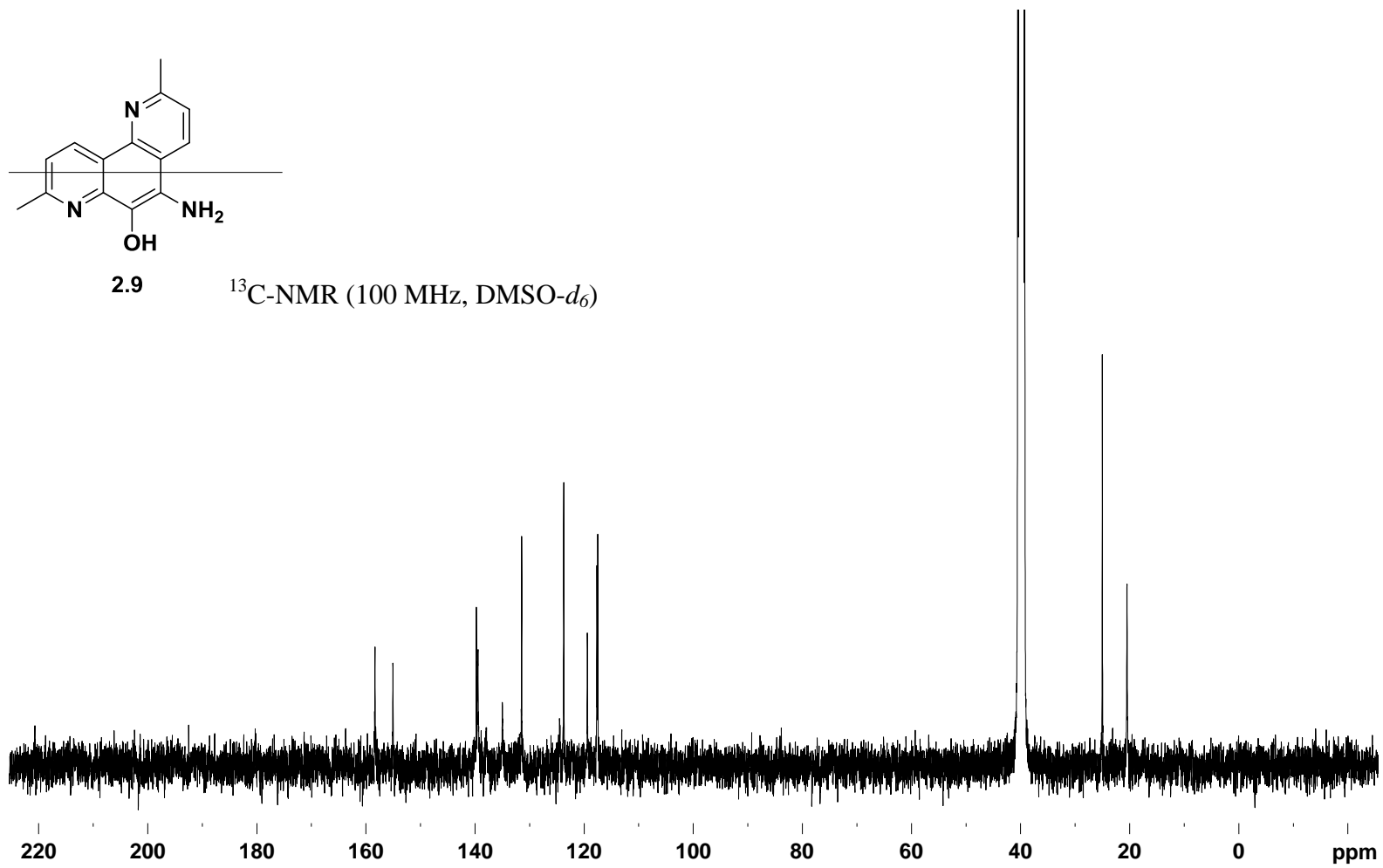
378

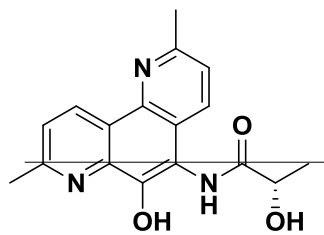




2.9

$^{13}\text{C}$ -NMR (100 MHz, DMSO- $d_6$ )

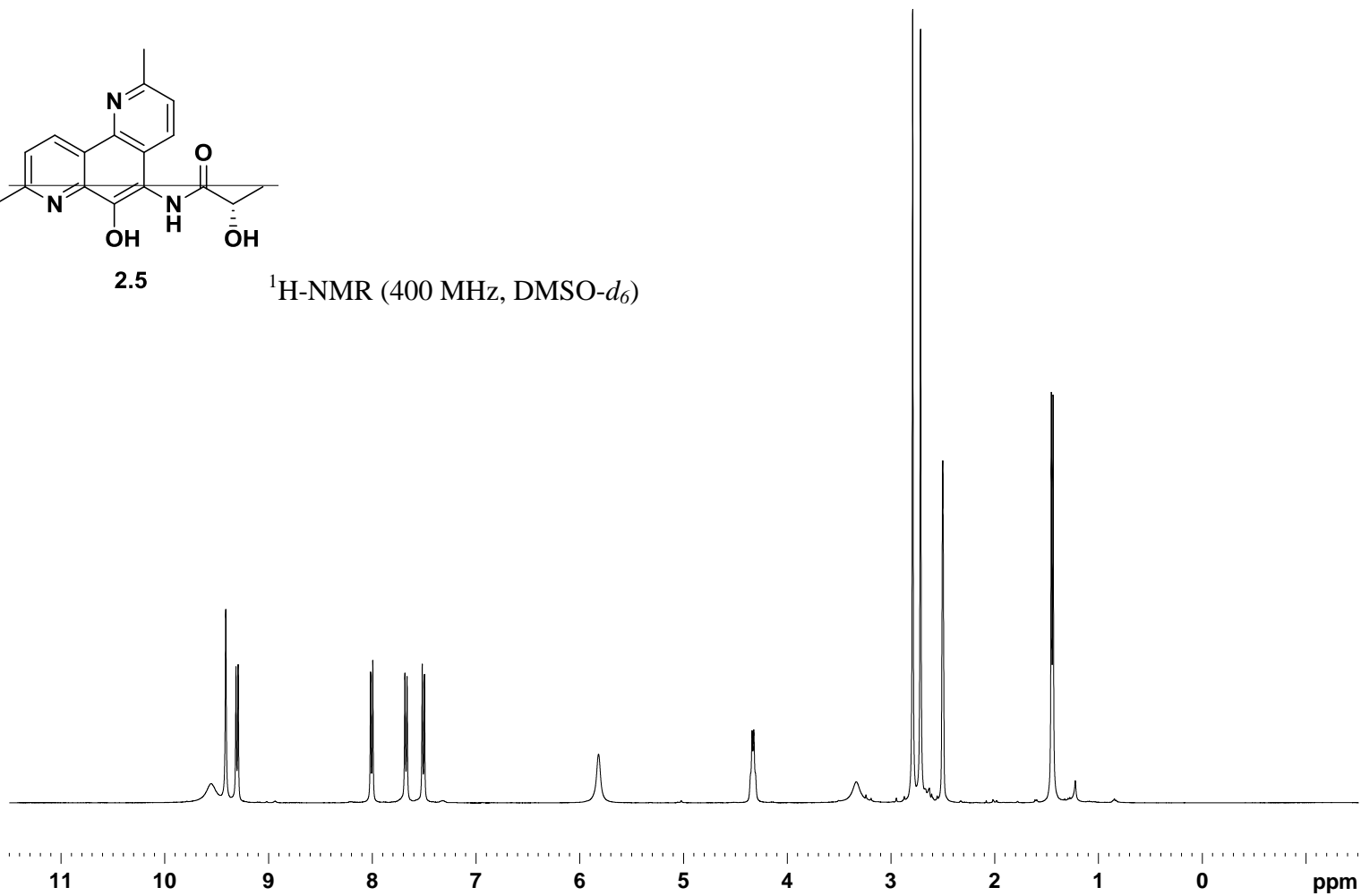


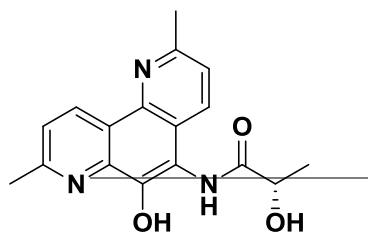


2.5

<sup>1</sup>H-NMR (400 MHz, DMSO-*d*<sub>6</sub>)

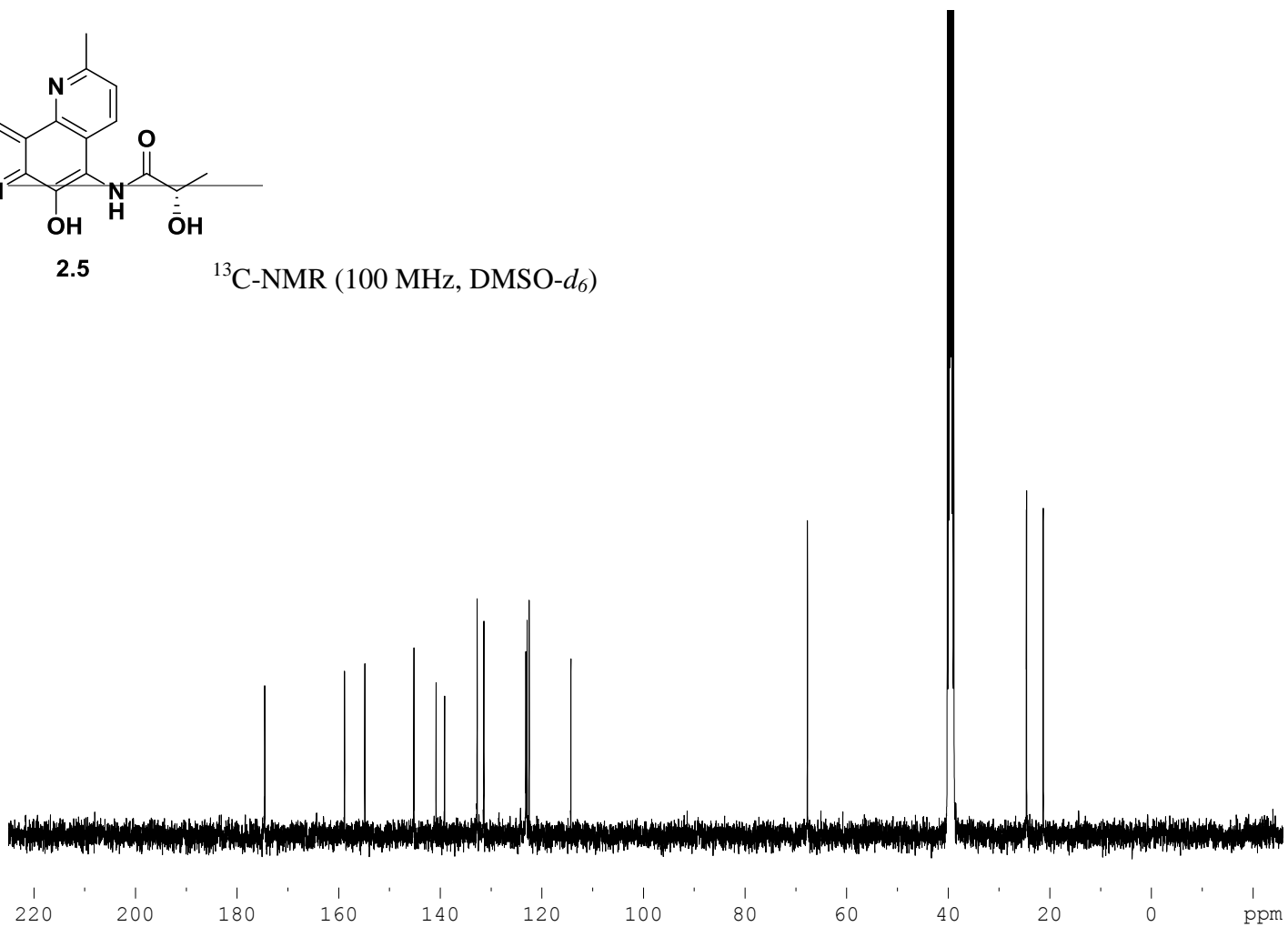
380





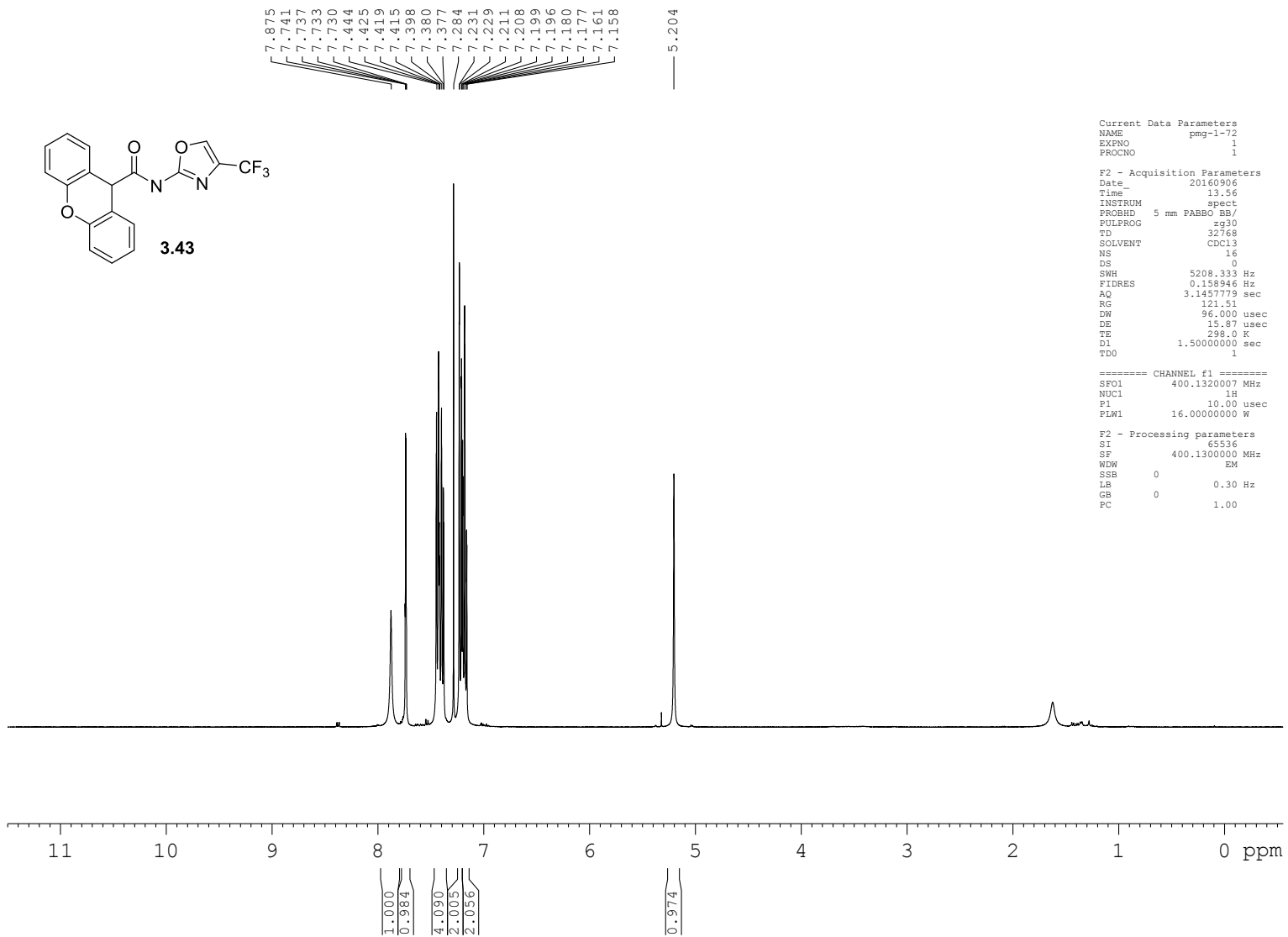
2.5

$^{13}\text{C-NMR}$  (100 MHz,  $\text{DMSO-}d_6$ )

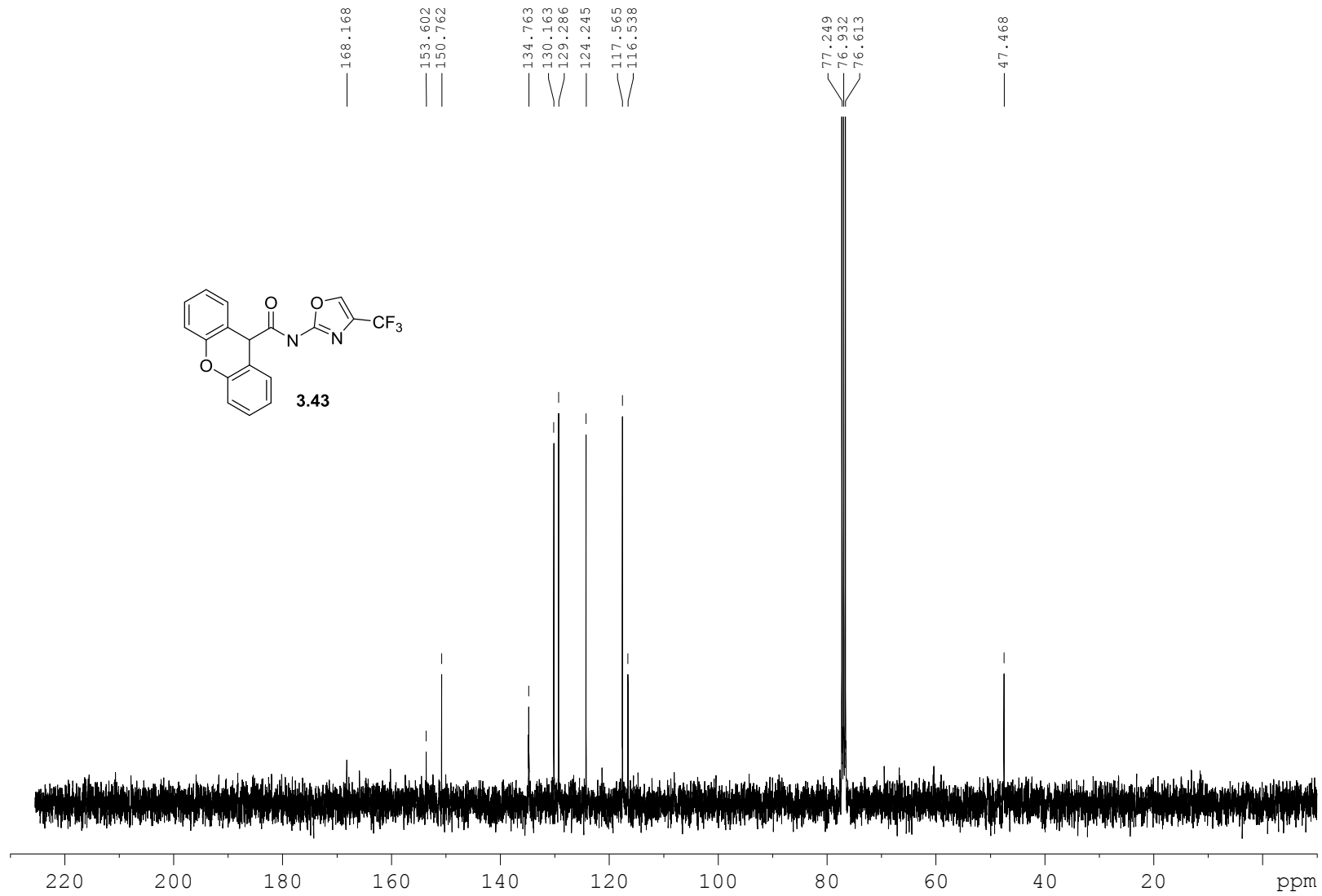


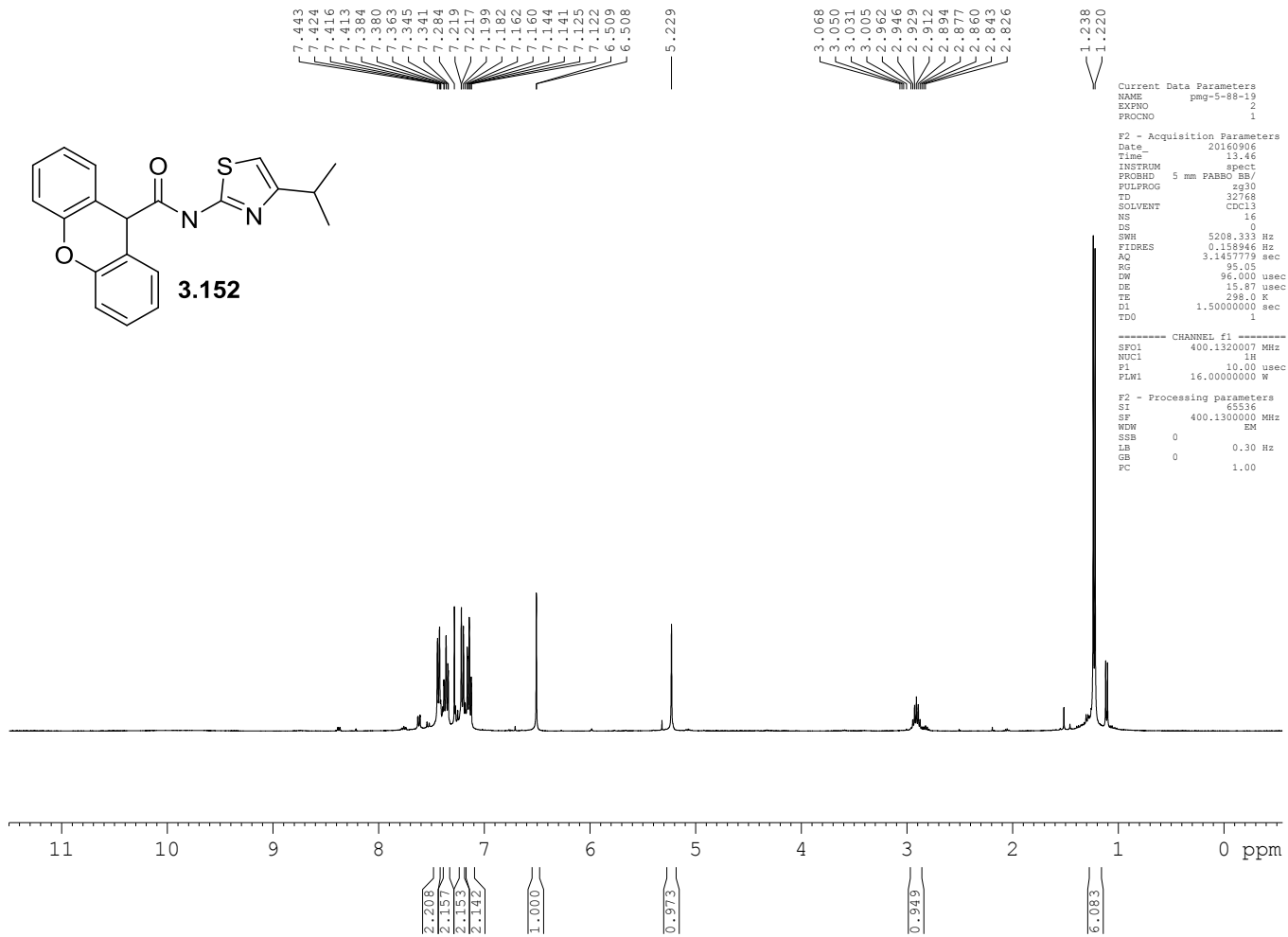
## **Appendix C**

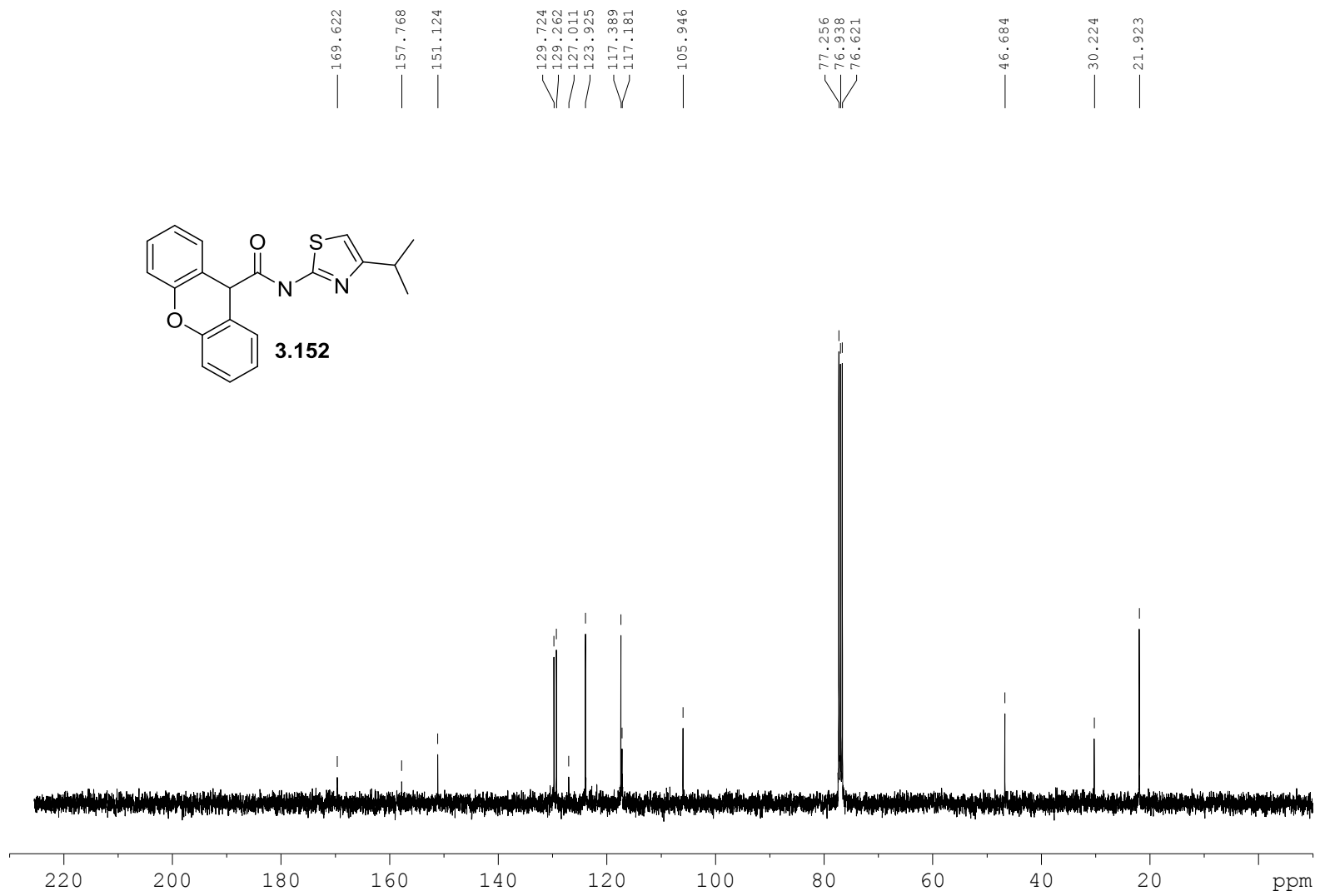
Relevant spectra for chapter III

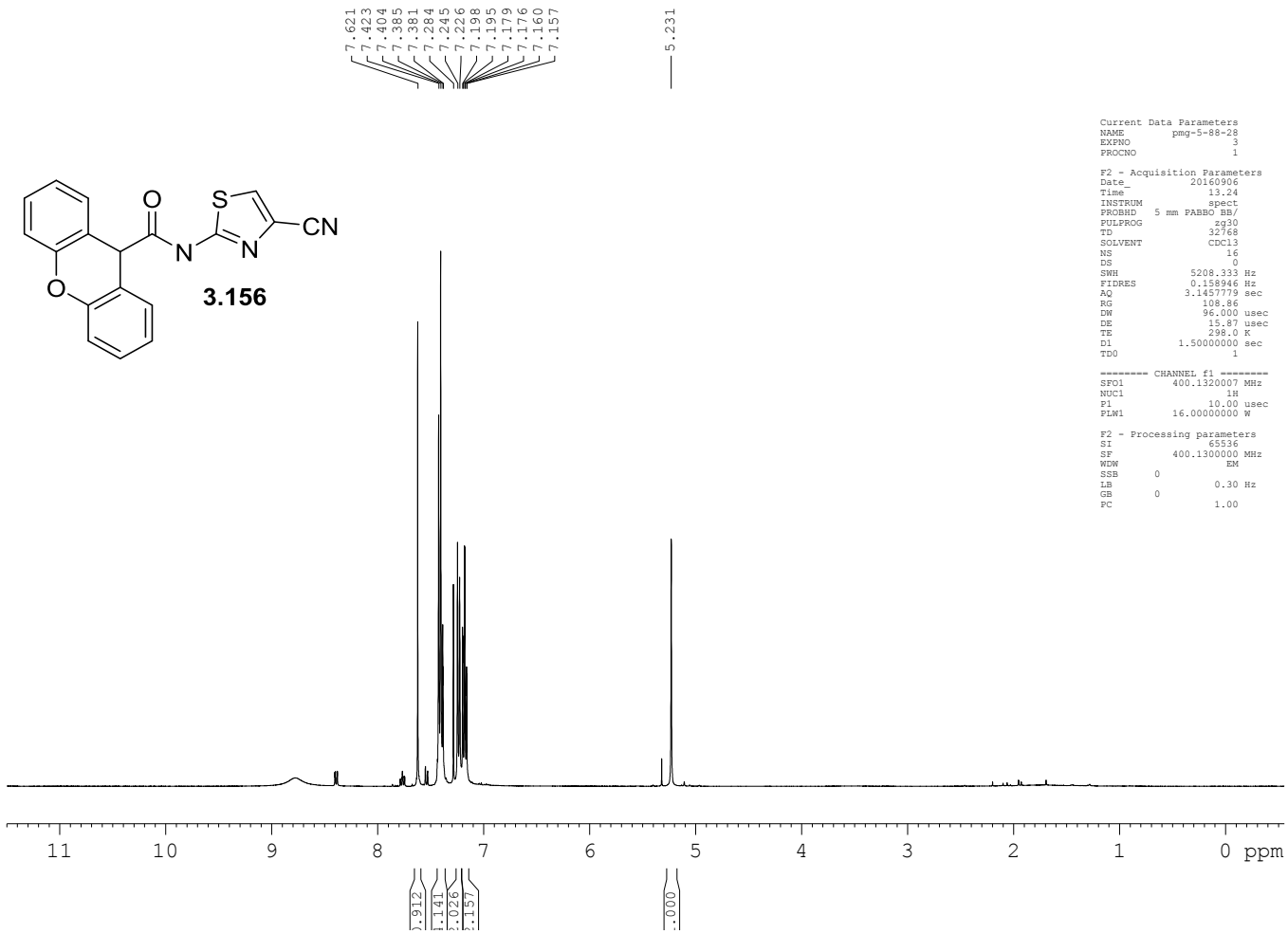


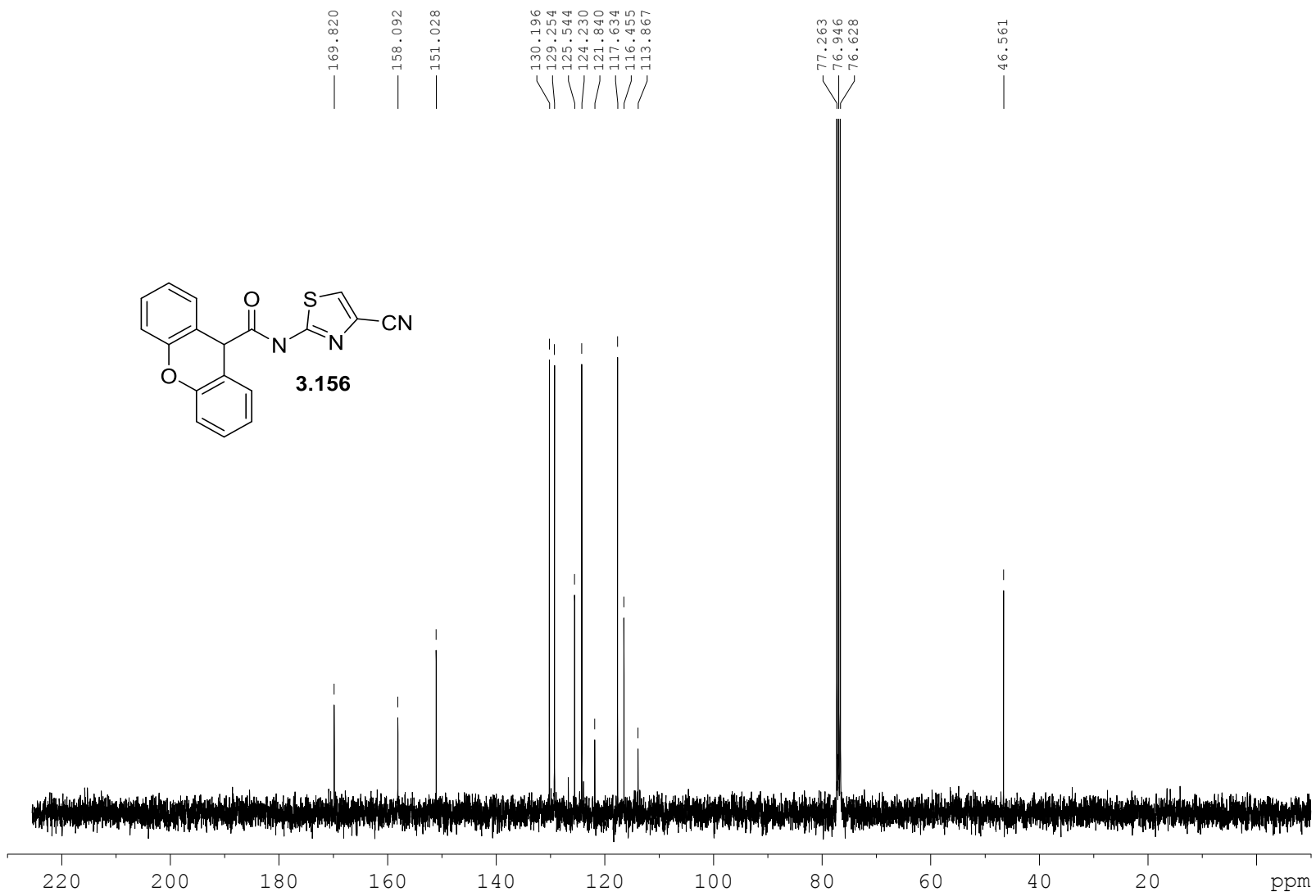
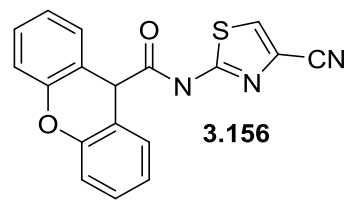








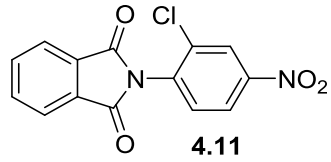




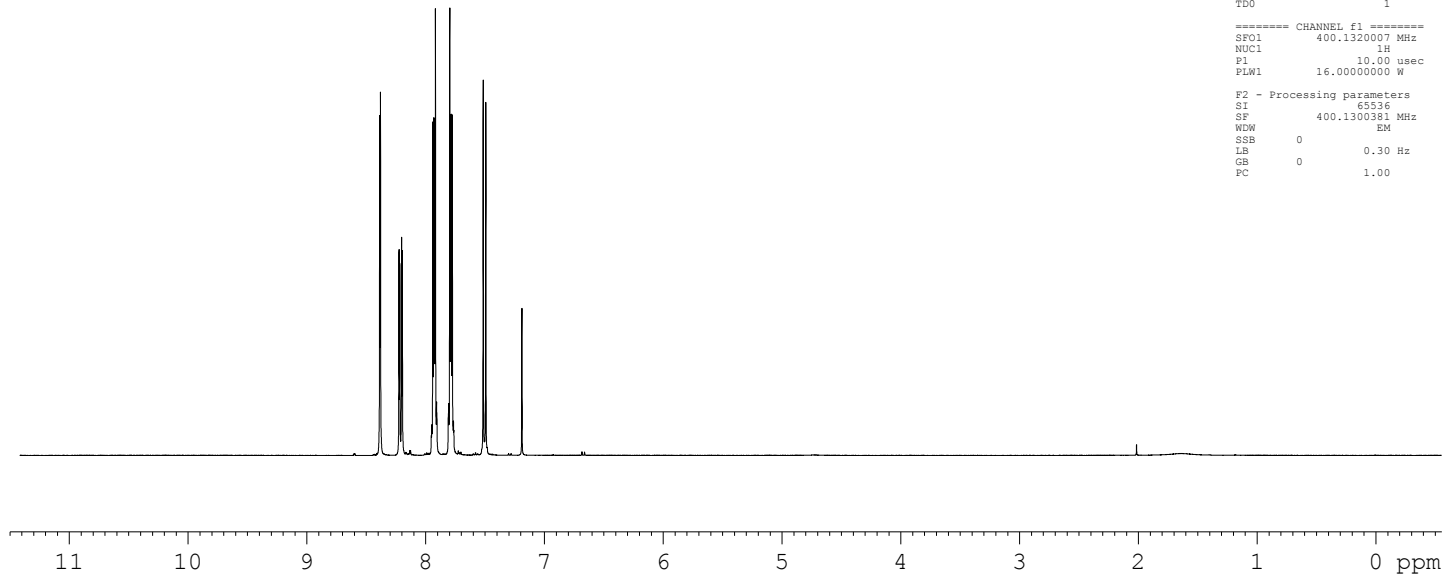
## **Appendix D**

Relevant spectra for chapter IV

390



8.386  
8.380  
8.223  
8.217  
8.202  
8.195  
7.939  
7.931  
7.925  
7.917  
7.786  
7.789  
7.783  
7.775  
7.515  
7.493  
7.189



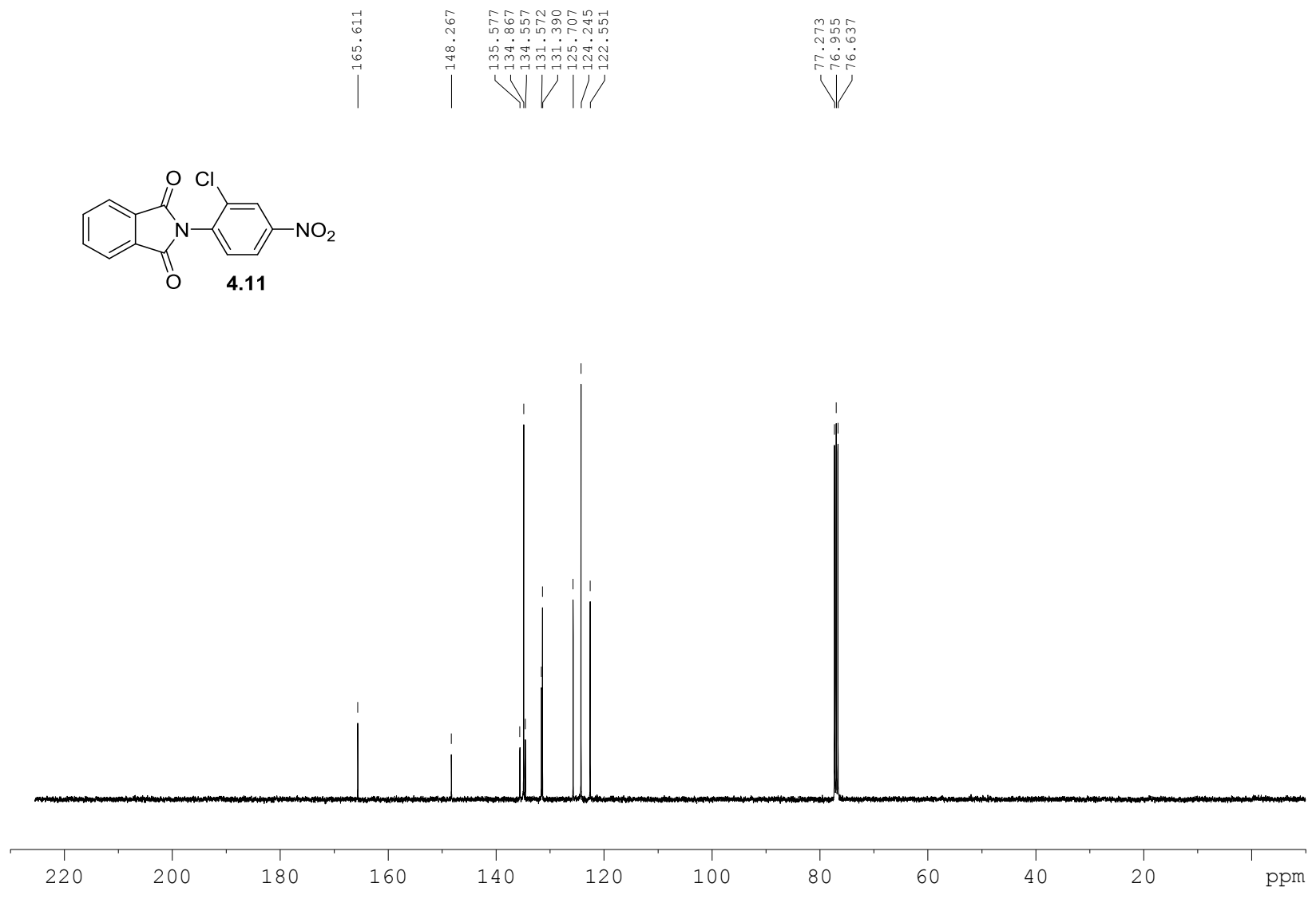
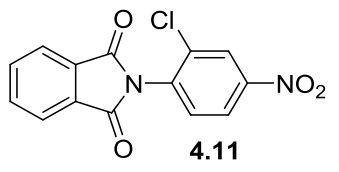
1.000  
1.076  
2.168  
2.214  
1.086

Current Data Parameters  
NAME pmg-1-149  
EXPNO 1  
PROCNO 1

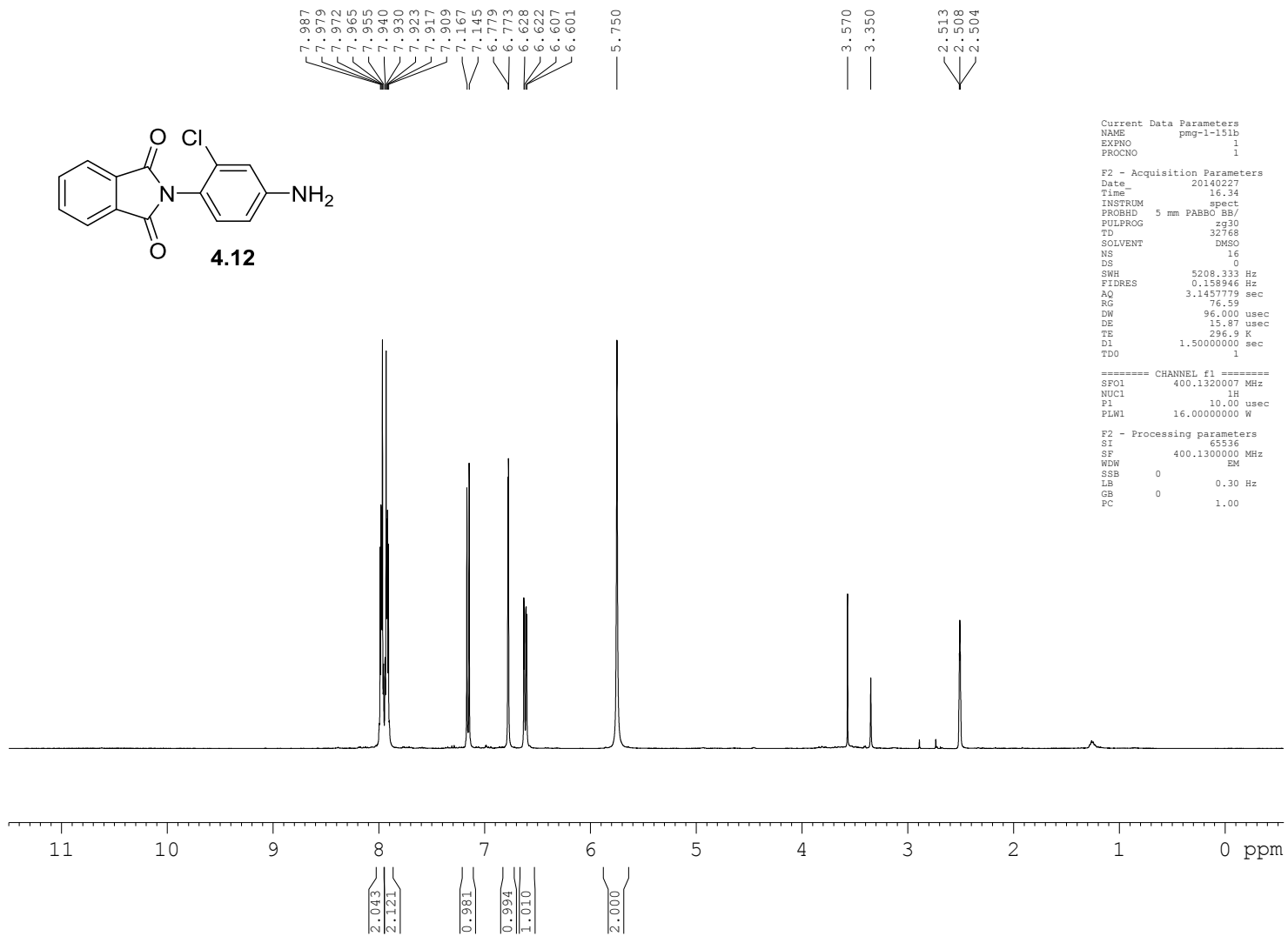
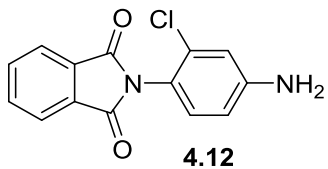
F2 - Acquisition Parameters  
Date\_ 20140227  
Time 16.30  
INSTRUM spect  
PROBHD 5 mm PABBO BB/  
PULPROG zg30  
TD 32768  
SOLVENT CDCl3  
NS 16  
DS 0  
SWH 5208.333 Hz  
FIDRES 0.158946 Hz  
AQ 3.1457779 sec  
RG 86.04  
DW 96.000 usec  
DE 15.87 usec  
TE 297.0 K  
D1 1.50000000 sec  
TDO 1

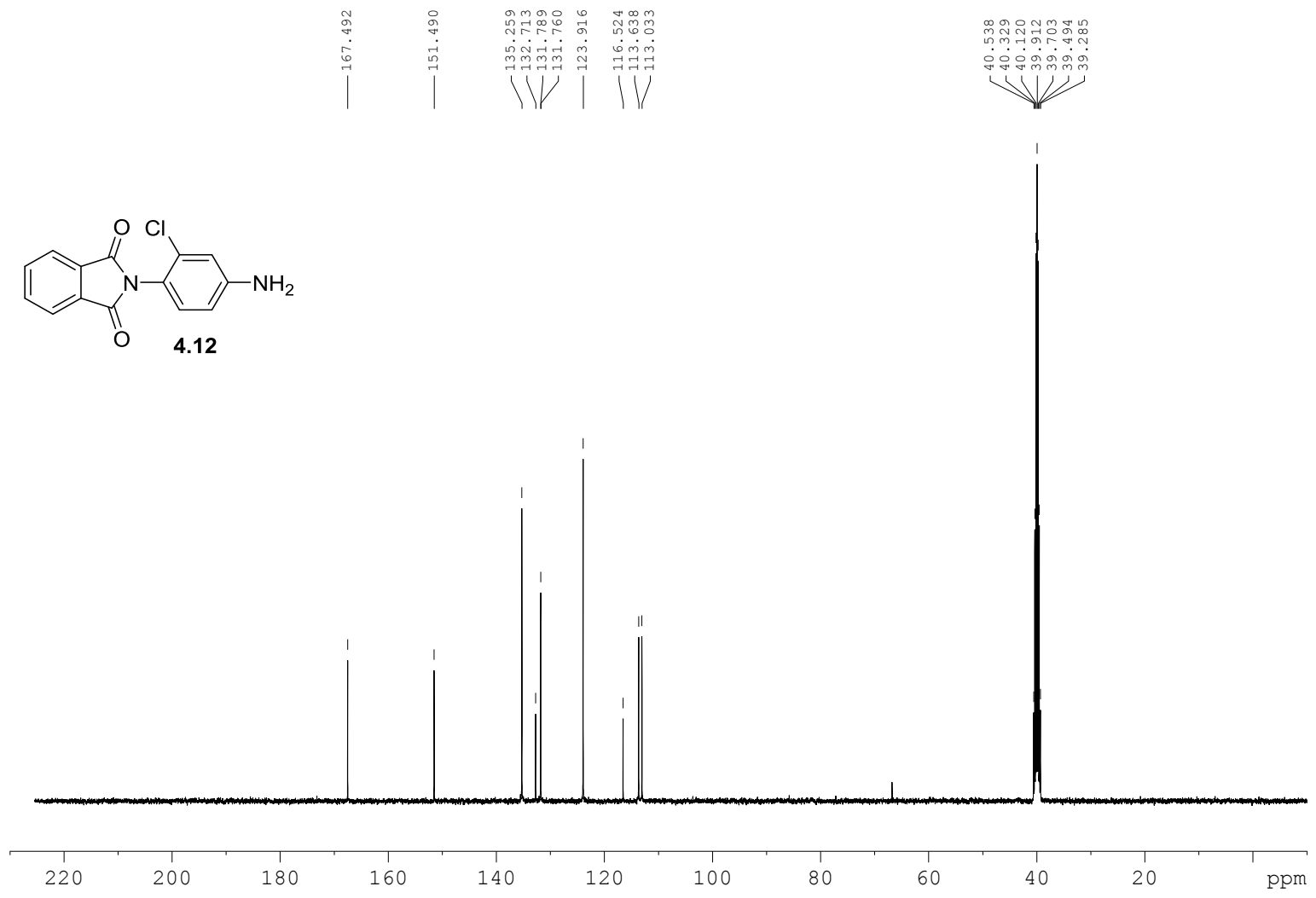
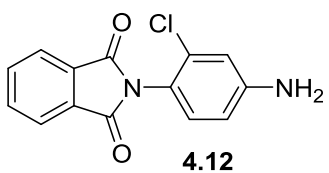
\*\*\*\*\* CHANNEL f1 \*\*\*\*\*  
SFO1 400.1320007 MHz  
NUC1 1H  
P1 10.00 usec  
PLW1 16.00000000 W

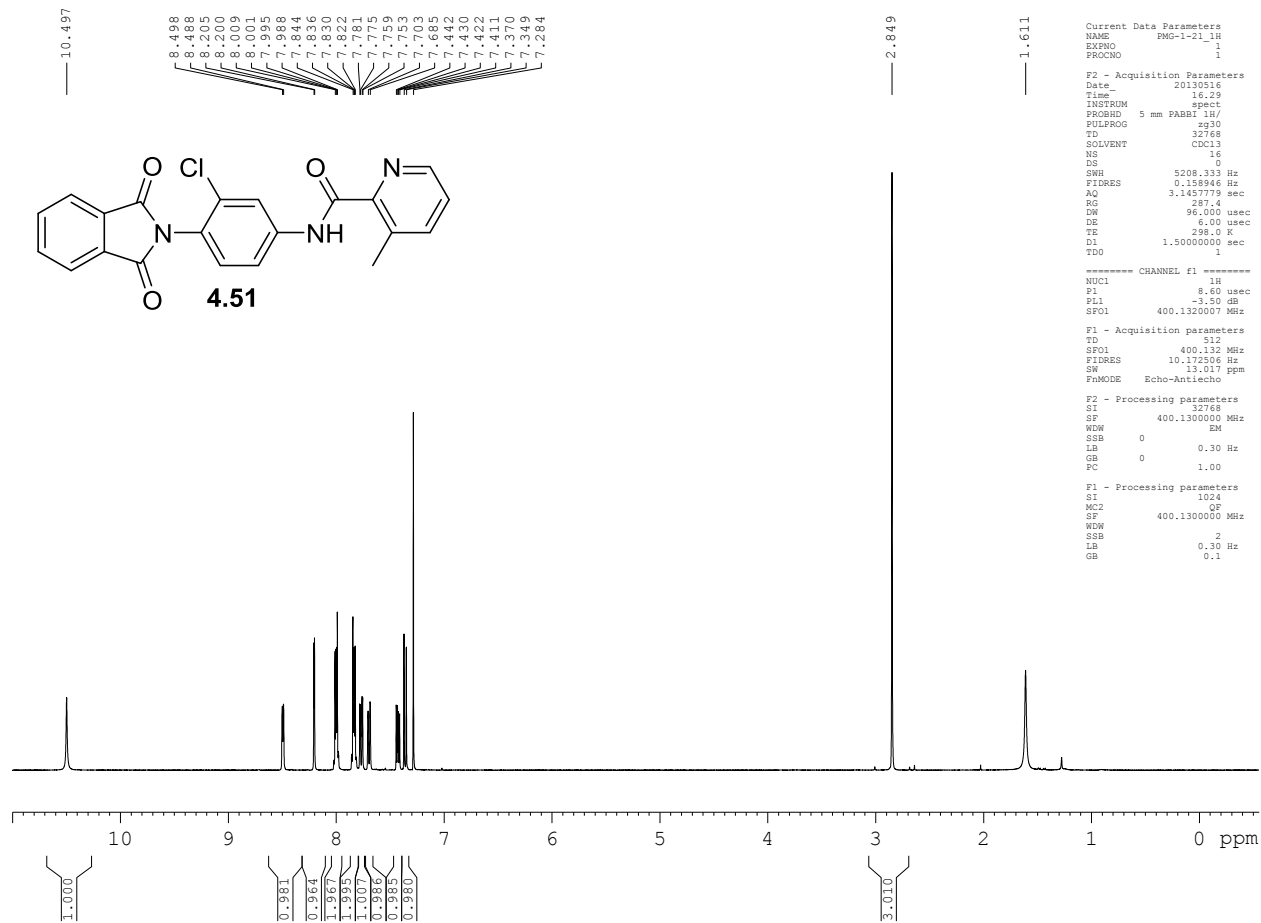
F2 - Processing parameters  
SI 65536  
SF 400.1300381 MHz  
WDW EM  
SSB 0  
LB 0.30 Hz  
GB 0  
PC 1.00











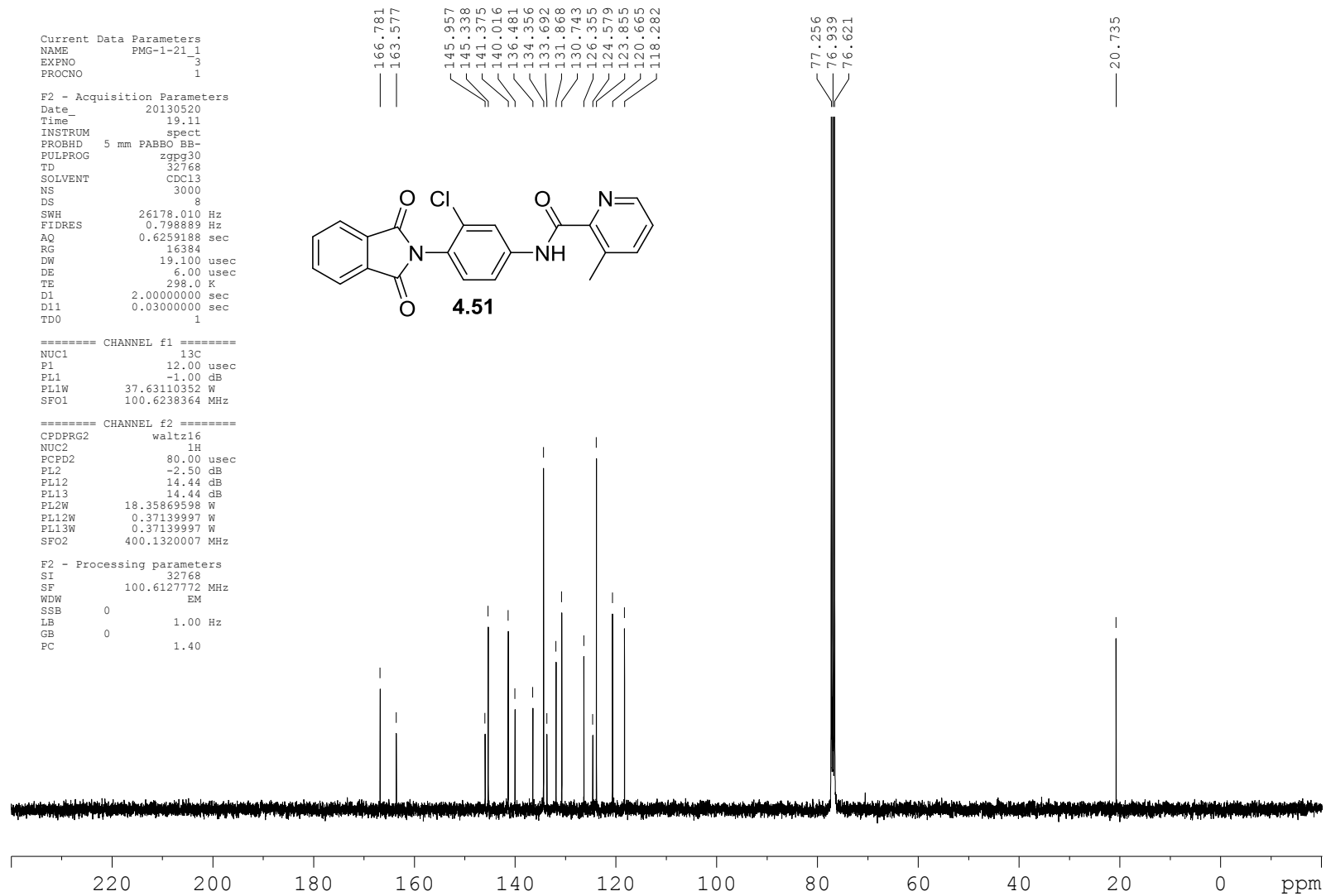
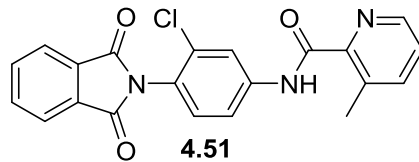
Current Data Parameters  
 NAME PMG-1-21\_1  
 EXPNO 3  
 PROCNO 1

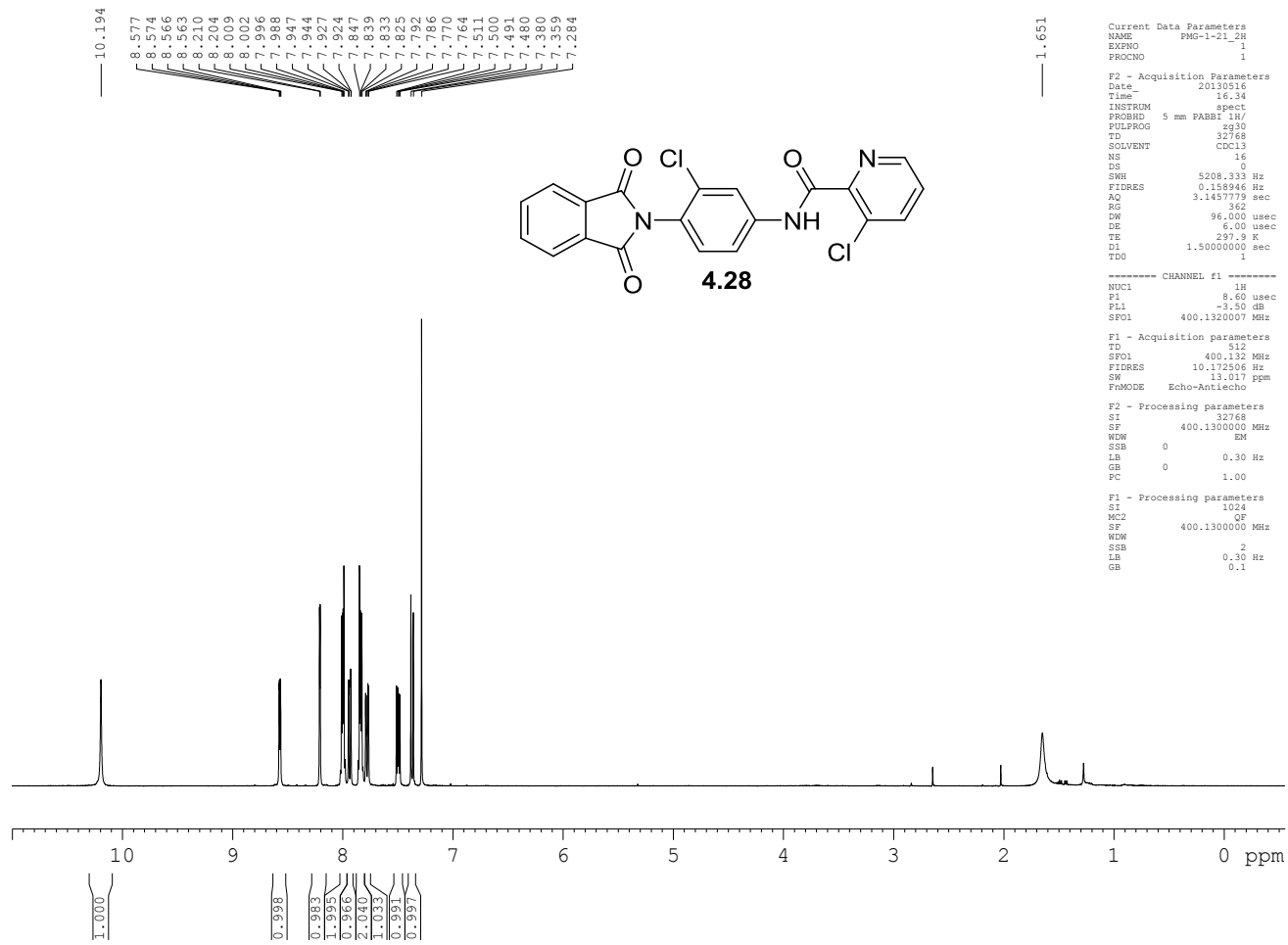
F2 - Acquisition Parameters  
 Date\_ 20130520  
 Time\_ 19.11  
 INSTRUM spect  
 PROBHD 5 mm PABBO BB-  
 PULPROG zgpg30  
 TD 32768  
 SOLVENT CDCl3  
 NS 3000  
 DS 8  
 SWH 26178.010 Hz  
 FIDRES 0.798889 Hz  
 AQ 0.6259188 sec  
 RG 16384  
 DW 19.100 usec  
 DE 6.00 usec  
 TE 298.0 K  
 D1 2.00000000 sec  
 D11 0.03000000 sec  
 TD0 1

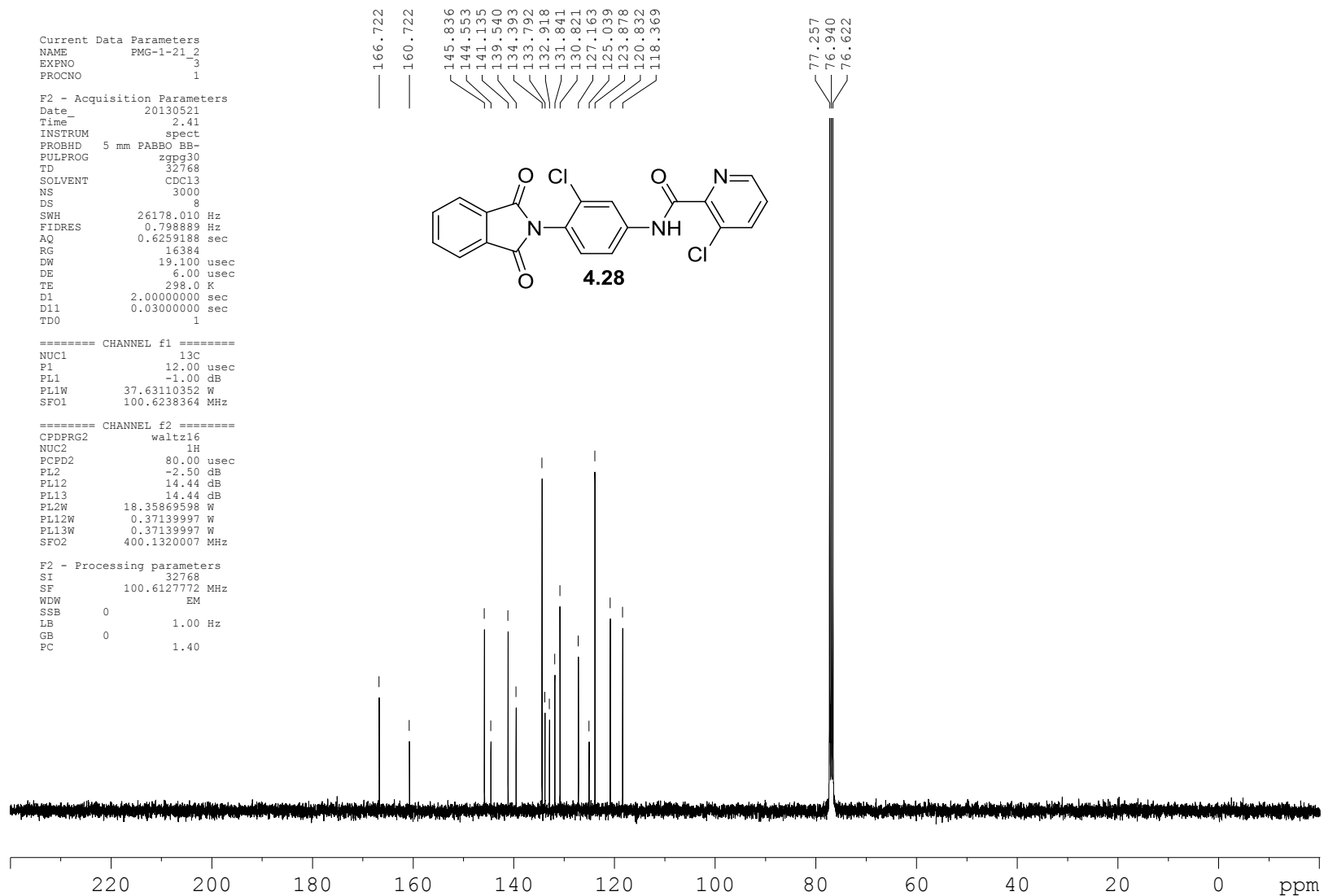
===== CHANNEL f1 =====  
 NUC1 13C  
 P1 12.00 usec  
 PL1 -1.00 dB  
 PL1W 37.63110352 W  
 SFO1 100.6238364 MHz

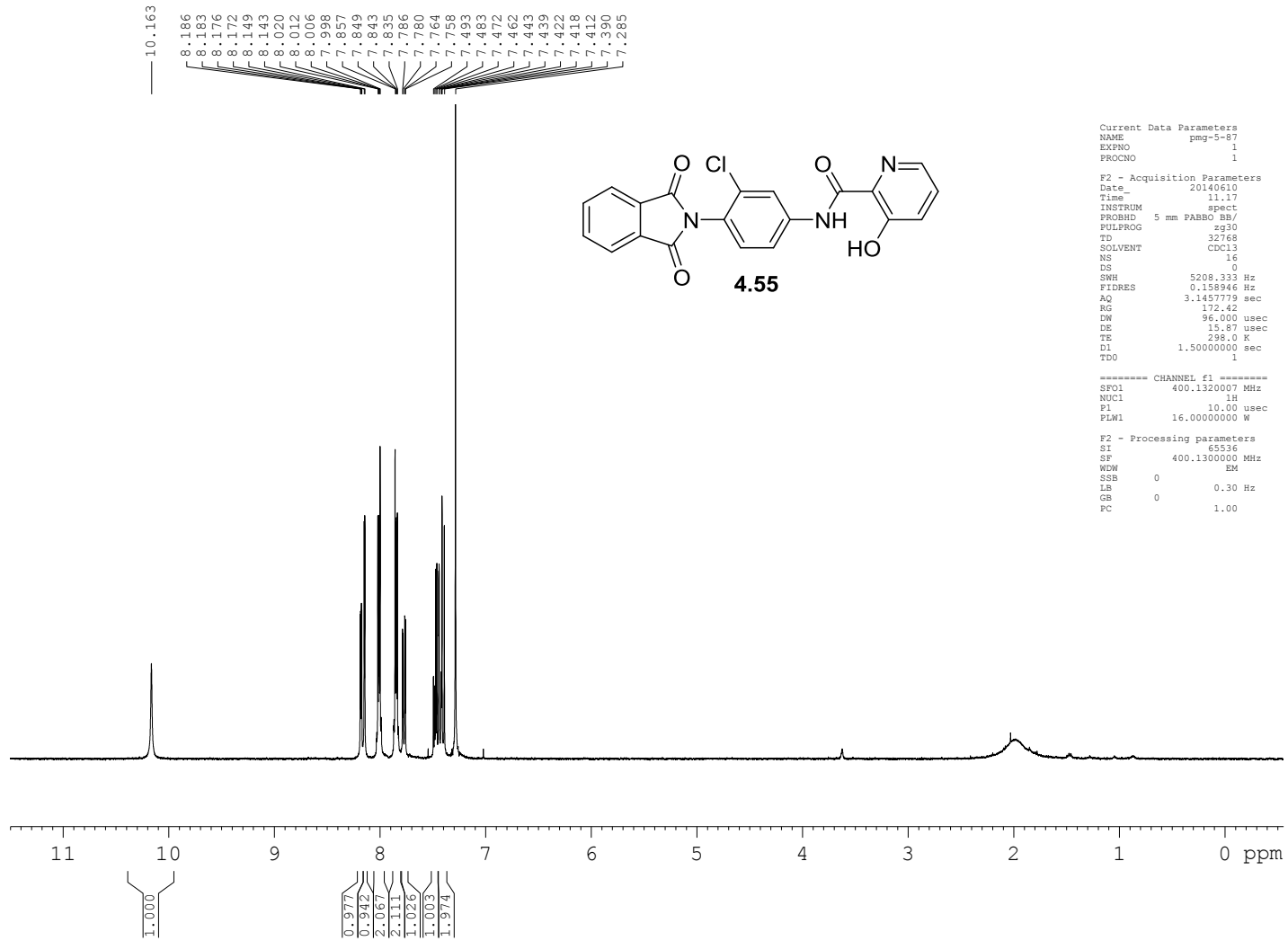
===== CHANNEL f2 =====  
 CPDPRG2 waltz16  
 NUC2 1H  
 PCPD2 80.00 usec  
 PL2 -2.50 dB  
 PL12 14.44 dB  
 PL13 14.44 dB  
 PL2W 18.35869598 W  
 PL12W 0.37139997 W  
 PL13W 0.37139997 W  
 SFO2 400.1320007 MHz

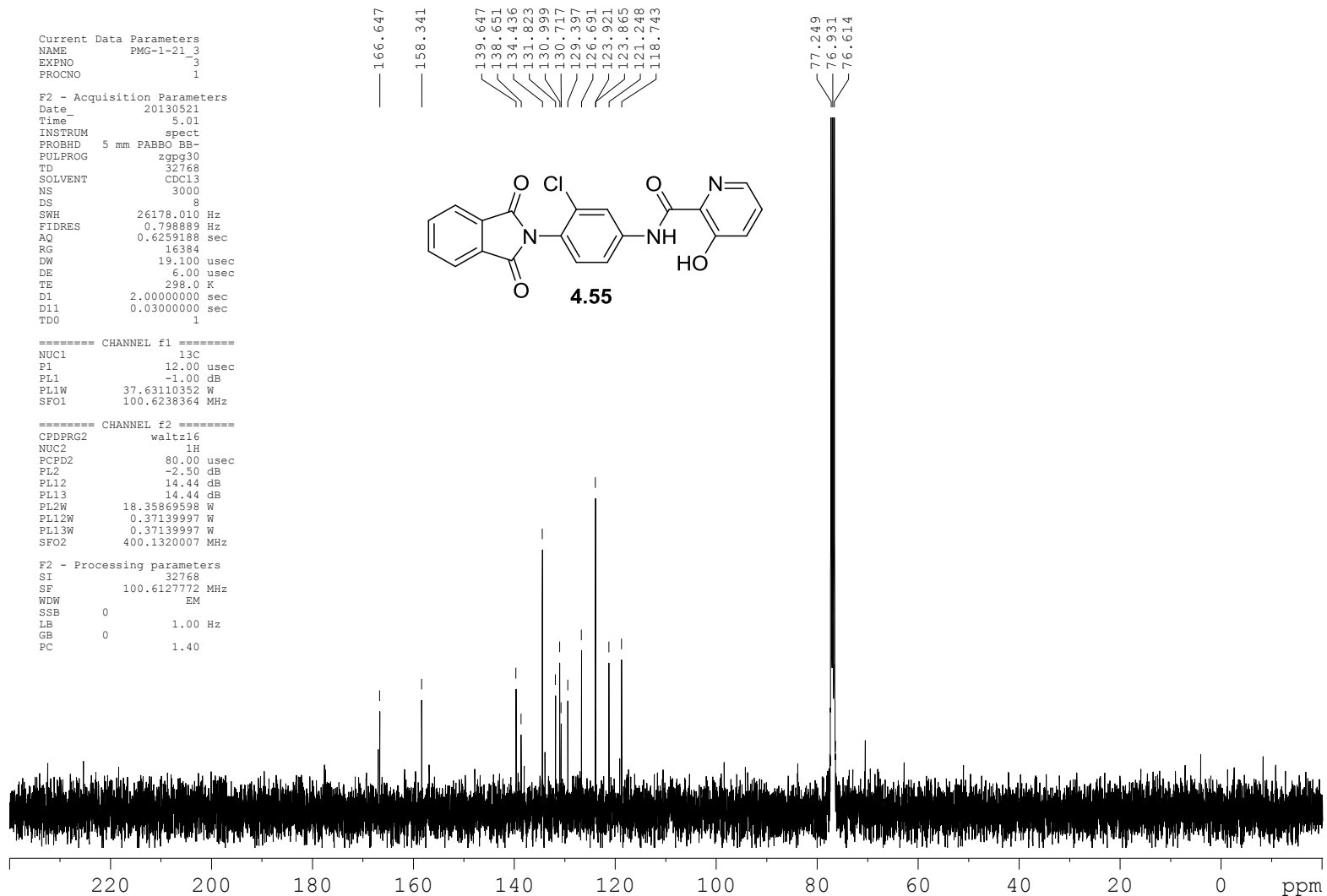
F2 - Processing parameters  
 SI 32768  
 SF 100.612772 MHz  
 WDW EM  
 SSB 0  
 LB 1.00 Hz  
 GB 0  
 PC 1.40





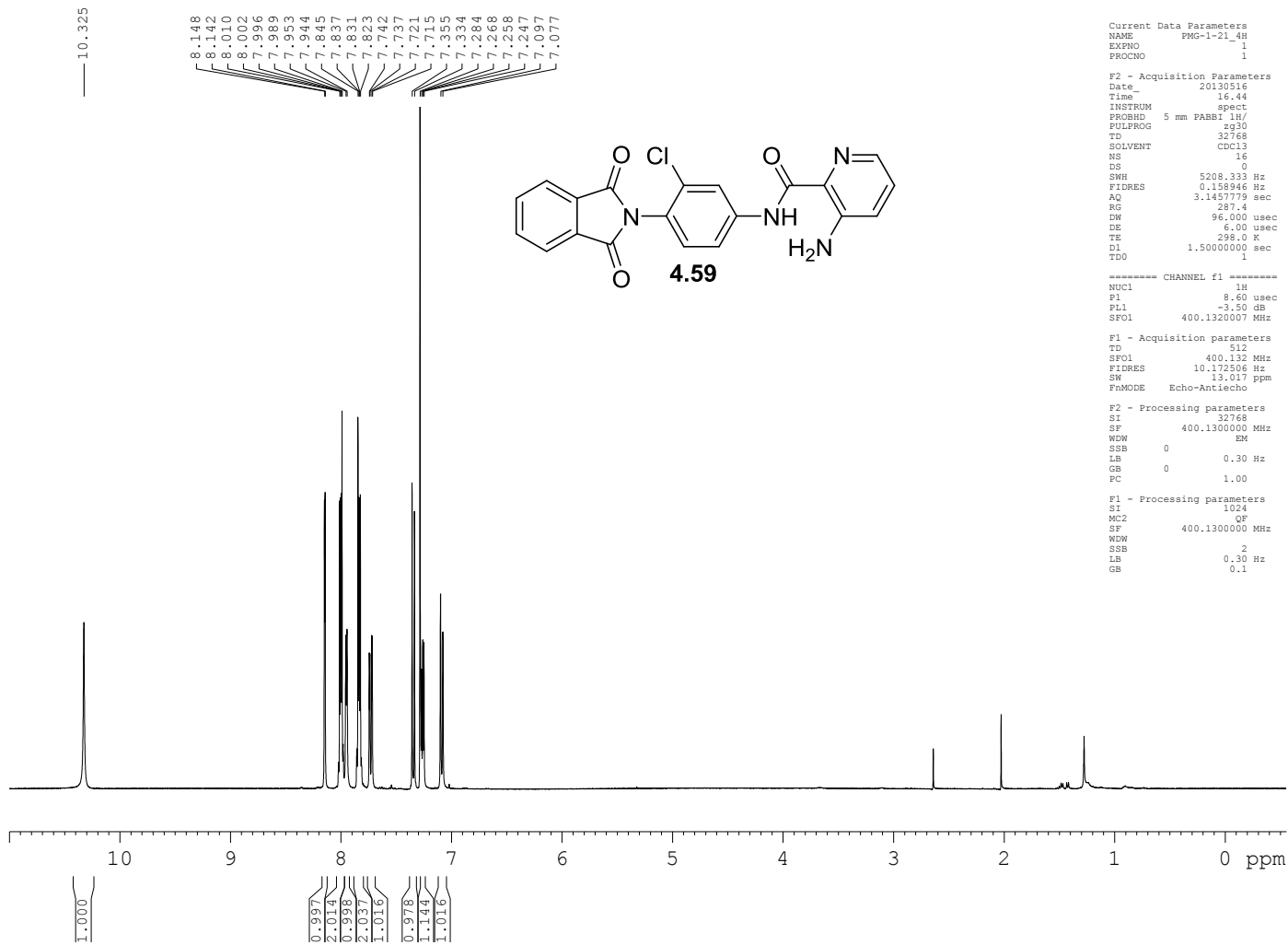








400



Current Data Parameters  
NAME PMG-1-21\_4  
EXPNO 3  
PROCNO 1

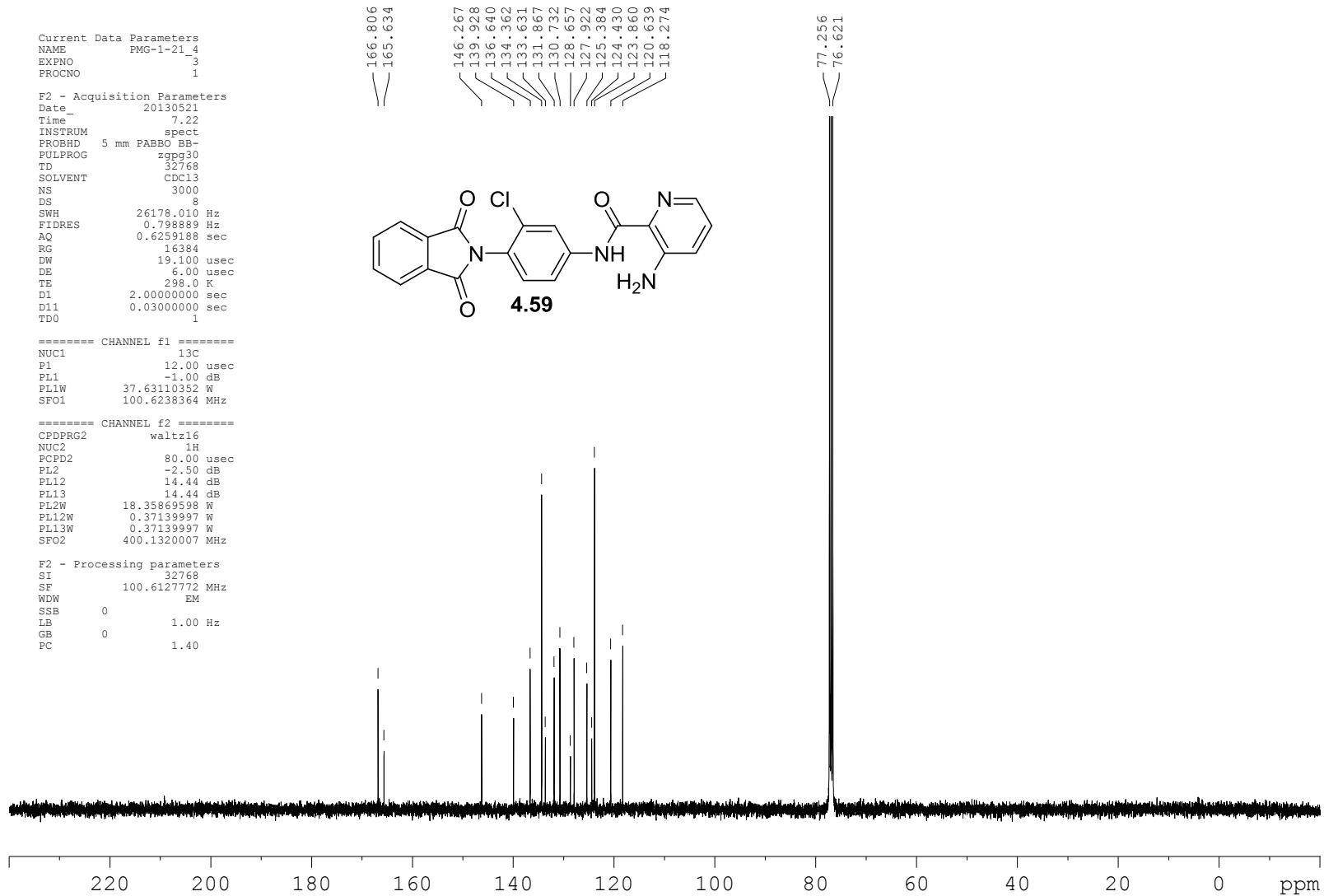
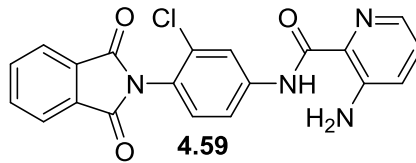
F2 - Acquisition Parameters  
Date\_ 20130521  
Time 7.22  
INSTRUM spect  
PROBHD 5 mm PABBO BB-  
PULPROG zgpg30  
TD 32768  
SOLVENT CDCl3  
NS 3000  
DS 8  
SWH 26178.010 Hz  
FIDRES 0.798889 Hz  
AQ 0.6259188 sec  
RG 16384  
DW 19.100 usec  
DE 6.00 usec  
TE 298.0 K  
D1 2.00000000 sec  
D11 0.03000000 sec  
TD0 1

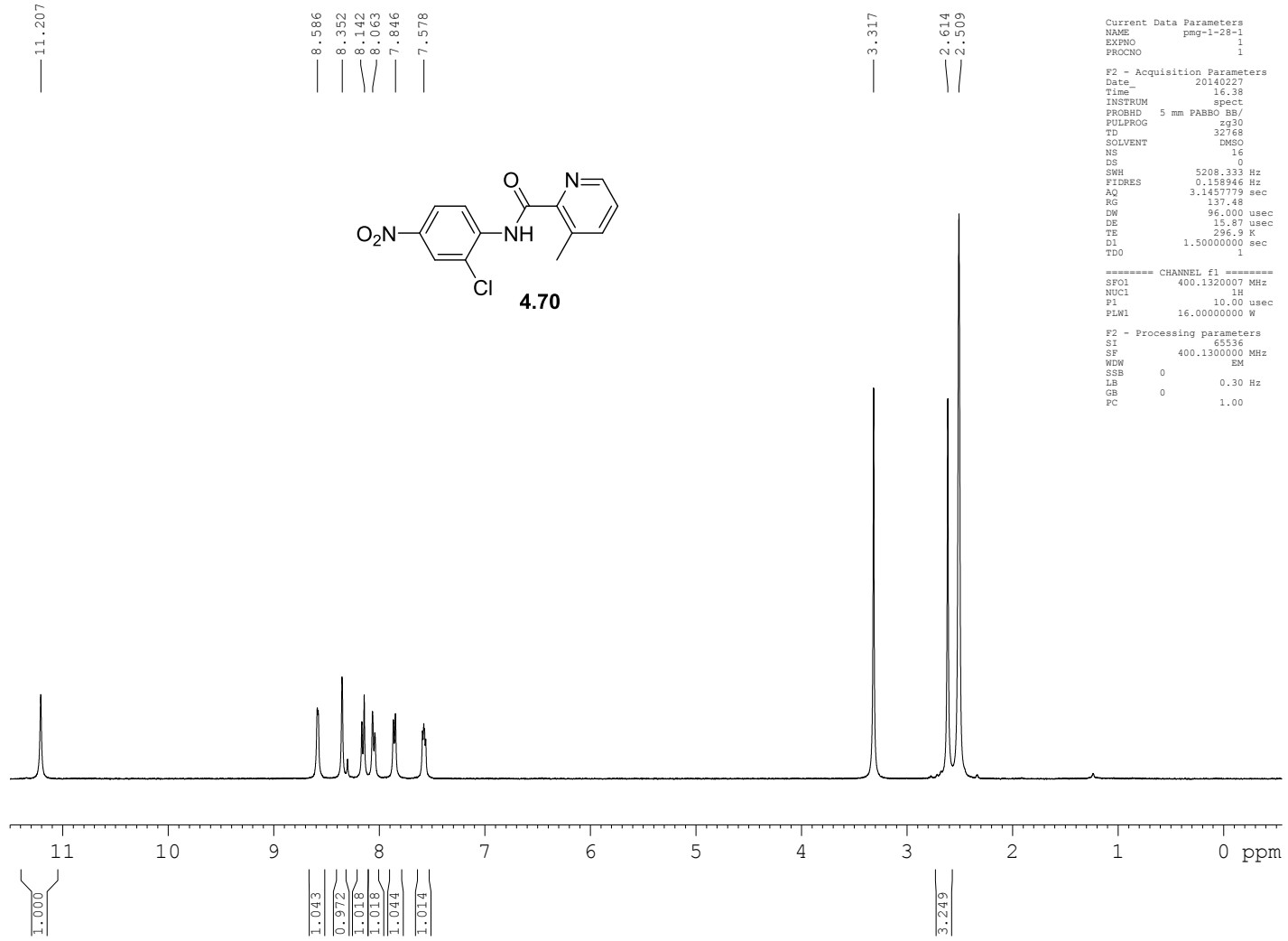
===== CHANNEL f1 =====  
NUC1 13C  
P1 12.00 usec  
PL1 -1.00 dB  
PL1W 37.63110352 W  
SFO1 100.6238364 MHz

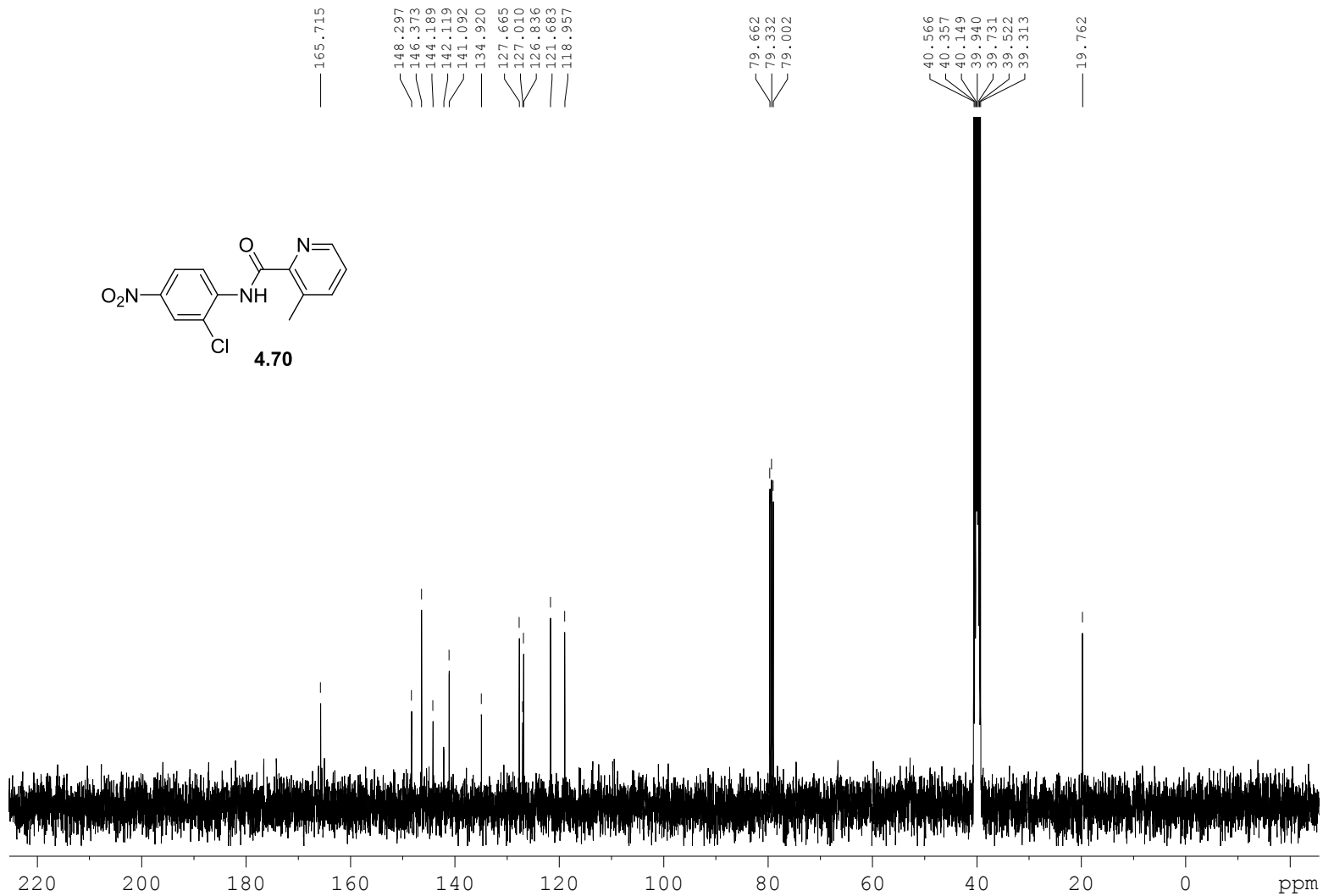
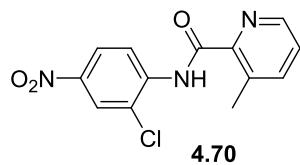
===== CHANNEL f2 =====  
CPDPRG2 waltz16  
NUC2 1H  
PCPD2 80.00 usec  
PL2 -2.50 dB  
PL12 14.44 dB  
PL13 14.44 dB  
PL2W 18.35869598 W  
PL12W 0.37139997 W  
PL13W 0.37139997 W  
SFO2 400.1320007 MHz

F2 - Processing parameters  
SI 32768  
SF 100.6127772 MHz  
WDW EM  
SSB 0  
LB 1.00 Hz  
GB 0  
PC 1.40

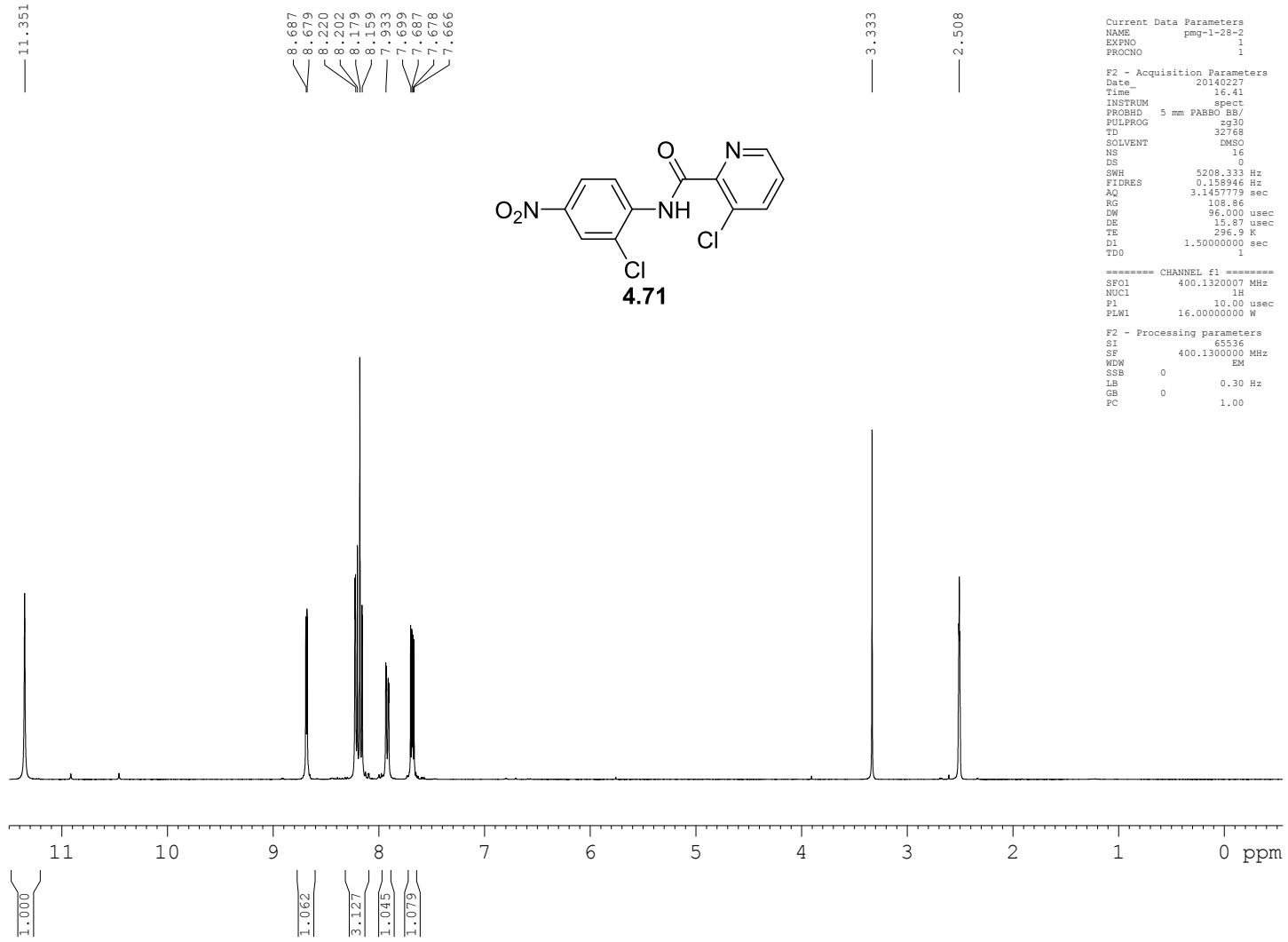
166.806  
165.634  
146.267  
139.928  
136.640  
134.362  
133.631  
131.867  
130.732  
128.657  
127.922  
125.384  
124.430  
123.860  
120.639  
118.274  
77.256  
76.621

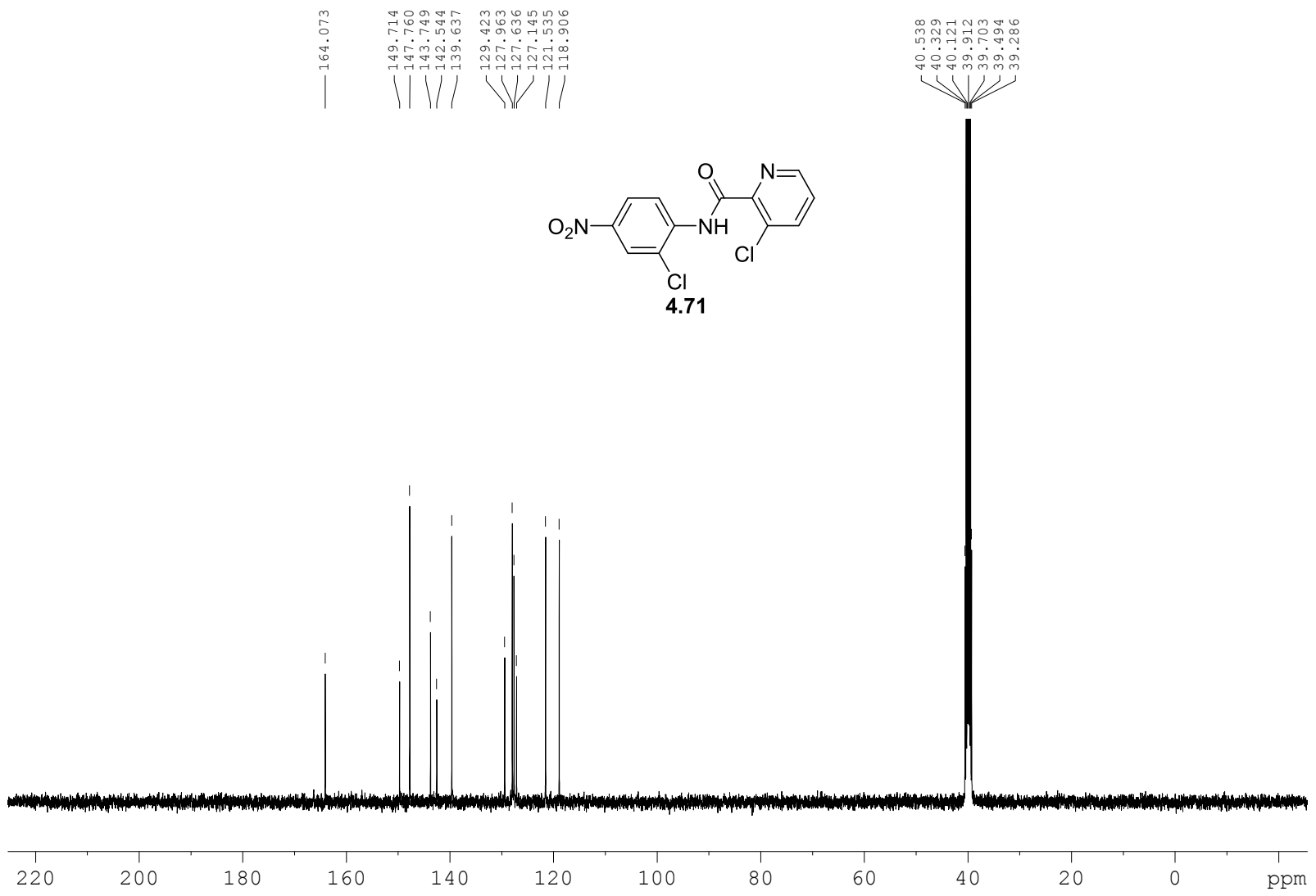


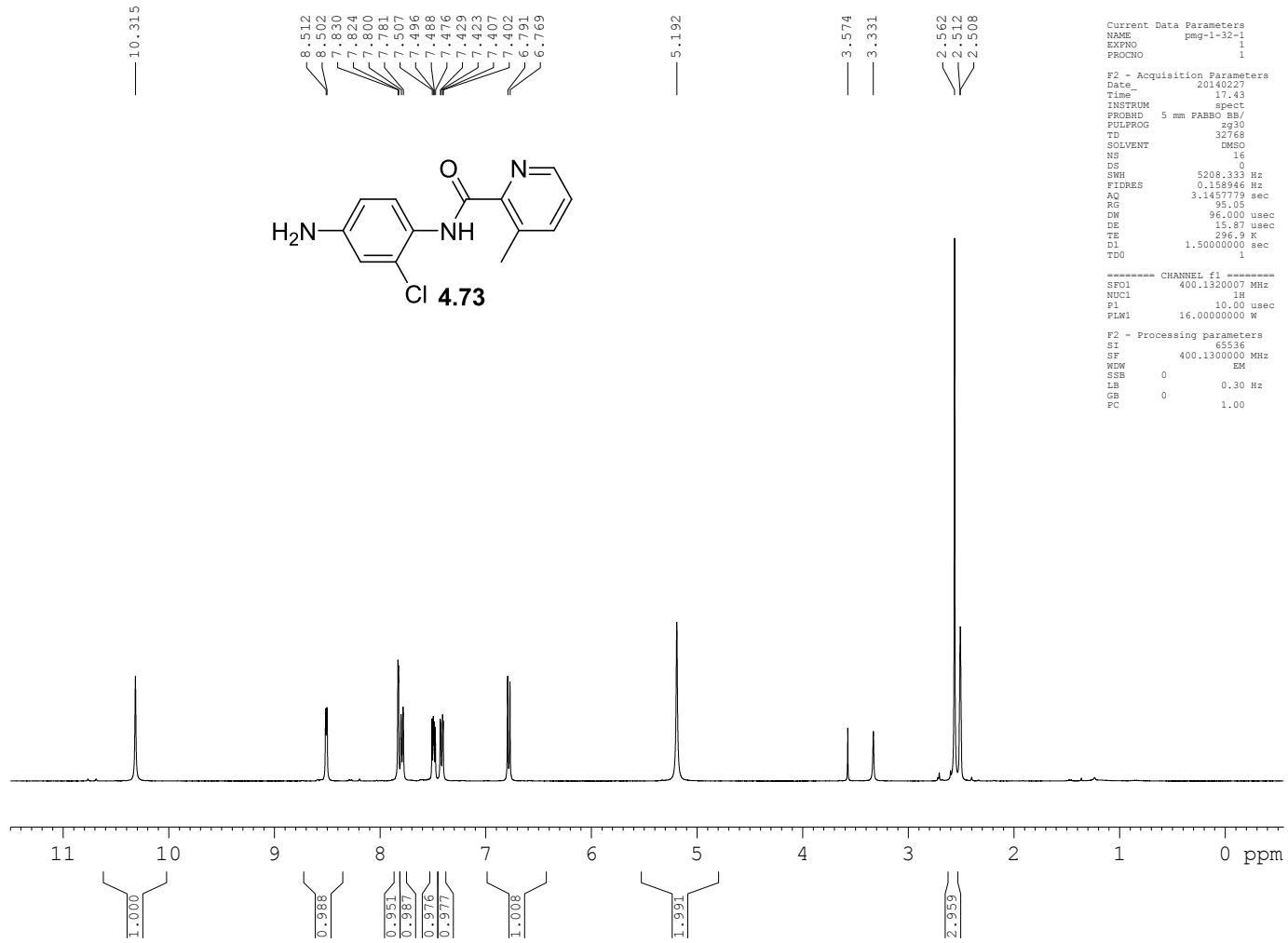


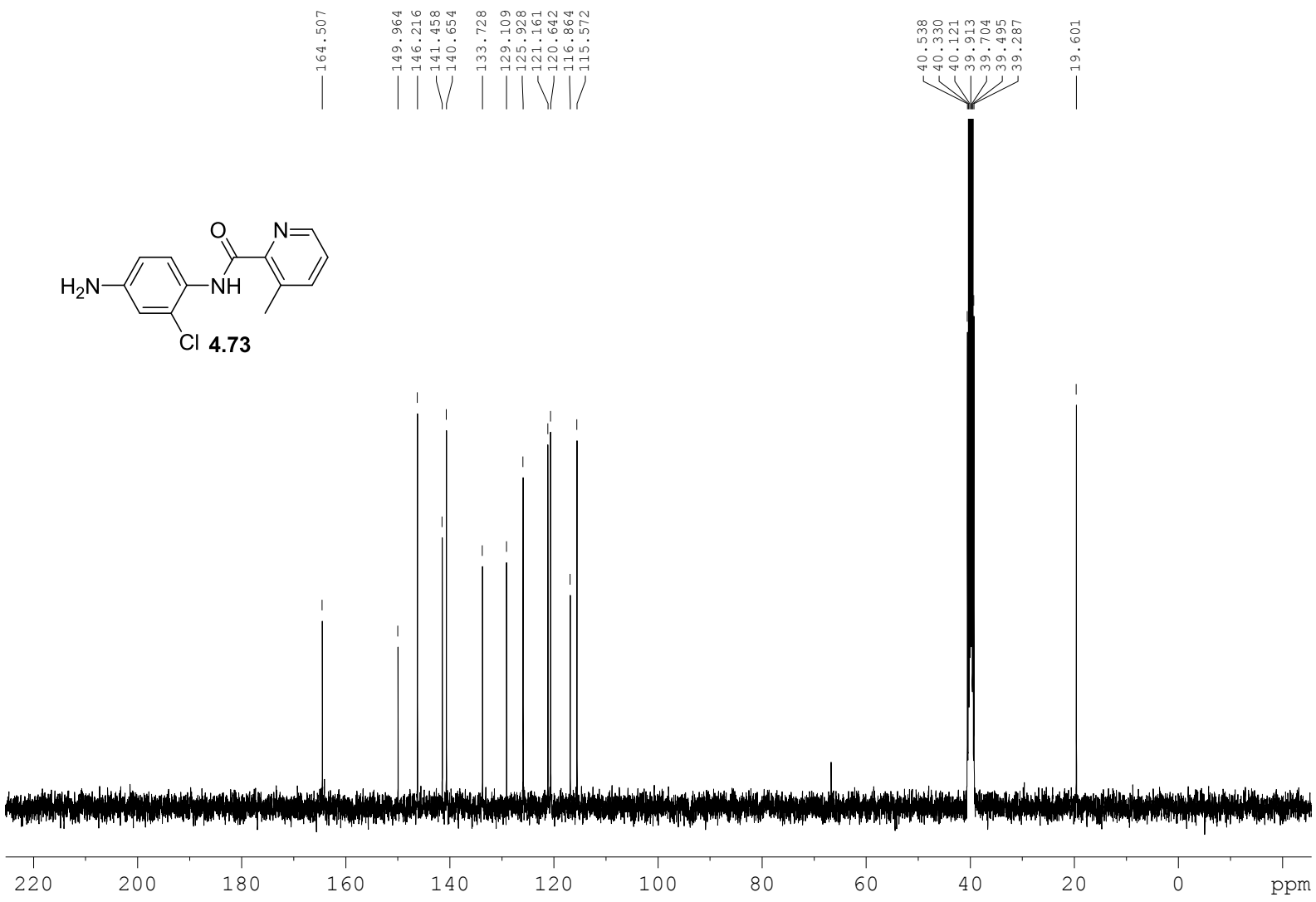


404

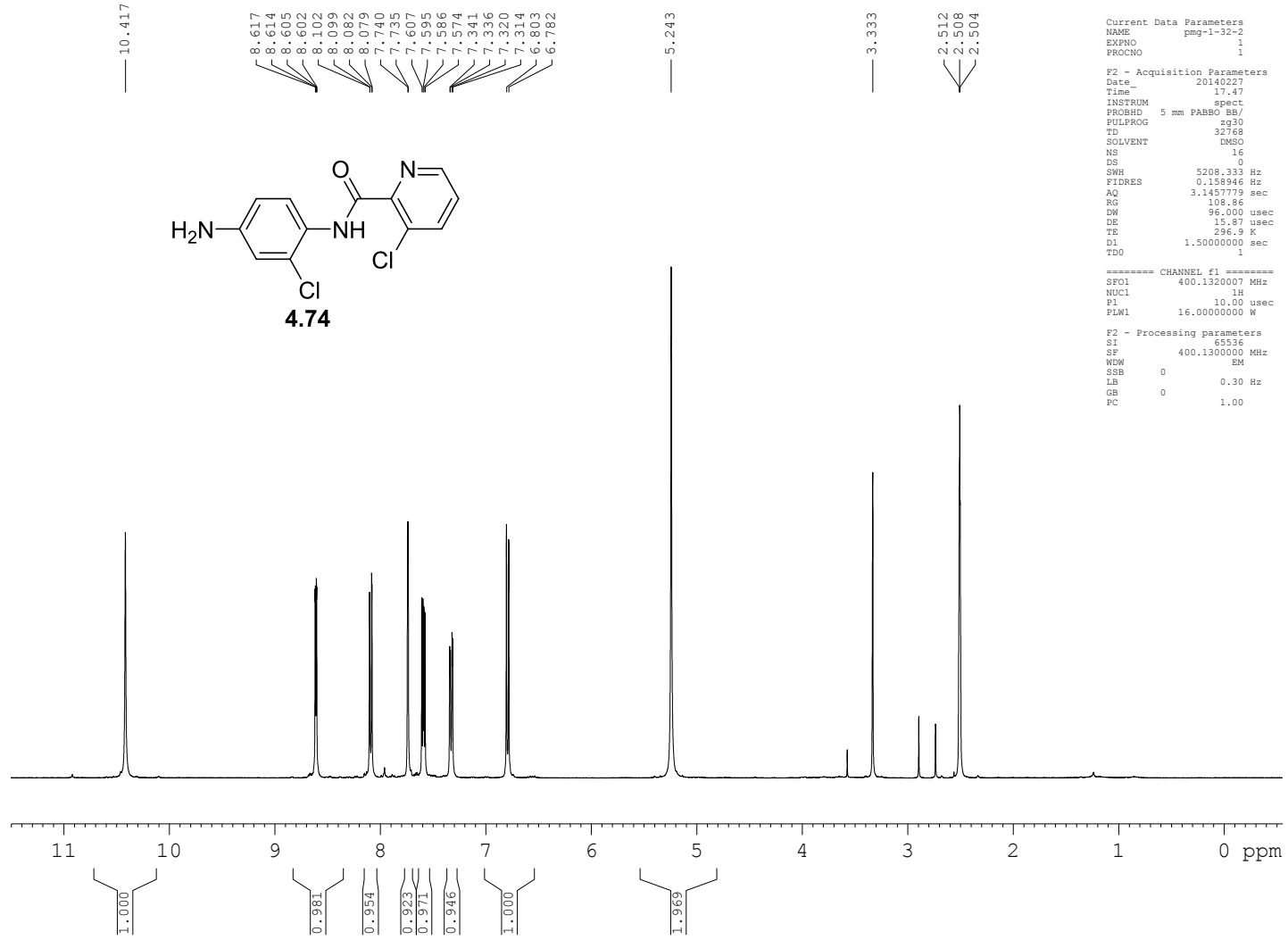












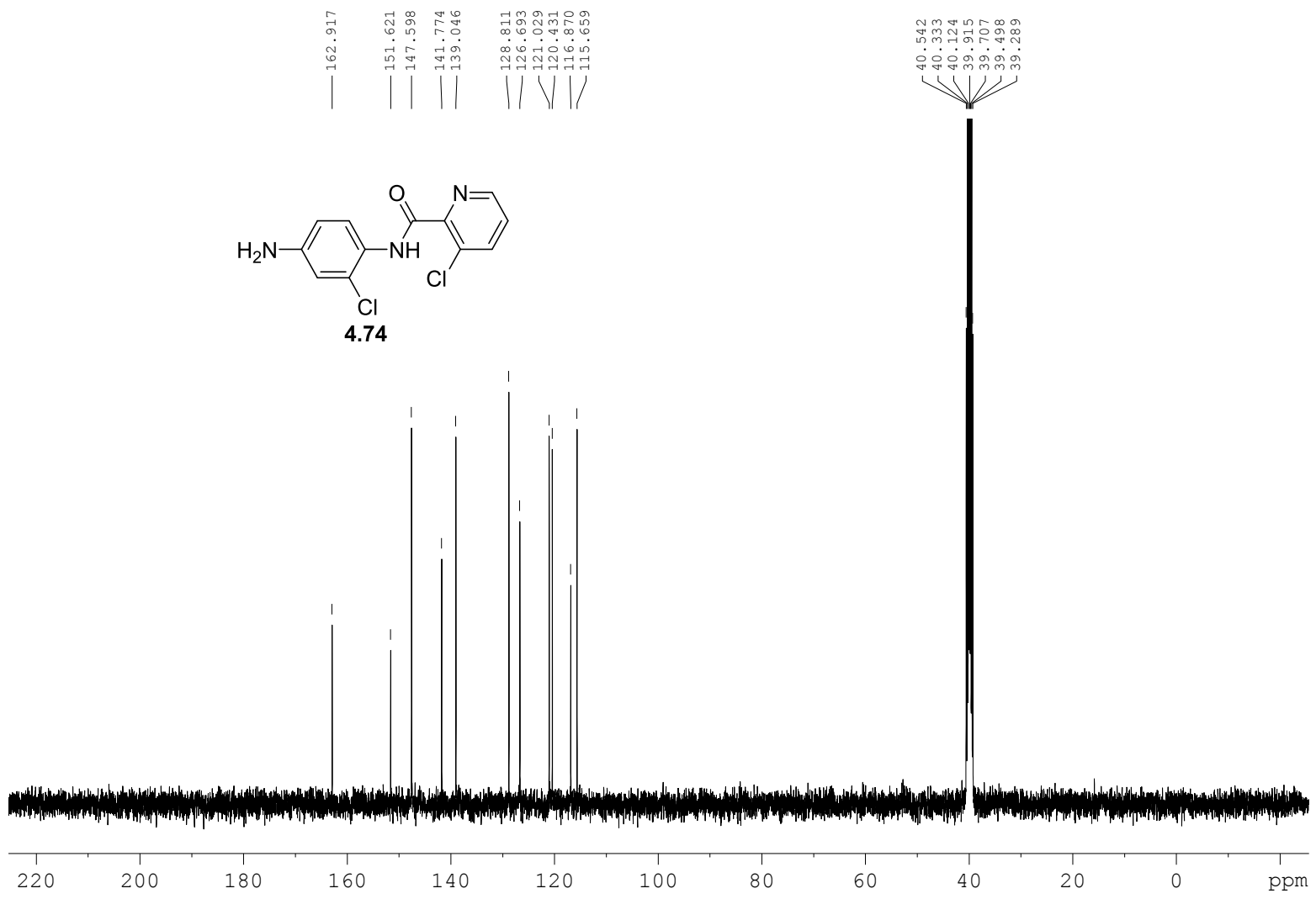
```

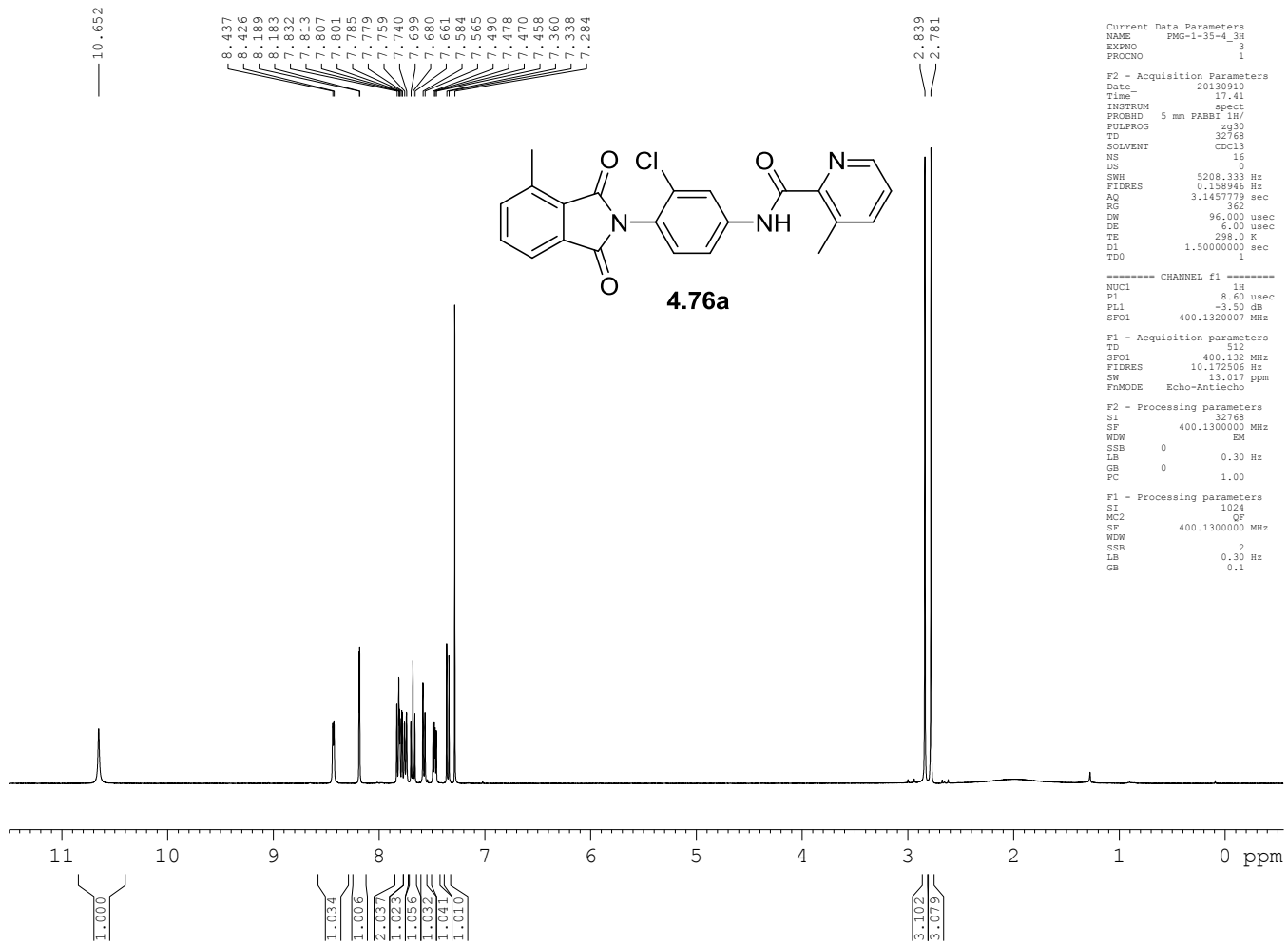
Current Data Parameters
NAME      pmg-132-2
EXPNO    1
PROCNO   1

F2 - Acquisition Parameters
Date_    20140227
Time     17.47
INSTRUM  spect
PROBHD   5 mm PABBO BB/
PULPROG  zg30
TD       32768
SOLVENT  DMSO
NS       16
DS       0
SWH      5208.333 Hz
FIDRES   0.158946 Hz
AQ       3.1457779 sec
RG       108.86
DW       96.000 usec
DE       15.87 usec
TE       296.9 K
DL       1.5000000 sec
TDO      1

===== CHANNEL f1 =====
SFO1    400.1320007 MHz
NUC1    1H
PI      10.00 usec
PLW1    16.00000000 W

F2 - Processing parameters
SI      65536
SF      400.1300000 MHz
WDW     EM
SSB     0
LB      0.30 Hz
GB      0
PC      1.00
    
```





```

Current Data Parameters
NAME      PMG-1-35-4
EXPNO    2
PROCNO   1

F2 - Acquisition Parameters
Date_    20130627
Time     8.45
INSTRUM  spect
PROBHD   5 mm PABBO BB/
PULPROG  zgpg30
TD       32768
SOLVENT  CDCl3
NS       1834
DS       0
SWH      31446.541 Hz
FIDRES   0.959672 Hz
AQ       0.5210612 sec
RG       16384
DW       15.900 usec
DE       6.00 usec
TE       298.0 K
D1       2.00000000 sec
d11      0.03000000 sec
DELTA    1.89999998 sec
TD0      1

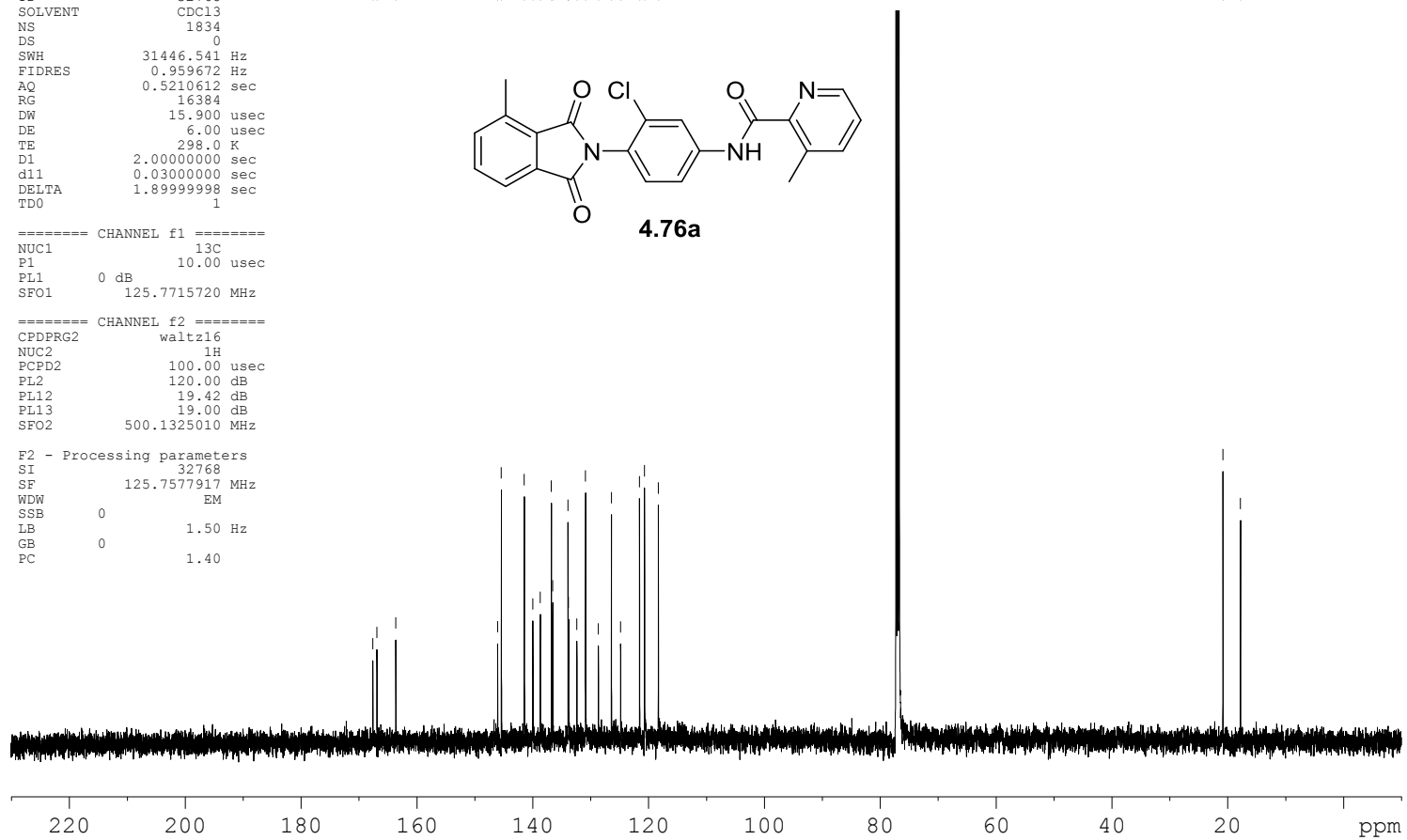
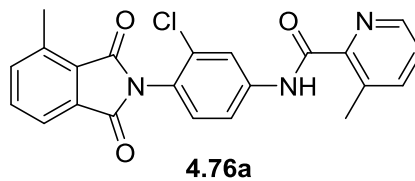
===== CHANNEL f1 =====
NUC1     13C
P1       10.00 usec
PL1      0 dB
SFO1     125.7715720 MHz

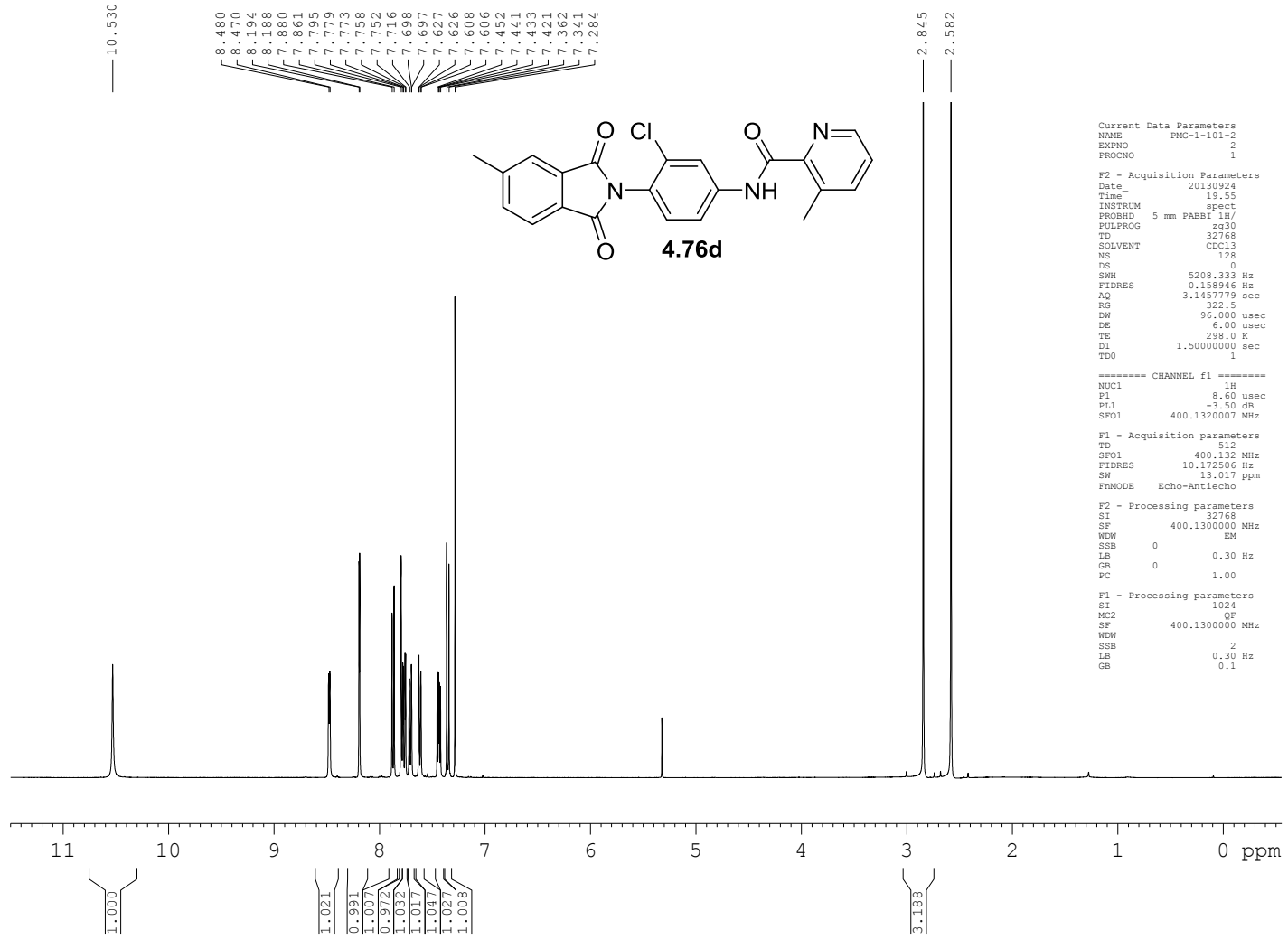
===== CHANNEL f2 =====
CPDPRG2  waltz16
NUC2     1H
PCPD2    100.00 usec
PL2      120.00 dB
PL12     19.42 dB
PL13     19.00 dB
SFO2     500.1325010 MHz

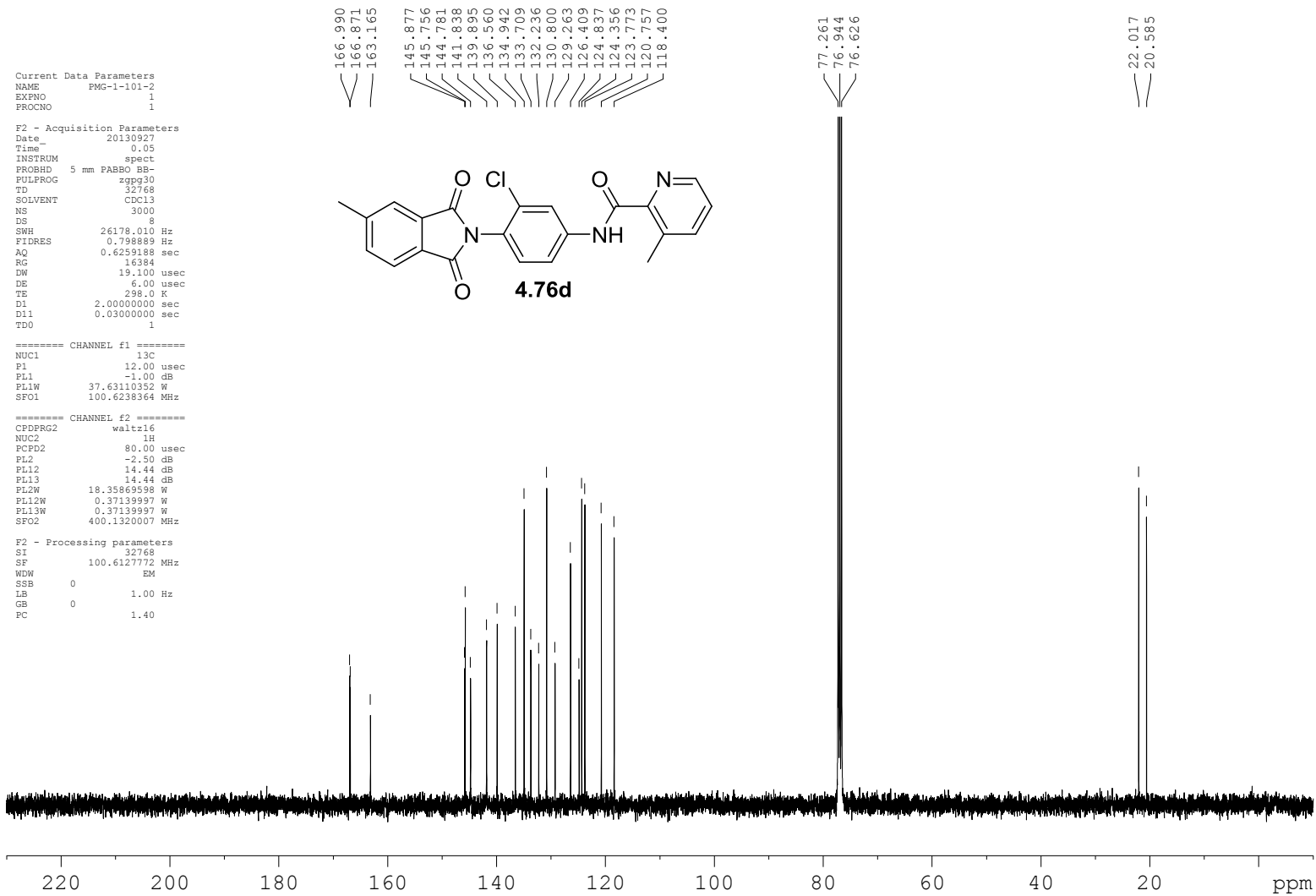
F2 - Processing parameters
SI       32768
SF       125.7577917 MHz
WDW      EM
SSB      0
LB       1.50 Hz
GB       0
PC       1.40

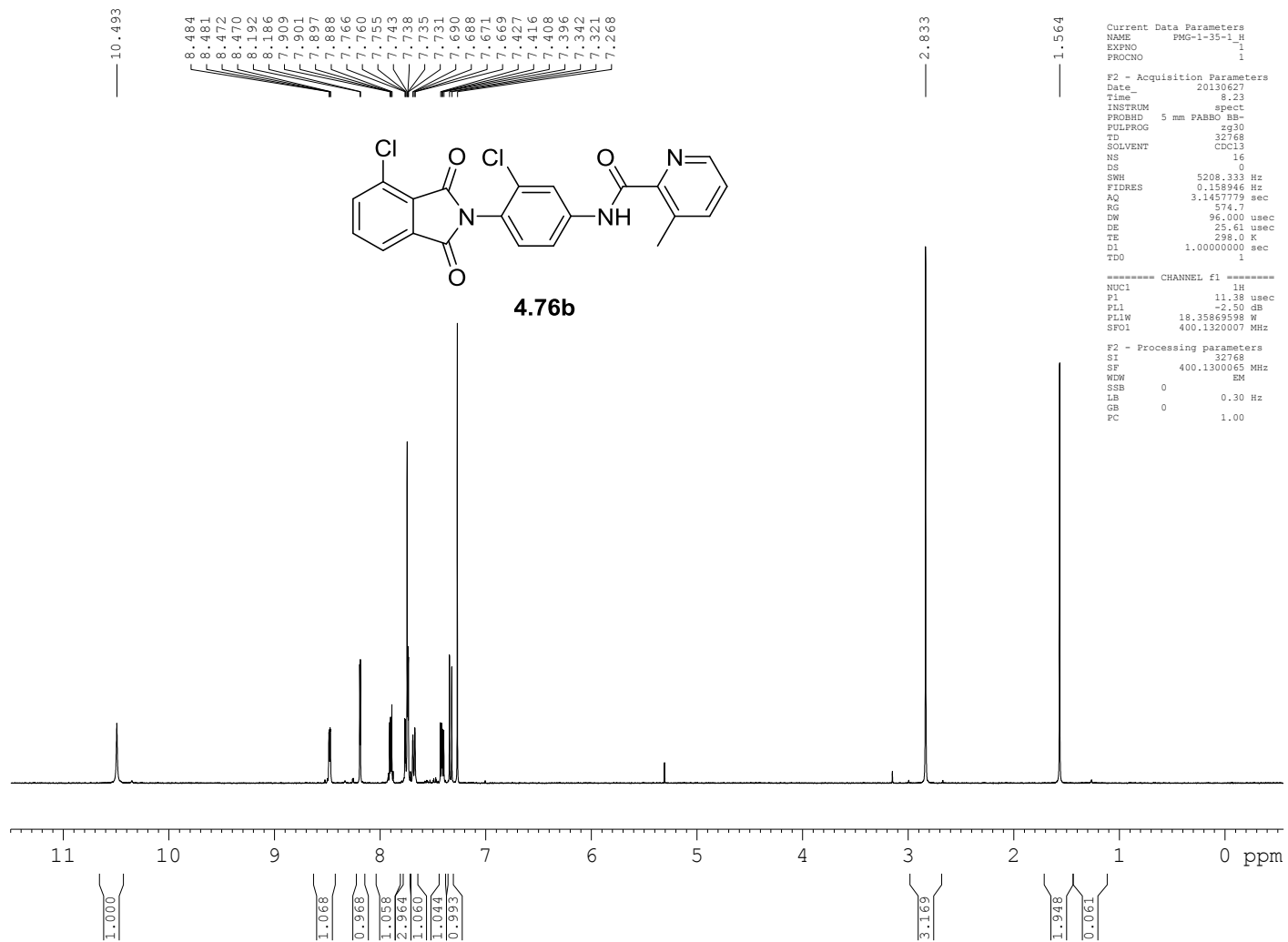
```

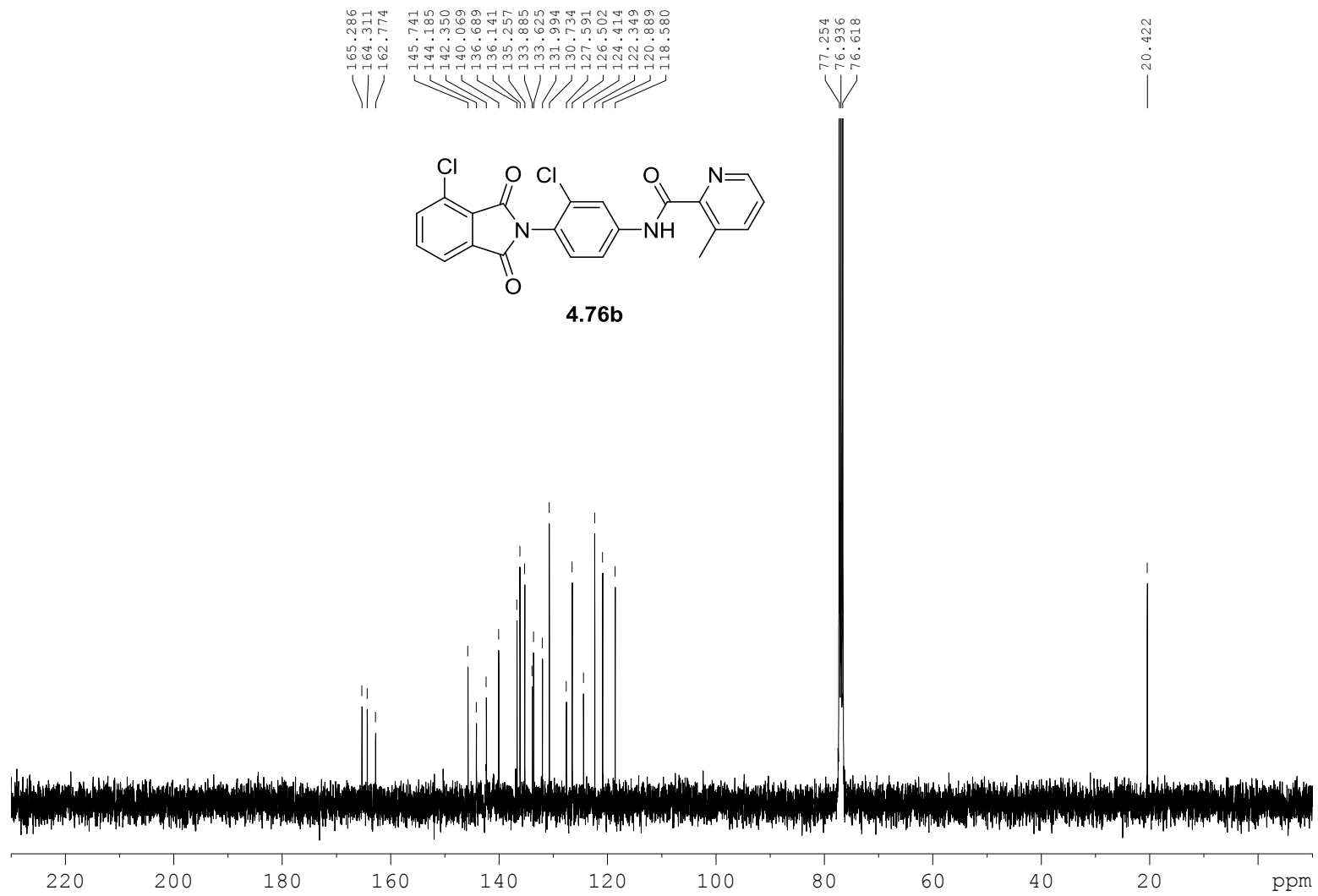
167.595  
166.875  
163.627  
146.048  
145.393  
141.427  
139.964  
138.673  
136.763  
136.522  
133.897  
133.794  
132.359  
130.859  
128.644  
126.396  
124.803  
121.541  
120.678  
118.294



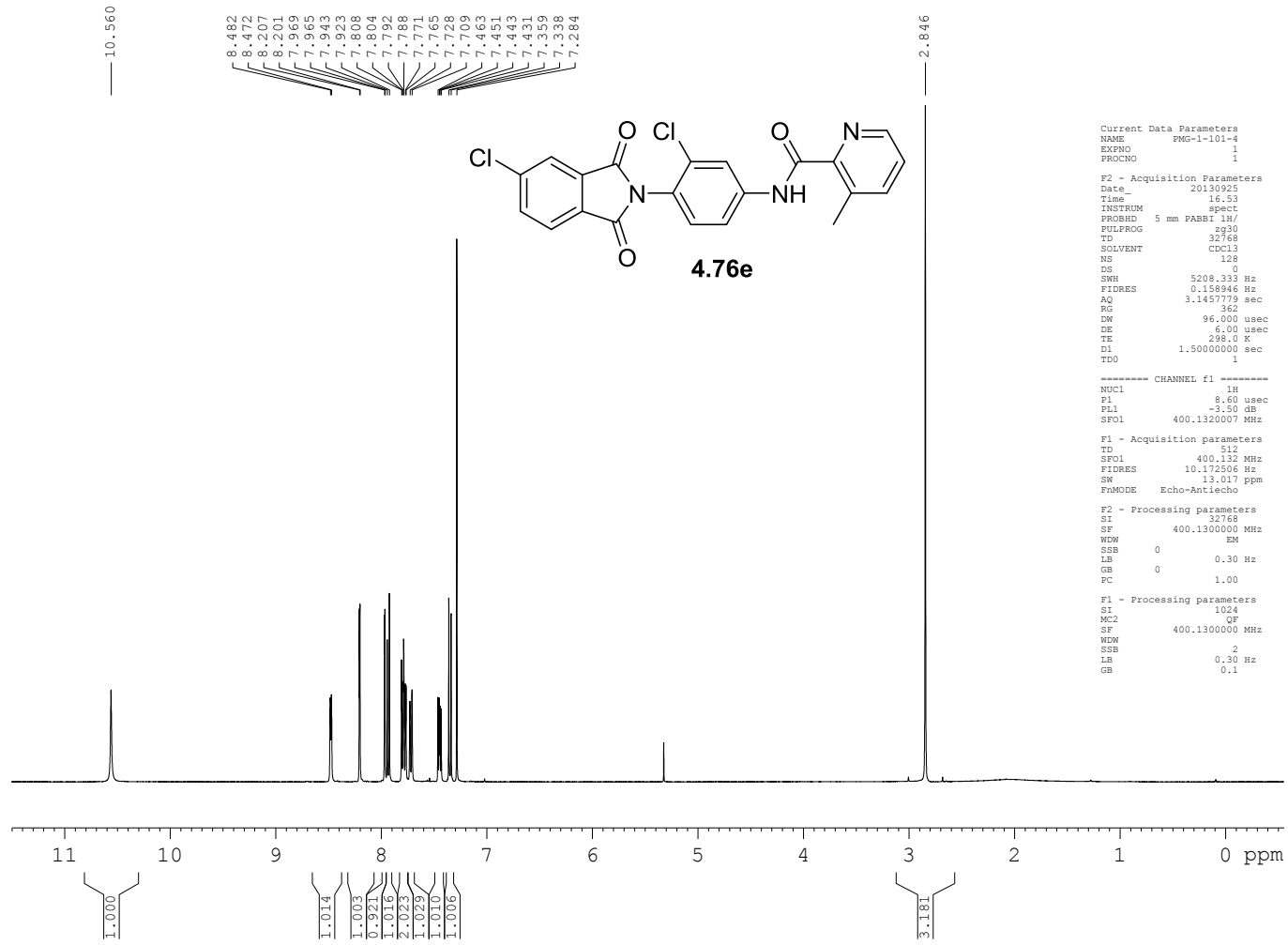












Current Data Parameters  
 NAME PMG-1-101-4  
 EXPNO 1  
 PROCNO 1

F2 - Acquisition Parameters  
 Date\_ 20130927  
 Time 2.27  
 INSTRUM spect  
 PROBHD 5 mm PABBO BB-  
 FULPROG zgpg30  
 TD 32768  
 SOLVENT CDCl3  
 NS 3000  
 DS 8  
 SWH 26178.010 Hz  
 FIDRES 0.798888 Hz  
 AQ 0.6259188 sec  
 RG 16384  
 DW 19.100 usec  
 DE 6.00 usec  
 TE 298.0 K  
 D1 2.00000000 sec  
 D11 0.03000000 sec  
 TDO 1

===== CHANNEL f1 =====  
 NUC1 13C  
 P1 12.00 usec  
 PL1 -1.00 dB  
 PL1W 37.63110352 W  
 SFO1 100.628364 MHz

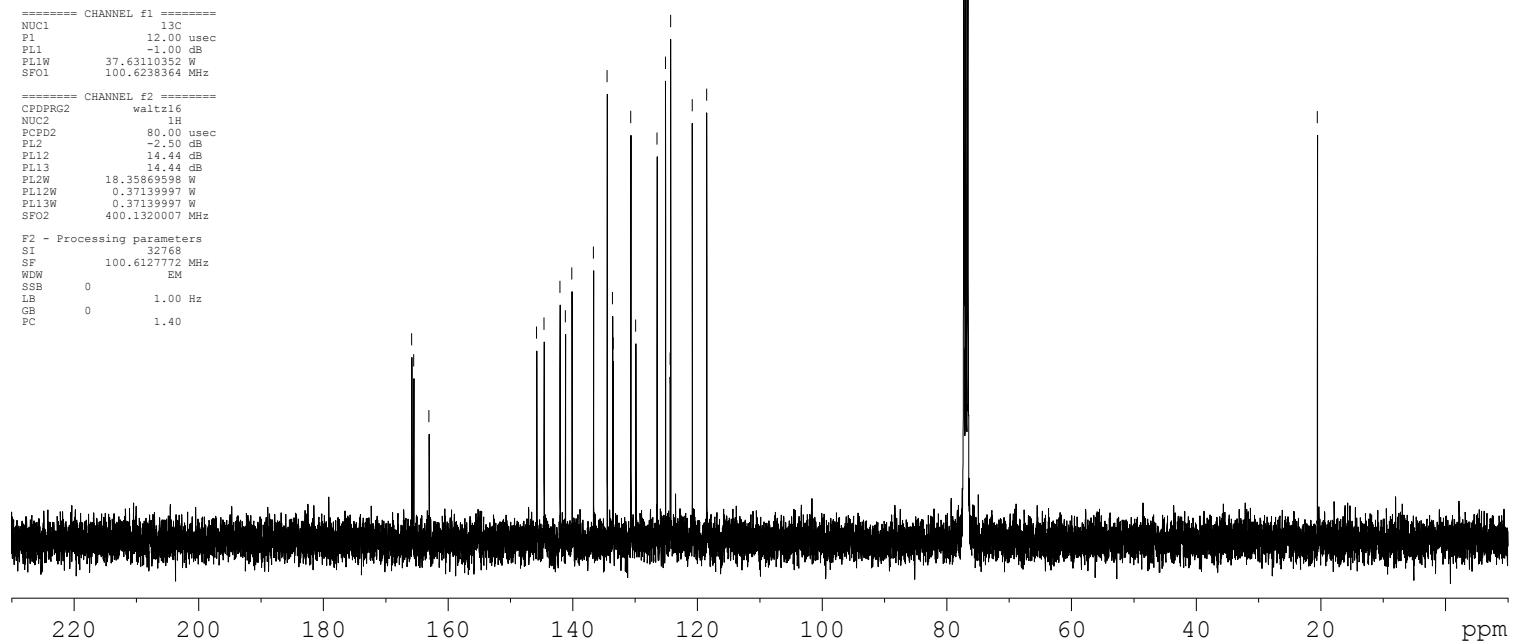
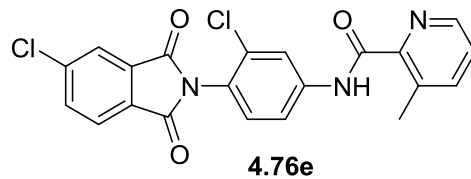
===== CHANNEL f2 =====  
 CPDPRG2 waltz16  
 NUC2 1H  
 PCPD2 80.00 usec  
 PL2 -2.50 dB  
 PL12 14.44 dB  
 PL13 14.44 dB  
 PL2W 18.35869598 W  
 PL12W 0.37139997 W  
 PL13W 0.37139997 W  
 SFO2 400.1320007 MHz

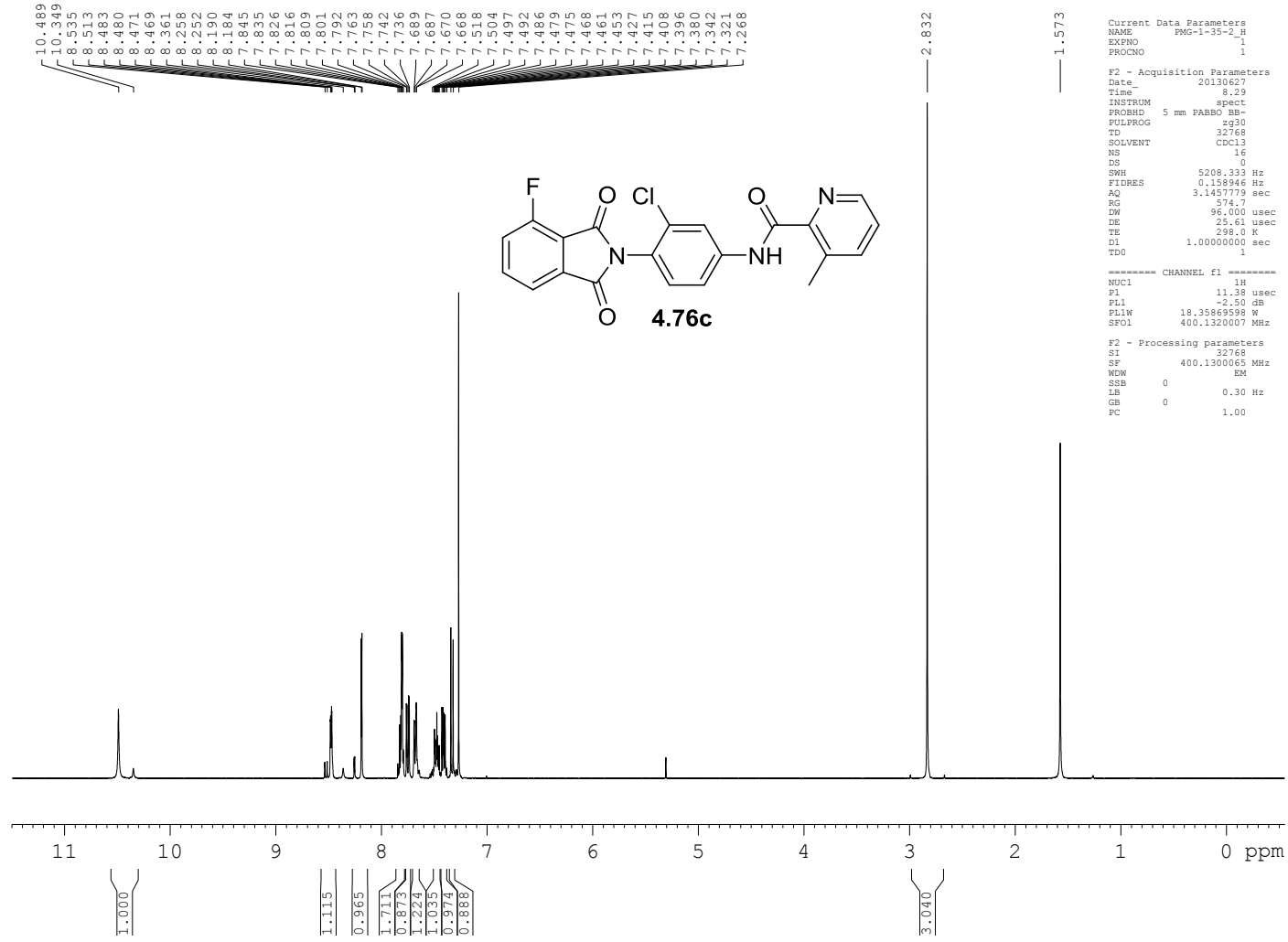
F2 - Processing parameters  
 SI 32768  
 SF 100.6127772 MHz  
 WDW EM  
 SSB 0  
 LB 1.00 Hz  
 GB 0  
 PC 1.40

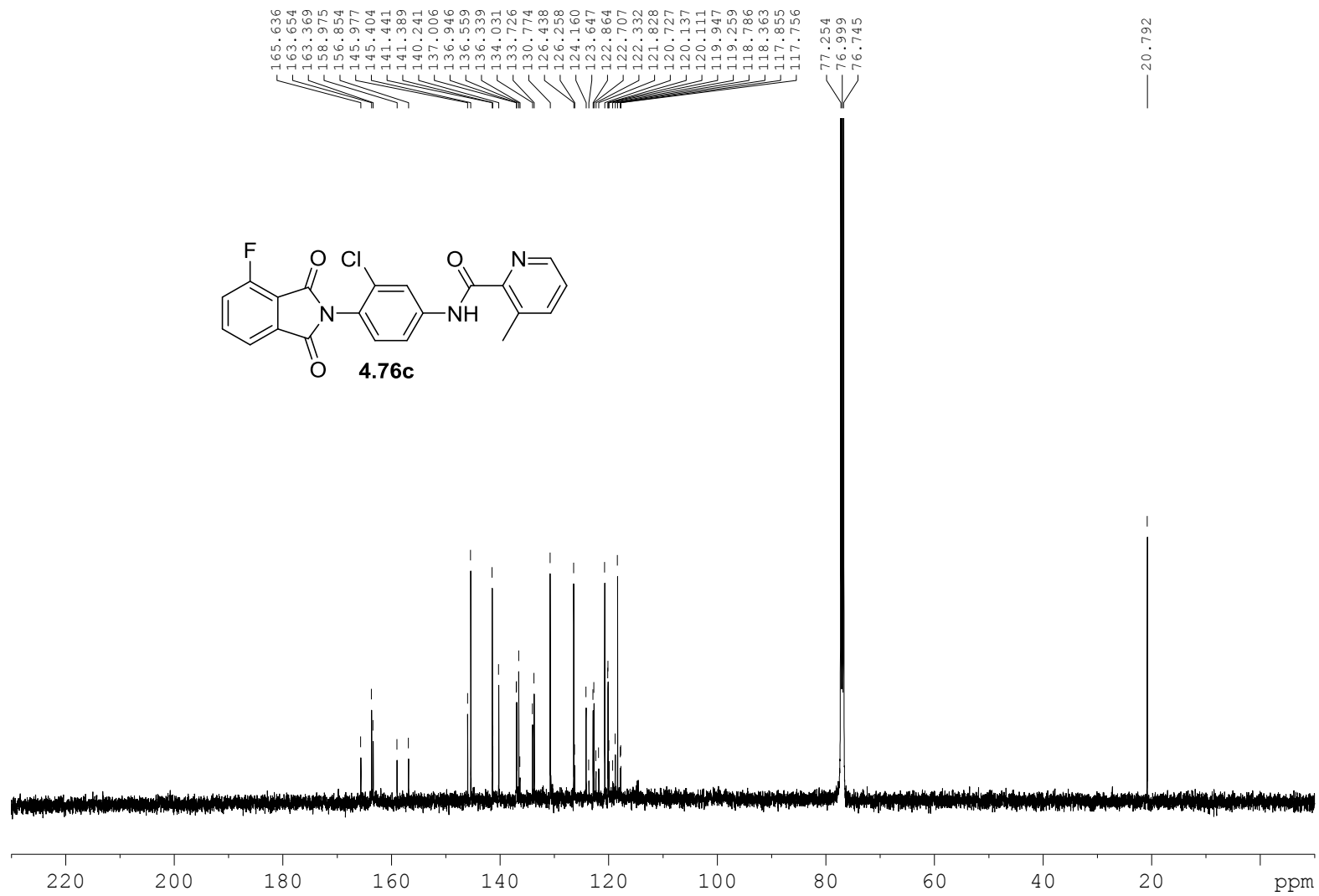
165.805  
 165.488  
 163.040  
 145.772  
 144.591  
 142.040  
 141.174  
 140.122  
 136.665  
 134.474  
 133.582  
 133.486  
 130.675  
 129.875  
 126.468  
 125.119  
 124.371  
 124.295  
 120.829  
 118.506

77.255  
 76.937  
 76.620

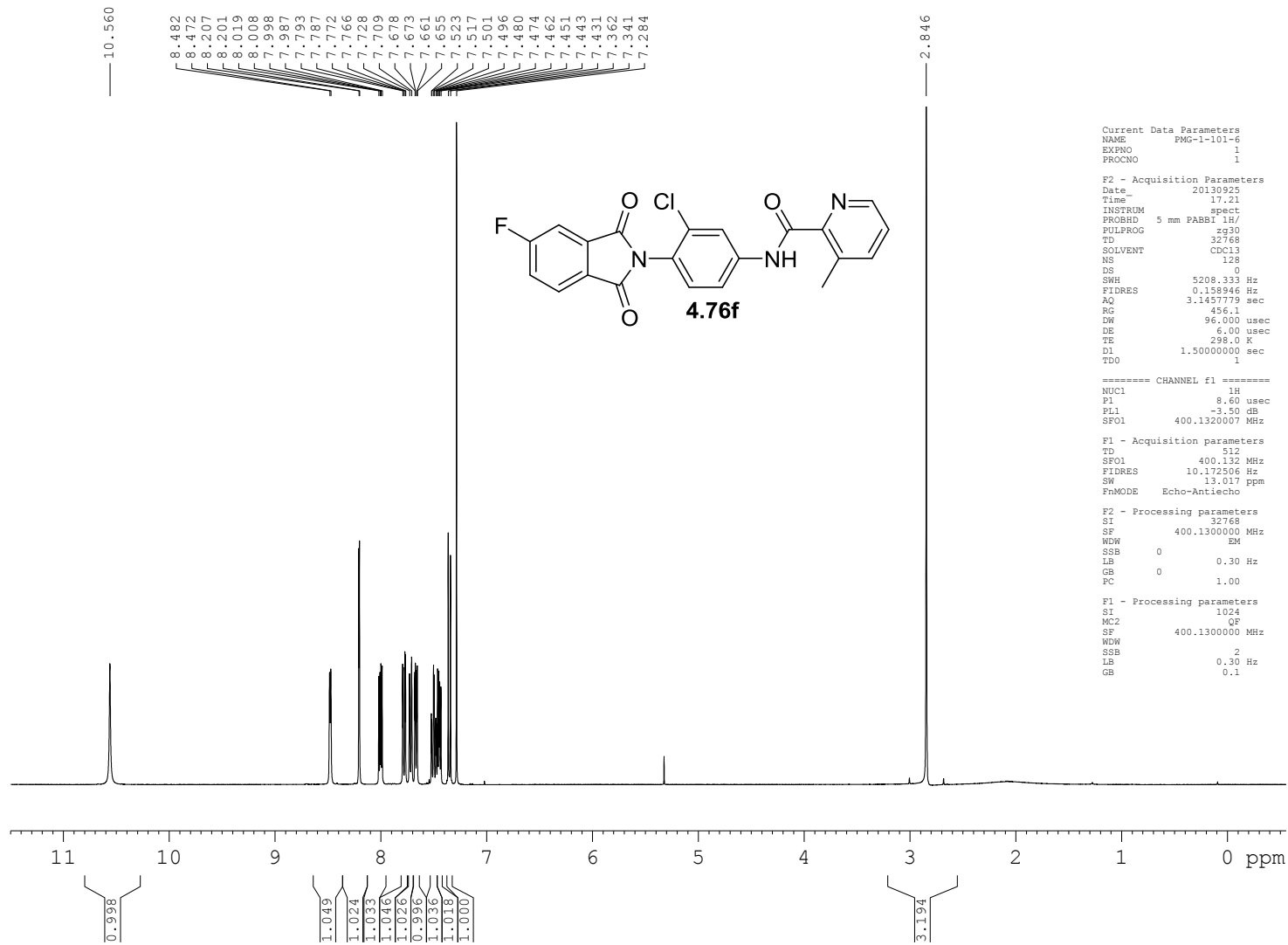
20.538







420



Current Data Parameters  
NAME PMG-1-101-6  
EXPNO 1  
PROCNO 1

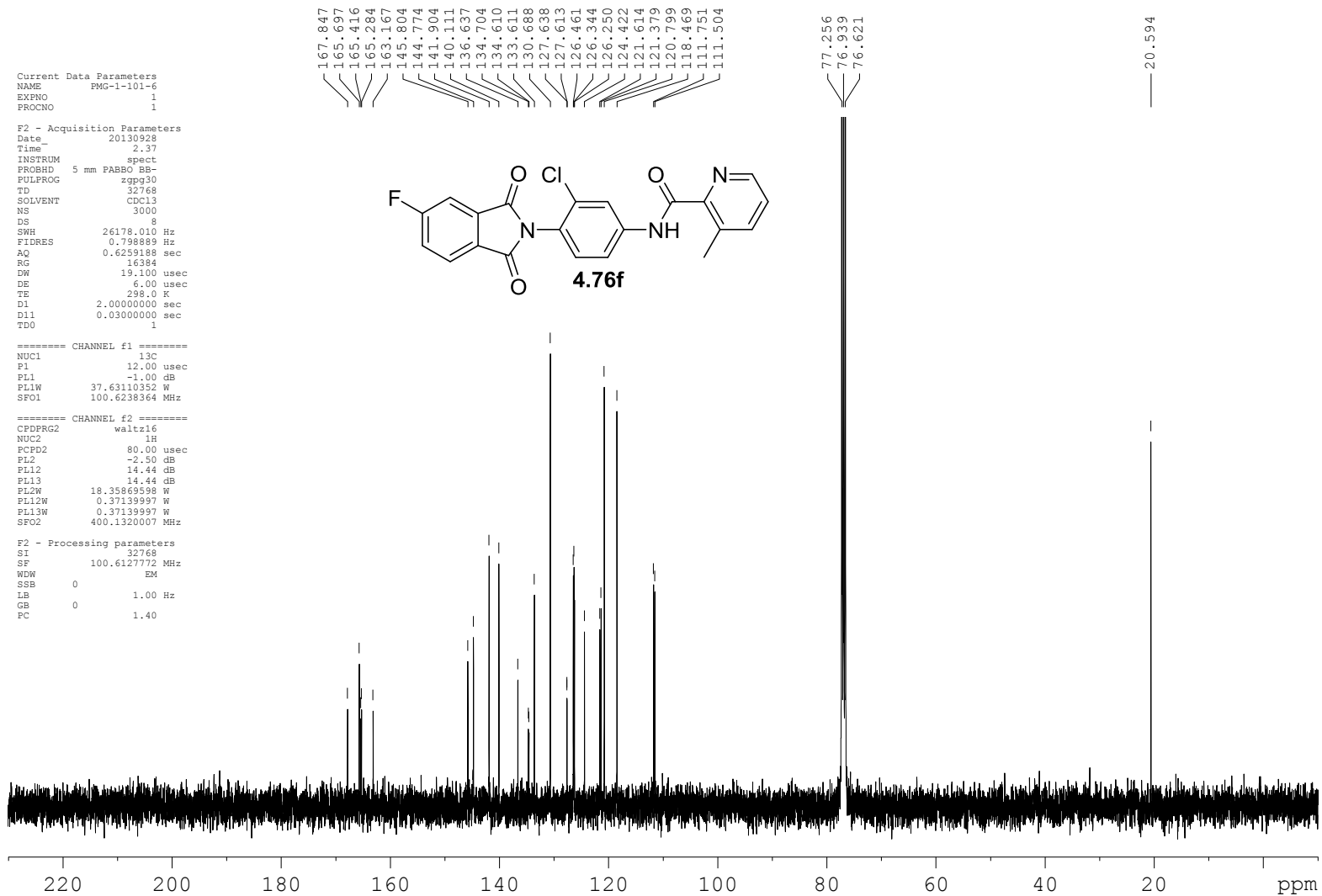
F2 - Acquisition Parameters  
Date\_ 20130925  
Time 17.21  
INSTRUM spect  
PROBHD 5 mm PABBI 1H/  
PULPROG zg30  
TD 32768  
SOLVENT CDCl3  
NS 128  
DS 0  
SWH 5208.333 Hz  
FIDRES 0.158946 Hz  
AQ 3.1457779 sec  
RG 456.1  
DW 96.000 usec  
DE 6.00 usec  
TE 298.0 K  
D1 1.5000000 sec  
TDO 1

\*\*\*\*\* CHANNEL f1 \*\*\*\*\*  
NUC1 1H  
P1 8.60 usec  
PL1 -3.50 dB  
SFO1 400.1320007 MHz

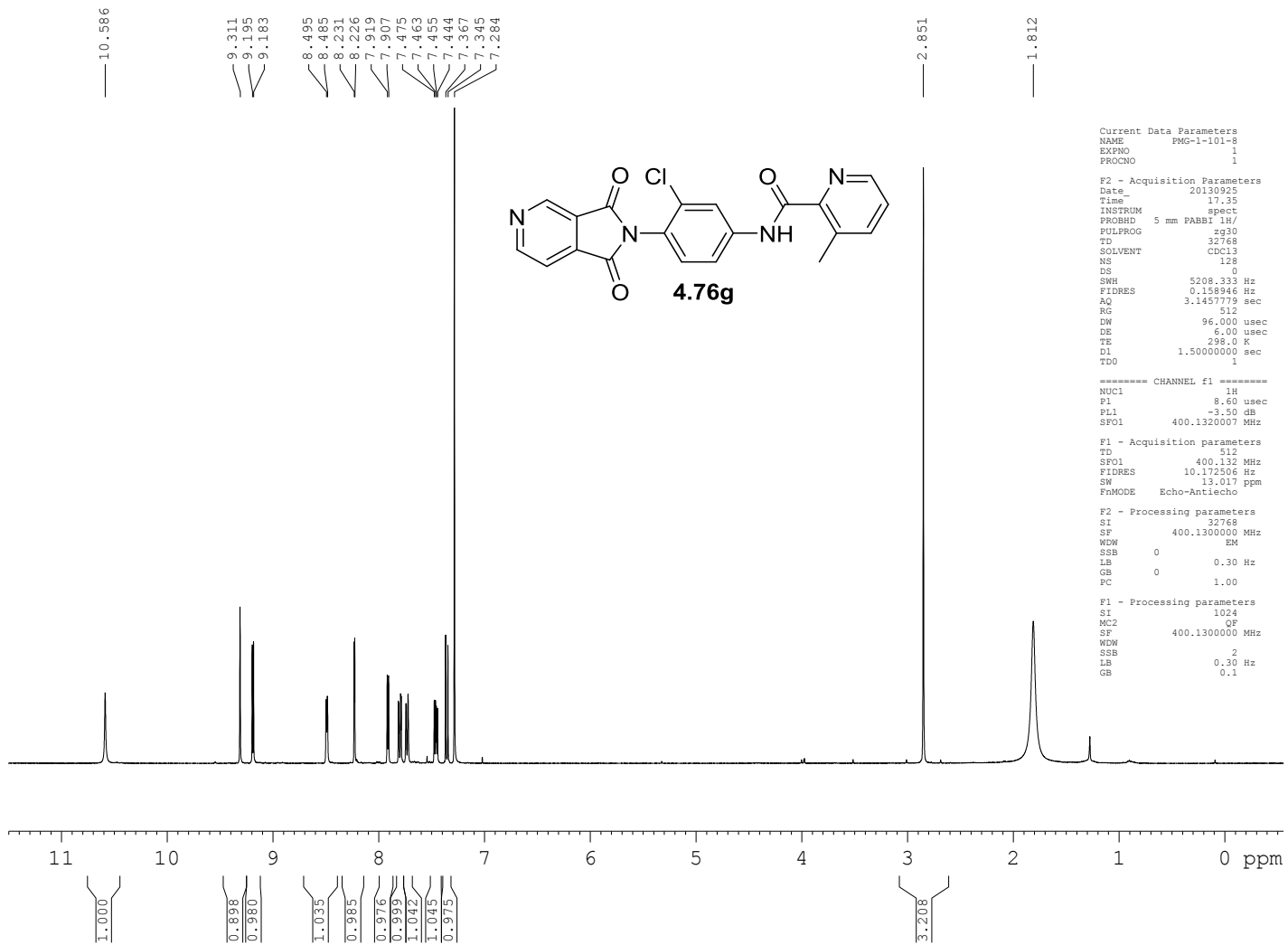
F1 - Acquisition parameters  
TD 512  
SFO1 400.132 MHz  
FIDRES 10.172506 Hz  
SW 15.017 ppm  
FhMODE Echo-Antiecho

F2 - Processing parameters  
SI 32768  
SF 400.1300000 MHz  
WDW EM  
SSB 0  
LB 0.30 Hz  
GB 0  
PC 1.00

F1 - Processing parameters  
SI 1024  
MC2 GF  
SF 400.1300000 MHz  
WDW 2  
SSB 0.30 Hz  
LB 0.1



422



423

Current Data Parameters  
NAME PMG-1-101-8  
EXPNO 1  
PROCNO 1

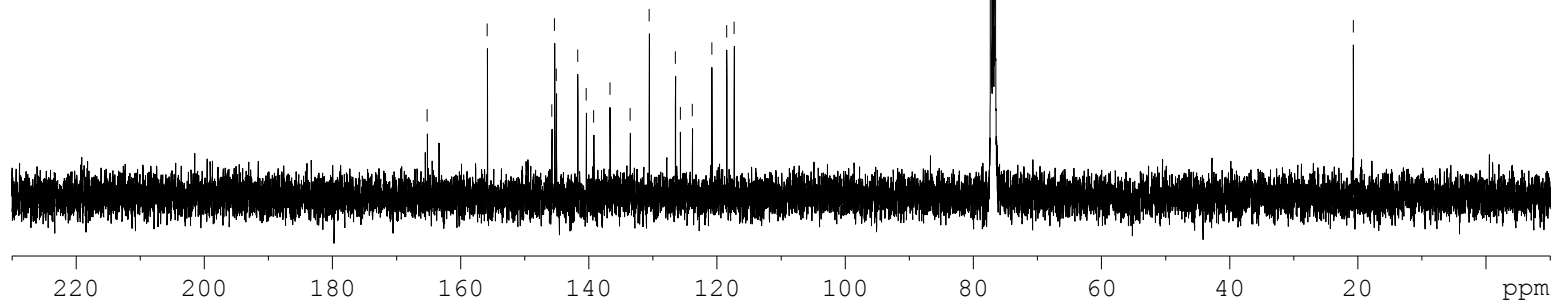
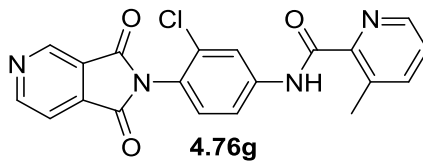
F2 - Acquisition Parameters  
Date\_ 20130928  
Time\_ 4.57  
INSTRUM spect  
PROBHD 5 mm PABBO BB-  
PULPROG zgpg30  
TD 32768  
SOLVENT CDC13  
NS 3000  
DS 8  
SWH 26178.010 Hz  
FIDRES 0.798889 Hz  
AQ 0.6259188 sec  
RG 16384  
DW 19.100 usec  
DE 6.00 usec  
TE 298.0 K  
D1 2.00000000 sec  
D11 0.03000000 sec  
TDO 1

===== CHANNEL f1 =====  
NUC1 13C  
P1 12.00 usec  
PL1 -1.00 dB  
PL1W 37.63110352 W  
SFO1 100.6238364 MHz

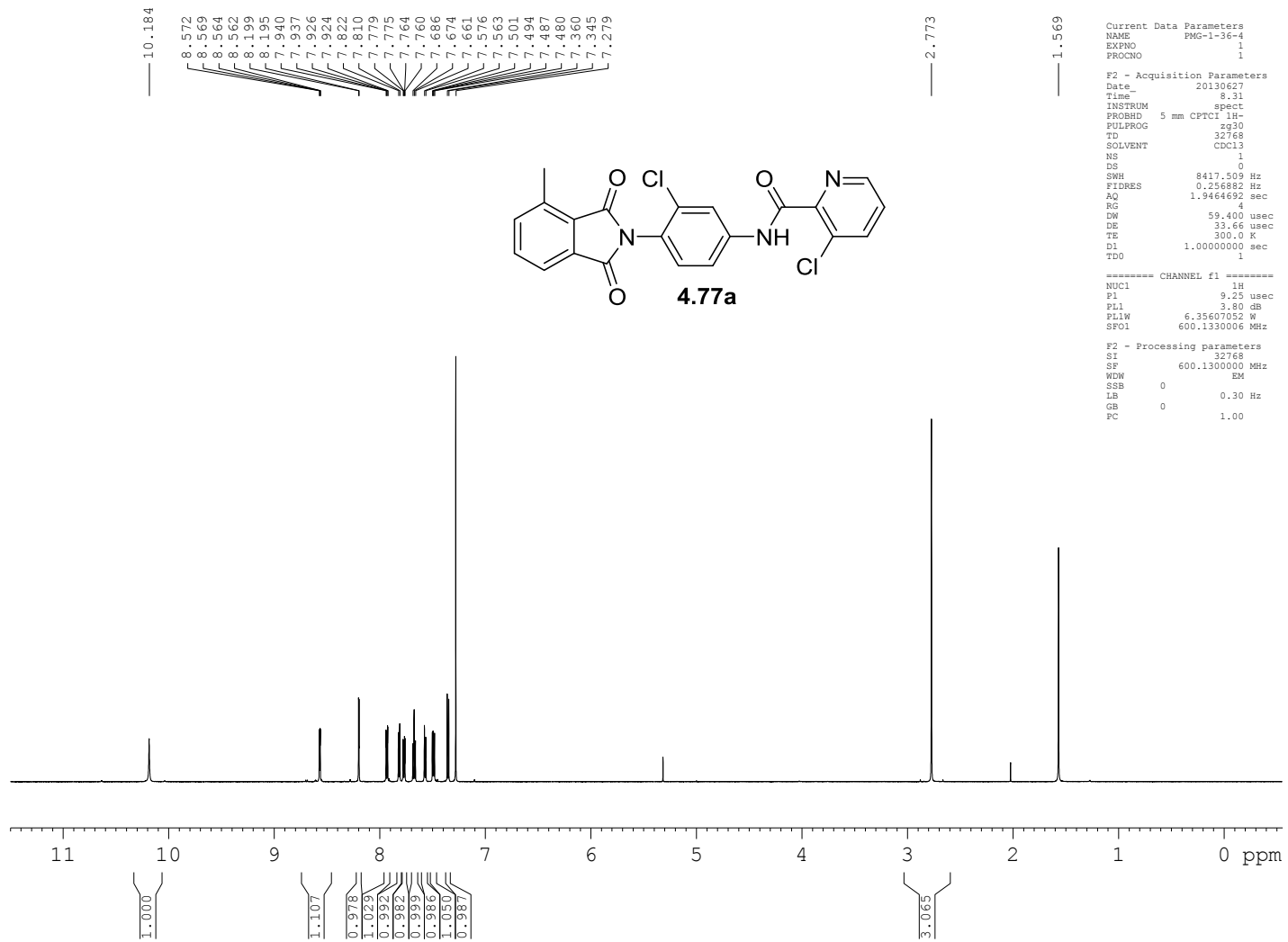
===== CHANNEL f2 =====  
CFDPRG2 waltz16  
NUC2 1H  
PCPD2 80.00 usec  
PL2 -2.50 dB  
PL12 14.44 dB  
PL13 14.44 dB  
PL2W 18.35869598 W  
PL12W 0.37139997 W  
PL13W 0.37139997 W  
SFO2 400.1320007 MHz

F2 - Processing parameters  
SI 32768  
SF 100.6127772 MHz  
WDW EM  
SSB 0  
LB 1.00 Hz  
GB 0  
PC 1.40

165.189  
163.347  
155.810  
145.756  
145.317  
145.055  
141.724  
140.380  
139.216  
136.681  
133.516  
130.559  
126.472  
125.698  
123.825  
120.788  
118.464  
117.305  
77.251  
76.934  
76.617  
20.679







Current Data Parameters  
NAME PMG-1-36-4  
EXPNO 3  
PROCNO 1

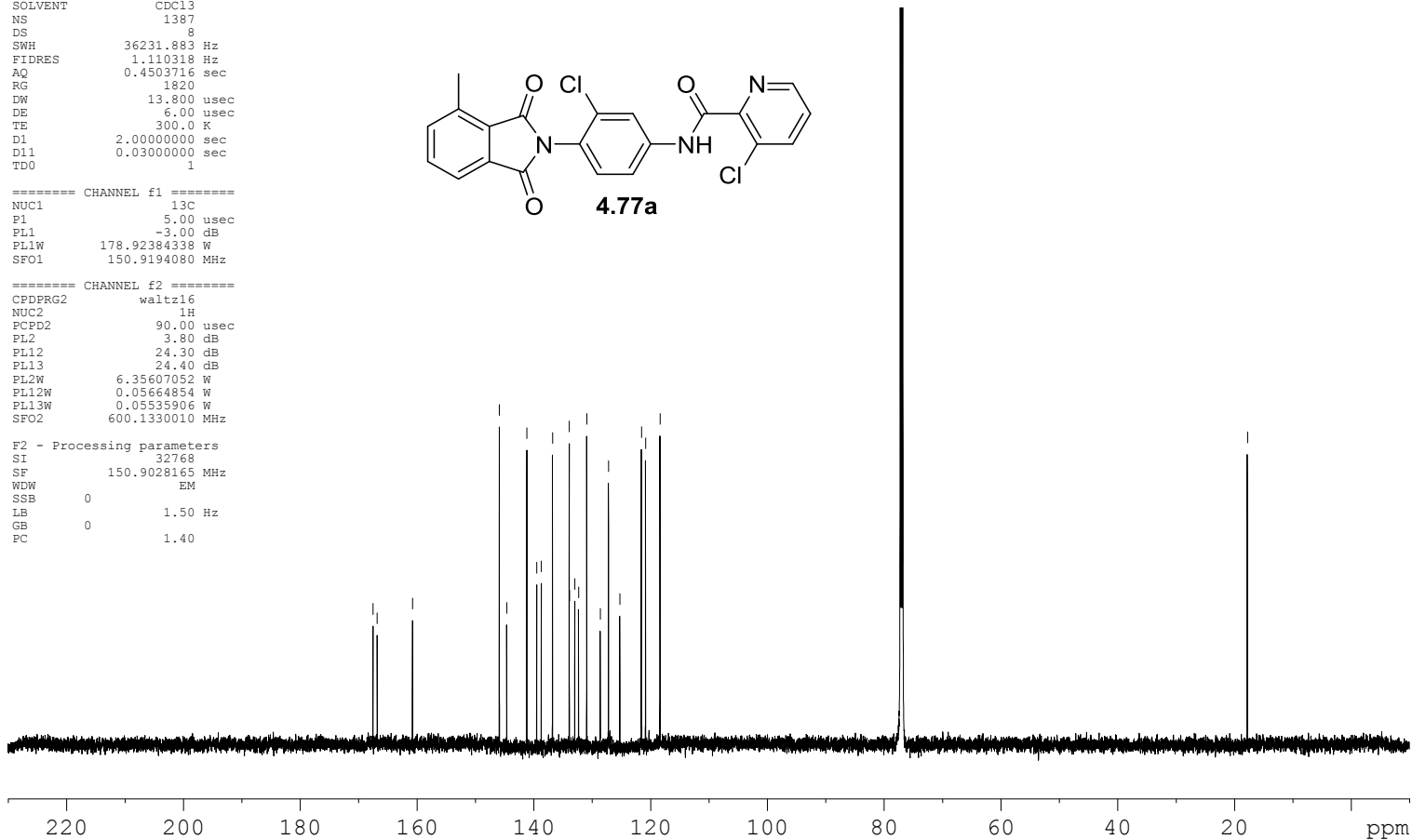
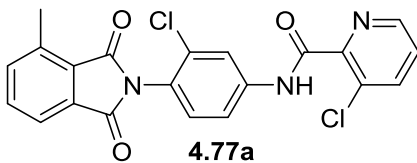
F2 - Acquisition Parameters  
Date\_ 20130627  
Time\_ 8.36  
INSTRUM spect  
PROBHD 5 mm CPTCI 1H-  
PULPROG zgpg  
TD 32632  
SOLVENT CDCl3  
NS 1387  
DS 8  
SWH 36231.883 Hz  
FIDRES 1.110318 Hz  
AQ 0.4503716 sec  
RG 1820  
DW 13.800 usec  
DE 6.00 usec  
TE 300.0 K  
D1 2.00000000 sec  
D11 0.03000000 sec  
TDO 1

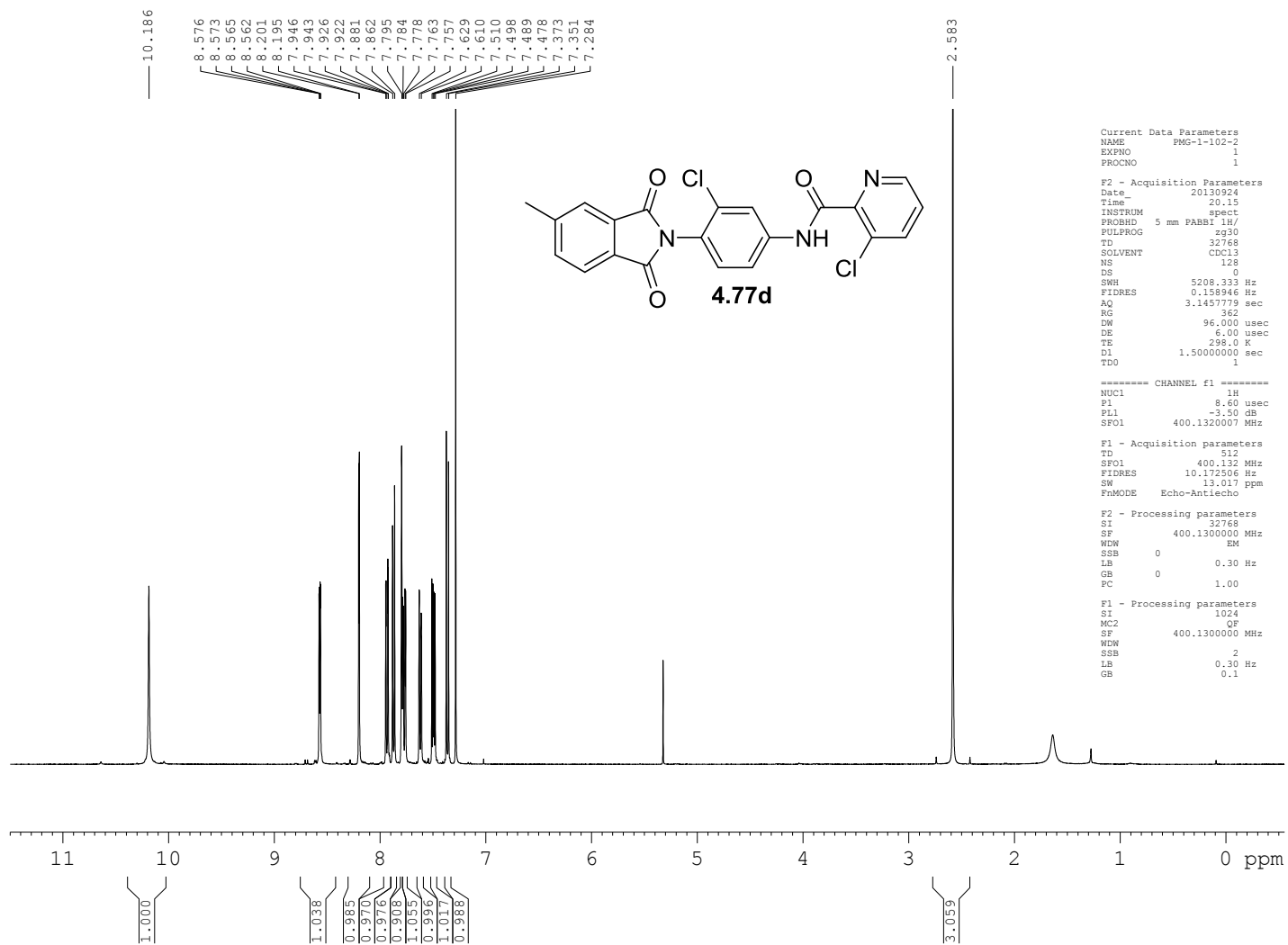
==== CHANNEL f1 =====  
NUC1 13C  
P1 5.00 usec  
PL1 -3.00 dB  
PL1W 178.92384338 W  
SFO1 150.9194080 MHz

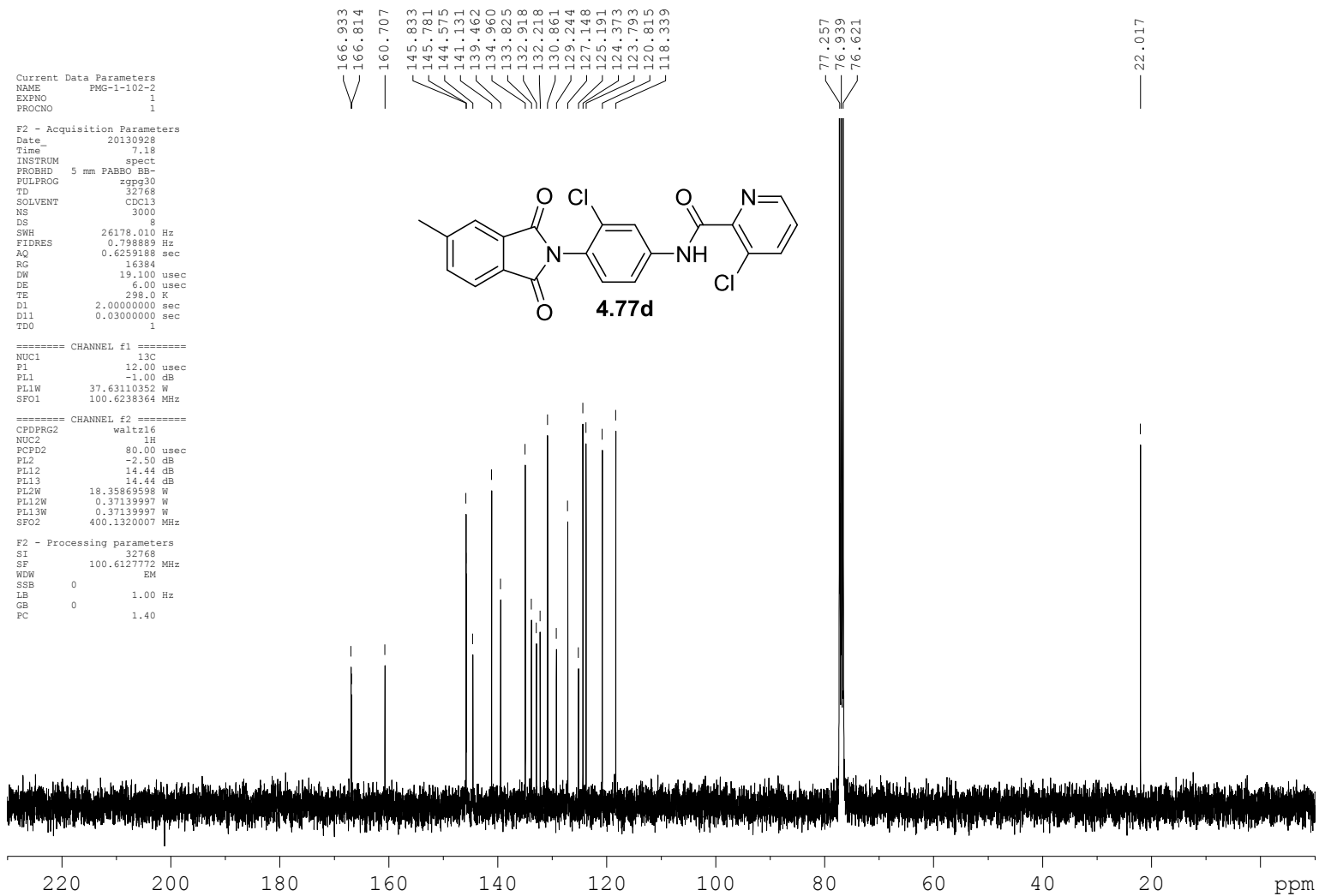
==== CHANNEL f2 =====  
CPDPRG2 waltz16  
NUC2 1H  
PCPD2 90.00 usec  
PL2 3.80 dB  
PL12 24.30 dB  
PL13 24.40 dB  
PL2W 6.35607052 W  
PL12W 0.05664854 W  
PL13W 0.05535906 W  
SFO2 600.1330010 MHz

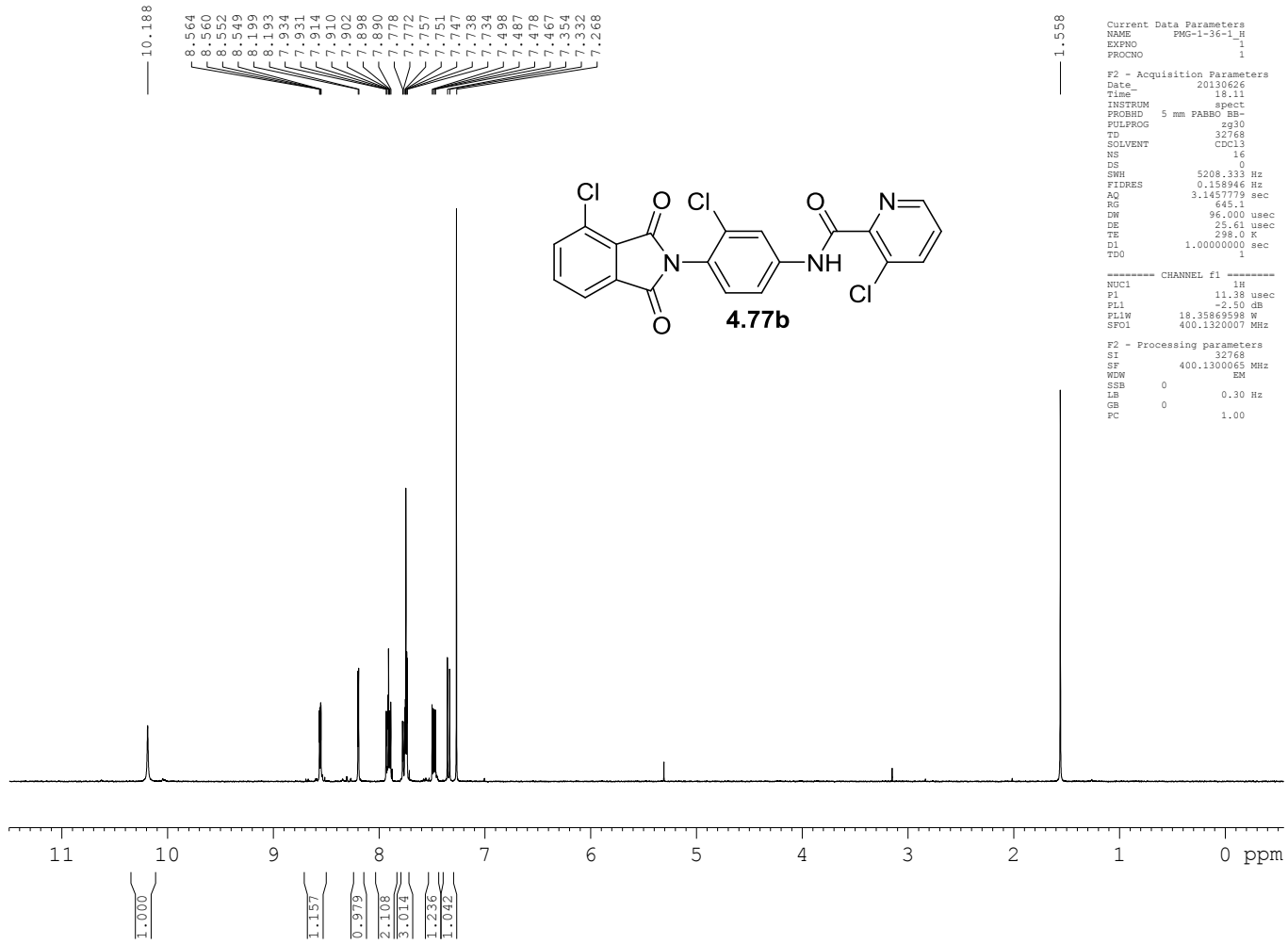
F2 - Processing parameters  
SI 32768  
SF 150.9028165 MHz  
WDW EM  
SSB 0  
LB 1.50 Hz  
GB 0  
PC 1.40

167.509  
166.784  
160.733  
145.856  
144.609  
141.160  
139.459  
138.676  
136.762  
133.898  
133.866  
132.945  
132.301  
130.906  
128.588  
127.169  
125.230  
121.534  
120.821  
118.350









```

Current Data Parameters
NAME      PMG-1-36-1_C
EXPNO    2
PROCNO   1

F2 - Acquisition Parameters
Date_    20130626
Time     20.05
INSTRUM  spect
PROBHD   5 mm PABBO BB-
FULPROG  zgpg30
TD       32768
SOLVENT  CDCl3
NS       2500
DS       8
SWH      26178.010 Hz
FIDRES   0.798889 Hz
AQ       0.6259188 sec
RG       16384
DW       19.100 usec
DE       6.00 usec
TE       298.0 K
D1       2.00000000 sec
D11      0.03000000 sec
TD0      1

===== CHANNEL f1 =====
NUC1     13C
P1       12.00 usec
PL1      -1.00 dB
PL1W     37.63110352 W
SFO1     100.6238364 MHz

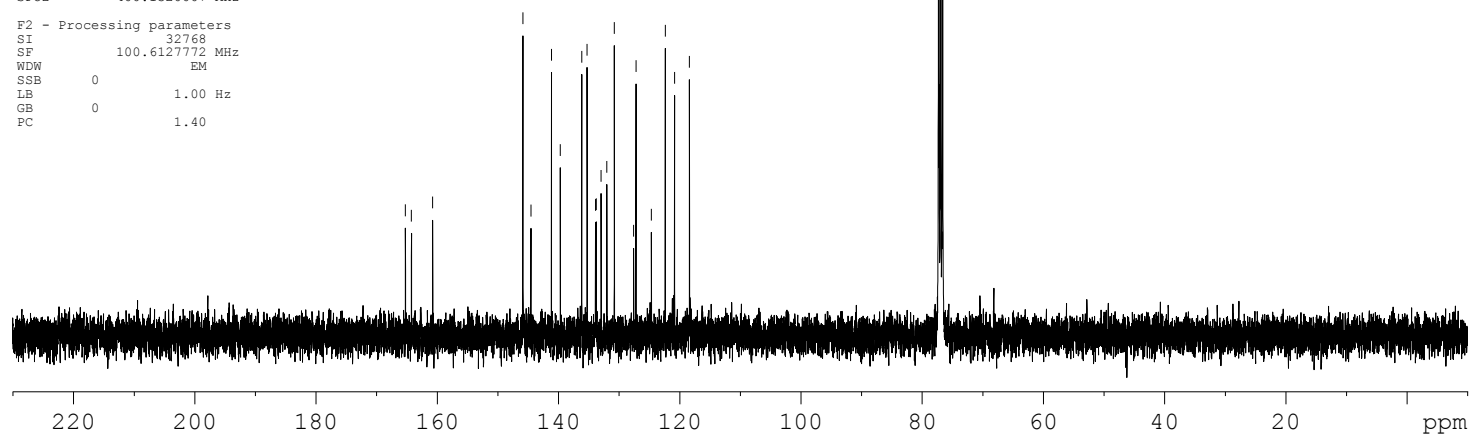
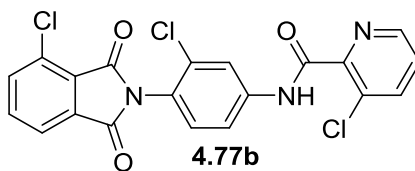
===== CHANNEL f2 =====
CPDPRG2  waltz16
NUC2     1H
PCPD2    80.00 usec
PL2      -2.50 dB
PL12     14.44 dB
PL13     14.44 dB
PL2W     18.35869598 W
PL12W    0.37139997 W
PL13W    0.37139997 W
SFO2     400.1320007 MHz

F2 - Processing parameters
SI       32768
SF       100.6127772 MHz
WDW      EM
SSB      0
LB       1.00 Hz
GB       0
PC       1.40

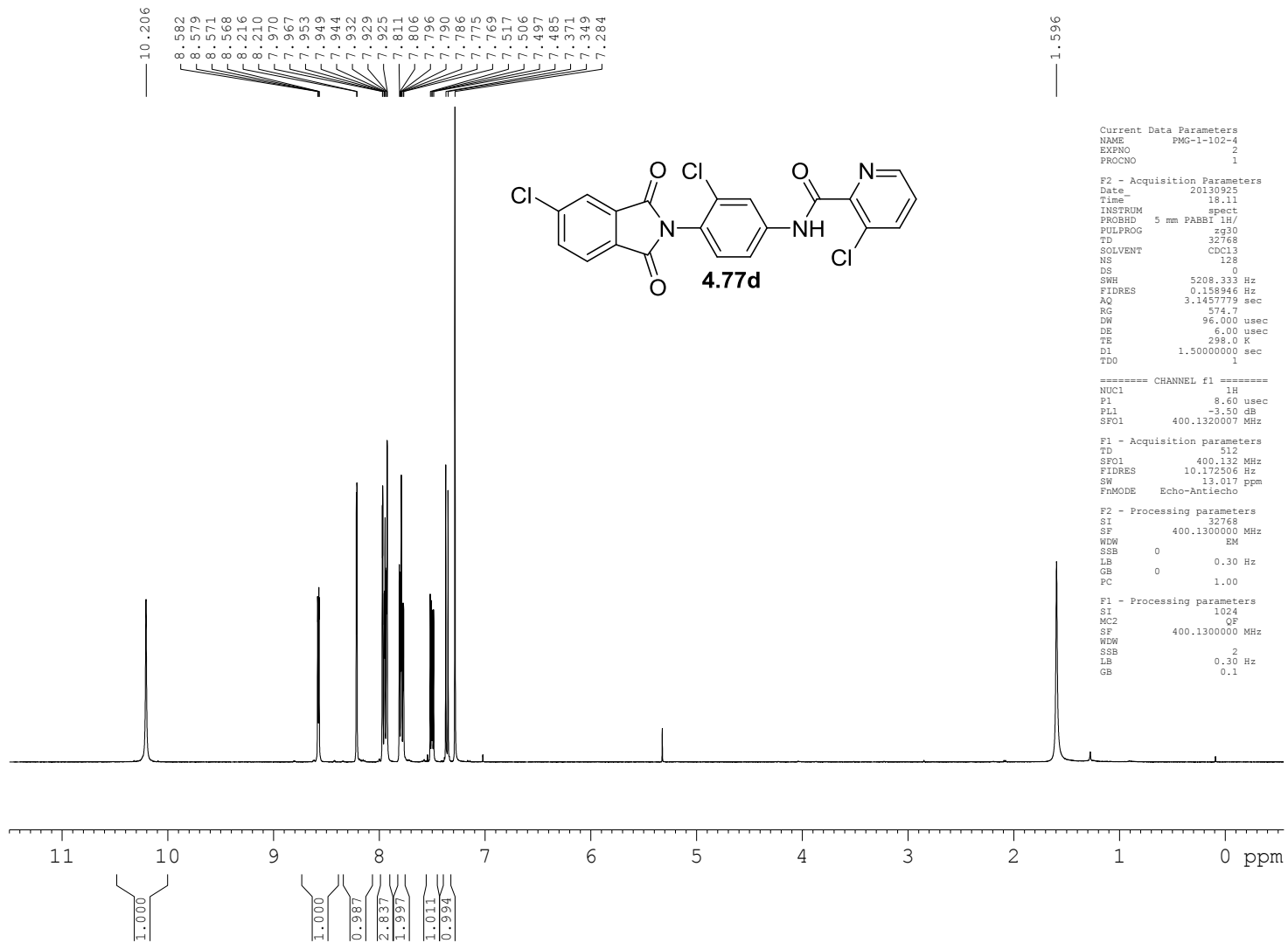
```

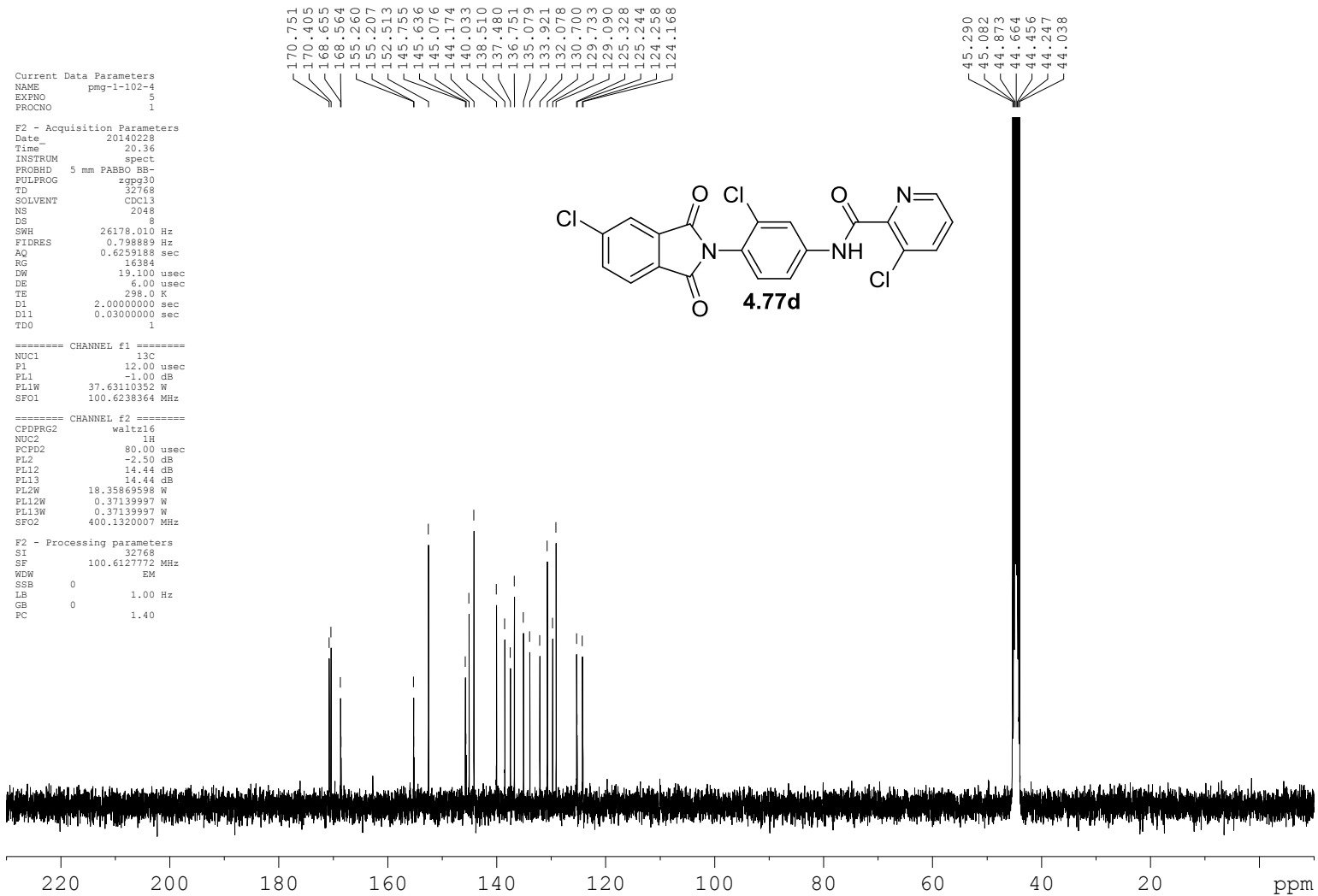
165.226  
 164.236  
 160.733  
 145.837  
 144.520  
 141.145  
 139.675  
 136.141  
 135.253  
 133.866  
 133.746  
 132.943  
 132.003  
 130.766  
 127.575  
 127.178  
 124.650  
 122.350  
 120.820  
 118.365

77.251  
 76.933  
 76.616



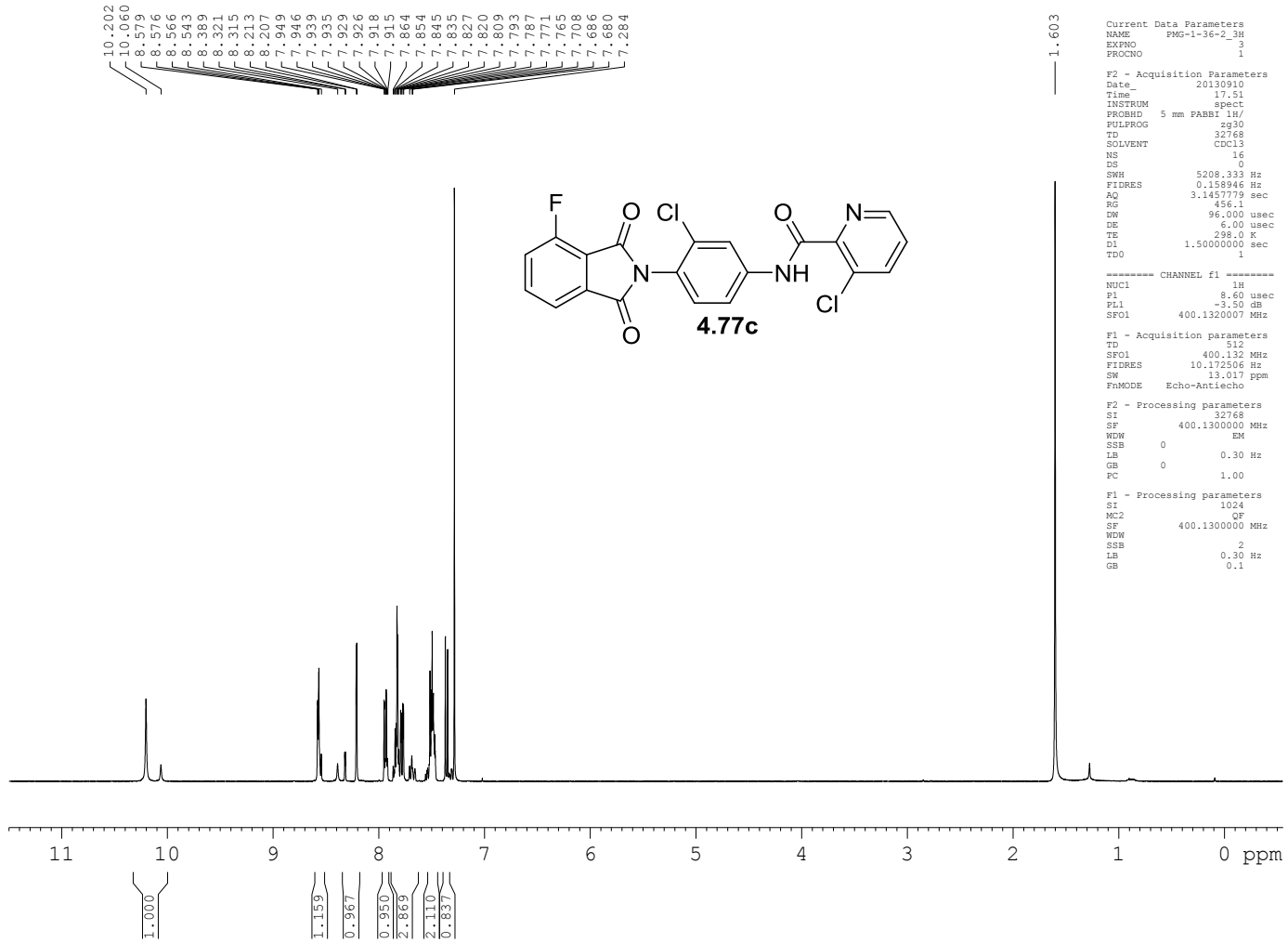
430







432



Current Data Parameters  
NAME PMG-1-36-2\_C  
EXPNO 2  
PROCNO 1

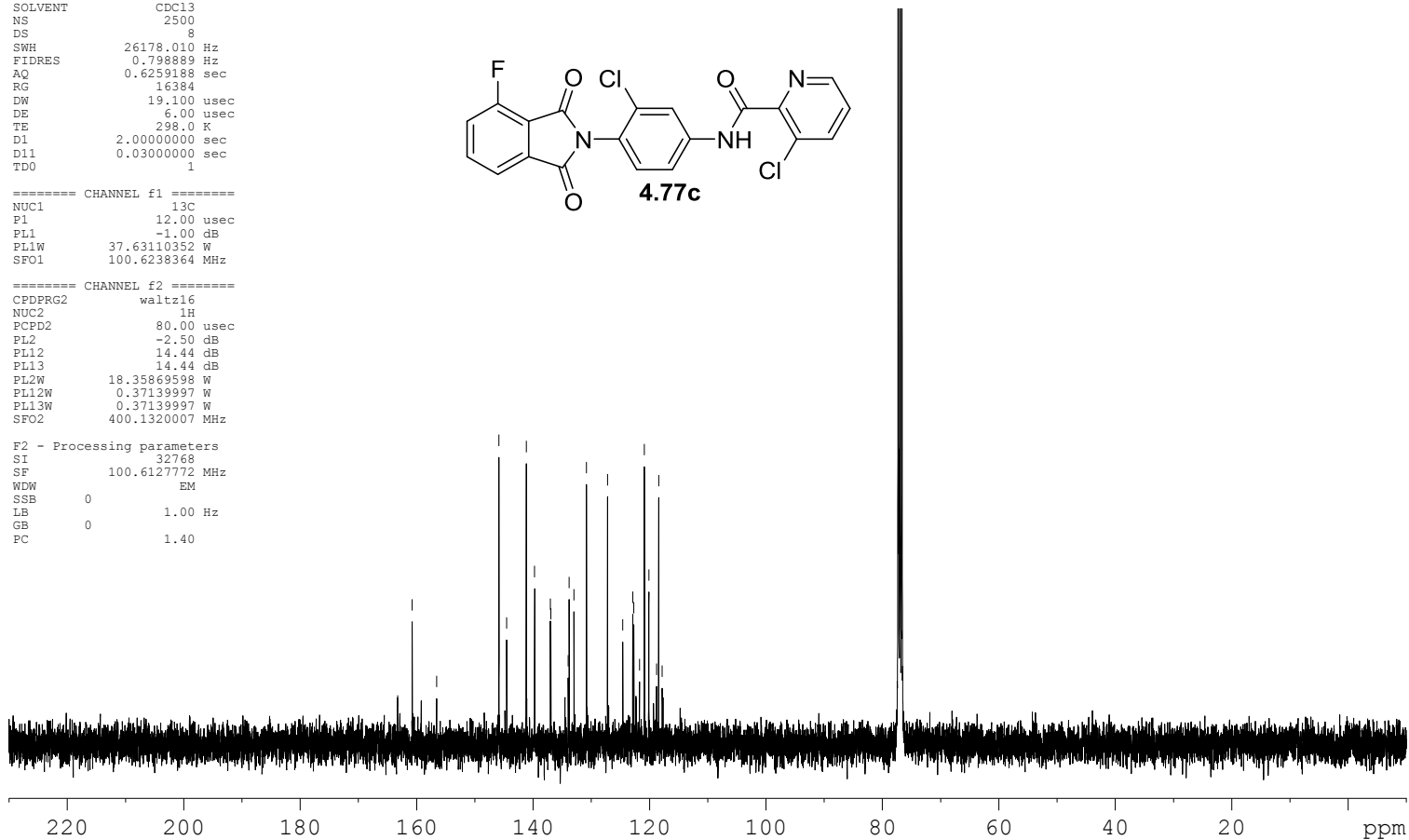
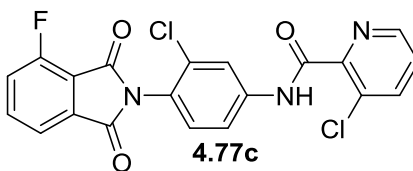
F2 - Acquisition Parameters  
Date 20130627  
Time 7.53  
INSTRUM spect  
PROBHD 5 mm PABBO BB-  
PULPROG zgpg30  
TD 32768  
SOLVENT CDCl3  
NS 2500  
DS 8  
SWH 26178.010 Hz  
FIDRES 0.798889 Hz  
AQ 0.6259188 sec  
RG 16384  
DW 19.100 usec  
DE 6.00 usec  
TE 298.0 K  
D1 2.00000000 sec  
D11 0.03000000 sec  
TDO 1

===== CHANNEL f1 =====  
NUC1 13C  
P1 12.00 usec  
PL1 -1.00 dB  
PL1W 37.63110352 W  
SFO1 100.6238364 MHz

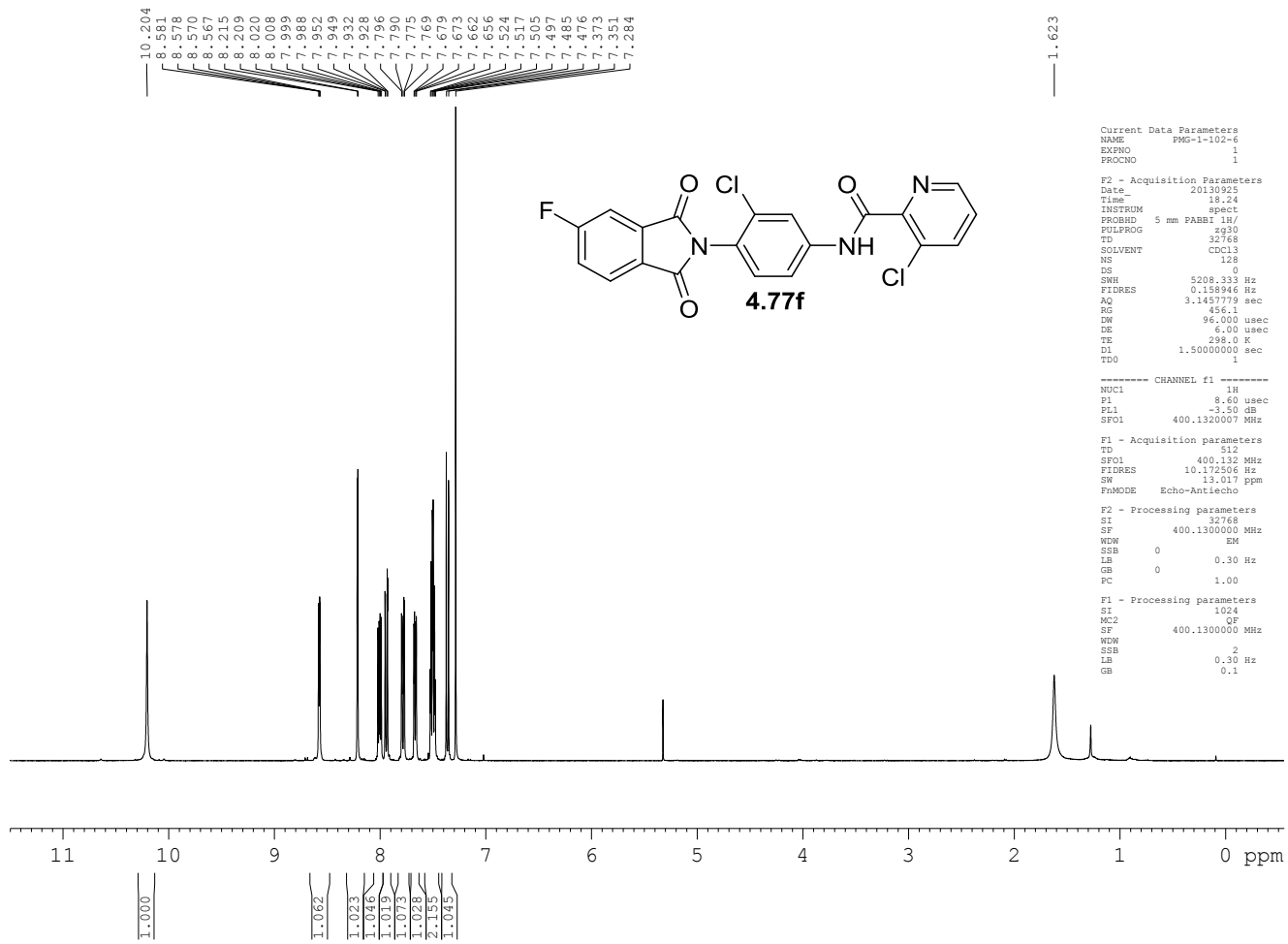
===== CHANNEL f2 =====  
CPDPRG2 waltz16  
NUC2 1H  
PCPD2 80.00 usec  
PL2 -2.50 dB  
PL12 14.44 dB  
PL13 14.44 dB  
PL2W 18.35869598 W  
PL12W 0.37139997 W  
PL13W 0.37139997 W  
SFO2 400.1320007 MHz

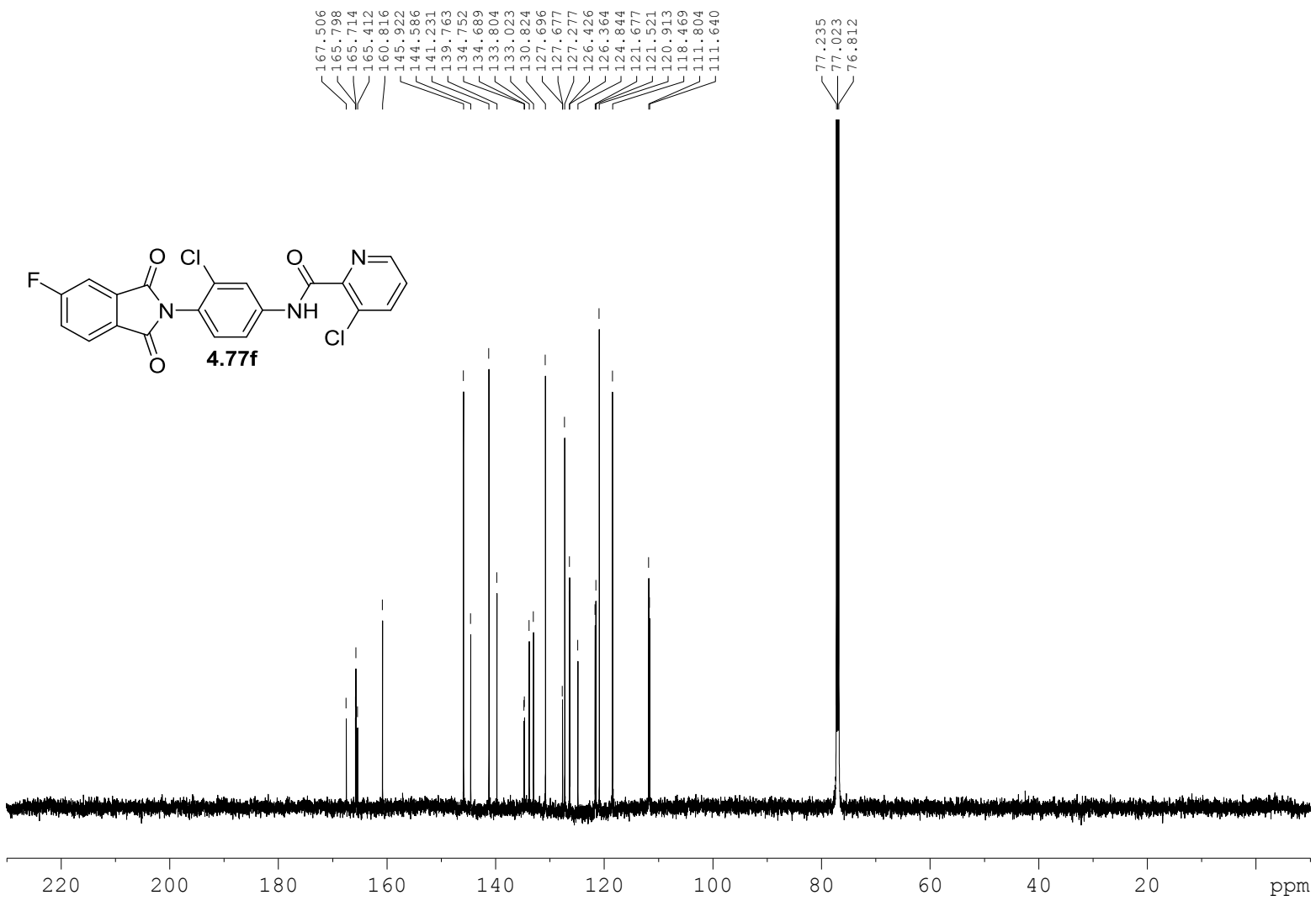
F2 - Processing parameters  
SI 32768  
SF 100.6127772 MHz  
WDW EM  
SSB 0  
LB 1.00 Hz  
GB 0  
PC 1.40

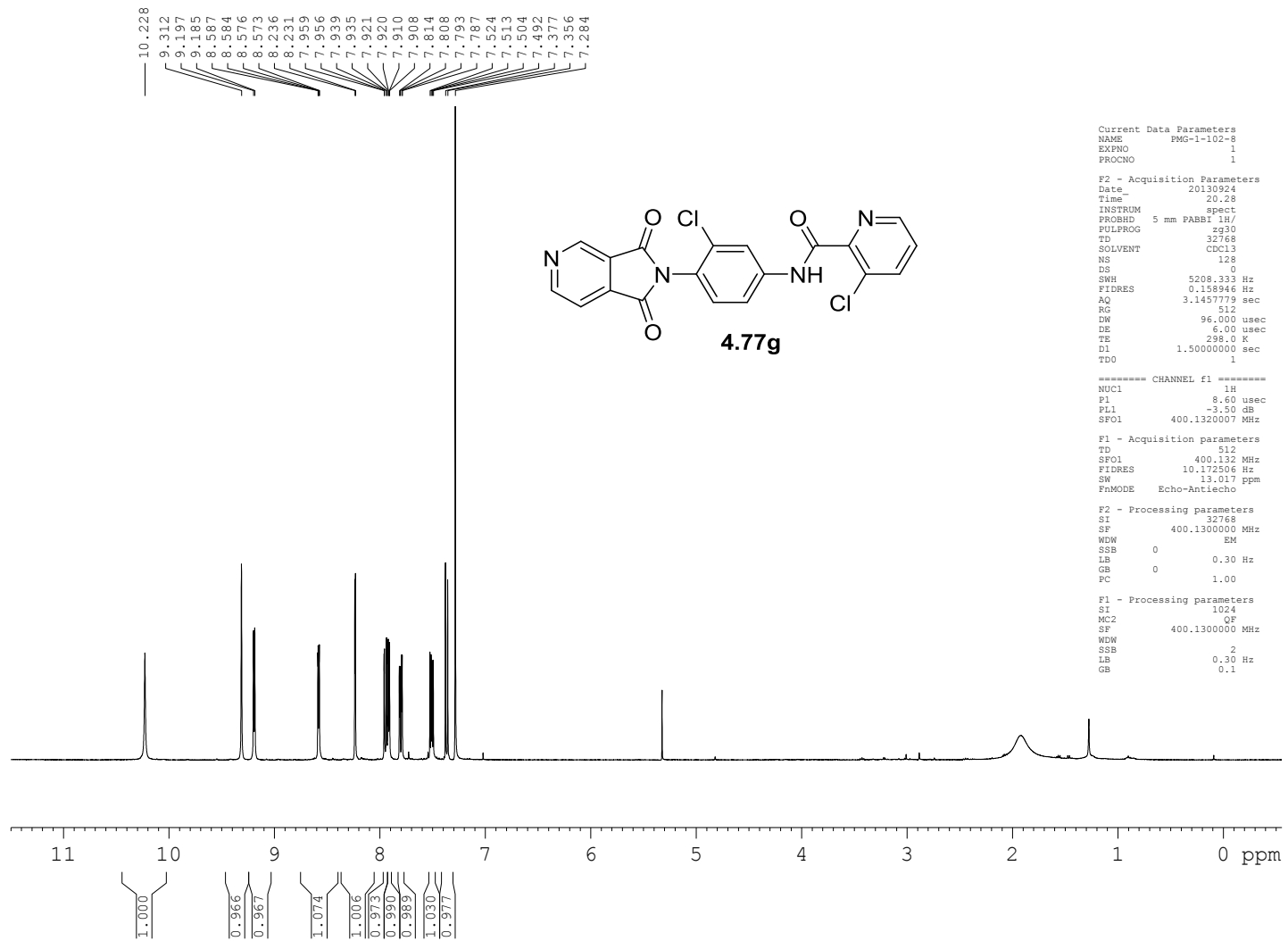
163.231  
160.733  
159.259  
156.529  
145.839  
144.517  
141.144  
139.706  
136.990  
136.914  
134.523  
133.946  
133.768  
132.942  
130.794  
127.183  
124.558  
122.855  
122.660  
121.696  
120.841  
120.071  
118.758  
118.391  
117.783



434







```

Current Data Parameters
NAME      PMG-1-102-8
EXPNO    2
PROCNO   1

F2 - Acquisition Parameters
Date      20130928
Time     20.12
INSTRUM  spect
PROBHD   5 mm PABBO BB-
PULPROG  zgpg30
TD       32768
SOLVENT  CDCl3
NS       3000
DS       8
SWH      26178.010 Hz
FIDRES   0.798889 Hz
AQ       0.6259188 sec
RG       16384
DW       19.100 usec
DE       6.00 usec
TE       298.0 K
D1       2.00000000 sec
D11      0.03000000 sec
TDO      1

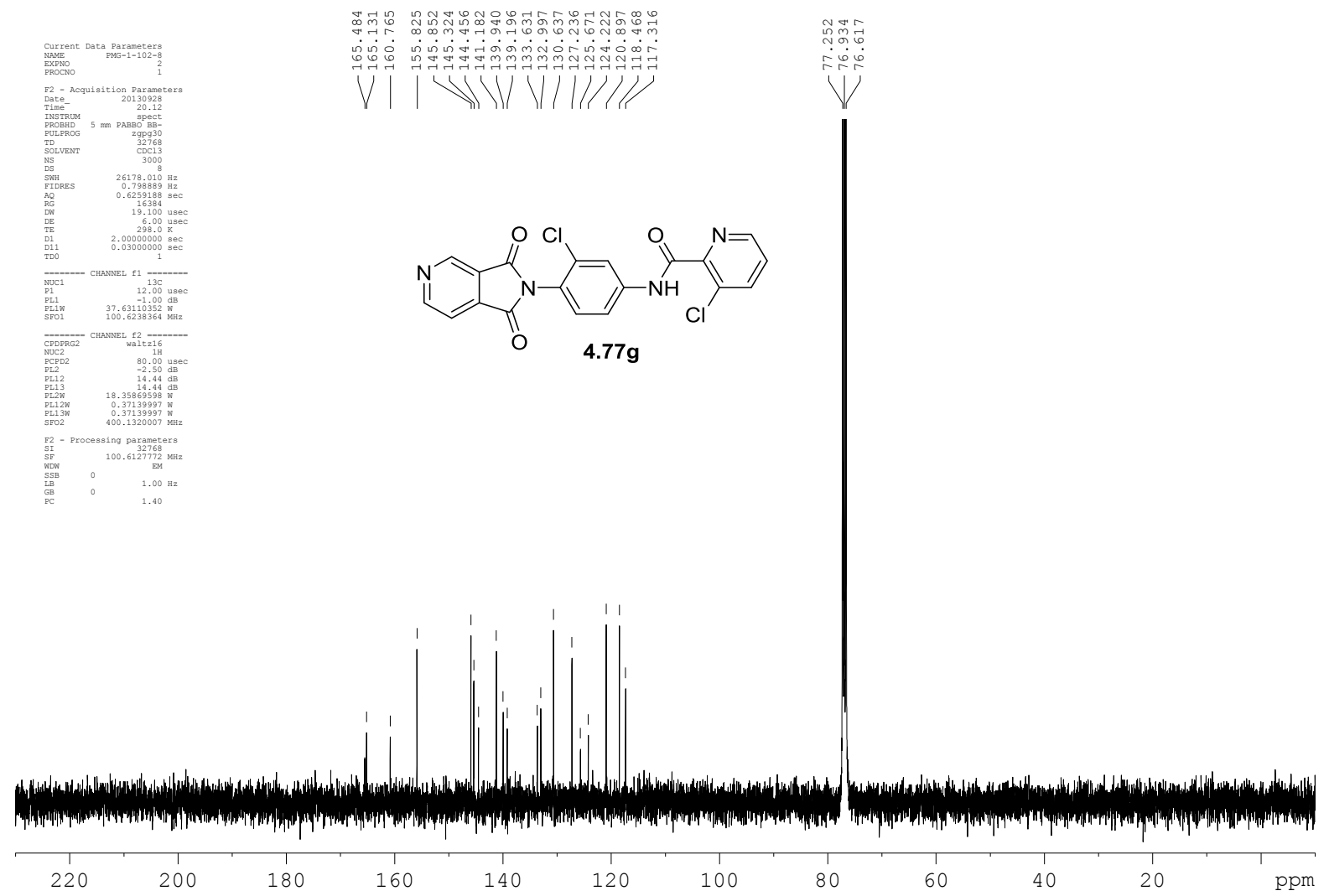
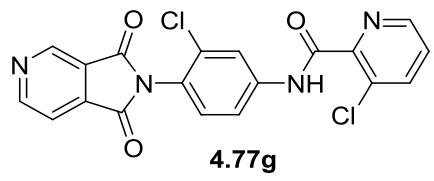
----- CHANNEL f1 -----
NUC1     13C
P1       12.00 usec
PL1      -1.00 dB
PL1W     37.63110352 W
SFO1     100.628364 MHz

----- CHANNEL f2 -----
CPDPRG2  walz16
NUC2     1H
PCPD2    80.00 usec
PL2      -2.50 dB
PL12     14.44 dB
PL13     14.44 dB
PL2W     18.35866858 W
PL12W    0.37139997 W
PL13W    0.37139997 W
SFO2     400.1320007 MHz

F2 - Processing parameters
SI       32768
SF       100.6127772 MHz
WDW      EM
SSB      0
LB       1.00 Hz
GB       0
PC       1.40

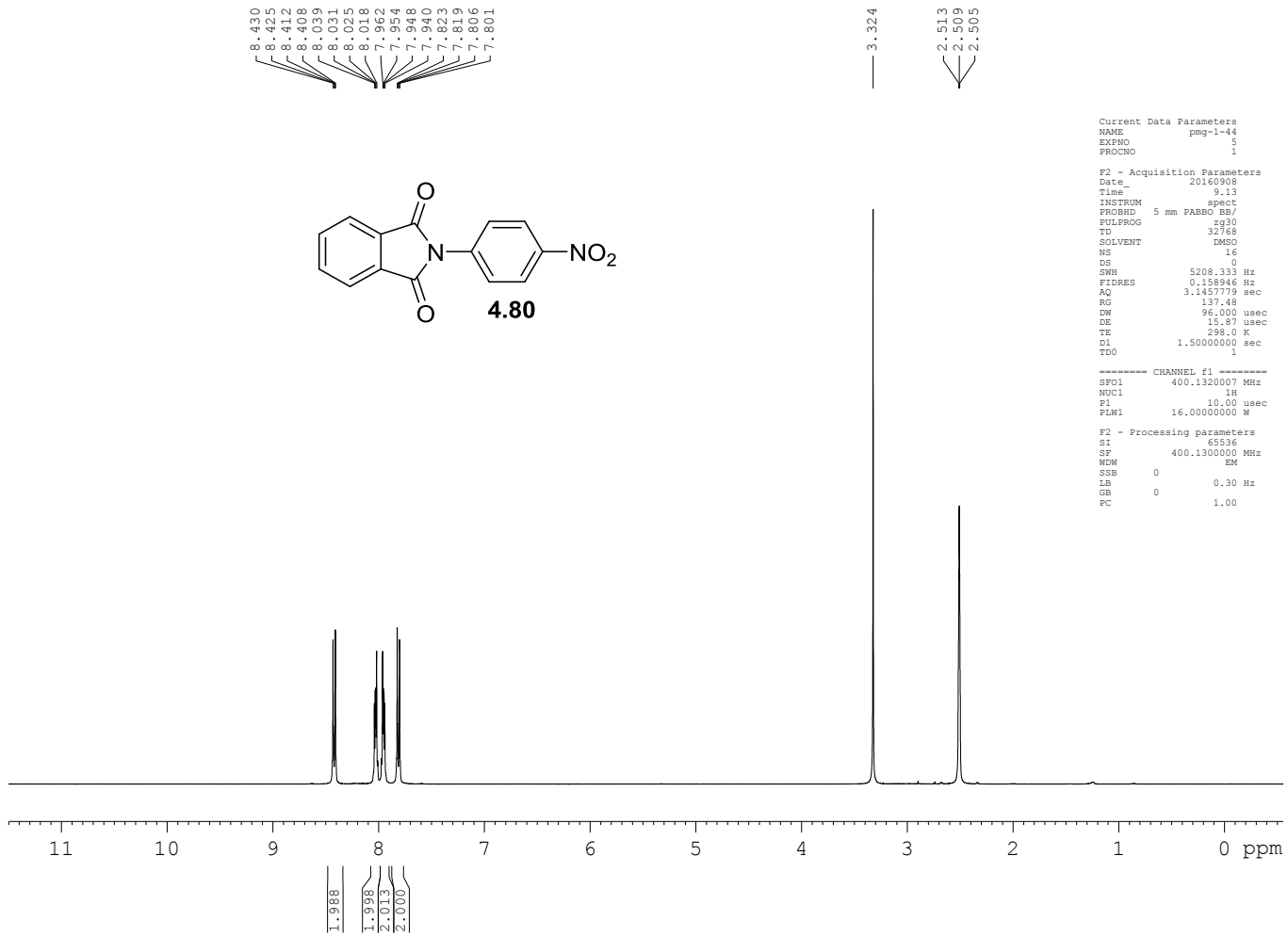
```

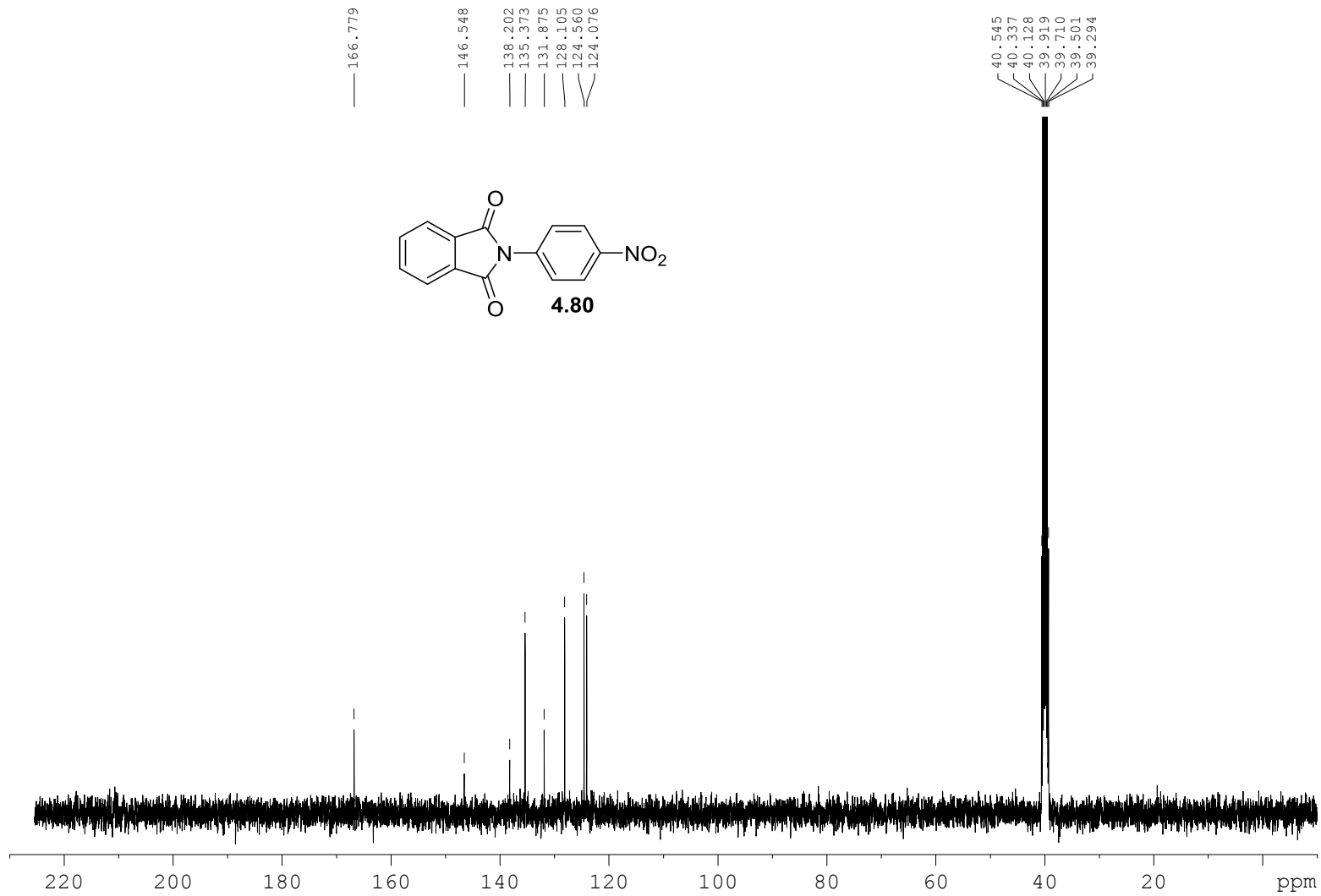
165.484  
 165.131  
 160.765  
 155.825  
 145.852  
 145.324  
 144.456  
 141.182  
 139.940  
 139.196  
 133.631  
 132.937  
 130.637  
 127.236  
 125.671  
 124.222  
 120.897  
 118.468  
 117.316  
 77.252  
 76.934  
 76.617



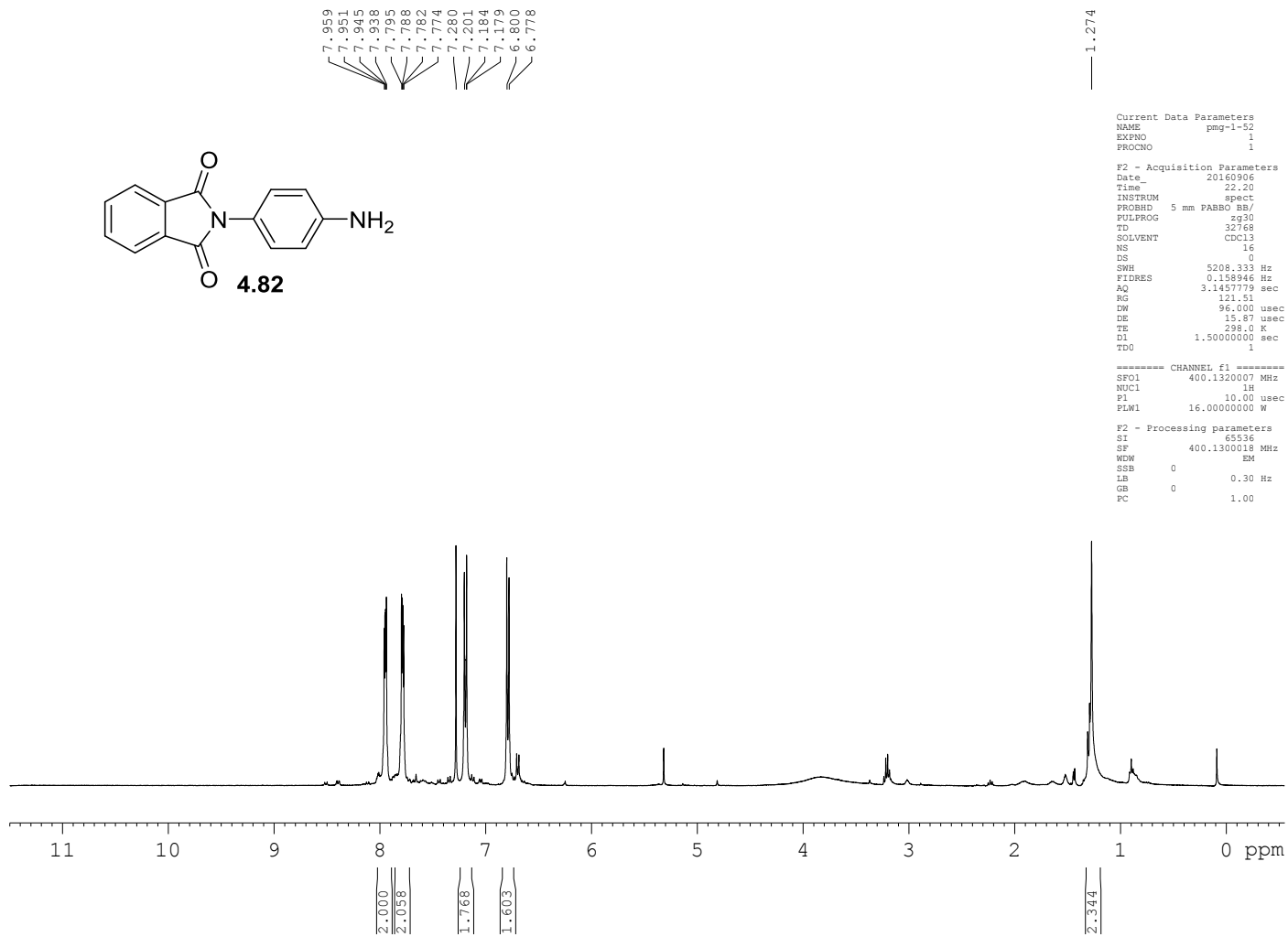
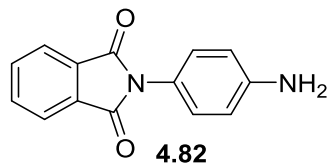
437

438

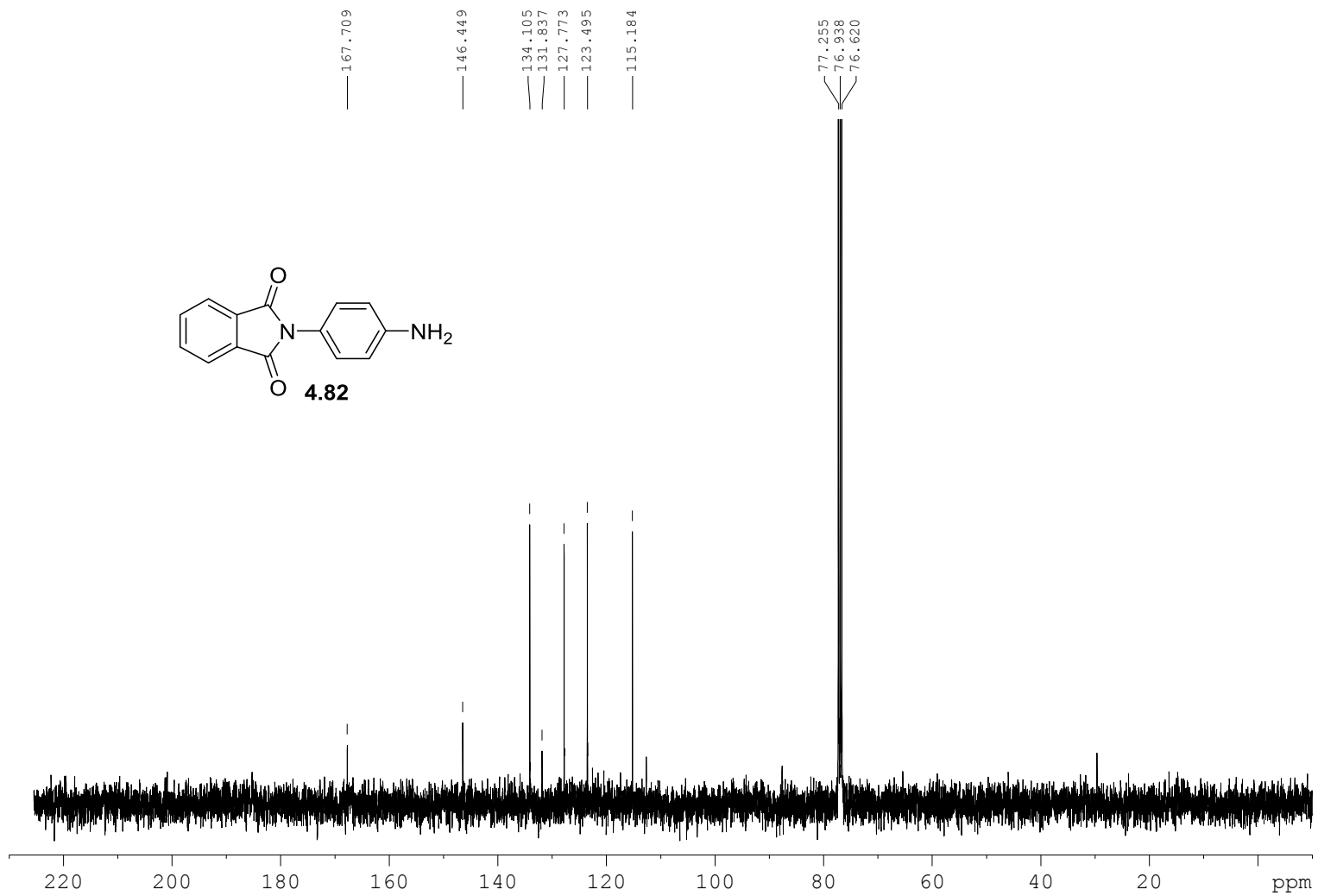
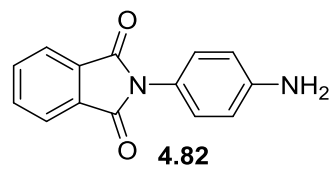




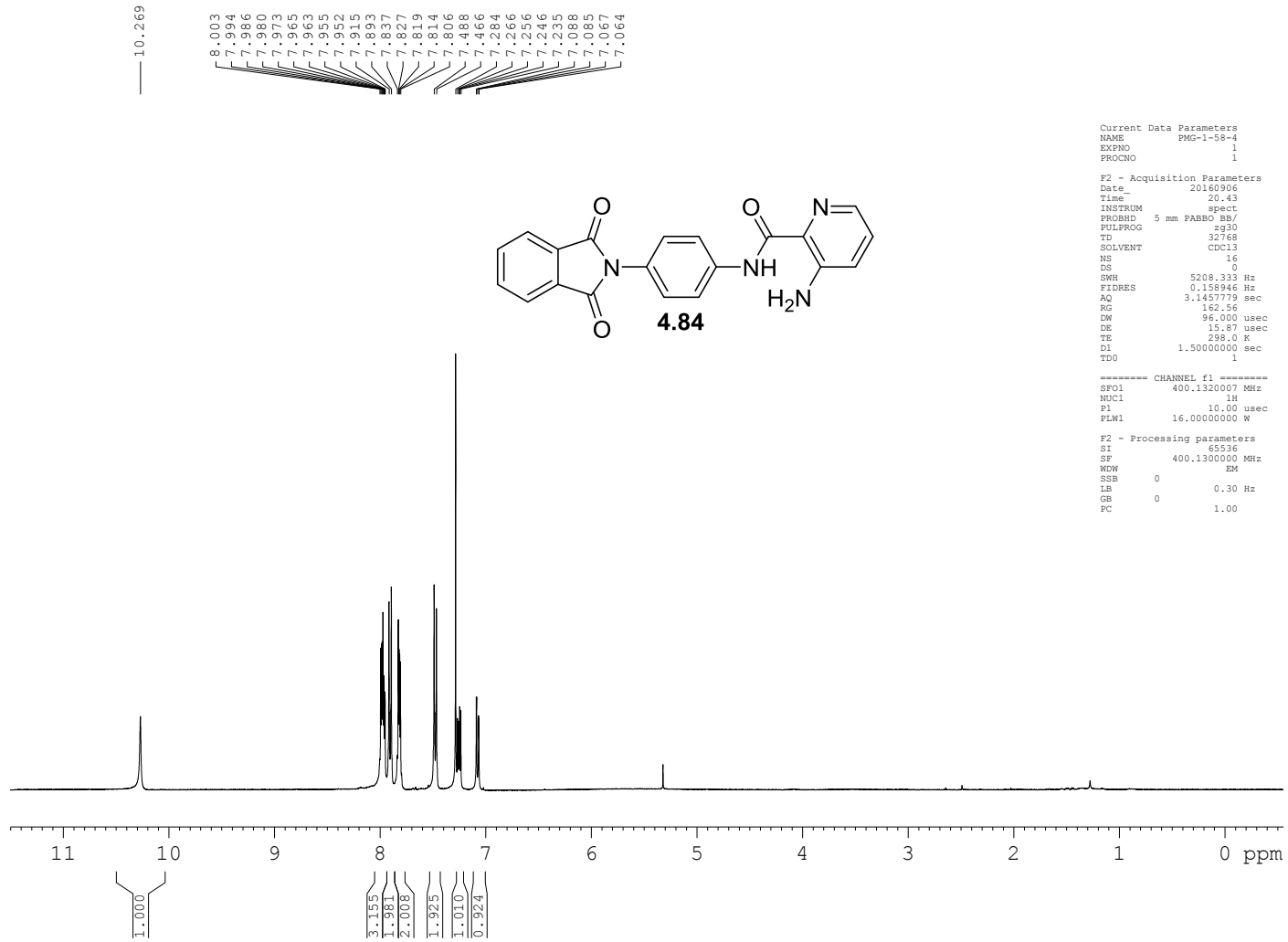


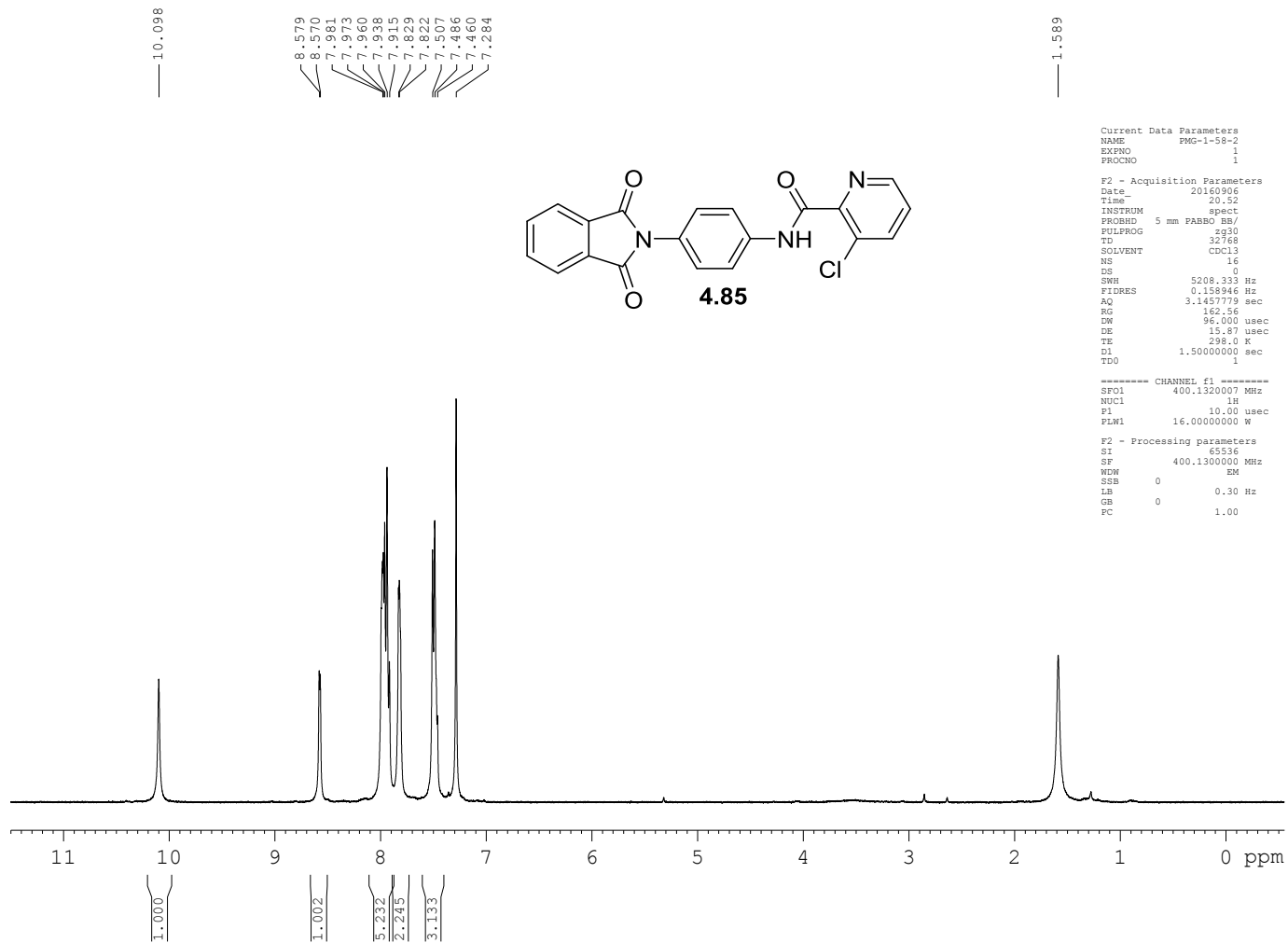


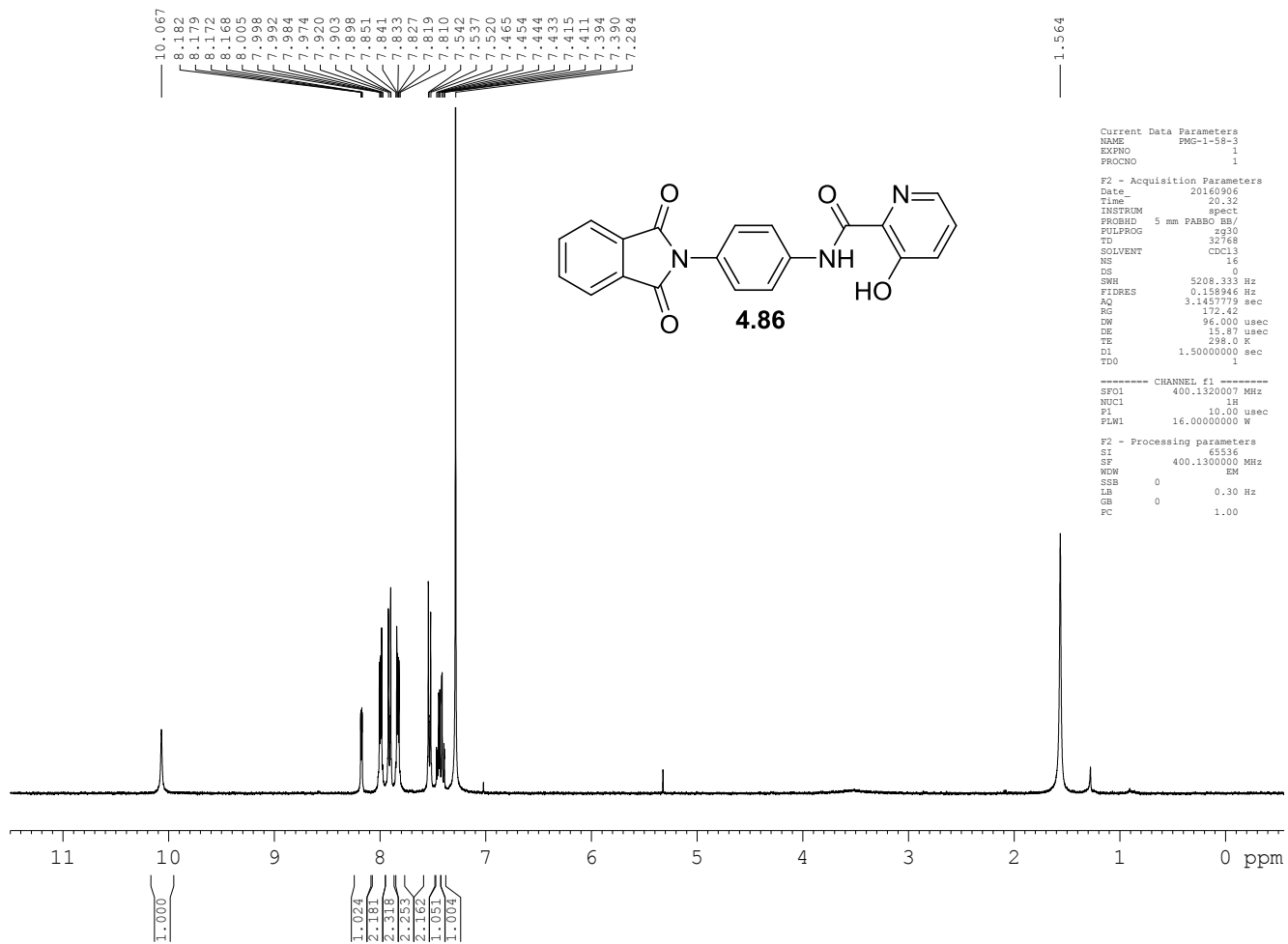
441

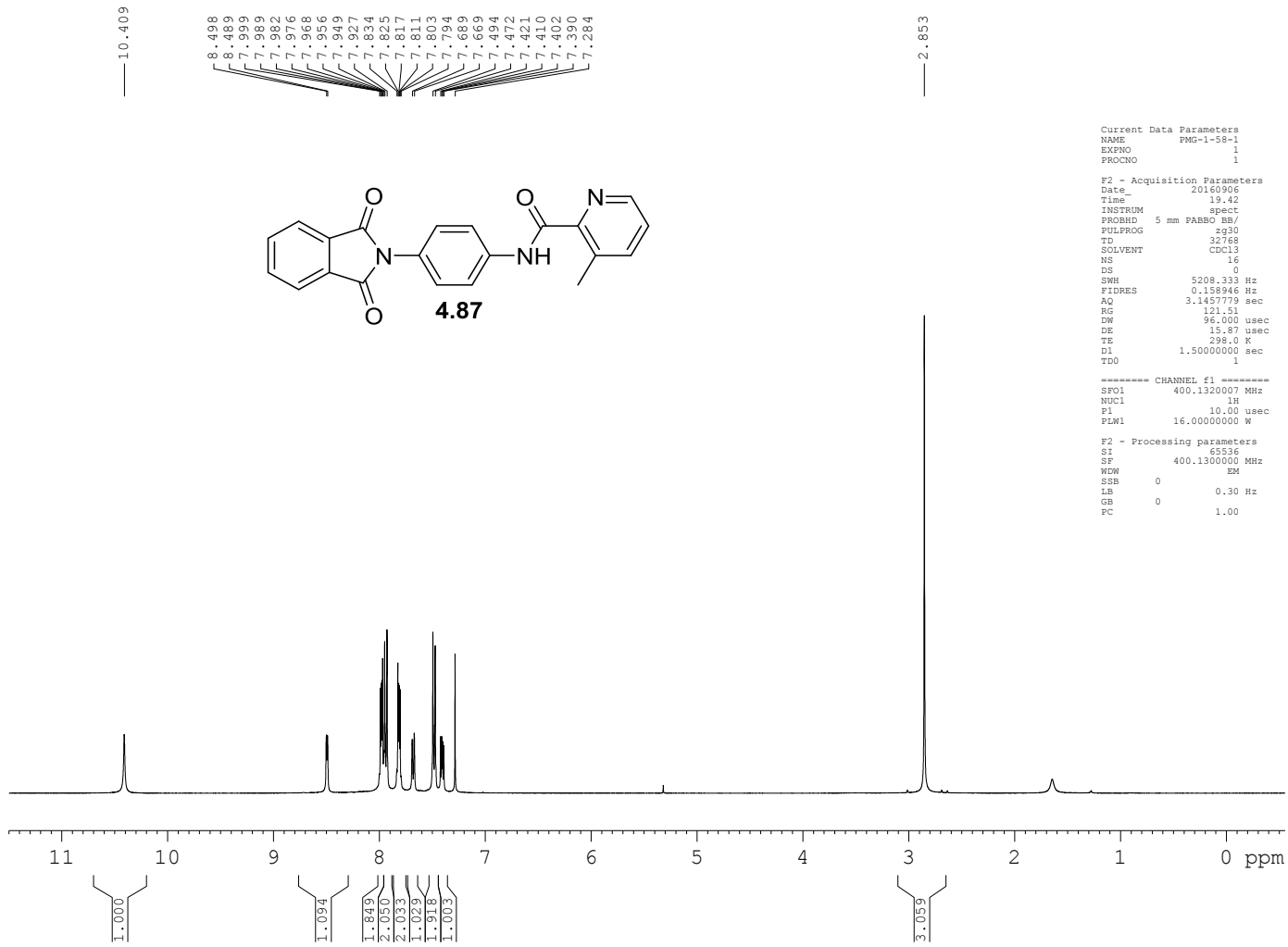


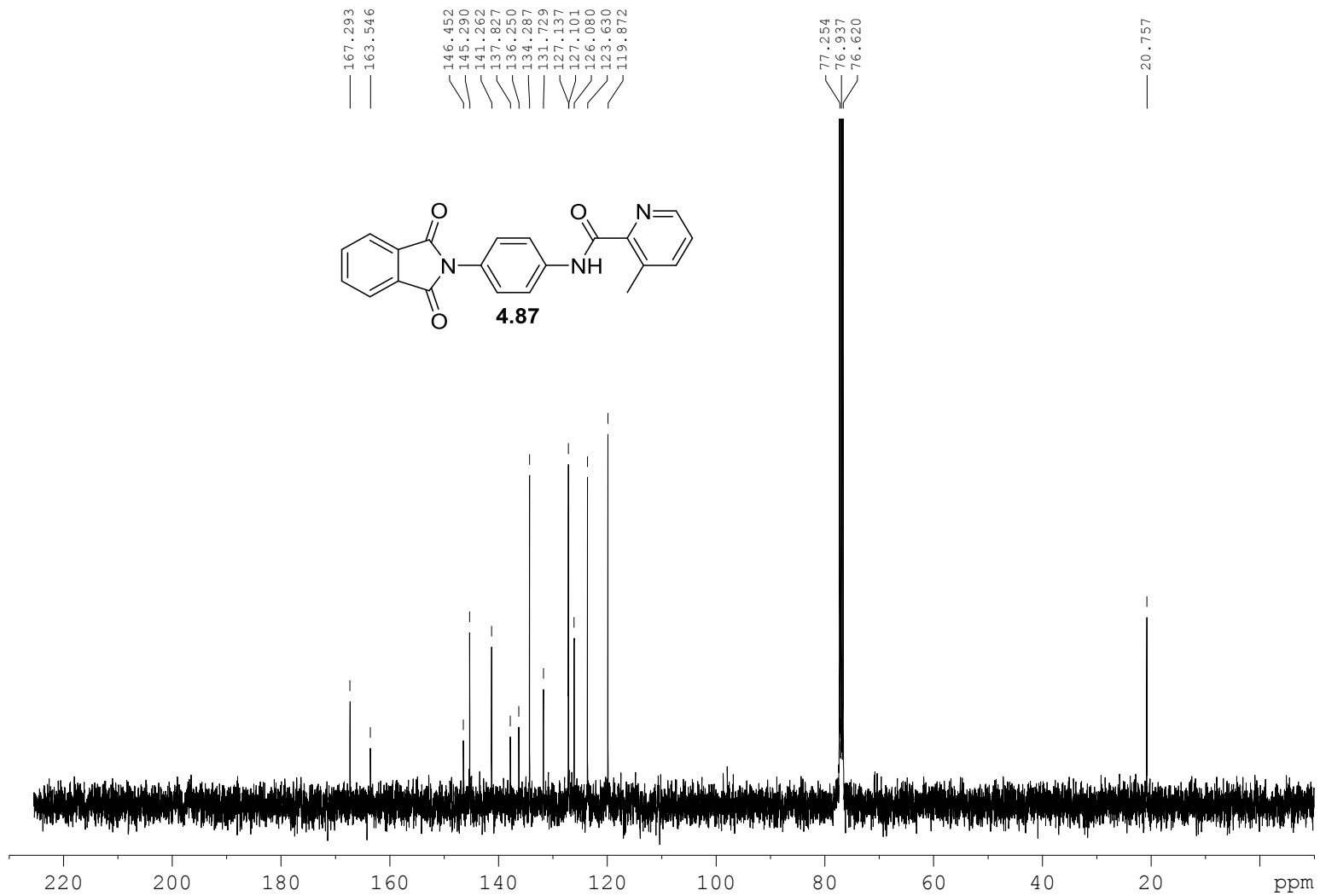
442

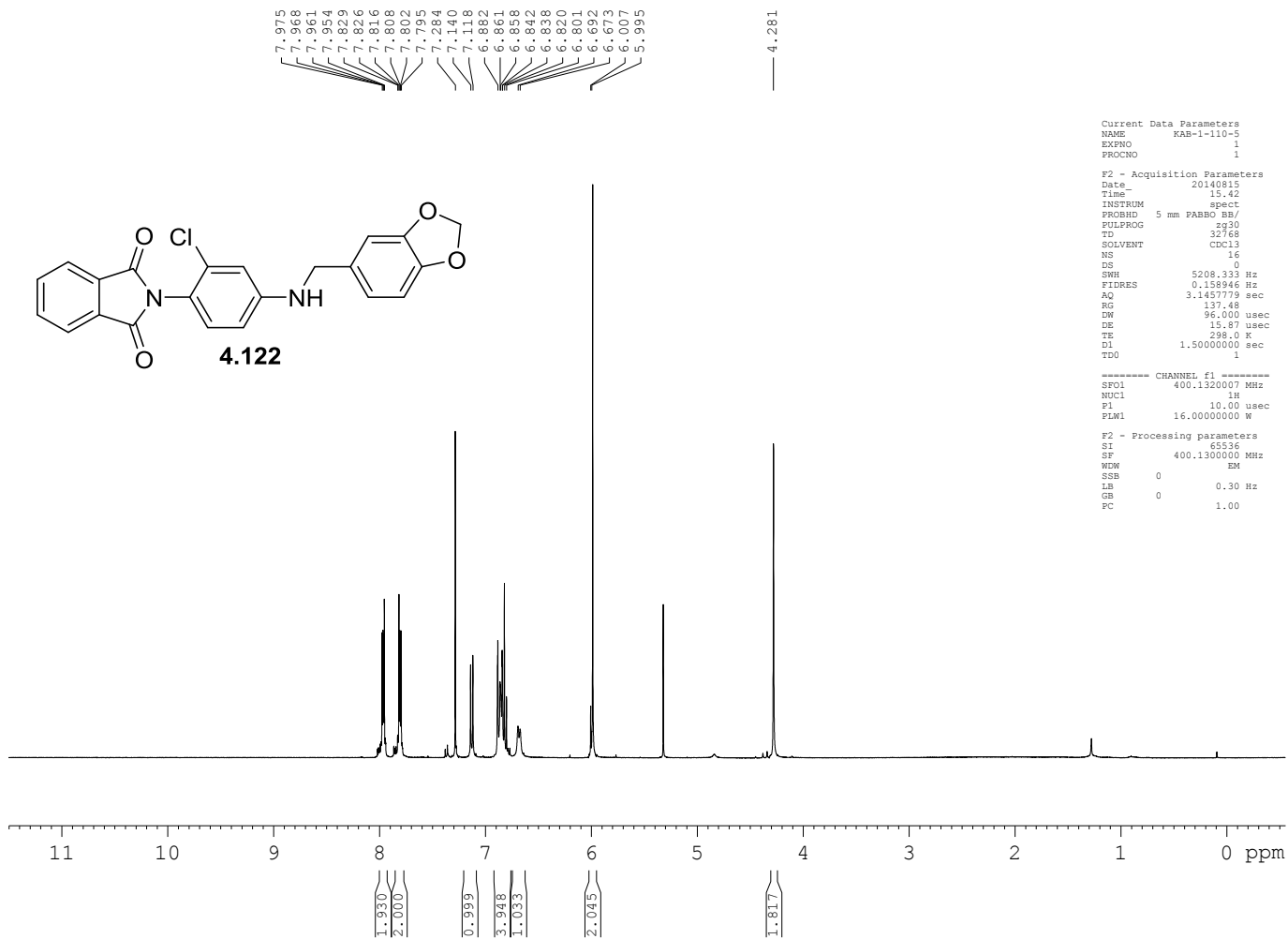






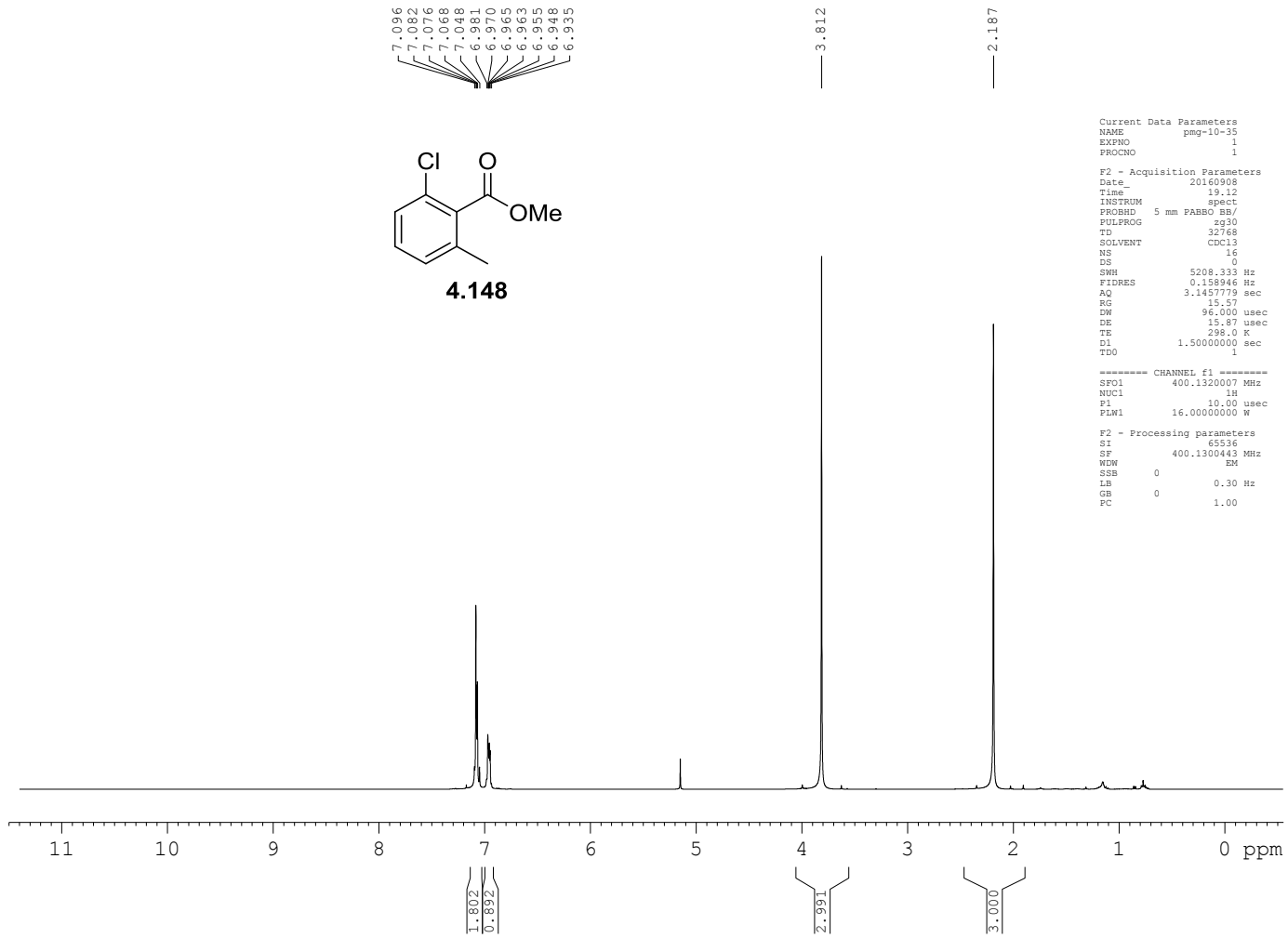


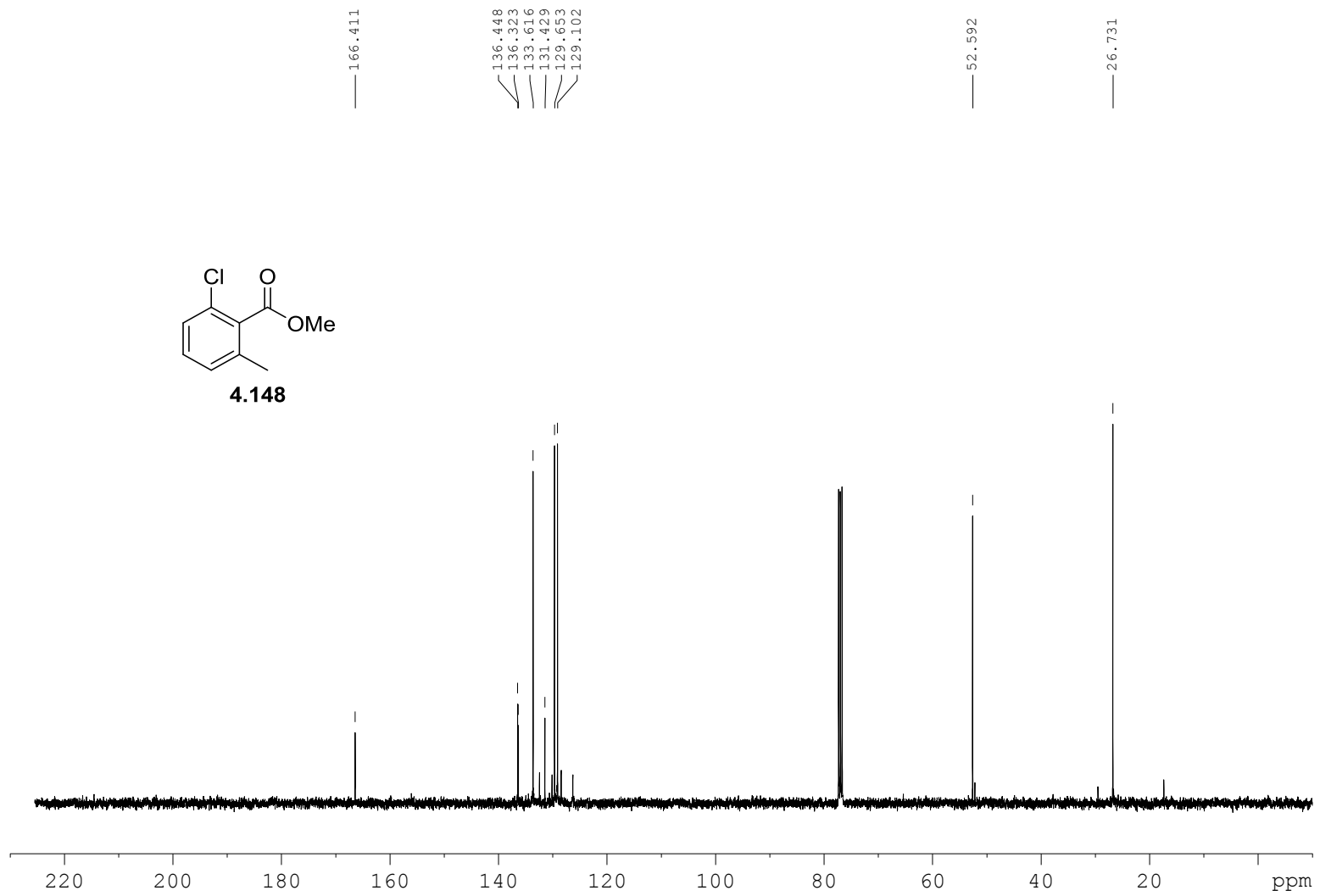




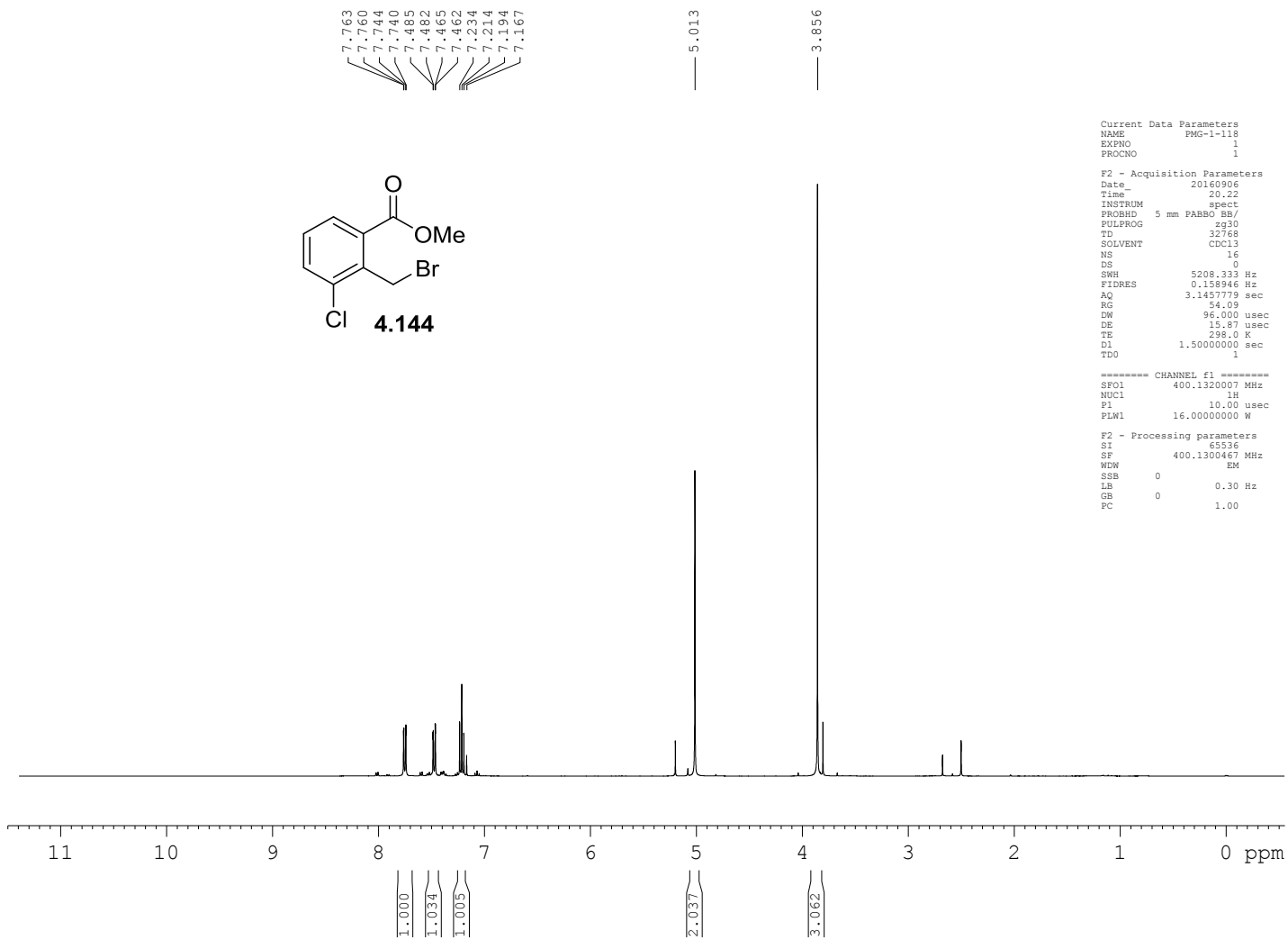


448

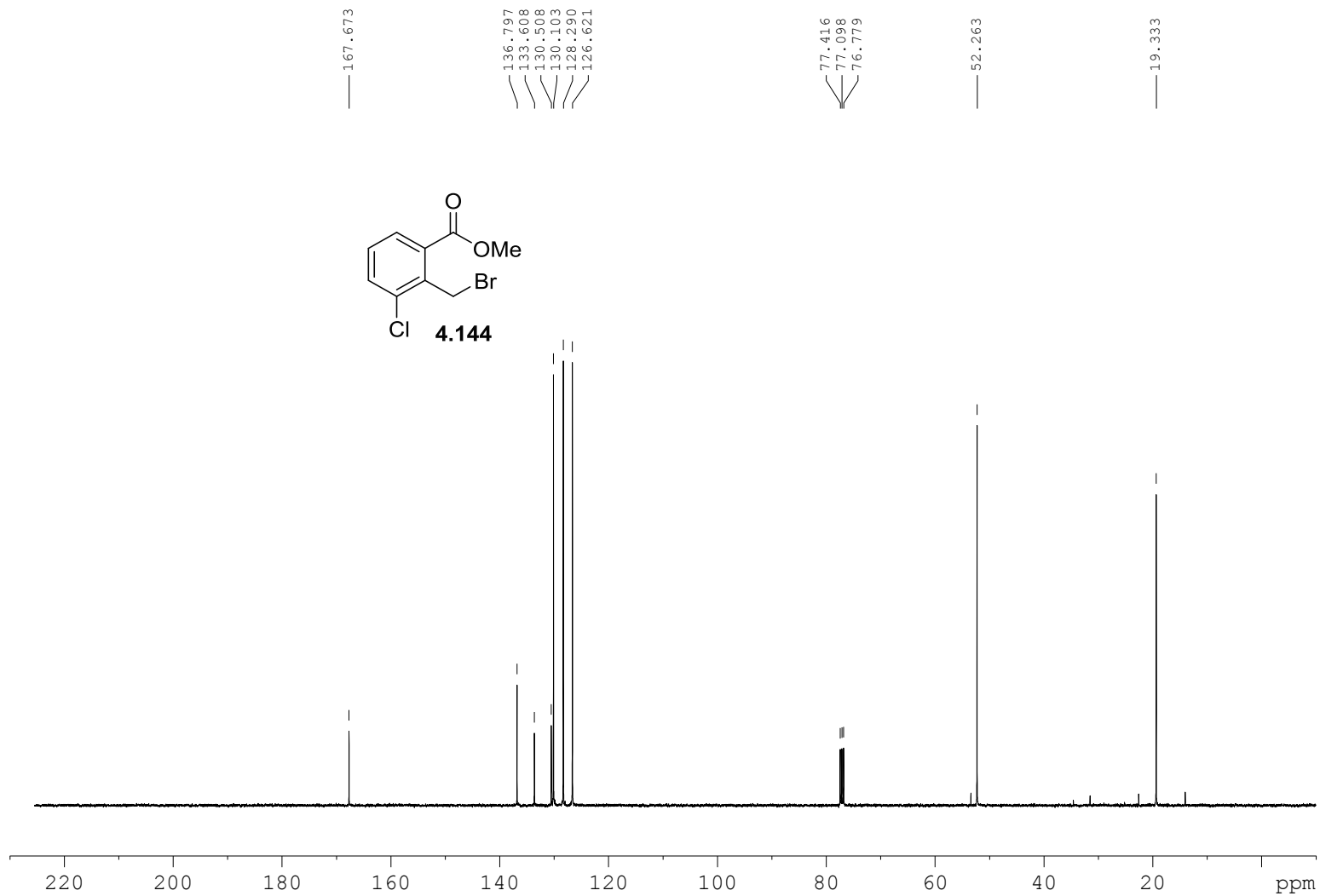


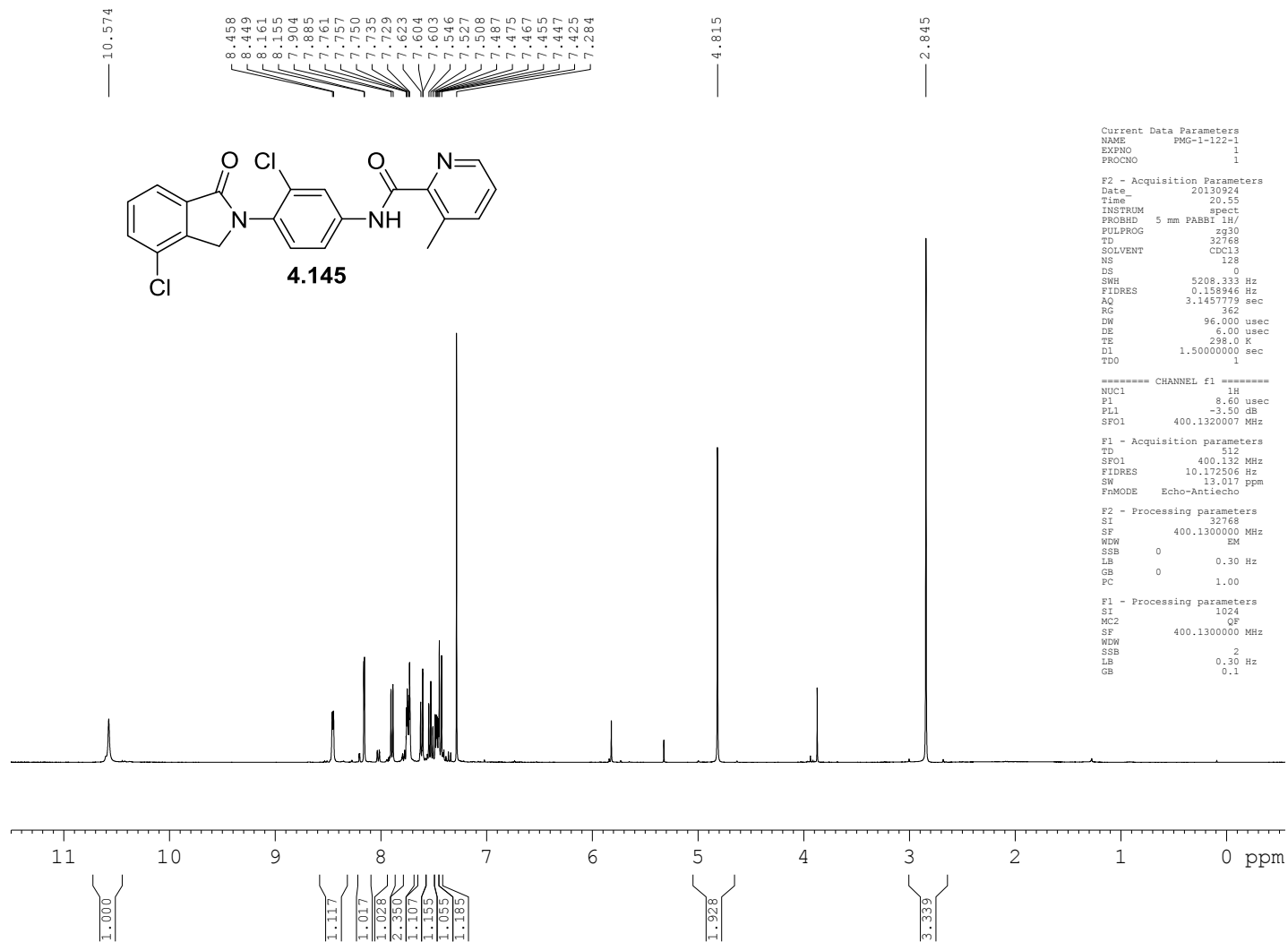


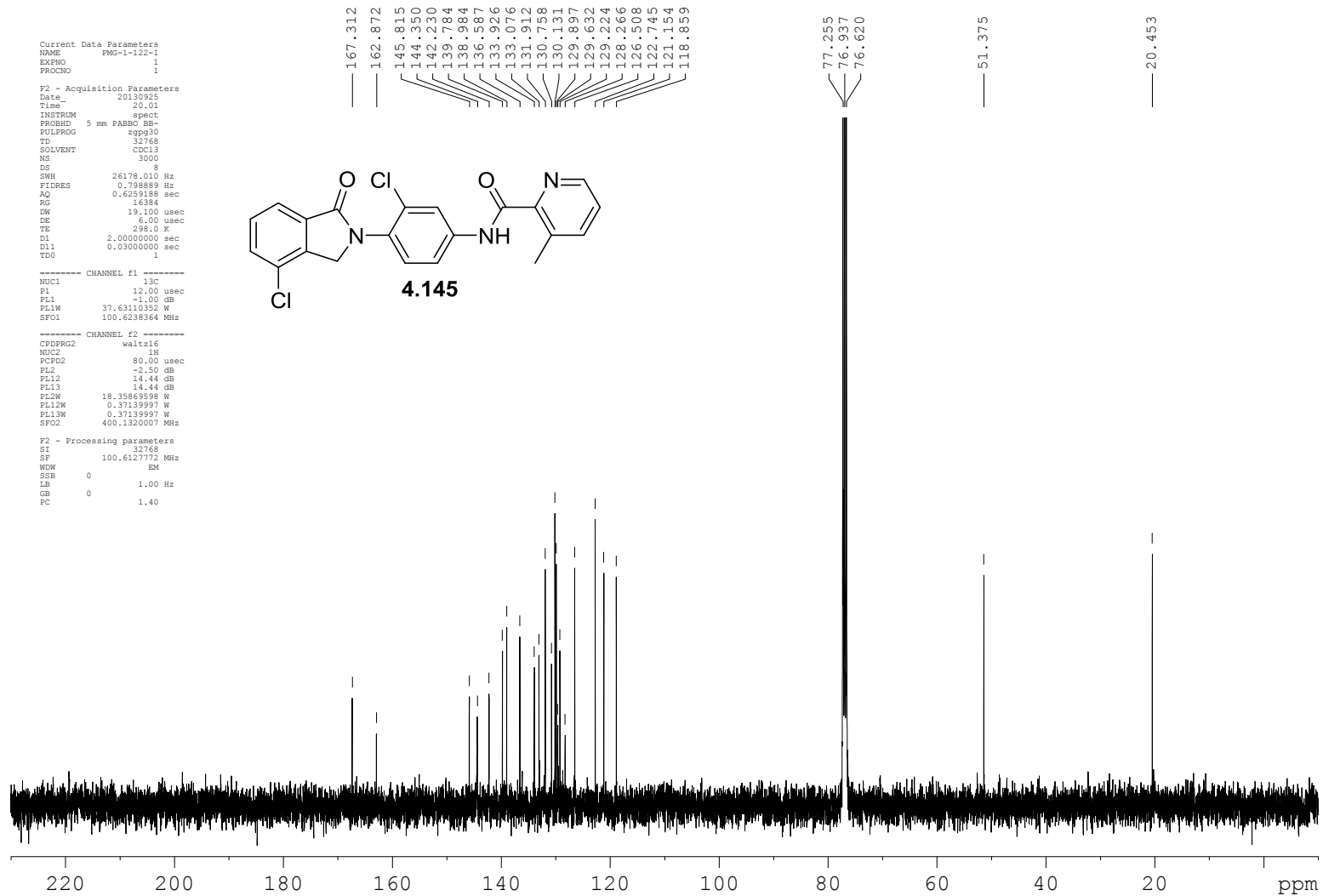
450



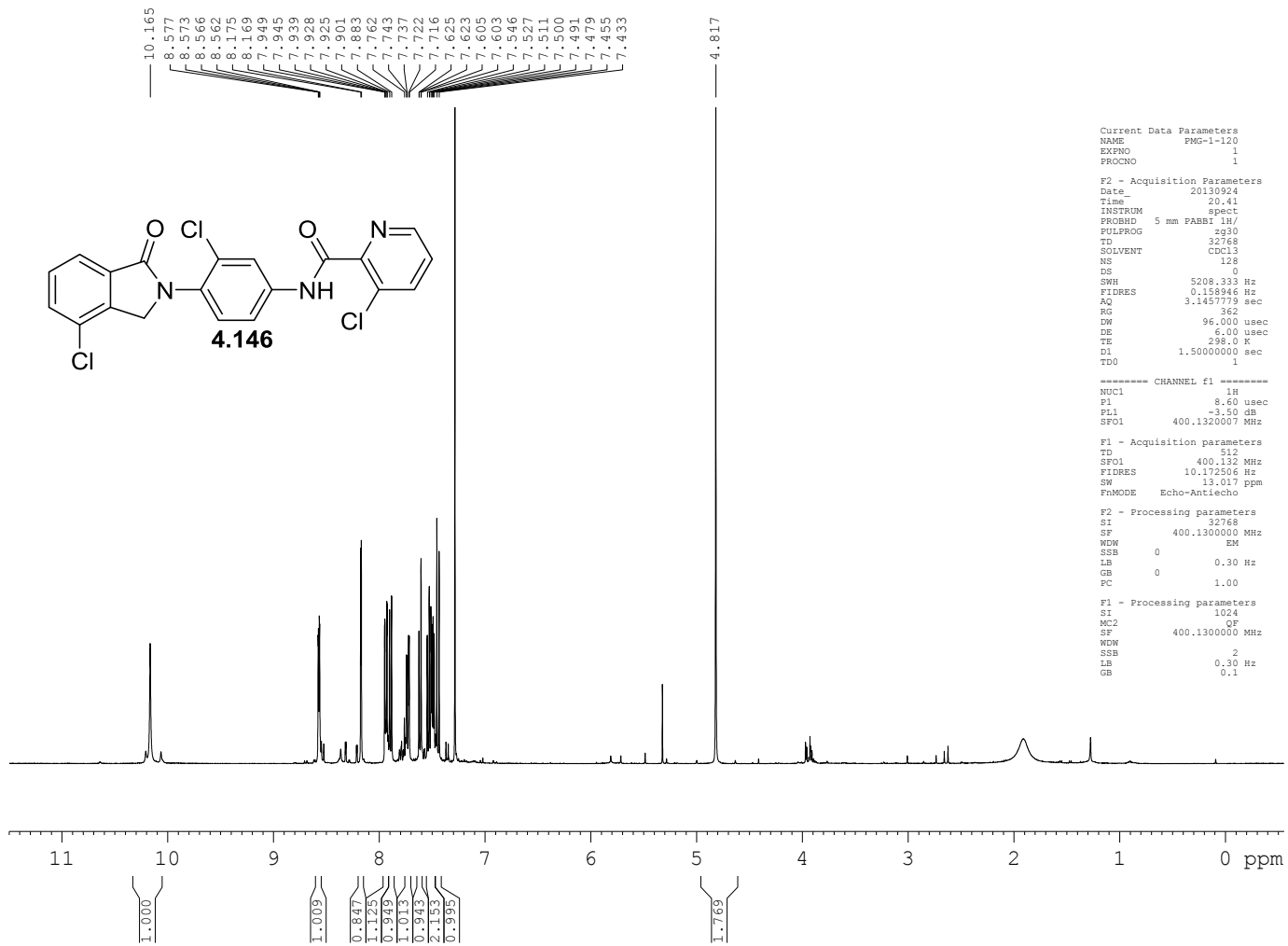
451

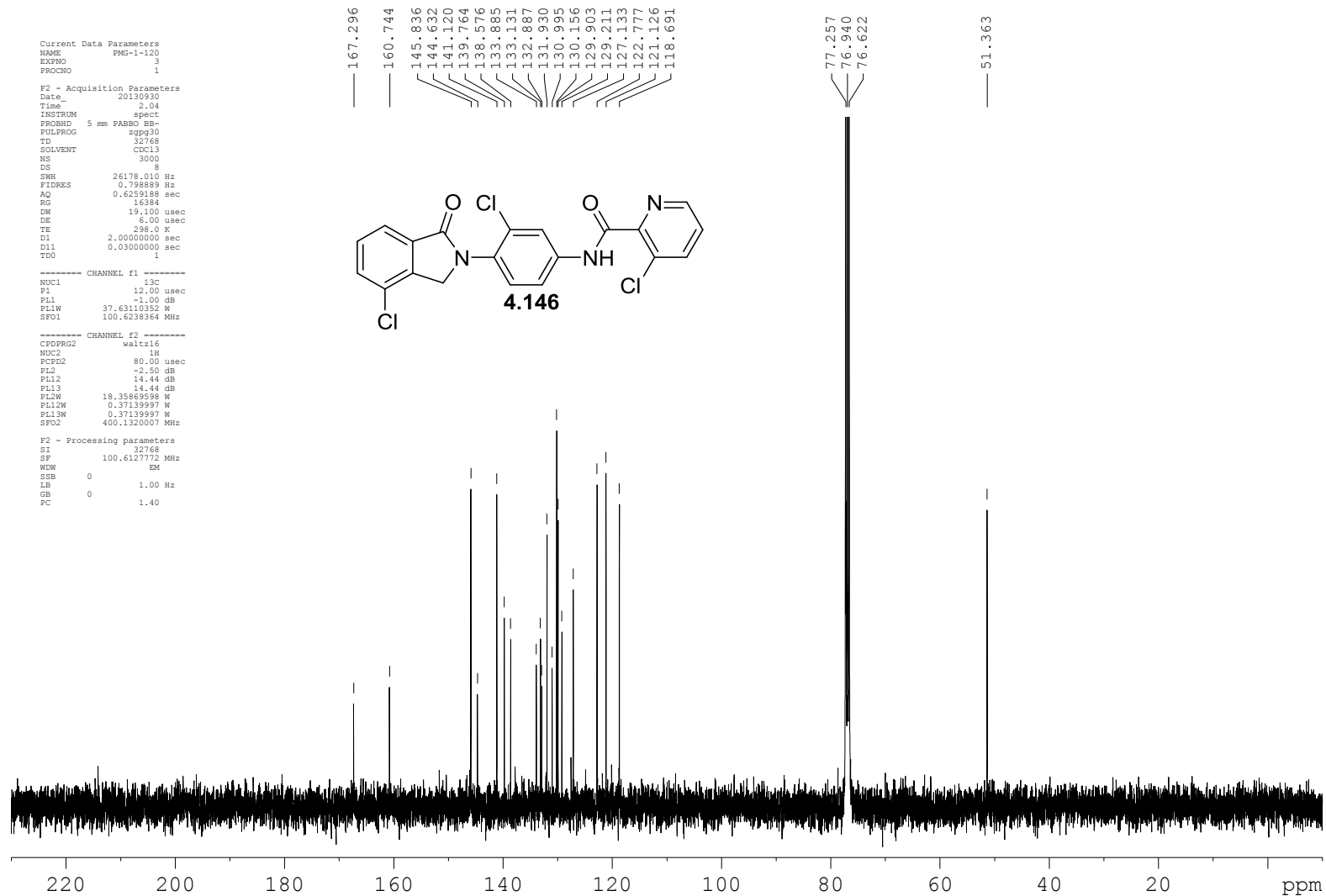






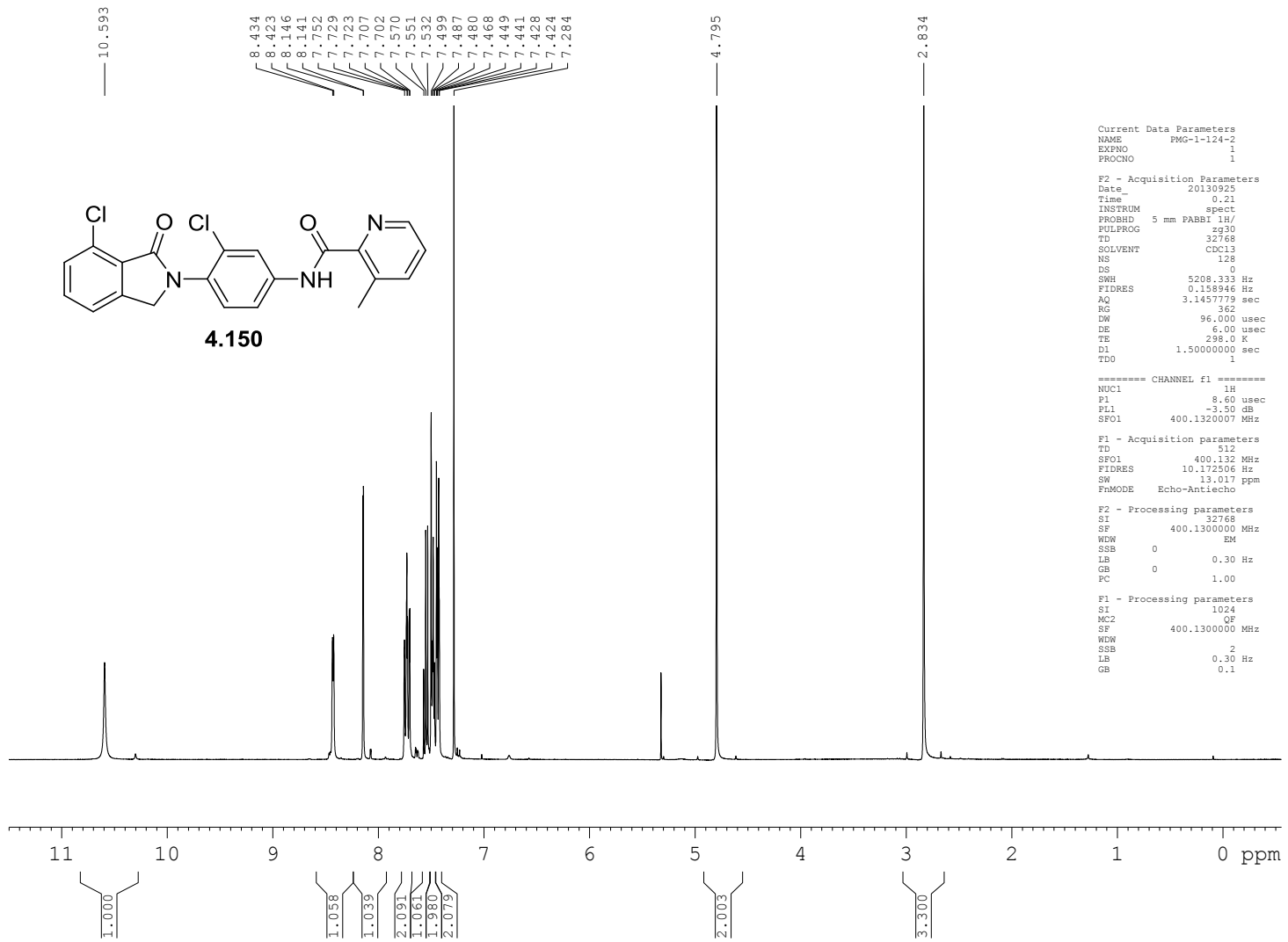
454

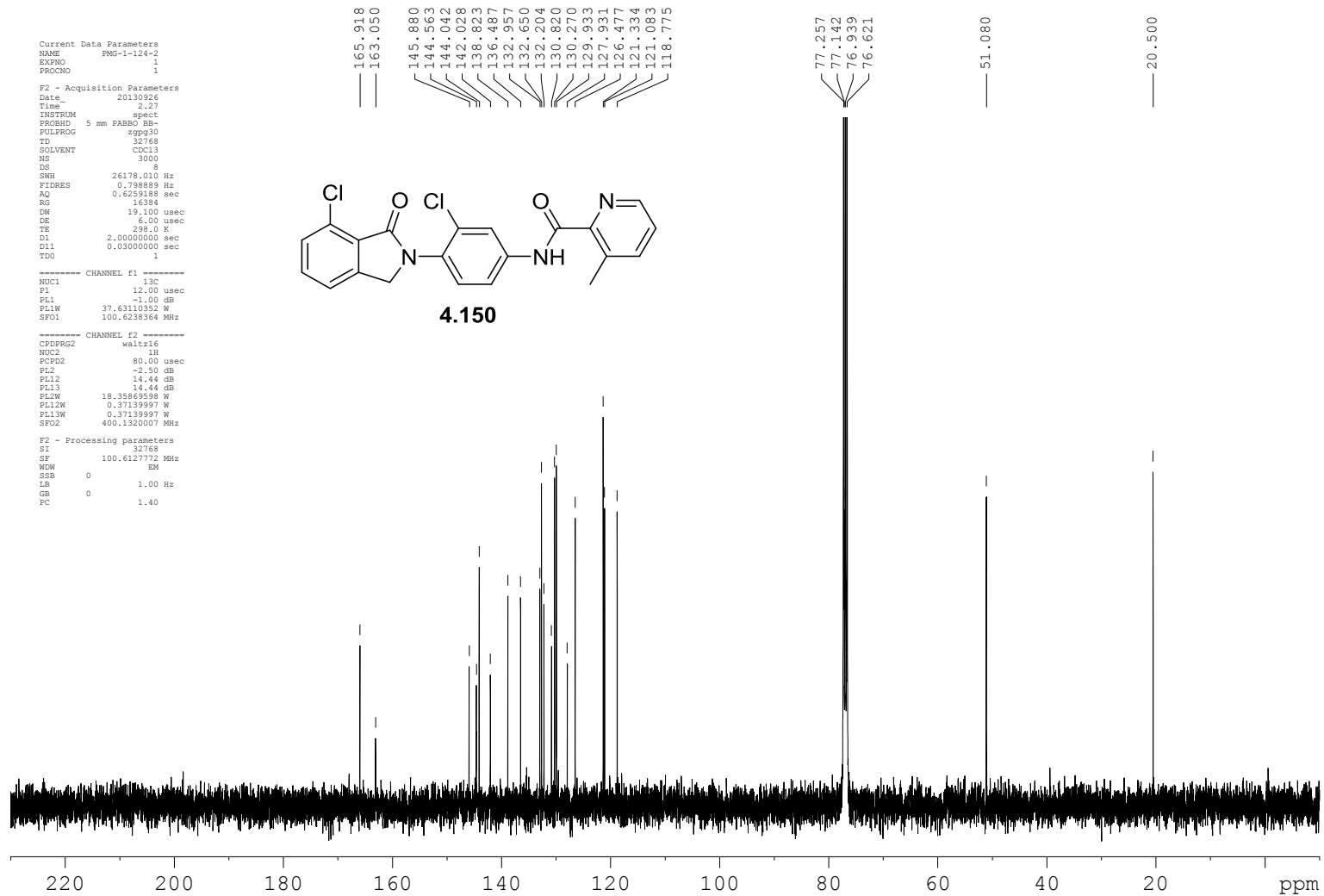






456

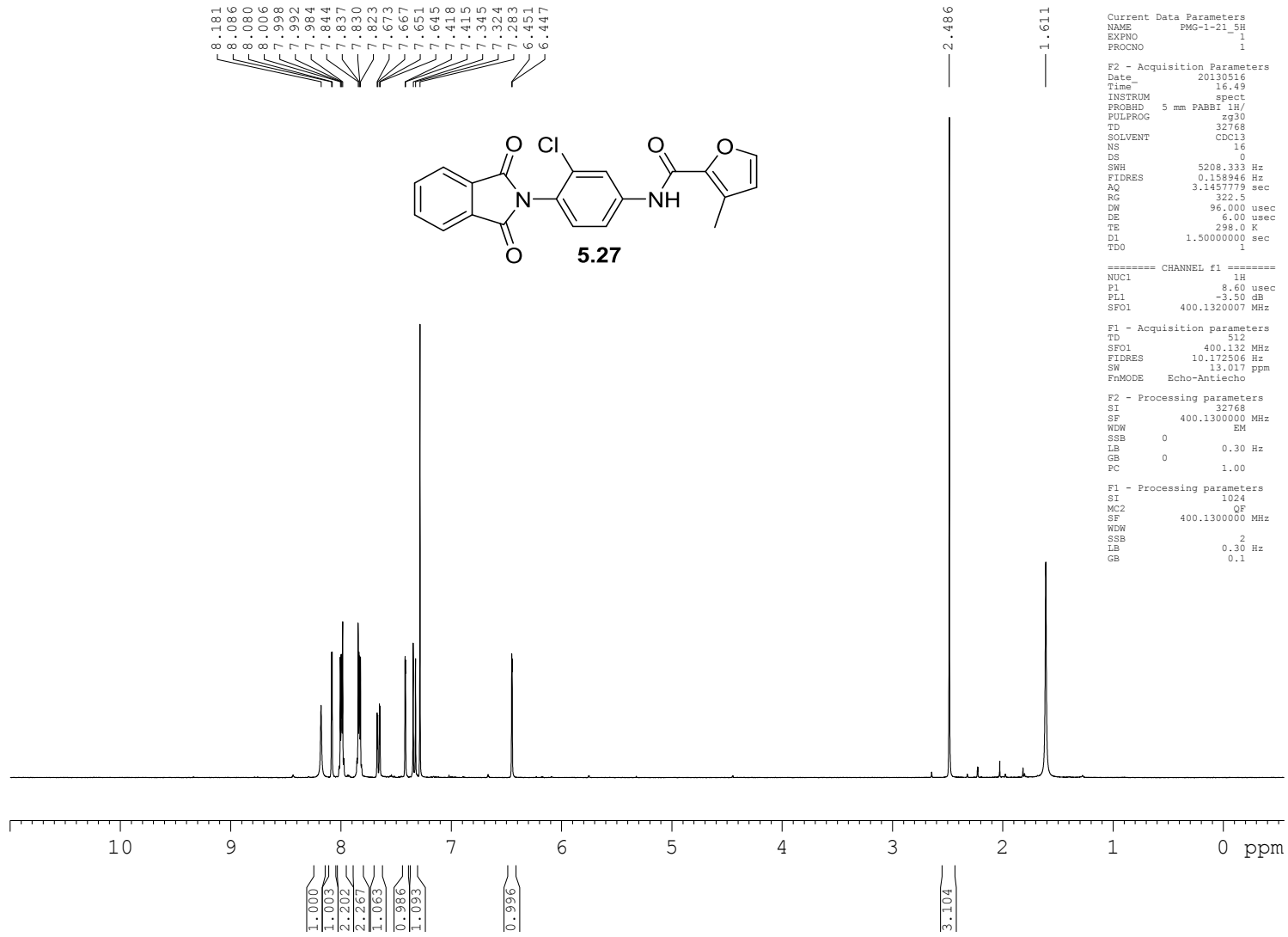




## **Appendix E**

Relevant spectra for chapter V

459



460

Current Data Parameters  
NAME PMG-1-21\_5  
EXPNO 3  
PROCNO 1

F2 - Acquisition Parameters  
Date\_ 20130521  
Time 9.43  
INSTRUM spect  
PROBHD 5 mm PABBO BB-  
PULPROG zgpg30  
TD 32768  
SOLVENT CDC13  
NS 3000  
DS 8  
SWH 26178.010 Hz  
FIDRES 0.798889 Hz  
AQ 0.6259188 sec  
RG 16384  
DW 19.100 usec  
DE 6.00 usec  
TE 298.0 K  
D1 2.00000000 sec  
D11 0.03000000 sec  
TD0 1

===== CHANNEL f1 =====  
NUC1 13C  
P1 12.00 usec  
PL1 -1.00 dB  
PL1W 37.63110352 W  
SFO1 100.6238364 MHz

===== CHANNEL f2 =====  
CPDPRG2 waltz16  
NUC2 1H  
PCPD2 80.00 usec  
PL2 -2.50 dB  
PL12 14.44 dB  
PL13 14.44 dB  
PL2W 18.35869598 W  
PL12W 0.37139997 W  
PL13W 0.37139997 W  
SFO2 400.1320007 MHz

F2 - Processing parameters  
SI 32768  
SF 100.6127772 MHz  
WDW EM  
SSB 0  
LB 1.00 Hz  
GB 0  
PC 1.40

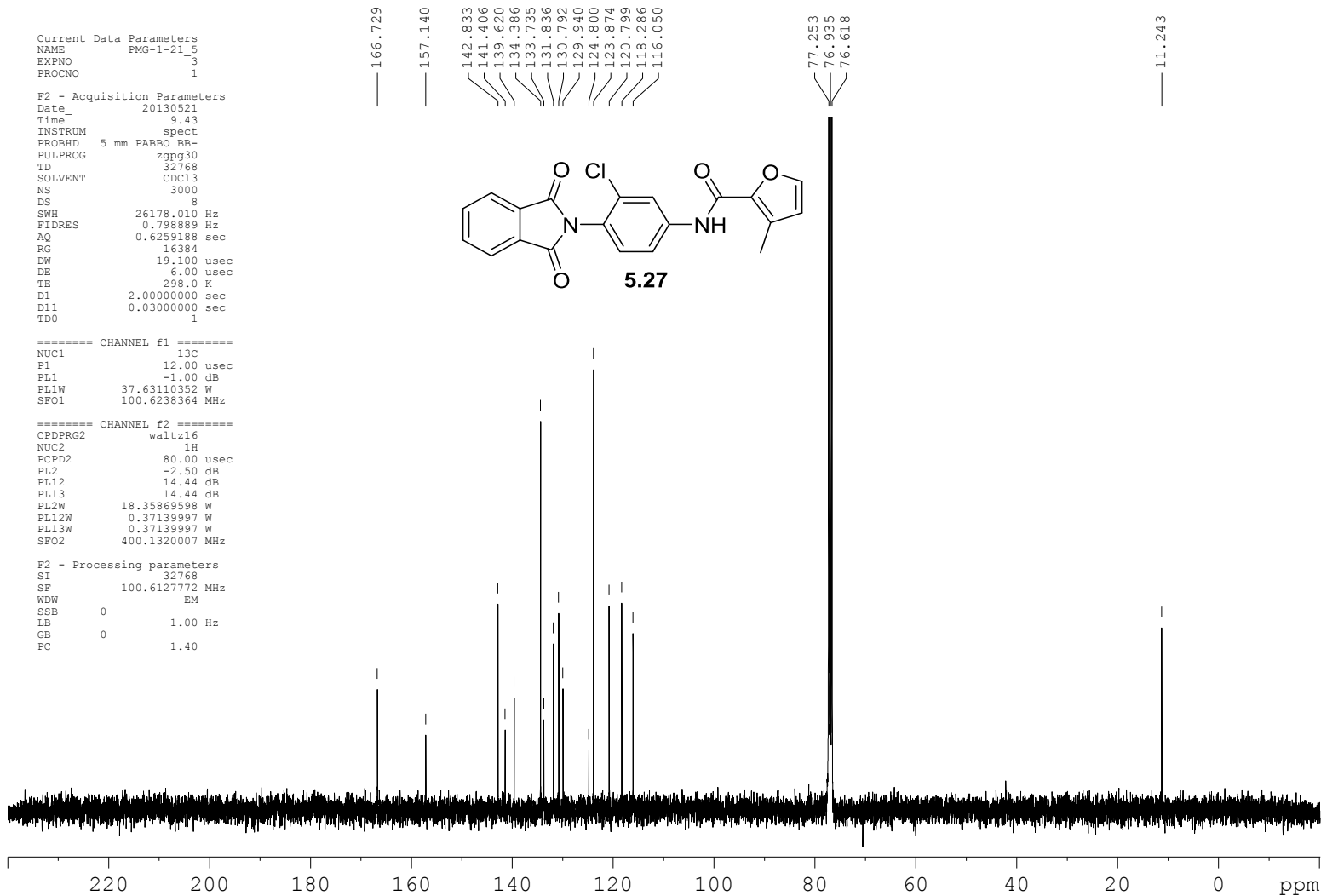
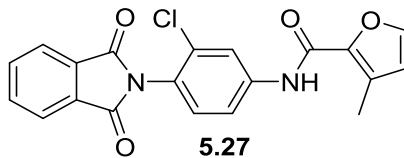
166.729

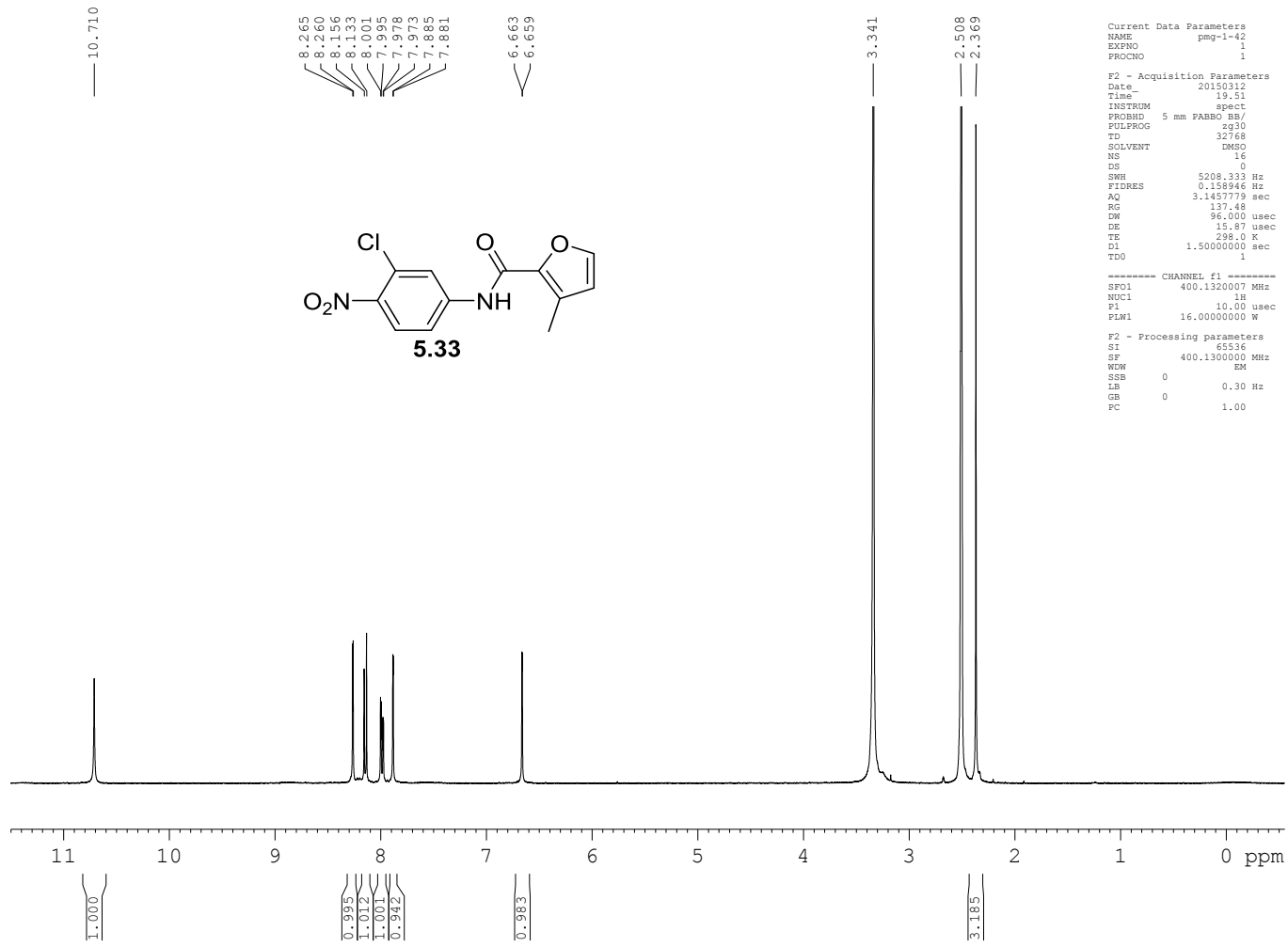
157.140

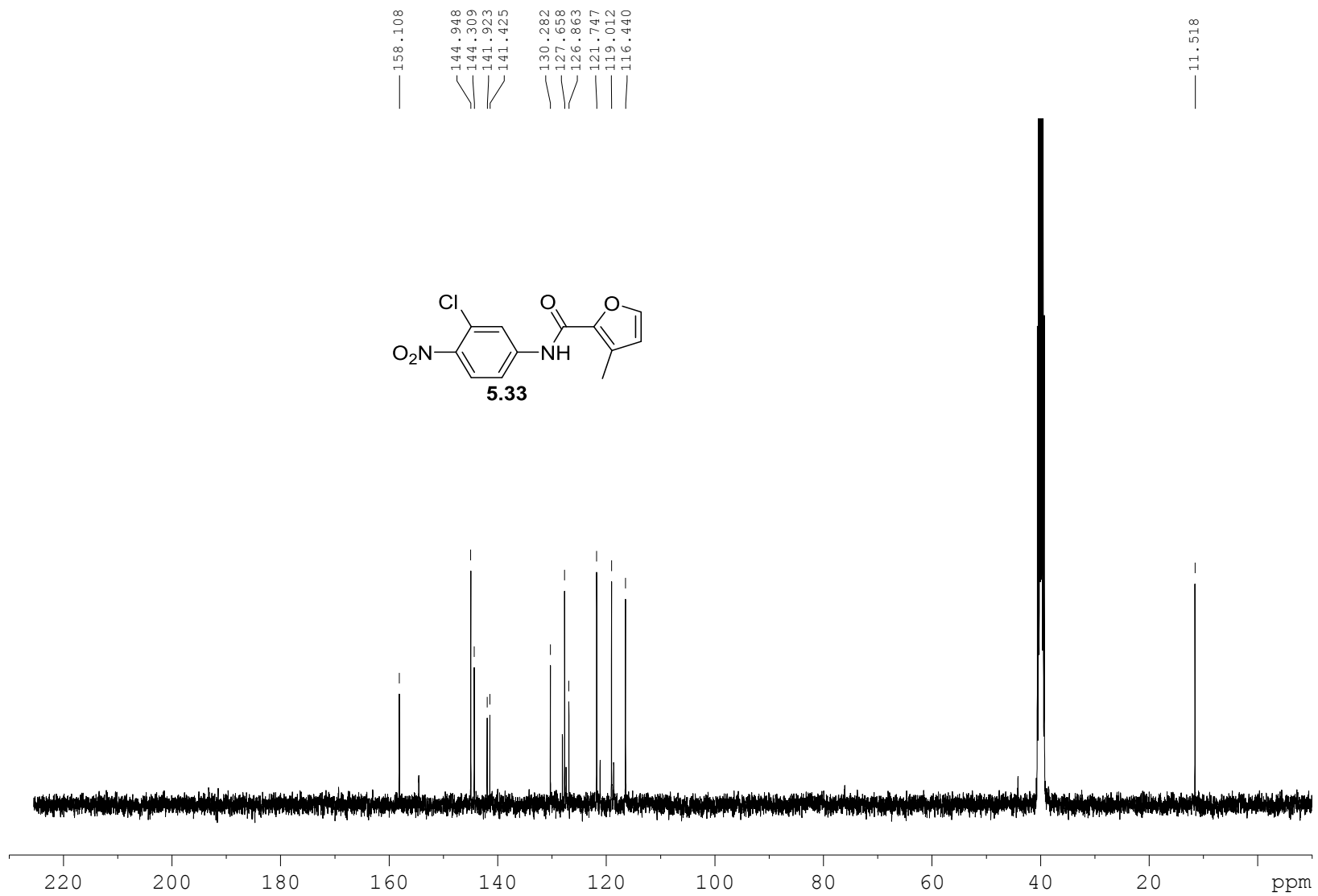
142.833  
141.406  
139.620  
134.386  
133.735  
131.836  
130.792  
129.940  
124.800  
123.874  
120.799  
118.286  
116.050

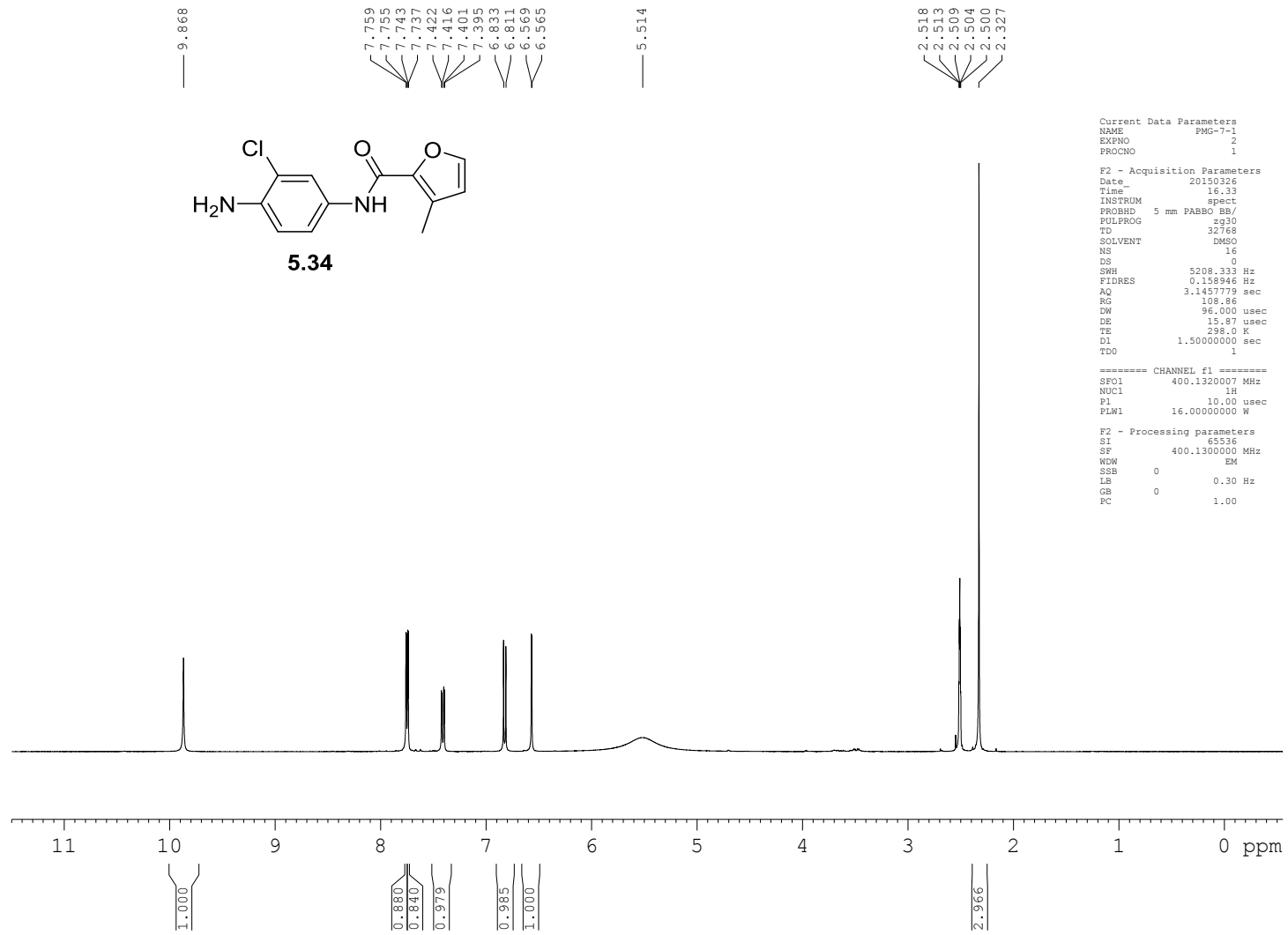
77.253  
76.935  
76.618

11.243

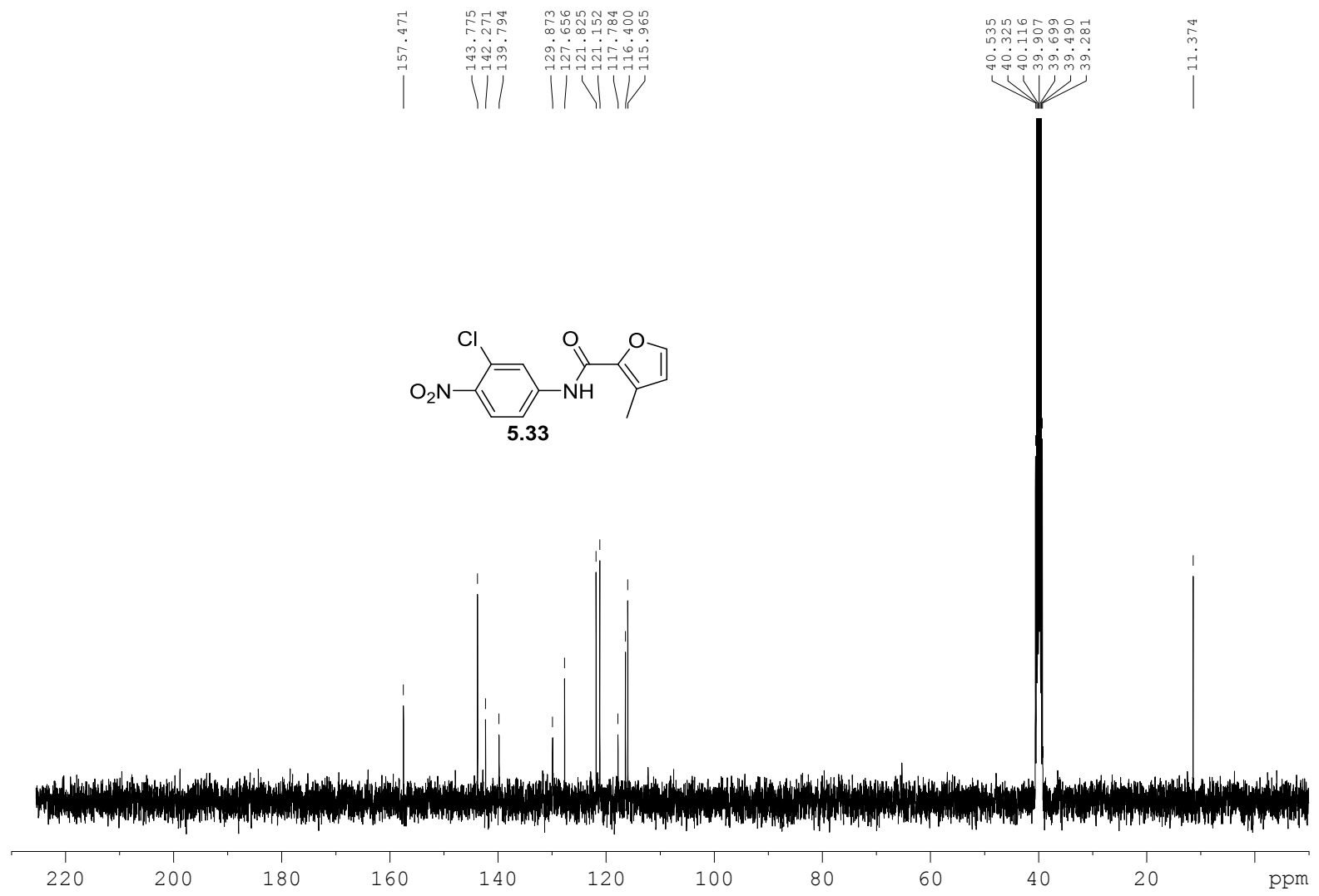


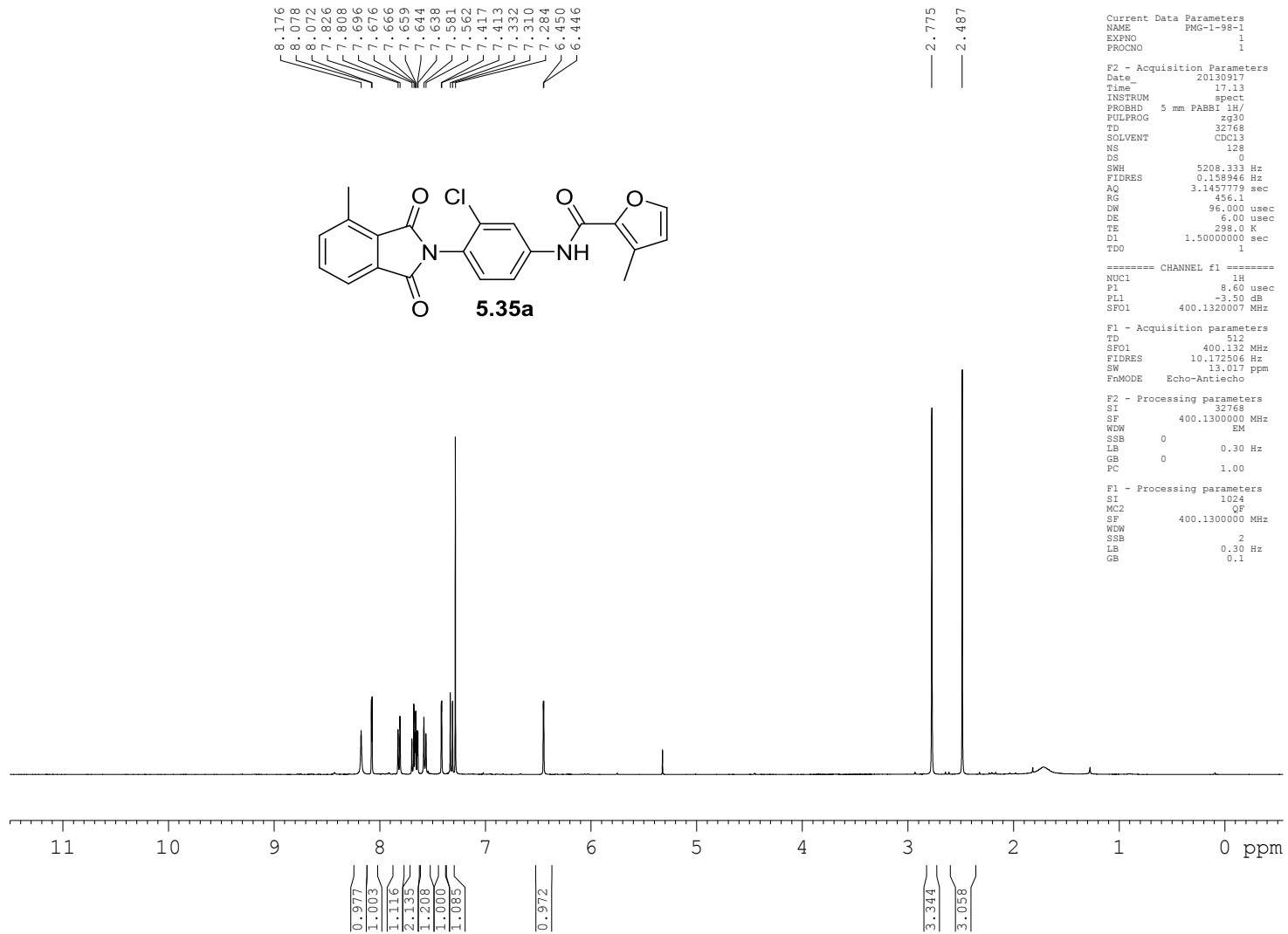












Current Data Parameters  
NAME PMG-1-98-1  
EXPNO 2  
PROCNO 1

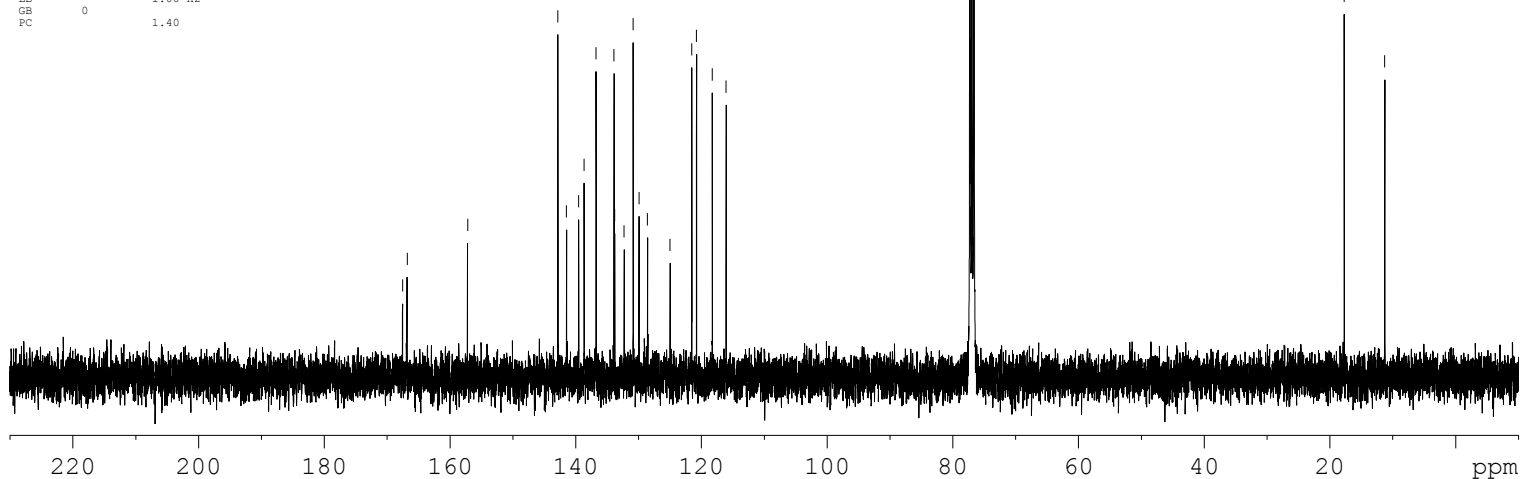
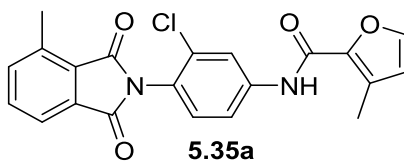
F2 - Acquisition Parameters  
Date\_ 20130918  
Time 16.51  
INSTRUM spect  
PROBHD 5 mm PABBO BB-  
PULPROG zgpg30  
TD 32768  
SOLVENT CDCl3  
NS 3000  
DS 8  
SWH 26178.010 Hz  
FIDRES 0.798889 Hz  
AQ 0.6259188 sec  
RG 16384  
DW 19.100 usec  
DE 6.00 usec  
TE 298.0 K  
D1 2.00000000 sec  
D11 0.03000000 sec  
TDO 1

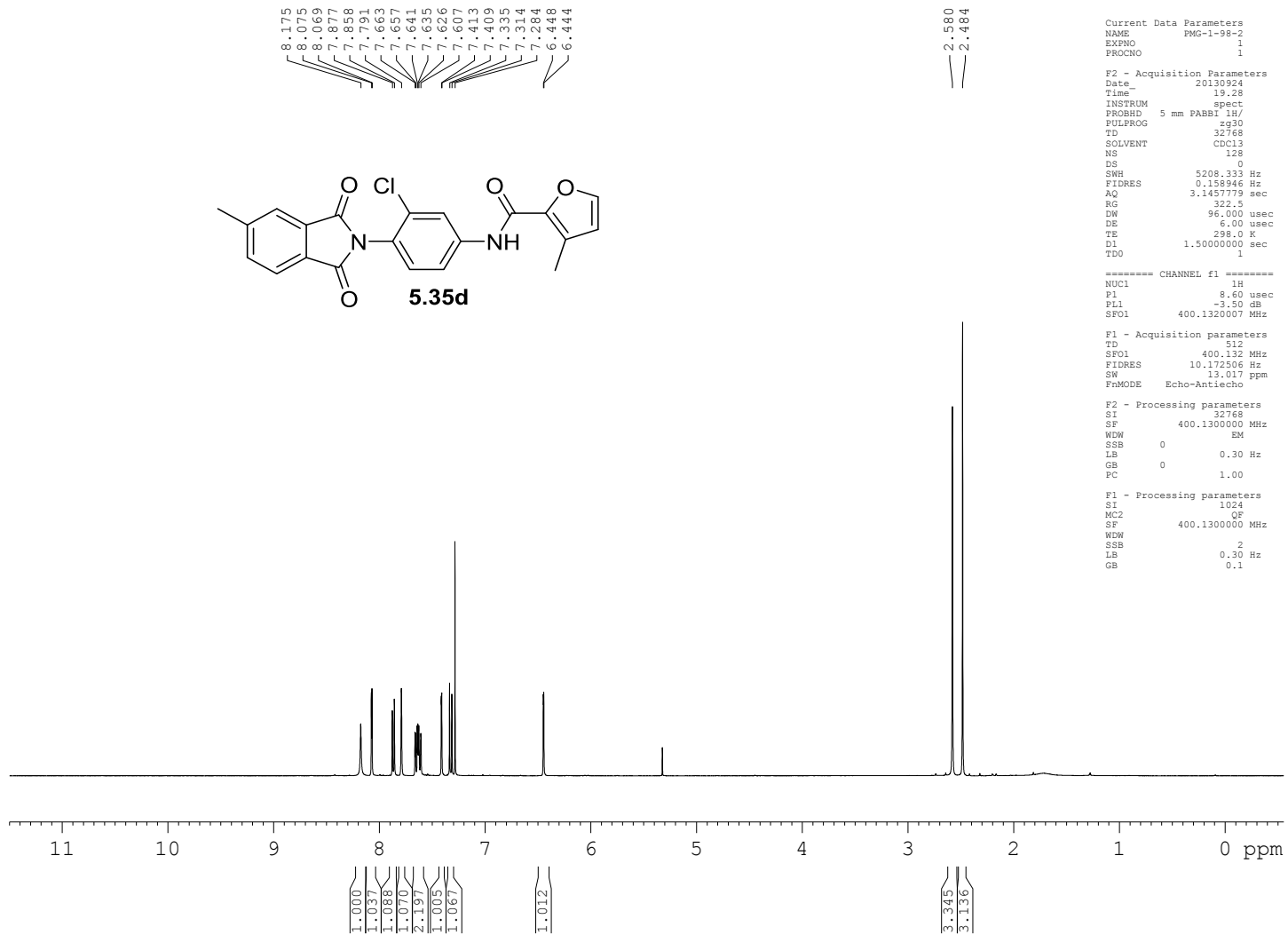
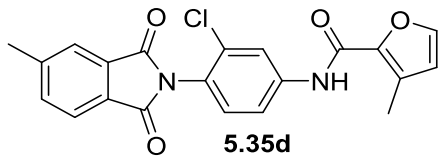
===== CHANNEL f1 =====  
NUC1 13C  
P1 12.00 usec  
PL1 -1.00 dB  
PL1W 37.63110352 W  
SFO1 100.6238364 MHz

===== CHANNEL f2 =====  
CPDPRG2 waltz16  
NUC2 1H  
PCPD2 80.00 usec  
PL2 -2.50 dB  
PL12 14.44 dB  
PL13 14.44 dB  
PL2W 18.35869598 W  
PL12W 0.37139997 W  
PL13W 0.37139997 W  
SFO2 400.1320007 MHz

F2 - Processing parameters  
SI 32768  
SF 100.6127772 MHz  
WDW EM  
SSB 0  
LB 1.00 Hz  
GB 0  
PC 1.40

167.492  
166.776  
157.149  
142.812  
141.430  
139.513  
138.649  
136.737  
133.871  
133.774  
132.264  
130.846  
129.897  
128.551  
124.955  
121.505  
120.755  
118.247  
116.042  
77.253  
76.935  
76.618  
17.704  
11.242





```

Current Data Parameters
NAME      PWS-1-98-2
EXPNO    1
PROCNO   1

F2 - Acquisition Parameters
Date_    20130924
Time     19.28
INSTRUM  spect
PROBHD   5 mm PABBI 1H/
PULPROG  zg30
TD       32768
SOLVENT  CDC13
NS       128
DS       0
SWH      5208.333 Hz
FIDRES   0.158946 Hz
AQ       3.1457779 sec
RG       327.5
DW       96.000 usec
DE       6.00 usec
TE       298.0 K
D1       1.5000000 sec
TD0      1

===== CHANNEL f1 =====
NUC1     1H
P1       8.60 usec
PI1      -3.50 dB
SF01     400.1320007 MHz

F1 - Acquisition parameters
TD       512
SF01     400.132 MHz
FIDRES   10.172506 Hz
SW       13.017 ppm
FMODE    Echo-Antiecho

F2 - Processing parameters
SI       32768
SF       400.1300000 MHz
WDW      EM
SSB      0
LB       0.30 Hz
GB       0
PC       1.00

F1 - Processing parameters
SI       1024
MC2      0
SF       400.1300000 MHz
WDW      2
SSB      2
LB       0.30 Hz
GB       0.1
    
```

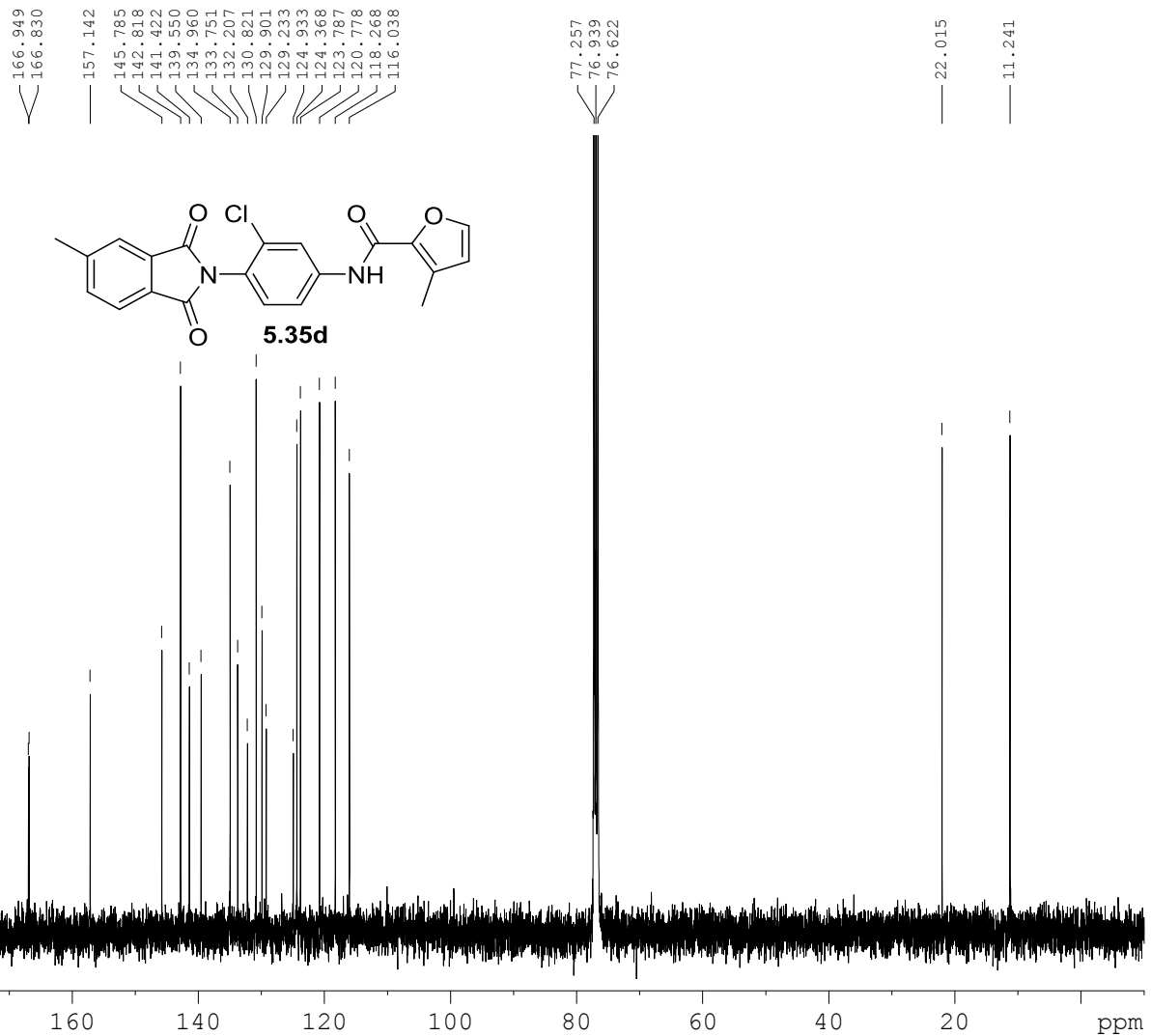
Current Data Parameters  
 NAME PMG-1-98-2  
 EXPNO 1  
 PROCNO 1

F2 - Acquisition Parameters  
 Date\_ 20130929  
 Time 21.13  
 INSTRUM spect  
 PROBHD 5 mm PABBO BB-  
 PULPROG zgpg30  
 TD 32768  
 SOLVENT cdcl3  
 NS 3000  
 DS 8  
 SWH 26178.010 Hz  
 FIDRES 0.798899 Hz  
 AQ 0.6259188 sec  
 RG 16384  
 DW 19.100 usec  
 DE 6.00 usec  
 TE 298.0 K  
 D1 2.00000000 sec  
 D11 0.03000000 sec  
 TD0 1

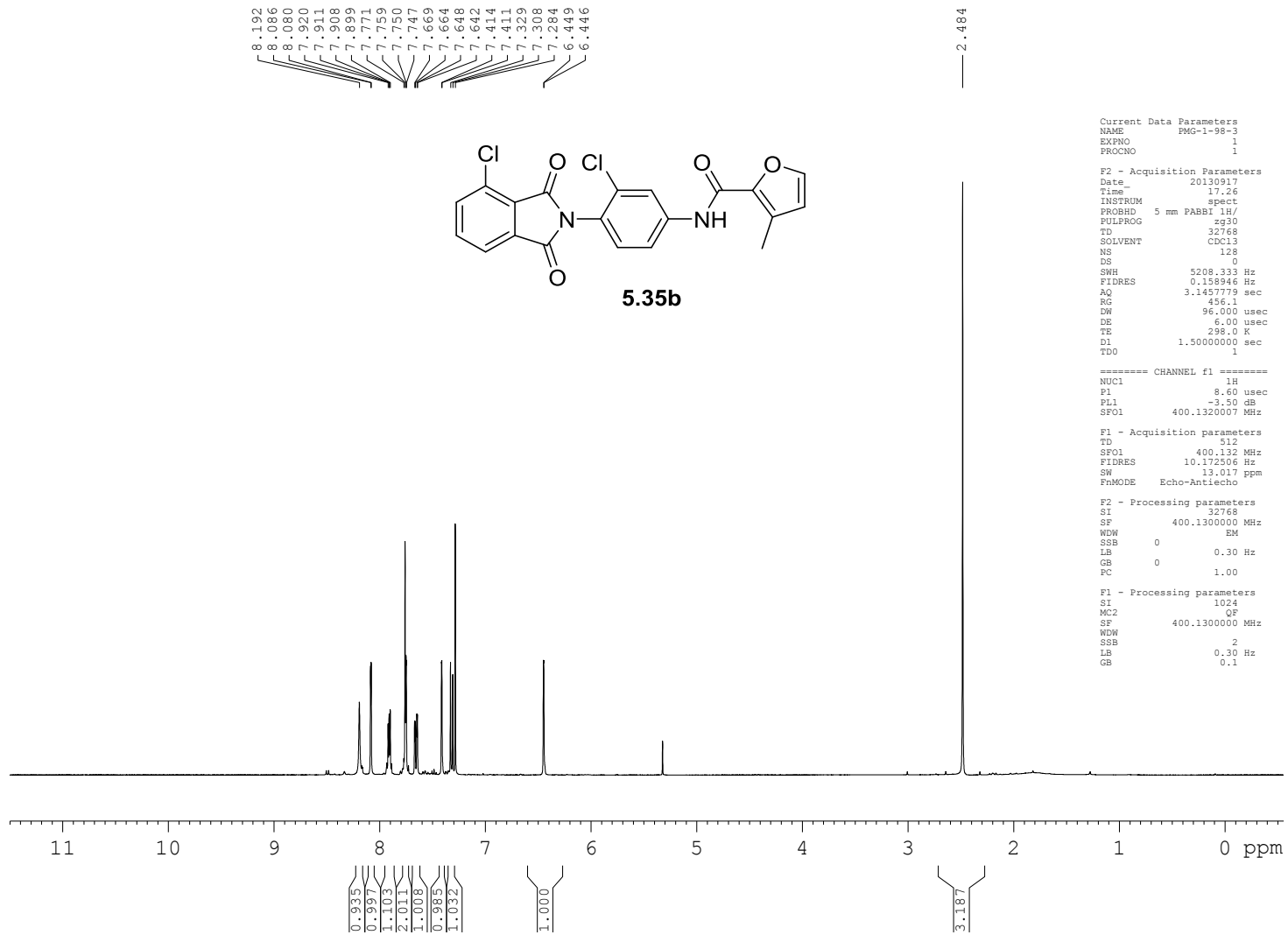
===== CHANNEL f1 =====  
 NUC1 13C  
 P1 12.00 usec  
 PL1 -1.00 dB  
 PL1W 37.63110352 W  
 SFO1 100.6238364 MHz

===== CHANNEL f2 =====  
 CPDPRG2 waltz16  
 NUC2 1H  
 PCPD2 80.00 usec  
 PL2 -2.50 dB  
 PL12 14.44 dB  
 PL13 14.44 dB  
 PL2W 18.35869598 W  
 PL12W 0.37139997 W  
 PL13W 0.37139997 W  
 SFO2 400.1320007 MHz

F2 - Processing parameters  
 SI 32768  
 SF 100.6127772 MHz  
 WDW EM  
 SSB 0  
 LB 1.00 Hz  
 GB 0  
 FC 1.40



469



470

Current Data Parameters  
NAME PMG-1-98-3  
EXPNO 2  
PROCNO 1

F2 - Acquisition Parameters  
Date\_ 20130918  
Time 21.20  
INSTRUM spect  
PROBHD 5 mm PABBO BB-  
PULPROG zgpg30  
TD 32768  
SOLVENT CDCl3  
NS 3000  
DS 8  
SWH 26178.010 Hz  
FIDRES 0.798889 Hz  
AQ 0.6259188 sec  
RG 16384  
DW 19.100 usec  
DE 6.00 usec  
TE 298.0 K  
D1 2.0000000 sec  
D11 0.0300000 sec  
TD0 1

===== CHANNEL f1 =====  
NUC1 13C  
P1 12.00 usec  
PL1 -1.00 dB  
PL1W 37.63110352 W  
SFO1 100.6238364 MHz

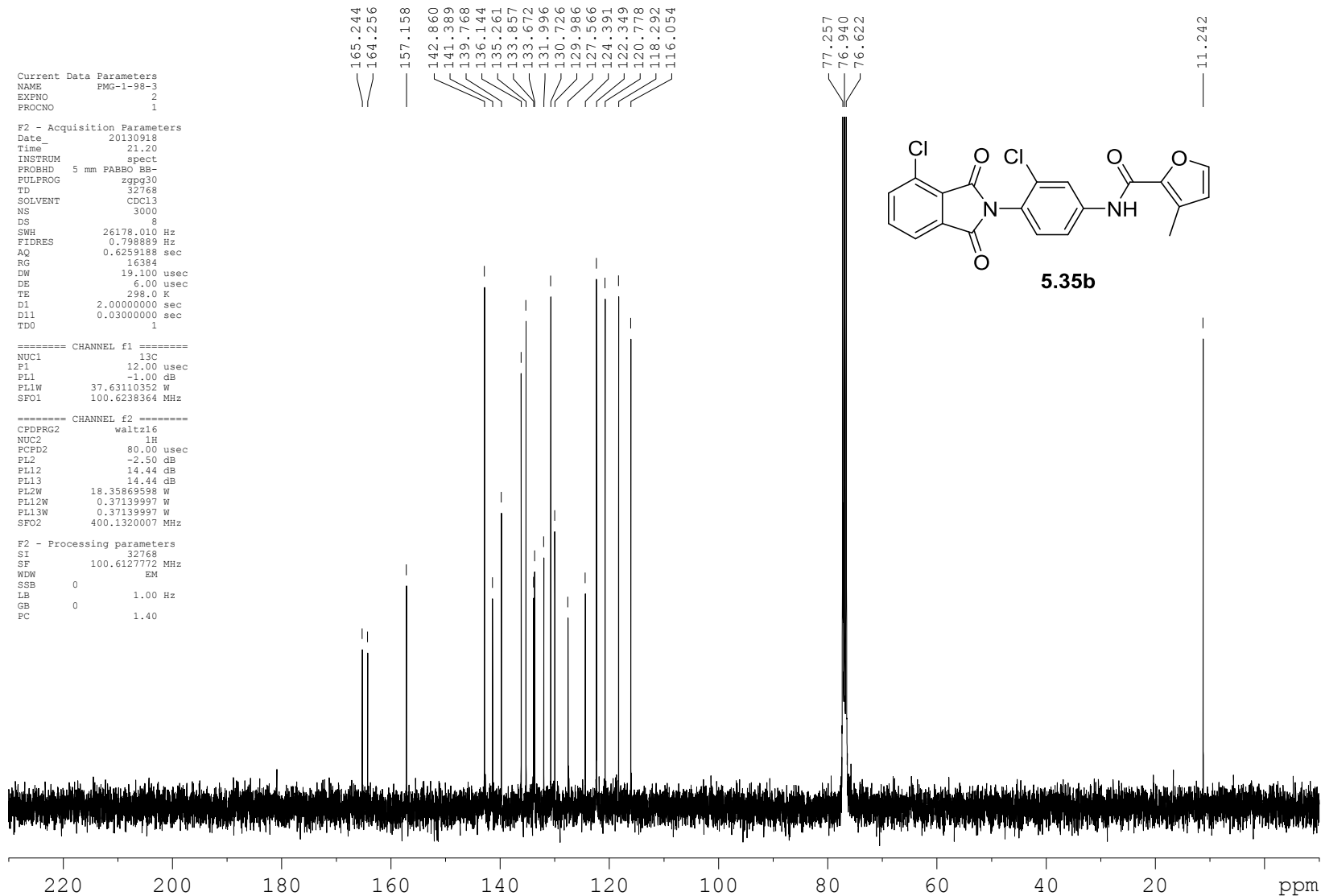
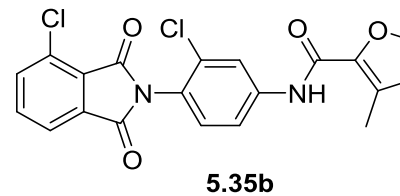
===== CHANNEL f2 =====  
CPDPRG2 waltz16  
NUC2 1H  
PCPD2 80.00 usec  
PL2 -2.50 dB  
PL12 14.44 dB  
PL13 14.44 dB  
PL2W 18.35869598 W  
PL12W 0.37139997 W  
PL13W 0.37139997 W  
SFO2 400.1320007 MHz

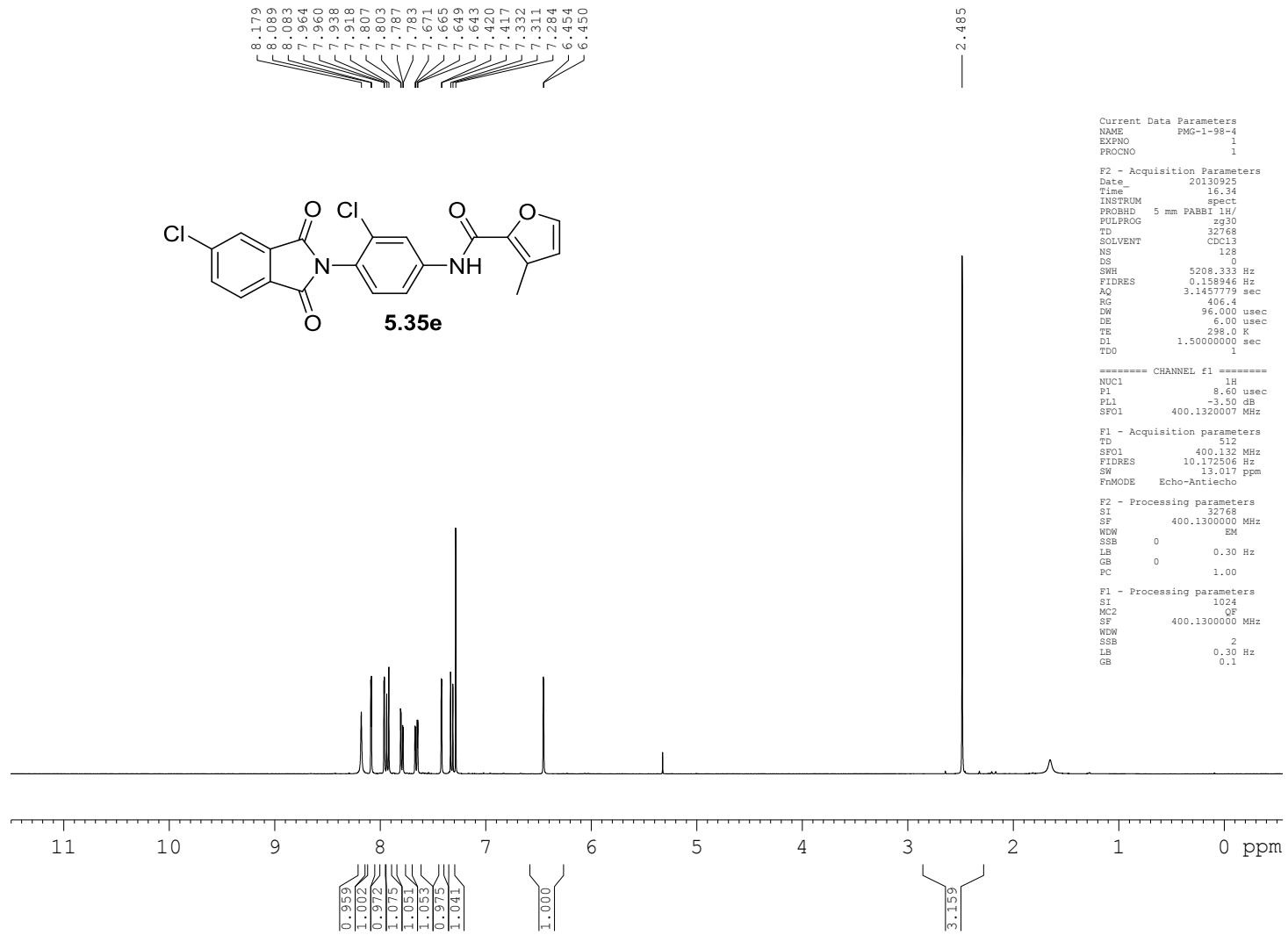
F2 - Processing parameters  
SI 32768  
SF 100.6127772 MHz  
WDW EM  
SSB 0  
LB 1.00 Hz  
GB 0  
FC 1.40

165.244  
164.256  
157.158  
142.860  
141.389  
139.768  
136.144  
135.261  
133.857  
133.672  
131.996  
130.726  
129.986  
127.566  
124.391  
122.349  
120.778  
118.292  
116.054

77.257  
76.940  
76.622

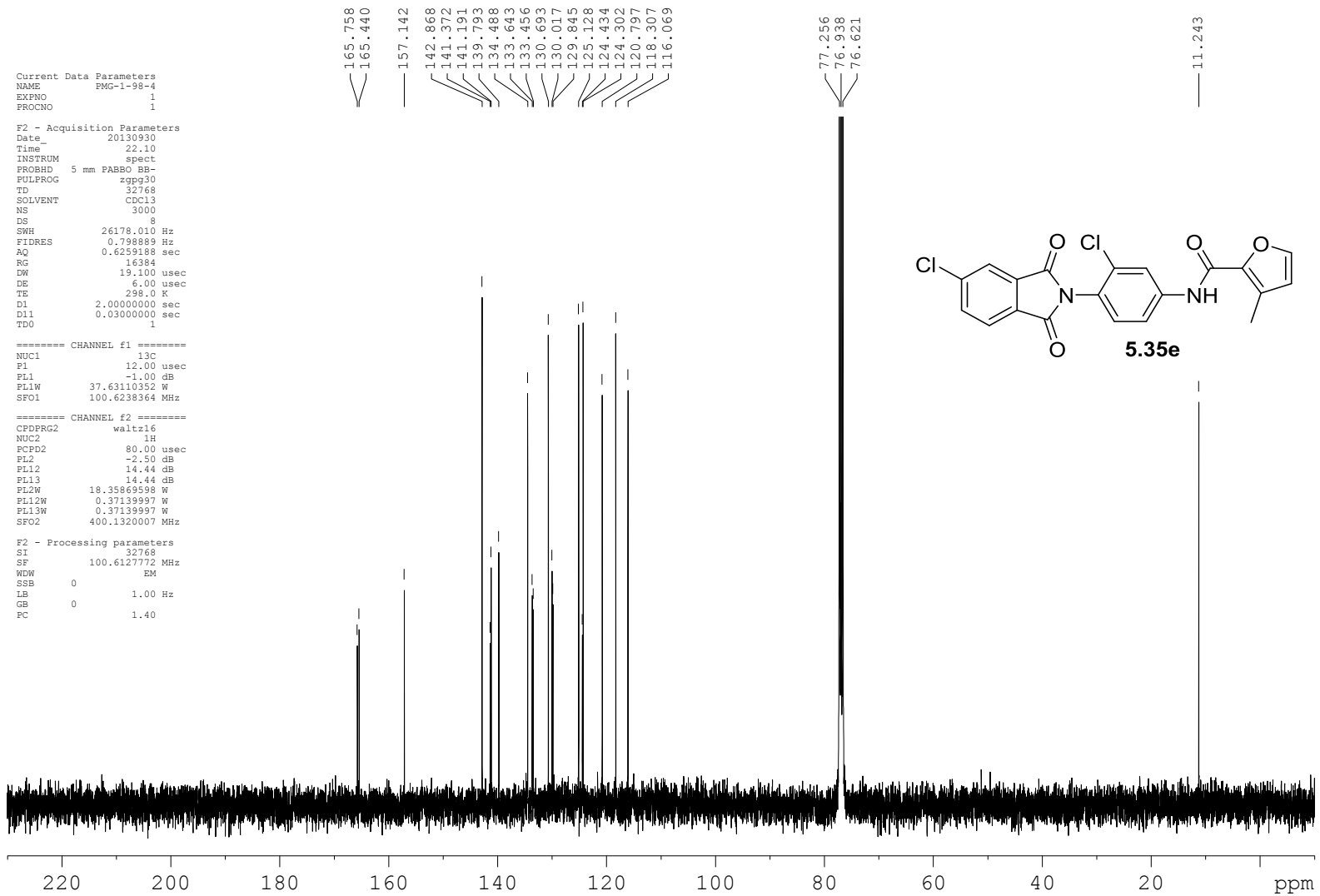
11.242

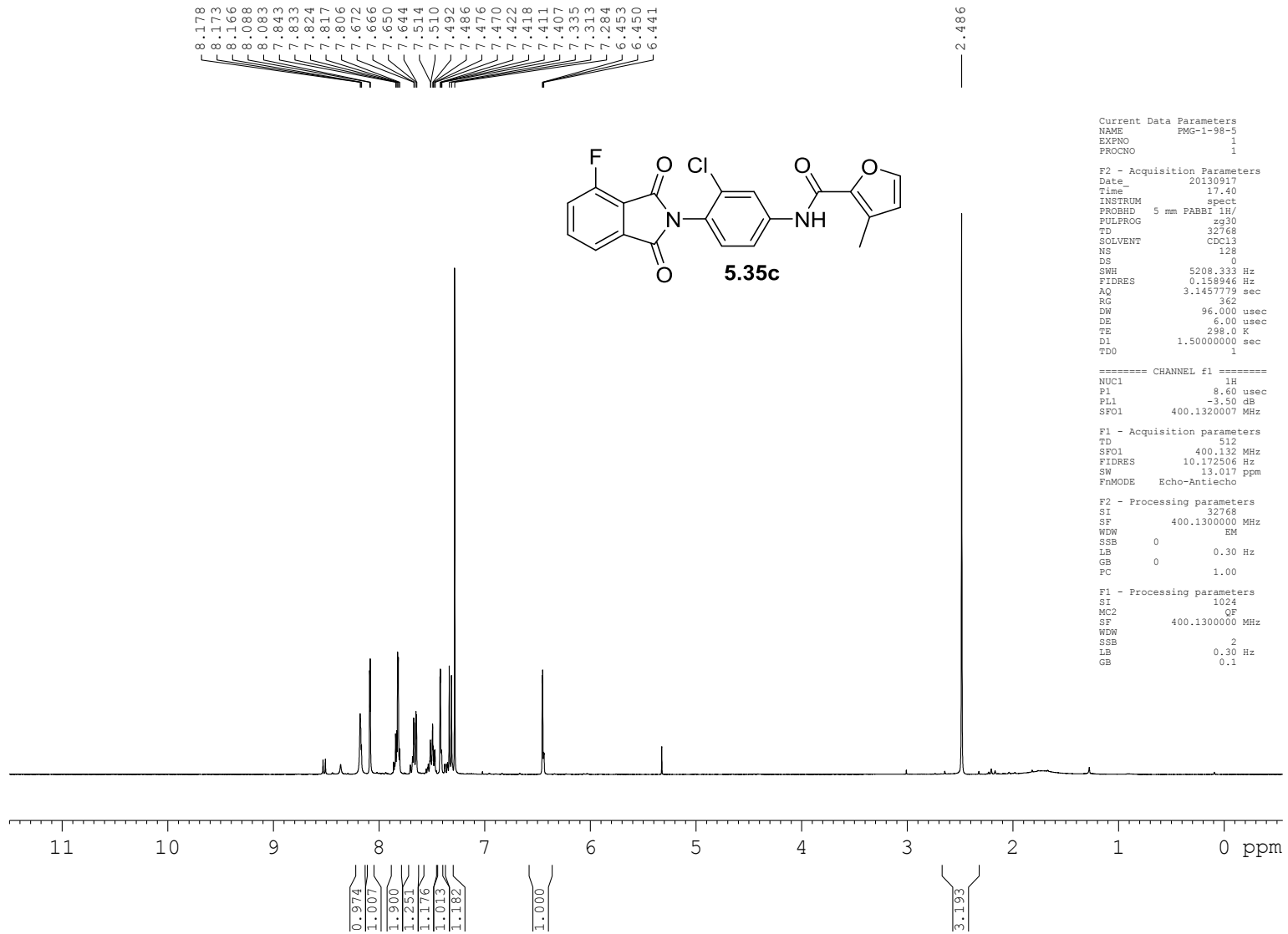






472





474

Current Data Parameters  
NAME PMG-1-98-5  
EXPNO 2  
PROCNO 1

F2 - Acquisition Parameters  
Date\_ 20130918  
Time\_ 23.40  
INSTRUM spect  
PROBHD 5 mm PABBO BB-  
PULPROG zgpg30  
TD 32768  
SOLVENT cdcl3  
NS 3000  
DS 8  
SWH 26178.010 Hz  
FIDRES 0.798889 Hz  
AQ 0.6259188 sec  
RG 16384  
DW 19.100 usec  
DE 6.00 usec  
TE 298.0 K  
D1 2.00000000 sec  
D11 0.03000000 sec  
TD0 1

===== CHANNEL f1 =====  
NUC1 13C  
P1 12.00 usec  
PL1 -1.00 dB  
PL1W 37.63110352 W  
SFO1 100.6238364 MHz

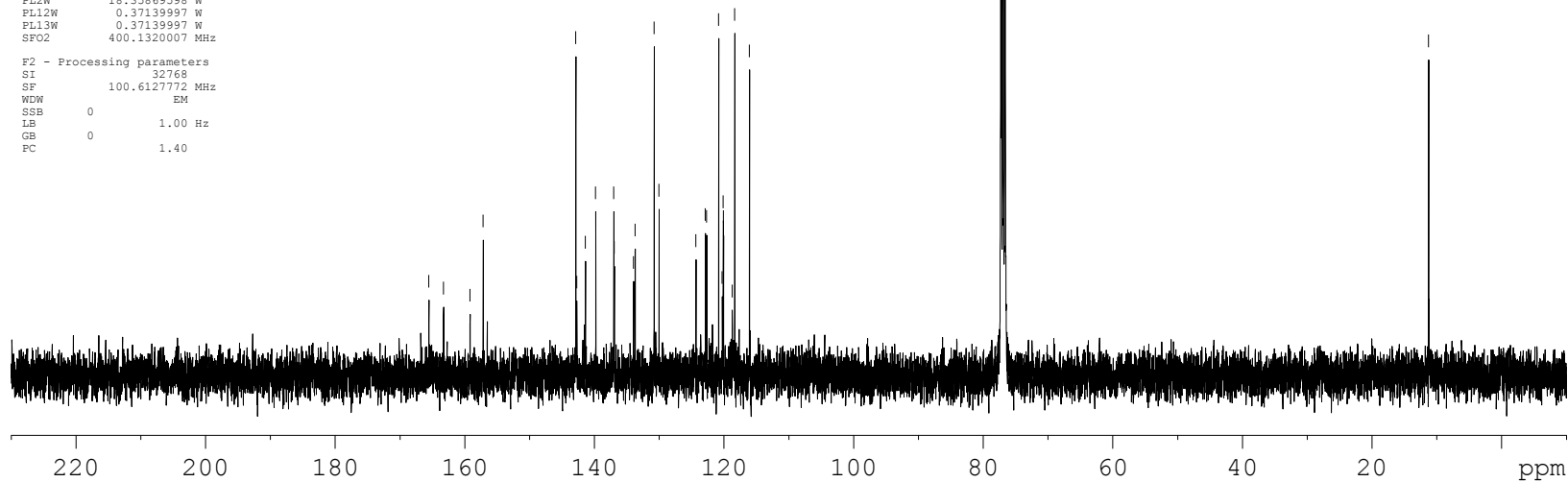
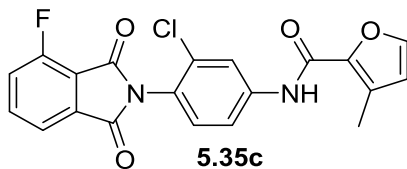
===== CHANNEL f2 =====  
CPDPRG2 waltz16  
NUC2 1H  
PCPD2 80.00 usec  
PL2 -2.50 dB  
PL12 14.44 dB  
PL13 14.44 dB  
PL2W 18.35869598 W  
PL12W 0.37139997 W  
PL13W 0.37139997 W  
SFO2 400.1320007 MHz

F2 - Processing parameters  
SI 32768  
SF 100.6127772 MHz  
WDW EM  
SSB 0  
LB 1.00 Hz  
GB 0  
PC 1.40

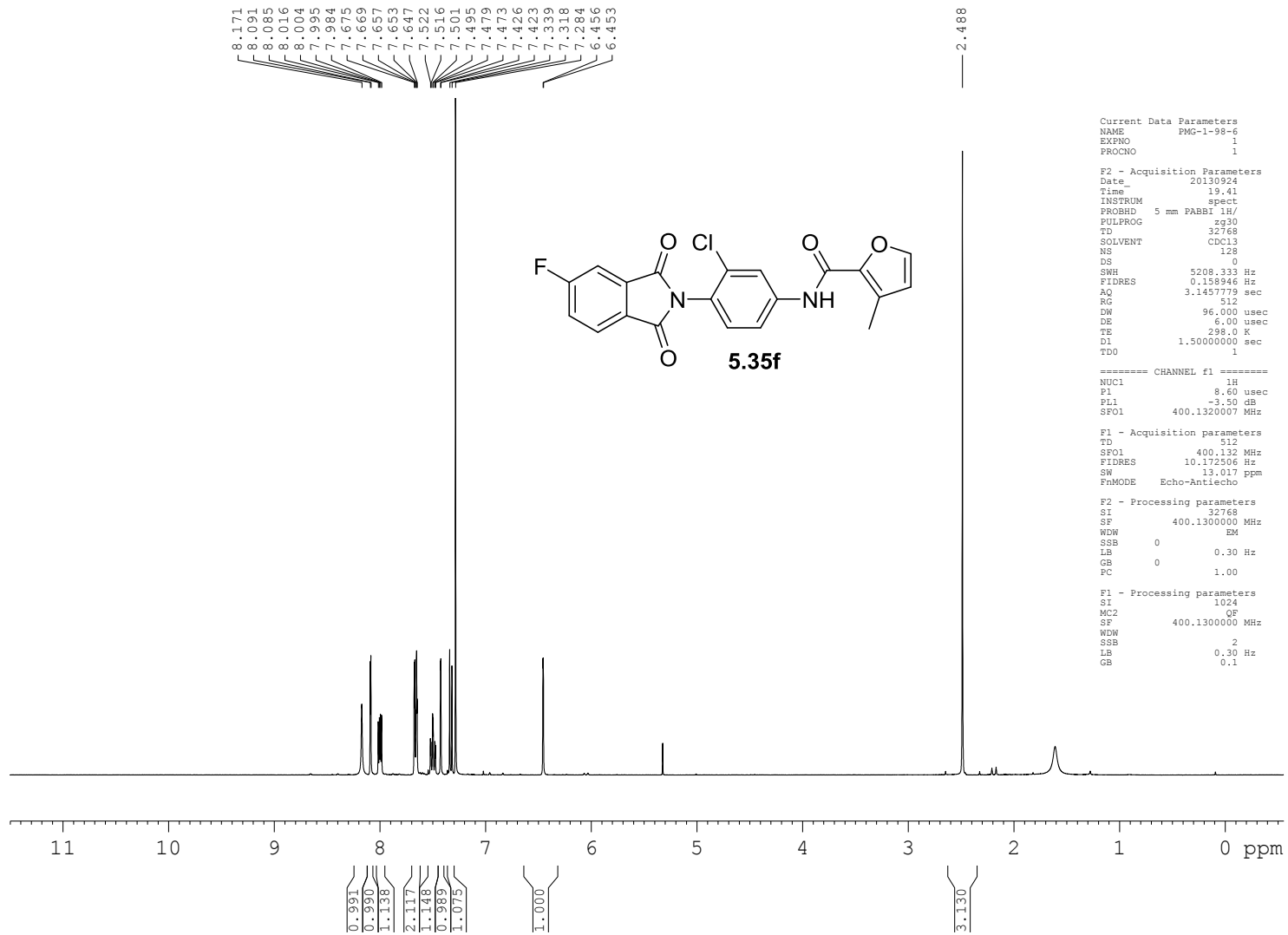
165.527  
163.275  
159.187  
157.151  
142.869  
142.709  
141.379  
139.791  
136.993  
136.917  
133.935  
133.708  
130.766  
130.006  
124.318  
122.857  
122.662  
120.810  
120.254  
120.107  
120.070  
118.712  
118.317  
116.061

77.255  
76.937  
76.620

11.242



475



```
Current Data Parameters
NAME      FMG-1-98-6
EXPNO     1
PROCNO    1

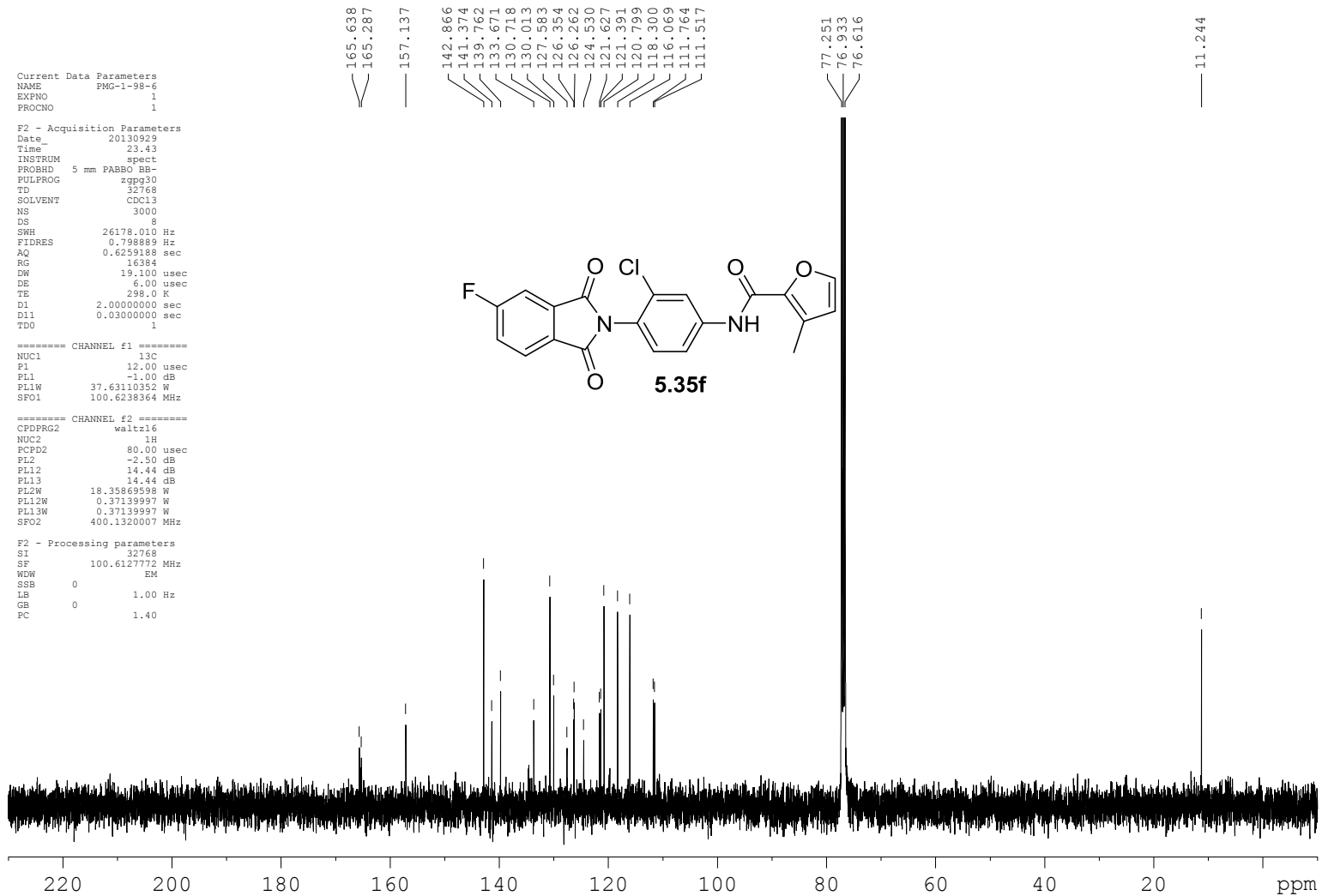
F2 - Acquisition Parameters
Date_     20130924
Time      19.41
INSTRUM   spect
PROBHD    5 mm PABBI 1H/
PULPROG   zg30
TD         32768
SOLVENT   CDCl3
NS         128
DS         0
SWH        5208.333 Hz
FIDRES     0.158946 Hz
AQ         3.1457779 sec
RG         512
DW         96.000 usec
DE         6.00 usec
TE         298.0 K
D1         1.5000000 sec
TDO        1

===== CHANNEL f1 =====
NUC1       1H
P1         8.60 usec
PL1        -3.50 dB
SFO1       400.1320007 MHz

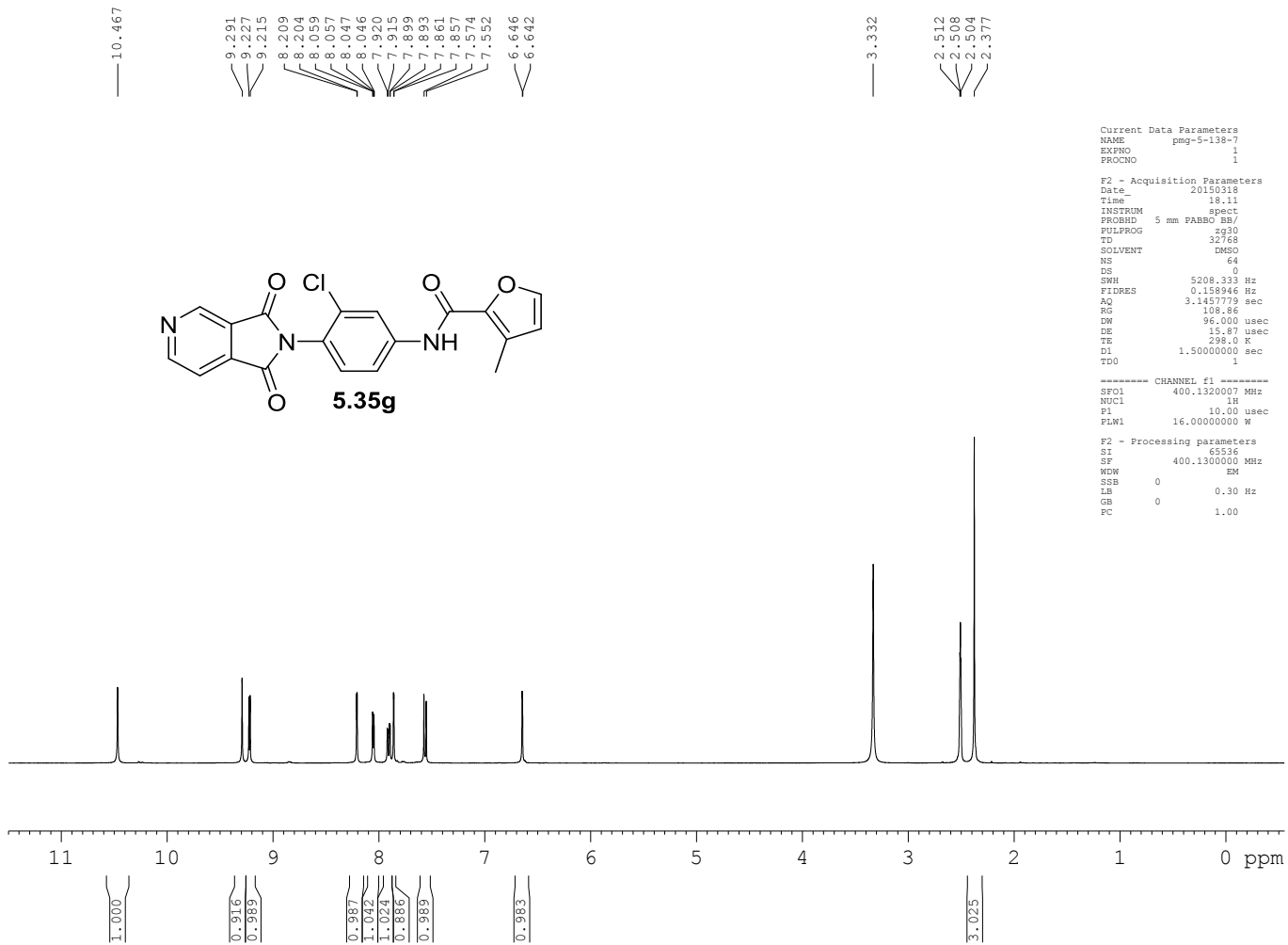
F1 - Acquisition parameters
TD         512
SFO1       400.132 MHz
FIDRES     10.172506 Hz
SW         13.017 ppm
FnMODE     Echo-Antiecho

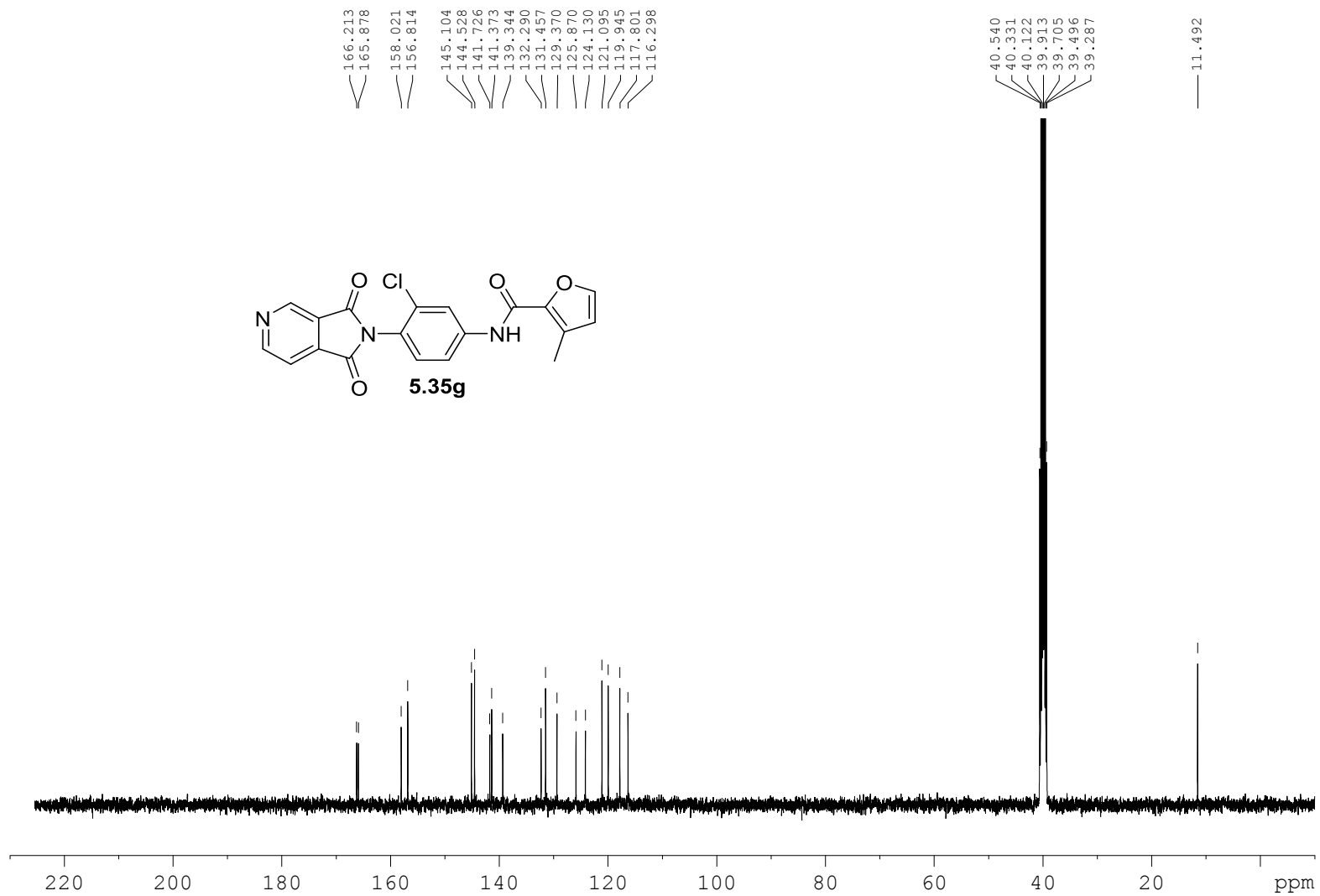
F2 - Processing parameters
SI         32768
SF         400.1300000 MHz
WDW        EM
SSB        0
LB         0.30 Hz
GB         0
PC         1.00

F1 - Processing parameters
SI         1024
MC2        QF
SF         400.1300000 MHz
WDW        SSB
SSB        2
LB         0.30 Hz
GB         0.1
```



477



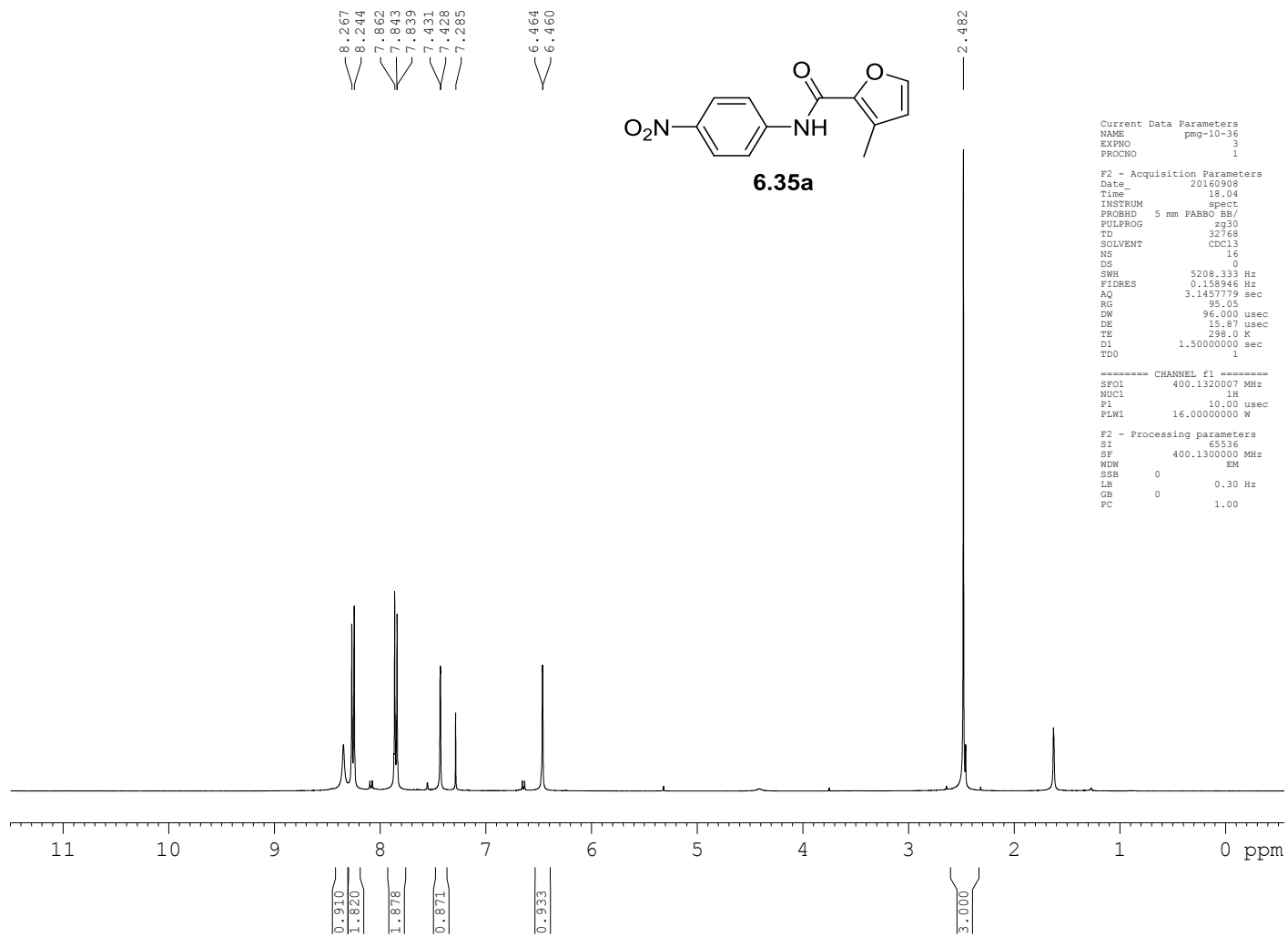


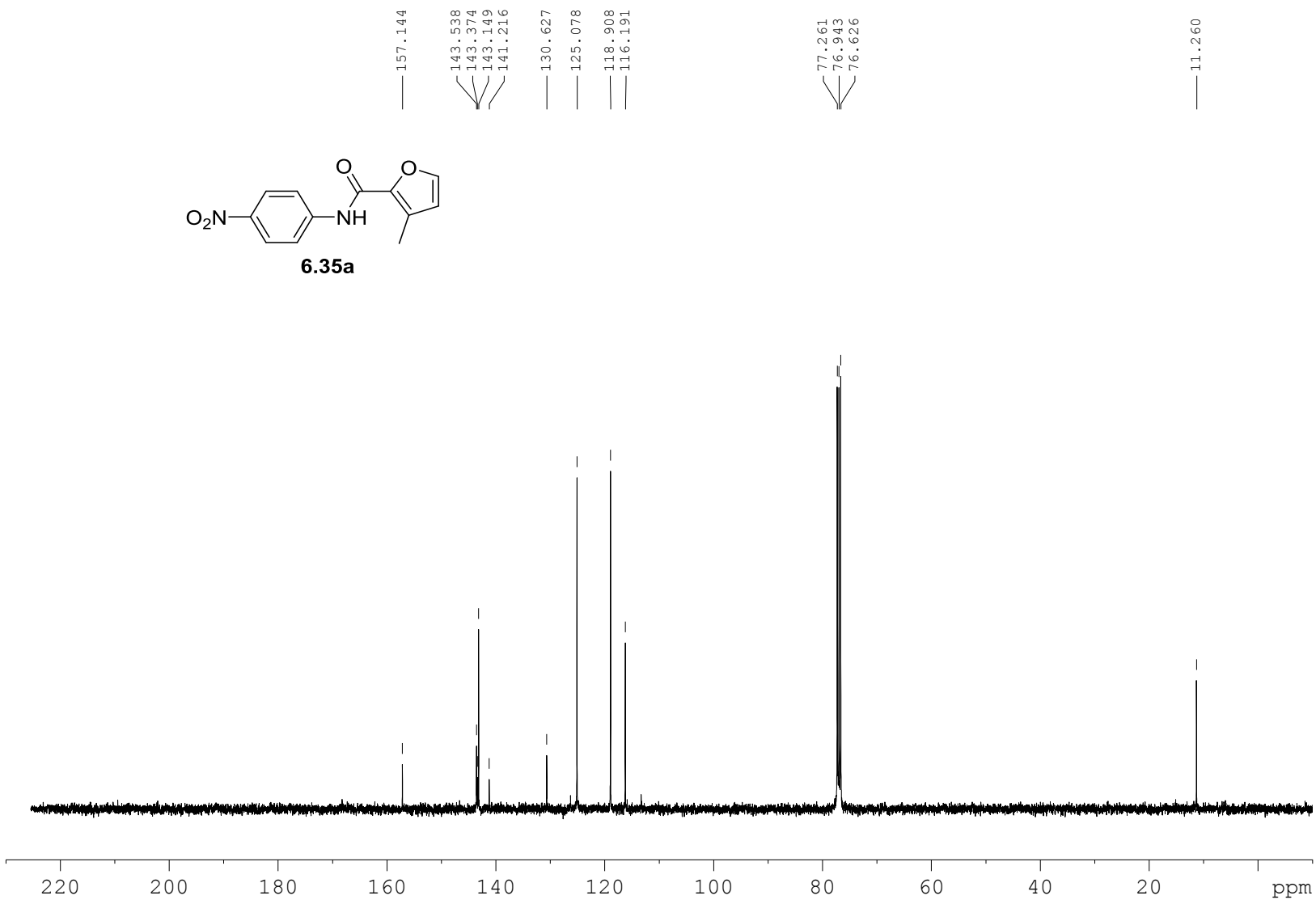
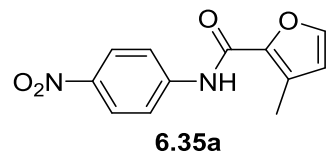
# Appendix F

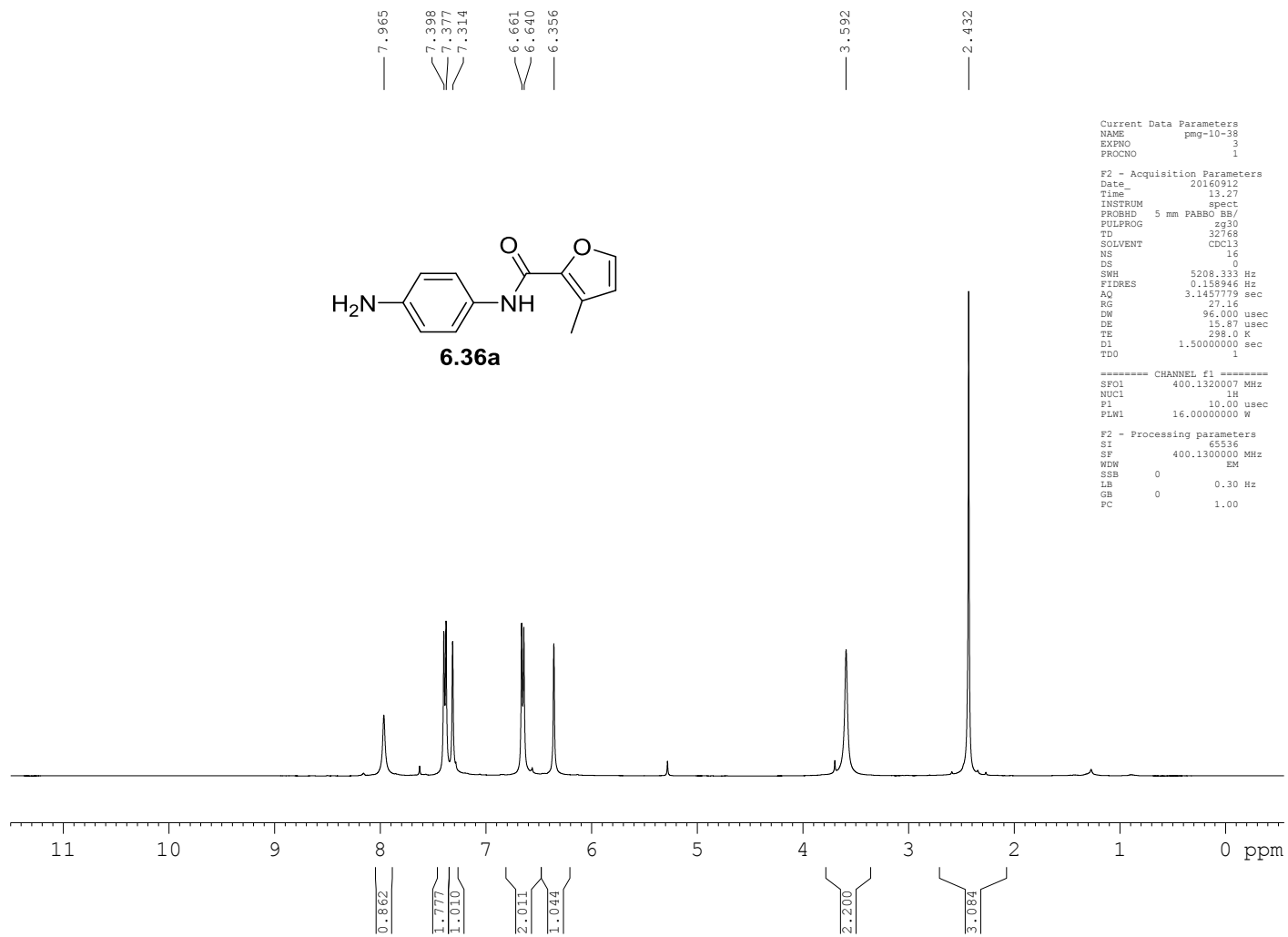
Relevant spectra for chapter VI

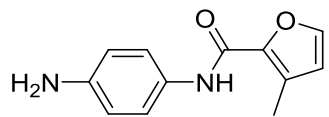
1



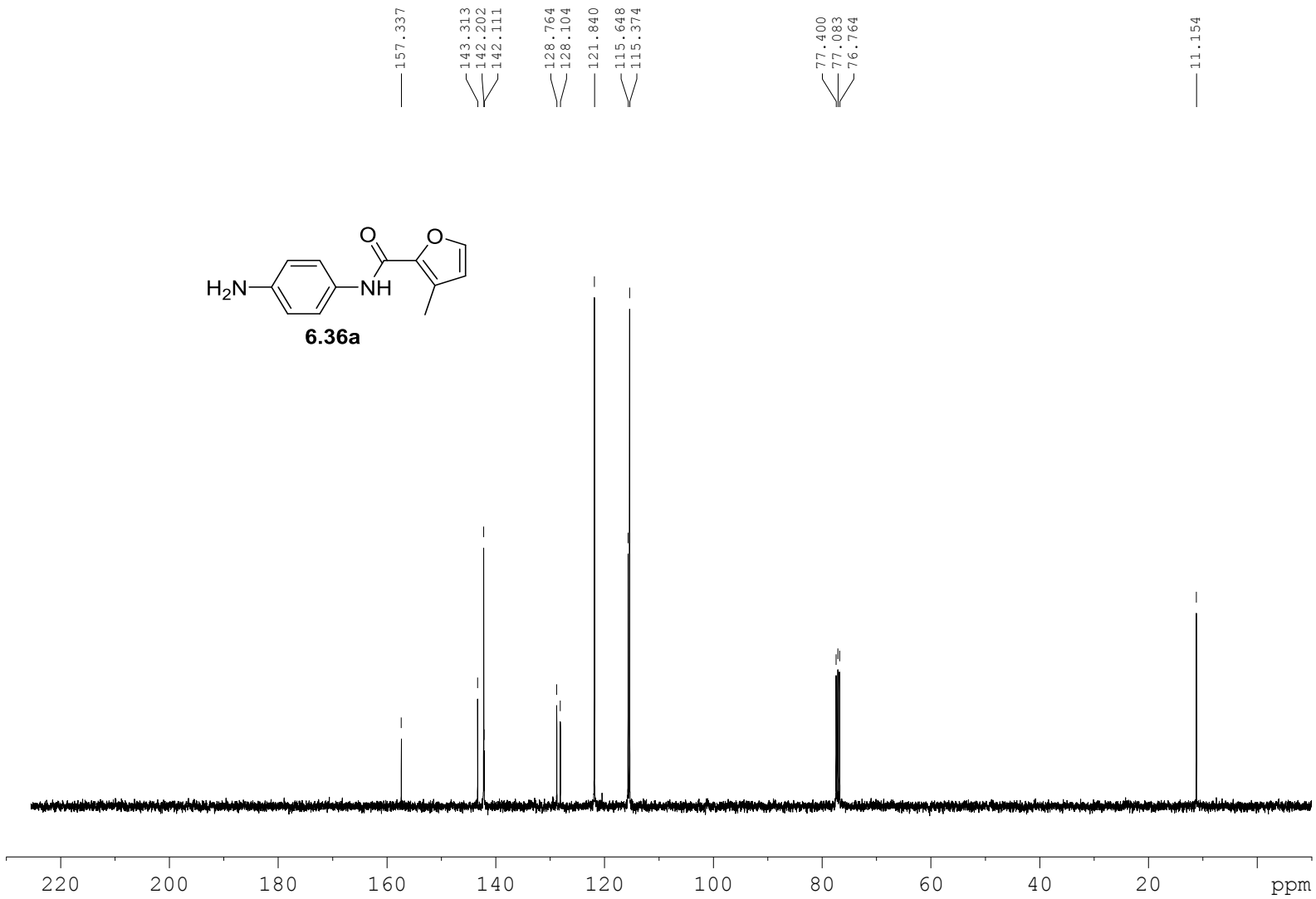




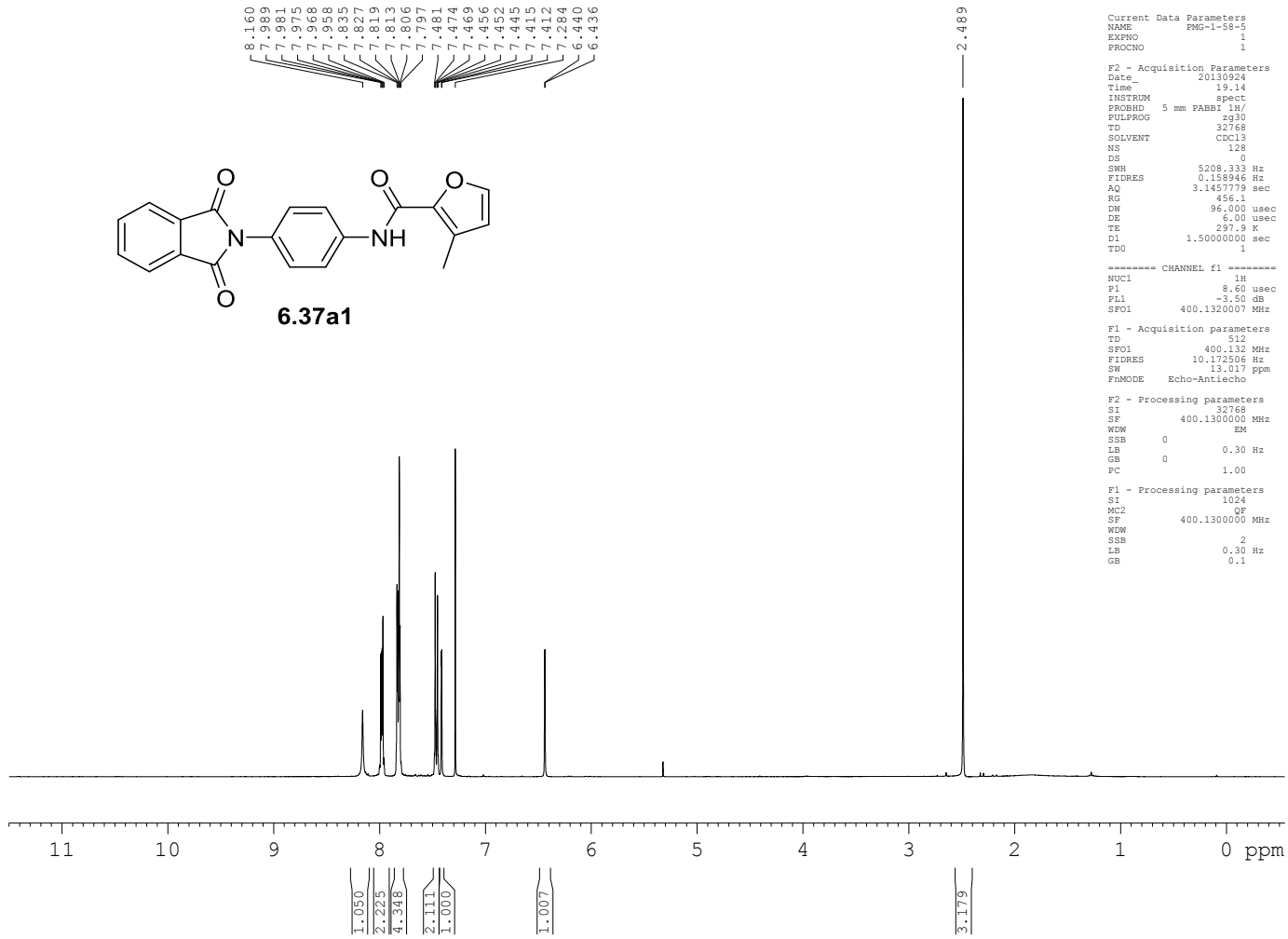
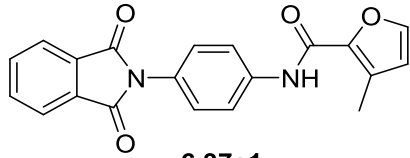




**6.36a**



484



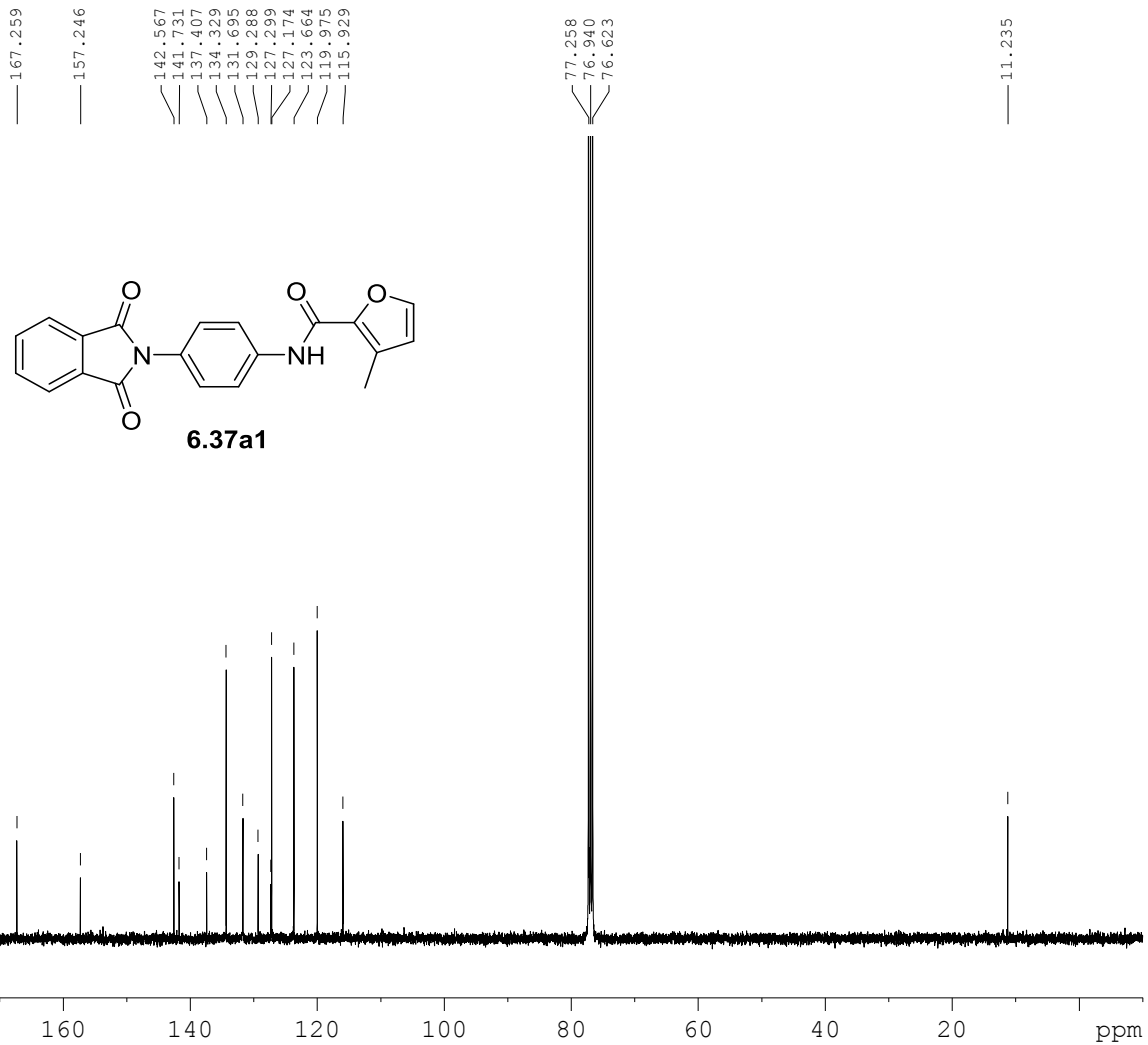
Current Data Parameters  
 NAME PMG-1-58-5  
 EXPNO 1  
 PROCNO 1

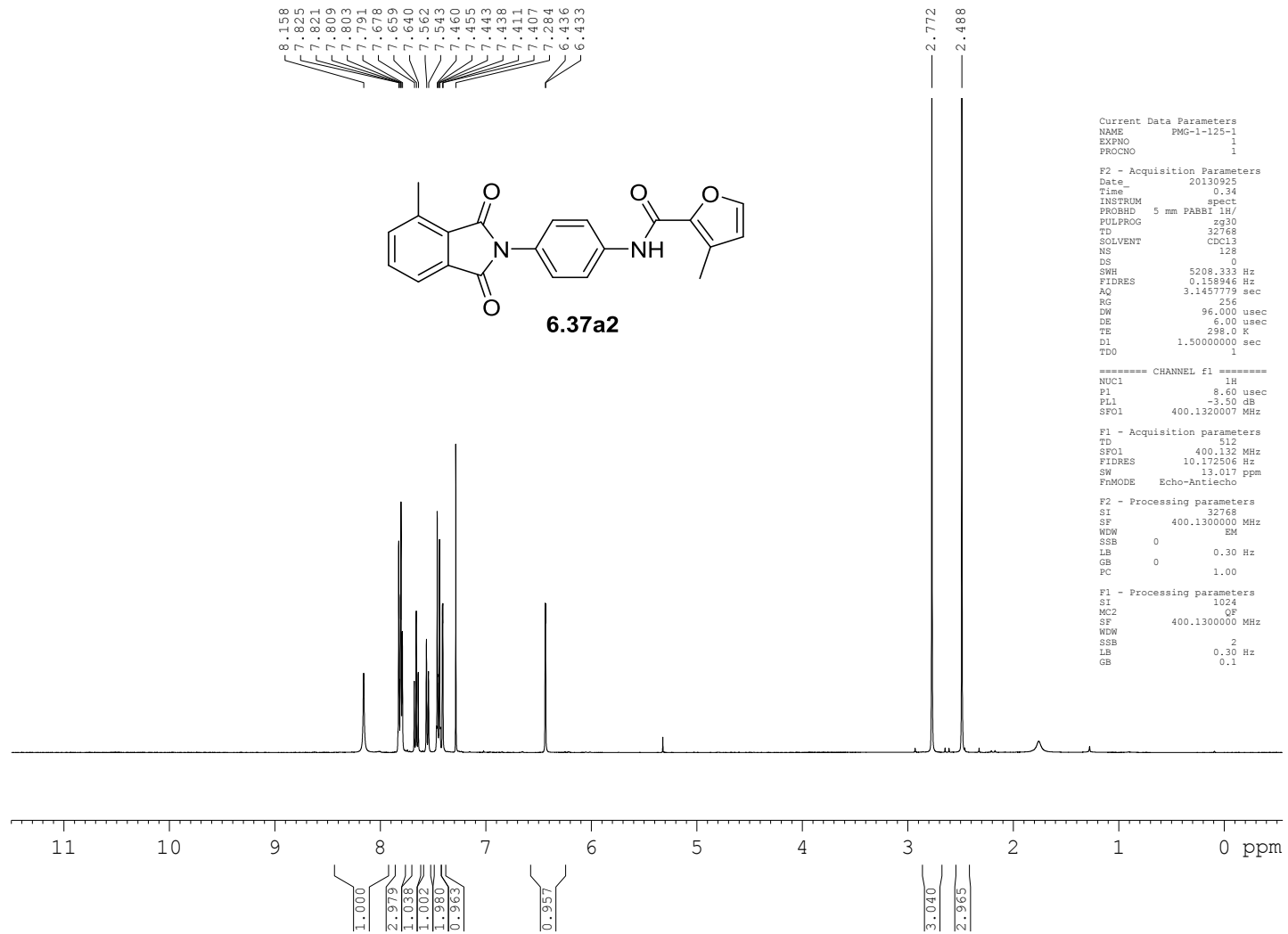
F2 - Acquisition Parameters  
 Date\_ 20130928  
 Time 22.32  
 INSTRUM spect  
 PROBHD 5 mm PABBO BB-  
 PULPROG zgpg30  
 TD 32768  
 SOLVENT CDCl3  
 NS 3000  
 DS 8  
 SWH 26178.010 Hz  
 FIDRES 0.798889 Hz  
 AQ 0.6259188 sec  
 RG 16384  
 DW 19.100 usec  
 DE 6.00 usec  
 TE 298.0 K  
 D1 2.00000000 sec  
 D11 0.03000000 sec  
 TDO 1

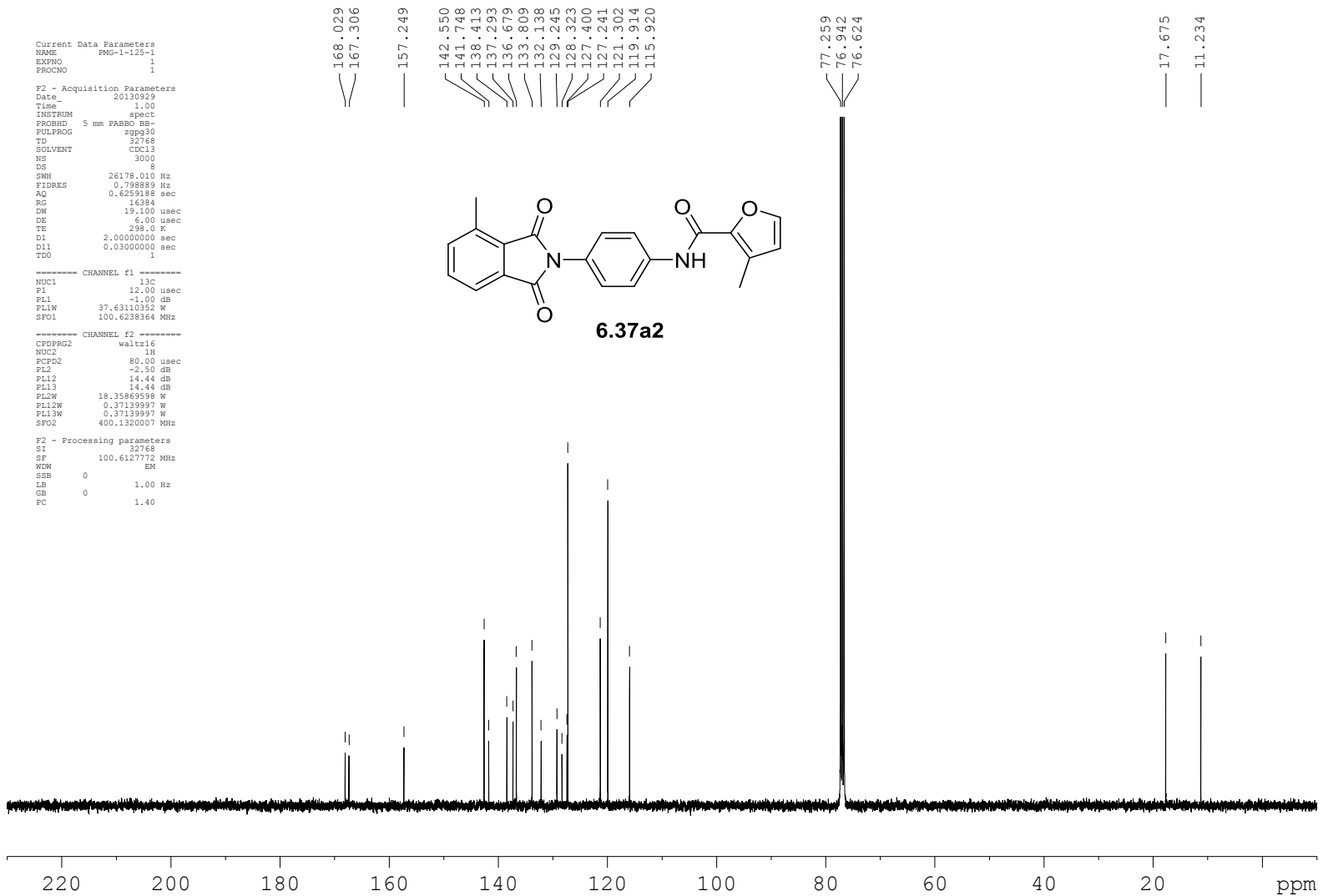
===== CHANNEL f1 =====  
 NUC1 13C  
 P1 12.00 usec  
 PL1 -1.00 dB  
 PL1W 37.63110352 W  
 SFO1 100.6238364 MHz

===== CHANNEL f2 =====  
 CPDPRG2 waltz16  
 NUC2 1H  
 PCPD2 80.00 usec  
 PL2 -2.50 dB  
 PL12 14.44 dB  
 PL13 14.44 dB  
 PL2W 18.35869598 W  
 PL12W 0.37139997 W  
 PL13W 0.37139997 W  
 SFO2 400.1320007 MHz

F2 - Processing parameters  
 SI 32768  
 SF 100.6127772 MHz  
 WDW EM  
 SSB 0  
 LB 1.00 Hz  
 GB 0  
 PC 1.40

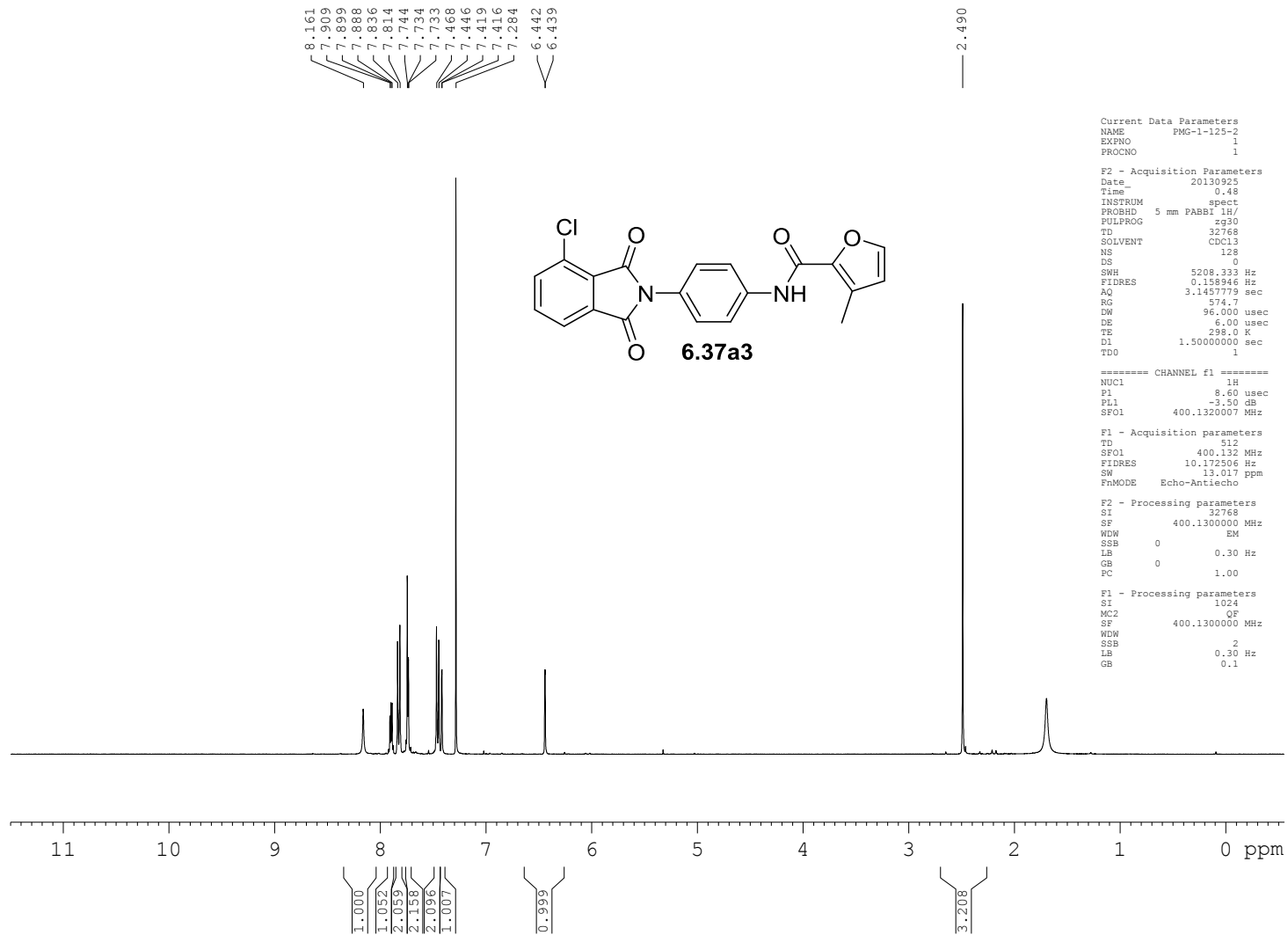








488



Current Data Parameters  
NAME PWS-1-123-2  
EXPNO 1  
PROCNO 1

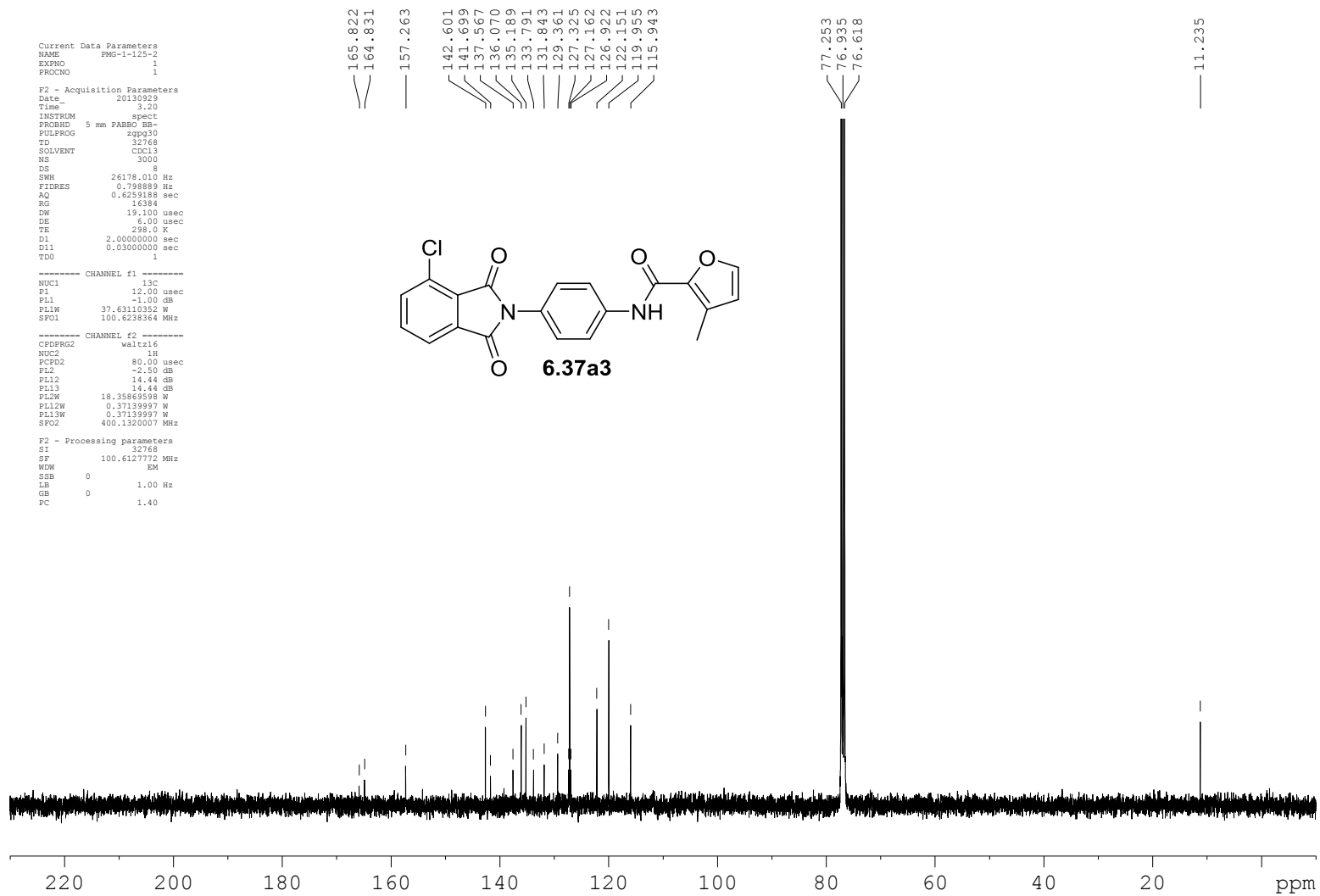
F2 - Acquisition Parameters  
Date\_ 20130925  
Time 0.48  
INSTRUM spect  
PROBHD 5 mm PABBI 1H/  
PULPROG zg30  
TD 32768  
SOLVENT CDCl3  
NS 128  
DS 0  
SWH 5208.333 Hz  
FIDRES 0.158946 Hz  
AQ 3.1457779 sec  
RG 574.7  
DW 96.000 usec  
DE 6.00 usec  
TE 298.0 K  
D1 1.50000000 sec  
TDO 1

===== CHANNEL f1 =====  
NUC1 1H  
P1 8.60 usec  
PL1 -3.50 dB  
SFO1 400.1320007 MHz

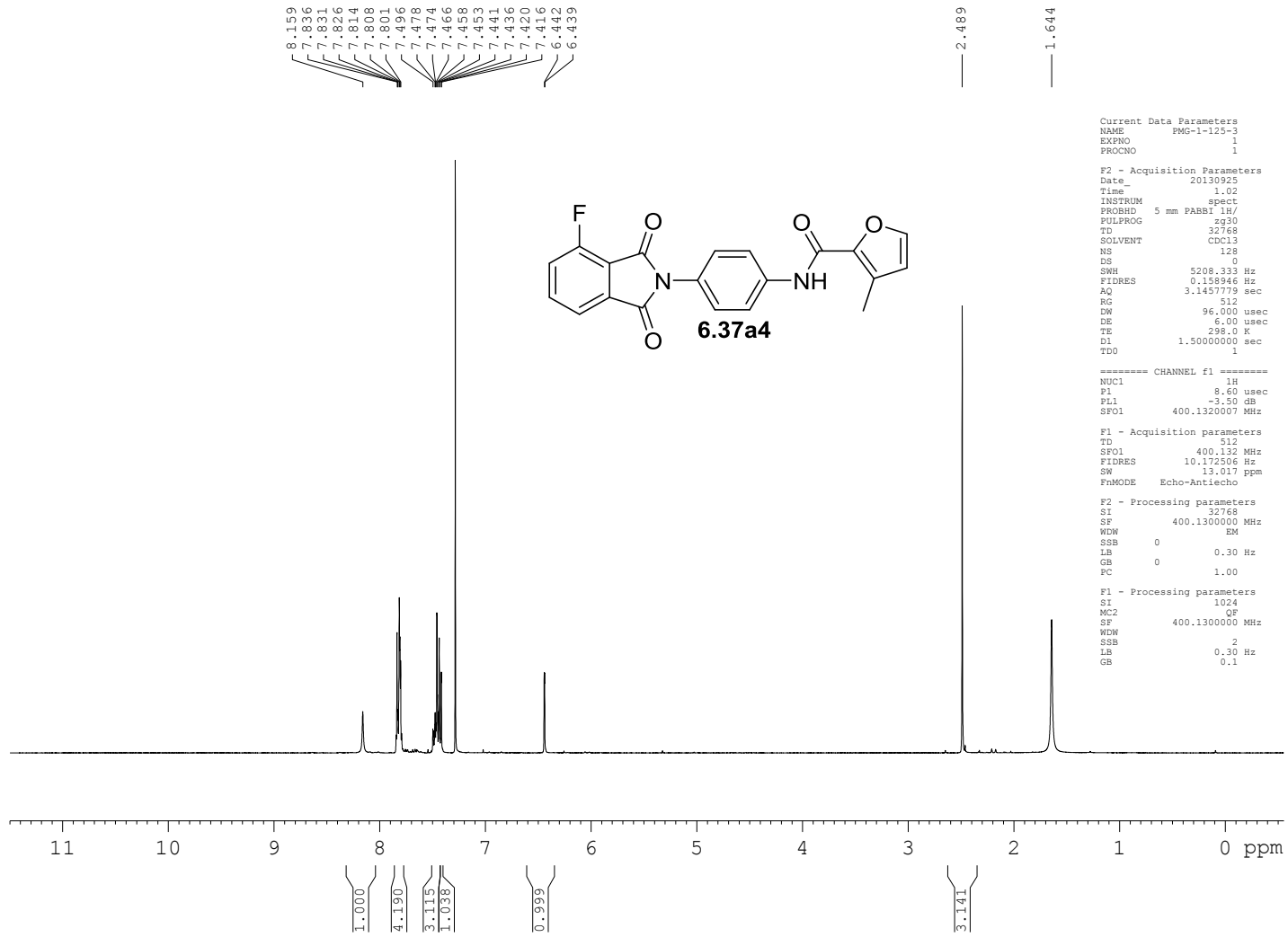
F1 - Acquisition parameters  
TD 512  
SFO1 400.132 MHz  
FIDRES 10.172506 Hz  
SW 13.017 ppm  
FMODE Echo-Antischo

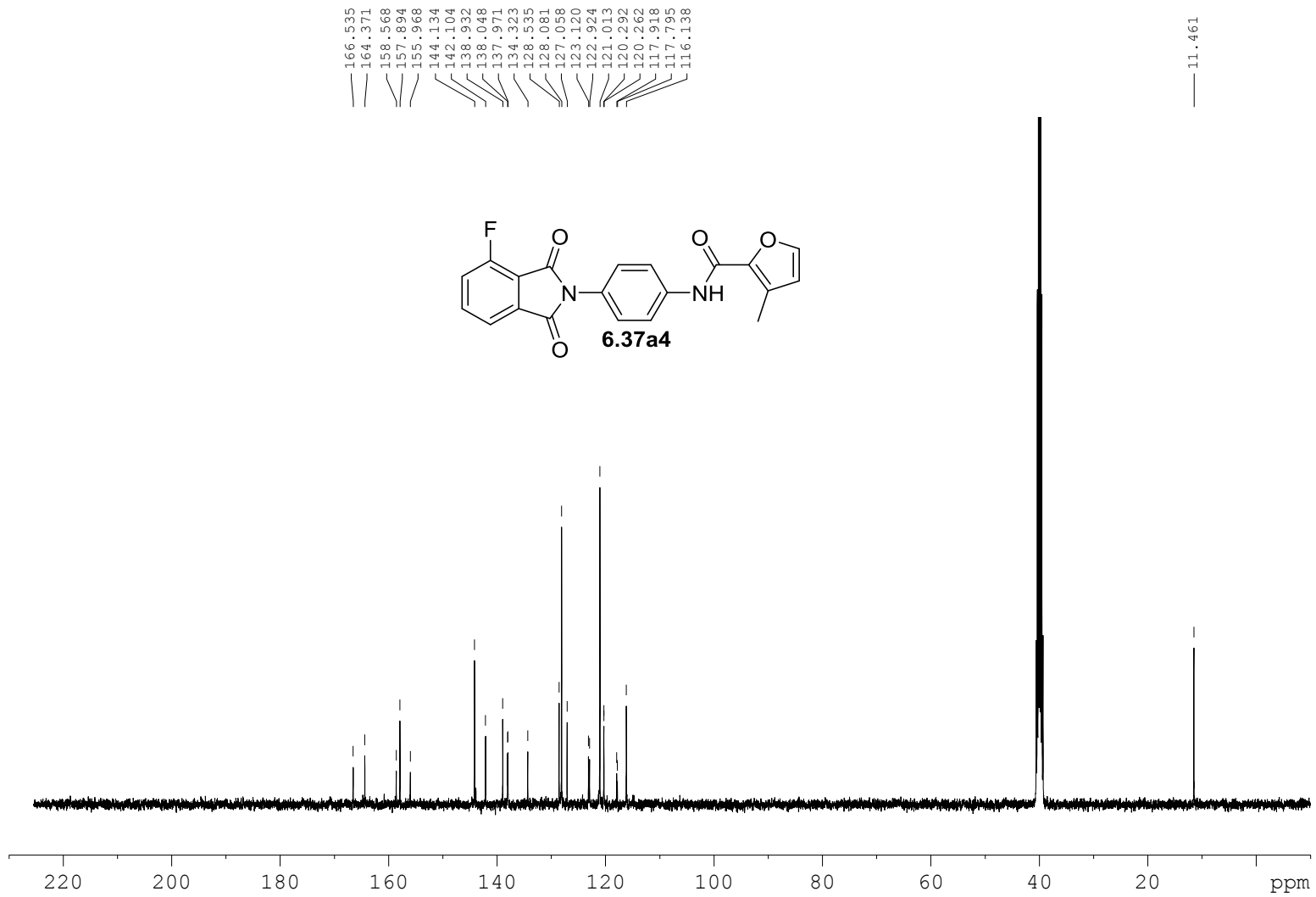
F2 - Processing parameters  
SI 32768  
SF 400.1300000 MHz  
WDW EM  
SSB 0  
LB 0.30 Hz  
GB 0  
PC 1.00

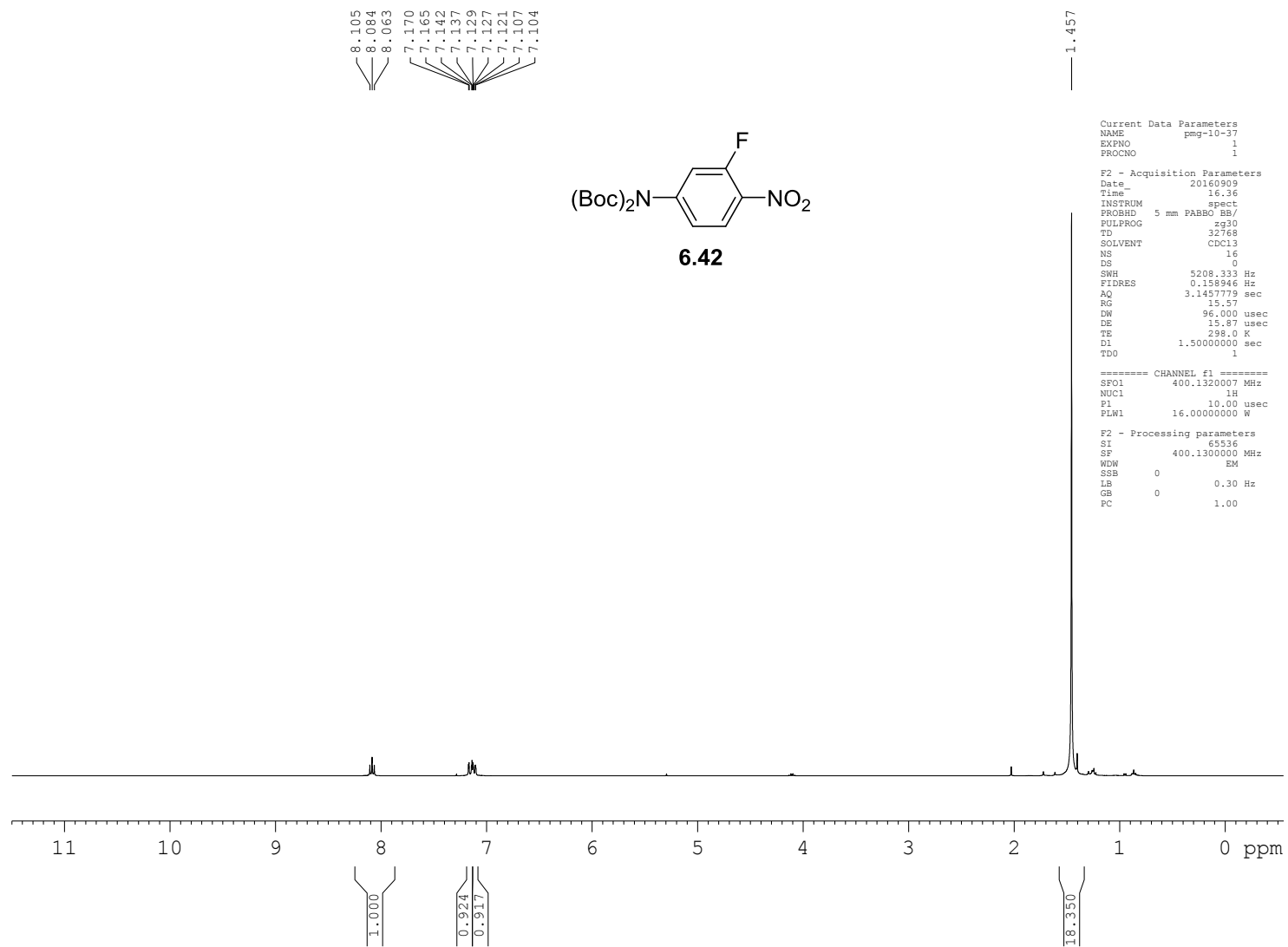
F1 - Processing parameters  
SI 1024  
MC2 0  
SF 400.1300000 MHz  
WDW 2  
SSB 0.30 Hz  
LB 0.1

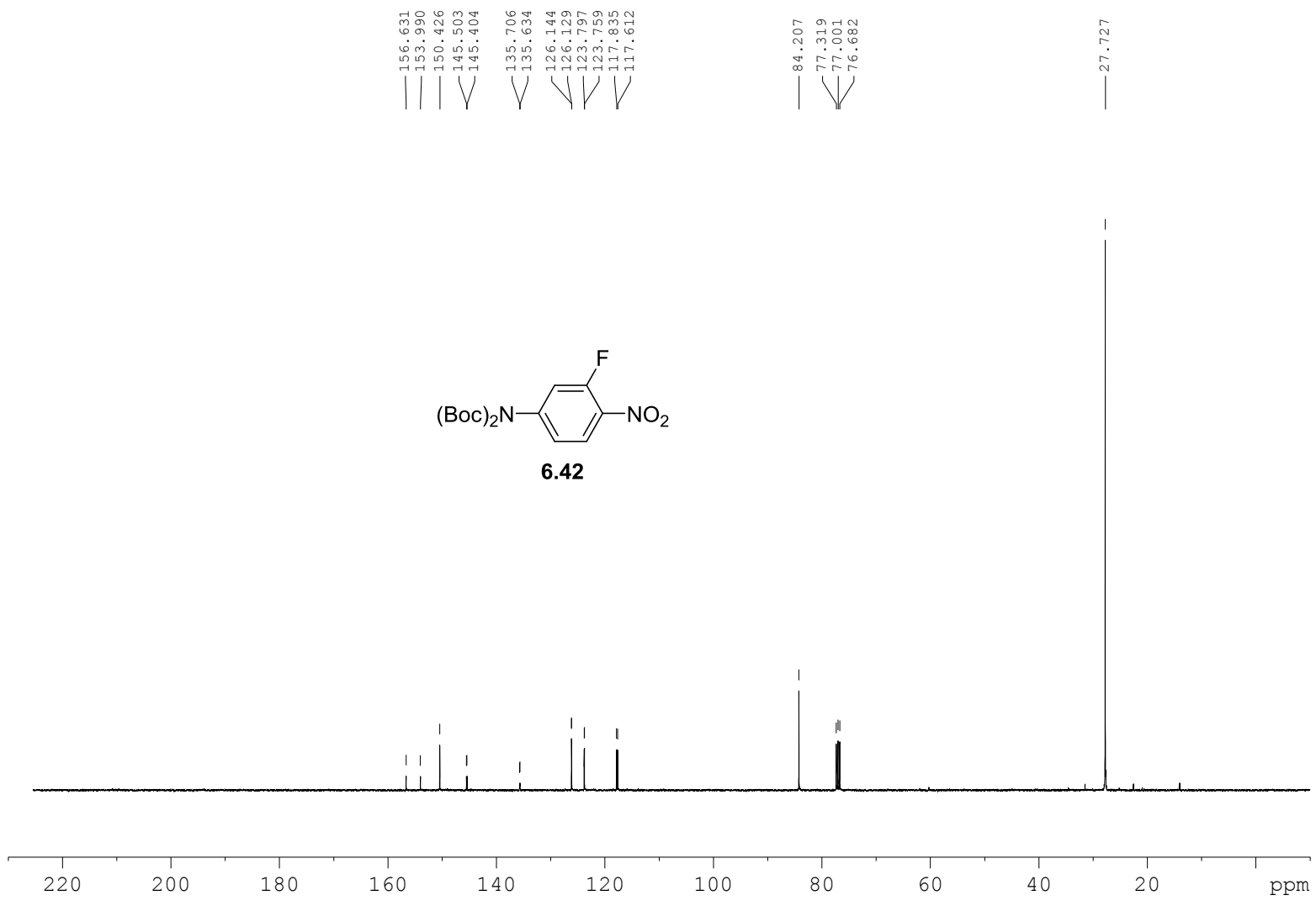


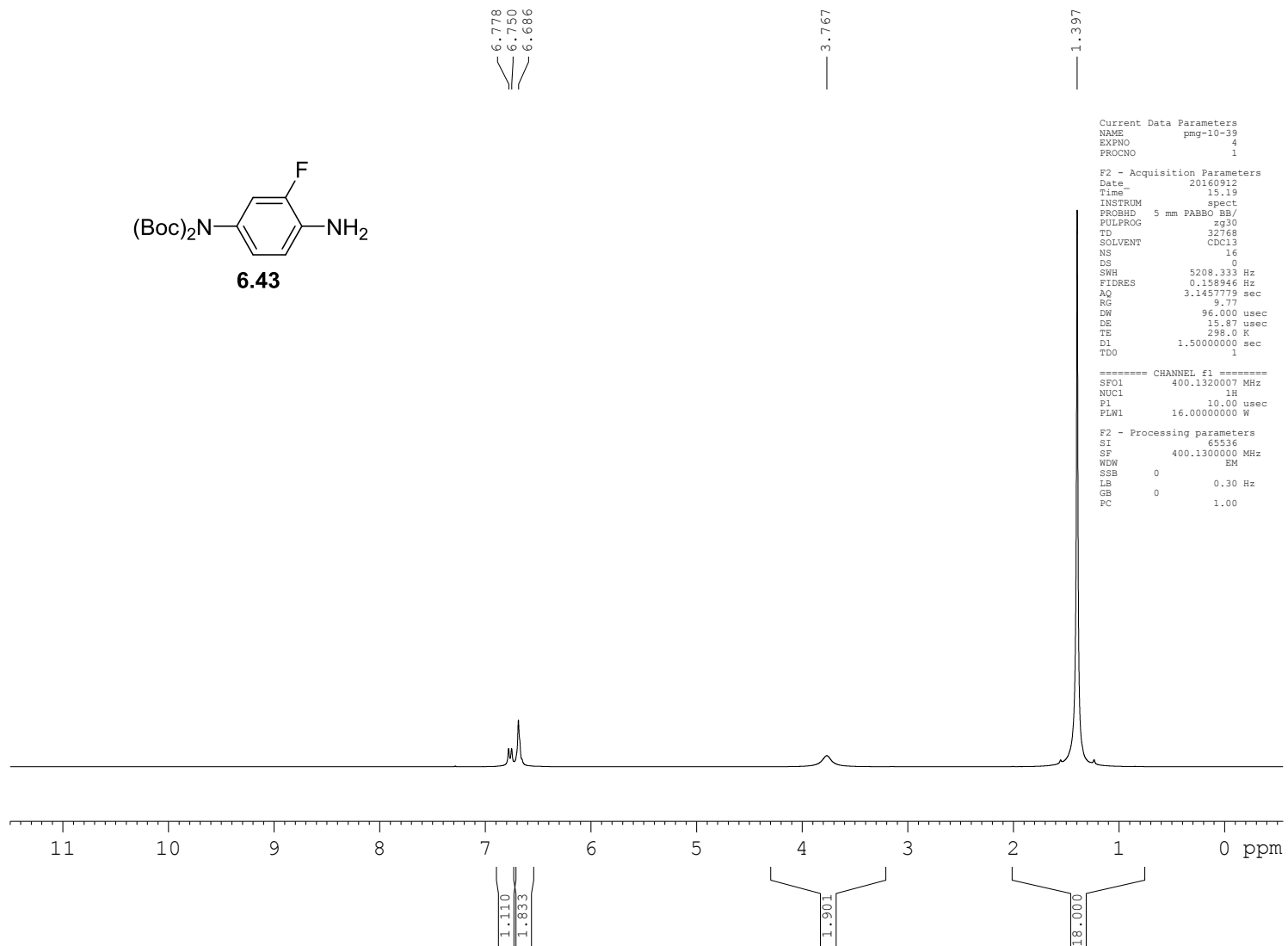
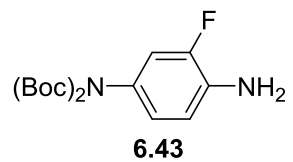
490

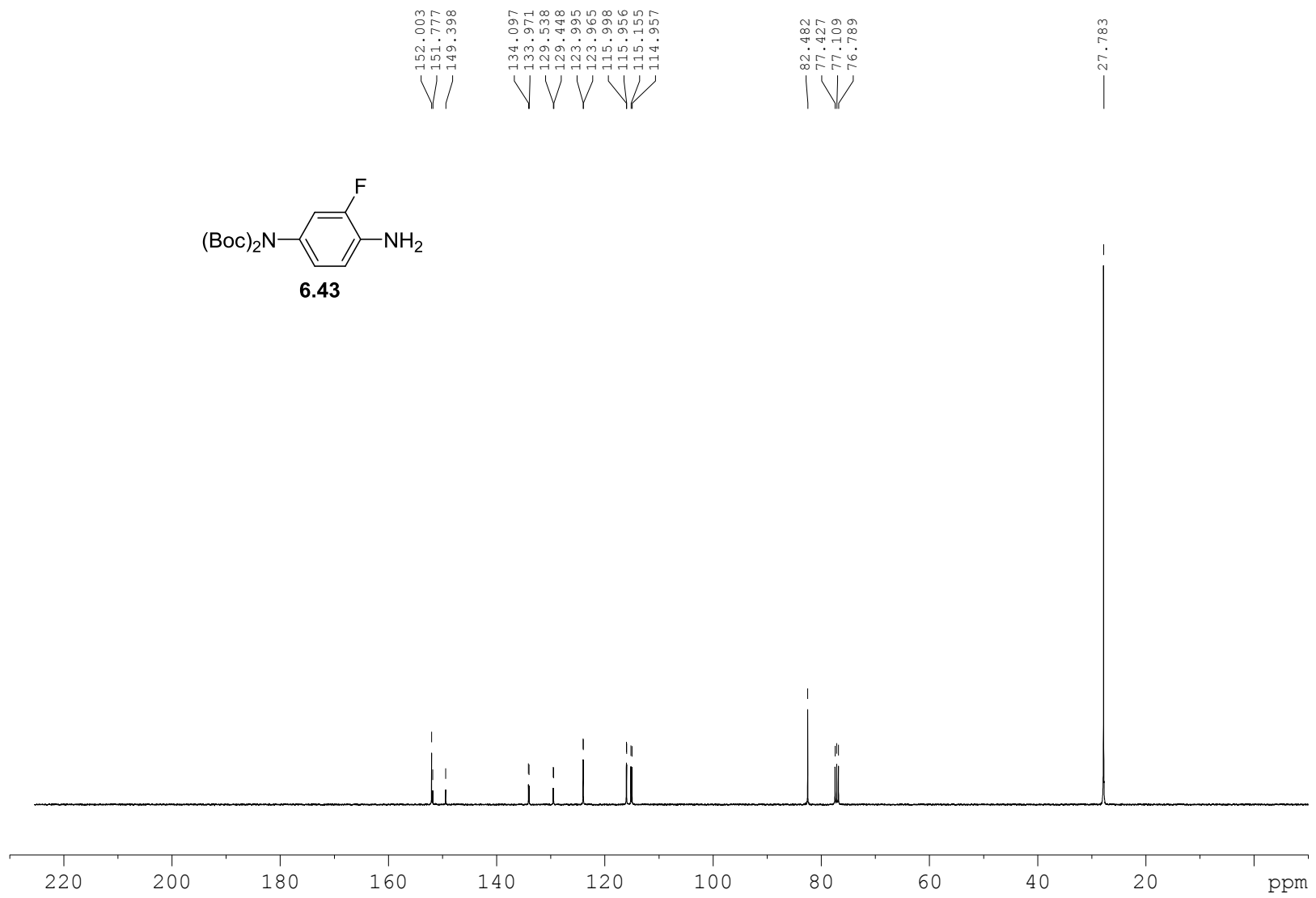
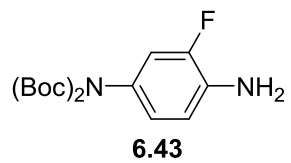




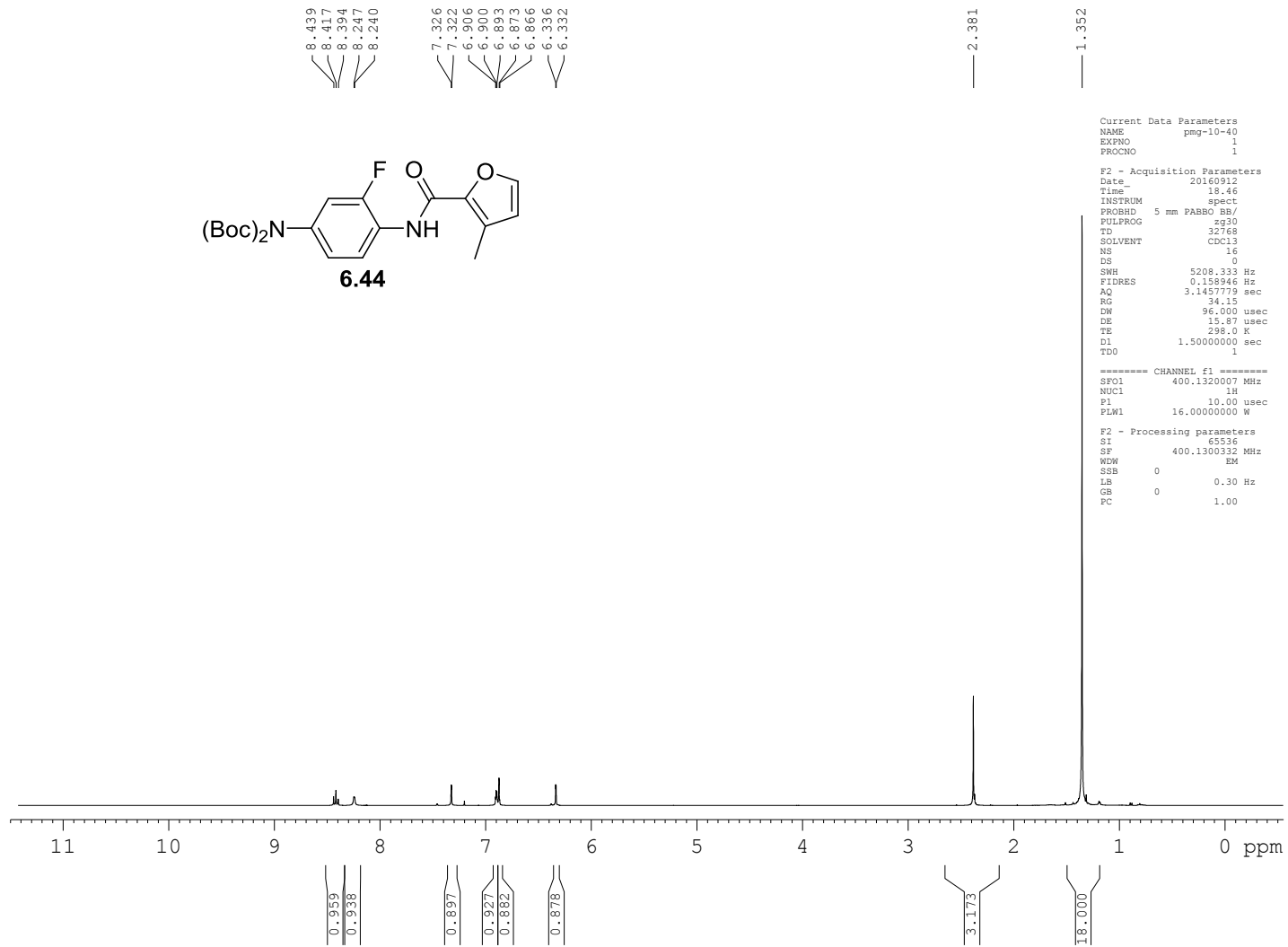


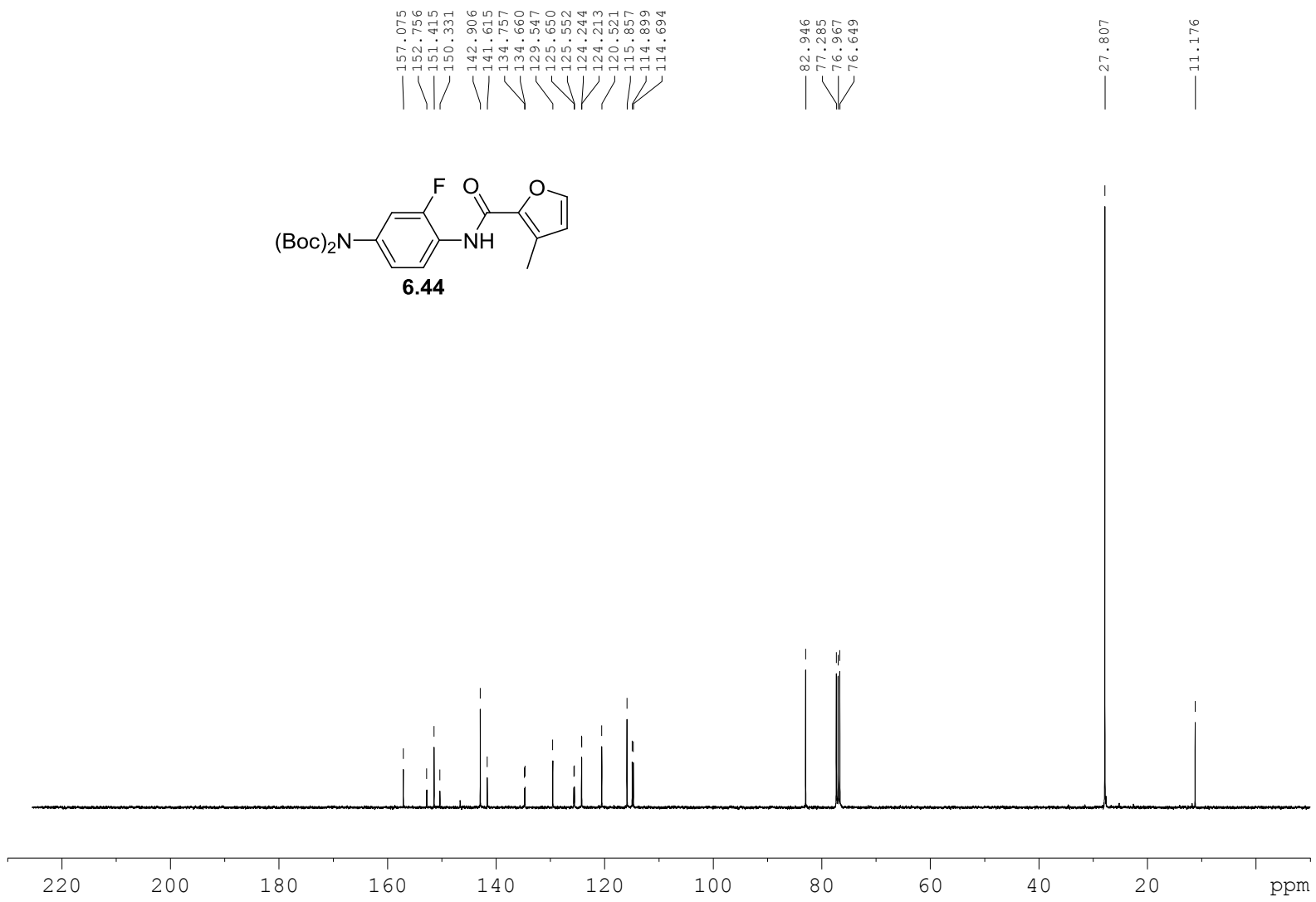
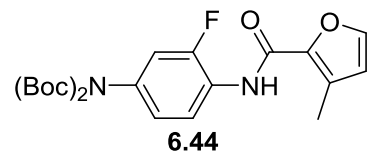


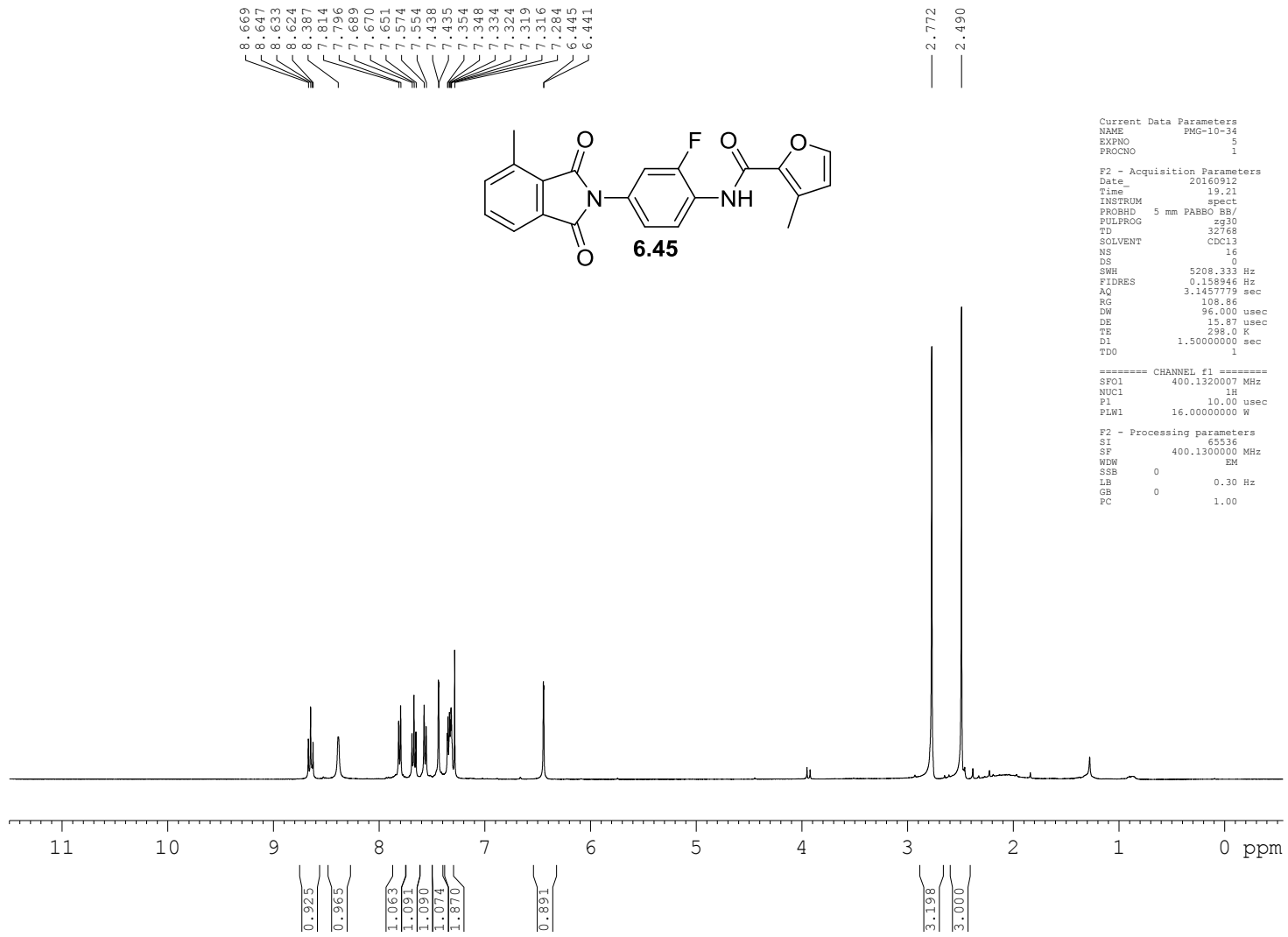


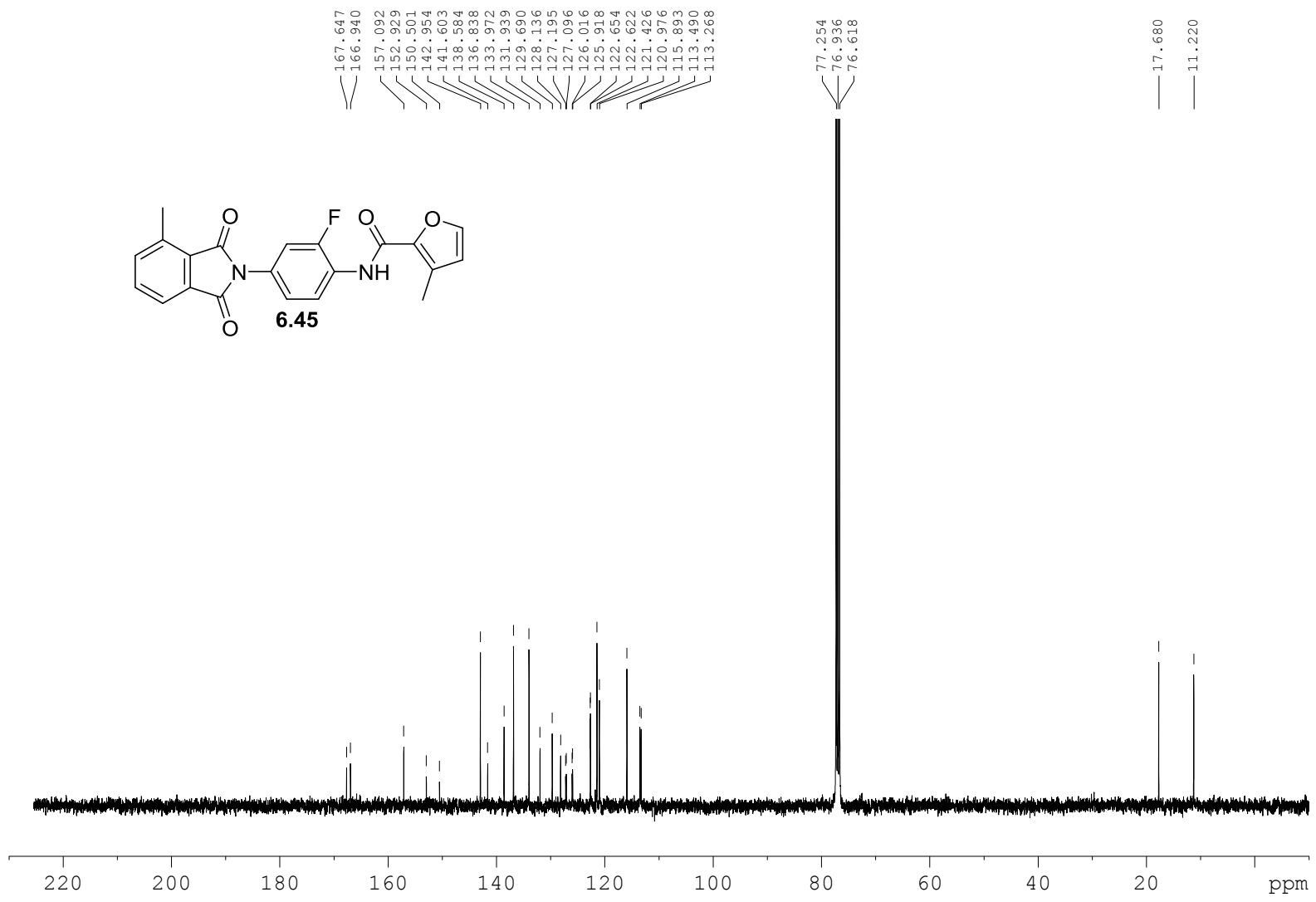




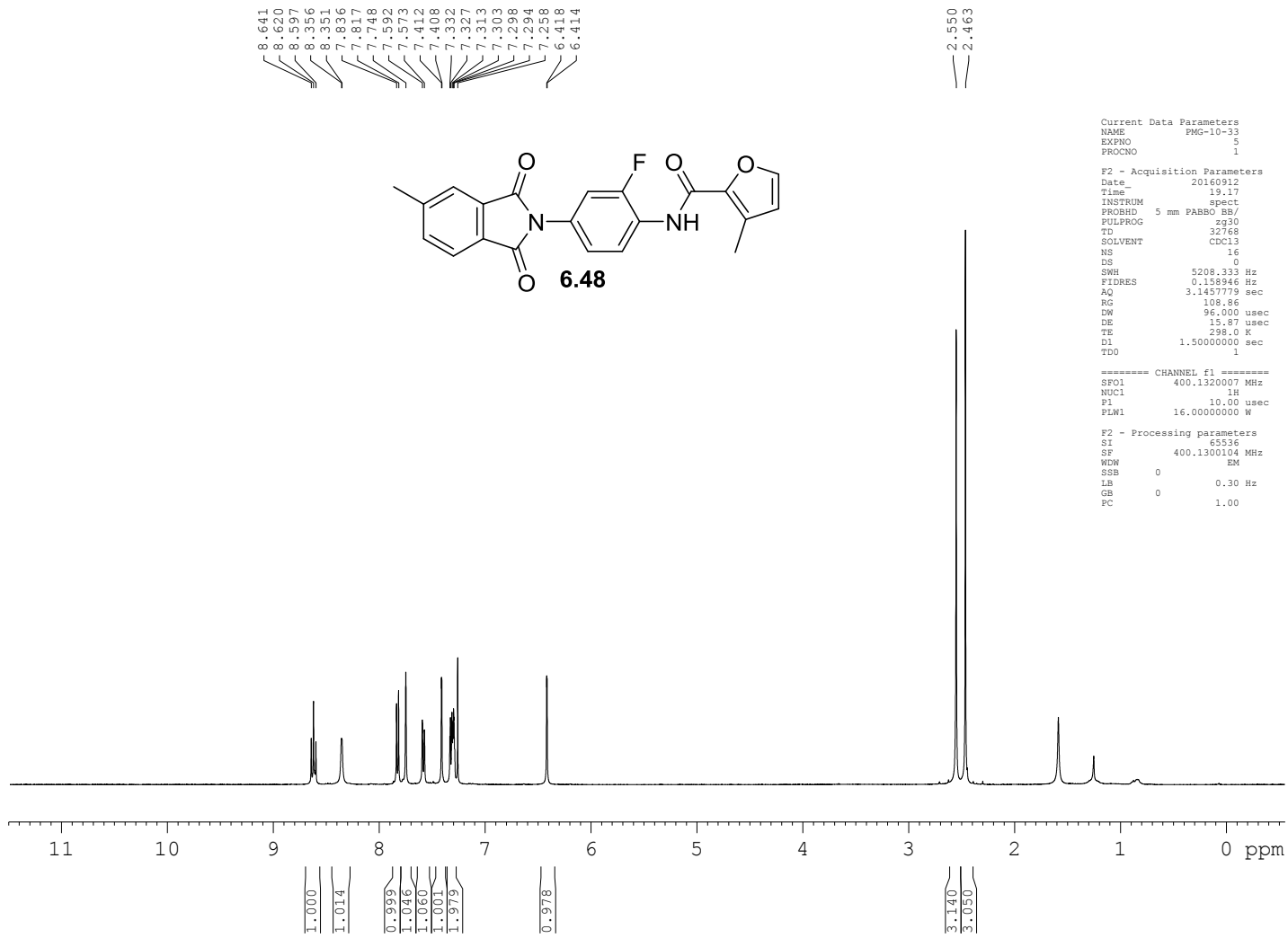








500

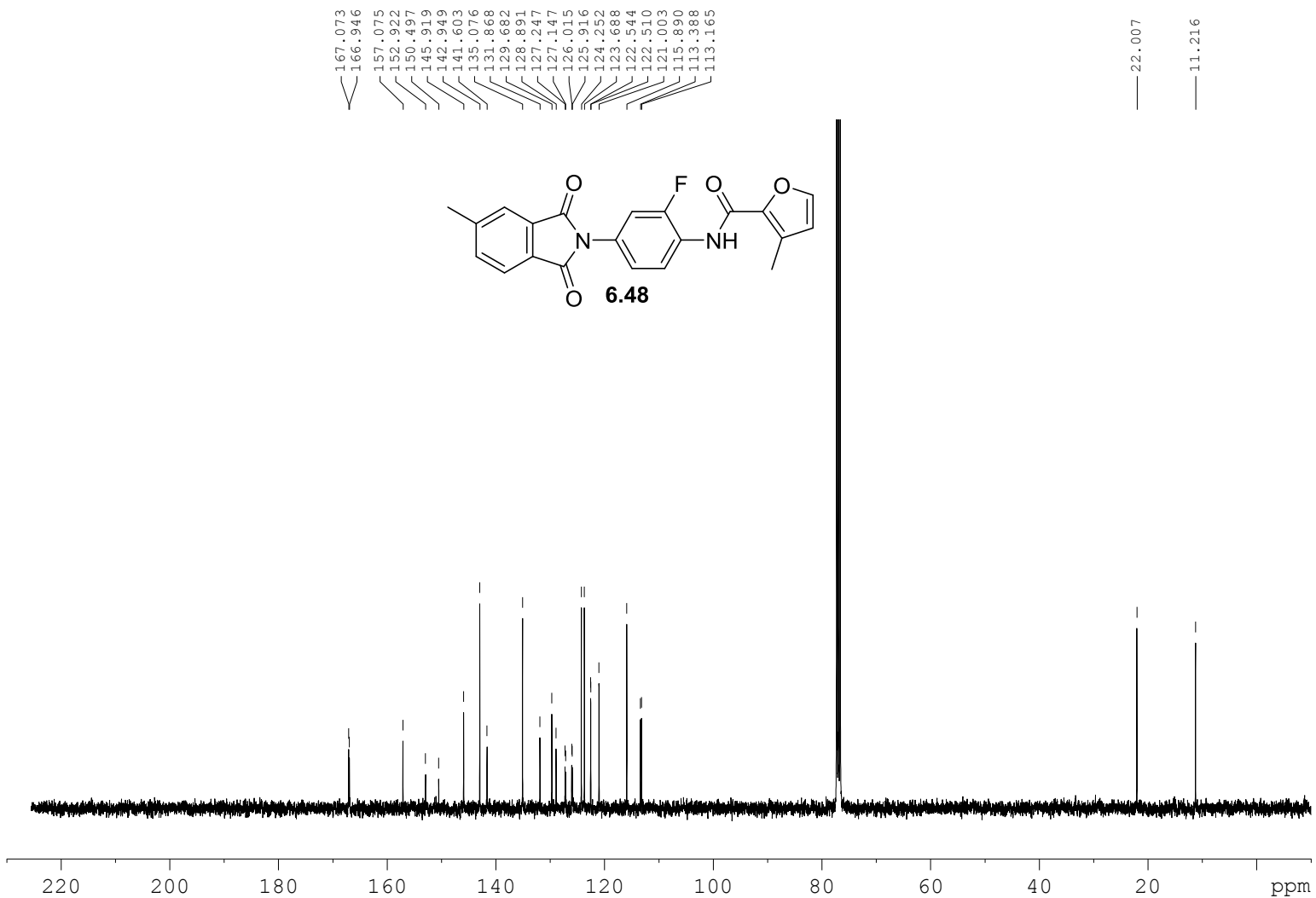


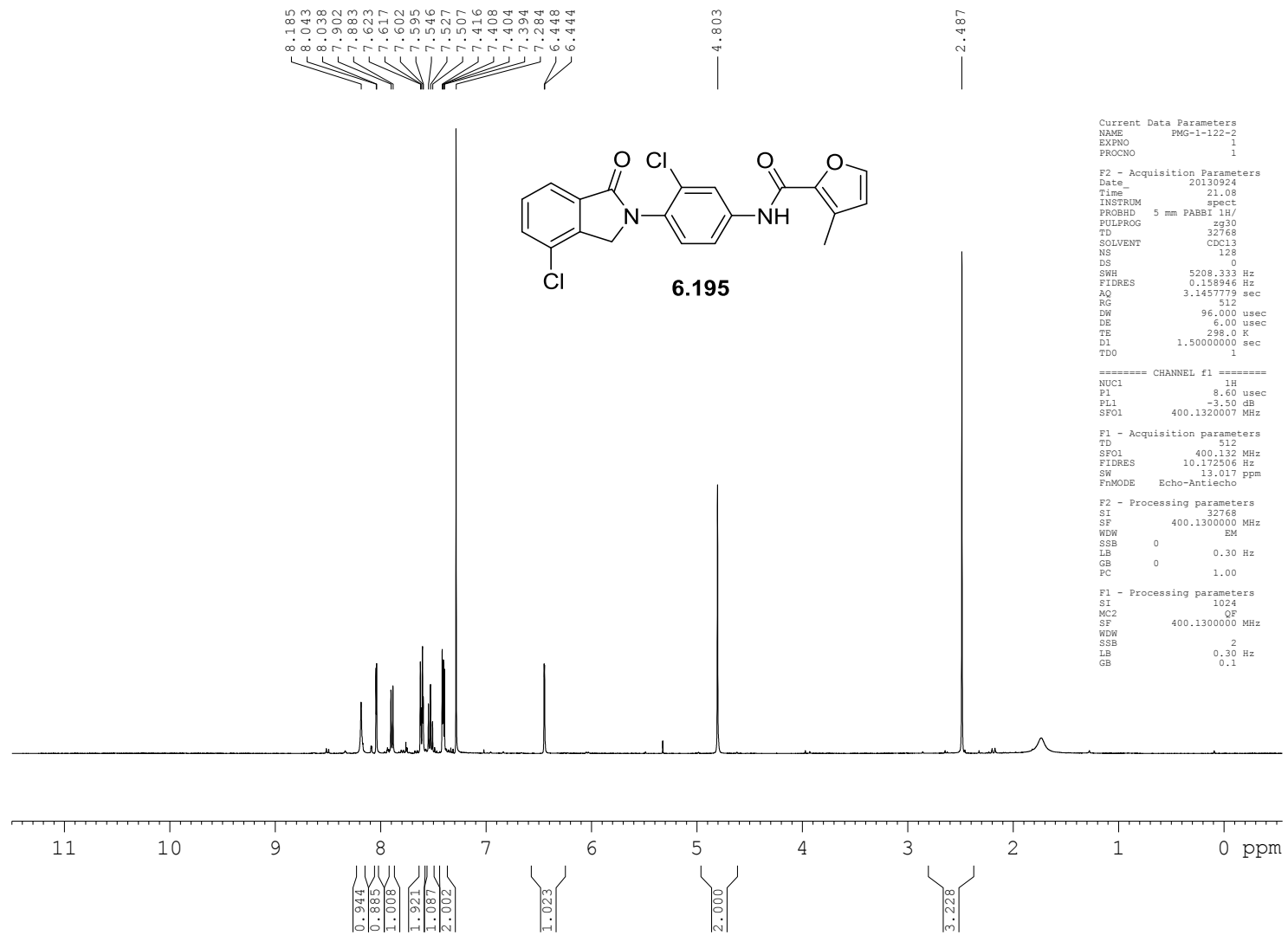
Current Data Parameters  
NAME PMG-10-33  
EXPNO 5  
PROCNO 1

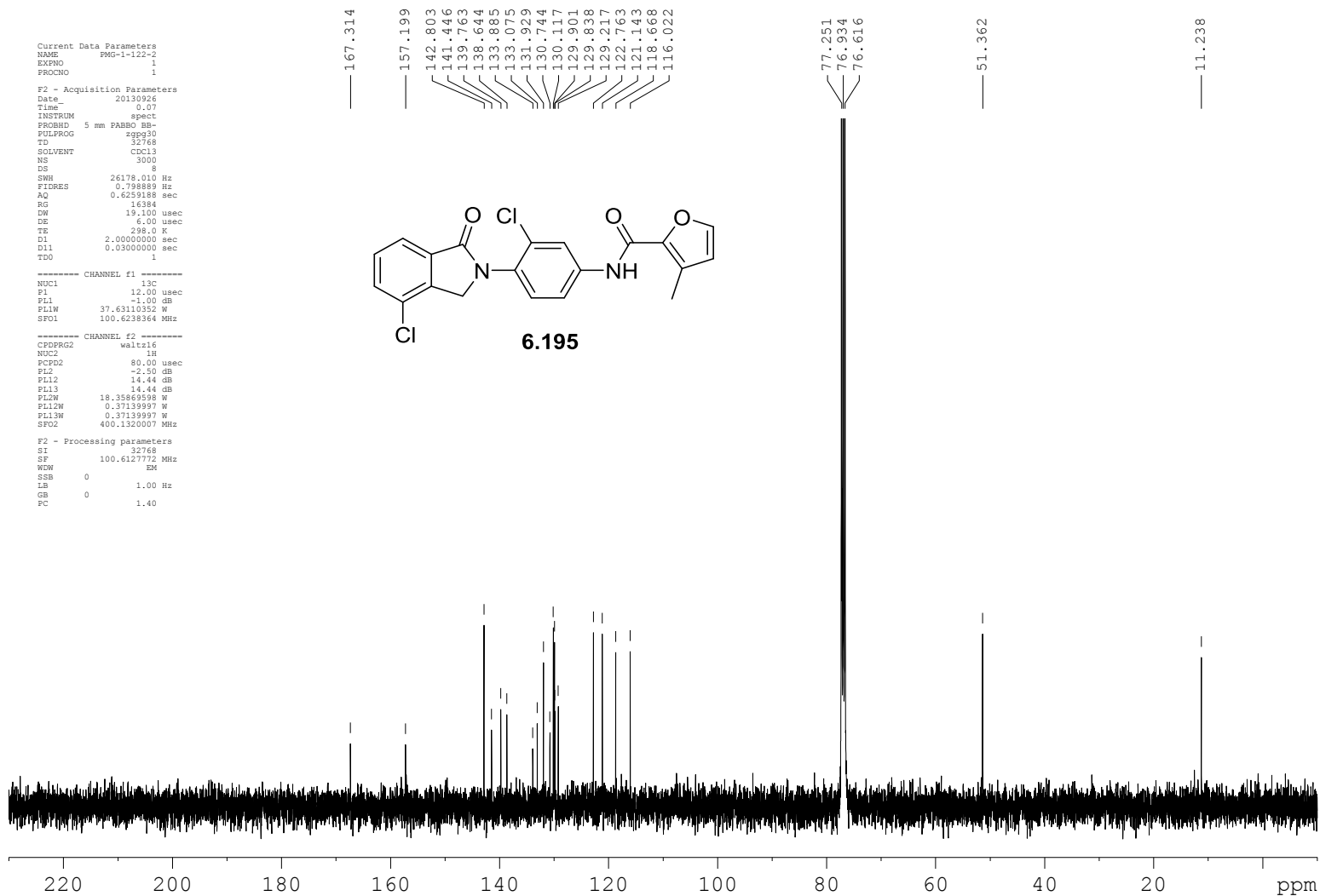
F2 - Acquisition Parameters  
Date\_ 20160912  
Time 19.17  
INSTRUM spect  
PROBHD 5 mm PABBO BB/  
PULPROG zg30  
TD 32768  
SOLVENT CDCl3  
NS 16  
DS 0  
SWH 5208.333 Hz  
FIDRES 0.158946 Hz  
AQ 3.1457773 sec  
RG 108.86  
DW 96.000 usec  
DE 15.87 usec  
TE 298.0 K  
D1 1.5000000 sec  
TDO 1

==== CHANNEL f1 =====  
SFO1 400.1320007 MHz  
NUC1 1H  
P1 10.00 usec  
PLW1 16.00000000 W

F2 - Processing parameters  
SI 65536  
SF 400.1300104 MHz  
WDW EM  
SSB 0  
LB 0.30 Hz  
GB 0  
PC 1.00

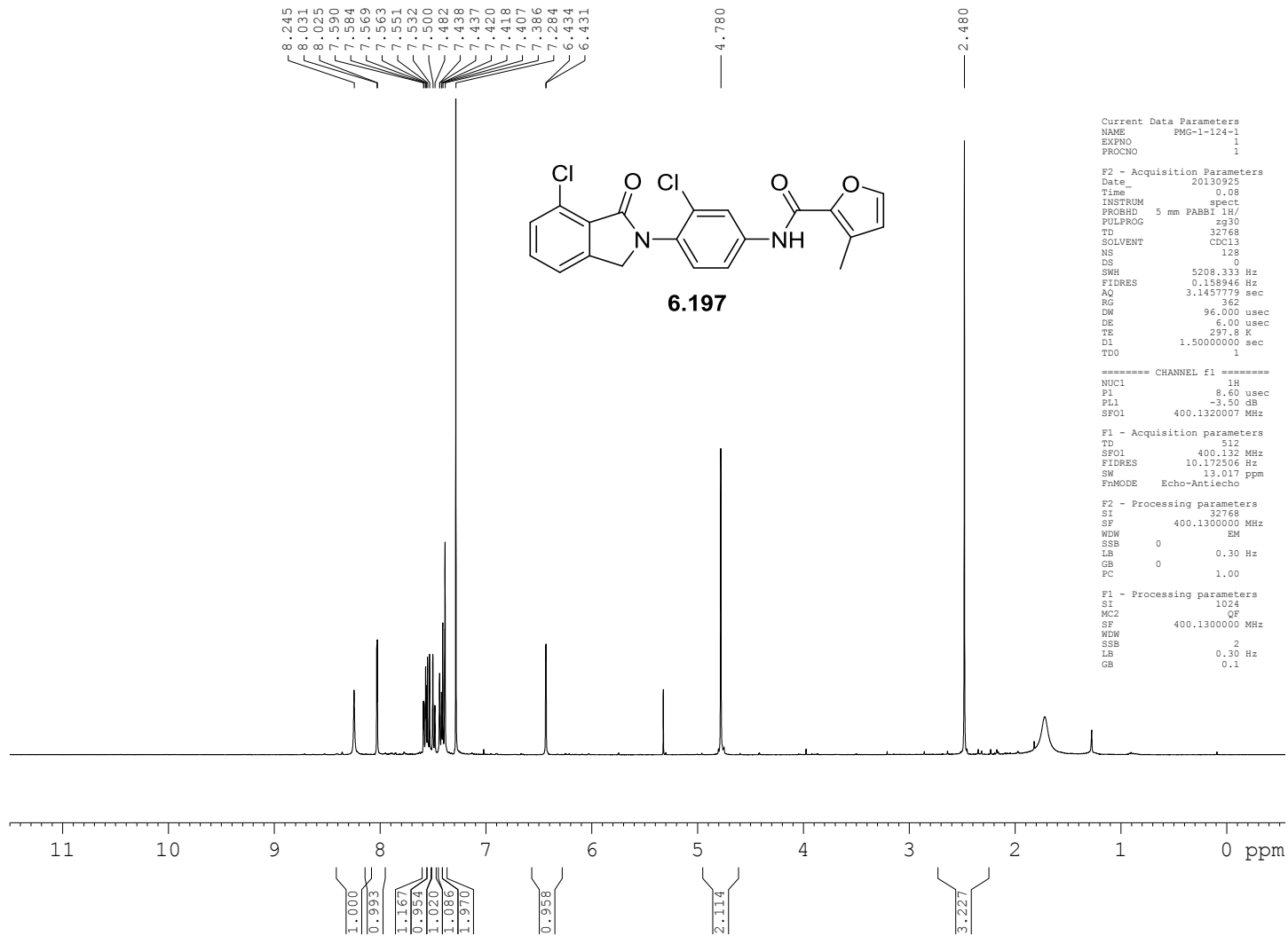


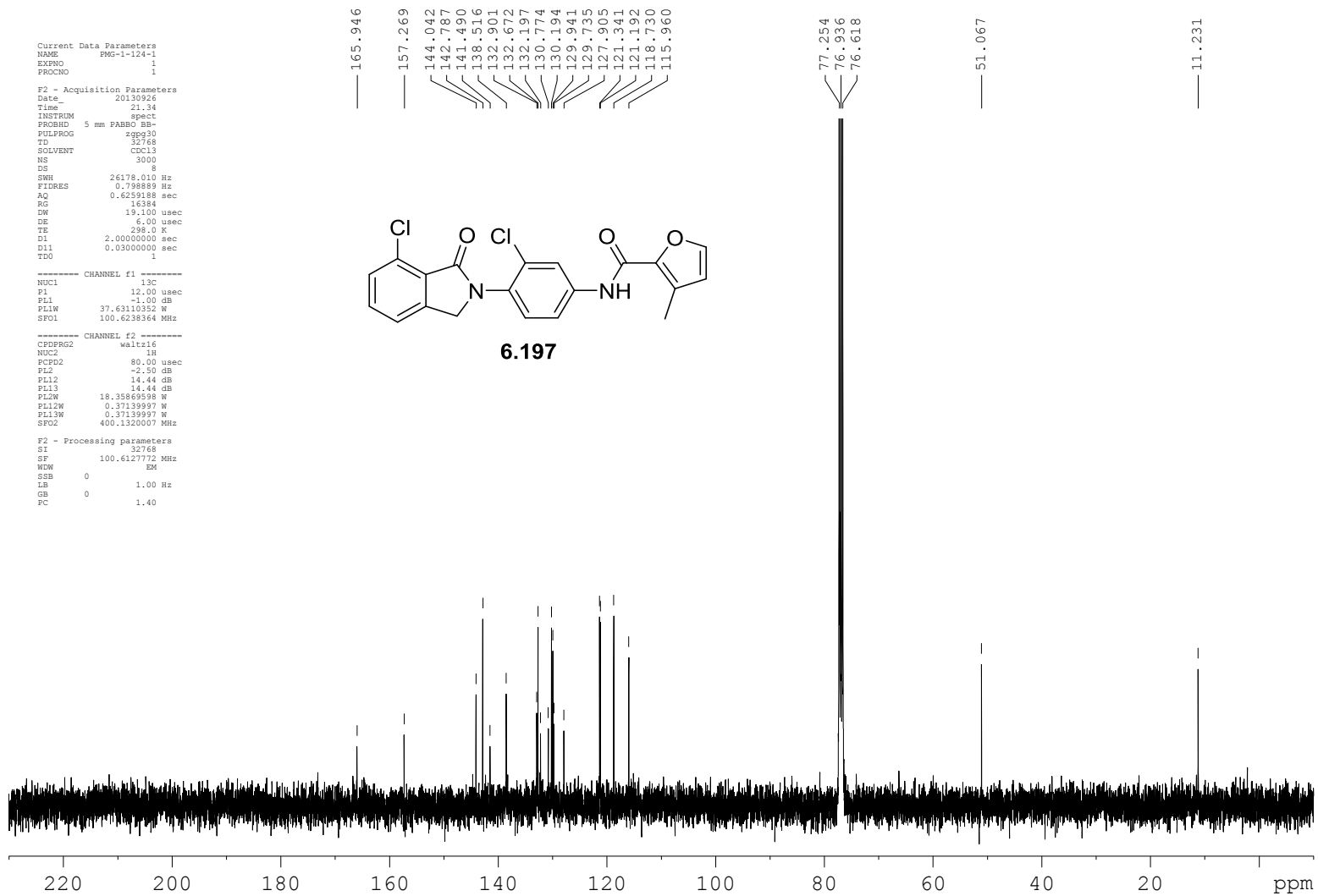






504





## REFERENCES

- (1) Long, S.; Sousa, E.; Kijjoa, A.; Pinto, M. Marine Natural Products as Models to Circumvent Multidrug Resistance. *Molecules* **2016**, *21* (7), 892.
- (2) Zhang, G.; Li, J.; Zhu, T.; Gu, Q.; Li, D. ScienceDirect Advanced Tools in Marine Natural Drug Discovery Anti-Cancer Hyper Triglyceridemia. *Curr. Opin. Biotechnol.* **2016**, *42*, 13–23.
- (3) Blunt, J. W.; Copp, B. R.; Keyzers, R. A.; Munro, M. H. G.; Prinsep, M. R. Marine Natural Products. *Nat. Prod. Rep.* **2016**, *33* (3), 382–431.
- (4) Anjum, K.; Abbas, S. Q.; Shah, S. A. A.; Akhter, N.; Batool, S.; Hassan, S. S. ul. Marine Sponges as a Drug Treasure. *Biomol. Ther. (Seoul)*. **2016**, *24* (4), 347–362.
- (5) Annapoorani, A.; Jabbar, A. K. K. A.; Musthafa, S. K. S.; Pandian, S. K.; Ravi, A. V. Inhibition of Quorum Sensing Mediated Virulence Factors Production in Urinary Pathogen *Serratia Marcescens* PS1 by Marine Sponges. *Indian J. Microbiol.* **2012**, *52* (2), 160–166.
- (6) Ravichandran, S.; Wahidullah, S.; D'souza, L.; Anbuezhian, R. M. Antimicrobial Activity of Marine Sponge *Clathria Indica* (Dendy, 1889). *Russ. J. Bioorganic Chem.* **2011**, *37* (4), 428–435.
- (7) Mendiola, J.; Regalado, E. L.; Diaz-Garcia, A.; Thomas, O. P.; Fernandez-Calienes, A.; Rodriguez, H.; Laguna, A.; Valdes, O. In Vitro Antiplasmodial Activity, Cytotoxicity and Chemical Profiles of Sponge Species of Cuban Coasts. *Nat Prod Res* **2014**, *28* (5), 312–317.
- (8) Mendiola, J. [ In Vivo Antiplasmodial Activity of *Mycale Laxissima* and *Clathria Echinata* Sponges ] *Laxissima Y Clathria Echinata*. **2013**, No. February.
- (9) Rudi, A.; Yosief, T.; Loya, S.; Hizi, A.; Schleyer, M.; Kashman, Y. Clathsterol, a Novel Anti-HIV-1 RT Sulfated Sterol from the Sponge *Clathria* Species. *J. Nat. Prod.* **2001**, *64* (11), 1451–1453.
- (10) Capon, R. J.; Miller, M.; Rooney, F. Mirabilin G: A New Alkaloid from a Southern Australian Marine Sponge, *Clathria* Species. *J. Nat. Prod.* **2001**, *64* (5), 643–644.
- (11) Keyzers, R. A.; Northcote, P. T.; Webb, V. Clathriol, a Novel Polyoxygenated 14?? Steroid Isolated from the New Zealand Marine Sponge *Clathria Lissosclera*. *J. Nat. Prod.* **2002**, *65* (4), 598–600.
- (12) Davis, R. A.; Mangalindan, G. C.; Bojo, Z. P.; Antemano, R. R.; Rodriguez, N. O.; Concepcion, G. P.; Samson, S. C.; De Guzman, D.; Cruz, L. J.; Tasdemir, D.; et al. Microcionamides A and B, Bioactive Peptides from the Philippine Sponge *Clathria* (*Thalysias*) *Abietina*. *J. Org. Chem.* **2004**, *69* (12), 4170–4176.
- (13) Laville, R.; Thomas, O. P.; Berru e, F.; Marquez, D.; Vacelet, J.; Amade, P. Bioactive Guanidine Alkaloids from Two Caribbean Marine Sponges. *J. Nat. Prod.* **2009**, *72* (9), 1589–1594.
- (14) Gupta, P.; Sharma, U.; Schulz, T. C.; McLean, A. B.; Robins, A. J.; West, L. M. Bicyclic C21 Terpenoids from the Marine Sponge *Clathria Compressa*. *J. Nat. Prod.* **2012**, *75* (6), 1223–1227.
- (15) Sun, X.; Sun, S.; Ference, C.; Zhu, W.; Zhou, N.; Zhang, Y.; Zhou, K. A Potent Antimicrobial Compound Isolated from *Clathria Cervicornis*. *Bioorganic Med. Chem. Lett.* **2015**, *25* (1), 67–69.
- (16) Woo, J. K.; Kim, C. K.; Kim, S. H.; Kim, H.; Oh, D. C.; Oh, K. B.; Shin, J. Gombaspiroketal A-C, Sesterterpenes from the Sponge *Clathria Gombawuiensis*. *Org.*

- Lett.* **2014**, *16* (11), 2826–2829.
- (17) Woo, J. K.; Kim, C. K.; Ahn, C. H.; Oh, D. C.; Oh, K. B.; Shin, J. Additional Sesterterpenes and a Nortriterpene Saponin from the Sponge *Clathria Gombawuiensis*. *J. Nat. Prod.* **2015**, *78* (2), 218–224.
  - (18) Woo, J. K.; Jeon, J. E.; Kim, C. K.; Sim, C. J.; Oh, D. C.; Oh, K. B.; Shin, J. Gombamide A, a Cyclic Thiopeptide from the Sponge *Clathria Gombawuiensis*. *J. Nat. Prod.* **2013**, *76* (7), 1380–1383.
  - (19) Bhat, K. L.; Madeleine, M. Cyclopeptide Alkaloids. **1997**, *64* (1), 21–27.
  - (20) Joullié, M. M.; Richard, D. J. Cyclopeptide Alkaloids: Chemistry and Biology. *Chem. Commun. (Camb)*. **2004**, 2011–2015.
  - (21) Tan, N. H.; Zhou, J. Plant Cyclopeptides. *Chem. Rev.* **2006**, *106* (3), 840–895.
  - (22) Kazlauskas, R.; Lidgard, R. O.; Murphy, P. T.; Wells, R. J. Brominated Tyrosine-Derived Metabolites from the Sponge *Ianthella Basta*. *Tetrahedron Lett.* **1980**, *21* (23), 2277–2280.
  - (23) Casapullo, A.; Finamore, E.; Minale, L.; Zollo, F. A Dimeric Peptide Alkaloid of a Completely New Type, Anchinopeptolide A, from the Marine Sponge *Anchinoe Tenacior*. *Tetrahedron Lett.* **1993**, *34* (39), 6297–6300.
  - (24) Palermo, J. A.; Brasco, M. F. R.; Seldes, A. M. Storniamides A–D: Alkaloids from a Patagonian Sponge *Cliona* Sp. *Tetrahedron* **1996**, *52* (8), 2727–2734.
  - (25) Rao, M. R.; Faulknert, D. J. Botryllamides E–H, Four New Tyrosine Derivatives from the Ascidian *Botrylloides Tyreum*. *J. Nat. Prod.* **2004**, *67* (6), 1064–1066.
  - (26) McKay, M. J.; Carroll, A. R.; Quinn, R. J. Perspicamides A and B, Quinolinecarboxylic Acid Derivatives from the Australian Ascidian *Botrylloides Perspicuum*. *J. Nat. Prod.* **2005**, *68* (12), 1776–1778.
  - (27) Guella, G.; Frassanito, R.; Mancini, I.; Sandron, T.; Modeo, L.; Verni, F.; Dini, F.; Petroni, G. Keronopsamides, a New Class of Pigments from Marine Ciliates. *European J. Org. Chem.* **2010**, No. 3, 427–434.
  - (28) Yin, S.; Cullinane, C.; Carroll, A. R.; Quinn, R. J.; Davis, R. A. Botryllamides K and L, New Tyrosine Derivatives from the Australian Ascidian *Aplidium Altarium*. *Tetrahedron Lett.* **2010**, *51* (26), 3403–3405.
  - (29) Stonard, R. J.; Andersen, R. J. Celenamide-a and Celenamide-B, Linear Peptide Alkaloids from the Sponge *Cliona Celata*. *J. Org. Chem.* **1980**, *45* (4), 3687–3691.
  - (30) Oltz, E. M.; Bruening, R. C.; Smith, M. J.; Kustin, K.; Nakanishi, K. The Tunichromes. A Class of Reducing Blood Pigments from Sea Squirts: Isolation, Structures, and Vanadium Chemistry. *J. Am. Chem. Soc.* **1988**, *110* (18), 6162–6172.
  - (31) Williams, D. E.; Austin, P.; Diaz-Marrero, A. R.; Van Soest, R.; Matainaho, T.; Roskelley, C. D.; Roberge, M.; Andersen, R. J. Neopetrosiamides, Peptides from the Marine Sponge *Neopetrosia* Sp. That Inhibit Amoeboid Invasion by Human Tumor Cells. *Org. Lett.* **2005**, *7* (19), 4173–4176.
  - (32) Li, H.; Bowling, J. J.; Fronczek, F. R.; Hong, J.; Jabba, S. V.; Murray, T. F.; Ha, N. C.; Hamann, M. T.; Jung, J. H. Asteropsin A: An Unusual Cystine-Crosslinked Peptide from Porifera Enhances Neuronal Ca<sup>2+</sup> Influx. *Biochim. Biophys. Acta - Gen. Subj.* **2013**, *1830* (3), 2591–2599.
  - (33) Whitson, E. L.; Ratnayake, A. S.; Bugni, T. S.; Harper, M. K.; Ireland, C. M. Isolation, Structure Elucidation, and Synthesis of Eudistomides A and B, Lipopeptides from a Fijian Ascidian *Eudistoma* Sp. *J. Org. Chem.* **2009**, *74* (3), 1156–1162.
  - (34) Sugawara, F.; Kim, K. W.; Uzawa, J.; Yoshida, S.; Takahashi, N.; Curtis, R. W. Structure of Malformin A2, Reinvestigation of Phytotoxic Metabolites Produced by *Aspergillus Niger*. *Tetrahedron Lett.* **1990**, *31* (30), 4337–4340.

- (35) Kim, K. W.; Sugawara, F.; Uzawa, J.; Yoshida, S.; Murofushi, N.; Takahashi, N.; Curtis, R. W.; Kanai, M. Structure of Malformin B, Phytotoxic Metabolites Produced by *Aspergillus Niger*. *Tetrahedron Lett.* **1991**, 32 (46), 6715–6718.
- (36) Nakaya, M.; Oguri, H.; Takahashi, K.; Fukushi, E.; Watanabe, K.; Oikawa, H. Relative and Absolute Configuration of Antitumor Agent SW-163D. *Biosci. Biotechnol. Biochem.* **2007**, 71 (12), 2969–2976.
- (37) Burgess, E. M.; Penton, H. R.; Taylor, E. a. Thermal Reactions of Alkyl N-Carbomethoxysulfamate Esters. *J. Org. Chem.* **1973**, 38 (1), 26–31.
- (38) Martin, J. C.; Arhart, R. J. Sulfuranes. III. Reagent for the Dehydration of Alcohols. *J. Am. Chem. Soc.* **1971**, 93 (17), 4327–4329.
- (39) Izawa, T.; Nishiyama, S.; Yamamura, S. Total Syntheses of Makaluvamines A, B, C and D, Cytotoxic Pyrroloiminoquinone Alkaloids Isolated from Marine Sponge Bearing Activities against Topoisomerase II. *Tetrahedron* **1994**, 50 (48), 13593–13600.
- (40) El-Faham, A.; Albericio, F. Peptide Coupling Reagents, More than a Letter Soup. *Chem. Rev.* **2011**, 111 (11), 6557–6602.
- (41) Han, Y.; Albericio, F.; Barany, G. Occurrence and Minimization of Cysteine Racemization during Stepwise Solid-Phase Peptide Synthesis. *J. Org. Chem.* **1997**, 62 (c), 4307–4312.
- (42) Varma, R. S.; Chatterjee, A. K.; Varma, M. Alumina-Mediated Microwave Thermolysis: A New Approach to Deprotection of Benzyl Esters. *Tetrahedron Lett.* **1993**, 34 (29), 4603–4606.
- (43) Schmidt, U.; Kroner, M.; Griesser, H. No Title No Title. *Synthesis (Stuttg.)* **1991**, 53 (9), 294–300.
- (44) Tsuji, T.; Kataoka, T.; Yoshioka, M.; Sendo, Y.; Nishitani, Y.; Hirai, S.; Maeda, T.; Nagata, W. Synthetic Studies on  $\beta$ -Lactam Antibiotics. VII. Mild Removal of the Benzyl Ester Protecting Group with Aluminum Trichloride. *Tetrahedron Lett.* **1979**, 20 (30), 2793–2796.
- (45) Koide, T.; Otaka, A.; Suzuki, H.; Fujii, N. Selective Conversion of S-Protected Cysteine Derivatives to Cystine by Various Sulphoxide-Silyl Compound / Trifluoroacetic Acid Systems. *SYNLETT* **1991**, 1.
- (46) Akaji, K.; Tatsumi, T.; Yoshida, M.; Kimura, T.; Fujiwara, Y.; Kiso, Y. Synthesis of Cystine-Peptide. **1991**, 15–16.
- (47) Akaji, K.; Tatsumi, T.; Yoshida, M.; Kimura, T.; Fujiwara, Y.; Kiso, Y. Disulfide Bond Formation Using the Silyl Chloride-Sulfoxide System for the Synthesis of a Cystine Peptide. *J. Am. Chem. Soc.* **1992**, 114 (11), 4137–4143.
- (48) Boger, D. L.; Ichikawa, S. Total Syntheses of Thiocoraline and BE-22179: Establishment of Relative and Absolute Stereochemistry [7]. *J. Am. Chem. Soc.* **2000**, 122 (12), 2956–2957.
- (49) Boger, D. L.; Ichikawa, S.; Tse, W. C.; Hedrick, M. P.; Jin, Q. Total Syntheses of Thiocoraline and BE-22179 and Assessment of Their DNA Binding and Biological Properties. *J. Am. Chem. Soc.* **2001**, 123 (4), 561–568.
- (50) Babu, S. N. N.; Srinivasa, G. R.; Santhosh, D. C.; Gowda, D. C. The Hydrogenolysis of N-Benzyl Groups with Magnesium and Ammonium Formate. *J. Chem. Res.* **2004**, 2004 (1), 66–67.
- (51) Manning, M.; Lammek, B.; Bankowski, K.; Seto, J.; Sawyer, W. H. Synthesis and Some Pharmacological Properties of 18 Potent O- Alkyltyrosine-Substituted Antagonists of the Vasopressor Responses to Arginine-Vasopressin. *J. Med. Chem.* **1985**, 28 (Table I), 1485–1491.

- (52) Theodoropoulos, D.; Mizrahi, J.; Dalietos, D.; Francisco, S. Conformationally Restricted C-Terminal Peptides of Substance P. Synthesis, Mass Spectral Analysis and Pharmacological Properties. **1985**, No. 10, 1536–1539.
- (53) Jiang, L.; Job, G. E.; Klapars, A.; Buchwald, S. L. Copper-Catalyzed Coupling of Amides and Carbamates with Vinyl Halides. *Org. Lett.* **2003**, 5 (20), 3667–3669.
- (54) Shen, R.; Porco, J. Synthesis of Enamides Related to the Salicylate Antitumor Macrolides Using Copper-Mediated Vinylic Substitution. *Org. Lett.* **2000**, 2 (9), 1333–1336.
- (55) Shen, R.; Lin, C. T.; Porco, J. A. Total Synthesis and Stereochemical Assignment of the Salicylate Antitumor Macrolide Lobatamide C. *J. Am. Chem. Soc.* **2002**, 124 (20), 5650–5651.
- (56) Takai, K.; Nitta, K.; Utimoto, K. Simple and Selective Method for Aldehydes (RCHO) to (E)-Haloalkenes (RCH:CHX) Conversion by Means of a Haloform-Chromous Chloride System. *J. Am. Chem. Soc.* **1986**, 108 (23), 7408–7410.
- (57) Toumi, M.; Evano, G.; Saint, D. V.; Etats-unis, V.; Cedex, V. Total Synthesis of the Cyclopeptide Alkaloid Paliurine E. Insights into Macrocyclization by Ene - Enamide RCM. **2008**, No. 3, 1270–1281.
- (58) Schmidt, U.; Lieberknecht, A.; Boekens, H.; Griesser, H. Total Synthesis of Zizyphine A. Synthesis of Peptide Alkaloids, Amino Acids and Peptides. *J. Org. Chem.* **1983**, 48 (16), 2680–2685.
- (59) Ono, N.; Kamimura, A.; Kawai, T.; Kaji, A. A Convenient Procedure for the Conversion of (E)-Nitroalkenes to (Z)-Nitroalkenes via Erythro-B-Nitroselenides. *J. Chem. Soc. Chem. Commun.* **1987**, No. 20, 1550–1551.
- (60) Tingoli, M.; Tiecco, M.; Chianelli, D.; Balducci, R.; Temperini, A. Novel Azido-Phenylselenenylation of Double Bonds. Evidence for a Free-Radical Process. *J. ...* **1991**, 56 (4), 6809–6813.
- (61) Tingoli, M.; Tiecco, M.; Testaferri, L.; Andrenacci, R.; Balducci, R. Synthesis of Nitrogen-Containing Heterocycles from the Azido-Selenenylation Products of Unsaturated Carbonyl Compounds. *J. Org. Chem.* **1993**, 58 (22), 6097–6102.
- (62) Czernecki, S.; Randriamandimby, D. Azido-Phenylselenenylation of Protected Glycols. *Tetrahedron Lett.* **1993**, 34 (49), 7915–7916.
- (63) Gupta, V.; Besev, M.; Engman, L. Pyrrolidines from Olefins via Radical Cyclization. *Tetrahedron Lett.* **1998**, 39 (16), 2429–2432.
- (64) Mironov, Y. V.; Sherman, A. A.; Nifantiev, N. E. Homogeneous Azidophenylselenenylation of Glycols Using TMSN<sub>3</sub>-Ph<sub>2</sub>Se<sub>2</sub>-Ph(OAc)<sub>2</sub>. *Tetrahedron Lett.* **2004**, 45 (49), 9107–9110.
- (65) Mironov, Y. V.; Grachev, A. A.; Lalov, A. V.; Sherman, A. A.; Egorov, M. P.; Nifantiev, N. E. A Study of the Mechanism of the Azidophenylselenenylation of Glycols. *Russ. Chem. Bull.* **2009**, 58 (2), 284–290.
- (66) Fenical, W.; Jensen, P. R. Developing a New Resource for Drug Discovery: Marine Actinomycete Bacteria. *Nat. Chem. Biol.* **2006**, 2 (12), 666–673.
- (67) Prieto-Davó, A.; Fenical, W.; Jensen, P. R. Comparative Actinomycete Diversity in Marine Sediments. *Aquat. Microb. Ecol.* **2008**, 52 (1), 1–11.
- (68) Williams, D. E.; Dalisay, D. S.; Li, F.; Amphlett, J.; Maneerat, W.; Chavez, M. A. G.; Wang, Y. A.; Matainaho, T.; Yu, W.; Brown, P. J.; et al. Nahuolic Acid A Produced by a Streptomyces Sp. Isolated from a Marine Sediment Is a Selective SAM-Competitive Inhibitor of the Histone Methyltransferase SETD8. *Org. Lett.* **2013**, 15 (2), 414–417.
- (69) Nam, S. J.; Kauffman, C. A.; Paul, L. A.; Jensen, P. R.; Fenical, W. Actinoranone, a Cytotoxic Meroterpenoid of Unprecedented Structure from a Marine Adapted

- Streptomyces Sp. *Org. Lett.* **2013**, *15* (21), 5400–5403.
- (70) Nam, S. J.; Kauffman, C. A.; Jensen, P. R.; Fenical, W. Isolation and Characterization of Actinoramides A-C, Highly Modified Peptides from a Marine Streptomyces Sp. *Tetrahedron* **2011**, *67* (35), 6707–6712.
- (71) Boonlarpadab, C.; Kauffman, C. A.; Jensen, P. R.; Fenical, W. Marineosins A and B, Cytotoxic Spiroaminals from a Marine-Derived Actinomycete. *Org. Lett.* **2008**, *10* (24), 5505–5508.
- (72) Nam, S. J.; Kauffman, C. A.; Jensen, P. R.; Moore, C. E.; Rheingold, A. L.; Fenical, W. Actinobenzoquinoline and Actinophenanthrolines A-C, Unprecedented Alkaloids from a Marine Actinobacterium. *Org. Lett.* **2015**, *17* (13), 3240–3243.
- (73) Groundwater, P. W.; Ali, M. Synthesis of Pyrido [ 2 , 3- c ] Acridines. **1997**, 3381–3385.
- (74) Saeki, K.; Kawai, H.; Kawazoe, Y.; Hakura, A. Dual Stimulatory and Inhibitory Effects of Fluorine-Substitution on Mutagenicity: An Extension of the Enamine Epoxide Theory for Activation of the Quinoline Nucleus. *Biol. Pharm. Bull.* **1997**, *20* (6), 646–650.
- (75) Prado, S.; Michel, S.; Tillequin, F.; Koch, M.; Pfeiffer, B.; Pierré, A.; Léonce, S.; Colson, P.; Baldeyrou, B.; Lansiaux, A.; et al. Synthesis and Cytotoxic Activity of benzo[c][1,7] and [1,8]phenanthrolines Analogues of Nitidine and Fagaronine. *Bioorganic Med. Chem.* **2004**, *12* (14), 3943–3953.
- (76) Yamada, K.; Suzuki, T.; Kohara, A.; Hayashi, M.; Mizutani, T.; Saeki, K. I. In Vivo Mutagenicity of Benzo[f]quinoline, Benzo[h]quinoline, and 1,7-Phenanthroline Using the lacZ Transgenic Mice. *Mutat. Res. - Genet. Toxicol. Environ. Mutagen.* **2004**, *559* (1-2), 83–95.
- (77) Monchaud, D.; Allain, C.; Teulade-Fichou, M. P. Development of a Fluorescent Intercalator Displacement Assay (G4-FID) for Establishing Quadruplex-DNA Affinity and Selectivity of Putative Ligands. *Bioorganic Med. Chem. Lett.* **2006**, *16* (18), 4842–4845.
- (78) Hounsou, C.; Guittat, L.; Monchaud, D.; Jourdan, M.; Saettel, N.; Mergny, J. L.; Teulade-Fichou, M. P. G-Quadruplex Recognition by Quinacridines: A SAR, NMR, and Biological Study. *ChemMedChem* **2007**, *2* (5), 655–666.
- (79) ??erbet??i, T.; Gen??s, C.; Depauw, S.; Prado, S.; Por??e, F. H.; Hildebrand, M. P.; David-Cordonnier, M. H.; Michel, S.; Tillequin, F. Synthesis and Biological Evaluation of Dialkylaminoalkylamino benzo[c][1,7] and [1,8]phenanthrolines as Antiproliferative Agents. *Eur. J. Med. Chem.* **2010**, *45* (6), 2547–2558.
- (80) Genès, C.; Lenglet, G.; Depauw, S.; Nhili, R.; Prado, S.; David-Cordonnier, M.-H.; Michel, S.; Tillequin, F.; Porée, F.-H. Synthesis and Biological Evaluation of N-Substituted Benzo[c]phenanthrolines and Benzo[c]phenanthrolinones as Antiproliferative Agents. *Eur. J. Med. Chem.* **2011**, *46* (6), 2117–2131.
- (81) Steinhauer, T. N.; Girreser, U.; Meier, C.; Cushman, M.; Clement, B. One-Step Synthetic Access to Isosteric and Potent Anticancer Nitrogen Heterocycles with the Benzo[ c ]Phenanthridine Scaffold. *Chem. - A Eur. J.* **2016**, 1–9.
- (82) Duszyk, M.; MacVinish, L.; Cuthbert, a W. Phenanthrolines--a New Class of CFTR Chloride Channel Openers. *Br. J. Pharmacol.* **2001**, *134*, 853–864.
- (83) CARR, B. A.; FRANKLIN\*, M. R. Drug-Metabolizing Enzyme Induction by 2,2'-Dipyridyl, 1,7-Phenanthroline, 7,8-Benzoquinoline and Oltipraz in Mouse. *Xenobiotica* **1998**, *28* (10), 949–956.
- (84) Carr, B. A.; Franklin, M. R. Induction of Drug Metabolizing Enzymes by 1 , 7-Phenanthroline and Oltipraz in Mice Is Unrelated to. **1999**, *13* (2), 77–82.
- (85) Wang, S.; Hartley, D. P.; Ciccotto, S. L.; Vincent, S. H.; Franklin, R. B.; Kim, M. S.

- Induction of Hepatic Phase II Drug-Metabolizing Enzymes by 1,7-Phenanthroline in Rats Is Accompanied by Induction of Mrp3. *Drug Metab. Dispos.* **2003**, *31* (6), 773–775.
- (86) MacKenzie, A. E.; Caltabiano, G.; Kent, T. C.; Jenkins, L.; McCallum, J. E.; Hudson, B. D.; Nicklin, S. A.; Fawcett, L.; Markwick, R.; Charlton, S. J.; et al. The Antiallergic Mast Cell Stabilizers Lodoxamide and Bufrolin as the First High and Equipotent Agonists of Human and Rat GPR35. *Mol. Pharmacol.* **2013**, *85* (1), 91–104.
- (87) Danac, R.; Daniloaia, T.; Antoci, V.; Vasilache, V.; Ionel, I. Design , Synthesis and Antimycobacterial Activity of Some New Azahetero- Cycles : Phenanthroline with P-Halo -Benzoyl Skeleton . Part V. **2015**, *1684*, 14–19.
- (88) Yapi, A. D.; Valentin, A.; Chezal, J. M.; Chavignon, O.; Chaillot, B.; Gerhardt, R.; Teulade, J. C.; Blache, Y. In Vitro and in Vivo Antimalarial Activity of Derivatives of 1,10-Phenanthroline Framework. *Arch. Pharm. (Weinheim)*. **2006**, *339* (4), 201–206.
- (89) Neamati, N.; Hong, H.; Mazumder, A.; Wang, S.; Sunder, S.; Nicklaus, M. C.; Milne, G. W. A.; Proksa, B.; Pommier, Y. Depsides and Depsidones as Inhibitors of HIV-1 Integrase: Discovery of Novel Inhibitors through 3D Database Searching. *J. Med. Chem.* **1997**, *40* (6), 942–951.
- (90) Mustata, G. I.; Brigo, A.; Briggs, J. M. HIV-1 Integrase Pharmacophore Model Derived from Diverse Classes of Inhibitors. *Bioorganic Med. Chem. Lett.* **2004**, *14* (6), 1447–1454.
- (91) Pratt, Y. T.; Drake, N. L. Quinolinequinones. V. 6-Chloro- and 7-Chloro-5,8-Quinolinequinones. *J. Am. Chem. Soc.* **1960**, *82* (5), 1155–1161.
- (92) González-Vera, J. A.; Luković, E.; Imperiali, B. Synthesis of Red-Shifted 8-Hydroxyquinoline Derivatives Using Click Chemistry and Their Incorporation into Phosphorylation Chemosensors. *J. Org. Chem.* **2009**, *74* (19), 7309–7314.
- (93) Belov, A. V.; Nichvoloda, V. M. Quinone Imines with a Fused Azine Ring: I. Synthesis and Hydrochlorination of 5-(P-Tolylsulfonylimino)quinolin-8-One. *Russ. J. Org. Chem.* **2004**, *40* (1), 93–96.
- (94) Chavan, P.; Simlasan, L. oo4o4mqsa pergamIn 53.00+.00. **1986**, *6* (2).
- (95) Kitahara, Y.; Nagaoka, Y.; Matsumura, T.; Kubo, A. SYNTHESIS OF 6-METHOXY-5,8-QUINOLINEDIONES AND 8-METHOXY-5,6-QUINOLINEDIONES USING OXIDATIVE DEMETHYLATION WITH CERIUM 0 AMMONIUM NITRATE. *Heterocycles* **1994**, *38* (3), 659–678.
- (96) Buchowiecki, W.; Zjawiony, J. An Improved , High-Yield Synthesis of 8-Hydroxy-2-Methylquinoline. **1985**, No. 3, 1015–1016.
- (97) Hayashi, T. A Physiological Study of Epileptic Seizures Following Cortical Stimulation in Animals and Its Application to Human Clinics. *Jpn. J. Physiol.* **1952**, *3* (1), 46–64.
- (98) Curtis, D. R.; Watkins, J. C. The Excitation and Depression of Spinal Neurones by Structurally Related Amino Acids. *J. Neurochem.* **1960**, *6*, 117–141.
- (99) D'Souza, M. S. Glutamatergic Transmission in Drug Reward: Implications for Drug Addiction. *Front. Neurosci.* **2015**, *9* (NOV).
- (100) Miladinovic, T.; Nashed, M. G.; Singh, G. Overview of Glutamatergic Dysregulation in Central Pathologies. *Biomolecules* **2015**, *5* (4), 3112–3141.
- (101) Meldrum, B. S. Glutamate as a Neurotransmitter in the Brain: Review of Physiology and Pathology. *J. Nutr.* **2000**, *130* (4S Suppl), 1007S – 15S.
- (102) Herman, M. A.; Jahr, C. E. Extracellular Glutamate Concentration in Hippocampal Slice. *J. Neurosci.* **2007**, *27* (36), 9736–9741.
- (103) Moussawi, K.; Riegel, A.; Nair, S.; Kalivas, P. W. Extracellular Glutamate: Functional Compartments Operate in Different Concentration Ranges. *Front. Syst. Neurosci.* **2011**, *5* (November), 94.



- (104) Chapman, A. G.; Nanan, K.; Williams, M.; Meldrum, B. S. Anticonvulsant Activity of Two Metabotropic Glutamate Group I Antagonists Selective for the mGlu5 Receptor: 2-Methyl-6-(Phenylethynyl)-Pyridine (MPEP), and (E)-6-Methyl-2-Styryl-Pyridine (SIB 1893). *Neuropharmacology* **2000**, *39* (9), 1567–1574.
- (105) Traynelis, S. F.; Wollmuth, L. P.; McBain, C. J.; Menniti, F. S.; Vance, K. M.; Ogden, K. K.; Hansen, K. B.; Yuan, H.; Myers, S. J.; Dingledine, R. Glutamate Receptor Ion Channels: Structure, Regulation, and Function. *Pharmacol. Rev.* **2010**, *62*, 405–4.
- (106) Deutschenbaur, L.; Beck, J.; Kiyhankhadiv, A.; Mühlhauser, M.; Borgwardt, S.; Walter, M.; Hasler, G.; Sollberger, D.; Lang, U. E. Role of Calcium, Glutamate and NMDA in Major Depression and Therapeutic Application. *Prog. Neuro-Psychopharmacology Biol. Psychiatry* **2016**, *64*, 325–333.
- (107) Yin, S.; Niswender, C. M. Progress toward Advanced Understanding of Metabotropic Glutamate Receptors: Structure, Signaling and Therapeutic Indications. *Cell. Signal.* **2014**, *26* (10), 2284–2297.
- (108) Niswender, C. M.; Conn, P. J. Metabotropic Glutamate Receptors: Physiology, Pharmacology, and Disease. *Annu Rev Pharmacol Toxicol* **2010**, *50*, 295–322.
- (109) Hermans, E.; Challiss, R. a. Structural, Signalling and Regulatory Properties of the Group I Metabotropic Glutamate Receptors: Prototypic Family C G-Protein-Coupled Receptors. *Biochem. J.* **2001**, *359* (Pt 3), 465–484.
- (110) Kunishima, N.; Shimada, Y.; Tsuji, Y.; Sato, T.; Yamamoto, M.; Kumasaka, T.; Nakanishi, S.; Jingami, H.; Morikawa, K. Structural Basis of Glutamate Recognition by a Dimeric Metabotropic Glutamate Receptor. *Nature* **2000**, *407*, 971–977.
- (111) Zhang, X. C.; Liu, J.; Jiang, D. Why Is Dimerization Essential for Class-C GPCR Function? New Insights from mGluR1 Crystal Structure Analysis. *Protein Cell* **2014**, *5* (7), 492–495.
- (112) Huixian Wu, 1\* Chong Wang, 1\* Karen J. Gregory, 2, 3 Gye Won Han, 1 Hyekyung P. Cho, 2 Yan Xia, 4 Colleen M. Niswender, 2 Vsevolod Katritch, 1 Huixian Wu, 1\* Chong Wang, 1\* Karen J. Gregory, 2, 3 Gye Won Han, 1 Hyekyung P. Cho, 2 Yan Xia, 4 Colleen M. Nis, 2 Raymond C. Stevens. Structure of a Class C GPCR Metabotropic Glutamate Receptor 1 Bound to an Allosteric Modulator. *Science (80-. )*. **2014**, *344* (March), 58–64.
- (113) Ciruela, F.; Soloviev, M. M.; McIlhinney, R. A. J. Cell Surface Expression of the Metabotropic Glutamate Receptor Type L Alpha Is Regulated by the C-Terminal Tail. *FEBS Lett.* **1999**, *448* (1), 91–94.
- (114) Tateyama, M.; Kubo, Y. Regulatory Role of C-Terminus in the G-Protein Coupling of the Metabotropic Glutamate Receptor 1. *J. Neurochem.* **2008**, *107* (4), 1036–1046.
- (115) DiRaddo, J. O.; Pshenichkin, S.; Gelb, T.; Wroblewski, J. T. Two Newly Identified Exons in Human GRM1 Express a Novel Splice Variant of Metabotropic Glutamate 1 Receptor. *Gene* **2013**, *519* (2), 367–373.
- (116) Joly, C.; Gomeza, J.; Brabet, I.; Curry, K.; Bockaert, J.; Pin, J. P. Molecular, Functional, and Pharmacological Characterization of the Metabotropic Glutamate Receptor Type 5 Splice Variants: Comparison with mGluR1. *J. Neurosci.* **1995**, *15* (5 Pt 2), 3970–3981.
- (117) Aramori, I.; Nakanishi, S. Signal Transduction and Pharmacological Characteristics of a Metabotropic Glutamate Receptor, mGluR1, in Transfected CHO Cells. *Neuron* **1992**, *8* (4), 757–765.
- (118) Emery, A. C.; DiRaddo, J. O.; Miller, E.; Hathaway, H. a; Pshenichkin, S.; Takoudjou, G. R.; Grajkowska, E.; Yasuda, R. P.; Wolfe, B. B.; Wroblewski, J. T. Ligand Bias at Metabotropic Glutamate 1a Receptors: Molecular Determinants That Distinguish  $\beta$ -Arrestin-Mediated from G Protein-Mediated Signaling. *Mol. Pharmacol.* **2012**, *82* (2),

291–301.

- (119) Heuss, C.; Scanziani, M.; Gähwiler, B. H.; Gerber, U. G-Protein-Independent Signaling Mediated by Metabotropic Glutamate Receptors. *Nat. Neurosci.* **1999**, *2* (12), 1070–1077.
- (120) Thandi, S.; Blank, J. L.; Challiss, R. A. J. Group-I Metabotropic Glutamate Receptors, mGlu1a and mGlu5a, Couple to Extracellular Signal-Regulated Kinase (ERK) Activation via Distinct, but Overlapping, Signalling Pathways. *J. Neurochem.* **2002**, *83* (5), 1139–1153.
- (121) Martin, L. J.; Blackstone, C. D.; Haganir, R. L.; Price, D. L. Cellular Localization of a Metabotropic Glutamate Receptor in Rat Brain. *Neuron* **1992**, *9* (2), 259–270.
- (122) Lavreysen, H.; Pereira, S. N.; Leysen, J. E.; Langlois, X.; Lesage, A. S. J. Metabotropic Glutamate 1 Receptor Distribution and Occupancy in the Rat Brain: A Quantitative Autoradiographic Study Using [3H]R214127. *Neuropharmacology* **2004**, *46* (5), 609–619.
- (123) Stephan, D.; Bon, C.; Holzwarth, J. a; Galvan, M.; Pruss, R. M. Human Metabotropic Glutamate Receptor 1: mRNA Distribution, Chromosome Localization and Functional Expression of Two Splice Variants. *Neuropharmacology* **1996**, *35* (12), 1649–1660.
- (124) Luján, R.; Ciruela, F. Immunocytochemical Localization of Metabotropic Glutamate Receptor Type 1 Alpha and Tubulin in Rat Brain. *Neuroreport* **2001**, *12* (6), 1285–1291.
- (125) Luján, R.; Roberts, J. D. B.; Shigemoto, R.; Ohishi, H.; Somogyi, P. Differential Plasma Membrane Distribution of Metabotropic Glutamate Receptors mGluR1, mGluR2 and mGluR5, Relative to Neurotransmitter Release Sites. *J. Chem. Neuroanat.* **1997**, *13* (4), 219–241.
- (126) Petralia, R. S.; Wang, Y. X.; Singh, S.; Wu, C.; Shi, L.; Wei, J.; Wenthold, R. J. A Monoclonal Antibody Shows Discrete Cellular and Subcellular Localizations of mGluR1 Metabotropic Glutamate Receptors. *J. Chem. Neuroanat.* **1997**, *13* (2), 77–93.
- (127) Shigemoto, R.; Nakanishi, S.; Mizuno, N. Distribution of the mRNA for a Metabotropic Glutamate Receptor (mGluR1) in the Central Nervous System: An in Situ Hybridization Study in Adult and Developing Rat. *J. Comp. Neurol.* **1992**, *322* (1), 121–135.
- (128) Minakami, R.; Hirose, E.; Yoshioka, K.; Yoshimura, R.; Misumi, Y.; Sakaki, Y.; Tohyama, M.; Kiyama, H.; Sugiyama, H. Postnatal Development of mRNA Specific for a Metabotropic Glutamate Receptor in the Rat Brain. *Neurosci Res* **1992**, *15* (1-2), 58–63.
- (129) Jones, E. G.; Liu, X.; Mun, A. Changes in Subcellular Localization of Metabotropic Glutamate Receptor Subtypes During Postnatal. **1998**, *465* (February), 450–465.
- (130) Mick, G.; Yoshimura, R.; Ohno, K.; Kiyama, H.; Tohyama, M. The Messenger RNAs Encoding Metabotropic Glutamate Receptor Subtypes Are Expressed in Different Neuronal Subpopulations of the Rat Suprachiasmatic Nucleus. *Neuroscience* **1995**, *66* (1), 161–173.
- (131) Simonyi, A.; Ngomba, R. T.; Storto, M.; Catania, M. V.; Miller, L. A.; Youngs, B.; DiGorgi-Gerevini, V.; Nicoletti, F.; Sun, G. Y. Expression of Groups I and II Metabotropic Glutamate Receptors in the Rat Brain during Aging. *Brain Res.* **2005**, *1043* (1-2), 95–106.
- (132) Fotuhi, M.; Standaert, D. G.; Testa, C. M.; Penney, J. B.; Young, a B.; Penney, Y.; Ab. Differential Expression of Metabotropic Glutamate Receptors in the Hippocampus and Entorhinal Cortex of the Rat. *Brain Res Mol Brain Res* **1994**, *21*, 283–292.
- (133) Lujan, R.; Nusser, Z.; Roberts, J. D.; Shigemoto, R.; Somogyi, P. Perisynaptic Location of Metabotropic Glutamate Receptors mGluR1 and mGluR5 on Dendrites and Dendritic Spines in the Rat Hippocampus. *Eur. J. Neurosci.* **1996**, *8* (7), 1488–1500.
- (134) Shigemoto, R.; Kinoshita, A. Differential Presynaptic Localization of Metabotropic Glutamate Receptor Subtypes in the Rat Hippocampus. ... *Neurosci.* **1997**, *17* (19), 7503–

7522.

- (135) Gereau, R. W.; Conn, P. J. Roles of Specific Metabotropic Glutamate Receptor Subtypes in Regulation of Hippocampal CA1 Pyramidal Cell Excitability. *J. Neurophysiol.* **1995**, *74* (1), 122–129.
- (136) Rae, M. G.; Irving, A. J. Both mGluR1 and mGluR5 Mediate Ca<sup>2+</sup> Release and Inward Currents in Hippocampal CA1 Pyramidal Neurons. *Neuropharmacology* **2004**, *46* (8), 1057–1069.
- (137) Bortolotto, Z. A.; Collett, V. J.; Conquet, F.; Jia, Z.; Van Der Putten, H.; Collingridge, G. L. The Regulation of Hippocampal LTP by the Molecular Switch, a Form of Metaplasticity, Requires mGlu5 Receptors. *Neuropharmacology* **2005**, *49* (SUPPL.), 13–25.
- (138) Aiba, A.; Chen, C.; Herrup, K.; Rosenmund, C.; Stevens, C. F.; Tonegawa, S. Reduced Hippocampal Long-Term Potentiation and Context-Specific Deficit in Associative Learning in mGluR1 Mutant Mice. *Cell* **1994**, *79* (2), 365–375.
- (139) Manahan-Vaughan, D. The Metabotropic Glutamate Receptor, mGluR5, Is a Key Determinant of Good and Bad Spatial Learning Performance and Hippocampal Synaptic Plasticity. *Cereb. Cortex* **2005**, *15* (11), 1703–1713.
- (140) Tigaret, C. M.; Olivo, V.; Sadowski, J. H. L. P.; Ashby, M. C.; Mellor, J. R. Coordinated Activation of Distinct Ca<sup>2+</sup> Sources and Metabotropic Glutamate Receptors Encodes Hebbian Synaptic Plasticity. *Nat. Commun.* **2016**, *7*, 10289.
- (141) Neyman, S.; Manahan-Vaughan, D. Metabotropic Glutamate Receptor 1 (mGluR1) and 5 (mGluR5) Regulate Late Phases of LTP and LTD in the Hippocampal CA1 Region in Vitro. *Eur. J. Neurosci.* **2008**, *27* (6), 1345–1352.
- (142) Lapointe, V.; Morin, F.; Ratté, S.; Croce, A.; Conquet, F.; Lacaille, J.-C. Synapse-Specific mGluR1-Dependent Long-Term Potentiation in Interneurons Regulates Mouse Hippocampal Inhibition. *J. Physiol.* **2004**, *555* (Pt 1), 125–135.
- (143) Le Vasseur, M.; Ran, I.; Lacaille, J. C. Selective Induction of Metabotropic Glutamate Receptor 1- and Metabotropic Glutamate Receptor 5-Dependent Chemical Long-Term Potentiation at Oriens/alveus Interneuron Synapses of Mouse Hippocampus. *Neuroscience* **2008**, *151* (1), 28–42.
- (144) Topolnik, L.; Azzi, M.; Morin, F.; Kougioumoutzakis, A.; Lacaille, J.-C. mGluR1/5 Subtype-Specific Calcium Signalling and Induction of Long-Term Potentiation in Rat Hippocampal Oriens/alveus Interneurons. *J. Physiol.* **2006**, *575* (Pt 1), 115–131.
- (145) Tan, Y.; Hori, N.; Carpenter, D. O. The Mechanism of Presynaptic Long-Term Depression Mediated by Group I Metabotropic Glutamate Receptors. *Cell. Mol. Neurobiol.* **2003**, *23* (2), 187–203.
- (146) Le Duigou, C.; Holden, T.; Kullmann, D. M. Short- and Long-Term Depression at Glutamatergic Synapses on Hippocampal Interneurons by Group I mGluR Activation. *Neuropharmacology* **2011**, *60* (5), 748–756.
- (147) Volk, L. J.; Daly, C. a; Huber, K. M. Differential Roles for Group 1 mGluR Subtypes in Induction and Expression of Chemically Induced Hippocampal Long-Term Depression. *J. Neurophysiol.* **2006**, *95* (January 2006), 2427–2438.
- (148) Wang, W.; Zhang, Z.; Shang, J.; Jiang, Z.-Z.; Wang, S.; Liu, Y.; Zhang, L.-Y. Activation of Group I Metabotropic Glutamate Receptors Induces Long-Term Depression in the Hippocampal CA1 Region of Adult Rats in Vitro. *Neurosci. Res.* **2008**, *62* (1), 43–50.
- (149) Chaouloff, F.; Hemar, A.; Manzoni, O. Acute Stress Facilitates Hippocampal CA1 Metabotropic Glutamate Receptor-Dependent Long-Term Depression. *J. Neurosci.* **2007**, *27* (27), 7130–7135.

- (150) Bordi, F.; Reggiani, A.; Conquet, F. Regulation of Synaptic Plasticity by mGluR1 Studied in Vivo in mGluR1 Mutant Mice. *Brain Res.* **1997**, *761* (1), 121–126.
- (151) Naie, K.; Manahan-Vaughan, D. Pharmacological Antagonism of Metabotropic Glutamate Receptor 1 Regulates Long-Term Potentiation and Spatial Reference Memory in the Dentate Gyrus of Freely Moving Rats via N-Methyl-D-Aspartate and Metabotropic Glutamate Receptor-Dependent Mechanisms. *Eur. J. Neurosci.* **2005**, *21* (2), 411–421.
- (152) Naie, K.; Tsanov, M.; Manahan-Vaughan, D. Group I Metabotropic Glutamate Receptors Enable Two Distinct Forms of Long-Term Depression in the Rat Dentate Gyrus in Vivo. *Eur. J. Neurosci.* **2007**, *25* (11), 3264–3275.
- (153) Nahir, B.; Lindsly, C.; Frazier, C. J. mGluR-Mediated and Endocannabinoid-Dependent Long-Term Depression in the Hilar Region of the Rat Dentate Gyrus. *Neuropharmacology* **2010**, *58* (4-5), 712–721.
- (154) Gravius, A.; Pietraszek, M.; Schmidt, W. J.; Danysz, W. Functional Interaction of NMDA and Group I Metabotropic Glutamate Receptors in Negatively Reinforced Learning in Rats. *Psychopharmacology (Berl.)* **2006**, *185* (1), 58–65.
- (155) Riedel, G.; Sandager-Nielsen, K.; Macphail, E. M. Impairment of Contextual Fear Conditioning in Rats by Group I mGluRs: Reversal by the Nootropic Nefiracetam. *Pharmacol. Biochem. Behav.* **2002**, *73* (2), 391–399.
- (156) Gravius, A.; Pietraszek, M.; Schafer, D.; Schmidt, W. J.; Danysz, W. Effects of mGlu1 and mGlu5 Receptor Antagonists on Negatively Reinforced Learning. *Behav Pharmacol* **2005**, *16* (2), 113–121.
- (157) Gravius, A.; Barberi, C.; Sch??fer, D.; Schmidt, W. J.; Danysz, W. The Role of Group I Metabotropic Glutamate Receptors in Acquisition and Expression of Contextual and Auditory Fear Conditioning in Rats - a Comparison. *Neuropharmacology* **2006**, *51* (7-8), 1146–1155.
- (158) Rudy, J. W.; Matus-Amat, P. DHPG Activation of Group 1 mGluRs in BLA Enhances Fear Conditioning. *Learn. Mem.* **2009**, *16* (7), 421–425.
- (159) Gil-Sanz, C.; Delgado-Garc??a, J. M.; Fair??n, A.; Gruart, A. Involvement of the mGluR1 Receptor in Hippocampal Synaptic Plasticity and Associative Learning in Behaving Mice. *Cereb. Cortex* **2008**, *18* (7), 1653–1663.
- (160) Baker, K. D.; Edwards, T. M.; Rickard, N. S. Inhibition of mGluR1 and IP3Rs Impairs Long-Term Memory Formation in Young Chicks. *Neurobiol. Learn. Mem.* **2008**, *90* (1), 269–274.
- (161) Gieros, K.; Sobczuk, A.; Salinska, E. Differential Involvement of mGluR1 and mGluR5 in Memory Reconsolidation and Retrieval in a Passive Avoidance Task in 1-Day Old Chicks. *Neurobiol. Learn. Mem.* **2012**, *97* (1), 165–172.
- (162) Schr??der, U. H.; M??ller, T.; Schreiber, R.; Stolle, A.; Zuschratter, W.; Balschun, D.; Jork, R.; Reymann, K. G. The Potent Non-Competitive mGlu1 Receptor Antagonist BAY 36-7620 Differentially Affects Synaptic Plasticity in Area Cornu Ammonis 1 of Rat Hippocampal Slices and Impairs Acquisition in the Water Maze Task in Mice. *Neuroscience* **2008**, *157* (2), 385–395.
- (163) Cinque, C.; Zuena, A. R.; Casolini, P.; Ngomba, R. T.; Melchiorri, D.; Maccari, S.; Nicoletti, F.; Di Giorgi Gerevini, V.; Catalani, A. Reduced Activity of Hippocampal Group-I Metabotropic Glutamate Receptors in Learning-Prone Rats. *Neuroscience* **2003**, *122* (1), 277–284.
- (164) Petersen, S.; Bomme, C.; Baastrup, C.; Kemp, A.; Christoffersen, G. R. J. Differential Effects of mGluR1 and mGluR5 Antagonism on Spatial Learning in Rats. *Pharmacol. Biochem. Behav.* **2002**, *73* (2), 381–389.

- (165) Sukhotina, I. A.; Dravolina, O. A.; Novitskaya, Y.; Zvartau, E. E.; Danysz, W.; Bepalov, A. Y. Effects of mGlu1 Receptor Blockade on Working Memory, Time Estimation, and Impulsivity in Rats. *Psychopharmacology (Berl)*. **2008**, *196* (2), 211–220.
- (166) Christoffersen, G. R.; Christensen, L. H.; Harrington, N. R.; Macphail, E. M.; Riedel, G. Task-Specific Enhancement of Short-Term, but Not Long-Term, Memory by Class I Metabotropic Glutamate Receptor Antagonist 1-Aminoindan-1,5-Dicarboxylic Acid in Rats. *Behav. Brain Res.* **1999**, *101* (2), 215–226.
- (167) Davarniya, B.; Hu, H.; Kahrizi, K.; Musante, L.; Fattahi, Z.; Hosseini, M.; Maqsood, F.; Farajollahi, R.; Wienker, T. F.; Ropers, H. H.; et al. The Role of a Novel TRMT1 Gene Mutation and Rare GRM1 Gene Defect in Intellectual Disability in Two Azeri Families. *PLoS One* **2015**, *10* (8), 1–13.
- (168) Conquet, F.; Bashir, Z. I.; Davies, C. H.; Daniel, H.; Ferraguti, F.; Bordi, F.; Franz-Bacon, K.; Reggiani, A.; Matarese, V.; Condé, F. Motor Deficit and Impairment of Synaptic Plasticity in Mice Lacking mGluR1. *Nature* **1994**, *372* (6503), 237–243.
- (169) Lalonde, R.; Strazielle, C. Brain Regions and Genes Affecting Postural Control. *Prog. Neurobiol.* **2007**, *81* (1), 45–60.
- (170) Ichise, T. mGluR1 in Cerebellar Purkinje Cells Essential for Long-Term Depression, Synapse Elimination, and Motor Coordination. *Science (80-. )*. **2000**, *288* (5472), 1832–1835.
- (171) Nakao, H.; Nakao, K.; Kano, M.; Aiba, A. Metabotropic Glutamate Receptor Subtype-1 Is Essential for Motor Coordination in the Adult Cerebellum. *Neurosci. Res.* **2007**, *57* (4), 538–543.
- (172) Aiba, A.; Kano, M.; Chen, C.; Stanton, M. E.; Fox, G. D.; Herrup, K.; Zwingman, T. A.; Tonegawa, S. Deficient Cerebellar Long-Term Depression and Impaired Motor Learning in mGluR1 Mutant Mice. *Cell* **1994**, *79* (2), 377–388.
- (173) Catania, M. V.; Bellomo, M.; Di Giorgi-Gerevini, V.; Seminara, G.; Giuffrida, R.; Romeo, R.; De Blasi, A.; Nicoletti, F. Endogenous Activation of Group-I Metabotropic Glutamate Receptors Is Required for Differentiation and Survival of Cerebellar Purkinje Cells. *J. Neurosci.* **2001**, *21* (19), 7664–7673.
- (174) Rampello, L.; Casolla, B.; Rampello, L.; Pignatelli, M.; Battaglia, G.; Gradini, R.; Orzi, F.; Nicoletti, F. The Conditioned Eyeblink Reflex: A Potential Tool for the Detection of Cerebellar Dysfunction in Multiple Sclerosis. *Mult. Scler. J.* **2011**, *17* (10), 1155–1161.
- (175) Conti, V.; Aghaie, A.; Cilli, M.; Martin, N.; Caridi, G.; Musante, L.; Candiano, G.; Castagna, M.; Fairen, A.; Ravazzolo, R.; et al. Crv4, a Mouse Model for Human Ataxia Associated with Kyphoscoliosis Caused by an mRNA Splicing Mutation of the Metabotropic Glutamate Receptor 1 (Grm1). *Int. J. Mol. Med.* **2006**, *18* (4), 593–600.
- (176) Katz, M. L.; Johnson, G. C.; Coates, J. R.; Brien, D. P. O. A Truncated R Etr Otrans Poson Disrupts the GRM1 Coding Sequence IN C O t on de T Ule Ar Dogs W I T H B a N D E R a ' S N E O N a T a L A T a X I a. **2011**, 267–272.
- (177) Notartomaso, S.; Zappulla, C.; Biagioni, F.; Cannella, M.; Bucci, D.; Mascio, G.; Scarselli, P.; Fazio, F.; Weisz, F.; Lionetto, L.; et al. Pharmacological Enhancement of mGlu1 Metabotropic Glutamate Receptors Causes a Prolonged Symptomatic Benefit in a Mouse Model of Spinocerebellar Ataxia Type 1. *Mol. Brain* **2013**, *6* (1), 48.
- (178) Rossi, P. I. A.; Musante, I.; Summa, M.; Pittaluga, A.; Emionite, L.; Ikehata, M.; Rastaldi, M. P.; Ravazzolo, R.; Puliti, A. Compensatory Molecular and Functional Mechanisms in Nervous System of the Grm1crv4 Mouse Lacking the mGlu1 Receptor: A Model for Motor Coordination Deficits. *Cereb. Cortex* **2013**, *23* (9), 2179–2189.
- (179) Rossi, P. I. A.; Vaccari, C. M.; Terracciano, A.; Doria-Lamba, L.; Facchinetti, S.; Priolo, M.; Ayuso, C.; De Jorge, L.; Gimelli, S.; Santorelli, F. M.; et al. The Metabotropic

- Glutamate Receptor 1, GRM1: Evaluation as a Candidate Gene for Inherited Forms of Cerebellar Ataxia. *J. Neurol.* **2010**, 257 (4), 598–602.
- (180) Marignier, R.; Chenevier, F.; Rogemond, V.; Sillevius Smitt, P.; Renoux, C.; Cavillon, G.; Androdias, G.; Vukusic, S.; Graus, F.; Honnorat, J.; et al. Metabotropic Glutamate Receptor Type 1 Autoantibody–Associated Cerebellitis. *Arch. Neurol.* **2010**, 67 (5), 627–630.
- (181) Guerguelcheva, V.; Azmanov, D. N.; Angelicheva, D.; Smith, K. R.; Chamova, T.; Florez, L.; Bynevelt, M.; Nguyen, T.; Cherninkova, S.; Bojinova, V.; et al. Autosomal-Recessive Congenital Cerebellar Ataxia Is Caused by Mutations in Metabotropic Glutamate Receptor 1. *Am. J. Hum. Genet.* **2012**, 91 (3), 553–564.
- (182) Fazio, F.; Notartomaso, S.; Aronica, E.; Storto, M.; Battaglia, G.; Vieira, E.; Gatti, S.; Bruno, V.; Biagioni, F.; Gradini, R.; et al. Switch in the Expression of mGlu1 and mGlu5 Metabotropic Glutamate Receptors in the Cerebellum of Mice Developing Experimental Autoimmune Encephalomyelitis and in Autoptic Cerebellar Samples from Patients with Multiple Sclerosis. *Neuropharmacology* **2008**, 55 (4), 491–499.
- (183) Ta, E.; Stachowicz, K. The Anxiolytic-like Activity of Aida (1-Aminoindan-1,5-Dicarboxylic Acid), an mGlu1 Receptor Antagonist. *Sci. York* **2004**, 113–126.
- (184) Steckler, T.; Lavreysen, H.; Oliveira, A. M.; Aerts, N.; Van Craenendonck, H.; Prickaerts, J.; Megens, A.; Lesage, A. S. J. Effects of mGlu1 Receptor Blockade on Anxiety-Related Behaviour in the Rat Lick Suppression Test. *Psychopharmacology (Berl.)* **2005**, 179 (1), 198–206.
- (185) Pietraszek, M.; Sukhanov, I.; Maciejak, P.; Szyndler, J.; Gravius, A.; Wisniewska, A.; Puzosnik, A.; Bepalov, A. Y.; Danysz, W. Anxiolytic-like Effects of mGlu1 and mGlu5 Receptor Antagonists in Rats. *Eur. J. Pharmacol.* **2005**, 514 (1), 25–34.
- (186) Kotlinska, J.; Bochenski, M. The Influence of Various Glutamate Receptors Antagonists on Anxiety-like Effect of Ethanol Withdrawal in a plus-Maze Test in Rats. *Eur. J. Pharmacol.* **2008**, 598 (1-3), 57–63.
- (187) Zhang, F.; Liu, B.; Lei, Z.; Wang, J.-H. mGluR1,5 Activation Improves Network Asynchrony and GABAergic Synapse Attenuation in the Amygdala: Implication for Anxiety-like Behavior in DBA/2 Mice. *Mol. Brain* **2012**, 5 (1), 20.
- (188) Ieraci, A.; Mallei, A.; Popoli, M. Social Isolation Stress Induces Anxious-Depressive-Like Behavior and Alterations of Neuroplasticity-Related Genes in Adult Male Mice. *Neural Plast.* **2016**, 2016.
- (189) Bianchi, R.; Chuang, S.-C.; Zhao, W.; Young, S. R.; Wong, R. K. S. Cellular Plasticity for Group I mGluR-Mediated Epileptogenesis. *J. Neurosci.* **2009**, 29 (11), 3497–3507.
- (190) Zhao, W.; Bianchi, R.; Wang, M.; Wong, R. K. S. Extracellular Signal-Regulated Kinase 1 / 2 Is Required for the Induction of Group I Metabotropic Glutamate Receptor-Mediated Epileptiform Discharges. *J. Neurosci.* **2004**, 24 (1), 76–84.
- (191) Al-Ghoul, W. M.; Meeker, R. B.; Greenwood, R. S. Kindled Seizures Increase Metabotropic Glutamate Receptor Expression and Function in the Rat Supraoptic Nucleus. *J Neurosci Res* **1998**, 54 (3), 412–423.
- (192) Karr, L.; Rutecki, P. A. Activity-Dependent Induction and Maintenance of Epileptiform Activity Produced by Group I Metabotropic Glutamate Receptors in the Rat Hippocampal Slice. *Epilepsy Res.* **2008**, 81 (1), 14–23.
- (193) Wang, M.; Bianchi, R.; Chuang, S. C.; Zhao, W.; Wong, R. K. S. Group I Metabotropic Glutamate Receptor-Dependent TRPC Channel Trafficking in Hippocampal Neurons. *J. Neurochem.* **2007**, 101 (2), 411–421.
- (194) Thuault, S. J.; Davies, C. H.; Randall, A. D.; Collingridge, G. L. Group I mGluRs

- Modulate the Pattern of Non-Synaptic Epileptiform Activity in the Hippocampus. *Neuropharmacology* **2002**, *43* (2), 141–146.
- (195) Stoop, R.; Conquet, F.; Pralong, E. Determination of Group I Metabotropic Glutamate Receptor Subtypes Involved in the Frequency of Epileptiform Activity in Vitro Using mGluR1 and mGluR5 Mutant Mice. *Neuropharmacology* **2003**, *44* (2), 157–162.
- (196) Lee, A. C.; Wong, R. K. S.; Chuang, S.-C.; Shin, H.-S.; Bianchi, R. Role of Synaptic Metabotropic Glutamate Receptors in Epileptiform Discharges in Hippocampal Slices. *J. Neurophysiol.* **2002**, *88* (4), 1625–1633.
- (197) Moldrich, R. X.; Chapman, A. G.; De Sarro, G.; Meldrum, B. S. Glutamate Metabotropic Receptors as Targets for Drug Therapy in Epilepsy. *Eur. J. Pharmacol.* **2003**, *476* (1-2), 3–16.
- (198) Wong, R. K. S.; Bianchi, R.; Chuang, S.-C.; Merlin, L. R. Group I mGluR-Induced Epileptogenesis: Distinct and Overlapping Roles of mGluR1 and mGluR5 and Implications for Antiepileptic Drug Design. *Epilepsy Curr.* **2005**, *5* (2), 63–68.
- (199) Chapman, A. G.; Yip, P. K.; Yap, J. S.; Quinn, L. P.; Tang, E.; Harris, J. R.; Meldrum, B. S. Anticonvulsant Actions of LY 367385 ((+)-2-Methyl-4-Carboxyphenylglycine) and AIDA ((RS)-1-Aminoindan-1,5-Dicarboxylic Acid). *Eur. J. Pharmacol.* **1999**, *368* (1), 17–24.
- (200) Akbar, M. T.; Rattray, M.; Powell, J. F.; Meldrum, B. S. Altered Expression of Group I Metabotropic Glutamate Receptors in the Hippocampus of Amygdala-Kindled Rats. *Mol. Brain Res.* **1996**, *43* (1-2), 105–116.
- (201) Avallone, J.; Gashi, E.; Magrys, B.; Friedman, L. K. Distinct Regulation of Metabotropic Glutamate Receptor (mGluR1 Alpha) in the Developing Limbic System Following Multiple Early-Life Seizures. *Exp. Neurol.* **2006**, *202* (1), 100–111.
- (202) Kirschstein, T.; Bauer, M.; Müller, L.; Rüschemschmidt, C.; Reitze, M.; Becker, A. J.; Schoch, S.; Beck, H. Loss of Metabotropic Glutamate Receptor-Dependent Long-Term Depression via Downregulation of mGluR5 after Status Epilepticus. *J. Neurosci.* **2007**, *27* (29), 7696–7704.
- (203) Aronica, E. M.; Gorter, J. a; Paupard, M. C.; Grooms, S. Y.; Bennett, M. V.; Zukin, R. S. Status Epilepticus-Induced Alterations in Metabotropic Glutamate Receptor Expression in Young and Adult Rats. *J. Neurosci.* **1997**, *17* (21), 8588–8595.
- (204) Guo, F.; Sun, F.; Yu, J. L.; Wang, Q. H.; Tu, D. Y.; Mao, X. Y.; Liu, R.; Wu, K. C.; Xie, N.; Hao, L. Y.; et al. Abnormal Expressions of Glutamate Transporters and Metabotropic Glutamate Receptor 1 in the Spontaneously Epileptic Rat Hippocampus. *Brain Res. Bull.* **2010**, *81* (4-5), 510–516.
- (205) Ngomba, R. T.; Santolini, I.; Biagioni, F.; Molinaro, G.; Simonyi, A.; Van Rijn, C. M.; D'Amore, V.; Mastroiacovo, F.; Olivieri, G.; Gradini, R.; et al. Protective Role for Type-1 Metabotropic Glutamate Receptors against Spike and Wave Discharges in the WAG/Rij Rat Model of Absence Epilepsy. *Neuropharmacology* **2011**, *60* (7-8), 1281–1291.
- (206) D'Amore, V.; Von Randow, C.; Nicoletti, F.; Ngomba, R. T.; Van Luijckelaar, G. Anti-Absence Activity of mGlu1 and mGlu5 Receptor Enhancers and Their Interaction with a GABA Reuptake Inhibitor: Effect of Local Infusions in the Somatosensory Cortex and Thalamus. *Epilepsia* **2015**, *56* (7), 1141–1151.
- (207) D'Amore, V.; Santolini, I.; Celli, R.; Lionetto, L.; De Fusco, A.; Simmaco, M.; Van Rijn, C. M.; Vieira, E.; Stauffer, S. R.; Conn, P. J.; et al. Head-to Head Comparison of mGlu1 and mGlu5 Receptor Activation in Chronic Treatment of Absence Epilepsy in WAG/Rij Rats. *Neuropharmacology* **2014**, *85*, 91–103.
- (208) Meyers, J. L.; Salling, M. C.; Almlı, L. M.; Ratanatharathorn, A.; Uddin, M.; Galea, S.; Wildman, D. E.; Aiello, A. E.; Bradley, B.; Ressler, K.; et al. Frequency of Alcohol

- Consumption in Humans; the Role of Metabotropic Glutamate Receptors and Downstream Signaling Pathways. *Transl. Psychiatry* **2015**, 5 (6), e586.
- (209) Simonyi, A.; Christian, M. R.; Sun, A. Y.; Sun, G. Y. Chronic Ethanol-Induced Subtype- and Subregion-Specific Decrease in the mRNA Expression of Metabotropic Glutamate Receptors in Rat Hippocampus. *Alcohol. Clin. Exp. Res.* **2004**, 28 (9), 1419–1423.
- (210) Bird, M. K.; Lawrence, A. J. Group I Metabotropic Glutamate Receptors: Involvement in Drug-Seeking and Drug-Induced Plasticity. *Curr. Mol. Pharmacol.* **2009**, 2 (1), 83–94.
- (211) Cozzoli, D. K.; Courson, J.; Wroten, M. G.; Greentree, D. I.; Lum, E. N.; Campbell, R. R.; Thompson, A. B.; Maliniak, D.; Worley, P. F.; Jonquieres, G.; et al. Binge Alcohol Drinking by Mice Requires Intact Group 1 Metabotropic Glutamate Receptor Signaling within the Central Nucleus of the Amygdala. *Neuropsychopharmacology* **2014**, 39 (2), 435–444.
- (212) Kotlinska, J. H.; Bochenski, M.; Danysz, W. The Role of Group I mGlu Receptors in the Expression of Ethanol-Induced Conditioned Place Preference and Ethanol Withdrawal Seizures in Rats. *Eur. J. Pharmacol.* **2011**, 670 (1), 154–161.
- (213) Reynolds, A. R.; Williams, L. A.; Saunders, M. A.; Prendergast, M. A. Group 1 mGlu-Family Proteins Promote Neuroadaptation to Ethanol and Withdrawal-Associated Hippocampal Damage. *Drug Alcohol Depend.* **2015**, 156, 213–220.
- (214) Olive, M. F. Metabotropic Glutamate Receptor Ligands as Potential Therapeutics for Addiction. *Curr. Drug Abuse Rev.* **2009**, 2 (1), 83–98.
- (215) Besheer, J.; Faccidomo, S.; Grondin, J. J. M.; Hodge, C. W. Effects of mGlu1-Receptor Blockade on Ethanol Self-Administration in Inbred Alcohol-Preferring Rats. *Alcohol* **2008**, 42 (1), 13–20.
- (216) Besheer, J.; Faccidomo, S.; Grondin, J. J. M.; Hodge, C. W. Regulation of Motivation to Self-Administer Ethanol by mGluR5 in Alcohol-Preferring (P) Rats. *Alcohol. Clin. Exp. Res.* **2008**, 32 (2), 209–221.
- (217) Besheer, J.; Grondin, J. J.; Salling, M. C.; Spanos, M.; Stevenson, R. A.; Hodge, C. W. Interoceptive Effects of Alcohol Require mGlu5 Receptor Activity in the Nucleus Accumbens. *J Neurosci* **2009**, 29 (30), 9582–9591.
- (218) Herrold, A. A.; Voigt, R. M.; Napier, T. C. mGluR5 Is Necessary for Maintenance of Methamphetamine-Induced Associative Learning. *Eur. Neuropsychopharmacol.* **2013**, 23 (7), 691–696.
- (219) Clewa, R. M.; Olive, M. F. mGlu Receptors and Drug Addiction. *Wiley Interdiscip. Rev. Membr. Transp. Signal.* **2012**, 1 (3), 281–295.
- (220) Schmidt, H. D.; Kimmey, B. A.; Arreola, A. C.; Pierce, R. C. Group I Metabotropic Glutamate Receptor-Mediated Activation of PKC Gamma in the Nucleus Accumbens Core Promotes the Reinstatement of Cocaine Seeking. *Addict. Biol.* **2015**, 20 (2), 285–296.
- (221) Ben-Shahar, O.; Sacramento, A. D.; Miller, B. W.; Webb, S. M.; Wroten, M. G.; Silva, H. E.; Caruana, A. L.; Gordon, E. J.; Ploense, K. L.; Ditzhazy, J.; et al. Deficits in Ventromedial Prefrontal Cortex Group 1 Metabotropic Glutamate Receptor Function Mediate Resistance to Extinction during Protracted Withdrawal from an Extensive History of Cocaine Self-Administration. *J Neurosci* **2013**, 33 (2), 495–506a.
- (222) Timmer, K. M.; Steketee, J. D. Group I Metabotropic Glutamate Receptors in the Medial Prefrontal Cortex: Role in Mesocorticolimbic Glutamate Release in Cocaine Sensitization. *Synapse* **2013**, 67 (12), 887–896.
- (223) Rphu, L. Q. Evidence for a Relationship between Group 1 mGluR Hypofunction and Increased Cocaine and Ethanol Sensitivity in Homer2 Null Mutant Mice. *5*, 9–12.



- (224) Mitrano, D. A.; Arnold, C.; Smith, Y. Subcellular and Subsynaptic Localization of Group I Metabotropic Glutamate Receptors in the Nucleus Accumbens of Cocaine-Treated Rats. *Neuroscience* **2008**, *154* (2), 653–666.
- (225) Swanson, C. J.; Baker, D. A.; Carson, D.; Worley, P. F.; Kalivas, P. W. Repeated Cocaine Administration Attenuates Group I Metabotropic Glutamate Receptor-Mediated Glutamate Release and Behavioral Activation: A Potential Role for Homer. *J. Neurosci.* **2001**, *21* (22), 9043–9052.
- (226) McCutcheon, J. E.; Loweth, J. A.; Ford, K. A.; Marinelli, M.; Wolf, M. E.; Tseng, K. Y. Group I mGluR Activation Reverses Cocaine-Induced Accumulation of Calcium-Permeable AMPA Receptors in Nucleus Accumbens Synapses via a Protein Kinase C-Dependent Mechanism. *J. Neurosci.* **2011**, *31* (41), 14536–14541.
- (227) Loweth, J. a; Scheyer, A. F.; Milovanovic, M.; LaCrosse, A. L.; Flores-Barrera, E.; Werner, C. T.; Li, X.; Ford, K. a; Le, T.; Olive, M. F.; et al. Synaptic Depression via mGluR1 Positive Allosteric Modulation Suppresses Cue-Induced Cocaine Craving. *Nat. Neurosci.* **2014**, *17* (1), 73–80.
- (228) Loweth, J. A.; Tseng, K. Y.; Wolf, M. E. Using Metabotropic Glutamate Receptors to Modulate Cocaine's Synaptic and Behavioral Effects: MGluR1 Finds a Niche. *Curr. Opin. Neurobiol.* **2013**, *23* (4), 500–506.
- (229) Yuan, T.; Mameli, M.; O'Connor, E. C.; Dey, P.; Verpelli, C.; Sala, C.; Perez-Otano, I.; Lüscher, C.; Bellone, C. Expression of Cocaine-Evoked Synaptic Plasticity by GluN3A-Containing NMDA Receptors. *Neuron* **2013**, *80* (4), 1025–1038.
- (230) Bakshi, K.; Parihar, R.; Goswami, S. K.; Walsh, M.; Friedman, E.; Wang, H. Y. Prenatal Cocaine Exposure Uncouples mGluR1 from Homer1 and Gq Proteins. *PLoS One* **2014**, *9* (3), 1–10.
- (231) Bellone, C.; Mameli, M.; Lüscher, C. In Utero Exposure to Cocaine Delays Postnatal Synaptic Maturation of Glutamatergic Transmission in the VTA. *Nat. Neurosci.* **2011**, *14* (11), 1439–1446.
- (232) Gupta, D. S.; McCullumsmith, R. E.; Beneyto, M.; Haroutunian, V.; Davis, K. L.; Meador-Woodruff, J. H. Metabotropic Glutamate Receptor Protein Expression in the Prefrontal Cortex and Striatum in Schizophrenia. *Synapse* **2005**, *57* (3), 123–131.
- (233) Richardson-Burns, S. M.; Haroutunian, V.; Davis, K. L.; Watson, S. J.; Meador-Woodruff, J. H. Metabotropic Glutamate Receptor mRNA Expression in the Schizophrenic Thalamus. *Biol. Psychiatry* **2000**, *47* (1), 22–28.
- (234) Volk, D. W.; Eggan, S. M.; Lewis, D. A. Alterations in Metabotropic Glutamate Receptor 1alpha and Regulator of G Protein Signaling 4 in the Prefrontal Cortex in Schizophrenia. *Am. J. Psychiatry* **2010**, *167* (12), 1489–1498.
- (235) Brody, S. A.; Conquet, F.; Geyer, M. A. Disruption of Prepulse Inhibition in Mice Lacking mGluR1. *Eur. J. Neurosci.* **2003**, *18* (12), 3361–3366.
- (236) Pietraszek, M.; Gravius, A.; Schäfer, D.; Weil, T.; Trifanova, D.; Danysz, W. mGluR5, but Not mGluR1, Antagonist Modifies MK-801-Induced Locomotor Activity and Deficit of Prepulse Inhibition. *Neuropharmacology* **2005**, *49* (1), 73–85.
- (237) Varty, G. B.; Grilli, M.; Forlani, A.; Fredduzzi, S.; Grzelak, M. E.; Guthrie, D. H.; Hodgson, R. A.; Lu, S. X.; Nicolussi, E.; Pond, A. J.; et al. The Antinociceptive and Anxiolytic-like Effects of the Metabotropic Glutamate Receptor 5 (mGluR5) Antagonists, MPEP and MTEP, and the mGluR1 Antagonist, LY456236, in Rodents: A Comparison of Efficacy and Side-Effect Profiles. *Psychopharmacology (Berl)*. **2005**, *179* (1), 207–217.
- (238) Kim, W. Y.; Vezina, P.; Kim, J. H. Blockade of Group II, but Not Group I, mGluRs in the Rat Nucleus Accumbens Inhibits the Expression of Conditioned Hyperactivity in an Amphetamine-Associated Environment. *Behav. Brain Res.* **2008**, *191* (1), 62–66.

- (239) Kim, J. H.; Vezina, P. Metabotropic Glutamate Receptors in the Rat Nucleus Accumbens Contribute to Amphetamine-Induced Locomotion. *J. Pharmacol. Exp. Ther.* **1998**, *284* (1), 317–322.
- (240) Bhardwaj, S. K.; Ryan, R. T.; Wong, T. P.; Srivastava, L. K. Loss of Dysbindin-1, a Risk Gene for Schizophrenia, Leads to Impaired Group 1 Metabotropic Glutamate Receptor Function in Mice. *Front. Behav. Neurosci.* **2015**, *9* (March), 72.
- (241) Frank, R. A. W.; McRae, A. F.; Pocklington, A. J.; van de Lagemaat, L. N.; Navarro, P.; Croning, M. D. R.; Komiyama, N. H.; Bradley, S. J.; Challiss, R. A. J.; Armstrong, J. D.; et al. Clustered Coding Variants in the Glutamate Receptor Complexes of Individuals with Schizophrenia and Bipolar Disorder. *PLoS One* **2011**, *6* (4).
- (242) Ayoub, M. A.; Angelicheva, D.; Vile, D.; Chandler, D.; Morar, B.; Cavanaugh, J. A.; Visscher, P. M.; Jablensky, A.; Pflieger, K. D. G.; Kalaydjieva, L. Deleterious GRM1 Mutations in Schizophrenia. *PLoS One* **2012**, *7* (3).
- (243) Downey, P. M.; Petr??, R.; Simon, J. S.; Devlin, D.; Lozza, G.; Veltri, A.; Beltramo, M.; Bertorelli, R.; Reggiani, A. Identification of Single Nucleotide Polymorphisms of the Human Metabotropic Glutamate Receptor 1 Gene and Pharmacological Characterization of a P993S Variant. *Biochem. Pharmacol.* **2009**, *77* (7), 1246–1253.
- (244) Mutel, V.; Ellis, G. J.; Adam, G.; Chaboz, S.; Nilly, A.; Messer, J.; Bleuel, Z.; Metzler, V.; Malherbe, P.; Schlaeger, E. J.; et al. Characterization of [3H]quisqualate Binding to Recombinant Rat Metabotropic Glutamate 1a and 5a Receptors and to Rat and Human Brain Sections. *J. Neurochem.* **2000**, *75* (6), 2590–2601.
- (245) Kingston, A. E.; Lowndes, J.; Evans, N.; Clark, B.; Tomlinson, R.; Burnett, J. P.; Mayne, N. G.; Cockerham, S. L.; Lodge, D. Sulphur-Containing Amino Acids Are Agonists for Group 1 Metabotropic Receptors Expressed in Clonal RGT Cell Lines. *Neuropharmacology* **1998**, *37* (3), 277–287.
- (246) Desai, M. A.; Burnett, J. P.; Mayne, N. G.; Schoepp, D. Pharmacological Characterization of Desensitization in a Humand mGluR1a-Expressing Non-Neuronal Cell Line Co-Transfected with a Glutamate Transporter. *Br J Pharmacol* **1996**, *118*, 1558–1564.
- (247) Brabet, I.; Parmentier, M. L.; De Colle, C.; Bockaert, J.; Acher, F.; Pin, J. P. Comparative Effect of L-CCG-I, DCG-IV and Gamma-Carboxy-L-Glutamate on All Cloned Metabotropic Glutamate Receptor Subtypes. *Neuropharmacology* **1998**, *37* (8), 1043–1051.
- (248) Saugstad, J. A.; Segerson, T. P.; Westbrook, G. L. L-2-Amino-3-Phosphonopropionic Acid Competitively Antagonizes Metabotropic Glutamate Receptors 1?? And 5 in *Xenopus* Oocytes. *Eur. J. Pharmacol. Mol. Pharmacol.* **1995**, *289* (2), 395–397.
- (249) Madsen, U.; Bräuner-Osborne, H.; Frydenvang, K.; Hvene, L.; Johansen, T. N.; Nielsen, B.; Sánchez, C.; Stensbøl, T. B.; Bischoff, F.; Krogsgaard-Larsen, P. Synthesis and Pharmacology of 3-Isoxazolol Amino Acids as Selective Antagonists at Group I Metabotropic Glutamic Acid Receptors. *J. Med. Chem.* **2001**, *44* (7), 1051–1059.
- (250) Sekiyama, N.; Hayashi, Y.; Nakanishi, S.; Jane, D. E.; Tse, H.-W.; Birse, E. F.; Watkins, J. C. Structure-Activity Relationships of New Agonists and Antagonists of Different Metabotropic Glutamate Receptor Subtypes. *Br. J. Pharmacol.* **1996**, *117*, 1493–1503.
- (251) Watkins, J.; Collingridge, G. Phenylglycine Derivatives as Antagonists of Metabotropic Glutamate Receptors. *Trends Pharmacol. Sci.* **1994**, *15* (9), 333–342.
- (252) Moroni, F.; Attucci, S.; Cozzi, A.; Meli, E.; Picca, R.; Scheideler, M. A.; Pellicciari, R.; Noe, C.; Sarichelou, I.; Pellegrini-Giampietro, D. E. The Novel and Systemically Active Metabotropic Glutamate 1 (mGlu1) Receptor Antagonist 3-MATIDA Reduces Post-Ischemic Neuronal Death. *Neuropharmacology* **2002**, *42* (6), 741–751.
- (253) Clark, B. P.; Baker, S. R.; Goldsworthy, J.; Harris, J. R.; Kingston, A. E. (+)-2-Methyl-4-

- Carboxyphenylglycine (LY367385) Selectively Antagonises Metabotropic Glutamate mGluR1 Receptors. *Bioorganic Med. Chem. Lett.* **1997**, 7 (21), 2777–2780.
- (254) Bedingfield, J. S.; Kemp, M. C.; Jane, D. E.; Tse, H. W.; Roberts, P. J.; Watkins, J. C. Structure-Activity Relationships for a Series of Phenylglycine Derivatives Acting at Metabotropic Glutamate Receptors (mGluRs). *Br. J. Pharmacol.* **1995**, 116 (8), 3323–3329.
- (255) Hermans, E.; Nahorski, S. R.; Challiss, R. A. J. Reversible and Non-Competitive Antagonist Profile of CPCCOEt at the Human Type 1?? Metabotropic Glutamate Receptor. *Neuropharmacology* **1998**, 37 (12), 1645–1647.
- (256) Litschig, S.; Gasparini, F.; Rueegg, D.; Stoehr, N.; Flor, P. J.; Vranesic, I.; Prézeau, L.; Pin, J. P.; Thomsen, C.; Kuhn, R. CPCCOEt, a Noncompetitive Metabotropic Glutamate Receptor 1 Antagonist, Inhibits Receptor Signaling without Affecting Glutamate Binding. *Mol. Pharmacol.* **1999**, 55 (3), 453–461.
- (257) Carroll, F. Y.; Stolle, a; Beart, P. M.; Voerste, a; Brabet, I.; Mauler, F.; Joly, C.; Antonicek, H.; Bockaert, J.; Müller, T.; et al. BAY36-7620: A Potent Non-Competitive mGlu1 Receptor Antagonist with Inverse Agonist Activity. *Mol. Pharmacol.* **2001**, 59 (5), 965–973.
- (258) Malherbe, P.; Kratochwil, N.; Knoflach, F.; Zenner, M. T.; Kew, J. N. C.; Kratzeisen, C.; Maerki, H. P.; Adam, G.; Mutel, V. Mutational Analysis and Molecular Modeling of the Allosteric Binding Site of a Novel, Selective, Noncompetitive Antagonist of the Metabotropic Glutamate 1 Receptor. *J. Biol. Chem.* **2003**, 278 (10), 8340–8347.
- (259) Lavreysen, H.; Janssen, C.; Bischoff, F.; Langlois, X.; Leysen, J. E.; Lesage, A. S. J. [3H]R214127: A Novel High-Affinity Radioligand for the mGlu1 Receptor Reveals a Common Binding Site Shared by Multiple Allosteric Antagonists. *Mol. Pharmacol.* **2003**, 63 (5), 1082–1093.
- (260) Lavreysen, H.; Wouters, R.; Bischoff, F.; N??brega Pereira, S.; Langlois, X.; Blokland, S.; Somers, M.; Dillen, L.; Lesage, A. S. J. JNJ16259685, a Highly Potent, Selective and Systemically Active mGlu1 Receptor Antagonist. *Neuropharmacology* **2004**, 47 (7), 961–972.
- (261) El-Kouhen, O.; Lehto, S. G.; Pan, J. B.; Chang, R.; Baker, S. J.; Zhong, C.; Hollingsworth, P. R.; Mikusa, J. P.; Cronin, E. a; Chu, K. L.; et al. Blockade of mGluR1 Receptor Results in Analgesia and Disruption of Motor and Cognitive Performances: Effects of A-841720, a Novel Non-Competitive mGluR1 Receptor Antagonist. *Br. J. Pharmacol.* **2006**, 149 (6), 761–774.
- (262) Wang, X.; Kolasa, T.; El Kouhen, O. F.; Chovan, L. E.; Black-Shaefer, C. L.; Wagenaar, F. L.; Garton, J. A.; Moreland, R. B.; Honore, P.; Lau, Y. Y.; et al. Rapid Hit to Lead Evaluation of pyrazolo[3,4-D]pyrimidin-4-One as Selective and Orally Bioavailable mGluR1 Antagonists. *Bioorganic Med. Chem. Lett.* **2007**, 17 (15), 4303–4307.
- (263) Sasikumar, T. K.; Qiang, L.; Burnett, D. A.; Greenlee, W. J.; Li, C.; Heimark, L.; Pramanik, B.; Grilli, M.; Bertorelli, R.; Lozza, G.; et al. Tricyclic Thienopyridine-Pyrimidones/thienopyrimidine-Pyrimidones as Orally Efficacious mGluR1 Antagonists for Neuropathic Pain. *Bioorganic Med. Chem. Lett.* **2009**, 19 (12), 3199–3203.
- (264) Van Hoorn, W. P.; Bell, A. S. Searching Chemical Space with the Bayesian Idea Generator. *J. Chem. Inf. Model.* **2009**, 49 (10), 2211–2220.
- (265) Mantell, S. J.; Gibson, K. R.; Osborne, S. A.; Maw, G. N.; Rees, H.; Dodd, P. G.; Greener, B.; Harbottle, G. W.; Million, W. A.; Poinard, C.; et al. In Vitro and in Vivo SAR of pyrido[3,4-D]pyrimidin-4-Ylamine Based mGluR1 Antagonists. *Bioorganic Med. Chem. Lett.* **2009**, 19 (8), 2190–2194.
- (266) Shannon, H. E.; Peters, S. C.; Kingston, A. E. Anticonvulsant Effects of LY456236, a

- Selective mGlu1 Receptor Antagonist. *Neuropharmacology* **2005**, *49* (SUPPL.), 188–195.
- (267) Suzuki, G.; Kimura, T.; Satow, A.; Kaneko, N.; Fukuda, J.; Hikichi, H.; Sakai, N.; Maehara, S.; Kawagoe-takaki, H.; Hata, M.; et al. Pharmacological Characterization of a New , Orally Active and Potent Allosteric Metabotropic Glutamate Receptor 1 Antagonist, 4-[1-(2-Fluoropyridin-3-Yl)-5-Methyl-1H-1,2,3-Triazol-4-Yl]-N-Isopropyl-N-Methyl-3,6-Dihydropyridine-1(2H)-Carboxamide (FTIDC). *Pharmacology* **2007**, *321* (3), 1144–1153.
- (268) Satow, A.; Maehara, S.; Ise, S.; Hikichi, H.; Fukushima, M.; Suzuki, G.; Kimura, T.; Tanak, T.; Ito, S.; Kawamoto, H.; et al. Pharmacological Effects of the Metabotropic Glutamate Receptor 1 Antagonist Compared with Those of the Metabotropic Glutamate Receptor 5 Antagonist and Metabotropic Glutamate Receptor 2 / 3 Agonist in Rodents : Detailed Investigations with a Selective All. *Pharmacology* **2008**, *326* (2), 577–586.
- (269) Satoh, A.; Nagatomi, Y.; Hirata, Y.; Ito, S.; Suzuki, G.; Kimura, T.; Maehara, S.; Hikichi, H.; Satow, A.; Hata, M.; et al. Discovery and in Vitro and in Vivo Profiles of 4-Fluoro-N-[4-[6-(Isopropylamino)pyrimidin-4-Yl]-1,3-Thiazol-2-Yl]-N-Methylbenzamide as Novel Class of an Orally Active Metabotropic Glutamate Receptor 1 (mGluR1) Antagonist. *Bioorganic Med. Chem. Lett.* **2009**, *19* (18), 5464–5468.
- (270) Xie, L.; Yui, J.; Fujinaga, M.; Hatori, A.; Yamasaki, T.; Kumata, K.; Wakizaka, H.; Furutsuka, K.; Takei, M.; Jin, Z. H.; et al. Molecular Imaging of Ectopic Metabotropic Glutamate 1 Receptor in Melanoma with a Positron Emission Tomography Radioprobe 18F-FITM. *Int. J. Cancer* **2014**, *135* (8), 1852–1859.
- (271) Micheli, F.; Cavanni, P.; Di Fabio, R.; Marchioro, C.; Donati, D.; Faedo, S.; Maffei, M.; Sabbatini, F. M.; Tranquillini, M. E. From Pyrroles to pyrrolo[1,2-A]pyrazinones: A New Class of mGluR1 Antagonists. *Bioorganic Med. Chem. Lett.* **2006**, *16* (5), 1342–1345.
- (272) Kohara, A.; Takahashi, M.; Yatsugi, S. ichi; Tamura, S.; Shitaka, Y.; Hayashibe, S.; Kawabata, S.; Okada, M. Neuroprotective Effects of the Selective Type 1 Metabotropic Glutamate Receptor Antagonist YM-202074 in Rat Stroke Models. *Brain Res.* **2008**, *1191*, 168–179.
- (273) Kohara, A.; Nagakura, Y.; Kiso, T.; Toya, T.; Watabiki, T.; Tamura, S.; Shitaka, Y.; Itahana, H.; Okada, M. Antinociceptive Profile of a Selective Metabotropic Glutamate Receptor 1 Antagonist YM-230888 in Chronic Pain Rodent Models. *Eur. J. Pharmacol.* **2007**, *571* (1), 8–16.
- (274) Kohara, A.; Toya, T.; Tamura, S.; Watabiki, T.; Nagakura, Y.; Shitaka, Y.; Hayashibe, S.; Kawabata, S.; Okada, M. Radioligand Binding Properties and Pharmacological Characterization of 6-Amino- N -Cyclohexyl- N , 3- 298198 ), a High-Affinity , Selective , and Noncompetitive Antagonist of Metabotropic Glutamate Receptor Type 1. *J. Pharmacol. Exp. Ther.* **2005**, *315* (1), 163–169.
- (275) Noeske, T.; Trifanova, D.; Kaus, V.; Renner, S.; Parsons, C. G.; Schneider, G.; Weil, T. Synergism of Virtual Screening and Medicinal Chemistry: Identification and Optimization of Allosteric Antagonists of Metabotropic Glutamate Receptor 1. *Bioorganic Med. Chem.* **2009**, *17* (15), 5708–5715.
- (276) Lovell, K. M.; Felts, A. S.; Rodriguez, A. L.; Venable, D. F.; Cho, H. P.; Morrison, R. D.; Byers, F. W.; Daniels, J. S.; Niswender, C. M.; Conn, P. J.; et al. N-Acyl-N'-Arylpiperazines as Negative Allosteric Modulators of mGlu1: Identification of VU0469650, a Potent and Selective Tool Compound with CNS Exposure in Rats. *Bioorganic Med. Chem. Lett.* **2013**, *23* (13), 3713–3718.
- (277) Annoura, H.; Fukunaga, A.; Uesugi, M.; Tatsuoka, T.; Horikawa, Y. A Novel Class of Antagonists for Metabotropic Glutamate Receptors, 7-(Hydroxyimino)cyclopropa[b]chromen-1a-Carboxylates. *Bioorganic Med. Chem. Lett.* **1996**, *6* (7), 763–766.

- (278) Fukuda, J.; Suzuki, G.; Kimura, T.; Nagatomi, Y.; Ito, S.; Kawamoto, H.; Ozaki, S.; Ohta, H. Identification of a Novel Transmembrane Domain Involved in the Negative Modulation of mGluR1 Using a Newly Discovered Allosteric mGluR1 Antagonist, 3-Cyclohexyl-5-Fluoro-6-Methyl-7-(2-Morpholin-4-Ylethoxy)-4H-Chromen-4-One. *Neuropharmacology* **2009**, *57* (4), 438–445.
- (279) Miller, T.; Krogan, N. J.; Dover, J.; Tempst, P.; Johnston, M.; Greenblatt, J. F.; Sherman, D. R.; Voskuil, M.; Schnappinger, D.; Harrell, M. I.; et al. Positive Allosteric Modulators of Metabotropic Glutamate 1 Receptor: Characterization, Mechanism of Action, and Binding Site. **2001**, *98* (26).
- (280) Hemstapat, K. A Novel Class of Positive Allosteric Modulators of Metabotropic Glutamate Receptor Subtype 1 Interact with a Site Distinct from That of Negative Allosteric Modulators. *Mol. Pharmacol.* **2006**, *70* (2), 616–626.
- (281) Vieira, E.; Huwyler, J.; Jolidon, S.; Knoflach, F.; Mutel, V.; Wichmann, J. Fluorinated 9H-Xanthene-9-Carboxylic Acid Oxazol-2-Yl-Amides as Potent, Orally Available mGlu1 Receptor Enhancers. *Bioorganic Med. Chem. Lett.* **2009**, *19* (6), 1666–1669.
- (282) Wichmann, J.; Bleicher, K.; Vieira, E.; Woltering, T.; Knoflach, F.; Mutel, V. Alkyl Diphenylacetyl, 9H-Xanthene- and 9H-Thioxanthene-Carbonyl Carbamates as Positive Allosteric Modulators of mGlu1 Receptors. *Farmaco* **2002**, *57* (12), 989–992.
- (283) Vieira, E.; Huwyler, J.; Jolidon, S.; Knoflach, F.; Mutel, V.; Wichmann, J. 9H-Xanthene-9-Carboxylic Acid [1,2,4]oxadiazol-3-Yl- and (2H-Tetrazol-5-Yl)-Amides as Potent, Orally Available mGlu1 Receptor Enhancers. *Bioorganic Med. Chem. Lett.* **2005**, *15* (20), 4628–4631.
- (284) Jain, A. N. Ligand-Based Structural Hypotheses for Virtual Screening. *J. Med. Chem.* **2004**, *47* (4), 947–961.
- (285) Jones, C. K.; Engers, D. W.; Thompson, A. D.; Field, J. R.; Blobaum, A. L.; Lindsley, S. R.; Zhou, Y.; Gogliotti, R. D.; Jadhav, S.; Zamorano, R.; et al. Discovery, Synthesis, and Structure-Activity Relationship Development of a Series of N-4-(2,5-Dioxopyrrolidin-1-Yl)phenylpicolinamides (VU0400195, ML182): Characterization of a Novel Positive Allosteric Modulator of the Metabotropic Glutamate Receptor 4 (. *J. Med. Chem.* **2011**, *54* (21), 7639–7647.
- (286) Bento, A. P.; Gaulton, A.; Hersey, A.; Bellis, L. J.; Chambers, J.; Davies, M.; Krüger, F. A.; Light, Y.; Mak, L.; McGlinchey, S.; et al. The ChEMBL Bioactivity Database: An Update. *Nucleic Acids Res.* **2014**, *42* (D1), 1083–1090.
- (287) Gasteiger, J.; Rudolph, C.; Sadowski, J. Automatic Generation of 3D-Atomic Coordinates for Organic Molecules. *Tetrahedron Comput. Methodol.* **1990**, *3* (6 PART C), 537–547.
- (288) Mendenhall, J.; Meiler, J. Improving Quantitative Structure-Activity Relationship Models Using Artificial Neural Networks Trained with Dropout. *J. Comput. Aided. Mol. Des.* **2016**, *30* (2), 177–189.
- (289) Bemis, G. W.; Murcko, M. A. The Properties of Known Drugs. 1. Molecular Frameworks. *J. Med. Chem.* **1996**, *39* (15), 2887–2893.
- (290) Willett, P.; Barnard, J. M.; Downs, G. M. Chemical Similarity Searching. *J. Chem. Inf. Model.* **1998**, *38* (6), 983–996.
- (291) De Paulis, T.; Hemstapat, K.; Chen, Y.; Zhang, Y.; Saleh, S.; Alagille, D.; Baldwin, R. M.; Tamagnan, G. D.; Conn, P. J. Substituent Effects of N-(1,3-Diphenyl-1H-Pyrazol-5-Yl)benzamides on Positive Allosteric Modulation of the Metabotropic Glutamate-5 Receptor in Rat Cortical Astrocytes. *J. Med. Chem.* **2006**, *49* (11), 3332–3344.
- (292) Carmichael, O.; Lockhart, S. The Role of Diffusion Tensor Imaging in the Study of Cognitive Aging. *Brain Imaging Behav. Neurosci.* **2012**, No. November 2011, 289–320.

- (293) Lindsley, C. W.; Emmitte, K. A.; Hopkins, C. R.; Bridges, T. M.; Gregory, K. J.; Niswender, C. M.; Conn, P. J. Practical Strategies and Concepts in GPCR Allosteric Modulator Discovery: Recent Advances with Metabotropic Glutamate Receptors. *Chem. Rev.* **2016**, acs.chemrev.5b00656.
- (294) Lindsley, C. W. 2013 Philip S. Portoghese Medicinal Chemistry Lectureship: Drug Discovery Targeting Allosteric Sites. *J. Med. Chem.* **2014**, *57* (18), 7485–7498.
- (295) Engers, D. W.; Lindsley, C. W. Allosteric Modulation of Class C GPCRs: A Novel Approach for the Treatment of CNS Disorders. *Drug Discov. Today Technol.* **2013**, *10* (2), e269–e276.
- (296) Conn, P. J.; Lindsley, C. W.; Meiler, J.; Niswender, C. M. Opportunities and Challenges in the Discovery of Allosteric Modulators of GPCRs for Treating CNS Disorders. *Nat. Rev. Drug Discov.* **2014**, *13* (9), 692–708.
- (297) Conn, P. J.; Lindsley, C. W.; Jones, C. K. Activation of Metabotropic Glutamate Receptors as a Novel Approach for the Treatment of Schizophrenia. *Trends Pharmacol. Sci.* **2009**, *30* (1), 25–31.
- (298) Noetzel, M. J.; Rook, J. M.; Vinson, P. N.; Cho, H. P.; Days, E.; Zhou, Y.; Rodriguez, A. L.; Lavreysen, H.; Stauffer, S. R.; Niswender, C. M.; et al. Functional Impact of Allosteric Agonist Activity of Selective Positive Allosteric Modulators of Metabotropic Glutamate Receptor Subtype 5 in Regulating Central Nervous System Function. *Mol. Pharmacol.* **2012**, *81* (2), 120–133.
- (299) Rook, J. M.; Noetzel, M. J.; Pouliot, W. A.; Bridges, T. M.; Vinson, P. N.; Cho, H. P.; Zhou, Y.; Gogliotti, R. D.; Manka, J. T.; Gregory, K. J.; et al. Unique Signaling Profiles of Positive Allosteric Modulators of Metabotropic Glutamate Receptor Subtype 5 Determine Differences in in Vivo Activity. *Biol. Psychiatry* **2013**, *73* (6), 501–509.
- (300) Bridges, T. M.; Rook, J. M.; Noetzel, M. J.; Morrison, R. D.; Zhou, Y.; Gogliotti, R. D.; Vinson, P. N.; Xiang, Z.; Jones, C. K.; Niswender, C. M.; et al. Biotransformation of a Novel Positive Allosteric Modulator of mGlu5 Contributes to Seizures in Rats Involving a Receptor Agonism-Dependent Mechanism. *Drug Metab. Dispos.* **2013**.
- (301) Rook, J. M.; Noetzel, M. J.; Pouliot, W. A.; Bridges, T. M.; Vinson, P. N.; Cho, H. P.; Zhou, Y.; Gogliotti, R. D.; Manka, J. T.; Gregory, K. J.; et al. Unique Signaling Profiles of Positive Allosteric Modulators of Metabotropic Glutamate Receptor Subtype 5 Determine Differences in in Vivo Activity. *Biol. Psychiatry* **2013**, *73* (6), 501–509.
- (302) Racine, R. J. Modification of Seizure Activity by Electrical Stimulation: II. Motor Seizure. *Electroencephalogr. Clin. Neurophysiol.* **1972**, *32* (3), 281–294.
- (303) Gillis, E. P.; Eastman, K. J.; Hill, M. D.; Donnelly, D. J.; Meanwell, N. A. Applications of Fluorine in Medicinal Chemistry. *J. Med. Chem.* **2015**, *58* (21), 8315–8359.